Proceedings

11^{th} International Conference on Mathematical and Numerical Aspects of Waves

WAVES 2013

June 3-7, 2013

Gammarth, Tunisia

Proceedings of the 11^{th} International Conference on Mathematical and Numerical Aspects of Waves (WAVES 2013)

June 3-7, 2013, Gammarth, Tunisia

Conference homepage
http://www.enit.rnu.tn/waves2013

Slides at
http://www.enit.rnu.tn/waves2013

Online Proceedings at
http://www.enit.rnu.tn/waves2013

Scientific committee

Chair

Patrick Joly

International Program Committee

Mark Ainsworth
Xavier Antoine
Alex Barnett
Héléne Barucq
Eliane Bécache
Abderrahmane Bendali
Marc Bonnet
Anne-Sophie Bonnet-Bendhia
Liliana Borcea
Oscar Bruno
Anna-Lisa Buffa
Fioralba Cakoni
Simon Neil Chandler-Wilde
Francis Collino
Martin Costabel
Laurent Demanet
Julien Diaz
Rabia Djellouli
Sonia Fliss
Josselin Garnier
Dan Givoli
Nabil Gmati
Houssem Haddar
Thomas Hagstrom
Laurence Halpern
Christophe Hazard
Jan Hesthaven
Ralf Hiptmair
Thorsten Hohage
Manfred Kaltenbacher
Andreas Kirsch
Olivier Lafitte
Armin Lechleiter
Eric Lunéville
Paul Martin
Peter Monk
Jean-Claude Nédélec
David Peter Nicholls
Nilima Nigam
Naoshi Nishimura
George C. Papanicolaou
Joseph E. Pasciak
Roland Potthast
Jeffrey Rauch
Jerónimo Rodríguez García
Olof Runborg
Dominik Schoetzau
Geza Seriani
Ricardo Weder

Preface

The 11th International Conference on Mathematical and Numerical Aspects of Waves Propagation is jointly organized and supported by ENIT-LAMSIN, ENSTA and INRIA. This conference is the main venue where significant advances in the analysis and computational modeling of wave phenomena and exciting new applications are presented. This book summarizes the works that have been selected for presentation at the conference and is composed of extended abstracts for invited plenary talks, two-pages abstracts for invited minisymposia talks and two-pages abstracts for selected contributed talks. The selection has been done based on reports by members of the scientific committee and we are very grateful for their valuable help with this issue.

These contributions cover major themes related to waves, that include forward and inverse scattering, nonlinear wave phenomena, fast computational techniques, high performance computing, numerical analysis, absorbing layers and approximate boundary conditions, analytic and semi-analytic techniques for wave problems, domain decomposition, guided waves, periodic and random media etc... We believe that they provide a rather complete and up-to-date overview of the state of the art in the domain.

The organization of the meeting was done in a full coordination between the organizing committee and the local organizing committee. We thank all of them for their contribution to the success of this event. A special thank goes to Skander Belhaj who set up the web page, to Ibrahim Trabelsi who did the technical editing of the book of abstracts and to Sonia Fliss who took care of all technicalities related to elaborating the conference program.

Nabil Gmati and Houssem Haddar
On behalf of the organizing committee.

Table of contents

Invited Talks

Explicit Local Time-Stepping Methods For Wave Propagation

Marcus J. Grote
Institute of Mathematics, University of Basel, Basel, Switzerland.
Email: Marcus.Grote@unibas.ch

Abstract

Semi-discrete Galerkin formulations of transient wave equations, either with conforming or discontinuous Galerkin finite element discretizations, typically lead to large systems of ordinary differential equations. For any explicit time integration method, the time-step will then be constrained by the smallest elements in the mesh, possibly very high a price to pay. Explicit local time-stepping schemes (LTS) permit to overcome the crippling effect of locally refined meshes without resorting to implicit methods.

For wave equations without damping, leap-frog based LTS methods lead to high-order explicit LTS schemes, which also conserve the energy. For damped wave equations, Adams-Bashforth or Runge-Kutta based LTS methods lead to efficient LTS schemes of arbitrarily high accuracy. When combined with a finite element discretization in space with an essentially diagonal mass matrix, the resulting time-marching schemes are fully explicit and thus inherently parallel. Numerical experiments with continuous and discontinuous Galerkin finite element discretizations validate the theory and illustrate the usefulness of these local time-stepping methods.

Finite Element Discretization

Consider the (damped) wave equation

$$u_{tt} + \sigma u_t - \nabla \cdot (c^2 \nabla u) = f \ \text{ in } \ \Omega \times (0,T)\,, \qquad (1)$$

with appropriate initial and boundary conditions in a bounded domain $\Omega \subset \mathbb{R}^d$. Here the damping coefficient, $\sigma = \sigma(x) \geq 0$, is non-negative but possibly zero, the speed of propagation, $c = c(x) > 0$, is piecewise smooth and strictly positive, and $f(x,t)$ is a known source term. Spatial discretization of (1) with continuous finite elements (with mass lumping) [1] or discontinuous Galerkin (DG) methods [6], [8] leads to the second-order system of ordinary differential equations

$$\mathbf{M}\,\frac{d^2\mathbf{U}}{dt^2}(t) + \mathbf{M}_\sigma\,\frac{d\mathbf{U}}{dt}(t) + \mathbf{K}\,\mathbf{U}(t) = \mathbf{R}(t)\ , \qquad (2)$$

or to the alternative first-order system

$$\mathbf{M}\frac{d\mathbf{Q}}{dt}(t) + \mathbf{M}_\sigma\,\mathbf{Q}(t) + \mathbf{C}\,\mathbf{Q}(t) = \mathbf{R}(t)\,, \qquad (3)$$

both with an essentially diagonal mass matrix $\mathbf{M}$. Thus, when combined with explicit time integration, the resulting fully discrete scheme for the solution of (1), or any other similar wave equation from electromagnetics or elasticity, will be truly explicit.

Local Time Stepping

Locally refined meshes impose severe stability constraints on explicit time-stepping methods for the numerical solution of (1). Local time stepping (LTS) methods overcome that bottleneck by using smaller time-steps precisely where the smallest elements in the mesh are located.

In the absence of damping, that is $\sigma = 0$, explicit second-order LTS integrators for (2) were proposed in [2], [3], which are based on the standard leap-frog scheme. By combining these time-stepping schemes with the modified equation approach, the resulting LTS methods achieve arbitrarily high (even) order of convergence.

In the presence of damping, LTS methods based on Adams-Bashforth multi-step schemes for (3) were derived in [4], which achieve arbitrarily high accuracy while remaining fully explicit. In contrast to Adams-Bashforth methods, Runge-Kutta (RK) methods are one-step methods; hence, they do not require a starting procedure and easily accommodate adaptive time-step selection. Although RK methods do require additional evaluations per time-step, that additional work is compensated by a less stringent CFL stability condition. Recently, LTS methods based either on classical RK or low-storage RK methods were derived for (3) in [5]. In particular, the resulting LTS-RK schemes achieve the same rate of convergence as the original classical or low-storage RK methods; hence, they also yield efficient LTS methods with optimal stability properties.

Since the above LTS methods are truly explicit, their parallel implementation is straightforward; in particular, it requires no adjacency or coherence in the numbering of the degrees of freedom nor any special data structures. In the presence of multi-level mesh refinement, each local time-step in the fine region can itself include further local time-steps inside

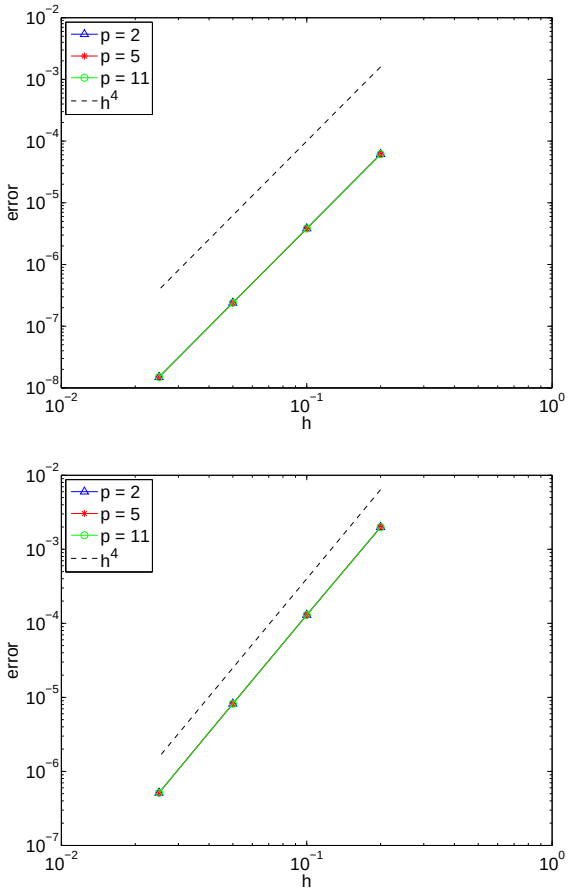

Figure 1: The error at $T = 10$ vs. the mesh size $h = h^{\text{coarse}}$ is shown for the LTS-RK4(p) method with $p = 2, 5, 11$ and either continuous (top) or nodal DG (bottom) $\mathcal{P}^3$ finite elements.

a smaller subregion with an even higher degree of local mesh refinement. The explicit local time-stepping schemes for the scalar (damped) wave equation immediately apply to other wave equations from electromagnetics or elasticity [4]; in fact, they can be used for general linear first-order hyperbolic systems.

Numerical Experiments

Convergence Study

To validate the optimal convergence rate of the RK4 based LTS scheme, for instance, we now consider (1) in one space dimension with constant wave speed $c = 1$ and damping coefficient $\sigma = 0.1$ on the interval $\Omega = [0, 6]$. The initial conditions are chosen to yield the exact solution $u_{ex}(x, t) = \cos(t) \cdot \sin(\pi x)$. Next, we divide Ω into three equal parts. The left and right intervals, $[0, 2]$ and $[4, 6]$, are discretized with an equidistant mesh of size h^{coarse}, whereas the interval $[2, 4]$ is discretized with an equidistant mesh of size $h^{\text{fine}} = h^{\text{coarse}}/p$. Hence, the two outer intervals correspond to the coarse region and the inner interval $[2, 4]$ to the refined region. For each time-step Δt in the coarse region, we take p local time-steps of size $\Delta\tau = \Delta t/p$.

For spatial discretization, we consider either a standard H^1-conforming FE or a nodal DG discretization with $\mathcal{P}^3$ elements. For a sequence of meshes, we monitor the L^2 space-time error in the numerical solution until the final time $T = 10$. Independently of the number of local time-steps $p = 2, 5, 11$, we observe the expected overall fourth-order convergence with respect to the L^2-norm, see Fig. 1.

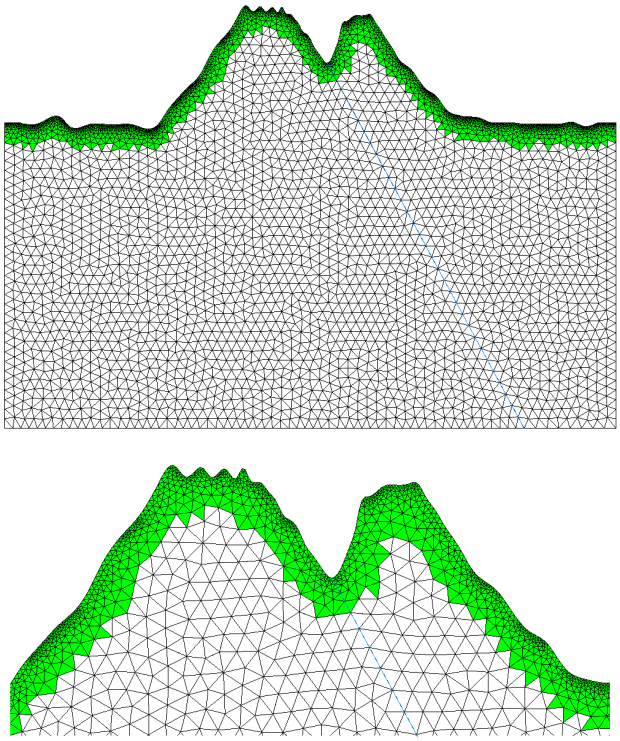

Figure 2: Merapi volcano: the initial triangular mesh is shown. The green triangles near the surface belong to the "fine" mesh.

Two-Dimensional Example

To illustrate the versatility of our approach, we now consider a 2D model of the Merapi volcano (Indonesia) which requires a highly refined mesh near the surface of the Earth, as shown in Fig. 2. We set $c = 1$ on its Eastern and $c = 2$ on its Western ridge. At the surface, we impose a homogeneous

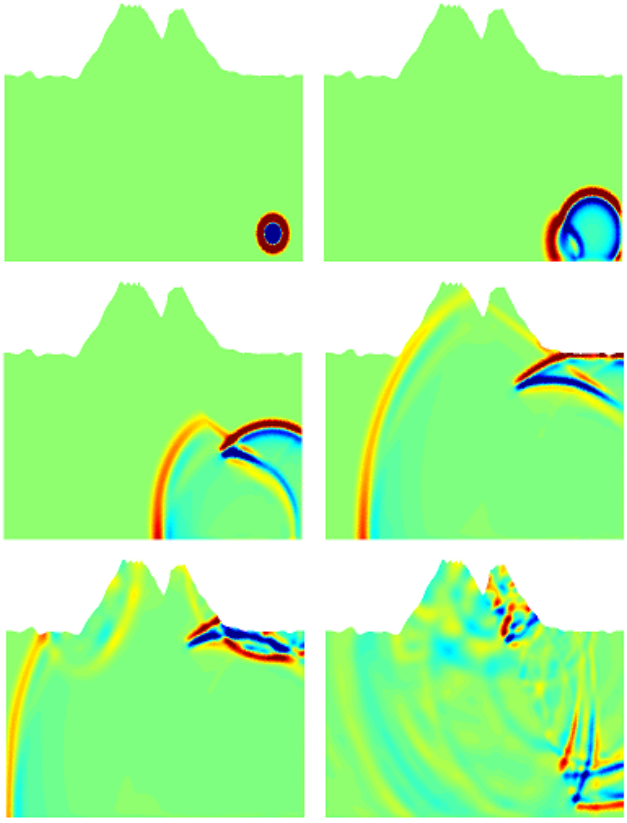

Figure 3: Merapi volcano: the numerical solution is shown at times $t = 0.2, 0.5, 1, 1.6, 1.9, 3.5$.

Neumann condition, whereas at the lateral and lower boundaries we truncate the computational domain with an efficient PML formulation for second-order wave equations [7].

For the spatial discretization we use standard H^1-conforming $\mathcal{P}^2$ elements whereas for the time discretization, we choose the third-order LTS-RK3 scheme. Thus, the numerical method is third-order accurate both in space and time with respect to the L^2-norm. Since the typical mesh size inside the refined region is about twelve times smaller than that in the surrounding coarser region, we take $p = 12$ local time steps of size $\Delta\tau = \Delta t/p$ for every time step Δt inside the coarser region.

In Fig. 3 we display snapshots of the numerical solution as the initial Gaussian pulse propagates upwards and impinges on the discontinuity in the velocity field. At the lateral and lower boundaries, the waves leave the computational domain without any spurious reflection.

References

[1] G. Cohen, *High-order numerical methods for transient wave equations*, Springer, 2002.

[2] J. Diaz and M.J. Grote, *Energy conserving explicit local time-stepping for second-order wave equations*, SIAM J. Sci. Comput., **31** (2009), pp. 1985–2014.

[3] M.J. Grote and T. Mitkova, *Explicit local time-stepping for Maxwell's equations*, J. Comput. Appl. Math., **234** (2010), pp. 3283–3302.

[4] M.J. Grote and T. Mitkova, *High-order explicit local time-stepping methods for damped wave equations*, J. Comput. Appl. Math., **239** (2013), pp. 270–289.

[5] M.J. Grote, M. Mehlin and T. Mitkova, *Runge-Kutta based explicit local time-stepping methods*, in preparation.

[6] M.J. Grote, A. Schneebeli and D. Schötzau, *Discontinuous Galerkin finite element method for the wave equation*, SIAM J. Num. Analysis, **44** (2006), pp. 2408–2431.

[7] M.J. Grote and I. Sim, *Perfectly matched layer for the second-order wave equation*, in Proc. of 9th Internat. Conf. on Math. and Numerical Aspects of Wave Propagation (WAVES 2009), pp. 370-371, held at INRIA, Pau, France, June 15-19, 2009.

[8] J.S. Hesthaven and T.Warburton, *Nodal Discontinuous Galerkin Methods*, Springer, 2008.

Array imaging in heavy clutter

C. Tsogka[1,2,*], L. Borcea[3], G. Papanicolaou[4]
[1] Applied Mathematics, University of Crete, Heraklion, Greece.
[2] Institute of Applied and Computational Mathematics, FORTH, Heraklion, Greece.
[3] Computational and Applied Mathematics, Rice University, Houston, TX, USA
[4] Mathematics, Stanford University, Stanford, CA, USA
[*]Email: tsogka@tem.uoc.gr

Abstract

We consider the problem of imaging in heavy clutter, *i.e.*, strongly backscattering media in which the echoes from the objects that we wish to image are overwhelmed by the background medium reflections. In such regimes the signal (coherent echoes) to noise (incoherent backscatter) ratio (SNR) of the data is very low and because of this coherent imaging fails. One solution is to assume that there is no coherence left in the data and use incoherent methods which rely only on intensities [3]. Incoherent imaging however, has very low resolution unless *a priori* information is available or very large arrays are used. Alternatively, we propose the use of data processing techniques that enhance the SNR of the coherent echoes by filtering out the clutter backscatter. We review here such an approach which adaptively selects the time-frequency windows that contain the coherent echoes [1], [9], and present some recent developments towards its application to the case of multiple reflectors.

1 Array imaging

1.1 Problem setup

In array imaging the data is the array response matrix $\mathbb{P}(t)$ whose elements are the traces $P(t,\vec{\mathbf{x}}_r,\vec{\mathbf{x}}_s)$. They are obtained by emitting probing pulses $f(t)$ from sources located at $\vec{\mathbf{x}}_s$, $s=1,\ldots,N_s$, and by recording the medium response at the array receivers $\vec{\mathbf{x}}_r$ for $r=1,\ldots,N_r$. We assume here that sources and receivers are collocated and $N_s=N_r=N$. To model the data we consider the scalar acoustic wave equation in an open, unbounded domain Ω,

$$\begin{aligned}\frac{1}{v^2(\vec{\mathbf{x}})}\frac{\partial^2 p(t,\vec{\mathbf{x}})}{\partial t^2}-\Delta p(t,\vec{\mathbf{x}})&=f(t)\delta(\vec{\mathbf{x}}-\vec{\mathbf{x}}_s),\\ p(0,\vec{\mathbf{x}})=0,\quad \frac{\partial p(0,\vec{\mathbf{x}})}{\partial t}&=0.\end{aligned}\tag{1}$$

Each element of the response matrix, $P(t,\vec{\mathbf{x}}_r,\vec{\mathbf{x}}_s)$, equals $p(t,\vec{\mathbf{x}}_r)$, the solution of (1) for a point source located at $\vec{\mathbf{x}}_s$ emitting the pulse $f(t)$, where

$$f(t)=e^{-i\omega_0 t}f_{B_0}(t),$$

and with Fourier transform

$$\hat{f}(\omega)=\int_{-\infty}^{\infty}e^{i(\omega-\omega_0)t}f_{B_0}(t)dt=\hat{f}_{B_0}(\omega-\omega_0),\tag{2}$$

supported in the frequency interval centered at ω_0 with bandwidth B_0.

In (1), $v(\vec{\mathbf{x}})$ is the wave speed that can be decomposed as,

$$\frac{1}{v^2(\vec{\mathbf{x}})}=\frac{1}{c^2(\vec{\mathbf{x}})}\left(1+\varepsilon\mu\left(\frac{\mathbf{x}}{\ell},\frac{z}{\ell_z}\right)+\nu(\vec{\mathbf{x}})\right),\tag{3}$$

Here z denotes the direction of propagation, or range, and $\mathbf{x}$ the cross-range. The reflectivity of the object that we wish to image is the unknown $\nu(\vec{\mathbf{x}})$. Our goal in imaging is to determine the support of $\nu(\vec{\mathbf{x}})$ given the array data $\mathbb{P}(t)$ and assuming that we know $c(\vec{\mathbf{x}})$, which is the smooth part of the velocity.

To model clutter we introduced, in (3), $\mu(\frac{\mathbf{x}}{\ell},\frac{z}{\ell_z})$, a statistically homogeneous random process with zero mean. This expresses our uncertainty about the inhomogeneities in the propagation medium, which are not known and cannot be estimated in detail. The strength of the inhomogeneities is controlled by the parameter ε, and the scale of the inhomogeneities is given by the correlation length ℓ which can be different in the range and cross-range directions.

1.2 Coherent imaging methods

The simplest coherent imaging method is Kirchhoff migration (KM) which can be written as,

$$\mathcal{J}^{\mathrm{KM}}(\vec{\mathbf{y}}^s)=\sum_{r=1}^{N}\sum_{s=1}^{N}\int d\omega\,\widehat{Q}(\vec{\mathbf{y}}^s;\vec{\mathbf{x}}_s,\vec{\mathbf{x}}_r,\omega),\tag{4}$$

where $\widehat{Q}(\vec{\mathbf{y}}^s;\vec{\mathbf{x}}_s,\vec{\mathbf{x}}_r,\omega)$ are the backpropagated traces at point $\vec{\mathbf{y}}^s$,

$$\begin{aligned}\widehat{Q}(\vec{\mathbf{y}}^s;\vec{\mathbf{x}}_s,\vec{\mathbf{x}}_r,\omega)=\widehat{P}(\vec{\mathbf{x}}_r,\vec{\mathbf{x}}_s,\omega)\times\\ \exp\left[-i\omega(\tau(\vec{\mathbf{x}}_r,\vec{\mathbf{y}}^s)+\tau(\vec{\mathbf{x}}_s,\vec{\mathbf{y}}^s))\right].\end{aligned}\tag{5}$$

KM forms the image at points $\vec{\mathbf{y}}^s$ in the imaging window, by summing over the array elements the back-propagated traces. The back-propagation from the receiver, $\vec{\mathbf{x}}_r$, to the image point, $\vec{\mathbf{y}}^s$, and then back to the source, $\vec{\mathbf{x}}_s$, is done approximately, with travel times τ computed in a fictitious medium with sound speed $c(\vec{\mathbf{x}})$, which is the smooth part of $v(\vec{\mathbf{x}})$.

Kirchhoff migration works well in smooth media when there is no clutter or the clutter is weak. It does not give satisfactory results in clutter, however, where the KM images become noisy and statistically unstable, *i.e.*, they change unpredictably with the realization of the clutter [4]. This is because the effect of the random inhomogeneities on the waves propagating through clutter is cumulative, and, for long distances of propagation, the traces have long and noisy codas even when ε in (3) is small ($\sim$ 2-3%).

To image in such regimes, we developed the coherent interferometric (CINT) methodology [4], [5], [6], [7], [8]. CINT forms images by superposing time delayed, local cross-correlations of the array traces, instead of the traces themselves. The cross-correlations are computed over time windows of width $1/\Omega_d$ and over source and receiver offsets that do not exceed X_d. The two parameters that control the size of the windows are the decoherence frequency (Ω_d) and length (X_d) and depend on the random medium and the distance of propagation. The decoherence length, X_d, depends on the frequency as well [4],

$$X_d(\omega) = \frac{c_0}{\omega \kappa_d}. \tag{6}$$

Both Ω_d and X_d (*i.e.*, κ_d) can be estimated adaptively during the image formation process (cf. [5]). The CINT imaging functional is given by

$$\mathcal{J}^{\rm CINT}(\vec{\mathbf{y}}^s;\Omega_d,\kappa_d) = \int\int_{|\omega-\omega'|\le\Omega_d} d\omega d\omega' \sum_{r=1}^{N}\sum_{\substack{r'=1 \\ |\vec{\mathbf{x}}_r-\vec{\mathbf{x}}_{r'}|\le X_d\left(\frac{\omega+\omega'}{2}\right)}}^{N} \sum_{s=1}^{N}\sum_{\substack{s'=1 \\ |\vec{\mathbf{x}}_r-\vec{\mathbf{x}}_{r'}|\le X_d\left(\frac{\omega+\omega'}{2}\right)}}^{N} \widehat{Q}(\vec{\mathbf{y}}^s;\vec{\mathbf{x}}_s,\vec{\mathbf{x}}_r,\omega)\overline{\widehat{Q}(\vec{\mathbf{y}}^s;\vec{\mathbf{x}}_{s'},\vec{\mathbf{x}}_{r'},\omega')}$$

with $\widehat{Q}(\vec{\mathbf{y}}^s;\vec{\mathbf{x}}_s,\vec{\mathbf{x}}_r,\omega)$ defined in (5).

2 Illustration of heavy clutter effects on coherent imaging

We consider here imaging in heavy clutter, that we model by allowing ε in (3) to take large values of the order of 10-20%. For moderate clutter ($\varepsilon \sim$ 3-5%), the SNR of the coherent signal is relatively high and imaging can be done successfully with coherent interferometry (CINT) [4], [6]. In heavy clutter, however, CINT does not work well. To illustrate this, let us consider the configuration depicted in Figure 1, where two small scatterers are embedded in a strongly scattering medium. Remark that the second reflector is hidden behind the first one and this makes its detection and imaging quite challenging. We choose the simulation parameters so as to be in a regime that is typical in ultrasonic nondestructive testing experiments [2]. The velocity of the background medium fluctuates around the constant $c(\vec{\mathbf{x}}) = 1$Km/s. The strength of the fluctuations is $\varepsilon = 10\%$ and the medium is obtained by combining an isotropic random medium with correlation length $\ell = \ell_z = \lambda_0/4$ and a layered medium with $\ell_z = \lambda_0/50$.

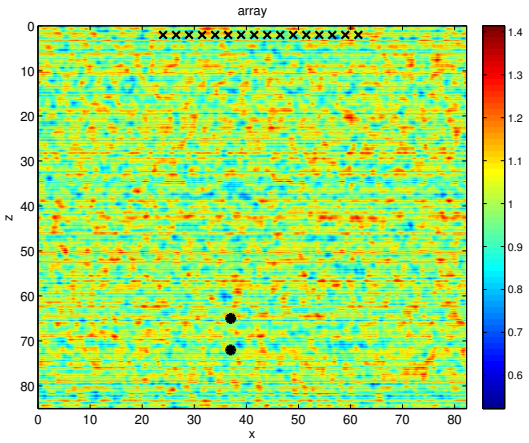

Figure 1: Two reflectors embedded in a strongly scattering medium. The array is on the top. The velocity of the medium fluctuates around the constant $c(\vec{\mathbf{x}}) = 1$Km/s. The horizontal axis is cross-range and the vertical is range, measured in units of $\lambda_0 = 0.1$mm.

To obtain the array response matrix we solve numerically the wave equation (1) in the heterogeneous medium with velocity $v(\vec{\mathbf{x}})$ shown in Figure 1. The pulse $f(t)$ is a second derivative of a Gaussian with central frequency $f_0 = 10$MHz. The reflectors are small disks of diameter $\lambda_0/2$ and are modelled as soft scatterers, *i.e.*, the acoustic field is zero at their boundary. Length is measured in units of the central wavelength $\lambda_0 = 0.1$mm.

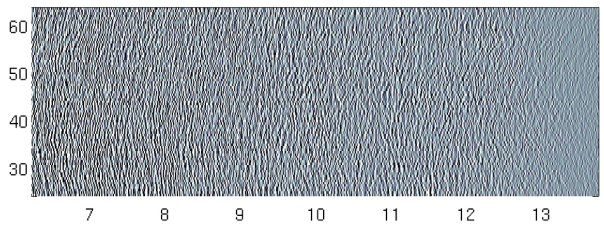

Figure 2: Data traces obtained on the array for a pulse emitted by the central array element for the configuration shown on Figure 1. It is impossible to distinguish in the traces any coherent echo arriving from the scatterers we wish to image.

The data traces obtained when the pulse is emitted from the central array element are shown on Figure 2. We cannot observe in the traces any coherent echo arriving from the scatterers we wish to image. That is why coherent imaging methods fail to produce a good image in that setup.

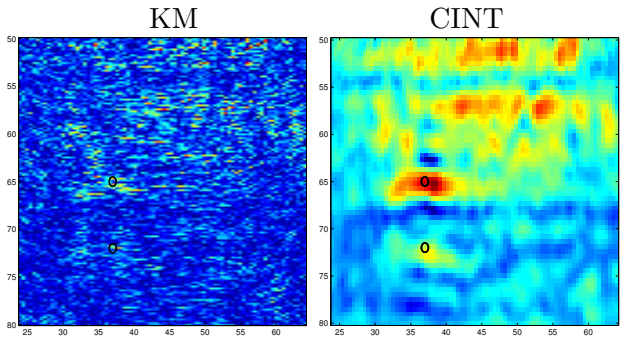

Figure 3: KM (left) and CINT (right) images obtained for the data shown on Figure 2. The true location of the scatterers is shown with black circles.

The Kirchhoff migration and CINT images are shown on Figure 3. CINT is computed with $\kappa_d = 0.05$ and $\Omega_d = 3$MHz. We observe that both images are very noisy and have maxima (red pixels in the picture) at several locations that do not correspond to the reflectors. As a result, we cannot distinguish the objects we wish to image from the background noise.

To improve these results and be able to image with coherent techniques in heavy clutter we follow the approach of [9] that consists in detecting the presence of the coherent signal and then amplifying its SNR by adequate filtering.

3 Adaptive time-frequency filtering

Our filtering algorithm is the one proposed in [9] and is based on the following remark: the coherent echoes due to a reflector take the form of a hyperbola whose support is limited and contained in a small time window. The question is how to find this window in the noisy data traces without having any *a priori* information on the location of the reflector.

We perform the window search on a binary tree (see Figure 4). Each node of the tree is associated with the local cosine coefficients of the response matrix. Our detection is based on the behavior of the singular values of this matrix. Starting from the root, we seek for an anomalous behavior of the largest singular values. Once a window is selected, it is refined by continuing the search to its children, and so on. Filtering consists in zeroing the LC coefficients in all other windows but the selected ones, and in projecting the matrix of LC coefficients on to the low rank subspace associated with the singular values with anomalous behavior.

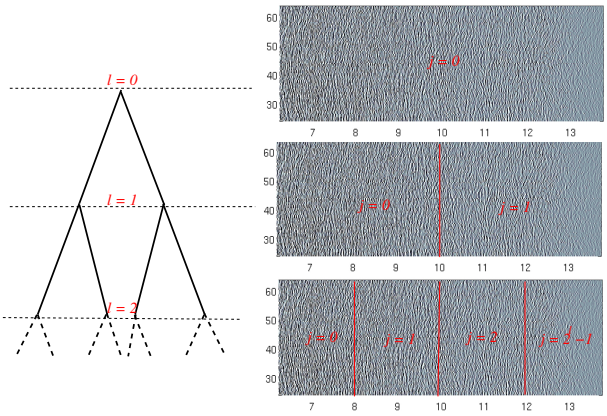

Figure 4: Illustration of the time windowing segmentations of the array data traces at different tree levels l. The schematic on the left illustrates the binary tree. On the right we show the segmentation of the data traces in the time windows indexed by j, with $j = 0, 1, \ldots, 2^{l-1}$, at tree levels denoted by l.

The input of the algorithm is the array response matrix $\mathbb{P}(t)$, for time $t \in [T_o, T_f]$, sampled on a mesh with $N_T = 2^m$ points. We also need to specify the maximum level of the tree, $D \leq m$, to be used in the LCT. This is chosen so that we have enough samples of the signal at each level of the tree. The detection and filtering algorithm consists of the following steps.

T.1 LCT of the response matrix. At first we compute the binary tree of the local cosine coefficients of the response matrix. At each level l of

the tree, with $0 \leq l \leq D$, we compute the real $N \times N$ matrices of coefficients $\hat{\mathbb{P}}^l(t_j^l, \omega_n^l)$ given by

$$\hat{\mathbb{P}}^l(t_j^l, \omega_n^l) = \left\{ \hat{P}^l(t_j^l, \omega_n^l, \vec{\mathbf{x}}_r, \vec{\mathbf{x}}_s) \right\}_{r,s=1,\ldots,N}, \quad (7)$$

with

$$\hat{P}^l(t_j^l, \omega_n^l, \vec{\mathbf{x}}_r, \vec{\mathbf{x}}_s) = \int dt\, P(t, \vec{\mathbf{x}}_r, \vec{\mathbf{x}}_s) \sqrt{\frac{2}{\Delta t_l}} \times \chi\left(\frac{t - t_j}{\Delta t_l}\right) \cos[\omega_n^l (t - t_j)].$$

Here t_j^l are the mesh points that define the width and location of the time windows at level l,

$$t_j^l = j\Delta t_l = \frac{jT}{2^l}, \quad j = 0, 1, \ldots, 2^l, \quad (8)$$

and ω_n^l are the frequencies associated with the decomposition in the smooth windows χ,

$$\omega_n^l = \frac{\pi\,(n + 1/2)}{\Delta t_l}, \quad n \in \mathbb{N}. \quad (9)$$

This is the usual LCT algorithm and more information about it can be found in [11].

T.2 Singular value decomposition of the local cosine matrices of coefficients. For each l and t_j^l we compute the SVD of $\hat{\mathbb{P}}^l(t_j^l, \omega_n^l)$, frequency by frequency. Let us denote by $\sigma_q^{l,j}(\omega_n^l)$ the singular values, for $q = 1, \ldots N$.

We then form the matrices of the first Q normalized singular values,

$$\mathbb{S}^{l,j} = \left\{ \tilde{\sigma}_q^{l,j}(\omega_n^l) \right\}_{1 \leq q \leq Q,\, n \in \mathcal{N}^l},$$

$$\text{where } \tilde{\sigma}_q^{l,j}(\omega_n^l) = \frac{\sigma_q^{l,j}(\omega_n^l)}{\max_{n'} \sigma_q^{l,j}(\omega_{n'_l})},$$

over the set of frequency indices

$$\mathcal{N}^l = \left\{ n = 0, 1, \ldots, N_T/2^l - 1, \;\; \text{s.t. } \omega_n^l \in B \right\},$$

with cardinality $|\mathcal{N}^l|$.

We then compute the SVD of matrices $\mathbb{S}^{l,j}$, for $j = 0, \ldots, 2^l - 1$ and $l = 0, \ldots, D$, and calculate

$$\lambda^{l,j} = \gamma_2^{l,j} / \gamma_1^{l,j}, \quad (10)$$

where $\gamma_q^{l,j}$, for $1 \leq q \leq \min\{Q, |\mathcal{N}^l|\}$, are the singular values of $\mathbb{S}^{l,j}$.

T.3 Detection and Filtering. We select the time window of interest as follows:

For $l = 0 : D$

If $\lambda^{l,j}$ has a maximum above a predetermined threshold, let l_0 be this l and stop.

Next, initialise $j_\star^{l_0} = \arg\max_j \lambda^{l_0,j}$.

For $l = l_0 + 1 : D$

Compute $j_\star^l = \arg\max_{j \in \{2j_\star^{l-1}, 2j_\star^{l-1}+1\}} \lambda^{l,j}$.

If $j_\star^l$ is a maximum of $\lambda^{l,j}$ above a predetermined threshold, for j in the vicinity of $j_\star^l$, continue. Otherwise, set $l = l - 1$ and stop.

Select the window at $t_{j_\star^l}^l$.

In the selected time window, define the filter $\mathcal{F}^{j_\star^l}$, that sets to zero the LC coefficients in the windows that have not been selected, at level l,

$$\mathcal{F}^{j_\star^l} \hat{\mathbb{P}}^l(t_j^l, \omega_n^l) = 0, \text{ for } j = 0, 1, \ldots, 2^l - 1, \; j \neq j_\star^l \text{ and } n = 0, 1, \ldots N_T/2^l - 1.$$

Additional filtering is done by the filter $\mathcal{Q}$, which projects $\mathcal{F}^{j_\star^l} \hat{\mathbb{P}}^l(t_j^l, \omega_n^l)$ on the subspace of low rank matrices with singular vectors corresponding to the "anomalous" top singular values. The projection is done for frequency indices n in the set $\mathcal{N}^l$. All other coefficients are set to zero.

The output of the algorithm is the filtered response matrix in the time domain which is obtained by the inverse LCT of the entries $\mathcal{Q}\mathcal{F}^{j_\star^l} \hat{\mathbb{P}}^l(t_{j_\star}^l, \omega_n^l)$, at the selected tree level l.

This algorithm was presented in detail in [9] together with several results for imaging one reflector in various types of clutter. Its theoretical analysis has been carried out in [1] in the case of finely layered media. The key idea is to detect an anomaly pattern in the singular values of $\hat{\mathbb{P}}^l(t_{j_\star}^l, \omega_n^l)$ (the matrix of LC coefficients) that suggests the presence of a coherent echo in the data.

Indeed, in the windows that contain only clutter echoes, the top singular values follow a similar pattern and they are clustered across frequencies. This observation was analytically proven in the layered case [1], and seems to hold for more general random media. It implies, in particular, that the matrices $\mathbb{S}^{l,j}$ of normalized singular values have almost rank one in these windows.

The rank of $\mathbb{S}^{l,j}$ is expected to change and become at least two in windows that contain detectable

coherent echoes. More precisely, a reflector is detectable by our algorithm when the largest singular value of $\hat{\mathbb{P}}^l(t^l_{j_\star}, \omega^l_n)$ can be bound away from those due to clutter. In this case $\mathbb{S}^{l,j}$ has at least rank two and that is why in our selection criterion we seek for a maximum of $\lambda^{l,j}$, the ratio between the second and the first singular value of $\mathbb{S}^{l,j}$. We call the singular values associated to the coherent echoes "anomalous" as they have a different behavior compared to the other ones that correspond to clutter (and are clustered together).

Remark that the time window refinement is crucial: a reflector might become detectable at a lower level in the tree although it is not detectable at higher levels. Indeed, in heavy clutter, at higher tree levels, the reflector is not detectable because the energy of the coherent signal is small compared to the energy of the clutter echoes. As we go to lower levels in the tree the coherent energy remains the same while the one associated to the clutter diminishes, that is why the reflector can now be detected and imaged.

After the time-window selection step is finished, our filtering consists in removing the contributions of all the windows except the selected ones. It also projects the matrix of coefficients, in the selected windows, on the subspace of low rank matrices with singular vectors corresponding to the "anomalous" singular values. The projection is done with the truncated SVD.

There are two parameters in the algorithm that we have to choose. The number of singular values Q and the frequency band B. Typically we should have $2M \leq Q \leq N$, where M is the number of scatterers we are searching for, and N is the dimension of the response matrix. The results of the algorithm are not very sensible to the value of Q and we take $Q = 10$ in practice. The bandwidth B is the part of the frequency spectrum on which the scatterers are detectable and this is usually the lower part of the spectrum.

4 Detection and filtering results

Let us now apply the filtering algorithm previously described to the array data for the imaging problem considered in section 2. The first important step is the selection of the time windows. We show in Figure 5(top) the selection criterion (10) at level $l = 4$. It suggests that coherent echoes are present in windows 7 and 9. On the bottom plots of the same figure we show the normalized singular values $\tilde{\sigma}^{l,j}_q(\omega^l_n)$ in these windows. We used $Q = 10$ and $B = [0, 5]$MHz. The number of "anomalous" singular values is 2 for window 7 and 1 for window 9.

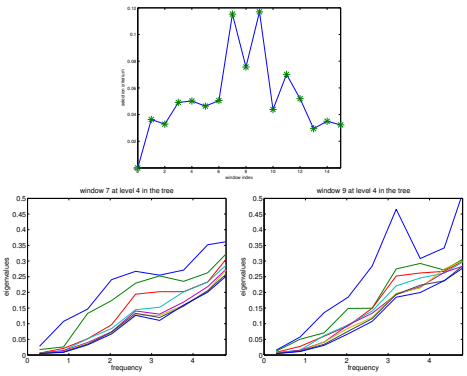

Figure 5: Time window selection. Top: the selection criterion (10) suggests that there are two windows that contain coherent echoes, windows 7 and 9. On the bottom left and right plots we display the first $Q = 10$ normalized singular values $\tilde{\sigma}^{l,j}_q(\omega^l_n)$ for $\omega^l_n \in B = [0, 5]$MHz in the selected windows 7 and 9 respectively. Observe that there are two anomalous singular values at window 7 and one at window 9.

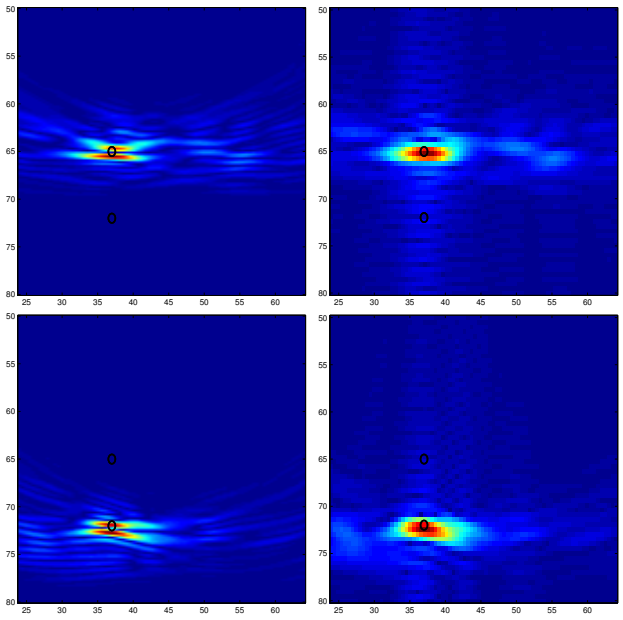

Figure 6: Imaging results using the filtered data. On the left we show the KM image and on the right the CINT image computed with $\kappa_d = 0.02$ and $\Omega_d =$ 3MHz. On the top row we display the images for the first reflector (selected window 7 at level 4) and on the bottom row the ones for the second reflector (selected window 9 at level 4).

After selecting the time windows of interest we filter the data as described in Step T.3 of our algorithm. We show the images obtained with the filtered data in Figure 6. The improvement with respect to Figure 3 is dramatic. The results are now extremely good, the images have clear peaks on the reflectors that we wish to image and their location is correctly estimated. Remark that the detection of the second reflector is unambiguous (see Figure 5) which results in its accurate imaging (see Figure 6, bottom row). One can use either KM or CINT for imaging, the results of both methods are excellent now as the SNR of the data has been significantly increased after the application of our filtering algorithm.

Conclusions

We reviewed in this paper a filtering algorithm that allows for detecting and imaging reflectors embedded in strongly scattering media. This is a challenging problem that appears in applications such as nondestructive testing of materials [2], land mine detection [10] and foliage penetrating radar. The algorithm uses the local cosine coefficients of the response matrix, $\hat{\mathbb{P}}^l(t_j^l, \omega_n^l)$, on a binary tree. It selects the level l and the windows j in the tree that contain coherent echoes from detectable scatterers by seeking for a break in the pattern of the singular values of matrices $\hat{\mathbb{P}}^l(t_j^l, \omega_n^l)$. We refer to [9], for a more detailed description of the algorithm, and to [1] for its theoretical analysis in the case of finely layered media. In [1], [9], the problem of imaging one reflector in heavy clutter was considered. Here, the more challenging problem of multiple reflectors is addressed. In the oral presentation, the robustness of the algorithm is illustrated with more results for various configurations of reflectors.

5 Acknowledgements

The work of L. Borcea was partially supported by the AFSOR Grant FA9550-12-1-0117, the ONR Grants N00014-12-1-0256, N00014-09-1-0290 and N00014-05-1-0699, and by the NSF Grants DMS-0907746, DMS-0934594, DMS-0604008.

The work of G. Papanicolaou was partially supported by the US Army grant W911NF-07-2-0027-1 and by AFOSR grant FA9550-11-1-0266.

The work of C. Tsogka was partially supported by the European Research Council under the European Union's Seventh Framework Programme (FP7/2007-2013) / ERC grant agreement n. 239959.

References

[1] R. Alonso, L. Borcea, G. Papanicolaou, and C. Tsogka. Detection and imaging in strongly backscattering randomly layered media. *Inverse Problems*, 27:025004, 2011.

[2] A. Aubry and A. Derode. Random matrix theory applied to acoustic backscattering and imaging in complex media. *Phys. Rev. Lett.*, 102(8):084301, Feb 2009.

[3] G. Bal and K. Ren. Transport-based imaging in random media. *SIAM Applied Mathematics*, 68:1738–1762, 2008.

[4] L. Borcea, G. Papanicolaou, and C. Tsogka. Interferometric array imaging in clutter. *Inverse Problems*, 21(4):1419–1460, 2005.

[5] L. Borcea, G. Papanicolaou, and C. Tsogka. Adaptive interferometric imaging in clutter and optimal illumination. *Inverse Problems*, 22(4):1405–1436, 2006.

[6] L. Borcea, G. Papanicolaou, and C. Tsogka. Coherent interferometric imaging. *Geophysics*, 71(4):SI165–SI175, 2006.

[7] L. Borcea, G. Papanicolaou, and C. Tsogka. Coherent interferometry in finely layered random media. *SIAM J. on Multiscale Model. Simul.*, 5:62–83, 2006.

[8] L. Borcea, G. Papanicolaou, and C. Tsogka. Asymptotics for the space-time Wigner transform with applications to imaging. In P. H. Baxendale and S. V. Lototsky, editors, *Stochastic Differential Equations: Theory and Applications. Volume in Honor of Professor Boris L. Rozovskii*, volume 2 of *Interdisciplinary Mathematical Sciences*, pages 91–112. World Scientific, 2007.

[9] L. Borcea, G. Papanicolaou, and C. Tsogka. Adaptive time-frequency detection and filtering for imaging in heavy clutter. *SIAM Imaging Science*, 4(3):827–849, 2011.

[10] M. Carrasco L. Robledo and D. Mery. A survey of land mine detection technology. *International Journal of Remote Sensing*, 30(9):2399–2410, 2009.

[11] S. Mallat. *A wavelet tour of signal processing*. Academic Press, second edition, 1999.

A primer in the theory of Time Domain Boundary Integral Equations

F.J. Sayas[1,*]
[1] Department of Mathematical Sciences, University of Delaware, Newark DE – USA
*Email: fjsayas@math.udel.edu

Abstract

We sketch some of the techniques and results about time domain boundary integral operators associated to the acoustic wave equation.

Introduction

In this paper we will describe some of the techniques and results about time domain (retarded) boundary integral equations for the acoustic wave equation. The exposition will be limited to the single layer potential and the associated single layer boundary integral operator in three space dimensions. Instead of showing mapping properties of the operators we will focus on two problems related to Galerkin semidiscretization in space, studying mapping properties of the discrete inverse of the single layer retarded integral equation (and, at the same time, of the continuous inverse), and of the associated error operator (a sort of Céa estimate for the space semidiscretization).

Similar work can be carried out for all the layer potentials and integral operators for the acoustic wave equation in any space dimension and, with minor changes, for the elastic wave equations.

In a language very close to the one used here, these results can be found –with fully detailed proofs and step by step presentation of all functional elements– in the lecture notes [8]. The results shown here are valid for full Galerkin discretization of the equations as well as for combined Galerkin-in-space Convolution-Quadrature-in-time discretization. For the latter, see [3].

The style of the exposition will be narrative, with results presented in the body of the text. Some prior knowledge of classical Sobolev spaces is assumed. As for vector-valued distributions, the only needed facts are exposed in a final appendix.

1 A very weak layer potential

Let Γ be a closed orientable Lipschitz surface in the space, separating a bounded region Ω_- from its exterior Ω_+. Whenever needed, traces and normal derivatives from both sides of Γ will be tagged with a $\pm$ superscript, depending on what side of Γ they are coming from. Let now $\lambda : \Gamma \times \mathbb{R} \to \mathbb{R}$ be a causal function, i.e.,

$$\lambda(t) := \lambda(\cdot, t) \equiv 0 \qquad t < 0.$$

The acoustic (retarded) single layer potential, with density λ, is formally defined by the integral expression

$$(\mathcal{S} * \lambda)(\mathbf{x}, t) = \int_\Gamma \frac{\lambda(\mathbf{y}, t - |\mathbf{x} - \mathbf{y}|)}{4\pi|\mathbf{x} - \mathbf{y}|} \mathrm{d}\Gamma(\mathbf{y}) \qquad (1)$$

for any $\mathbf{x} \in \mathbb{R}^3 \setminus \Gamma$ and $t \in \mathbb{R}$. Note that it is again a causal function. This potential can also be understood as a (weak) solution of a transmission problem, namely $u := \mathcal{S} * \lambda$ is a causal solution of

$$\ddot{u} = \Delta u \qquad (2a)$$
$$[\![\gamma u]\!] = 0 \qquad (2b)$$
$$[\![\partial_\nu u]\!] = \lambda. \qquad (2c)$$

Let us first explain what these equations mean. We understand u as a distribution with values in the Hilbert space

$$H^1_\Delta(\mathbb{R}^3 \setminus \Gamma) := \{U \in H^1(\mathbb{R}^3 \setminus \Gamma) \,:\, \Delta U \in L^2(\mathbb{R}^3 \setminus \Gamma)\}.$$

The Laplacian is then understood in the sense of distributions in $\mathbb{R}^3 \setminus \Gamma$, and therefore as a bounded operator $H^1_\Delta(\mathbb{R}^3 \setminus \Gamma) \to L^2(\mathbb{R}^3 \setminus \Gamma) \equiv L^2(\mathbb{R}^3)$. The double dot in (2a) is second order differentiation of $H^1_\Delta(\mathbb{R}^3 \setminus \Gamma)$-valued distributions, and (2a) is an equation in the sense of distributions with values in $L^2(\mathbb{R}^3 \setminus \Gamma)$. The equation (2b) contains the jump of the trace

$$[\![\gamma U]\!] := \gamma^- U - \gamma^+ U,$$

which defines a bounded operator $H^1(\mathbb{R}^3 \setminus \Gamma) \to H^{1/2}(\Gamma)$. Therefore (2b) is an equation in the sense of distributions with values in $H^{1/2}(\Gamma)$. Similarly

$$[\![\partial_\nu U]\!] := \partial_\nu^- U - \partial_\nu^+ U$$

is an operator that measures the jump of the normal derivative for functions in $H^1_\Delta(\mathbb{R}^3 \setminus \Gamma)$, and (2c)

can be seen as an equation in the sense of $H^{-1/2}(\Gamma)$-valued distributions. We can thus go very far in the conditions for definition of the layer potential $\mathcal{S} * \lambda$: given a causal $H^{-1/2}(\Gamma)$-valued distribution λ, $\mathcal{S} * \lambda$ is a formal causal $H^1_\Delta(\mathbb{R}^3 \setminus \Gamma)$-valued solution of (2) (note how the vanishing initial conditions are hidden in the request of causality).

It is however not clear how (2) has a unique solution. A simple idea to enforce uniqueness is to reduce the set of distributions on which we are allowed to work. A quite wide family of such distributions is the set of causal X-valued distributions f (here X is any Banach space), whose Laplace transform F exists in

$$\mathbb{C}_+ := \{s \in \mathbb{C} \,:\, \operatorname{Re} s > 0\},$$

and can be bounded as follows

$$\|\mathrm{F}(s)\|_X \leq C_{\mathrm{F}}(\operatorname{Re} s)|s|^\mu \qquad \forall s \in \mathbb{C}_+,$$

where $\mu \in \mathbb{R}$ and $C_{\mathrm{F}} : (0,\infty) \to (0,\infty)$ is non-increasing and bounded by a rational function at the origin. This set of distributions corresponds to the derivatives of arbitrary order of causal continuous X-valued functions with polynomial growth at infinity. We will refer to it as $\mathrm{TD}(X)$ (TD as in time-domain). (Some authors [1] prefer to extend the set of causal distributions to any distribution having a Laplace transform. The more restricted setting that we are going to use does not seem to lose any interesting set of data and handles the inversion process in a quite natural way.)

Using standard techniques of Laplace transforms and resolvent estimates, it can be proved that if $\lambda \in \mathrm{TD}(H^{-1/2}(\Gamma))$, then problem (2) has a unique solution $u \in \mathrm{TD}(H^1_\Delta(\mathbb{R}^3 \setminus \Gamma))$. We will refer to it as $u = \mathcal{S} * \lambda$. The Laplace domain analysis justifies the convolutional notation, which we will exploit later on. We can also define

$$\mathcal{V} * \lambda := \gamma(\mathcal{S} * \lambda),$$

by taking the trace on Γ of the solution of (2). We thus obtain an element of $\mathrm{TD}(H^{1/2}(\Gamma))$.

2 An even weaker semidiscrete equation

Let us now deal with the possibility of inverting the equation

$$\mathcal{V} * \lambda = \beta. \tag{3}$$

One of thew possible aims of this inversion process is the representation of the solution of a transient scattering problem with an indirect boundary integral ansatz. Assume that we want to find the scattered field for a sound-soft obstacle hit by an incoming incident wave:

$$\ddot{u} = \Delta u, \tag{4a}$$
$$\gamma^+ u = \beta := -\gamma u^{\mathrm{inc}}. \tag{4b}$$

The practical way to proceed (the Boundary Element way) consists of trying to represent the solution of (4) in the form $u = \mathcal{S} * \lambda$, and use unique solvability of (3) to provide the correct density. However, the analysis of the inverse operator for $\lambda \mapsto \mathcal{V} * \lambda$ works in quite the opposite direction.

Instead of explaining the invertibility process at the continuous level, let us use a Galerkin semidiscretization in space to study a more general problem that will be useful at the stage of numerical discretization as well.

Let X_h be any closed subspace of $H^{-1/2}(\Gamma)$ and take $\beta \in \mathrm{TD}(H^{1/2}(\Gamma))$ as data. We then look for a distribution $\lambda^h \in \mathrm{TD}(H^{-1/2}(\Gamma))$ such that

$$\lambda^h \in X_h, \tag{5a}$$
$$\langle \mu^h, \mathcal{V} * \lambda^h \rangle_\Gamma = \langle \mu^h, \beta \rangle_\Gamma \quad \forall \mu^h \in X_h, \tag{5b}$$

and postprocess the solution as a single layer potential

$$u^h = \mathcal{S} * \lambda^h. \tag{5c}$$

Once again, we have to read these equations with some care. Being an element of X_h has to be understood in a weak sense: if $\Pi^h : H^{-1/2}(\Gamma) \to X_h \subset H^{-1/2}(\Gamma)$ is any bounded projection onto X_h, condition (5a) can be equivalently read as $\Pi^h \lambda^h = \lambda^h$, that is, as a distributional equation in $H^{-1/2}(\Gamma)$. Equations (5b) –where angled brackets represent the $H^{-1/2}(\Gamma) \times H^{1/2}(\Gamma)$ duality product–, can be understood in the sense of scalar valued distributions (one equation for each $\mu^h \in X_h$), but they can also be read in a more compact form

$$\mathcal{V} * \lambda_h - \beta \in X_h^\circ, \tag{6}$$

where

$$X_h^\circ := \{\xi \in H^{1/2}(\Gamma) \,:\, \langle \mu^h, \xi \rangle_\Gamma = 0 \quad \forall \mu^h \in X_h\},$$

is the polar set or annihilator of X_h.

What we next do is reverting the order in which equations (5) are considered. The potential u^h takes

now the lead, as an element of $\mathrm{TD}(H^1_\Delta(\mathbb{R}^3 \setminus \Gamma))$ satisfying:

$$\ddot{u}^h = \Delta u^h, \tag{7a}$$
$$[\![\gamma u^h]\!] = 0, \tag{7b}$$
$$\gamma^+ u^h - \beta \in X_h^\circ, \tag{7c}$$
$$[\![\partial_\nu u^h]\!] \in X_h. \tag{7d}$$

Equations (7) are understood as distributional equations with values in $L^2(\mathbb{R}^3 \setminus \Gamma)$, $H^{1/2}(\Gamma)$, $H^{1/2}(\Gamma)$, and $H^{-1/2}(\Gamma)$ respectively. The density is then defined as $\lambda^h := [\![\partial_\nu u^h]\!]$.

If we momentarily forget about the semidiscrete space X_h (which can be done by setting $X_h = H^{-1/2}(\Gamma)$, thus making condition (7d) void), a Laplace domain analysis of this problem is what appears in the seminal work of Alain Bamberger and Toung Ha–Duong [1] (with a second part [2] dealing with the associated double layer potential operators). This idea of studying the potential to analyse the integral operator is behind the development of variationall tools for boundary integral equations of the first kind, and can be traced back to another seminal paper, this time by Jean-Claude Nédélec and Jacques Planchard [6]. The realization that the semidiscrete equations are related to the exotic transmission conditions in (7) was part of what I developed in collaboration with my then student Antonio Laliena [5].

3 More semidiscrete concepts

The operator $\beta \mapsto u^h \mapsto \lambda^h$ (which in practice is understood as $\beta \mapsto \lambda^h \mapsto u^h$) can be considered as a sort of Galerkin solver for equation (3). These operators can be easily shown to be convolution operators and we can thus write

$$\lambda^h = \mathcal{G}^h_\lambda * \beta \qquad u^h = \mathcal{G}^h_u * \beta = \mathcal{S} * \mathcal{G}^h_\lambda * \beta, \tag{8}$$

while realizing that the study is more about $\beta \mapsto \mathcal{G}^h_u * \beta$ and that

$$\lambda^h = [\![\partial_\nu \cdot]\!](\mathcal{G}^h_u * \beta).$$

A related operator is the one that starts with the exact solution of (3) and compares it with the solution of (5). Let thus $\lambda \in \mathrm{TD}(H^{-1/2}(\Gamma))$, and consider the solution of

$$\lambda^h \in X_h, \tag{9a}$$
$$\langle \mu^h, \mathcal{V} * (\lambda^h - \lambda)\rangle_\Gamma = 0 \quad \forall \mu^h \in X_h. \tag{9b}$$

Instead of paying attention to λ^h and to the potential $\mathcal{S}*\lambda^h$, it is advantageous to think in terms of the error of the potential

$$\varepsilon^h := \mathcal{S} * (\lambda^h - \lambda). \tag{9c}$$

This distribution is a causal $H^1_\Delta(\mathbb{R}^3 \setminus \Gamma)$-valued distributional solution of

$$\ddot{\varepsilon}^h = \Delta \varepsilon^h, \tag{10a}$$
$$[\![\gamma \varepsilon^h]\!] = 0, \tag{10b}$$
$$\gamma^+ \varepsilon^h \in X_h^\circ, \tag{10c}$$
$$[\![\partial_\nu \varepsilon^h]\!] + \lambda \in X_h. \tag{10d}$$

Once again, we have related convolution operators

$$\begin{aligned} \varepsilon^h &= \mathcal{E}^h_u * \lambda = \mathcal{G}^h_u * \mathcal{V} * \lambda - \mathcal{S} * \lambda \\ &= \mathcal{S} * (\mathcal{G}^h_\lambda * \mathcal{V} * \lambda - \lambda), \end{aligned} \tag{11a}$$

and

$$\mathcal{E}^h_\lambda * \lambda = \mathcal{G}^h_\lambda * \mathcal{V} * \lambda - \lambda, \tag{11b}$$

both of them satisfying a sort of Galerkin orthogonality property, namely, if $\Pi^h : H^{-1/2}(\Gamma) \to X^h$ is any projection onto X^h (for instance, the orthogonal projection), then

$$\mathcal{E}^h_u * (\Pi^h \lambda) = 0, \qquad \mathcal{E}^h_\lambda * (\Pi^h \lambda) = 0, \tag{12}$$

implying that any bound for the operators

$$\lambda \mapsto \varepsilon^h \quad \text{and} \quad \lambda \mapsto \lambda^h - \lambda = [\![\partial_\nu \varepsilon^h]\!]$$

is automatically a bound for the difference $\lambda - \Pi^h \lambda$.

4 Transfer function analysis

As already mentioned, the analysis of the convolution operators (for the Galerkin solver in Section 2 and for the Galerkin approximation error operator in Section 3) can be carried out by taking Laplace transforms. For the Galerkin solver, what we need to study is the influence of the parameter s in the operator that takes $\mathrm{B} \in H^{1/2}(\Gamma)$, solves the equation

$$\Lambda^h \in X_h, \tag{13a}$$
$$\langle \mu^h, \mathrm{V}(s)\Lambda^h - \mathrm{B}\rangle_\Gamma = 0 \quad \forall \mu^h \in X_h \tag{13b}$$

(see (5)), and then builds

$$\mathrm{U}^h := \mathrm{S}(s)\Lambda^h. \tag{13c}$$

In (13) we are using the single layer potential for the resolvent Laplace equation (defined for $\mathbf{x} \in \mathbb{R}^3 \setminus \Gamma$ and any $s \in \mathbb{C}$)

$$(\mathrm{S}(s)\Lambda)(\mathbf{x}) := \int_\Gamma \frac{e^{-\iota\, s|\mathbf{x}-\mathbf{y}|}}{4\pi|\mathbf{x}-\mathbf{y}|}\Lambda(\mathbf{y})\mathrm{d}\Gamma(\mathbf{y}),$$

which is the Laplace transform of (1). We are also using the associated single layer operator $\mathrm{V}(s) = \gamma\mathrm{S}(s)$. Denoting

$$\Lambda^h = \mathrm{G}^h_\lambda(s)\mathrm{B}, \quad \mathrm{U}^h = \mathrm{G}^h_u(s)\Lambda^h = \mathrm{S}(s)\mathrm{G}^h_\lambda(s)\mathrm{B},$$

the Laplace domain analysis yields bounds of the form

$$\|\mathrm{G}^h_u(s)\|_{H^{1/2}(\Gamma)\to H^1(\mathbb{R}^3)} \le C_\Gamma \frac{|s|^{3/2}}{\sigma\,\underline{\sigma}^{3/2}}, \qquad (14a)$$

$$\|\mathrm{G}^h_\lambda(s)\|_{H^{1/2}(\Gamma)\to H^{-1/2}(\Gamma)} \le C_\Gamma \frac{|s|^2}{\sigma\,\underline{\sigma}}, \qquad (14b)$$

where

$$s \in \mathbb{C}_+, \quad \sigma := \mathrm{Re}\, s, \qquad \underline{\sigma} := \min\{1, \sigma\}.$$

(From now on, the constant C_Γ is a generic constant depending on the domain Γ but not on the particular subspace X_h.) An analysis of the associated Galerkin error operators

$$\mathrm{E}^h_\lambda(s) := \mathrm{G}^h_\lambda(s)\mathrm{V}(s) - \mathrm{I}, \qquad \mathrm{E}^h_u(s) := \mathrm{S}(s)\mathrm{E}^h_\lambda(s),$$

yields

$$\|\mathrm{E}^h_u(s)\|_{H^{1/2}(\Gamma)\to H^1(\mathbb{R}^3)} \le C_\Gamma \frac{|s|}{\sigma\,\underline{\sigma}^2}, \qquad (14c)$$

$$\|\mathrm{E}^h_\lambda(s)\|_{H^{1/2}(\Gamma)\to H^{-1/2}(\Gamma)} \le C_\Gamma \frac{|s|^{3/2}}{\sigma\,\underline{\sigma}^{3/2}}. \qquad (14d)$$

The bounds given in (14) imply that the convolution operators (8) and (11) correspond to convolutions with elements

$$\begin{aligned}
&\mathcal{G}^h_\lambda \in \mathrm{TD}(\mathcal{B}(\,H^{1/2}(\Gamma), H^{-1/2}(\Gamma)\,)),\\
&\mathcal{E}^h_\lambda \in \mathrm{TD}(\mathcal{B}(\,H^{-1/2}(\Gamma), H^{-1/2}(\Gamma)\,)),\\
&\mathcal{G}^h_u \in \mathrm{TD}(\mathcal{B}(\,H^{1/2}(\Gamma), H^{1}(\mathbb{R}^3)\,),\\
&\mathcal{E}^h_u \in \mathrm{TD}(\mathcal{B}(\,H^{-1/2}(\Gamma), H^{1}(\mathbb{R}^3)\,),
\end{aligned}$$

where $\mathcal{B}(X,Y)$ is the space of bounded linear operators from X to Y. This means that behind the actual operators are operator-valued causal distributions. There is actually more information that can be extracted from (14). For instance, careful inversion of the Laplace transform leads to the following bound [4]: if $a \in \mathrm{TD}(\mathcal{B}(X,Y))$ and its Laplace A satisfies

$$\|\mathrm{A}(s)\|_{X\to Y} \le C_\mathrm{A}(\sigma)\,|s|^\mu, \quad \mu \ge 0, \quad \forall s \in \mathbb{C}_+,$$

then for sufficiently smooth causal input g, the convolution operator $g \mapsto a * g$ can be bounded as follows:

$$\|(a*g)(t)\|_Y \le 2^\mu C_\varepsilon(t) C_\mathrm{A}(t^{-1}) \int_0^t \|(\mathcal{P}_k g)(\tau)\|_X \mathrm{d}\tau,$$

where

$$k := \lfloor \mu + 2 \rfloor, \qquad \varepsilon := k - (\mu+1) \in (0,1],$$

$$C_\varepsilon(t) := \frac{1+\varepsilon}{\pi\varepsilon}\,\frac{t^\varepsilon}{(1+t)^\varepsilon}$$

and

$$(\mathcal{P}_k g)(t) := \sum_{\ell=0}^k \binom{k}{\ell} g^{(\ell)}(t).$$

This abstract (black-box) result delivers time-domain bounds for the convolution operators associated to the Galerkin solver and error operator. Note that (12) means that we can actually obtain bounds of the form

$$\|u^h(t) - u(t)\|_{H^1(\mathbb{R}^3)} \le \alpha(t)\, B_\lambda(t), \qquad (15a)$$

where

$$\alpha(t) := \frac{4C_\Gamma}{\pi}\, t\, \min\{1, t^2\}\frac{t}{1+t} \qquad (15b)$$

and

$$B_\lambda(t) := \int_0^t \|\mathcal{P}_3\lambda(t) - \Pi^h\mathcal{P}_3\lambda(t)\|_{H^{-1/2}(\Gamma)}\mathrm{d}\tau. \qquad (15c)$$

5 Time domain analysis

We now sketch an alternative form of studying the above convolution operators. The techniques shown in this section are distilled from recent work in [4], [7] and [3]. For simplicity we will focus on the problem (10), which deals with the Galerkin approximation error at the level of the potential. (The arguments for the discrete inverse, a.k.a., the Galerkin solver, are slightly more involved.) The first thing we do is to cut off the domain far enough from Γ. In order to do that we choose $R > 0$ such that

$$\Gamma \subset B(\mathbf{0}; R) := \{\mathbf{x} \in \mathbb{R}^3 \,:\, |\mathbf{x}| < R\},$$

and consider the truncated domain $B_T := B(\mathbf{0}; R+T)$. We then study a cut-off smooth version of (10) looking for $\varepsilon_T : [0,\infty) \to H^1_\Delta(B_T \setminus \Gamma)$ such that

$$\begin{aligned}
\ddot{\varepsilon}_T(t) &= \Delta\varepsilon_T(t) && \forall t \geq 0, && \text{(16a)}\\
\gamma_T\varepsilon_T(t) &= 0 && \forall t \geq 0, && \text{(16b)}\\
[\![\gamma\varepsilon_T(t)]\!] &= 0 && \forall t \geq 0, && \text{(16c)}\\
\gamma^+\varepsilon_T(t) &\in X_h^\circ && \forall t \geq 0, && \text{(16d)}\\
[\![\partial_\nu\varepsilon_T(t)]\!] + \lambda(t) &\in X_h && \forall t \geq 0, && \text{(16e)}\\
\varepsilon_T(0) = \dot{\varepsilon}_T(0) &= 0. && && \text{(16f)}
\end{aligned}$$

Some explanations about (16) are in order. The symbol γ_T is used for the trace operator $\gamma_T : H^1(B_T \setminus \Gamma) \to H^{1/2}(\partial B_T)$. Differentiation in (16a) and in the second initial condition in (16f) is strong (classical). In principle, we are looking for a solution of (16) that is twice continuously differentiable with values in the space where (16a) takes place, e.g., in $L^2(B_T \setminus \Gamma)$ and at least continuous with values in $H^1_\Delta(B_T \setminus \Gamma)$ so that all other conditions can be imposed pointwise in time.

The next step is the identification of an abstract setting for a second order problem associated to (16). We need three spaces

$$\begin{aligned}
H &:= L^2(B_T),\\
V &:= \{v \in H^1_0(B_T) \,:\, \gamma^+ v \in X_h^\circ\},\\
D(A) &:= \{v \in V \,:\, \Delta u \in L^2(B_T \setminus \Gamma),\, [\![\partial_\nu v]\!] \in X_h\},
\end{aligned}$$

and the operator $A := \Delta : D(A) \to H$. The non-homogeneous transmission condition (16e) does not allow the solution to be in the domain of A, so we proceed to lift it by solving time-independent problems

$$\begin{aligned}
u_0(t) &\in V,\\
(u_0(t), v_0)_{H^1(B_T)} &= \langle \lambda(t), \gamma v\rangle_\Gamma \quad \forall v \in V.
\end{aligned}$$

We then look for $v_0 : [0,\infty) \to D(A)$ such that

$$\begin{aligned}
\ddot{v}_0(t) &= Av_0(t) + f(t) \qquad \forall t \geq 0,\\
v_0(0) = \dot{v}_0(0) &= 0,
\end{aligned}$$

where $f := u_0 - \ddot{u}_0 : [0,\infty) \to V$. The sum $\varepsilon_T := u_0 + v_0$ is the solution of (16) and some careful work allows us to bound

$$\begin{aligned}
\|\varepsilon_T(t)\|_{H^1(B_T)} \leq & C_\Gamma \Big(\|\lambda(t)\|_{H^{-1/2}(\Gamma)} \\
& + c_T B(\lambda, t) \Big) \qquad \forall t \geq 0,
\end{aligned} \tag{17}$$

where $c_T^2 := 1 + T^2$ and

$$B(\lambda, t) := \int_0^t \|\lambda(\tau) - \ddot{\lambda}(\tau)\|_{H^{-1/2}(\Gamma)} \mathrm{d}\tau.$$

The difficulty at this moment is recognizing that $\varepsilon_T = \varepsilon^h$ in B_T for a limited time interval. This is done in several steps. If $\delta := \operatorname{dist}(\partial B_0, \Gamma)$, we first show that

$$\partial_\nu\varepsilon_T(t) = 0 \quad \text{in } H^{-1/2}(\partial B_T), \qquad \forall t \leq T + \delta.$$

Note that this can be easily hand-waved with a causality argument, but that this is quite similar to proving finite speed of propagation of compactly supported initial data in the solution of a wave equation written with separation of variables. (It is true, but the property is invisible in the formula.) Once this has been established, the next step is to compute the jump of the normal derivative on Γ with a simultaneous propagation of the T-dependent dynamical system (16),

$$\varepsilon^h_\lambda(T) := [\![\partial_\nu\varepsilon_T(T)]\!], \qquad T \geq 0,$$

and then show that

$$\varepsilon^h_\lambda(t) = [\![\partial_\nu\varepsilon_T(t)]\!], \qquad 0 \leq t \leq T + \delta.$$

The function ε^h_λ is extended by zero to negative values of the time variable and used to construct a potential $\varepsilon^h := \mathcal{S} * \varepsilon^h_\lambda$. This has to be compared with

$$\underline{\varepsilon}_T(t) := \begin{cases} \varepsilon_T(t), & \text{in } B_T,\\ 0, & \text{in } \mathbb{R}^3 \setminus \overline{\Omega}_-, \end{cases}$$

providing the identification

$$\underline{\varepsilon}_T(t) = (\mathcal{S} * \varepsilon_\lambda)(t) \qquad 0 \leq t < T + \delta.$$

This necessary (and quite cumbersome) work on comparison of strong and weak solutions is needed to ensure that we are not producing solutions that somehow cannot be 'smoothly' extended to negative times or to the exterior domain (at least for a finite amount of time) and thus identified with the layer potentials. Once these details have been settled, we can use the bound in (17) and (12) to obtain a bound

$$\begin{aligned}
\|u^h(t) - u(t)\|_{H^1(\mathbb{R}^3)} \leq C \Big(& \|\lambda(t) - \Pi^h\lambda(t)\|_{H^{-1/2}(\Gamma)} \\
& + c_t\, B(\lambda - \Pi^h\lambda, t) \Big),
\end{aligned}$$

which is definitely a tighter bound than (15). We can even make this look somewhat better by using a shifting argument that hides the constant $c_t^2 = 1+t^2$ in a bound of the form

$$\|u^h(t) - u(t)\|_{H^1(\mathbb{R}^3)} \leq C\, H(\partial^{-1}(\lambda - \Pi^h\lambda), t)$$

where

$$H(\xi, t) := \sum_{\ell=0}^{2} \int_0^t \|\xi(\tau)\|_{H^{-1/2}(\Gamma)} \mathrm{d}\tau,$$

and

$$\partial^{-1}\xi(t) := \int_0^t \xi(\tau)\mathrm{d}\tau.$$

Appendix

A Vector-valued distributions

Let X be a Banach space and $\mathcal{D}(\mathbb{R})$ be the space of infinitely often differentiable functions with compact support, endowed with its usual concept of convergence. An X-valued distribution is a sequentially continuous map $\mathcal{D}(\mathbb{R}) \to X$. If $f : \mathbb{R} \to X$ is a continuous function, then the Bochner integral

$$\int_{-\infty}^{\infty} \varphi(t) f(t) \mathrm{d}t$$

defines a distribution with values in X. If f is an X-valued distribution, then we can define its derivative

$$\langle \dot{f}, \varphi\rangle := -\langle f, \dot{\varphi}\rangle,$$

which is a distribution as well. If f is an X-valued distribution and $A : X \to Y$ is linear and bounded, then Af defines a Y-valued distribution. A distribution is said to be causal when $\langle f, \varphi\rangle = 0$ for all φ with support in $(-\infty, 0)$. A distribution is said to be tempered when it can be extended to act on the elements of the Schwartz class $\mathcal{S}(\mathbb{R})$. Given a causal tempered distribution f, its Laplace transform is defined as

$$\mathrm{F}(s) = \mathcal{L}\{f\}(s) := \langle f, \exp(-s\cdot)\rangle \qquad s \in \mathbb{C}_+.$$

The Laplace transform $\mathrm{F} : \mathbb{C}_+ \to X$ is an holomorphic X-valued function. In some conditions on the decay of an holomorphic X-valued function $\mathrm{F} : \mathbb{C}_+ \to X$, we can define the functions

$$f(t) := \frac{1}{2\pi\imath} \int_{\sigma-\imath\infty}^{\sigma+\imath\infty} e^{s\,t} \mathrm{F}(s) \mathrm{d}s,$$

show that they are independent of $\sigma > 0$, and that they define a causal continuous tempered function whose Laplace transform is F.

Acknowledgments

This work is an extract of a long term project including collaboration with Antonio Laliena (Universidad de Zaragoza, Spain), Víctor Domínguez (Universidad Pública de Navarra, Spain), Lehel Banjai (Heriot-Watt University, UK), Christian Lubich (Universität Tübingen, Germany) and my students at the University of Delaware (Sijiang Lu, Zhixing Fu, Tonatiuh Sánchez-Vizuet, Tianyu Qiu, and Matthew Hassell). My research is partially funded by the National Science Foundation (Grant DMS 1216356).

References

[1] A. Bamberger and T. Ha-Duong. *Formulation variationelle espace-temps pour le calcul par potentiel rétardé de la diffraction d'une onde acoustique I.* Math. Methods Appl. Sci. 8(3) (1986) 405-435.

[2] A. Bamberger and T. Ha-Duong. *Formulation variationelle espace-temps pour le calcul par potentiel rétardé de la diffraction d'une onde acoustique II.* Math. Methods Appl. Sci. 8(4) (1986) 598-608.

[3] L. Banjai, A.R. Laliena, and F.J. Sayas. *Fully discrete Kirchhoff formulas with CQ and BEM.* Submitted.

[4] V. Domínguez and F.J. Sayas. *Some properties of layer potentials and boundary integral operators for the wave equation.* J. Integral Equations Appl. To appear.

[5] A.R. Laliena and F.J. Sayas. *Theoretical aspects of the application of convolution quadrature to the scattering of acoustic waves.* Numer. Math. 112(4) 637–768.

[6] J.C. Nédélec and J. Planchard. *Une méthode variationelle d'éléments finis pour la résolution numérique d'un problème extérieur dans R^3*, RAIRO, Sér Rouge 7 (R-3) (1073) 105–129.

[7] F.J. Sayas. *Energy estimates for Galerkin semidiscretizations of time domain boundary integral equations.* Numer. Math. To appear.

[8] F.J. Sayas. *Retarded potentials and time domain boundary integral equations: a road map.*

Dynamical Dirichlet to Neumann map for the anisotropic wave equations and application to the inverse spectral problem

Mourad Bellassoued,
[1] University of Carthage,
Department of Mathematics
Faculty of Sciences of Bizerte
7021 Jarzouna Bizerte, Tunisia
*Email: mourad.bellassoued@fsb.rnu.tn

In this talk we seek stability estimates in the inverse problem of determining the potential or the velocity in a wave equation in an anisotropic medium from measured Neumann boundary observations. This information is enclosed in the dynamical Dirichlet-to-Neumann map associated to the wave equation. We prove in dimension $n \geq 2$ that the knowledge of the Dirichlet-to-Neumann map for the wave equation uniquely determines the electric potential and we prove Hölder-type stability in determining the potential. We prove similar results for the determination of velocities close to 1.
Keywords: Stability estimates, Hyperbolic inverse problem, Dirichlet-to-Neumann map.

1 Introduction

In this talk, we are interested in the following inverse boundary value problem: on a Riemannian manifold with boundary, determine the potential or the velocity — i.e. the conformal factor within a conformal class of metrics — in a wave equation from the vibrations measured at the boundary. Let $(\mathcal{M}, \mathrm{g})$ be a compact Riemannian manifold with boundary $\partial\mathcal{M}$. All manifolds will be assumed smooth (which means $\mathcal{C}^\infty$). We denote by Δ_g the Laplace-Beltrami operator associated to the metric g. In local coordinates,

$$\mathrm{g}(x) = \sum_{j,k=1}^{n} \mathrm{g}_{jk}(x)\mathrm{d}x^j \otimes \mathrm{d}x^k,$$

Δ_g is given by

$$\Delta_\mathrm{g} = \frac{1}{\sqrt{\det \mathrm{g}}} \sum_{j,k=1}^{n} \frac{\partial}{\partial x_j}\left(\sqrt{\det \mathrm{g}}\, \mathrm{g}^{jk} \frac{\partial}{\partial x_k}\right). \quad (1.1)$$

Here (g^{jk}) is the inverse of the metric g and $\det \mathrm{g} = \det(\mathrm{g}_{jk})$. Let us consider the following initial boundary value problem for the wave equation with bounded electric potential $q \in L^\infty(\mathcal{M})$

$$\begin{cases} \left(\partial_t^2 - \Delta_\mathrm{g} + q(x)\right) u = 0, & \text{in } (0,T)\times\mathcal{M}, \\ u(0,\cdot) = 0, \quad \partial_t u(0,\cdot) = 0 & \text{in } \mathcal{M}, \\ u = f, & \text{on } (0,T)\times\partial\mathcal{M}, \end{cases} \quad (1.2)$$

where $f \in H^1((0,T)\times\partial\mathcal{M})$ such that $f(0,\cdot) = 0$. Denote by $\nu = \nu(x)$ the outward normal vector field to $\partial\mathcal{M}$ at $x \in \partial\mathcal{M}$, normalized so that $\sum_{j,k=1}^n \mathrm{g}_{jk}\nu^j\nu^k = 1$ if $\nu = \sum_{j=1}^n \nu^j \frac{\partial}{\partial x_j}$. We may define the dynamical Dirichlet-to-Neumann map $\Lambda_{\mathrm{g},q}$ by

$$\Lambda_{\mathrm{g},q} f = \sum_{j,k=1}^{n} \nu_j \mathrm{g}^{jk} \frac{\partial u}{\partial x_k}\Big|_{(0,T)\times\partial\mathcal{M}} \quad (1.3)$$

where the $\nu_j = \sum_{k=1}^n \mathrm{g}_{jk}\nu^k$ are the coefficients of the outward conormal.

It is clear that one cannot hope to uniquely determine the metric $\mathrm{g} = (\mathrm{g}_{jk})$ from the knowledge of the Dirichlet-to-Neumann map $\Lambda_{\mathrm{g},q}$. As was noted in [23], the Dirichlet-to-Neumann map is invariant under a gauge transformation of the metric g. Namely, given a diffeomorphism $\Psi : \mathcal{M} \to \mathcal{M}$ such that $\Psi|_{\partial\mathcal{M}} = \mathrm{Id}$ one has $\Lambda_{\Psi^*\mathrm{g},q} = \Lambda_{\mathrm{g},q}$ where $\Psi^*\mathrm{g}$ denotes the pullback of the metric g under Ψ. The inverse problem should therefore be formulated modulo the natural gauge invariance. Nevertheless, when the problem is restricted to a conformal class of metrics, there is no such gauge invariance and the inverse problem now takes the form: knowing $\Lambda_{c\mathrm{g},q}$, can one determine the conformal factor c and the potential q?

Belishev and Kurylev gave an affirmative answer in [3] to the general problem of finding a smooth metric from the Dirichlet-to-Neumann map. Their approach is based on the boundary control method introduced by Belishev [2] and uses in an essential way an unique continuation property. Unfortunately

it seems unlikely that this method would provide stability estimates even under geometric and topological restrictions. Their method also solves the problem of recovering g through boundary spectral data. The boundary control method gave rise to several refinements of the results of [3]: one can cite for instance [19], [18] and [1].

The importance of control theory for inverse problems was first understood by Belishev [2]. He used control theory to develop the first variant of the boundary control (BC) method. Later, the idea based on control theory were combined with the geometrical ones. The importance of the geometry for inverse problems follows the fact that any elliptic second-order differential operator gives rise to a Riemannian metric in the corresponding domain. The role of this metric becomes clearer if we consider the solutions of the corresponding wave equation. Indeed, these waves propagate with the unit speed along geodesics of this Riemannian metric. These geometric ideas where introduced to the boundary control method in [19], [18].

In this , the inverse problem under consideration is whether the knowledge of the Dirichlet-to-Neumann map $\Lambda_{\mathrm{g},\,q}$ on the boundary uniquely determines the electric potential q (with a fixed metric g) and whether the knowledge of the Dirichlet-to-Neumann map $\Lambda_{\mathrm{g}} = \Lambda_{\mathrm{g},0}$ uniquely determines the conformal factor of the metric g within a conformal class. From the physical viewpoint, our inverse problem consists in determining the properties (e.g. a dispersion term) of an inhomogeneous medium by probing it with disturbances generated on the boundary. The data are responses of the medium to these disturbances which are measured on the boundary, and the goal is to recover the potential $q(x)$ and the velocity $c(x)$ which describes the property of the medium. Here we assume that the medium is quiet initially, and f is a disturbance which is used to probe the medium. Roughly speaking, the data is $\partial_\nu u$ measured on the boundary for different choices of f.

In the Euclidian case ($\mathrm{g} = e$) Rakesh and Symes [21], [20] used complex geometrical optics solutions concentrating near lines with any direction $\omega \in S^{n-1}$ to prove that $\Lambda_{e,q}$ determines $q(x)$ uniquely in the wave equation. In [21], $\Lambda_{e,q}$ gives equivalent information to the responses on the whole boundary for all the possible input disturbances. Ramm and Sjöstrand [22] extended the results in [21] to the case of a potential q depending both on space x and time t. Isakov [15] considered the simultaneous determination of a potential and a damping coefficient. A key ingredient in the existing results, is the construction of complex geometric optics solutions of the wave equation in the Euclidian case, concentrated along a line, and the relationship between the hyperbolic Dirichlet-to-Neumann map and the X-ray transform plays a crucial role.

Regarding stability estimates, Sun [25] established in the Euclidean case stability estimates for potentials from the Dirichlet-to-Neumann map. In [23] and [24] Stefanov and Uhlmann considered the inverse problem of determining a Riemannian metric on a Riemannian manifold with boundary from the hyperbolic Dirichlet-to-Neumann map associated to solutions of the wave equation $(\partial_t^2 - \Delta_{\mathrm{g}})u = 0$. A Hölder type of conditional stability estimate was proven in [23] for metrics close enough to the Euclidean metric in $\mathcal{C}^k$, $k \geq 1$ or for generic simple metrics in [24].

Uniqueness properties for local Dirichlet-to-Neumann maps associated with the wave equation are rather well understood (e.g., Belishev [2], Katchlov, Kurylev and Lassas [18], Kurylev and Lassas [19]) but stability for such operators is far from being apprehended. For instance, one may refer to Isakov and Sun [17] where a local Dirichet-to-Neumann map yields a stability result in determining a coefficient in a subdomain. As for results involving a finite number of data in the Dirichlet-to-Neumann map, see Cheng and Nakamura [10], Rakesh [20]. There are quite a few works on Dirichlet-to-Neumann maps, so our references are far from being complete: see also Cardoso and Mendoza [9], Eskin [12]-[13]-[14], Uhlmann [26] as related papers.

The main goal of this paper is to study the stability of the inverse problem for the dynamical anisotropic wave equation. The approach that we develop is a dynamical approach. Our inverse problem corresponds to a formulation with boundary measurements at infinitely many frequencies. On the other hand, the main methodology for formulations of inverse problems involving a measurement at a fixed frequency, is based on L^2-weighted inequalites called Carleman estimates. For such applications of Carleman inequalities to inverse problems we refer for instance to Bellassoued [4], Isakov [16]. Most papers treat the determination of spatially varying functions by a single measurement. As for observability inequalities by

means of Carleman estimates, see [5], [6], [7].

Our proof is inspired by techniques used by Stefanov and Uhlmann [24], and Dos Santos Ferreira, Kenig, Salo and Uhlmann [11]. In the last reference, an uniqueness theorem for an inverse problem for an elliptic equation is proved following ideas which in turn go back to the work of Calderón [8]. The heuristic underlying idea is that one can (at least formally) translate techniques used in solving the elliptic equation $\partial_t^2 + \Delta_g$ (which is the prototype of equations studied in [11]) to the case of the wave equation $\partial_t^2 - \Delta_g$ by changing t into it. Our problem turns out to be somehow easier because we don't need to construct complex geometrical solutions, but can rely on classical WKB solutions.

Our problem turns out to be easier because geometrical optics solutions interact with the interior of $\mathcal{M}$ in the dynamical case but not in the elliptic case. The main idea is to probe the medium by real geometric optics solutions of the wave equation, concentrated along a geodesic line, starting on one side of the boundary, and measure responses of the medium on other side of the boundary.

References

[1] M. Anderson, A. Katsuda,Y. Kurylev,M. Lassas,M. Taylor, *Boundary regularity for the Ricci equation, geometric convergence and Gel'fand's inverse boundary problem*, Inventiones Math. 158 (2004), 261-321.

[2] M. Belishev, *Boundary control in reconstruction of manifolds and metrics (BC method)*, Inverse Problems 13 (1997), R1 - R45.

[3] M. Belishev, Y.V. Kurylev, *To the reconstruction of a Riemannian manifold via its spectral data (BC- method).* Commun. Partial Differ. Equations 17, No.5-6, 767-804 (1992).

[4] M. Bellassoued, *Uniqueness and stability in determining the speed of propagation of second-order hyperbolic equation with variable coefficients*, Applicable Analysis 83 (2004), 983-1014.

[5] M. Bellassoued, M. Choulli, *Stability estimate for an inverse problem for the magnetic Schrödinger equation from the Dirichlet-to-Neumann map*, J. Funct. Anal. 258, No. 1, 161-195 (2010).

[6] M. Bellassoued, D. Jellali, M. Yamamoto, *Lipschitz stability for a hyperbolic inverse problem by finite local boundary data,* Applicable Analysis 85 (2006), 1219-1243.

[7] M. Bellassoued, D. Jellali, M. Yamamoto, *Stability Estimate for the hyperbolic inverse boundary value problem by local Dirichlet-to-Neumann map*, J. Math. Anal. Appl. 343, No. 2, 1036-1046, (2008).

[8] A. P. Calderón, *On an inverse boundary value problem,* in Seminar on Numerical Analysis and its Applications to Continuum Physics, Rio de Janeiro, (1988), 65-73.

[9] F. Cardoso and R. Mendoza, *On the hyperbolic Dirichlet-to-Neumann functional,* Comm. Partial Diff. Equations 21 (1996), 1235-1252.

[10] J. Cheng and G. Nakamura, *Stability for the inverse potential problem by finite measurements on the boundary,* Inverse Problems 17 (2001), 273-280.

[11] D. Dos Santos Ferreira, C. E. Kenig, M. Salo, and G. Uhlmann, *Limiting Carleman weihts and anisotropic inverse problems*, Inventiones Math. 178 (2009), 119-171.

[12] G. Eskin, *A new approach to hyperbolic inverse problems*, arXiv:math/0505452v3 [math.AP], 2006.

[13] G. Eskin, *Inverse hyperbolic problems with time-dependent coefficients*, arXiv:math/0508161v2 [math.AP], 2006.

[14] G. Eskin, *Global uniqueness in the inverse scattering problem for the Schrödinger operator with external Yang-Mills potentials*, Comm. Math. Phys. 222 (2001), no. 3, 503-531.

[15] V. Isakov, *An inverse hyperbolic problem with many boundary measurements*, Comm. Part. Dif. Equations 16 (1991), 1183-1195.

[16] V. Isakov, *Inverse Problems for Partial Differential Equations*, Springer-Verlag, Berlin, (1998).

[17] V. Isakov and Z. Sun, *Stability estimates for hyperbolic inverse problems with local boundary data*, Inverse Problems 8 (1992), 193-206.

[18] A. Katchalov, Y. Kurylev and M. Lassas, *Inverse Boundary Spectral Problems,* Chapman & Hall/CRC, Boca Raton, (2001).

[19] Y.V. Kurylev and M. Lassas, *Hyperbolic inverse problem with data on a part of the boundary,* in "Differential Equations and Mathematical Physics", AMS/IP Stud. Adv. Math. 16, Amer. Math. Soc., Providence, (2000), 259-272.

[20] Rakesh, *Reconstruction for an inverse problem for the wave equation with constant velocity*, Inverse Problems 6 (1990), 91-98.

[21] Rakesh and W. Symes, *Uniqueness for an inverse problems for the wave equation*, Comm. Partial Diff. Equations 13 (1988), 87-96.

[22] A. Ramm and J. Sjöstrand, *An inverse problem of the wave equation*, Math. Z. 206 (1991), 119-130.

[23] P. Stefanov and G. Uhlmann, *Stability estimates for the hyperbolic Dirichlet-to-Neumann map in anisotropic media,* J. Functional Anal. 154 (1998), 330-358.

[24] P. Stefanov and G. Uhlmann, *Stable Determination of Generic Simple Metrics from the Hyperbolic Dirichlet-to-Neumann Map*, International Math. Research Notices, 17 (2005), 1047-1061.

[25] Z. Sun, *On continous dependence for an inverse initial boundary value problem for the wave equation*, J. Math. Anal. App. 150 (1990), 188-204.

[26] G. Uhlmann, *Inverse boundary value problems and applications*, Astérisque 207, (1992), 153-221.

Seismology of the Sun

L. Gizon
Max-Planck-Institut für Sonnensystemforschung, 37191 Katlenburg-Lindau, Germany
and Institut für Astrophysik, Georg-August-Universität Göttingen, 37073 Göttingen, Germany
Email: gizon@mps.mpg.de

Abstract

In order to solve the mysteries of the solar dynamo, we must understand the plasma motions that maintain the magnetic field in the solar interior. Helioseismology, the science of solar oscillations, can in principle enable us to see inside the sun and provide this information. I will review the basic methods of helioseismology and discuss important findings based on observations from the SOHO and SDO satellites. Methods of local helioseismology, which rely on the two-point correlations of the wave field, enable us to probe vector flows in three dimensions and subsurface magnetic structures. A new method is presented to compute the spatial sensitivity of helioseismic travel times to weak perturbations to a background solar model.

1 Solar Oscillations

Solar seismic waves are continuously excited by turbulent motions in the upper layers of the convection zone. Oscillations of the solar atmosphere with periods near five minutes can be measured as fluctuations in the solar spectrum, either in velocity (Doppler shift of absorption lines) or in intensity. Since the mid 1990's dedicated observatories from space (SOHO) and from the ground (global network GONG) have provided time series of spatially resolved images of the visible solar hemisphere. The most recent experiment is the Helioseismic and Magnetic Imager onboard NASA's SDO spacecraft. HMI/SDO data consist of full-disk Doppler velocity images of 4000^2 pixels recorded at a cadence of 45 seconds, which give access to the full spectrum of solar seismic waves, from global acoustic oscillations of the entire solar volume to short-lived near-surface waves.

2 Probing the Solar Dynamo

The propagation of acoustic waves is sensitive to the local conditions of the solar plasma, e.g. sound speed and density, and is affected by the plasma flow velocity, e.g. rotation, meridional circulation, and large-scale convective velocities. Waves also interact with the magnetic field, particularly strong in active regions and sunspots. The goal of helioseismology is to retrieve as much information as possible about the solar interior from the surface observations of solar oscillations, on time scales ranging from days to years. One of the most important question in solar physics is the origin of the solar magnetic field. Why does solar magnetic activity change with a period of eleven years? What are the processes that lead to the formation of sunspots? In order to answer such questions, one should probe the internal flows that maintain the solar dynamo.

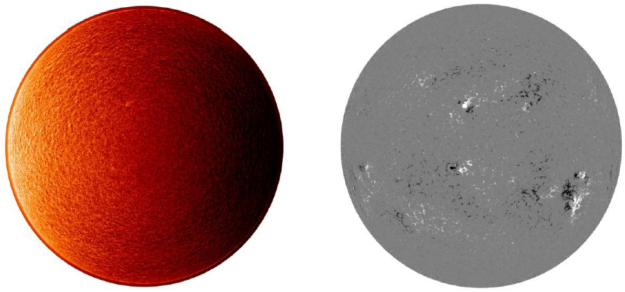

Figure 1: Left: Line-of-sight component of velocity (HMI Dopplergram). The east-west gradient across the image is due to solar rotation ($\sim 2\ \mathrm{km\,s^{-1}}$); the fine details are due to solar oscillations and convective motions. Right: Line-of-sight component of the magnetic field (HMI magnetogram). The strong concentrations of magnetic field at mid latitudes is due to magnetic active regions and sunspots.

3 Methods of Helioseismology

Methods of helioseismology are organized according to two classes: global and local. Global helioseismology is the interpretation of the frequencies of the normal modes of oscillation, extracted from the power spectrum of solar oscillations. Starting from a 1D reference solar model, one asks how the model should be perturbed in order to have frequencies of oscillations that are consistent with the observed frequencies. This linear inverse problem is solved using

standard techniques. Global mode helioseismology has been extremely successful, in particular to infer the angular velocity as a function of radius and (unsigned) latitude. However, global helioseismology is limited as it cannot provide information about flows in the north-south direction nor can it tell us about structural heterogeneities in all three dimensions. In order to overcome these limitations, techniques of *local* helioseismology are being developed. The most basic quantity in local helioseismology is the cross-covariance between two locations on the solar surface,

$$C(\boldsymbol{r}_1, \boldsymbol{r}_2, t) = \frac{1}{T}\int_0^T \mathrm{d}t'\, \phi(\boldsymbol{r}_1, t')\, \phi(\boldsymbol{r}_2, t'+t), \quad (1)$$

where ϕ is the observed wavefield, i.e. the Doppler velocity. In terms of the wave displacement $\boldsymbol{\xi}(\boldsymbol{r}, t)$, we have $\phi = \boldsymbol{\ell}\cdot\partial_t\boldsymbol{\xi}$, where ℓ is a unit vector in the direction of the line of sight. The duration of the observations, T, may be hours to weeks depending on the application. The cross-covariance function is a fundamental quantity as it is closely related to the Green's function and gives the travel time of wave packets between $\boldsymbol{r}_1$ and $\boldsymbol{r}_2$. In practice, a large set of travel times are measured and then inverted for 3D solar structure and vector flows. This last operation is not trivial as the 3D kernel functions that give the spatial sensitivity of travel times to a solar model are not straightforward to compute.

In the following sections an overview of the formalism used in local helioseismology is presented as well as a new, convenient method to solve the linear forward problem.

Normal Modes of Oscillation

Stellar oscillations are described by the displacement $\boldsymbol{\xi}(\boldsymbol{r}, t)$ of a fluid element originally at position $\boldsymbol{r}$ and t in the unperturbed fluid. The linearized equations of conservation of momentum, mass and energy can be combined into a single equation:

$$\mathcal{L}(\boldsymbol{\xi}) = \boldsymbol{S}, \quad (2)$$

where $\mathcal{L} = \partial_t^2 + \mathcal{H}$ and

$$\begin{aligned}\rho\mathcal{H}(\boldsymbol{\xi}) \;=\; & -\boldsymbol{\nabla}(\rho c^2\boldsymbol{\nabla}\cdot\boldsymbol{\xi}) \\ & +(\boldsymbol{\nabla}\cdot\boldsymbol{\xi})\boldsymbol{\nabla}p + (\boldsymbol{\xi}\cdot\boldsymbol{\nabla})\boldsymbol{\nabla}p - \boldsymbol{\nabla}(\boldsymbol{\xi}\cdot\boldsymbol{\nabla}p) \\ & -\rho\Delta\boldsymbol{g}' - \rho\Delta(\boldsymbol{F}/\rho)' \end{aligned} \quad (3)$$

for adiabatic oscillations and no background flow. The quantities ρ, c and p are the background (time-independent) density, sound speed and pressure. The last two terms in $\mathcal{H}$ account for the wave perturbations to the gravitational and magnetic forces. The source term, $\boldsymbol{S}(\boldsymbol{r}, t)$ on the right-hand side of the wave equation, describes the random forcing by turbulent convection; it is a realization drawn from a random process. The wave equation is (often) supplemented by a free-surface boundary condition at the top of the solar model.

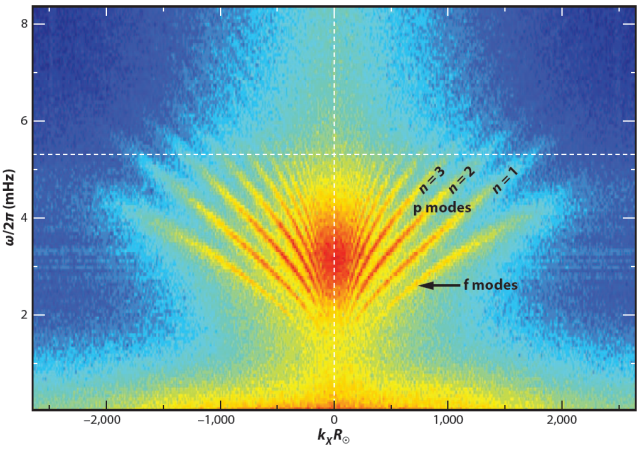

Figure 2: Observed power spectrum of solar oscillations as a function of frequency and horizontal wavenumber k_x at fixed $k_y = 0$, showing surface-gravity waves (f modes) and acoustic waves (p modes). The radial order, n, corresponds to the number of nodes of the eigenfunctions. The power below 1.5 mHz is due to solar convection.

Modes of free oscillation, $\boldsymbol{s}^\alpha(\boldsymbol{r})e^{-\mathrm{i}\omega_\alpha t}$, solve the eigenvalue problem $\mathcal{H}(\boldsymbol{s}^\alpha) = \omega_\alpha^2\boldsymbol{s}^\alpha$. Eigenfunctions are often normalized according to $\langle\boldsymbol{s}^\alpha, \boldsymbol{s}^\alpha\rangle = 1$, where the inner product is defined by $\langle\boldsymbol{u}, \boldsymbol{v}\rangle = \int_\odot \boldsymbol{u}^*\cdot\boldsymbol{v}\,\rho\mathrm{d}^3\boldsymbol{r}$. For a non-rotating 1D solar model, the eigenmode $\alpha = (l, m, n)$ is of the form

$$\boldsymbol{s}^{lmn}(\boldsymbol{r}) = \boldsymbol{T}_{\boldsymbol{r}}^{ln}[Y_{lm}(\hat{\boldsymbol{r}})] \quad (4)$$

where Y_{lm} are spherical harmonics and

$$\boldsymbol{T}_{\boldsymbol{r}}^{ln} = R_{ln}(r)\hat{\boldsymbol{r}} + \frac{H_{ln}(r)}{\sqrt{l(l+1)}}\boldsymbol{\nabla}_\perp, \quad (5)$$

where $R(r)$ and $H(r)$ are the radial and horizontal eigenfunctions and $\boldsymbol{\nabla}_\perp = \hat{\boldsymbol{\theta}}\partial_\theta + \hat{\boldsymbol{\phi}}(\sin\theta)^{-1}\partial_\phi$ in a spherical-polar coordinate system where θ is co-latitude and ϕ is longitude.

Modes have finite lifetimes due to their interaction with turbulence and/or to radiative damping, both difficult to model. Traditionally, ad-hoc attenuation is introduced in the wave equation, $(\partial_t +$

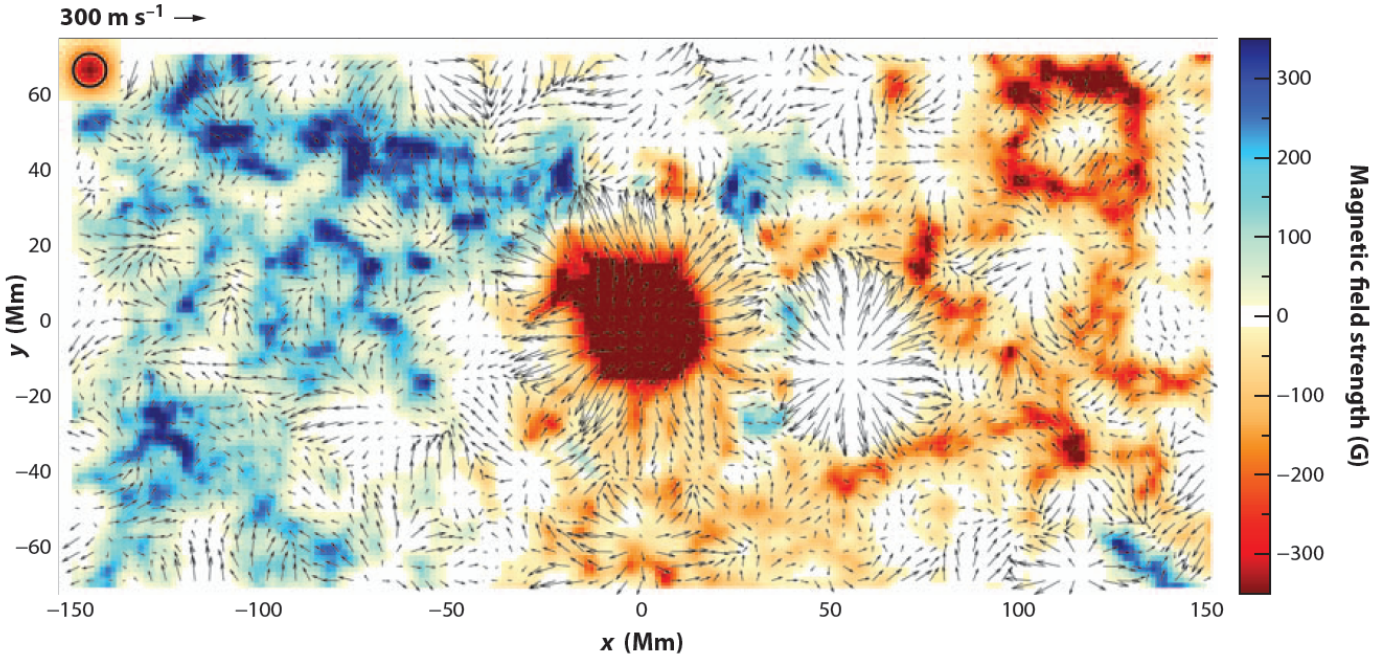

Figure 3: Map of horizontal flows (arrows) in the vicinity of a sunspot obtained by local helioseismology. The depth is 1 Mm and the observation time is $T = 1$ day. The background colors show the line-of-sight component of the magnetic field at the surface for context.

$\gamma)^2\boldsymbol{\xi} + \mathcal{H}(\boldsymbol{\xi}) = 0$, where γ represents the half width at half maximum of a Lorentzian line profile in the power spectrum. With this correction, the modes of oscillation of the damped equation have that the same eigenfunctions but complex frequencies $\sigma_\alpha = \omega_\alpha - \mathrm{i}\gamma_\alpha$.

4 Formulation of Linear Forward Problem

Here we ask how the cross-covariance function is perturbed by a small change in the solar model, for example a localized change in the sound speed, $\delta c(\boldsymbol{r})$, or the presence of a flow, $\boldsymbol{U}(\boldsymbol{r})$. This change in the solar model is implemented as a change in the wave operator, $\mathcal{L} \to \mathcal{L} + \delta\mathcal{L}$. Note that we consider only steady perturbations, so that the problem may be solved at fixed temporal frequency, ω.

4.1 Zero-Order Problem

Let us define the Fourier transform of the displacement vector by

$$\boldsymbol{\xi}(\boldsymbol{r},\omega) = \frac{1}{2\pi}\int_{-\infty}^{\infty} \mathrm{d}t\; \boldsymbol{\xi}(\boldsymbol{r},t)e^{\mathrm{i}\omega t}. \qquad (6)$$

In Fourier space,

$$\mathcal{L}\boldsymbol{\xi}(\boldsymbol{r},\omega) = \boldsymbol{S}(\boldsymbol{r},\omega), \qquad (7)$$

where $\mathcal{L} = -\omega^2 + \mathcal{H}$ is the unperturbed (or zero-order) wave operator. In general, the solution to the above equation can be written in the form

$$\boldsymbol{\xi}(\boldsymbol{r},\omega) = 2\pi\int_\odot \mathrm{d}^3\boldsymbol{r}_\mathrm{s}\; \boldsymbol{G}^j(\boldsymbol{r},\boldsymbol{r}_\mathrm{s},\omega)S_j(\boldsymbol{r}_\mathrm{s},\omega), \qquad (8)$$

where the sum over repeated indices $j \in \{x,y,z\}$ is implicit and $\boldsymbol{G}^j(\boldsymbol{r},\boldsymbol{r}_\mathrm{s},\omega)$ is the displacement at $\boldsymbol{r}$ that results from a delta-function source at $\boldsymbol{r}_\mathrm{s}$ acting in the j-th direction:

$$\mathcal{L}_{\boldsymbol{r}}\boldsymbol{G}^j(\boldsymbol{r},\boldsymbol{r}_\mathrm{s},\omega) = \frac{1}{2\pi}\hat{\boldsymbol{e}}_j(\boldsymbol{r}_\mathrm{s})\delta(\boldsymbol{r}-\boldsymbol{r}_\mathrm{s}). \qquad (9)$$

The Green's tensor may be computed either numerically or using a normal mode expansion:

$$\mathbf{G}(\boldsymbol{r},\boldsymbol{r}_\mathrm{s},\omega) = \frac{1}{2\pi}\sum_l \frac{2l+1}{4\pi}\sum_n \frac{\boldsymbol{T}^{ln}_{\boldsymbol{r}}\boldsymbol{T}^{ln}_{\boldsymbol{r}_\mathrm{s}}P_l(\cos\Delta)}{\omega_{ln}^2 - (\omega+\mathrm{i}\gamma_{ln})^2}. \qquad (10)$$

where Δ is the great circle distance between source $\boldsymbol{r}_\mathrm{s}$ and receiver $\boldsymbol{r}$.

Defining the observable by $\phi = -\mathrm{i}\omega\boldsymbol{\ell}\cdot\boldsymbol{\xi} := \mathrm{Obs}(\boldsymbol{\xi})$ and the observed Green's function by $\mathcal{G} = \mathrm{Obs}(\boldsymbol{G})$, then the zero-order wave field is given by

$$\phi(\boldsymbol{r},\omega) = 2\pi\int_\odot \mathrm{d}^3\boldsymbol{r}_\mathrm{s}\; \mathcal{G}^j(\boldsymbol{r},\boldsymbol{r}_\mathrm{s},\omega)S_j(\boldsymbol{r}_\mathrm{s},\omega). \qquad (11)$$

4.2 Perturbation to the Cross-Covariance Function

In frequency space, the expectation value of the cross-covariance between two points at the surface is

$$C(\boldsymbol{r}_1,\boldsymbol{r}_2,\omega)=\frac{2\pi}{T}\mathrm{E}[\phi^*(\boldsymbol{r}_1,\omega)\phi(\boldsymbol{r}_2,\omega)]. \qquad (12)$$

A change in the solar model (through $\delta\mathcal{L}$) causes a change in the observable, $\delta\phi=\mathrm{Obs}(\delta\boldsymbol{\xi})$. To first order, the perturbation to the cross-covariance is

$$\begin{aligned}\delta C(\boldsymbol{r}_1,\boldsymbol{r}_2,\omega) &= \frac{2\pi}{T}\mathrm{E}[\delta\phi^*(\boldsymbol{r}_1,\omega)\phi(\boldsymbol{r}_2,\omega)]\\ &\quad +(1\leftrightarrow 2)^*, \qquad (13)\end{aligned}$$

where the second term is obtained from the first by exchanging $\boldsymbol{r}_1$ and $\boldsymbol{r}_2$ and taking the complex conjugate. Using the first Born approximation,

$$\mathcal{L}(\delta\boldsymbol{\xi})=-\delta\mathcal{L}(\boldsymbol{\xi}), \qquad (14)$$

we obtain

$$\delta\phi(\boldsymbol{x},\omega)=-2\pi\int_\odot d^3\boldsymbol{r}\;\mathcal{G}^j(\boldsymbol{x},\boldsymbol{r},\omega)\left\{\delta\mathcal{L}\,\boldsymbol{\xi}(\boldsymbol{r},\omega)\right\}_j. \qquad (15)$$

Hence, the first-order perturbation to the cross-covariance can be written

$$\begin{aligned}&\delta C(\boldsymbol{r}_1,\boldsymbol{r}_2,\omega)=\\ &\quad -2\pi\int_\odot \mathrm{d}^3\boldsymbol{r}\;\mathcal{G}^{j*}(\boldsymbol{r}_1,\boldsymbol{r},\omega)\left\{\delta\mathcal{L}^*_{\boldsymbol{r}}\boldsymbol{X}(\boldsymbol{r},\boldsymbol{r}_2,\omega)\right\}_j\\ &\quad +(1\leftrightarrow 2)^* \qquad (16)\end{aligned}$$

where

$$\boldsymbol{X}(\boldsymbol{r},\boldsymbol{r}_2,\omega):=\frac{2\pi}{T}\mathrm{E}[\boldsymbol{\xi}^*(\boldsymbol{r},\omega)\phi(\boldsymbol{r}_2,\omega)] \qquad (17)$$

is the cross-covariance between $\boldsymbol{\xi}(\boldsymbol{r})$ and $\phi(\boldsymbol{r}_2)$.

4.3 Example Perturbation: Flows

Let us consider the case of a steady flow, $\boldsymbol{U}(\boldsymbol{r})$. Under the assumption that the flow amplitude is smaller than the wave speed, it is reasonable to expect that first-order perturbation theory will work. The flow-wave interaction is described by

$$\delta\mathcal{L}\boldsymbol{\xi}(\boldsymbol{r},\omega)=-2\mathrm{i}\omega\rho(\boldsymbol{r})\boldsymbol{U}(\boldsymbol{r})\cdot\boldsymbol{\nabla}\boldsymbol{\xi}(\boldsymbol{r},\omega), \qquad (18)$$

which consists of a Doppler shift. Inserting $\delta\mathcal{L}$ in equation (16), the perturbation to the cross-covariance becomes

$$\delta C(\boldsymbol{r}_1,\boldsymbol{r}_2,\omega)=\int_\odot \mathrm{d}^3\boldsymbol{r}\,\boldsymbol{U}(\boldsymbol{r})\cdot\boldsymbol{K}(\boldsymbol{r},\boldsymbol{r}_1,\boldsymbol{r}_2,\omega) \qquad (19)$$

where the vector-valued sensitivity kernel is defined by

$$\begin{aligned}&\boldsymbol{K}(\boldsymbol{r},\boldsymbol{r}_1,\boldsymbol{r}_2,\omega)=\\ &\quad -4\pi\mathrm{i}\omega\rho(\boldsymbol{r})\mathcal{G}^{j*}(\boldsymbol{r}_1,\boldsymbol{r},\omega)\,\boldsymbol{\nabla}_{\boldsymbol{r}}X_j(\boldsymbol{r},\boldsymbol{r}_2,\omega)\\ &\quad +(1\leftrightarrow 2)^*. \qquad (20)\end{aligned}$$

The kernel $\boldsymbol{K}$ provides the connection between helioseismology observables (cross-covariance or wave travel times) and internal flows. Two intermediate quantities are needed to compute $\boldsymbol{K}$, i.e. the Green's function $\mathcal{G}^j$ and the cross-covariance X_j. The Green's function can be computed either numerically or using a normal mode expansion, see equation (10). Notice that the seismic reciprocity theorem implies $\mathcal{G}^j(\boldsymbol{r}_1,\boldsymbol{r})=-\mathrm{i}\omega\,G^i_j(\boldsymbol{r},\boldsymbol{r}_1)\ell_i(\boldsymbol{r}_1)$, which depends on the response to a source at $\boldsymbol{r}_1$ pointing in the $\boldsymbol{\ell}(\boldsymbol{r}_1)$ direction. The computation of X_j relies on a realization of the random wave field $\boldsymbol{\xi}$, which may be obtained from a realistic simulation of solar convection or approximated by normal-mode summation. The approach described here for solving the linear forward problem maybe called 'computational local helioseismology'. Until now, only semi-analytical methods have been used, which are not very flexible and involve many more steps.

References

[1] L. Gizon, A. C. Birch, and H. C. Spruit, *Local Helioseismology: Three-Dimensional Imaging of the Solar Interior*, Annu. Rev. Astron. Astrophys., **48** (2010), pp. 289–338 (2010).

[2] L. Gizon and A. C. Birch, *A new method to compute sensitivity kernels for local helioseismology*, in Fourth HELAS International Conference: Seismological Challenges for Stellar Structure (2010).

The analysis of shifted Laplace and related preconditioners for finite element approximations of the Helmholtz equation

I.G. Graham[1]
[1] Department of Mathematical Sciences, University of Bath, Bath, UK
*Email: I.G.Graham@bath.ac.uk

Abstract

There has been much recent research on preconditioning (discretisations of) the Helmholtz operator $\Delta+k^2$ with the inverse of a discrete version of the so-called "shifted Laplacian" $\Delta+(k^2+\mathrm{i}\varepsilon)$ for some $\varepsilon > 0$. (In practice this inverse is replaced with a cheaper approximation, such as a multigrid V-cycle, to obtain a practically viable preconditioner.) Despite many numerical investigations there has been no rigorous analysis of how one should chose the shift for the type of Helmholtz problems arising in applications. In this talk we give sufficient conditions on ε so that the shifted matrix is a good preconditioner for the original matrix as $k \to \infty$. The results hold for finite element discretisation of both the interior impedance problem, and the sound-soft scattering problem (with radiation condition imposed as a far-field impedance boundary). We also investigate the properties of classical domain decomposition methods with coarse grid and local solves for approximating the inverse of the shifted problem, and analyse explicitly how this depends on ε and k. *The talk contains results obtained in collaboration with Paul Childs, Martin Gander, Douglas Shanks, Euan Spence and Eero Vainikko [4], [5], [9], [10].*

1 Overview

As a model problem for high-frequency wave scattering, we study the boundary value problem

$$\begin{cases} -\Delta u - k^2 u &= f \quad \text{in } \Omega, \\ \frac{\partial u}{\partial n} - \mathrm{i}ku &= g \quad \text{on } \Gamma, \end{cases} \tag{1}$$

where either (i) Ω is a bounded domain in $\mathbb{R}^d$ with boundary Γ or (ii) Ω is the exterior of a bounded scatterer, Γ denotes an appropriate far field boundary and the problem is appended with a Dirichlet condition on the boundary of the scatterer. Linear systems arising from finite element approximations of this problem for high wavenumber k are notoriously hard to solve. Because the system matrices are non-Hermitian and generally non-normal, general iterative methods like preconditioned (F)GMRES have to be employed. Analysing the convergence of these methods is hard, since an analysis of the spectrum of the system matrix alone is not sufficient to permit any conclusions to be drawn.

Quite a lot of recent research has focussed on preconditioning the discrete counterpart of (1) using the discrete countarpart of the problem

$$\begin{cases} -\Delta u - (k^2 + \mathrm{i}\varepsilon)u &= f \quad \text{in } \Omega, \\ \frac{\partial u}{\partial n} - \mathrm{i}\eta u &= g \quad \text{on } \Gamma, \end{cases} \tag{2}$$

for some η which depends on k and ε. It is generally observed that if the "absorption" parameter $\varepsilon > 0$, is taken sufficiently large, then standard iterative methods for (2) start to work, but ε needs to be sufficiently small for (2) to still provide a good preconditioner for (1). However to date there is only a rudimentary analysis of this question, e.g. for simple 1D or 2D problems, always using Fourier analysis, and assuming Dirichlet - rather than impedance - boundary conditions.

The use of absorption in preconditioning has been studied in various contexts by several authors. Let A_ε denote the system matrix arising from the finite element approximation of (2). Then, for example, Erlangga, Vuik & Oosterlee [6] sought to precondition A_0 with a multigrid approximation of A_ε^{-1} and typically used $\varepsilon \sim k^2$. Ernst and Gander [7] used Fourier analysis in 1D to show that ε needs to be taken to be $\mathcal{O}(k)$ for A_ε to be a good preconditioner for A_0 but needs to be $\mathcal{O}(k^2)$ for multigrid applied to A_ε to have a convergence factor less than unity. However the model problem considered in [7] was a very simplified one. Engquist and Ying [8] essentially used $\varepsilon = \mathcal{O}(k)$ to enhance the performance of their sweeping preconditioner. However none of these references give rigorous information on how ε should be chosen in general to obtain the best performance for preconditioning.

In this talk we give a new rigorous analysis which firstly provides sufficient conditions for convergence of GMRES for discretisations of problem (1) preconditioned by problem (2). The analysis developed to do this also allows us to then also analyse rather standard domain decomposition algorithms for (2) explic-

itly in k and ε and this analysis provides the ingredients for a fairly robust solver which is well disposed to parallel implementation.

The convergence theory for GMRES (see, e.g. [2] or [1]) tells us that $k-$independent convergence will be achieved for a system with matrix A_0 when preconditioned by A_ε^{-1}, provided as $k \to \infty$, the conditions :

$$\text{(G1)} \quad \|A_\varepsilon^{-1} A_0\| \text{ is uniformly bounded,}$$

and

$$\text{(G2)} \quad \text{dist}(0, W(A_\varepsilon^{-1} A_0)) \geq C > 0,$$

are satisfied, where $W(T)$ is the numerical range of the matrix T: $\{(T\mathbf{x}, \mathbf{x}) : \mathbf{x} \in \mathbb{C}^N, \|\mathbf{x}\| = 1\}$. Both these conditions can be attained if $\|I - A_\varepsilon^{-1} A_0\|$ can be made sufficiently small. The simple estimate

$$\|I - A_\varepsilon^{-1} A_0\| \ \leq \ \|A_\varepsilon^{-1}\| \, \|A_\varepsilon - A_0\| \tag{3}$$

then suggests the separate estimation of each of the norms on the right-hand side of (3). The second term is straightforward (in fact it reduces to $\varepsilon \|M\|$, where M is the domain mass matrix, when $\eta = k$). Our approach to bounding the harder first term is by first estimating the norm of the solution operator for the undiscretised problem (2) explicitly in k and ε, and then using this information and the variational theory of the finite element method to bound $\|A_\varepsilon^{-1}\|$. Bounding the solution operator requires a certain amount of PDE theory.

2 PDE Theory and Matrix Bounds

The following theorems are proved in [9]. The proof of Theorem 2.1 essentially uses Green's identity, while Theorem 2.2 uses classical multiplier theory (due to Morawetz and co-authors and summarised, e.g. in [3]). Here, for simplicity, we restict to the case $\eta = k$ in (2).

Theorem 2.1 *Suppose Ω is a Lipschitz domain, and that, as $k \to \infty$, ε/k is bounded below by a positive constant and ε/k^2 is bounded above. Then for any $k_0 > 0$ there exists a $C > 0$, independent of ε, k with*

$$\|\nabla u\|^2_{L^2(\Omega)} + k^2 \|u\|^2_{L^2(\Omega)} \leq C \left[\frac{k^2}{\varepsilon^2} \|f\|^2_{L^2(\Omega)} + \frac{k}{\varepsilon} \|g\|^2_{L^2(\Gamma)} \right] \tag{4}$$

for all $k \geq k_0$.

Theorem 2.2 *Suppose Ω is a star-shaped domain (or the annulus between two star-shaped domains in the case of the sound-soft scattering problem), and suppose that ε/k is bounded above as $k \to \infty$, Then for any $k_0 > 0$ there exists a $C > 0$, independent of ε, k with*

$$\|\nabla u\|^2_{L^2(\Omega)} + k^2 \|u\|^2_{L^2(\Omega)} \leq C \left[\|f\|^2_{L^2(\Omega)} + \|g\|^2_{L^2(\Gamma)} \right] \tag{5}$$

for all $k \geq k_0$.

Note that Theorem 2.2, which allows $\varepsilon = 0$ (and thus includes the Helmholtz wave scattering case) needs a starshaped domain (a special case of a "non-trapping" domain), whereas Theorem 2.1 has a larger ε and has no geometric restriction other than Lipschitz. "Trapping" is an important concept for scattering problems governed by the Helmholtz equation in exterior domains but not for problems with absorption and the theory reflects this.

Moreover Theorem 2.1 illustrates the better regularity properties of the problem with absorption: the constants which multiply the data in (4) decrease to zero as $k \to \infty$, if ε grows faster that $\mathcal{O}(k)$, while they are only bounded above in (5). This is important for the theory on domain decomposition described briefly below.

Most importantly for our discussion here, the estimate in Theorem 2.2 shows that if u is the solution to problem (2) then, provided ε/k is bounded above, we have the L^2 estimate:

$$\|u\|_{L^2(\Omega)} \leq \frac{C}{k} \left[\|f\|^2_{L^2(\Omega)} + \|g\|^2_{L^2(\Gamma)} \right]^{1/2}.$$

When the mesh is chosen so that the Galerkin method enjoys a quaisoptimality property, this estimate can be combined with a scaling argument to obtain the bound on the matrix inverse $\|A_\varepsilon^{-1}\| \leq C/(kh^d)$, where h is the mesh diameter (with the mesh assumed quasiuniform) and d is the space dimension. This estimates the first term on the right-hand side of (3). Moreover an elementary argument can be used to bound the second term in the form $C\varepsilon h^d$, and combination of these gives, finally,

$$\|I - A_\varepsilon^{-1} A_0\| \ \leq \ C \frac{\varepsilon}{k} \ , \tag{6}$$

and leads to the theorem:

Theorem 2.3 *If ε/k is bounded above by a sufficiently small constant then the number of GMRES iterations to solve systems with matrix $A_\varepsilon^{-1} A_0$ is bounded independently of k.*

Several remarks are in order here: (i) The assumption of mesh quasiuniformity is not essential. If the domain contains corners, standard shape-regular local refinement may be carried out and the result remains true, provided diagonal scaling as well as preconditioning is performed, i.e. to solve the system $A_0\mathbf{x} = \mathbf{b}$ with solution $\mathbf{x}$, we instead solve the system $D^{1/2}A_\varepsilon^{-1}A_0D^{-1/2}\mathbf{y} = D^{1/2}A_\varepsilon^{-1}\mathbf{b}$, with solution $\mathbf{y} = D^{1/2}\mathbf{x}$ where D is the diagonal of the mass matrix M; (ii) The assumption of star-shaped domains seems to be important here: in some experiments with trapping domains, the bound above on $\|A_\varepsilon^{-1}\|$ (and hence the guarantee of the smallness of $\|I - A_\varepsilon^{-1}A_0\|$) fails; (iii) The first condition (G1) for the convergence of GMRES holds for all choices of ε, up to $\mathcal{O}(k^2)$. However (G2) is much more delicate and in our theory at present we need ε/k sufficiently small for its proof. It is an interesting open question to try to relax this condition; (iv) We should bear in mind that we work here with sufficient conditions for the robust convergence of GMRES. These are by no means necessary and good convergence can sometimes also be achieved when the conditions identified here are not satisfied. These aspects will be illustrated in the talk by various numerical experiments.

3 Domain Decomposition

It is often claimed that the problem (2) becomes "elliptic" when $\varepsilon > 0$. We clarify this statement by giving a coercivity result for problem (2). This coercivity result is one of the ingredients for a new analysis of classical additive Schwarz domain decomposition methods, which use can fairly general subdomians and coarse mesh. The results give quite explicit criteria for the coarse mesh in order for the number of GMRES iterations to be bounded independently of k. Experiments with this preconditioner will be given in the talk. Proofs and further discussion will be in [10]. Related work on optimised non-overlapping Schwarz methods for problem (2) which gives convergence estimates explicitly in terms of k and ε will be given in the talk of Douglas Shanks [5].

In another talk in the conference [4], Paul Childs will describe the application of domain decomposition methods with absorption in conjunction with the sweeping preconditioner [8] providing a practical parallel 3D Helmholtz solver, and will apply these methods to substantial 3D problems of industrial significance.

References

[1] B. Beckermann, S. A. Goreinov , AND E. E. Tyrtyshnikov, *Some remarks on the Elman estimate for GMRES*, SIAM J. Matrix Anal. Appl. **27** (2006), 772–778.

[2] X.-C. Cai and O. B. Widlund. *Domain decomposition algorithms for indefinite elliptic problems.* SIAM Journal on Scientific and Statistical Computing, **13** (992), 243–258.

[3] S. N. Chandler-Wilde, I. G. Graham, S. Langdon, E.A. Spence, *Numerical-asymptotic boundary integral methods in high-frequency scattering*, Acta Numerica **21** (2012).

[4] P.N. Childs, I.G. Graham and J.D. Shanks, *Hybrid sweeping preconditioners for the Helmholtz equation* Proceedings WAVES 2013.

[5] J.D. Shanks, P.N. Childs, I.G. Graham, and *Shifted Laplace DDM preconditioners for the Helmholtz equation* Proceedings WAVES 2013.

[6] Y.A. Erlangga, C. Vuik and C.W. Oosterlee *On a class of preconditioners for solving the Helmholtz equation* Applied Numerical Mathematics **50** (2004), 409–425.

[7] O. G. Ernst and M. J. Gander, *Why it is difficult to solve Helmholtz problems with classical iterative methods.* In Numerical Analysis of Multiscale Problems, I.G. Graham, T.Y. Hou, O. Lakkis and R. Scheichl, editors, Proceedings of an LMS Durham Symposium 2010, LNCS **83**, Springer Verlag, 2012.

[8] B. Engquist and L. Ying, *Fast Algorithms for High Frequency Wave Propagation.* In Numerical Analysis of Multiscale Problems, I.G. Graham, T.Y. Hou, O. Lakkis and R. Scheichl, editors, Proceedings of an LMS Durham Symposium 2010, LNCS **83**, Springer Verlag, 2012.

[9] M.J. Gander, I.G. Graham, and E.A. Spence, *How should one choose the shift for the shifted Laplacian to be a good preconditioner for the Helmholtz equation?* in preparation, 2013.

[10] I.G. Graham, E.A. Spence and E. Vainikko *Additive Schwarz methods for the Helmholtz equation with and without absorption* in preparation, 2013.

Enforced stability of embedded eigenvalues and "invisible" obstacles in waveguides

Sergei A. Nazarov[1,*]
[1] Institute of Mechanical Engineering Problems, Russian Academy of Sciencies, StPetersburg, Russia
*Email: srgnazarov@yahoo.co.uk

Abstract

Based on the notion of the augmented scattering matrix and the corresponding criterion of the existence of trapped modes, an asymptotic procedure to keep an eigenvalue embedded into the continuous spectrum of a waveguide is presented. Similar technicalities and the asymptotic analysis of the standard scattering matrix provide the construction of elongated gently sloped obstacles in the cylindrical waveguide which become invisible at a finite set of prescribed frequencies.

1 Eigenvalues embedded into the continuous spectrum of a waveguide

The distinguishing feature of an eigenvalue embedded into the continuous spectrum of a waveguide is its natural instability, namely a small local perturbation of the waveguide may lead the eigenvalue outside the spectrum and turn it into a point of complex resonance. However under a proper but rather arbitrary choice of the small perturbation the eigenvalue stays in the spectrum. An asymptotic procedure to find out these appropriate perturbations of the waveguide walls and/or the shape of the obstacle is developed in [1]–[3] for different problems in mathematical physics. It requires to construct asymptotics of an artificial object, that is the augmented scattering matrix which becomes an algebraic identificator of the point spectrum and is determined through exponential wave packets of incoming and outgoing waves (see the original paper [4] as well as [1]–[3]). One may apply the procedure in two ways. First, cf. [1], to create the embedded eigenvalue near a fixed threshold point (these points give rise to standing waves) of the continuous spectrum. Second, cf. [2] and [3], to detect perturbations of the shape of an obstacle and/or a wall knob which are known to support trapped modes.

Let us formulate one of the obtained results for the two-dimensional acoustic waveguide with hard walls

$$\Pi(\varepsilon) = \{(x,y) : x \in (-\infty,+\infty), \varepsilon h(\varepsilon,x) < y < d\}, \tag{1}$$

where ε is a positive parameter, small in comparison the width $d > 0$ (we further set $d = 1$ and make the coordinates and geometric parameters dimensionless) while $h(\varepsilon, x)$ is a smooth function in x with a support in the interval $(-l, l)$ of length $2l > 0$. Moreover, the dependence of $h(\varepsilon, x)$ on the parameter ε is real analytic in a small neighborhood of the point $\varepsilon = 0$.

The pressure p satisfies the Helmholtz equation

$$-\Delta p(x,y) = \lambda p(x,y), \quad (x,y) \in \Pi(\varepsilon), \tag{2}$$

and the Neumann boundary conditions

$$\partial_n p(x,y) = 0, \quad (x,y) \in \partial\Pi(\varepsilon), \tag{3}$$

where Δ is the Laplace operator, λ is the spectral parameter proportional to the square of the frequency ω of harmonic in time oscillations, and ∂_n is the derivative along the outward normal.

The continuous spectrum σ_c of the problem (1), (2) coincides with the positive semi-axis $[0, +\infty)$ and is divided into the intervals $\Upsilon_k = \big(\pi^2 k^2, \pi^2 (k+1)^2\big)$ by the threshold points $\pi^2 k^2$; here $k = 0, 1, 2, \ldots$.

Theorem 1. *For any nonnegative integer k there exist $\varepsilon_k > 0$ and a profile function $f_k(\varepsilon, x)$ with the above-mentioned properties such that, for $\varepsilon \in (0, \varepsilon_k]$, the interval Υ_k of the continuous spectrum of the Neumann problem* (1), (2) *in the waveguide* (1) *with $d = 1$ includes exactly one eigenvalue λ_k^ε while the corresponding eigenfunction u_k^ε enjoys the exponential decay at infinity.*

Several questions remain open and the list of them is rather long. For example, it is not clear if it is possible to create simultaneously two eigenvalues in two given intervals Υ_k and Υ_j with $j \neq k$.

2 Invisible obstacles.

Asymptotic analysis of the standard scattering matrix, which is quite similar to the above-mentioned analysis of the augmented scattering matrix, can provide the construction of the profile function h of the waveguide wall such that, at given finite set of frequencies, all the propagative waves get only exponentially decaying perturbations after passing by the knob. In this way the obstacle becomes "invisible"

at these frequencies. Let us formulate one particular result in the two-dimensional linear theory of surface water-waves obtained recently in cooperation with A.-S. Bonnet-Ben Dhia and J. Taskinen.

We consider the planar channel (1) with the gently sloped warp described by the equation $y = \varepsilon h(\varepsilon, x)$ where the profile function keeps the properties mentioned above. The velocity potential $u(x, y)$ satisfies the Laplace equation

$$-\Delta u(x, y) = 0, \quad (x, y) \in \Pi(\varepsilon), \tag{4}$$

together with the Neumann (no–flow) condition at the bottom

$$\partial_n u(x, y) = 0, \quad x \in (-\infty, +\infty),\ y = \varepsilon h(\varepsilon, x), \tag{5}$$

and the Steklov (kinematic) condition at the free water surface

$$\partial_y u(x, d) = \lambda u(x, d), \quad x \in (-\infty, +\infty), \tag{6}$$

where $\lambda = g^{-1}\omega^2$ with the oscillation frequency $\omega > 0$ and the acceleration $g > 0$ due to gravity. The spectrum of the problem (4)–(6) is again absolutely continuous and coincides with the semi-axis $[0, +\infty)$. However, there is no positive thresholds since, for any $\lambda > 0$, exists only couple of propagative waves

$$w_\pm(x, y) = e^{\pm\mu i x}\left(e^{\mu y} + e^{-\mu y}\right)$$

where $\mu > 0$ is the unique root of the transcendental equation $\mu\left(e^{\mu d} - e^{-\mu d}\right)\left(e^{\mu d} + e^{-\mu d}\right)^{-1} = \lambda$.

If the channel bottom is flat, the wave w_+ travels along the channel in the positive direction of the x-axis. In the case of the warp this wave scatters and the problem (4)–(6) admits a solution in the form

$$u(x, y) = \chi_-(x) w_+(x, y) + \\ + \sum_{\pm} \chi_\pm(x) s_\pm w_\pm(x, y) + \widetilde{u}(x, y), \tag{7}$$

where the first term must be regarded as an incident wave from the left of the channel, the remainder $\widetilde{u}(x, y)$ decays exponentially as $|x| \to \infty$, $\chi_\pm$ are cut-off functions such that $\chi_\pm(x) = 0$ for $\pm x < l$ and $\chi_\pm(x) = 1$ for $\pm x > 2l$. The transmission s_+ and reflexion s_- coefficients are in the relationship $|s_+|^2 + |s_-|^2 = 1$. In the straight channel $\Pi(0) = (-\infty, +\infty) \times (0, d)$ we just have $u(x, y) = w_+(x, y)$ and hence

$$s_- = 0 \quad \text{and} \quad s_+ = 1. \tag{8}$$

Theorem 2. *For any $\lambda > 0$ there exist $\varepsilon_\lambda > 0$ and a nontrivial profile function $f_\lambda(\varepsilon, x)$ with the above-mentioned properties such that, for $\varepsilon \in (0, \varepsilon_\lambda]$, the problem (4)–(6) in the channel (1) admits the solution (7) with the coefficients (8) and the exponentially decaying remainder $\widetilde{u}(x, y)$.*

The equalities (8) mean that the incident wave w^+ from the left in the channel $\Pi(\varepsilon)$ gains only an exponentially small perturbation on the right of the channel. This fact ought to be interpreted as the invisibility of the warp. It is easy to verify that due to the evident relation $w_+(x, y) = \overline{w_-(x, y)}$ the invisibility property of the warp indicated in Theorem 2 is kept by the incident wave $w_-(x, y)$ coming from the right of the channel.

Notice that, similarly to embedded eigenvalues, the latter property is not stable with respect to small perturbations of the warp shape. However, the presented approach is able to give a rigorous reformulation of numerical simulations in terms of an appropriate proximity of the profile functions in both the cases under consideration.

Many other problems of the same type stay open but can be solved with the help of the developed method.

References

[1] S.A.Nazarov, *Asymptotic expansions of eigenvalues in the continuous spectrum of a regularly perturbed quantum waveguide* Theoretical and mathematical physics. **167** (2011) pp. 606–627.

[2] S.A.Nazarov, *Enforced stability of an eigenvalue in the continuous spectrum of a waveguide with an obstacle* Comput. Math. and Math. Physics. **52** (2012) pp. 448-464.

[3] S.A.Nazarov, *The enforced stability of embedded eigenvalues* Funct. Anal. Appl. **47** (2013) to appear.

[4] I.V. Kamotskii and S.A.Nazarov, *An augmented scattering matrix and exponentially decreasing solutions of an elliptic problem in a cylindrical domain* Zap. Nauchn. Sem. St.-Petersburg Otdel. Mat. Inst. Steklov. **264** (2000) pp. 66–82. (English transl.: Journal of Math. Sci.**111** (2002) pp. 3657–3666.

Diffraction effects for Bloch wave packets in periodic media

G. Allaire[1,*]
[1] CMAP, Ecole Polytechnique, 91128 Palaiseau, France.
*Email: gregoire.allaire@polytechnique.fr

Abstract

We report on a joint work with M. Palombaro and J. Rauch. We study the homogenization and singular perturbation of the wave equation in a periodic media for long times of the order of the inverse of the period. We consider inital data that are Bloch wave packets, i.e., that are the product of a fast oscillating Bloch wave and of a smooth envelope function. We prove that the solution is approximately equal to two waves propagating in opposite directions at a high group velocity with envelope functions which obey a Schrödinger type equation. Our analysis extends the usual WKB approximation by adding a dispersive, or diffractive, effect due to the non uniformity of the group velocity which yields the dispersion tensor of the homogenized Schrödinger equation.

1 Setting and results

The homogenization of the wave equation in periodic media is a well studied subject (see e.g. [7], [8]). It is known that, for non oscillating initial data (often called low frequency data), the homogenized limit is again a wave equation with effective coefficients that can be computed as in the static case. On the other hand, for oscillating initial data in resonance with the periodic medium (so-called high frequency data), the usual two-scale asymptotic method breaks down and one needs to use the famous WKB method (Wentzel, Kramers, Brillouin) to deduce that the asymptotic limit of the wave equation is described by geometric optics, i.e. eikonal equations for the phases and transport equations for the amplitudes of the waves (see e.g. [7], [9]).

The present work pertains to the second category, namely homogenization with high frequency data. However, the novelty is that we are interested in a much longer time scale, way beyond the geometric optic regime. In this new limit regime, called diffractive or dispersive regime [10], the phase is still the solution of the WKB eikonal equation but the amplitude, or envelope function, is not any longer solution of a transport equation but rather solution of a Schrödinger type equation (in a moving frame of reference). Therefore, our homogenized model describes dispersive properties of the wave equation for very long times.

There are many applications of wave propagation in periodic medium, including photonic crystals or optical fibers with a periodic transverse microstructure (see [13] and Figure 1).

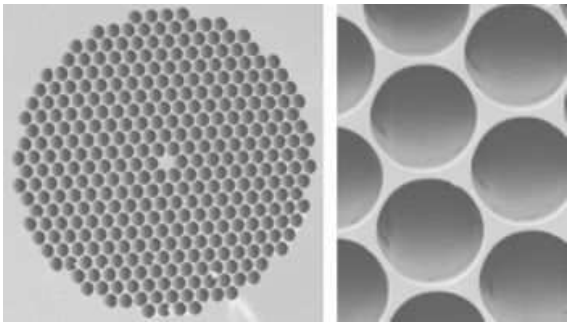

Figure 1: Cross section of a photonic optic fiber

More precisely, we study the homogenization of the singularly perturbed wave equation

$$\begin{cases} \varepsilon^2 \dfrac{\partial}{\partial t}\left(\rho_\varepsilon \dfrac{\partial u_\varepsilon}{\partial t}\right) - \operatorname{div}\left(A_\varepsilon \nabla u_\varepsilon\right) = 0 & \text{in } \mathbb{R}^N \times (0,T)\,, \\ u_\varepsilon(0,x) = u_\varepsilon^0(x) & \text{in } \mathbb{R}^N\,, \\ \dfrac{\partial u_\varepsilon}{\partial t}(0,x) = u_\varepsilon^1(x) & \text{in } \mathbb{R}^N\,, \end{cases} \tag{1}$$

where $T > 0$ is a final time, A_ε and ρ_ε are oscillating coefficients of the form

$$\begin{aligned} A_\varepsilon(x) &= A_0\left(\frac{x}{\varepsilon}\right) + \varepsilon^2 A_1\left(t, \frac{t}{\varepsilon}, x, \frac{x}{\varepsilon}\right), \\ \rho_\varepsilon(x) &= \rho_0\left(\frac{x}{\varepsilon}\right) + \varepsilon^2 \rho_1\left(t, \frac{t}{\varepsilon}, x, \frac{x}{\varepsilon}\right), \end{aligned} \tag{2}$$

with $\rho_0(y)$ and $A_0(y)$, real bounded periodic functions of period $(0,1)^N$ such that the density ρ_0 is strictly positive and the tensor A_0 is symmetric uniformly coercive. The macroscopic modulations $\rho_1(t,\tau,x,y)$ and $A_1(t,\tau,x,y)$ are smooth bounded functions which are periodic of period $(0,1)^N$ with respect to y (they also satisfy assumption (7) below). The second order time derivative in (1) has

been written in conservative form because the density ρ_ε may depend on time. Of course, if ρ_ε is independent of time, the inertial term is just equal to $\varepsilon^2\rho_\varepsilon(\partial^2 u_\varepsilon)/(\partial t^2)$ as usual. There is also an ε^2 scaling factor in front of the time derivative which corresponds to very long time. Indeed, upon introduction of a new time variable $\tau = \varepsilon^{-1}t$, the usual wave equation (without scaling) is recovered. Thus a time t of order 1 is equivalent to a long time τ of order ε^{-1}.

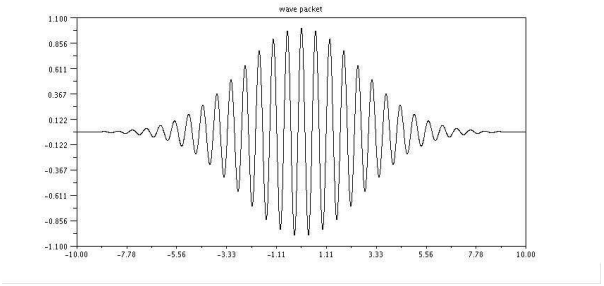

Figure 2: A wave packet

We consider initial data which are Bloch wave packets (see Figure 2) with a high-frequency linear phase

$$u_\varepsilon^0(x) = \psi_n\left(\frac{x}{\varepsilon},\theta_0\right) e^{2i\pi\frac{\theta_0\cdot x}{\varepsilon}} v_0(x)\,,$$
$$u_\varepsilon^1(x) = \frac{1}{\varepsilon^2}\psi_n\left(\frac{x}{\varepsilon},\theta_0\right) e^{2i\pi\frac{\theta_0\cdot x}{\varepsilon}} v_1(x)\,, \tag{3}$$

where v_0 and v_1 are sufficiently smooth functions and ψ_n is a so-called Bloch eigenfunction, solution of the following spectral cell equation in the unit torus $\mathbb{T}^N$

$$-(\mathrm{div}_y + 2i\pi\theta)\Big(A_0(y)(\nabla_y + 2i\pi\theta)\psi_n\Big) = \lambda_n(\theta)\rho_0(y)\,\psi_n\,, \tag{4}$$

corresponding to the n-th eigenvalue or energy level $\lambda_n(\theta)$. As usual the interpretation of the Bloch parameter θ is that it is a reduced wave number and the eigenvalue is the square of a time frequency $\omega_n(\theta_0)$ defined by

$$\omega_n(\theta_0) = \sqrt{\lambda_n(\theta_0)}.$$

The derivative of the frequency with respect to the wave number gives the group velocity

$$\mathcal{V} = \frac{1}{2\pi}\nabla\omega_n(\theta_0) = \frac{1}{4\pi}\frac{1}{\sqrt{\lambda_n(\theta_0)}}\nabla\lambda_n(\theta_0)\,, \tag{5}$$

and the divergence of the group velocity yields a dispersion tensor

$$A^* = \frac{1}{2\pi}\mathrm{div}_\theta\mathcal{V} = \frac{1}{4\pi^2}\nabla_\theta\nabla_\theta\omega_n(\theta_0)\,. \tag{6}$$

Our main assumptions is that $\lambda_n(\theta_0)$ is a simple eigenvalue and that the modulated coefficients ρ_1 and A_1 are "invariant along group lines", i.e.,

$$\frac{\partial\rho_1}{\partial\tau} \pm \mathcal{V}\cdot\nabla_x\rho_1 = 0\,, \quad \frac{\partial A_1}{\partial\tau} \pm \mathcal{V}\cdot\nabla_x A_1 = 0. \tag{7}$$

In truth, we can make a weaker but more technical assumption than (7). We prove that, as ε goes to 0, the solution of (1) is asymptotically the sum of two wave packets

$$u_\varepsilon(t,x) \approx e^{2i\pi\frac{\theta_0\cdot x}{\varepsilon}}\psi_n\left(\frac{x}{\varepsilon},\theta_0\right)\left(e^{i\frac{\omega_n(\theta_0)t}{\varepsilon^2}}v^+\left(t, x+\frac{\mathcal{V}}{\varepsilon}t\right)\right.$$
$$\left. + e^{-i\frac{\omega_n(\theta_0)t}{\varepsilon^2}}v^-\left(t, x-\frac{\mathcal{V}}{\varepsilon}t\right)\right), \tag{8}$$

in a sense of weak two-scale convergence. The envelope functions v^+ and v^-, in the right-hand side of (8), are solutions of two Schrödinger equations

$$\begin{cases} 2i\dfrac{\partial v^+}{\partial t} - \mathrm{div}\Big(A^*\nabla v^+\Big) + \gamma^* v^+ = 0 \ \text{ in } \mathbb{R}^N\times(0,T), \\ v^+(t=0,x) = \dfrac{1}{2}\Big(v_0(x) + \dfrac{1}{i\omega_n(\theta_0)}v_1(x)\Big) \ \text{ in } \mathbb{R}^N, \end{cases}$$

and

$$\begin{cases} -2i\dfrac{\partial v^-}{\partial t} - \mathrm{div}\Big(A^*\nabla v^-\Big) + \gamma^* v^- = 0 \ \text{ in } \mathbb{R}^N\times(0,T), \\ v^-(t=0,x) = \dfrac{1}{2}\Big(v_0(x) - \dfrac{1}{i\omega_n(\theta_0)}v_1(x)\Big) \ \text{ in } \mathbb{R}^N, \end{cases}$$

with

$$\gamma^*(t,x) = \frac{1}{2\omega_n(\theta_0)}\int_{\mathbb{T}^N}\Big(\tilde{A}_1\nabla\psi_n\cdot\nabla\overline{\psi}_n - \lambda_n(\theta_0)\tilde{\rho}_1|\psi_n|^2\Big)$$

Each of these two waves carries half of the initial data v^0 and opposite contributions in terms of the initial velocity v^1. The fact that the homogenized equations are of Schrödinger type is classical in the physics literature and is known in mathematics as dispersive geometric optics [10]. It is reminiscent of the so-called parabolic or paraxial approximation for waves propagating in a privileged direction.

Formula (8) yields a family of approximate travelling wave solutions of (1) with a coherent structure, even for long times. Remark that, when the group velocity $\mathcal{V}$ is zero (which happens, at least, at the bottom and top of each Bloch band), (8) is rather a stationary solution which is trapped by the periodic medium. Experimental exploitation of this phenomenon to slow light is a hot topic [12], [6], [11],

[5]. It is dreamed that the slow light technologies are a first step toward an all optical computer. As is well known there exists no propagating solution of the type of (8) with a frequency ω when ω^2 is in a gap of the Bloch spectrum, i.e. when $\omega^2 \neq \lambda_n(\theta)$ for all $n \geq 0$ and $\theta \in \mathbb{T}^N$. This property is a key feature of photonic crystals.

The fact that the homogenized equations for the envelope v^+ and v^- are Schrödinger equations is a confirmation of the dispersive properties (i.e. the nonlinear character of the effective dispersion relation) of periodic composite materials.

We give a weak convergence proof of (8) in [2] which is based on the notion of two-scale convergence with drift and on a simple, uniform in time, L^2 in space, estimate for the solution of (1). A strong convergence proof (for smooth coefficients), including the construction of infinite order asymptotic expansion of the solution, is given in a companion paper [3], while the case of Maxwell equations is treated in [4].

Eventually, if instead of periodic coefficients as in (2) we consider modulated coefficients $A_0\left(x, \frac{x}{\varepsilon}\right)$ and $\rho_0\left(x, \frac{x}{\varepsilon}\right)$, completely different results can be obtained. In [1], under very specific stationarity and geometric assumptions on the Bloch eigenvalue $\lambda_n(x, \theta)$ (which now depends on the space variable x), we prove that Bloch wave packets do not propagate and even more are exponentially localized.

References

[1] G. Allaire, L. Friz, *Localization of high frequency waves propagating in a locally periodic medium,* Proc. Roy. Soc. Edinburgh. 140A, pp.897-926 (2010).

[2] G. Allaire, M. Palombaro, J. Rauch, *Diffractive behavior of the wave equation in periodic media: weak convergence analysis,* Annali di Matematica Pura ed Applicata, **188**, pp.561-590 (2009).

[3] G. Allaire, M. Palombaro, J. Rauch, *Diffractive Geometric Optics for Bloch Wave Packets,* Archive Rat. Mech. Anal. **202**, pp.373-426 (2011).

[4] G. Allaire, M. Palombaro, J. Rauch, *Diffraction of Bloch Wave Packets for Maxwell's Equations,* submitted, arXiv:1202.6549 (2012).

[5] H. Altug, J. Vuckovic, *Experimental demonstration of the slow group velocity of light in two-dimensional coupled photonic crystal microcavity arrays,* Appl. Phys. Lett. **86**, 111102-1 to 111102-3 (2004).

[6] M. Bajcsy, A. Zibrov, M. Lukin, *Stationary pulses of light in an atomic medium,* Nature **426** (2003).

[7] A. Bensoussan, J.-L. Lions, G. Papanicolaou, *Asymptotic analysis for periodic structures,* North-Holland, Amsterdam (1978).

[8] S. Brahim-Otsmane, G. Francfort, F. Murat, *Correctors for the homogenization of the wave and heat equations,* J. Math. Pures Appl. (9) 71:197–231 (1992).

[9] L. Brillouin, *Propagation of Waves in Periodic Structures*, Dover, New York (1953).

[10] P. Donnat, J. Rauch, *Dispersive nonlinear geometric optics,* J. Math. Phys. 38 (1997), no. 3, 1484–1523.

[11] H. Gersen, T. Karle, R. Engelen, W. Bogaerts, J. Korterik, N. van Hulst, T. Krauss, and L. Kuipers, *Real-space observation of ultraslow light in photonic crystal waveguides,* Phys. Rev. Lett. 94(2005) 073903-1-073903-4.

[12] L.V. Hau, S. E. Harris, Z. Dutton, C. Behroozi, *Light speed reduction to 17 meters per second in an ultracold atomic gas,* Nature **397**, 594–598 (1999).

[13] P. St. J. Russell, *Photonic crystal fibers,* J. Lightwave. Technol., 24 (12), 4729–4749 (2006).

Minisymposia

3.1 Geophysics

Minisymposium organized by Sébastien Tordeux

Splitting schemes for geothermal processes simulation

K.V. Voronin[1,2,*], **Yu.M. Laevsky**[1,2]
[1] Institute of Computational Mathematics and Mathematical Geophysics SB RAS
[2] Novosibirsk State University
*Email: kvoronin@labchem.sscc.ru

Abstract

A few numerical algorithms for solving the nonstationary heat transfer equation in terms "temperature - heat flux" are discussed. Thereby, a nonstationary two- or three-dimensional parabolic problem in the mixed formulation is considered. Spatial discretization is implemented by the mixed finite element method with Raviart-Thomas finite elements of lowest order. For the vector equation for the mesh heat flow a few splitting schemes are analyzed. For the proposed schemes as long as for the reference scheme of Crank-Nicolson results of numerical experiments are presented. Special attention is given to the comparison of accuracy of different splitting schemes. Moreover, several application problems concerning thermochronology of certain geological regions are presented.
This work was supported by RFBR (No. 12-01-31046) and IP No. 76 SB RAS.

1 Problem statement

Consider the following system of first order differential equations written in terms "temperature - heat flux" which describes heat transfer process for $x \in \Omega \subset R^n, n = 2, 3$:

$$\begin{cases} c_p\rho\frac{\partial T}{\partial t} + div\,\mathbf{w} = f, x \in \Omega, \\ \frac{1}{\lambda}\mathbf{w} = -\nabla T, x \in \Omega. \end{cases}$$

Here T and $\mathbf{w}$ denote the unknown functions of temperature and heat flux, while c_p, ρ and λ are the coefficients of heat capacity, density and heat conductivity respectively; function f corresponds to the distributed heat source in the considered domain Ω. For this system we have an initial condition and Dirichlet or Neumann boundary conditions for T. Carrying out some simple manipulations one can obtain a mixed weak formulation of the problem

$$\begin{cases} \int_\Omega c_p\rho\frac{\partial T}{\partial t}\chi + \int_\Omega div\,\mathbf{w}\chi = \int_\Omega f\chi, \forall\chi \in L_2(\Omega) \\ \int_\Omega \frac{1}{\lambda}\mathbf{w}\cdot\mathbf{u} = \int_\Omega T\nabla\mathbf{u} - \int_{\partial\Omega} T\mathbf{u}\cdot\mathbf{n}, \forall\mathbf{u} \in \mathbf{H}_{div}(\Omega) \end{cases},$$

where unknown functions T and $\mathbf{w}$ are sought for as elements of functional spaces $L_2(\Omega)$ and $\mathbf{H}_{div}(\Omega)$ respectively.

2 Time and space discretization

Consider a rectangular grid covering the domain Ω. Space discretization is implemented by the mixed finite element method based on Raviart-Thomas finite elements of lowest order (for $\mathbf{H}_{div}$) and piecewise constant scalar functions (for L_2). Calculating the corresponding integrals in the mixed weak formulation one can obtain the following semidiscrete system:

$$\begin{cases} M\frac{dT_h}{dt} + B^T\mathbf{w}_h = f_h \\ A\mathbf{w}_h = BT_h + g_h \end{cases},$$

where M is a diagonal mass matrix for temperature, $\mathbf{A}$ - tridiagonal mass matrix for heat flux, $\mathbf{B}$ and $\mathbf{B}^T$ denote the discrete (mesh) counterparts of operators of gradient and divergence respectively; g_h arises from inhomogenious boundary conditions and will be omitted further, f_h corresponds to the differential righthand side f. Now it is straightforward to write the implicit α-weighted scheme in the following form:

$$\begin{cases} (\mathbf{A} + \alpha\tau\mathbf{H})\frac{\mathbf{w}^{n+1}-\mathbf{w}^n}{\tau} + \mathbf{H}\mathbf{w}^n = \frac{F^{n+1}+F^n}{2} \\ M\frac{T^{n+1}-T^n}{\tau} + B^T(\alpha\mathbf{w}^{n+1} + (1-\alpha)\mathbf{w}^n) = \frac{F^{n+1}+F^r}{2} \end{cases}$$

where $\mathbf{H} = \mathbf{B}M^{-1}\mathbf{B}^T$ approximates the second space derivatives tensor. To obtain the first equation for the heat flux only one should "differentiate" on the mesh level the Fourier law and make use of the mesh energy conservation law.

3 Splitting schemes

Taking $\alpha = 0$ one obtains the conditionally stable explicit scheme first order accurate in time and second order accurate in space, $\alpha = 0.5$ - the stable second-order accurate in time and space Crank-Nicolson scheme. Due to the rather complicated structure of matrix $\mathbf{H}$ Crank-Nicolson scheme can hardly be used for computations, especially in case of time-dependent coefficients. The first two splitting schemes proposed [1] are based on approximate factorizations of the operator $\mathbf{G} = \mathbf{A} + \alpha\tau\mathbf{H}$. Scheme 1 is based on the alternating-triangular factorization, scheme 2 - on the factorization of SSOR-type. Other

splitting schemes are closely connected to the splitting schemes for the mesh divergence of the heat flux with a specific choice of operators of second space derivatives. Scheme 3 (for $n = 2$) corresponds to the classical alternating-direction scheme, scheme 4 (for $n = 3$) - to the scheme of Douglas and Gunn of second order, scheme 5 - to the locally one-dimensional scheme based on Crank-Nicolson. Finally, we also consider scheme 6 - a splitting scheme proposed in [2] which is based on the so called Uzawa algorithm for the mixed formulation. Schemes 1-4 and 6 are second order accurate, scheme 5 is only of first order in time, in spite of the fact that the corresponding scheme for mesh divergence is of second order. The questions of stability for schemes 3-6 is still under study although the fact that these schemes are unconditionally stable for the mesh divergence is quite obvious. To obtain solution using proposed splitting schemes one requires only to invert block matrices with tridiagonal blocks which can be performed in an efficient way, especially for cluster machines.

4 Numerical experiments and applications

For the sake of brevity only few words are presented here concerning results of numerical experiments, namely only one test case is presented for comparison of the schemes mentioned above for $n = 2$. All the schemes were tested against the following analytical solution

$$T(x, y, t) = e^{-t} sin(2\pi x) cos(2\pi y) + y + 1$$

in the unit square with appropriate initial and boundary conditions. In figures (a) and (b) relative L_2-norms of the error for temperature and heat flux for the time moment $t = 1$ depending on the space step are shown for different 2D-schemes.

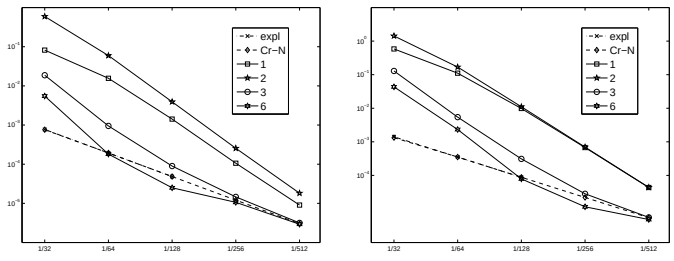

(a) (b)

In both figures "expl" stands for explicit, "Cr-N" - for Crank-Nicolson, line 1 corresponds to scheme 1, line 2 - to scheme 2, etc. The logarithmic scale is used for the axis of error values. For all implicit schemes the Courant number was taken 100, for the explicit scheme the maximum allowable time-step (due to the stability condition) was chosen. As one can notice, schemes 3 and 6 provide the best results similar to that of the Crank-Nicolson scheme, while schemes 1,2 and 5 are much less accurate. This holds true for both temperature and heat flux. The detailed comparison of the schemes for different test solutions with variable coefficients and nonuniform grids, as well as application problems (see, e.g.[3]) are omitted here due to the lack of space.

References

[1] Voronin K.V., Laevsky Yu.M. *On splitting schemes in the mixed finite element method*, Numerical Analysis and Applications, 5(2012), pp. 150-155.

[2] T. Arbogast, C.-S. Huang, and S.-M. Yang. *Improved accuracy for alternating-direction methods for parabolic equations based on regular and mixed finite elements*. Math. Models Methods Appl. Sci., 17 (8) (2007), pp.1279–1305.

[3] V.A. Vernikovsky, A.E. Vernikovskaya, O.P. Polyansky, Yu.M. Laevsky,N.Yu. Matushkin, K.V. Voronin, *A tectonothermal model for the formation of an orogen on the postcollisional stage (by the example of the Yenisei Ridge, Eastern Siberia)*, Russian geology and geophysics, **52** (2011), pp. 24-39.

Numerical simulation of filtration gas combustion

T. Kandryukova[1,*], **Yu. Laevsky**[1]
[1]Institute of Computational Mathematics and Mathematical Geophysics SB RAS
*Email: kandryukova@labchem.sscc.ru

Abstract

The problem under consieration is the filtration gas combustion. In particular we are interested in the numerical modelling of the propagation of region of gaseous exothermic reaction in chemically inert porous medium, as gaseous reactants are being supplied into the region of chemical transformation [1]. The aim of our work is the construction of efficient algorithms for calculating the motion of combustion wave. Several approaches will be used, namely the introduction of adaptive grids, the method of splitting into physical processes [2], parallelization on shared memory [3] and the use of external highly optimized libraries of Intel®MKL [4]. We obtain solutions of the problem that coincide with the experimental data. We also implement the parallelization of the constructed algorithms, which reduces the computational time by ten times compared to the original code.
This work was supported by RFBR (12-01-31046, 13-01-00019).

Introduction

Modeling of the processes of filtration gas combustion (FGC) is the problem of current interest that has wide practical application. Knowledge of the properties of FGC waves is essential in solving many problems of energy, chemical and construction technology, ecology, and fire safety. A physical model for FGC may be described as follows. Let there be a tube filled with a porous material, measuring about 10 cm. From one edge of it a combustible gas mixture is supplied at a rate of $\vec{v}$. Then the mixture is ignited, resulting in a combustion front, which can either be stationary or move in any direction, depending on the model parameters. If the combustion front moves, it may do so in a number of different fashions.

The simpliest one-dimensional FGC model in the enthalpy formulation includes three equations:

$$\frac{\partial T}{\partial t} = a_s \frac{\partial^2 T}{\partial x^2} + \alpha_s (H - T - \frac{Q}{c_g}\eta), \qquad (1)$$

$$\frac{\partial H}{\partial t} = a_g \frac{\partial^2 H}{\partial x^2} - v\frac{\partial H}{\partial x} + \alpha_g (T - H + \frac{Q}{c_g}\eta), \qquad (2)$$

$$\frac{\partial \eta}{\partial t} = a_g \frac{\partial^2 \eta}{\partial x^2} - v\frac{\partial \eta}{\partial x} - W(\eta, H). \qquad (3)$$

Here $a_i = \lambda_i / c_i \rho_i$ is the coefficient of thermal diffusivity of the i-th phase, c_i, ρ_i, λ_i are respectively, specific heat at constant pressure, density and thermal conductivity of i-th phase ($i = s$ for porous solid, $i = g$ for gas), $\alpha_s = \frac{\alpha}{(1-m)c_s\rho_s}, \alpha_g = \frac{\alpha}{m c_g \rho_g}$, m - porosity, α - interphase heat transfer rate, v - flow rate of the combustible mixture, $T \equiv T_s$, $Hc_g = T_g c_g + Q\eta$ is full gas enthalpy, where T_i is the temperature of the i-th phase, Q is energy release of the reaction, $W(\eta, H) = k_0 \eta e^{-E/R(H - \frac{Q}{c_g})}$ - the chemical reaction rate according to Arrhenius law, η - relative concentration of reactive component of the combustible mixture, k_0 - pre-exponential factor, E - activation energy, R - universal gas constant.

It is easy to see that the system is parabolic. However, due to the nonlinear components of the third equation solutions act as shock waves, which is typical for hyperbolic systems. It is also worth noting that the speed of the wave is a priori unknown. The Cauchy problem is stated by adding the Dirichlet boundary conditions on the left edge and the Neumann ones on the right edge.

1 Mathematical methods

1.1 Adaptive mesh

Jumps of the unknown functions in the area of chemical reactions require a significant refinement of the spatial step. This, in the case of explicit schemes, involves a further refinement of the time step, due to the Courant-type restriction. However, away from the flame front, the solution functions are smooth and close to a constant. Thus, one way to speed up the computation seems to be the introduction of an adaptive grid. It will depend on the solution of the previous time step and will be concentrated in the area of the chemical transformation.

We implemented two algorithms using adaptive

grids. In the first one in the vicinity of the chemical reaction zone a more dense grid is used. It then moves according to the movement of the combustion front. This approach saves time by increasing the spatial step for smooth areas. However, it does not affect the time step, which has to be chosen in accordance with the stability condition on the fine grid. An opportunity to increase the time step is implemented in the second algorithm. The basic idea is this: by doing one step of the uniformly coarse grid scheme (with the corresponding big time step), we obtain the initial data and boundary conditions for the fine mesh. This provides us with a subproblem with small spatial and time steps. Having executed all the steps of the subproblem, we replace values of coarse-grid solutions with the corresponding values of solutions of the embedded problem. This approach allows us to take big steps in space as well as in time outside the chemical reaction zone.

1.2 Splitting method

A significant proportion of the total computation time is devoted to the calculation of the exponent in the reactant-concentration equation. Method of splitting into physical parameters is based on the idea to isolate the summand with the exponential term. Thus, we count transfer and diffusion at the first half-step and chemical reaction at the second half-step. This approach opens tremendous opportunities for futher investigations and ways to reduce the execution time.

2 Programming methods

2.1 Parallelization (Modeling on machines with shared memory)

The simplest and most obvious way to implement the program on a multiprocessor node is implementation of OpenMP procedures for the inner loop of the program. However, when modeling small problems, the time required by the machine to transfer data is comparable to the time of the actual receipt of data. This parallelism is not always effective and in some cases even leads to a slowdown of the program execution. To reduce the time for the exchange of data flows, it may be useful to distribute the data between them, ie assign each thread its part of the spatial grid. Each thread creates its arrays to find a solution, fills them in accordance with the difference scheme, and outputs the results on its assigned grid nodes. On a regular grid we thus obtain practically independent tasks exchanging only boundary conditions.

2.2 Intel®MKL

The use of the external highly optimized libraries of Intel®MKL helped us to reduce the execution time. In our program we apply such functionalities as *vdExp* to calculate the exponent efficiently, *dgbtrf* and *dgbtrs* for solving a system of linear equations by a direct method at every time step of the implicit difference scheme.

Conclusion

We constructed various algorithms for the numerical solution of the FGC problem which provide solutions that are consistent with experimental data. Calculations were carried out for a small problem (tube length is 0.0125 m) and for a problem with characteristic dimensions (length of tube is 0.1 m). Modifications of the original algorithm have reduced the execution time by a factor of 10 in the case of small problems (for the physical time t = 0.1 sec) and almost 120 in the case of large ones (for the physical time t = 30 sec.) It's easy to see that the use of the adaptive grids for simulation of FGC provides significant gains. However, parallel implementation of such algorithms is not always effective and demands special approach. At the same time the number of processors on the computational node will grow and the influence of parallelism will increase, so construction of new algorithms that allow almost perfect scaling in the number of threads becomes rather actual problem. The algorithms based on the splitting method are expected to show good scalability since each thread can calculate the chemical reaction rate independently from the other ones.

References

[1] V. S. Babkin, Yu. M. Laevskii, *Seepage gas combustion*, Combustion, Explosion, and Shock Waves, Volume 23, Issue 5, September-October, 1987, pp 531-547.

[2] V. N. Snytnikov, E. M. Yurchenko, *Splitting scheme for the problems of gas filtration with chemical reactions*, Computational technologies, Volume 6, Issue 5, 2001, pp 95-105 (in Russian).

[3] http://openmp.org

[4] http://software.intel.com/ru-ru/articles/intel-mkl

Exploding Reflectors Revisited: 3D Multiscale Media

E. Landa[1], **G. Reshetova**[2,*], **V. Tcheverda**[3]
[1] OPERA, UFR Science et Techniques, Avenue l'Universite - BP 115, 64013 Pau Cedex - France
[2] Institute of Computational Mathematics and Mathematical Geophysics SB RAS, 6, prosp. Lavrentiev, 630090, Novosibirsk, Russia
[3] Institute of Petroleum Geology and Geophysics, SB RAS
Prosp. Koptyug 3, 630090 Novosibirsk, Russia

Abstract

Common Middle Point seismic sections provides important information about the internal structure of the 3D heterogeneous geological media and are a key element for seismic interpretation. It is therefore extremely important to be able to analyze in detail how the typical geological structures are manifested in these 3D seismic cubes. The most complete knowledge here is provided by full mathematical simulation, which takes into account all multiscale structure of the medium under study. Unfortunately, these simulations for realistic geological structures and 3D seismic surveys still can not be implemented on a modern, even the most powerful computer systems. In order to overcome this trouble we propose a different approach - modeling these 3D seismic cubes directly rather than shot-by-shot simulation with subsequent CMP stacking. In order to do that the well know "exploding reflectors principle" is modified for 3D heterogeneous multiscale media. Its parallel implementation allows modeling of 3D Common Middle Point stacks with reasonable computational costs.

1 Introduction

Common Middle Point (CMP) stack for the correct depth macrovelocity model will not only transform multi-shot multi-offset seismic data to zero-offset data, but also significantly reduce the multiples. In order to imitate this procedure we apply the exploding reflectors concepts (Claerbout, 1985) and keep in the mind the following key items:

1. The secondary sources should posses reasonable intensity;

2. The macrovelocity model should be properly smoothed, so barely to change the travel time, but essentially reduce reflections.

The smoothing is performed in vertical directions only

2 From the full model to the smooth propagator

To ensure the desired properties of the propagator the full velocity model is smoothed by its convolution with error function:

$$F < f > (z) = \beta \int\limits_{-z_0}^{z_0} f(z-\xi) e^{-\alpha \xi^2} d\xi \qquad (1)$$

This transform should reduce essentially reflections, but not perturb travel times to some extent. In order to guarantee the last property let parameters of transformation (1) are searched in order to save constant with given accuracy.

Straightforward computations give:

$$\beta \int\limits_{z-z_0}^{z+z_0} e^{-\alpha(z-\zeta)^2} d\zeta = \beta\sqrt{\alpha\pi}\ erf(\sqrt{\alpha} z_0)$$

Error function $erf(x)$ converges to unit with $x \to \infty$, so, in order to keep the constant we should choose $\beta\sqrt{\alpha\pi} = 1$. In our computations we choose $\sqrt{\alpha} z_0 = 4$, so $erf(\sqrt{\alpha} z_0) = 1 - 1.5 * 10^{-8}$ and any constant is saved up to single computer precision.

3 Secondary sources

Secondary sources are introduced by decomposition of the full model onto smooth propagator (with indicex 0) and rough reflectors (with indices 1):

$$\varrho = \rho_0 + \rho_1; \quad \lambda = \lambda_0 + \lambda_1; \quad \mu = \mu_0 + \mu_1.$$

This decomposition introduces incident (indices 0) and *reflected/scattered/diffracted* (indices 1) waves. The latter has the following integral representation:

$$\vec{U}_1(\vec{x};\omega) = \int\limits_{R^3} G(\vec{x};\vec{\xi};\omega) \left(\hat{L}_0 + \hat{L}_1\right) \vec{U}_0(\xi;\omega) d\xi$$

with elastic Green matrix $G(\vec{x};\vec{\xi};\omega)$ and linear differential operator

$$(L_1(\lambda_0,\mu_0)\vec{w})_k \equiv$$

$$\equiv \frac{\partial \lambda_0}{\partial x_k}\mathrm{div}\vec{w} + \sum_{j=1}^{3}\frac{\partial \mu_0}{\partial x_j}\left(\frac{\partial w_j}{\partial x_k}+\frac{\partial w_k}{\partial x_j}\right)$$

.

For smooth background volumetric source generates mainly incident P-wave. This allows to prove that wavefield $\vec{U}_1(x;x_0;x_s;\omega)$ generated by the source at $\vec{x}_s$ and scattered at $\vec{x}_0$ can be treated as the solution to the following equation:

$$\left(L_0+L_1+\varrho_0\omega_1^2\right)\vec{U}_1 = \\ -\frac{-\omega_1^2 F(\frac{\omega_1}{2})}{4v_p(x_0)}\lambda_1(x_0)A_{p0}(x_0,x_s)\mathrm{grad}\delta(x-x_0) \qquad (2)$$

and therefore is created by a secondary volumetric source at $\vec{x}_0$.

4 Numerical experiments

Numerical experiments were done for 3D heterogeneous multiscale model of the buried channel overlying cavernous-fractured reservoir (see Fig.1). For lack of space we do not present here the interim results, confirming the equivalence of zero-offset and exploding reflectors given by (2). But we represent 3D seismic cube of zero-offset/CMP data in Figure 2.

Acknowledgements

The research described in this publication is partially supported by RFBR grants 11-05-00947 and 13-05-00076.

References

[1] J.F.Claebout, *Imaging the Earth's interior*,Blackwell, 1985, 398 p. Geophysics, **66** (2001), pp. 845–860.

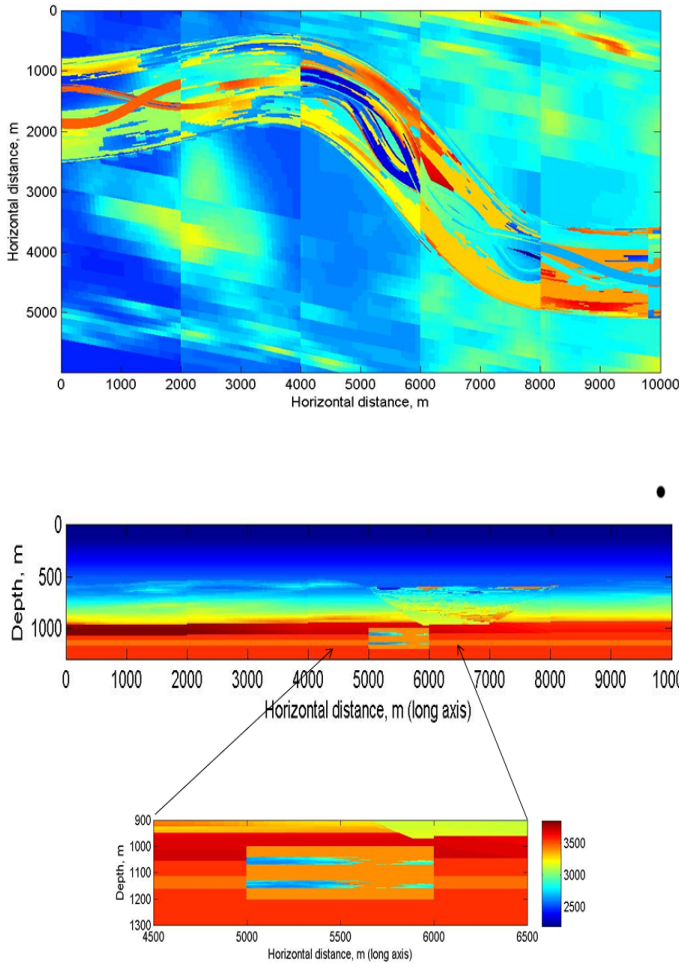

Figure 1: 3D seismic model used for simulation: the buried channal with fractured reservoir. a) Top view. b) Side view.

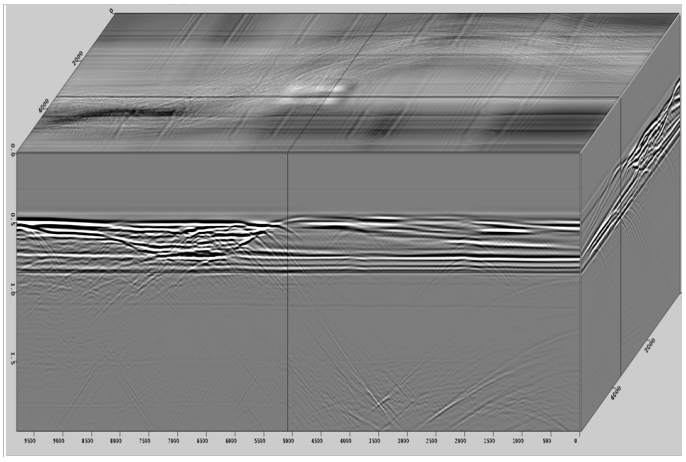

Figure 2: 3D zero-offset seismic cube. Simulation by exploding reflector.

Parallel algorithm for numerical simulation of wave propagation in presence of seismic attenuation

V. Lisitsa[1], G. Reshetova[2], V. Tcheverda[1], D. Vishnevsky[1,*]
[1] Institute of Petroleum Geology and Geophysics SB RAS, Novosibirsk, Russia.
[2] Institute of Computational Mathematics and Mathematical Geophysics SB RAS, Novosibirsk, Russia.
*Email: vishnevskydm@ipgg.sbras.ru

Abstract

This paper presents an algorithm oriented on the simulation of seismic wave propagation in models containing viscoelastic formations. These formations are typically relatively small (about 25 % of the model), however proper treatment of seismic attenuation doubles the computational intensity of the algorithm in comparison with ideally elastic models. Our suggestion is to use the attenuation oriented algorithm only in the vicinity of viscoelastic formations while efficient numerical approach to simulation of seismic waves propagation in ideally elastic media is applied elsewhere. In this paper we discuss both mathematical aspects of algorithm and peculiarities of its parallel implementation.

Introduction

Modern approaches to seismic processing such as full waveform inversion, reverse time migration are based on massive forward modeling. However, these techniques are used nowadays mostly in application to ideally elastic media. One of the main deterrent factors for their extension to viscoelasticity is the computational intensity of the forward modeling. Seismic attenuation is introduced in a model by convolution-like operator mapping strains into stresses. In order to localize this operator the generalized standard linear solid model (GSLS) is used [1], which is a rational approximation of the kernel in frequency domain. In time domain GSLS include additional memory variables and equations for them. As the result amount of RAM and floating point operation per grid cell needed for the simulation of wave propagation in viscoelastic models doubles with respect to those for ideally elastic media. At the same time these formations are typically small enough (less than 25% of the model) thus it is reasonable to use the GSLS only in the vicinity of the viscoelastic formations and couple it with the model of ideally elastic media which is used elsewhere.

1 The algorithm

Consider the GSLS model governing wave propagation in viscoelastic media:

$$\begin{gathered}\rho\frac{\partial u}{\partial t}=\nabla\cdot\sigma,\\ \frac{\partial\varepsilon}{\partial t}=\left(\nabla u+\nabla u^T\right),\\ \frac{\partial\sigma}{\partial t}=G_1\varepsilon+\sum_{l=1}^{L}r^l,\\ \tau_{\sigma,l}\frac{\partial r^l}{\partial t}=-G_2\varepsilon-r^l,\end{gathered}$$

where ρ is a mass density; G_1 and G_2 are fourth-order tensors, defining the model properties; u is a velocity vector; σ and ε are the stress and strain tensors; r^l tensor of memory variables. Note that the number of memory variables tensors is L, typically two or three. Proper initial and boundary conditions are assumed.

For the ideally elastic models the tensor G_2 equals to zero which means that solution of the last equation is trivial if zero initial conditions are used. Thus the memory variables tensors can be completely excluded from the equations. After that the system turns into that for ideally elastic wave equation. This means that there is no need to allocate random access memory (RAM) for the memory variables in the ideally elastic parts of the model.

Assume now a subdomain $\Omega\subseteq\mathbf{R}^3$ where full viscoelastic wave equation is stated, while ideally elastic wave equation is valid for the rest of the space. It is easy to prove that the conditions at the interface $\Gamma=\partial\Omega$ are

$$[\sigma\cdot\vec{n}]|_\Gamma=0,\quad [u]|_\Gamma=0,$$

where $\vec{n}$ is vector of outward normal and [] denote jumps of the function over the interface. These conditions are the same as those for elastic wave equation at an interface. Moreover if standard staggered grid scheme (SSGS) [2] is used these conditions are satisfied automatically. Thus the coupling of the models does not require any special treatment of conditions at the interface and can be implemented by allocation of RAM for memory variables and soling equations for them in viscoelastic part of the model.

2 Parallel implementation

Parallel implementation of the algorithm is done via domain decomposition technique. However, the amount of the computational job for elastic and viscoelastic parts of the model is different, which leads to the necessity to apply independent domain decomposition to design a well-balanced algorithm. Meanwhile the use of SSGS assumes two types of synchronization points. The first one is at instants just after the velocity components have been updated. This stage requires the same amount of flops per grid cell for both elastic and viscoelastic parts of the algorithm. The second type is after the stresses were computed. This part is strongly different for the named parts of the algorithm. This means that regardless to the ratio of the elementary subdomains associated with single core (node) for elastic and viscoelastic parts some of the cores will have latency period. This can be seen in fig. 1.

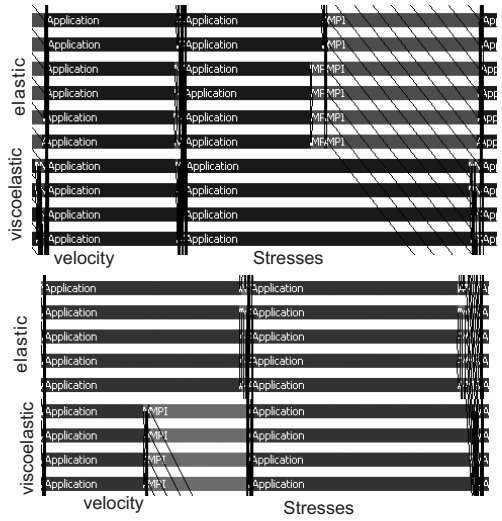

Figure 1: TraceAnalyzer images for equivolumetric (top) and optimal (bottom) domain decomposition. Dark bars correspond to computations, light bars represent waiting time.

As the result an optimal domain decomposition was suggested to minimize the overall computational time (core-hours) of the algorithm. The computational time can be estimated by the formula:

$$T(\alpha,\beta) = [\delta \max(1,\beta) + \max(1,\beta\gamma)] \left(\alpha + \frac{1-\alpha}{\beta}\right),$$

where $\gamma = 0.33$ and $\delta = 0.32$ are the ratios of computational time needed to update velocity and stresses respectively for elastic part per grid cell with respect to time for computing stresses for viscoelastic part. These values were measured experimentally. Parameters α is the relative volume of the viscoelastic part of the model and β is the ratio of the elementary volumes of elastic and viscoelastic parts. It is clear that the optimal domain decomposition is constructed if $\min_\beta T$ is achieved. Figure 2 represents the theoretical estimations of $T(\alpha,\beta)$ and numerical experiments. One may note that the optimal ratio of the elementary volumes for elastic and viscoelastic parts is equal to 3 for relatively small amount of viscoelasticity. In this case the speed-up of the hybrid algorithm is about 2 with respect to pure viscoelastic simulation.

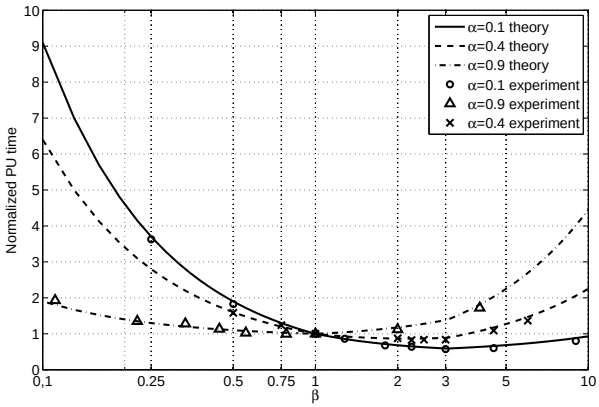

Figure 2: Normalized core-hours with respect to β.

3 Acknowledgements

This research was supported by RFBR grants no. 12-05-31008, 13-05-00076, 11-05-00947, grant MK-77.2013.5 and fellowship SP-150.2012.5 of President of Russian Federation, and Integration projects SB RAS 127 and 130.

References

[1] J.O. Blanch, A. Robertson, W.W. Symes, *Modeling of a constant Q: Methodology and algorithm for an efficient and optimally inexpensive viscoelastic technique*, Geophysics, **60** (1995), pp. 176–184.

[2] J. Virieux, *P-SV wave propagation in heterogeneous media: Velocity-stress finite-difference method*, Geophysics, **51** (1986), pp. 889–901.

High Order Time Discretization of the Wave Equation. Application to the Reverse Time Migration.

H. Barucq[1], H. Calandra[2], J. Diaz[1] and F. Ventimiglia[1,2]
[1] EPI Magique 3D, INRIA Bordeaux Sud-Ouest, IPRA-LMA.
[2] TOTAL Exploration & Production.
[1]Email: florent.ventimiglia@inria.fr

Abstract

Reverse Time Migration (RTM) is one of the most widely used techniques for Seismic Imaging, but it induces very high computational cost since it is based on many successive solutions to the full wave equation. High-Order Discontinuous Galerkin Methods (DGM), coupled with High Performance Computing techniques, can be used to solve accurately this equation in complex geophysical media without increasing the computational burden. However, to fully exploit the high-order space discretization, it is necessary to use a high-order time discretization. In this work, we propose a new high order time scheme, the so-called Nabla-p scheme. This scheme does not increase the storage costs since it is a single step method and does not require the storage of auxiliary unknowns. Numerical results show that it requires less storage than the ADER scheme for a given accuracy and that it can be efficiently implemented in an RTM algorithm.

Introduction

Geophysical exploration is undertaken on more and more complex media and we need advanced numerical methods to accurately image the subsurface. Indeed, Seismic Imaging algorithms, such as for instance Reverse Time Migration (RTM), generate high computational burden since they are iterative algorithms that require many successive solutions to the wave equation. To reduce these computational cost, we use High-Order Discontinuous Galerkin Methods, which are very accurate even with coarse meshes and can be combined with explicit time schemes. However, to take fully advantage of high-order space discretization, it is necessary to combine DGM with high order time discretization. This can be achieved by using DG-ADER methods [4], which are an extension of the Modified Equation Technique [2], [3]. They are single step methods, i.e., they only require to store the solution at the previous time step. Nevertheless, even when using advanced methods like DG-ADER schemes, we still have to store a huge number of unknowns. We then propose a new single step method, called Nabla-p schemes, which can be seen as an alternative to DG-ADER schemes. The original idea consists in inverting the discretization order, which introduce high order operators in space which require an appropriate space discretization. Fortunately, DG method are well adapted to deal with high order operators. This has already been successfully applied to the second order formulation of the acoustic wave equation and we focus here on the first order formulation of acoustic and elastodynamic wave equations. Numerical results show that the additional cost induced by the computation of the high order operator is counterbalanced by the accuracy of the method. Indeed, for a given accuracy, it allows for much coarser meshes than ADER, which considerably reduces the storage and the computational time.

1 Discretization of the wave equation

To simplify the presentation, we focus on the acoustic wave equation but the method can be applied to the elastodynamic wave equation too. We consider the following system in a bounded domain $\Omega \subset \mathbf{R}^n$, $n = 1, 2, 3$:

$$\left\{ \begin{array}{lll} \rho(\mathbf{x})\dfrac{\partial \mathbf{v}(\mathbf{x},t)}{\partial t} + & \boldsymbol{\nabla} p(\mathbf{x},t) & = 0 \quad \text{in} \quad \Omega \times [0,T] \\ \dfrac{1}{\mu(\mathbf{x})}\dfrac{\partial p(\mathbf{x},t)}{\partial t} + & \nabla \cdot (\mathbf{v}(\mathbf{x},t)) & = 0 \quad \text{in} \quad \Omega \times [0,T] \end{array} \right. \tag{1}$$

where ρ and μ are respectively the density and the compressibility modulus of Ω, p is the scalar pressure and $\mathbf{v}$ the velocity vector. By applying a DGM, we obtain the semi-discretized schemes:

$$\left\{ \begin{array}{l} \dfrac{dV}{dt} + \mathcal{M}_v^{-1} K_p P = \dfrac{dV}{dt} - \mathcal{A}_p P = 0 \\ \dfrac{dP}{dt} + \mathcal{M}_p^{-1} K_v V = \dfrac{dP}{dt} - \mathcal{A}_v V = 0 \end{array} \right. \tag{2}$$

where the mass matrices $\mathcal{M}_v$, $\mathcal{M}_p$ are easily invertible since they are diagonal and the stiffness matrices K_p, K_v are sparse. One of the most efficient way to discretize this system is to use ADER method [4]. It is equivalent to the MET, when using the same time step and the same order for the time discretization in the whole domain. The fourth order ADER scheme,

reads as:

$$\begin{cases} \dfrac{V^{n+1}-V^n}{\Delta t} &= \mathcal{A}_p P^{n+1/2} + \dfrac{\Delta t^2}{24}\mathcal{A}_p\mathcal{A}_v\mathcal{A}_p P^{n+1/2} \\ \dfrac{P^{n+3/2}-P^{n+1/2}}{\Delta t} &= \mathcal{A}_v V^{n+1} + \dfrac{\Delta t^2}{24}\mathcal{A}_v\mathcal{A}_p\mathcal{A}_v V^{n+1} \end{cases}$$

This scheme requires three times more multiplications by the stiffness matrices than the second order Leap Frog Scheme (LF), but the stability condition is multiplied by almost three. However, for higher order, the increase of the stability condition does not counterbalance rising multiplications. We propose here an alternative to ADER by applying the MET to the continuous wave equation (1). We then obtain the semi-discretized scheme:

$$\begin{cases} \dfrac{v(\mathbf{x})^{n+1}-v(\mathbf{x})^n}{\Delta t} &= -\boldsymbol{\nabla} p(\mathbf{x})^{n+\frac{1}{2}} - \dfrac{\Delta t^2}{24}\boldsymbol{\nabla}\boldsymbol{\nabla}\cdot\boldsymbol{\nabla} p(\mathbf{x})^{n+\frac{1}{2}} \\ \dfrac{p(\mathbf{x})^{n+1}-p(\mathbf{x})^{n+\frac{1}{2}}}{\Delta t} &= -\boldsymbol{\nabla}\cdot v(\mathbf{x})^{n+1} - \dfrac{\Delta t^2}{24}\boldsymbol{\nabla}\cdot\boldsymbol{\nabla}\boldsymbol{\nabla}\cdot v(\mathbf{x})^{n+1} \end{cases}$$

This method has already been applied to the second order formulation of the wave equation [1]. It is worth noting, that we obtain a third order operator in space, that we discretize with DGM.

2 Numerical Results

Our main goal is to limit the storage which is the main drawback of the RTM. The computational cost, can be controlled by new HPC techniques such that MPI, OpenMP or GPU. We have performed a comparison between classical LF scheme using $\mathcal{P}^6$-elements in space and fourth order time schemes. The length of the domain is 6 m, the simulation time is 6.0 sec. The original space step h varies from 0.2 to 0.03 m. We consider periodic boundary conditions and the initial data is:

$$U(x,t) = (x - x_0 - t)\, e^{-\left(\frac{(2\pi(x-x_0-t))^2}{r_0}\right)}.$$

In Fig. 1, we represent the relative L^2-error as a function of the number of unknowns. For a given accuracy, High Order schemes require less degrees of freedom (dof) than LF. Besides, the Nabla-p scheme requires three times less dofs than ADER.

In Fig. 2 we represent the relative L^2-error as a function of the number of operations. For a given accuracy, ADER and Nabla-p require approximatively the same number of operations. As a conclusion, Nabla-p scheme require less storage cost than ADER and the computional cost is similar. This indicates that Nabla-p scheme is more appropriate for the RTM.

We will present RTM results that will illustrate the performance of Nabla-p scheme in realistic 2D and 3D configurations.

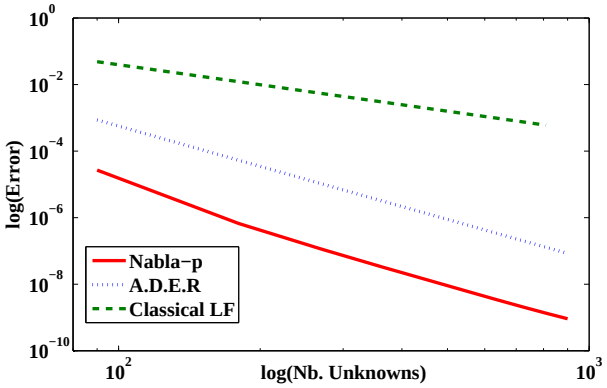

Figure 1: Number of Unknowns

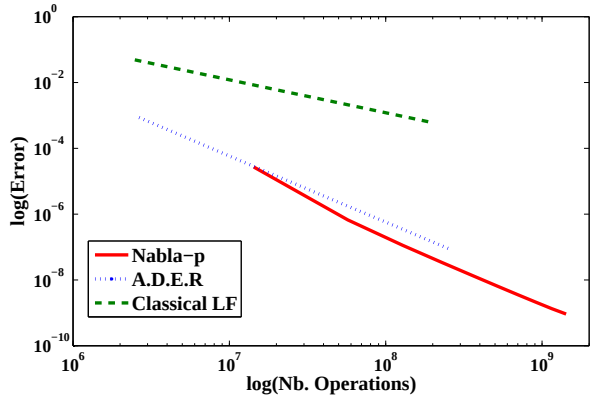

Figure 2: Number of operations

Acknowledgements

This work is supported by INRIA-TOTAL strategic action DIP. (http://dip.inria.fr)

References

[1] C. Agut, J. Diaz and A. Ezziani (2011) *High-Order Schemes Combining the Modified Equation Approach and Discontinuous Galerkin Approximations for the Wave Equation*, Computational Physics 11, 2 (2012) 691-708.

[2] M. A. Dablain (1986) *The application of high order differencing for the scalar wave equation*, Geophysics, Vol. 1, pp. 51:54-56.

[3] G. R. Shubin and J. B. Bell (1987) *A modified equation approach to constructing fourth-order methods for acoustic wave propagation*, SIAM J. Sci. Statist. Comput.,8:135-151.

[4] M. Dumbser and M. Käser (2000) *An arbitrary High-order discontinuous Galerkin method for elastic waves unstructured meshes - II.The three-dimensional isotropic case*, Geophys. J. Int. 142.

True Amplitude Imaging of Ocean Bottom Cable Data by Gaussian Beams Based Weighted Summation

Protasov M.I.[†,*], **Kutovenko M.P.**[†], **Tcheverda V.A.**[†]
[†]Institute of Petroleum Geology and Geophysics, 3, Koptyug st., Novosibirsk, Russia 630090
[*]Email:ProtasovMI@ipgg.sbras.ru

Abstract

An approach to true amplitude seismic imaging for Ocean Bottom Cable multicomponent (displacement and pressure) data is presented and discussed. This approach is a migration procedure based on weighted summation of prestack data.We use a pair of properly chosen Gaussian Beams with fixed dip and opening angles from each imaging point towards the acquisition system. Shooting from the image point overcomes some difficulties due to multiple arrivals of seismic energy which are common for complicated velocity models and provides uniform illumination and resolution in the target area. In addition, the global regularity of Gaussian beams stabilizes this approach in the presence of irregular ray fields. Numerical experiments with synthetic data set for the Gullfaks model (North Sea) are presented and discussed.

Introduction

We present the equations for true-amplitude elastic imaging of multi-component (4C) seismic Ocean Bottom Cable (OBC) data, and illustrate in the numerical examples how a linearized elastic inversion can retrieve perturbations in elastic parameters from the true-amplitude images. Our results extend the approach for elastic imaging of borehole seismic walkaway VSP data presented in the paper [3]. Our prestack migration procedure is based on weighted summation of the data, with weights computed by tracing Gaussian Beams (see [2]). The weights are functions of two angles; structural dip and opening angle for the pair of beams. Note that these beams are shot from the image points toward the acquisition surfaces, thus stabilizing the solution in complex models. Keeping the opening angle constant, while carrying out the summation over dip, provides so-called selective images of the rapid velocity variations, which we input to linearized (AVA-like) inversion for elastic parameters. We illustrate our imaging and inversion approaches with examples from a synthetic data set computed for Gullfaks field model.

Method

The 2d elastic model below is supposed to be decomposed as macro-model λ_0, μ_0, ρ_0 and reflectivity/scatterer component λ_1, μ_1, ρ_1. Let us suppose that along the bottom line Γ there is an Ocean Bottom Cable (OBC), registering the displacement vector and pressure scattered/reflected by underlying rocks: $\overrightarrow{d}(\overline{x}_r;\overline{x}_s;\omega) = (u_x, u_z, p)$. In order to describe scattered/reflected wave field Born's approximation is used. The problem we deal with is to recover functions λ_1, μ_1, ρ_1 or some their combinations from OBC data.

In order to construct a PP image at some target point $\overline{x}_i$ let us shoot from it a couple of P-rays, trace them through the smooth background towards the acquisition system and introduce a couple of P-wave Gaussian beams connected with these rays. Next, let us compute the Gaussian beam and the corresponding stresses at the receivers at the ocean bottom: $\overrightarrow{T}^p_{gb,r}(\overline{x}_r;\alpha,\beta;\omega)$, and the vertical derivative of the potential of another P-wave Gaussian beam at the source positions: $T^p_{gb,s}(\overline{x}_s;\alpha,\beta;\omega)$. Using these expressions as weights for the summation OBC data and applying the stationary phase method in the same manner as it was done in [3], we find that with accuracy to the first order the summation integral can be represented as:

$$f_{pp}(\beta) = \int d\overline{x}_r d\overline{x}_s d\omega d\alpha \, \overrightarrow{d}(\overline{x}_r;\overline{x}_s;\omega) \cdot$$
$$\cdot \overrightarrow{T}^p_{gb,r}(\overline{x}_r;\alpha,\beta;\omega) \cdot T^p_{gb,s}(\overline{x}_s;\alpha,\beta;\omega) + O(\omega^{-1}), \quad (1)$$

with the function

$$f_{pp}(\beta) = \frac{\lambda_1 + 2\mu_1 \cos^2 2\beta + \rho_1 V^2_{0,p} \cos 2\beta}{cos^2\beta}. \quad (2)$$

Here we use the fact that Gaussian beams are concentrated in the narrow vicinity of the corresponding ray which allows us to restrict the integration over a small area V around the imaging point.

Illustrations

To study the main features of the method and evaluate the limits of its applicability and resolution,

we have synthesized OBC data for the Gullfaks field model. Numerical simulation was done with a finite-difference scheme. The dataset consists of 81 shots and array of 161 3C receivers. We applied no pre-processing of these data before the Gaussian beam imaging; in particular no P- and S-wave separation was used. The result for opening angle $\beta = 0^0$ can be seen in Fig.1 (bottom) in comparison with the true model (top). The target structures are reconstructed with excellent quality, especially the fine layering of the reservoir (the shaded area). There are also no visible artifacts due to conversion (let us recall that we did not apply preliminary P- and S-wave separation). Next, we extract values of elastic parameters for the medium by inverting expression (2) for the function $f_{pp}(\beta)$. This inversion was carried out for two different sets of physically meaningful parameters: 1) AVO parameterization by R_0, G and C (see [1]); 2) Parameterization by P- and S-impedances and normalized density. In Fig.2(top) one can compare the recovered (red line) and real (blue line) functions $f_{pp}(\beta)$ and make sure that they match almost perfectly. Now these functions are used as the right-hand sides of a formally over determined system of linear equations: 20 equations for 3 parameters. This system is resolved by standard Least Squares optimization with the results presented in Fig.2(bottom) for both parameterizations. Under AVO parameterization R_0 recovery is almost ideal, parameter G is found with reasonable quality, but the third coefficient C is reconstructed poorly. At the same time, when parameterization by impedances and normalized density is used, only P-impedance is restored reliably, while neither S-impedance nor the density is determined with acceptable accuracy.

Conclusions

We presented theory and synthetic numerical results for a true amplitude Gaussian Beam elastic imaging and inversion procedure with application to Ocean Bottom Cable data. This research is based on our previous study performed for one component data and walk-away multicomponent VSP. The selective images obtained for a range of opening angles represent reflection coefficients in a linear approximation. If they can be computed for a range of opening angles, we can recover the elastic properties of the medium by AVA-like amplitude analysis and inversion. It is worth mentioning that our inversion results are obtained without preprocessing of the data,

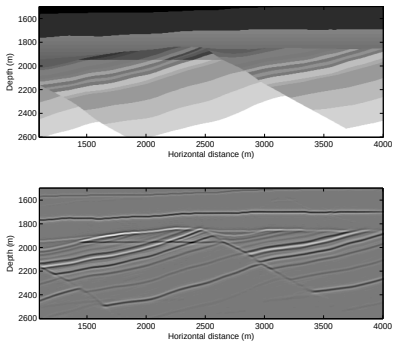

Figure 1: Velocity model (top) and its true-amplitude image (bottom).

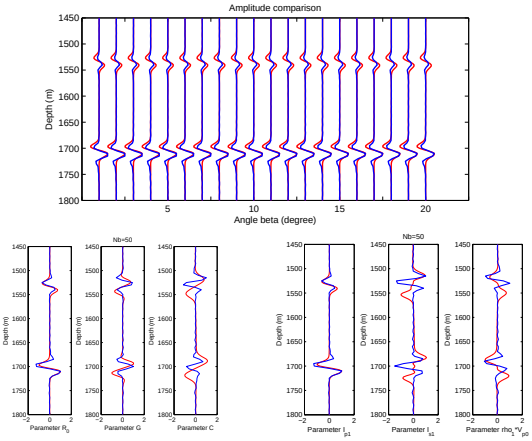

Figure 2: Input data for recovery of material parameters, the function f_{pp} (top). Inversion result for AVO parameters R_0, G, C (bottom left). Inversion results for P- and S-impedances and normalized density (bottom right).

and in particular no separation of P- and S-waves

Acknowledgments

The research described in this publication was done in cooperation with Moscow Schlumberger Research.

References

[1] Aki K., Richards P., *Quantitative Seismology*, Freeman, 1980.

[2] Popov M.M., *Ray theory and gaussian beam method for geophysicists*, EDUFBA, 2002.

[3] Protasov M.I., Tcheverda V.A., *True amplitude elastic Gaussian beam imaging of multicomponent walkaway VSP data*, Geophysical Prospecting, **v.60(6)**, 2012, pp. 1030 - 1042.

Absorbing Boundary Conditions for Tilted Transverse Isotropic waves in Reverse Time Migration context

H. Barucq[1], **L. Boillot**[1,*], **H. Calandra**[2], **J. Diaz**[1]
[1] INRIA - Magique3D team
[2] TOTAL company
*Email: lionel.boillot@inria.fr

Abstract

The construction of Absorbing Boundary Conditions (ABCs) for elastic media is an issue that is far from being solved. This is probably due to the very technical difficulties that arise when one wants to write higher-order conditions. In the isotropic case, we can nevertheless design conditions but the problem is not solved for general elastic media. Besides, a realistic representation of the Earth must include anisotropy and in most of cases, subsurface layers are Tilted Transverse Isotropic (TTI). That is why we propose a new low-order ABC for TTI media, that is constructed from the geometry profile of the slowness curves. We thus avoid technical issues that make the construction of ABCs impossible.

1 Problem setting

We are interested in the design of an efficient direct solver for elastodynamics that can be used for seismic imaging of heterogeneous media. Denoting $\mathbf{x} = (x, z)$ and $t \geqslant 0$, the space and time variables, the elastodynamics system reads as

$$\begin{cases} \rho(\mathbf{x})\partial_t \mathbf{v}(\mathbf{x},t) &= \nabla.\underline{\underline{\sigma}}(\mathbf{x},t), \\ \partial_t \underline{\underline{\sigma}}(\mathbf{x},t) &= \underline{\underline{C}}(\mathbf{x}) : \underline{\underline{\epsilon}}(\mathbf{v}(\mathbf{x},t)), \end{cases} \tag{1}$$

with $\rho > 0$ the density, $\mathbf{v}$ the velocity field, $\underline{\underline{\sigma}}$ the stress tensor, $\underline{\underline{C}}$ the stiffness tensor and $\underline{\underline{\epsilon}}$ the strain tensor. The coefficients of $\underline{\underline{C}}$ depend on the characteristics of the propagation medium. The simplest representation of $\underline{\underline{C}}$ corresponds to an isotropic medium but it does not adequately model waves in realistic cases. Transverse Isotropy (TI) models have more ability to reproduce waves into the Earth, see [7], [2]. Vertical Transverse Isotropy (VTI) assumes that there is a vertical axis of symmetry. In the more general case of TTI, the symmetry axis can be away from vertical, following an angle θ of rotation. (see Fig. 1 for a description of different wavefronts).

Isotropic media can be characterized by the P-waves and S-waves velocities V_p and V_s with the density ρ. VTI media are defined in the same manner by V_p, V_s and ρ, and in addition with the Thomsen VTI parameters ε and δ [5]. TTI media are described by the VTI parameters and by the characteristic angle of rotation θ.

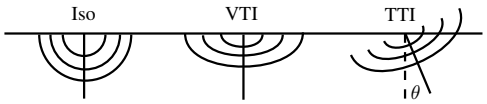

Figure 1: Wavefronts for isotropic (left), VTI (center) and TTI (right) media

A rigourous methodology for the construction of ABCs is based on the diagonalization of the system (1). This approach has been proposed by Enquist and Majda [3] for strongly hyberbolic systems. It provides a very elegant process for the derivation of ABCs on arbitrarily shaped boundaries [1]. Nevertheless, in practice, it can quickly become uneasy to use because of coupling terms that are difficult to handle in the first stage of the diagonalization. The coupling indeed, results in eigenvalues which are difficult to exploit for the construction of efficient ABCs. For instance, the VTI eigenvalues are [4]:

$$\lambda_{P/S} = \sqrt{\alpha k^2 - \beta\rho w^2 \pm \sqrt{\gamma k^4 - \eta\rho k^2 w^2 + \xi \rho^2 w^4}}$$

where k denotes the frequency related to the time variable by a Fourier transform, and $\alpha, \beta, \gamma, \eta, \xi$ are parameters depending on the tensor coefficients.

From a practical point of view, it is obvious that the numerical handling of λ is not feasible because of the composition of two square roots which show the coupling and are uneasy to localize. It reflects the coupling between P-waves and S-waves. A possible approach consists then in uncoupling these waves and constructing ABCs for each of them. By this way, ABCs for VTI can be constructed and, when the medium is isotropic, they are the same than the conditions derived in [6].

Next, the P-waves and S-waves VTI ABCs can be mixed in order to form unsplitted PS-waves low-order VTI ABCs. Unfortunately, considering the TTI case,

even the splitting of the PS-waves into P-waves and S-waves does not help anymore. This is due to the characteristic angle of rotation that prevents from obtaining a local ABC. In this work, we propose a new TTI ABC that includes any characteristic of the media providing this anisotropy is elliptic.

2 ABCs for elliptically TTI media

Elliptic anisotropy means that the TI coefficients are equal: $\delta = \varepsilon$. In this case, the slowness curve of S-waves forms a circle, as in the isotropic case, so that the same ABCs can be used. For example, for the left vertical boundary, S-waves ABC is

$$\begin{cases} \sigma_{xx} &= 0, \\ \sigma_{xz} &= \sqrt{\rho} V_s v_x. \end{cases} \tag{2}$$

However, P-waves curves are different (see Fig. 2). They form a circle for the isotropic case and a rotated ellipse for the TTI case.

The construction of the new ABC is then based on a change of coordinate that transforms a circle into a rotated ellipse. The ABC is then obtained by applying the coordinate change to the isotropic ABC. In case of a vertical boundary, isotropic P-waves ABC reads as

$$\begin{cases} \sigma_{xx} &= \pm \sqrt{\rho} V_p v_x, \\ \sigma_{xz} &= 0. \end{cases} \tag{3}$$

The sign is fixed by the orientation of the normal vector. Next, introducing $\kappa = \sqrt{1+2\varepsilon}$, TTI P-waves ABC is

$$\begin{cases} \sigma_{xx} &= \sqrt{\rho} V_p \frac{\kappa \cos^2\theta + \sin^2\theta}{\sqrt{\kappa^2 \cos^2\theta + \sin^2\theta}} \times \\ & \left[(\kappa \cos^2\theta + \sin^2\theta) v_x + (\kappa - 1) \cos\theta \sin\theta v_z \right], \\ \sigma_{xz} &= \sqrt{\rho} V_p \frac{(\kappa-1) \cos\theta \sin\theta}{\sqrt{\cos^2\theta + \kappa^2 \sin^2\theta}} \times \\ & \left[(1-\kappa) \cos\theta \sin\theta v_x + (\cos^2\theta + \kappa \sin^2\theta) v_z \right]. \end{cases} \tag{4}$$

Finally, the P-waves and S-waves ABCs are mixed in order to obtain unsplitted PS-waves low-order TTI ABCs for elliptic anisotropic media. The ellipticity hypothesis might be considered as restrictive. This is actually not the case because the simplest VTI ABC does not involve the parameter δ. We can thus suppose it is the same for any TI medium.

We will provide numerical results of Reverse Time Migration to assess the performance of the new ABC in anisotropic media.

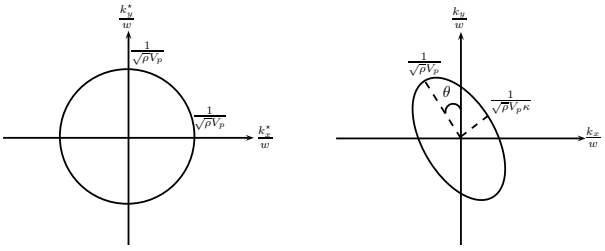

Figure 2: Slowness curves of isotropic (left) and TTI (right) cases – P-waves

Acknowledgments

The authors acknowledge the support by the INRIA-TOTAL strategic action DIP – Depth Imaging Partnership (`http://dip.inria.fr`).

References

[1] X. Antoine and H. Barucq. Microlocal diagonalization of strictly hyperbolic pseudodifferential systems and application to the design of radiation conditions in electromagnetism. *SIAM Journal on Applied Mathematics*, 61:1877–1905, 2001.

[2] E. Duveneck and M. P. Bakker. Stable p-wave modeling for reverse-time migration in tilted TI media. *Geophysics*, 76(2):65–75, 2011.

[3] B. Engquist and A. Majda. Absorbing boundary conditions for the numerical simulation of waves. *Math. Comp.*, 31:629–651, 1977.

[4] O. Podgornova. Transparent boundary conditions for elastic anisotropic (VTI) media: axially symmetric case. In *Waves*, 2009.

[5] L. Thomsen. Weak elastic anisotropy. *Geophysics*, 51(10):1954–1966, 1986.

[6] C. Tsogka. *Modélisation mathématique et numérique de la propagation des ondes élastiques tridimensionnelles dans des milieux fissurés*. PhD thesis, Paris IX Dauphine, 1999.

[7] I. Tsvankin. *Seismic signatures and analysis of reflection data in anisotropic media*. Elsevier, 2001.

Application of a preconditioned truncated Newton method to Full Waveform Inversion.

R. Brossier[1], L. Métivier[2,*], S. Operto[3], J. Virieux[1]
[1]ISTerre - Joseph Fourier University, UMR 5275, Grenoble, France.
[2]LJK- Joseph Fourier University - CNRS, UMR 5224, Grenoble, France.
[3]Géoazur - Nice Sophia Antipolis University - CNRS, UMR 7329, Villefranche-sur-mer , France.
* Email: ludovic.metivier@ujf-grenoble.fr

Abstract

Full Waveform Inversion (FWI) is a powerful seismic imaging method, based on the iterative minimization of the distance between simulated and recorded wavefields. The inverse Hessian operator related to this misfit function plays an important role in the reconstruction scheme. As conventional methods use direct approximations of this operator, we investigate an alternative optimization scheme: the truncated Newton method. This two-nested-loops algorithm is based on the resolution of the Newton linear system through a matrix-free iterative solver at each outer iteration. On the 2D BP 2004 model widely used as a benchmark for FWI, the contrasts in wave velocities between salt structures and the upper water layer generate high amplitude multiple reflections. These multiple reflections strengthen the need for quite accurate approximation of the inverse Hessian operator and the truncated Newton method is shown to outperform than more conventional algorithms (l-BFGS, nonlinear conjugate gradient).

Introduction

Full Waveform Inversion is a seismic imaging method dedicated to the computation of high resolution quantitative estimates of subsurface parameters such as pressure wave velocity, shear wave velocity, attenuation, or density. This method consists in computing a subsurface model p which minimizes a misfit function $f(p)$, defined by

$$f(p) = \frac{1}{2} \sum_{s=1}^{S} \|u_s(p) - d_s\|^2, \tag{1}$$

which measures the distance between the simulated wavefields $u_s(p)$ and the actual recorded wavefields d_s. Despite its early introduction in the 80s, only the recent development of computational capacities (computer clusters) and acquisition systems (wide-azimuth wide-offset broadband seismic surveys) have made possible its application to real data in oil and gas industry.

In this study, we particularly focus on the minimization method which is used to solve the FWI problem. As the large number of discrete unknowns prevents from using global optimization methods, state-of-the-art methods are local gradient-based methods such as the nonlinear conjugate gradient (CG) or the l-BFGS method. From an initial subsurface model p_0, a sequence p_k is built such that

$$p_{k+1} = p_k + \alpha_k \Delta p_k, \tag{2}$$

where α_k is computed through a linesearch method and Δp_k is the descent direction

$$\Delta p_k = -Q_k \nabla f(p_k). \tag{3}$$

The matrix Q_k is an approximation of the inverse Hessian matrix $(\nabla^2 f(p_k))^{-1}$. Pratt [2] clearly demonstrates the crucial role played by this operator in the FWI reconstruction scheme:

- it acts as a deconvolution operator that accounts for the limited bandwidth of the seismic data and corrects for the loss of amplitude of poorly illuminated subsurface parameters;
- it helps to remove artifacts that the second order reflected waves may generate on the gradient descent direction.

For multi-parameters FWI, the off-diagonal blocks of the Hessian matrix should also account for the trade-off between different classes of parameters. This suggests that it should be crucial to account accurately for the inverse Hessian operator within the minimization schemes, and leads us to the investigation of the truncated Newton method for FWI.

Methodology

The truncated Newton method only differs from standard descent method by the strategy used to compute the descent direction. Instead of using an approximation of the inverse Hessian operator, the descent direction Δp_k is computed through the resolution of the Newton linear system

$$\nabla^2 f(p_k) \Delta p_k = -\nabla f(p_k), \tag{4}$$

using a matrix-free CG solver, which results in a two-nested loops algorithm (inner linear CG iterations for the computation of Δp_k through (4) and outer nonlinear iterations for the construction of the sequence p_k through (2)). The incomplete resolution of the linear system (4) is referred as the truncation strategy. This presents several advantages over conventional procedures:

- the inverse Hessian operator is more accurately accounted for;
- the approximations of the inverse Hessian operator developed for the standard methods can be reintroduced within this framework as preconditioners of the linear system (4);
- the method is well suited for applications where the misfit function change over the iterations, as for instance using random combinations of data-sets d_s (source encoding techniques);
- the truncation strategy can be seen as an intrinsic regularization of the FWI problem (of particular interest for the interpretation of noisy data).

An efficient implementation of this algorithm for FWI is fully described in [1]. It mainly relies on the reduction of the computation cost associated with the inner loop. This is achieved using:

- second-order adjoint-state formulae for the computation of Hessian-vector products;
- an adaptive stopping criterion for the inner iterations, related to the truncation strategy, a crucial issue;
- an efficient preconditioning method based on the approximation of the diagonal terms of the inverse Hessian operator.

Numerical results

We compare the truncated Newton method with the nonlinear CG method and the l-BFGS method using the same preconditioning technique. This comparison is performed on the BP 2004 model, which exhibits complex subsurface patterns related to the presence of salt structures (figure 1). The high contrast in wave velocity between the water layer and these salt structures are responsible for the presence of high amplitude multi-reflected waves which renders an accurate estimation of the inverse Hessian operator crucial for a stable reconstruction of the subsurface model. These experiments are performed under the acoustic approximation, and we aim at recovering the pressure wave velocity model. We solve the wave equation in the frequency-domain (the forward problem is then described by the Helmholtz equation) and we adopt the so-called hierarchical approach: 6 groups of overlapping frequencies are inverted from 2.5 Hz to 20.5 Hz. The initial model p_0 (figure 1) is a smooth version of the exact one which shall be obtained using conventional tomography methods. The results provided by the three optimization schemes are presented in figure 2. As it can be seen, only the truncated Newton method provides a reliable estimation in this specific case of high contrasts.

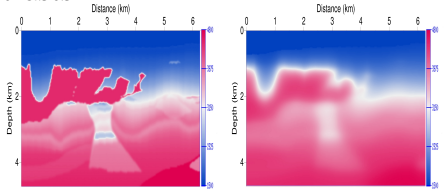

Figure 1. BP 2004 model (left), initial model (right).

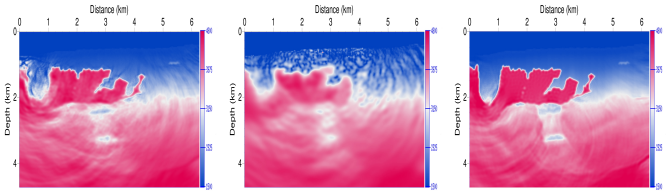

Figure 2. Nonlinear CG result (left), l-BFGS result (center), truncated Newton result (right).

Conclusion and perspectives

An accurate estimation of the inverse Hessian operator within the FWI reconstruction scheme is of particular importance for computing accurate estimations of the subsurface parameters. In the 2D acoustic approximation, when high amplitude multiple reflected waves have to be interpreted, the truncated Newton method provides a better alternative to conventional optimization methods. Application to real data is now the next step for investigating the interest of this method for FWI. This method will be also further investigated in anisotropic and elastic contexts, for multi-parameter reconstructions, in 2D and 3D experiments. The coupling of this method with source encoding strategies shall also be investigated.

References

[1] L. MÉTIVIER, R. BROSSIER, J. VIRIEUX, AND S. OPERTO, *Full waveform inversion and the truncated newton method*, SIAM Journal On Scientific Computing, in press (2012).

[2] R. G. PRATT, C. SHIN, AND G. J. HICKS, *Gauss-Newton and full Newton methods in frequency-space seismic waveform inversion*, Geophysical Journal International, 133 (1998), pp. 341–362.

3.2 Piano acoustics

Minisymposium organized by Antoine Chaigne

A non-smooth simulation of the dynamics of the grand piano action

A. Thorin[1,2,*], **X. Boutillon**[1], **X. Merlhiot**[3], **J. Lozada**[2]
[1] Laboratoire de Mécanique des Solides, École Polytechnique, Palaiseau, France.
[2] CEA, LIST, Sensorial and Ambient Interfaces Lab., F-91191 Gif-sur-Yvette Cedex, France.
[3] CEA, LIST, Interactive Simulation Lab., 18 route du Panorama, BP6, F-92265 Fontenay-aux-Roses, France.
*Email: anders.thorin@polytechnique.edu

Abstract

Two models of the grand piano key mechanism are presented: a single-degree-of-freedom model and a model based on 6 rotating bodies, 13 contact zones with nonlinear springs, 3 of them (hammer-jack, jack-escapement button, hammer-check) being also subject to Coulomb friction. The latter model introduces discontinuities on the velocities. The problems raised by the usual regular-dynamics formulation are discussed and a non-smooth dynamics approach is proposed. Based on the comparison between experimental and simulation results, it is discussed whether the simulation should be driven by the force exerted by the pianist or by the displacement of the key.

Introduction

The piano action is made of seven rotating bodies (Fig. 1) with parallel axes and felts at contact zones. Simulating the dynamics of the key mechanism (we retain this term for clarity purposes) has several purposes: to validate a mechanical model, to run numerical experiments which account for the effect of the mechanism on the player's finger, to study how modifications are "felt" by the player.

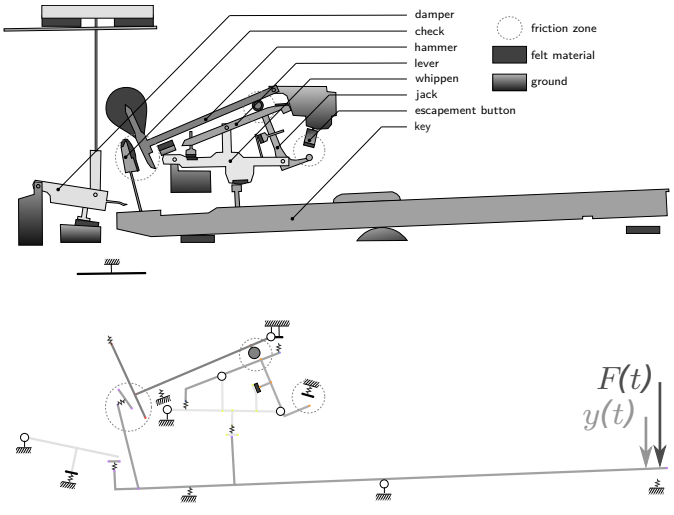

Figure 1: Top: scheme of the grand piano action. Bottom: rigid bodies model.

1 Model complexity and simulation input

The key motion $y(t)$ and the force $F(t)$ on the key are given by the dynamics of the mechanism and by the action imposed by the pianist (whose dynamics is also limited). If one does not describe the whole coupled system {mechanism – pianist}, which seems presently out of reach, the simulation of the mechanism only must be driven either by force data or by motion data. However, it has never been clarified whether the mechanism is better described as pseudo-impedance (force reacting to a motion imposed by the pianist) or as a pseudo-mobility (motion resulting from a force imposed by the pianist).

In order to validate a mechanical model, it is customary to compare simulation results with experimental observations. Since the dynamics of the mechanism is dominated by inertia, it appears that one can reduce the model of the whole mechanism to one single degree-of-freedom (following a dynamical equation of the form given by Eq. (1)) and yet obtain an excellent match between experimental measurements and *force-driven* simulation results. However, the corresponding motion-driven simulation results do not compare well with experiments: fine details in the time-evolution of the reacting force $F(t)$ are ignored. In other words, because of the inertia dominance, a force-driven simulation is not sufficient for accounting the details of the piano key mechanism.

2 Non-smooth formulation

Since an elementary model is not fully satisfactory, we used a model based on that proposed by Lozada [1]. The 7 bodies are considered as 6 rotating solids with dry and viscous friction on their axes and 13 non-linear and localized coupling springs representing the felts (Fig. 1). Any spring force is generically given by $F(g) = k\,g^r + b\,g^2\,\dot{g}$, where g is the compression length of the spring (felt). The equation describing the dynamics of any rigid body in the model is of generic form:

$$J\,\ddot{\theta} + c_v\,\dot{\theta} + c_d\,\mathrm{sign}(\dot{\theta}) + F(g(\mathbf{x}))\,l + \alpha = 0 \qquad (1)$$

where J is the inertia of the rigid body, c_v is a viscous friction coefficient, c_d is a dry friction coefficient, $\mathbf{x}$ is the vector of generalized coordinates (*i.e.* the 6 angles), $F(g(\mathbf{x}))\,l$ is the moment of the felt force (several such terms may be necessary when more than one felt act upon the considered rigid body) and α contains time-invariant terms such as the moment of gravity, in the small angles approximation. As usual, sign is the set-valued function defined by:

$$\text{sign}(\dot{\theta}) = \begin{cases} 1 & : \dot{\theta} > 0 \\ [-1,1] & : \dot{\theta} = 0 \\ -1 & : \dot{\theta} < 0 \end{cases} \qquad (2)$$

so that the dry friction is described by the Coulomb model.

Because of dry friction and intermittent contacts, the simulation of the model is complex. One difficulty is that Eq. (1) is not an ODE. Regularizing the sign set-valued function yields ODEs but the convergence to a physical solution when reducing the time step is not ensured. An example can be seen in the equilibrium position: null-velocities imply vanishing regularized friction forces whereas the Coulomb friction generally lets non-zero forces in the system. Another difficulty is that stick-slip transitions induce velocity discontinuities. Furthermore, the evaluation of the moment of the reaction contact forces $F(g(\mathbf{x}))$ is tedious. These difficulties can be overcome by using methods of non-smooth contact dynamics (NSCD).

Instead of writing the dynamics in the form of six coupled equations of the form (1), we use a Measure Differential Inclusion formulation [2]:

$$\begin{cases} \mathbf{M}\mathrm{d}\mathbf{v} &= \mathbf{F}^*(t)\mathrm{d}t + \mathbf{H}(\mathbf{x})\mathrm{d}\mathbf{i} \\ \mathbf{v}^+ &= (\dot{\mathbf{x}})^+ \\ (\mathbf{g}(\mathbf{x}),\ \mathbf{H}^T(\mathbf{x}).\mathbf{v}^+,\ \mathrm{d}\mathbf{i}) &\in K \end{cases} \qquad (3)$$

The first equation formulates the non-smooth dynamics where $\mathbf{M}$ is the mass matrix, $\mathbf{v}$ is the generalized velocity, $\mathbf{F}^*$ is the regular part of the sum of external forces, including gravity. $\mathrm{d}\mathbf{v}$ and $\mathrm{d}\mathbf{i}$ are vector-valued measures on $\mathbb{R}$ and can therefore be non-smooth. $\mathbf{H}$ relates the relative velocities to the generalized coordinates. The non-smooth laws (Coulomb and articular friction, impacts) and equality constraints are written as an inclusion in the fixed set K.

Eqs. (3) are discretized using a time-stepping scheme. Its solution is computed with an implicit scheme. As for smooth ODEs, it requires a root-finding algorithm (Newton's algorithm in our case). The time-discretization of the non-smooth dynamics and the non-smooth laws leads to a One-Step Non-Smooth Problem (OSNSP) [3]. This OSNSP is reformulated using a non-smooth augmented Lagrangian approach and solved using an iterative projective Gauss-Seidel-like method.

3 Results

We used XDE (eXtended Dynamic Engine), a software component developed at CEA, LIST. The inputs of the software are the geometrical and inertial descriptions of the pieces (here: the rigid bodies), the properties of the pivots (here: dry and viscous friction) and the contact laws (here: the coupling forces of the springs and the Coulomb friction). The software implements internally the non-smooth formulation of the dynamics and its solution, as described in Sec. 2.

An additional spring/damper association, aimed at representing the softness of the finger, has been inserted between the key mechanism and the (force- or motion-)driver of the mechanism. We measured the position of the key and the force applied by the pianist for several nuances, on one individual key. As for the results obtained with the one-degree-of-freedom model (Sec. 1), the results of a *force-driven* simulation compare correctly with the measured motion. Contrary to the results obtained with the one-degree-of-freedom model, the results of the *motion-driven* simulation compare also correctly with the measured force.

The calculation time ($\approx 20\times$ real-time) on an ordinary laptop computer could be largely improved by taking into account the particularities of the model of the key mechanism.

References

[1] J. Lozada, *Modélisation, contrôle haptique et nouvelles réalisation de claviers musicaux*, PhD thesis, École Polytechnique, France, 2007.

[2] X. Merlhiot, *On some industrial applications of time-stepping methods for nonsmooth mechanical systems: issues, successes and challenges*, in Euromech Colloquium [516] – Nonsmooth contact and impact laws in mechanics, 2011.

[3] V. Acary and B. Brogliato, *Numerical methods for nonsmooth dynamical systems: applications in mechanics and electronics*, Springer, 2008.

Vibration model of piano soundboards

X. Boutillon[1,*], **K. Ege**[2]
[1] Laboratoire de mécanique des solides, École polytechnique, F-91128 Palaiseau Cedex, France.
[2] Laboratoire Vibrations Acoustique, INSA-Lyon, 25 bis avenue Jean Capelle, F-69621 Villeurbanne Cedex, France.
*Email: boutillon@lms.polytechnique.fr

Abstract

Modal observations of a piano soundboard are compared with results predicted by a model consisting of weakly coupled homogeneous sub-structures. The model is entirely determined by the coarse geometry of the soundboard (main plate, ribs, bridges, cut-off corners) and by the elastic parameters of the wood species. It can also be used to predict the point-mobility at the bridge (where strings are attached) or far from it. The agreement between observations and model predictions is excellent, both in the low- and high-frequency regimes (respectively below and above $\approx$ 1 kHz). Applications include a comparison between the characteristics of different pianos as well as the influence of the wood properties on the point-mobility. Some consequences in terms of acoustical radiation will also be presented.

Introduction

In a piano, the soundboard is the plate-like structure on which the strings are attached. It radiates sound (the strings are too thin to radiate efficiently) and rules the sound-decay which is an essential part of the piano sound. Coupling between the string and the soundboard is described by the point-mobility $Y_Q(\omega) = V(\omega)/F(\omega)$ where, ω is the angular frequency, F the force applied by the string(s) at point Q and V the resulting velocity of the soundboard at that point. $Y_Q(\omega)$ can be written as the sum of the mobilities of the modes of the soundboard at a given point. We consider that modal shapes are sinusoids along the bridge and products of sinusoids across the soundboard (see § 1 for experimental observations and FEM results). Modal frequencies are obtained in average by a model presented in § 2. Modal dampings are given by observation. Ignoring fine geometrical details and local pecularities, these ingredients are sufficient to predict $Y_Q(\omega)$ at any point, according to Skudrzyk's theory of the mean-value of the point mobility [1]. Results pertaining to modal density and to the reciprocal of the frequency-averaged point-mobility are given in § 3, for different pianos.

1 Experimental and numerical observations

The following observations (see [2] for a complete report) have been made on an upright piano soundboard (Atlas, .91 m $\times$ 1.39 m) and result from a high-resolution modal analysis technique [3]. For results below 350 Hz, the soundboard was excited locally by a impact hammer and above that limit, the soundboard was excited globally by a strong acoustical field. The vibration was observed locally with accelerometers. The modal analysis also yielded the modal dampings with an excellent precision in a frequency range not accessible with Fourier-based techniques (modal overlap approaching 100%). It appears that above $\approx$1 kHz, not all the modes are observed at any given observation point, hence the use of the concept of *apparent* modal density, defined as the reciprocal of the average modal spacing and represented in Fig. 1. Below 1 kHz, the apparent modal density does not depend on the point of observation and looks similar to that of a plate (or a combination of plates). Above that limit, the apparent modal density decreases and depends on the point of observation.

A typical modal shape for the so-called low-frequency regime (below 1 kHz) is represented in the top of Fig. 2. The vibration extends over the whole soundboard except, eventually, in one or another cut-off corner. In the high-frequency regime

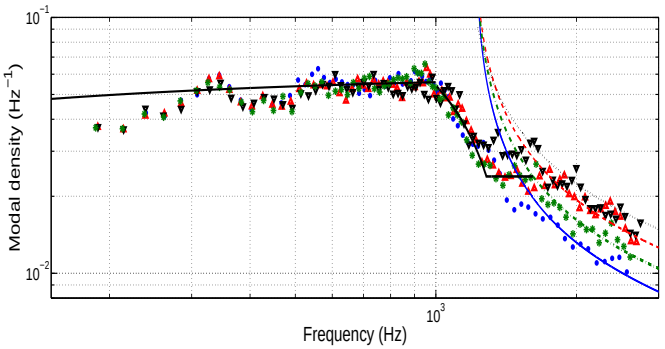

Figure 1: Modal density of the Atlas soundboard. Dots: observed values at various points of the soundboard. Lines: prediction of the model (§ 2).

(above 1 kHz), modal shapes have been obtained by finite-element modeling of the soundboard [2]. It appears (Fig. 2) that the vibration is both *confined* between ribs and, most often, *localised* in one or a very few areas of the ribbed parts of the soundboard, due presumably to the slightly irregular spacing of ribs across the soundboard.

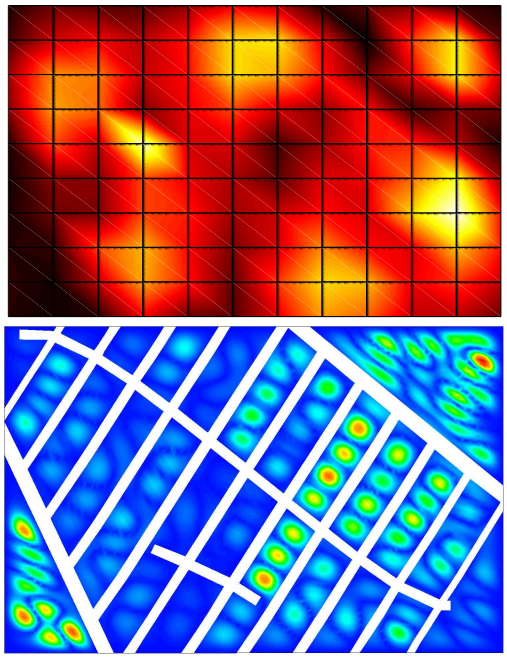

Figure 2: Typical modal shapes. Top: observed in the low-frequency regime (mode 10, 303 Hz). Bottom: numerically obtained in the high-frequency regime (mode 167, 2733 Hz).

2 Model

The different parts (cut-off corners, if any, the two main parts of the soundboard, as limited by the main bridge, the rim and the cut-off bars, the main bridge) are conidered as weakly coupled homogeneous substructures. The bass bridge is described as a simple mass added to the corresponding part of the soundboard. Each plate-like structure is considered with clamped boundary conditions. The main bridge is described as a bar, the cut-off corners as orthotropic plates, as well as the the ribbed parts of the soundboard in the low-frequency regime, following the homogenisation proposed by [4].

In the high frequency domain (where the apparent modal density depends on the point of observation), we consider that the two main parts of the soundboard (ribbed areas, extending on each side of the main bridge) vibrate only in the vicinity of the observation points, namely within three inter-rib spaces. Each inter-rib space of width p is seen as a structural wave-guide where the wave-number in the direction orthogonal to the ribs is $k_x = n\pi/p$, with $n \in \mathbb{N}^*$. A transition has been devised between the two regimes.

Under the weak-coupling hypothesis, the modal density is the sum of the modal densities of the substructures. The agreement between observations and the results given by the model (Fig. 1) is striking.

3 Applications

The model has been used to to analyse the influence of wood parameters (not shown here) and to characterise different pianos (Fig. 3).

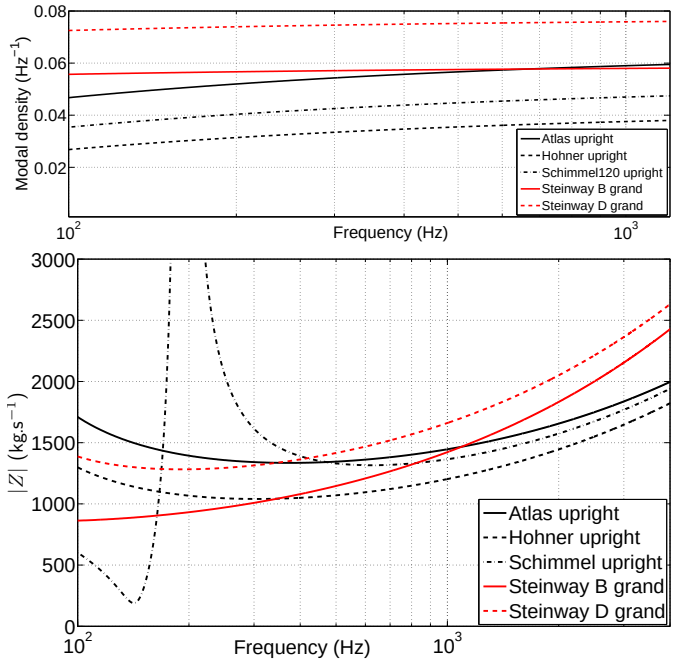

Figure 3: Comparison of three upright pianos and two grand pianos. Top: apparent modal density in low-frequency. Bottom: characteristic impedances (model artefact at 200 Hz for the Schimmel upright).

References

[1] E. J. Skudrzyk. *J.Acoust. Soc. Am.*, **67**(4):1105–1135, 1980.

[2] K. Ege, X. Boutillon, and M. Rébillat. *J. Sound Vibration*, **332**(5):1288-1305, 2013.

[3] K. Ege, X. Boutillon, and B. David. *J. Sound Vibration*, **325**(4-5): 852-869, 2009.

[4] J. Berthaut, M. N. Ichchou, and L. Jezequel. *Applied Acoustics*, **64**(11):1113–1136, 2003.

Modeling the grand piano

A. Chaigne[1,*], **J. Chabassier**[2], **P. Joly**[3]
[1] UME ENSTA, Palaiseau, France.
[2] Magique3d, Inria Sud Ouest, Talence, France.
[3] Poems, Inria, Palaiseau, France.
*Email: antoine.chaigne@ensta-paristech.fr

Abstract

A global model of a piano is presented. Its aim is to reproduce the main vibratory and acoustic phenomena involved in the generation of a piano sound from the initial blow of the hammer against the strings to the radiation from soundboard to the air. One first originality of the work is due to the string model which takes both geometrical nonlinear effects and stiffness into account. Other significant improvements are due to the combined modeling of the three main couplings between the constitutive parts of the instrument: hammer-string, string-soundboard and soundboard-air coupling.

1 Introduction

Simplifying assumptions were made in the model. The hammer is supposed to be perfectly aligned with the strings. The agraffe is assumed to be rigidly fixed. Both the string-soundboard and soundboard-air couplings are lossless. The soundboard is considered as simply supported along its edge, and the "listening" room is anechoic with no obstacle except the piano itself. The action of the mechanism prior to the shock of the hammer against the strings is ignored: the tone starts when the hammer hits the strings with an imposed velocity.

The physical parameters of hammers, strings and soundboards included in the model are obtained from standard string scaling and geometrical data from manufacturers, and complemented with our own measurements. For the losses in materials, approximate models based on experimental data are used. The numerical formulation of the model is based on a discrete formulation of the global energy of the system, which ensures stability (see [1]). This requires that the continuous energy of the problem is decaying with time. The global model of the piano is thus written according to this condition.

2 Strings

The string model accounts for large deformations, inducing geometrical nonlinearities, and intrinsic stiffness. The governing equations correspond to those of a nonlinear Timoshenko beam under axial tension. For the end conditions, we assume zero displacement (in both transverse and longitudinal directions) and zero moment at the agraffe. At the bridge, the end conditions are consecutive to coupling with the soundboard. The string is considered at rest at the origin of time. A source term accounts for the action of the hammer against the strings. A simple viscoelastic model accounts globally and approximately for the damping effects. The coefficients of this model are determined from measured sounds for each string, through comparisons between simulated and measured spectrograms. The global energy of this string model is preserved, under the condition $EA > T_0$ where E is the Young's modulus, A is the cross-sectional area of the string and T_0 its tension. This condition is always fulfilled in piano strings.

3 Hammer

The hammer's center of gravity is supposed to be moving along a straight line orthogonal to the strings at rest. The interaction force between the hammer and one string of a given note is distributed on a small portion of the string, through a spreading function localized around the impact point, and oriented in the transversal direction. The interaction force depends on the distance $d(t)$ between the hammer and the string: if $d(t)$ is larger than the mean hammer displacement $\overline{\xi}$, there is no contact and the force is zero. If $d(t) \leq \overline{\xi}$, the force is a function of the distance. According to previous studies, we define the function:

$$\Phi(d) = \left[\left(\overline{\xi} - d\right)^+\right]^p \qquad (1)$$

where $(\cdot)^+$ means "positive part of", and where p is a real positive nonlinear exponent. In practive, this coefficient varies between 1.5 and 3.5. In order to account further for the observed hysteretic behavior of the felt, a dissipative term is added in the expression of the force [2].

4 Soundboard

It is assumed that the only vibrating element is the soundboard, all other parts (rim, keybed, lid, iron frame...) being assumed to be perfectly rigid. A bidimensional Reissner-Mindlin plate model is considered. The bridge and ribs are considered as heterogeneities, and the orientation of the orthotropy axes can be space dependent. As a consequence, the density, thickness and elastic coefficients are functions of space. The soundboard is assumed to be simply supported on its edge. Finally, a source term is imposed in the transverse vertical direction. This term accounts for both the string's tension at the bridge and the air pressure jump. A modal approach has been adopted where the modal damping can be adjusted, mode by mode. This method is justified as long as the damping factor is small compared to the eigenfrequency and requires also that the modes are sufficiently well separated, a condition that is only strictly valid for the piano below 1 to 2 kHz [3]. The modal amplitudes are then solution of second-order uncoupled damped oscillators equations. Again, it is possible to exhibit an energy decaying with time for this part of the system.

5 Strings-soundboard coupling

A plausible, though not fully validated, model is used for the transformation of string longitudinal motion to bridge transverse motion. It is based on the observation that the strings form a slight angle with the horizontal plane due to both bridge height and soundboard curvature. It is assumed that the bridge moves in the vertical direction. When the hammer strikes the strings, it gives rise to a transversal wave which, in turn, induces a longitudinal wave, because of nonlinear geometrical coupling. The longitudinal wave travels 10 to 20 times faster than the transverse one, and comes first at the bridge. The resulting variation of tension is oriented in the direction of the string. Because of the angle formed by the string with the horizontal plane, this induces a vertical component of the longitudinal force at the bridge, in addition to the transverse force. The total bridge force is distributed in space in the soundboard by means of a rapidly decreasing regular function centered on the point where the string is attached on the soundboard. The associated kinematic boundary conditions are the continuity of string and soundboard velocities in the vertical direction, and the nullity of the velocity in the horizontal direction.

6 Soundboard-air coupling

For the propagation of piano sounds in free space, the rim is considered to be a rigid obstacle. The acoustic velocity and pressure are solutions of the linearized Euler equations in the unbounded domain which excludes the rim and the plate. Viscothermal losses in the air are ignored. The normal component of the acoustic velocity vanishes on the rim. The coupling between the 3D sound field and the vibrating soundboard obeys to the condition of continuity of the velocity normal components. Finally, the soundboard force is the pressure jump across both sides the plate. Again, this vibroacoustic system satisfies a property of energy decay.

Conclusion

This piano model accounts for the phenomena consecutive to amplitude dependence of string vibrations: presence of precursors [4], time-evolution of eigenfrequencies, transverse-longitudinal coupling and phantom partials. Due to the string-coupling, the presence of soundboard modes in the transients are reproduced in a natural way. Finally, due to the integration of ribs and bridges, the influence of soundboard modifications on the radiated sound can be investigated systematically.

References

[1] J. Chabassier, A. Chaigne, M. Duruflé and P. Joly, *Modeling the grand piano. Numerical Aspects*, in Proceedings of the 11th Int. Conf. on Math. and Num. Aspects of Waves (Waves 2013), Gammarth, Tunisia, 3-7 June 2013.

[2] A. Stulov, *Dynamic behavior and mechanical features of wool felt*, Acta Mechanica, **169(1)** (2004), pp. 13–21.

[3] K. Ege, X. Boutillon and M. Rébillat, *Vibroacoustics of the piano soundboard: (Non)linearity and modal properties in the low- and mid- frequency ranges*, J. Sound Vib., doi http://dx.doi.org/10.1016/j.jsv.2012.10.012.

[4] H. A. Conklin, J., *Generation of partials due to nonlinear mixing in a stringed instrument*, J. Acoust. Soc. Am., **105(1)** (1999), pp. 536–545.

Modeling the grand piano. Numerical Aspects.

J. Chabassier[1,*], **A. Chaigne**[2], **M. Duruflé**[1], **P. Joly**[3].
[1] Magique3d, Inria Sud Ouest, Talence, France.
[2] UME ENSTA, Palaiseau, France.
[3] Poems, Inria, Palaiseau, France.
*Email: juliette.chabassier@inria.fr

Abstract

This paper deals with the discretization of the global piano model described in [2]. We have to solve a complex system of coupled equations, where each subsystem has different spatial dimensions, which poses specific difficulties. The hammer-strings part is a 1D system governed by nonlinear equations. The soundboard is a 2D system with diagonal damping. The acoustic field is a 3D problem in an unbounded domain. Energy based methods allow to build an accurate and *a priori* stable scheme.

1 Introduction

The nonlinear parts of the problem (hammer-strings interaction, string vibration), the couplings between the subsystems and, more generally, the size of the problem in terms of computational burden, requires to guarantee the long-term numerical stability. In the context of wave equations, and in musical acoustics particularly, a classical and efficient technique to achieve this goal is to design numerical schemes based on the formulation of a discrete energy which is either constant or decreasing with time (see [7], [5]). Ensuring the positivity of the discrete energy, consistent with the continuous energy of the physical system, yields to a priori estimates for the unknowns of the problem, leading to the stability of the method. For most numerical schemes this imposes a restriction on the discretization parameters, as, for example, an upper bound for the time step.

In the discrete formulation, the coupling terms need a specific handling in order to guarantee a simple energy transfer, without any artificial introduction of dissipation or instabilities. Our choice here is to consider discrete coupling terms that cancel each other when computing the complete energy. In total, this method yields centered implicit couplings between the unknowns of the subsystems. The order of accuracy of the method is preserved, compared to the order of each subsystem taken independently, with no additional stability condition.

In view of the diversity of the various problems encountered in the full piano model, different discretization methods are chosen for each subsystem and for the coupling terms. We focus in the presentation on a general survey on the numerical resolution and on its main difficulties.

2 Strings

Standard high-order finite elements are used for the space discretization of the nonlinear system of equations that govern the vibrations of the strings. The spatial discretization parameters (mesh size and polynomial order) are selected to ensure a small numerical dispersion in the audio range. The time discretization of the strings system is probably the most novel and innovative method used in our piano numerical formulation. It combines a new scheme for nonlinear systems developped in [3], based on the expression of a discrete gradient, which ensures the conservation of an energy and an improved time discretisation for Timoshenko systems developped in [1]. A 1D nonlinear system must be solved at each time step. The solution is computed via an iterative modified Newton-Raphson method which needs the evaluation of both the scheme and its Jacobian with respect to the unknowns. It can be shown that a discrete energy is decaying, after extinction of the source. The stability of the numerical scheme can be derived from this property, with condition on the time step.

3 Hammer-strings coupling

Since the displacement of the hammer is a scalar function of time, we choose to solve the hammer-strings system by considering all together the unknowns of every strings belonging to the considered note, plus the hammer scalar unknown.The nonlinear hammer-strings interacting force is treated in a centered conservative way. A global discrete energy is shown to be decaying with respect to time when the hammer is given with an initial velocity.

4 Soundboard

The soundboard model assumes a diagonal damping in the modal basis. Its motion is first decomposed onto the modes of the undamped Reissner-Mindlin system belonging to the audio range, after semi-discretization in space with high-order finite elements as in [5]. These modes are only computed once for all, before starting the time iterations. This procedure yields decoupled equations which can be solved analytically in time, without introducing any additional approximation or numerical dispersion. The energy identity over time of the semi-discrete problem is also exactly satisfied with this method. However, one drawback of this choice is the loss of the local nature of the couplings with strings and air.

5 Strings-soundboard coupling at the bridge

The discrete formulation of the strings-soundboard continuity equations must ensure the stability of the resulting scheme, which couples the implicit three points nonlinear strings scheme described in 2 with the time semi-analytic soundboard model described in 4. New variables are introduced that represent the coupling forces associated to the conditions between strings and soundboard expressing the velocity continuity at the bridge. The strings and soundboard unknowns are evaluated on interleaved time grids : $\{n\,\Delta t\}$ for the strings, and $\{(n+1/2)\,\Delta t\}$ for the soundboard. The forces at the bridge are considered to be constant on time intervals of the form $[(n-1/2)\Delta t,\, (n+1/2)\Delta t]$. The discrete coupling condition is implicit and centered on times $n\,\Delta t$. Due to the linearity of the soundboard model, it is possible to express the soundboard unknowns as linear functions of the forces at the bridge. Thanks to this property, it is possible to perform Schur complements on the system which, originally, is globally implicit. An algorithm is then writen which updates first the unknowns of the strings and the forces at the bridge, and, in a second step, updates the unknowns of the soundboard.

6 Acoustic propagation and structural acoustics

The artifical truncation of the acoustic domain is done with with Perfectly Matched Layers [6]. The acoustical problem is solved in space with high-order finite elements and in time with an explicit leap-frog scheme, in view of the large number of degrees of freedom to consider. The acoustic velocity and pressure unknowns are calculated at times $\{n\,\Delta t\}$ and $\{(n+1/2)\,\Delta t\}$, respectively. In the variational formulation, the coupling between soundboard and air appears as source terms for the soundboard and the sound pressure equations. These terms are constructed in the discrete scheme so that they vanish when computing the energy, centered at times $n\,\Delta t$. An implicit coupling exists between the soundboard displacement and the acoustic pressure in the vicinity of the plate, which implies a change of basis between the physical and the modal representations of the soundboard. Due to the linearity of the equations, it is possible here to perform Schur complements, and to write an efficient algorithm that updates separately the plate (with a semi-analytic method) and the air variables (with the leap-frog scheme).

References

[1] J. Chabassier and S. Imperiale Stability and dispersion analysis of improved time discretisation for prestressed Timoshenko systems. Application to the stiff piano string. *Wave Motion*, to appear, doi : 10.1016/j.wavemoti.2012.11.002..

[2] Chabassier, J., Chaigne, A. and Joy, P. Modeling the grand piano. *Proceedings of Waves Conference*, 2013.

[3] J Chabassier, A Chaigne and P Joly. Energy preserving schemes for nonlinear Hamiltonian systems of wave equations: Application to the vibrating piano string. *Computer Methods in Applied Mechanics and Engineering*, vol 199, pp 2779–2795, 2010.

[4] J Chabassier and P Joly. Time domain simulation of a piano. Part I : model description. *Inria Research Report RR-8097*, Oct 2012.

[5] Derveaux, G., Chaigne, A., Joly, P., and Bécache, E. Time-domain simulation of a guitar: Model and method. *J. Acous. Soc. Am.*, 114(6):3368–3383, 2003.

[6] Imperiale, S. and Demaldent, E. (2011). Perfectly matched transmission problem with absorbing layers : application to anisotropic acoustics. *Int. J. Numer. Meth. Engng*, submitted.

[7] Rhaouti, L., Chaigne, A., and Joly, P. Time-domain modeling and numerical simulation of a kettledrum. *J. Acous. Soc. Am.*, 105(6):3545–3562, 1999.

3.3 Data assimilation for waves

Minisymposium organized by Philippe Moireau

Data assimilation: variational methods and back and forth nudging algorithm; Application to thermoacoustic tomography

D. Auroux[1,*], **J. Blum**[1], **S. Marinesque**[2]
[1] Laboratoire J. A. Dieudonné, Université de Nice Sophia Antipolis, Nice, France.
[2] Institut de Mathématiques de Toulouse, Université Paul Sabatier, Toulouse, France.
*Email: auroux@unice.fr

Abstract

We consider several data assimilation techniques for thermoacoustic tomography (TAT), which is a non invasive medical imaging technique. The inverse problem can be formulated as an initial condition reconstruction. Variational data assimilation schemes are compared with the back and forth nudging algorithm.

Introduction

ThermoAcoustic Tomography (TAT) is a hybrid imaging technique that uses ultrasound waves produced by a body submitted to a radiofrequency pulse, uniformly deposited throughout the body. The absorption of this initial energy causes a non-uniform thermal expansion, leading to the propagation of a pressure wave outside the body to investigate. This wave is then measured all around the body.

The physiological properties of the tissue are highly related to the absorption of the initial pulse. Considering that the initial illumination is a Dirac distribution in time, the problem of recovering the absorptivity of the investigated body from the thermoacoustic signal is equivalent to recovering the initial condition of a Cauchy problem involving the wave equation from the knowledge of the solution on a surface surrounding the imaging object [11].

Data assimilation consists in estimating the state of a system by combining via numerical methods two different sources of information: models and observations. Data assimilation makes it possible to answer a wide range of questions such as: optimal identification of the initial state of a system, perform reliable numerical forecasts, identify or extrapolate non observed variables by using a numerical model ... [6]. Most data assimilation methods are either variational methods such as 4D-VAR (based on optimal control theory) or sequential methods (filtering theory: Kalman filters). In linear situations, these two approaches are usually equivalent.

Variational data assimilation methods consider the equations governing the system as constraints and the problem is closed by using a variational principle. The well-known 4D-VAR, four dimensional variational data assimilation algorithm, is based on the minimization of a global cost function, which measures the discrepancy between the observations and the corresponding system states. Based on optimal control theory, the adjoint method allows one to compute the gradient of the cost function in a single numerical integration of the adjoint equation (see e.g. [8]). One iteration of the minimization process consists then in one forward integration of the model (in order to compute the cost function) and one backward integration of the adjoint model (in order to compute its gradient).

Nudging can be seen as a degenerate Kalman filter. Also known as the Luenberger or asymptotic observer [9], it consists in applying a Newtonian recall of the state value towards its direct observation. A main disadvantage of such sequential data assimilation methods is that it only takes into account past observations at a given time, and not future ones. Auroux and Blum proposed in [1] an original approach of backward and forward nudging (or *back and forth* nudging, BFN), which consists in initially solving the forward equations with a nudging term, and then, using the final state as an initial condition, in solving the same equations in a backward direction with a feedback term (with the opposite sign compared to the feedback term of forward nudging). This process is then repeated iteratively until convergence. The implementation of the BFN algorithm has been shown to be very easy, compared to other data assimilation methods [2].

This algorithm has been successfully applied to various problems: ODEs, PDEs, linear and nonlinear equations, ..., including viscous irreversible equations [2], [3], [4]. Note that for linear reversible systems, there has been a recent theoretical study of a similar algorithm [10].

From a practical point of view, these methods can be successfully used to manage the usual issues of the TAT inverse problem as incomplete data, external

source and variable sound speed (when given, however). So far, the theoretical convergence result for the nudging technique is based on a classical result about stabilization of the wave equation, which requires somehow a geometric optics condition. Numerical comparisons between variational and nudging algorithms, and also time reversal, have been performed.

Consider the following problem:

$$\begin{cases} \partial_{tt} u - \Delta u = 0, \quad (x,t) \in R^3 \times R_+, \\ u(x,0) = u_0(x), \quad x \in R^3, \\ \partial_t u(x,0) = 0, \quad x \in R^3, \end{cases} \tag{1}$$

where u_0 is the object to reconstruct. We assume that the support of u_0 is compact and included in the unit ball. The problem is the following: from the knowledge of u (possibly with noise) on a surface surrounding the unit ball, can we reconstruct u_0? Let u_{data} be the observed data.

The iterative BFN algorithm for TAT is the following [7]:

- Forward evolution:

$$\begin{cases} \partial_{tt} u_i - \Delta u_i = k \partial_t (u_{data} - u_i), \quad (x,t) \in R^3 \times [0;T], \\ u_i(x,0) = \tilde{u}_{i-1}(x,0), \quad x \in R^3, \\ \partial_t u_i(x,0) = \partial_t \tilde{u}_{i-1}(x,0), \quad x \in R^3, \end{cases} \tag{2}$$

  where T is such that the solution vanishes on the unit ball.

- Backward evolution:

$$\begin{cases} \partial_{tt} \tilde{u}_i - \Delta \tilde{u}_i = -\tilde{k} \partial_t (u_{data} - \tilde{u}_i), \quad (x,t) \in R^3 \times [0;T], \\ \tilde{u}_i(x,T) = u_i(x,T), \quad x \in R^3, \\ \partial_t \tilde{u}_i(x,0) = \partial_t u_i(x,T), \quad x \in R^3. \end{cases} \tag{3}$$

After each iteration, $\tilde{u}_i(x,0)$ is a new estimate of the object to reconstruct.

The nudging terms are added only on the observed domain, and parameters k and $\tilde{k}$ can be chosen equal as the considered equation (wave equation) is reversible. If we add a numerical or physical attenuation in the equation, then the backward nudging parameter might be increased, or one should refer to the recent improvement of the BFN algorithm in diffusive or attenuated situations [5].

In [7], the authors show that this algorithm converges (under standard hypotheses) with a geometric decay rate of the H_0^1 norm of the error.

References

[1] D. Auroux and J. Blum, *Back and forth nudging algorithm for data assimilation problems*, C. R. Acad. Sci. Sér. I, **340** (2005), pp. 873–878.

[2] D. Auroux and J. Blum, *A nudging-based data assimilation method: the Back and Forth Nudging (BFN) algorithm*, Nonlin. Proc. Geophys., **15** (2008), pp. 305–319.

[3] D. Auroux, P. Bansart, and J. Blum, *An evolution of the Back and Forth Nudging for geophysical data assimilation: application to Burgers equation and comparisons*, Inv. Prob. Sci. Eng., **21**(3) (2013), pp.399–419.

[4] D. Auroux and M. Nodet, *The back and forth nudging algorithm for data assimilation problems: theoretical results on transport equations*, ESAIM Control Optim. Calc. Var., **18**(2) (2012), pp.318–342.

[5] D. Auroux, J. Blum, and M. Nodet, *Diffusive Back and Forth Nudging algorithm for data assimilation*, C. R. Acad. Sci. Paris, Ser. I, **349**(15-16) (2011), pp.849-854.

[6] A. F. Bennett, *Inverse Modeling of the Ocean and Atmosphere*, Cambridge University Press, Cambridge, 2002.

[7] X. Bonnefond and S. Marinesque, *Application of a nudging technique to thermoacoustic tomography*, Inverse Problems Imaging, (2013), accepted for publication.

[8] F.-X. Le Dimet and O. Talagrand, *Variational algorithms for analysis and assimilation of meteorological. observations: theoretical aspects*, Tellus, **38A** (1986), pp. 97–110.

[9] D. Luenberger, *Observers for mutivariable systems*, IEEE Trans. Autom. Contr., **11** (1966), pp. 190–197.

[10] K. Ramdani, M. Tucsnak, and G. Weiss, *Recovering the initial state of an infinite-dimensional system using observers*, Automatica, **46** (2010), pp. 1616–1625.

[11] O. Scherzer, M. Grasmair, H. Grossauer, M. Haltmeier, and F. Lenzen, *Variational Methods in Imaging*, Appl. Math. Sci., vol. 167, Springer, New York, 2009.

Reconstructing initial data using iterative observers for wave type systems.

G. Haine[1,2,*]
[1] Université de Lorraine (Institut Élie Cartan),
[2] INRIA Nancy Grand-Est (CORIDA)
[*] Email: Ghislain.Haine@univ-lorraine.fr

Abstract

An iterative algorithm for solving initial data inverse problems from partial observations has been proposed in 2010 by Ramdani, Tucsnak and Weiss [1]. In this work, we are concerned with the convergence of this algorithm when the inverse problem is ill-posed, *i.e.* when the observations are not sufficient to reconstruct any initial data. We prove that the state space can be decomposed as a direct sum, stable by the algorithm, corresponding to the observable and unobservable part of the initial data. We show that this result holds for both locally distributed and boundary observation [2], [3].

Introduction

Let us start by briefly recalling the principle of the reconstruction method proposed in [1] in the simplified context of skew-adjoint generators and bounded observation operator. Given two Hilbert spaces X and Y (called *state* and *output* spaces respectively), let $A : \mathcal{D}(A) \to X$ be skew-adjoint operator generating a C_0-group $\mathbb{T}$ of isometries on X and let $C \in \mathcal{L}(X,Y)$ be a bounded observation operator. Consider the infinite dimensional linear system given by

$$\left\{ \begin{array}{ll} \dot{z}(t) = Az(t), & \forall t \geq 0, \\ y(t) = Cz(t), & \forall t \in [0,\tau]. \end{array} \right. \tag{1}$$

where z is the state and y the output function (where the dot symbol is used to denote the time derivative). Such systems are often used as models of vibrating systems.

The inverse problem considered here is to reconstruct the initial state $z(0) = z_0 \in X$ of system (1) knowing *the observation* $y(t)$ on the time interval $[0,\tau]$.

Then, let $z_0^+ \in X$ be a first arbitrary guess of z_0 and let us denote $A^+ = A - C^*C$ and $A^- = -A - C^*C$ and introduce the following initial and final Cauchy problems, for all $n \geq 1$, called respectively *forward* and *backward observers* of (1)

$$\left\{ \begin{array}{l} \dot{z}_n^+(t) = A^+ z_n^+(t) + C^* y(t), \quad \forall t \in [0,\tau], \\ z_1^+(0) = z_0^+, \\ z_n^+(0) = z_{n-1}^-(0), \quad \forall n \geq 2, \end{array} \right. \tag{2}$$

$$\left\{ \begin{array}{l} \dot{z}_n^-(t) = -A^- z_n^-(t) - C^* y(t), \quad \forall t \in [0,\tau], \\ z_n^-(\tau) = z_n^+(\tau), \quad \forall n \geq 2. \end{array} \right. \tag{3}$$

If we assume that (A,C) is exactly observable in time $\tau > 0$, i.e. that there exists $k_\tau > 0$ such that

$$\int_0^\tau \|y(t)\|^2 dt \geq k_\tau^2 \|z_0\|^2, \forall z_0 \in \mathcal{D}(A), \tag{4}$$

then, it is well-known that A^+ (respectively A^-) generate an exponentially stable C_0-semigroup $\mathbb{T}^+$ (respectively $\mathbb{T}^-$) on X. If we set $\mathbb{L} = \mathbb{T}_\tau^- \mathbb{T}_\tau^+$, then by [1, Proposition 3.7], we have $\delta := \|\mathbb{L}\|_{\mathcal{L}(X)} < 1$ and we obtain

$$\|z_n^-(0) - z_0\| \leq \delta^n \|z_0^+ - z_0\|, \quad \forall z_0 \in X, n \geq 1.$$

Note that since the choice of z_0^+ is arbitrary, we often choose zero in the applications.

1 Main results

In this work, we investigate the case without exact observability (for the wave equation for instance, this corresponds to the case where τ is too small for the geometric optic condition of Bardos, Lebeau and Rauch [4] to hold true). Remarking that systems (2) and (3) are still well defined in this case (at least when C is bounded), and that we still have

$$z_n^-(0) - z_0 = \mathbb{L}^n \left(z_0^+ - z_0 \right),$$

the following questions naturally arise : does the sequence $z_n^-(0)$ converge and if so, to what limit ?

Assume that $C \in \mathcal{L}(X,Y)$ is a bounded observation operator. Let us denote $\mathbb{S}$ the unitary C_0-group generated by A. Let $\Psi_\tau \in \mathcal{L}(X, L^2([0,\infty),Y)$ be the state-to-output operator defined by

$$\left(\Psi_\tau z_0\right)(t) = \left\{ \begin{array}{ll} C\mathbb{S}_t z_0, & \forall t \in [0,\tau], \\ 0, & \forall t > \tau. \end{array} \right.$$

Proposition 1. *We have the following decomposition of the state space X*

$$X = \operatorname{Ker} \Psi_\tau \oplus (\operatorname{Ker} \Psi_\tau)^\perp := \mathrm{V}_{\mathrm{Unobs}} \oplus \mathrm{V}_{\mathrm{Obs}},$$

and this decomposition is $\mathbb{L}$-stable.

Furthermore, $(\operatorname{Ker} \Psi_\tau)^\perp = \overline{\operatorname{Ran} \Phi_\tau}$, where

$$\Phi_\tau u = \int_0^\tau \mathbb{S}_{\tau-t}^* C^* u(t) dt,$$

is the input-to-state operator.

Theorem 2. *Denote by* Π *the orthogonal projection from* X *onto* $\mathrm{V_{Obs}}$*. Then the following statements hold true:*

1. *We have for all* $z_0 \in X, z_0^+ \in \mathrm{V_{Obs}}$*, and* $n \geq 1$*,*
$$\left\|(I-\Pi)\left(z_n^-(0)-z_0\right)\right\| = \left\|(I-\Pi)z_0\right\|.$$
2. *The sequence* $\left(\left\|\Pi\left(z_n^-(0)-z_0\right)\right\|\right)_{n\geq 1}$ *is strictly decreasing and verifies*
$$\left\|\Pi\left(z_n^-(0)-z_0\right)\right\| = \left\|z_n^-(0)-\Pi z_0\right\| \underset{n\to\infty}{\longrightarrow} 0.$$
3. *There exists a constant* $\alpha \in (0,1)$*, independent of* z_0 *and* z_0^+*, such that for all* $n \geq 1$*,*
$$\left\|\Pi\left(z_n^-(0)-z_0\right)\right\| \leq \alpha^n \left\|z_0^+ - \Pi z_0\right\|,$$
if and only if $\operatorname{Ran}\Phi_\tau$ *is closed in* X*.*

Using the framework of well-posed linear systems, we can use a result of Curtain and Weiss [5] to handle the case of (some) unbounded observation operators and derive a result similar to Theorem 2 (formally, we take $A^\pm = \pm A - \gamma C^* C$, with a suitably chosen $\gamma > 0$).

2 Application

Let Ω be a bounded open subset of $\mathbb{R}^N$, $N \geq 2$, with smooth boundary $\partial\Omega = \overline{\Gamma_0} \cup \overline{\Gamma_1}$, $\Gamma_0 \cap \Gamma_1 = \emptyset$ and Γ_0 and Γ_1 being relatively open in $\partial\Omega$. Denote by ν the unit normal vector of Γ_1 pointing towards the exterior of Ω. Consider the following wave system

$$\begin{cases} \ddot{w}(x,t) - \Delta w(x,t) = 0, & \forall x \in \Omega, t > 0, \\ w(x,t) = 0, & \forall x \in \Gamma_0, t > 0, \\ w(x,t) = u(x,t), & \forall x \in \Gamma_1, t > 0, \\ w(x,0) = w_0(x),\ \dot{w}(x,0) = w_1(x), & \forall x \in \Omega, \end{cases} \tag{5}$$

with u the input function (the control), and (w_0, w_1) the initial state. We observe this system on Γ_1, leading to

$$y(x,t) = -\frac{\partial(-\Delta)^{-1}\dot{w}(x,t)}{\partial\nu}, \quad \forall x \in \Gamma_1, t > 0. \tag{6}$$

Using a result of Guo and Zhang [6, Theorem 1.1], we can show that the system (5)–(6) fits into the framework described above and we can thus apply Theorem 2 (in its generalized version to unbounded observation operators) to recover the observable part of the initial data (w_0, w_1).

For instance, let us consider the configuration of Figure 1. We can easily obtain two subdomains of Ω (the striped ones on Figure 1), such that all initial data with support in the left (resp. right) one are in $\mathrm{V_{Obs}}$ (resp. in $\mathrm{V_{Unobs}}$).

We choose a suitable initial data to bring out these inclusions (in particular $w_1 \equiv 0$). We perform some simulations (using GMSH and GetDP) and obtain Figure 2, with 6% of relative error (in $L^2(\Omega)$) on the reconstruction of the observable part of the data after three iterations.

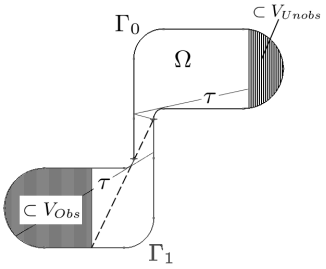

Figure 1: An example of configuration in 2D

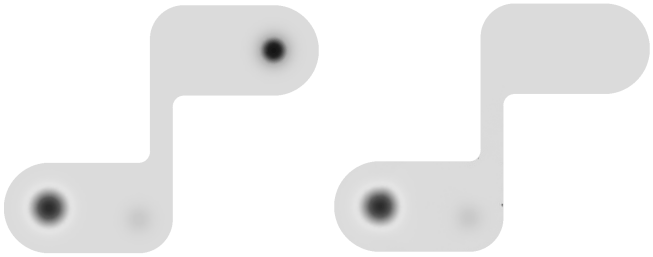

Figure 2: The initial position and its reconstruction after 3 iterations

References

[1] K. RAMDANI, M. TUCSNAK, AND G. WEISS, *Recovering the initial state of an infinite-dimensional system using observers*, Automatica, 46 (2010), pp. 1616–1625.

[2] G. HAINE, *Recovering the initial data of an evolution equation. Application to thermoacoustic tomography*, Submitted, (2012).

[3] G. HAINE, *Recovering the observable part of the initial data of an infinite-dimensional linear system*, Submitted, (2012).

[4] C. BARDOS, G. LEBEAU, AND J. RAUCH, *Sharp sufficient conditions for the observation, control, and stabilization of waves from the boundary*, SIAM J. Control Optim., 30 (1992), pp. 1024–1065.

[5] R. F. CURTAIN AND G. WEISS, *Exponential stabilization of well-posed systems by colocated feedback*, SIAM J. Control Optim., 45 (2006), pp. 273–297 (electronic).

[6] B.-Z. GUO AND X. ZHANG, *The regularity of the wave equation with partial dirichlet control and colocated observation*, SIAM J. Control Optim., 44 (2005), pp. 1598–1613.

Carleman estimates and applications to an inverse problem for waves

L. Baudouin[1], M. de Buhan[2], S. Ervedoza[3,*]
[1]CNRS, LAAS & Univ de Toulouse, Toulouse, France,
[2]CNRS, UMR 8145, MAP5, Univ. Paris Descartes, Paris, France,
[3]CNRS; IMT UMR 5219 & Univ. de Toulouse, Toulouse, France,
*Email: sylvain.ervedoza@math.univ-toulouse.fr

Abstract

In my talk, I will present some recent results obtained in [2] on an inverse problem for waves which consists of finding a potential in a wave equation through the knowledge of the flux of the solution of the equation. Our strategy is based on a Carleman estimate for the wave equation, see [5], [1], that we will use to design a convergent iterative process that yields the potential through the minimization of coercive quadratic functionals.

1 Introduction

1.1 Presentation of the inverse problem

The inverse problem we shall consider is the following.

Let Ω be a smooth bounded domain and Γ_0 be an open subdomain of $\partial\Omega$.

Given the source terms h and h_∂ and the initial data (w_0, w_1), considering the solution of

$$\begin{cases} \partial_t^2 W - \Delta W + QW = h, & \text{in } \Omega \times (0,T), \\ W = h_\partial, & \text{on } \partial\Omega \times (0,T), \\ W(0) = w_0,\ \partial_t W(0) = w_1, & \text{in } \Omega, \end{cases} \tag{1}$$

can we determine the unknown potential $Q = Q(x)$, assumed to depend only on $x \in \Omega$, from the additional knowledge of the flux

$$\mu = \partial_\nu W, \quad \text{on } \Gamma_0 \times (0,T) \tag{2}$$

of the solution?

1.2 Known results

As usual, this inverse problem consists in several questions:

• Uniqueness: is the map $Q \mapsto \mu$ injective?

• Stability: is the inverse of the map $Q \mapsto \mu$ continuous?

• Reconstruction: how can we compute Q from μ?

The question of uniqueness has been dealt with by Bukgheim and Klibanov in [4]. Later on, several works have been concerned with stability estimates, and in particular [7], [5], [1], [6] based on Carleman estimates provided the following conditions are satisfied:

$$\exists\, x_0 \notin \overline{\Omega},\ \Gamma_0 \supset \{x \in \partial\Omega,\ (x - x_0)\cdot\nu(x) \geq 0\}, \tag{3}$$

$$T > \sup_{x\in\Omega} |x - x_0|. \tag{4}$$

These *Geometric and Time* conditions, also known as the Γ conditions of J.-L. Lions, were first introduced in the context of controllability of waves when using multiplier techniques. Such conditions of geometrical nature are expected in such problem since the waves propagate at velocity one along the bicharacteristic rays and one should therefore guarantee that all the rays of Geometric Optics enter the observation domain to get nice uniqueness and stability results.

Under these conditions (3)–(4) indeed, [5], [1] prove Lipschitz stability results for this inverse problem.

However, despite the fact that the stability of this inverse problem is by now well-known, to our knowledge, no reconstruction process has been proposed in the literature. We intend to do so by using in a crucial way Carleman estimates.

2 Carleman estimates for waves

2.1 Results

We assume the following conditions

• the multipliers conditions (3)–(4).

• a regularity assumption:

$$W \in H^1((0,T); L^\infty(\Omega)), \tag{5}$$

• a positivity condition:

$$\exists \alpha > 0 \text{ such that } |w_0| > \alpha \text{ in } \Omega, \tag{6}$$

• An a priori bound on the potential Q:

$$\|Q\|_{L^\infty} \leq m. \tag{7}$$

And we propose the following algorithm:

• Initialization: $q^0 = 0$.

• Iteration: Given q^k, we set $\mu^k = \partial_t\left(\partial_\nu w[q^k] - \partial_\nu W[Q]\right)$ on $\Gamma_0 \times (0,T)$, where $w[q^k]$ denotes the solution of

$$\begin{cases} \partial_t^2 w - \Delta w + q^k w = h, & \text{in } \Omega\times(0,T),\\ w = h_\partial, & \text{on } \partial\Omega\times(0,T),\\ w(0) = w_0,\ \partial_t w(0) = w_1, & \text{in } \Omega, \end{cases} \quad (8)$$

corresponding to (1) with the potential q^k. We then introduce the functional J_{s,q^k} defined, for some $s>0$ that will be chosen independently of k, by

$$J_{s,q^k}(z) = \frac{1}{2s}\|e^{s\varphi}(\partial_t^2 z - \Delta z + q^k z)\|^2_{L^2(\Omega\times(0,T))} + \frac{1}{2}\|e^{s\varphi}(\partial_\nu z - \mu^k)\|^2_{L^2(\Gamma_0\times(0,T))}, \quad (9)$$

on the trajectories $z \in L^2(0,T;H_0^1(\Omega))$ such that $\partial_t^2 z - \Delta z + q^k z \in L^2(\Omega\times(0,T))$, $\partial_\nu z \in L^2(\Gamma_0\times(0,T))$ and $z(\cdot,0)=0$ in Ω, see (12) for the definition of φ. Let Z^k be a minimizer of the functional J_{s,q^k}, and then set

$$\tilde{q}^{k+1} = q^k + \frac{\partial_t Z^k(\cdot,0)}{w_0}, \quad (10)$$

where w_0 is the initial condition in (1).

Finally, using the function $T_m(q) = q$ if $|q|\le m$ and $T_m(q) = \text{sign}(q)m$ else, we set

$$q^{k+1} = T_m(\tilde{q}^{k+1}). \quad (11)$$

In the functional J_{s,q^k}, a weight function φ appears, which is the one coming from the Carleman estimate for the wave equation. It is chosen as follows. Let $\beta \in (0,1)$ (close to 1), and define, for $(x,t)\in\Omega\times(-T,T)$ and $\lambda>0$,

$$\varphi(x,t) = e^{\lambda\left(|x-x_0|^2-\beta t^2+C_0\right)}, \quad (12)$$

where $C_0>0$ is chosen such that $|x-x_0|^2-\beta t^2+C_0 \ge 1$ in $\Omega\times(-T,T)$.

We then obtain the following result:

Theorem 1 ([2]). *Assuming (3)–(7), there exist $\lambda>0$ and a constant $M>0$ such that for all $s\ge s_0(m)$ and $k\in\mathbb{N}$, the functional J_{s,q^k} is strictly coercive and therefore admits a unique minimizer Z^k, and*

$$\|e^{s\varphi(0)}(q^{k+1}-Q)\|_{L^2(\Omega)} \le \frac{M}{s^{1/4}}\|e^{s\varphi(0)}(q^k-Q)\|_{L^2(\Omega)}.$$

In particular, when s is large enough, the above algorithm converges: q^k converges to Q in $L^2(\Omega)$ as $k\to\infty$.

2.2 Comments

The proof of Theorem 1 relies upon a Carleman estimate for the wave equation, which can be found for instance in [5]. In [5], [1], it was used to derive Lipschitz stability estimates for the inverse problem under consideration, under the precise assumptions (3)–(7).

Our approach revisits these works by providing a constructing way to find the potential Q, based on the Carleman inequality directly. Note in particular that at each iteration, one only has to minimize the functional J_{s,q^k} which is strictly coercive and quadratic.

However, there are still numerical issues related to the fact that the weight functions are exponentials and may provide numerical overflow. Let us also mention the fact that even the convergence of the discrete inverse problem is not straightforward and requires to prove a discrete Carleman estimate, uniform with respect to the discretization parameters, see [3] for a detailed analysis in the 1-d setting.

References

[1] L. Baudouin. Lipschitz stability in an inverse problem for the wave equation. http://hal.archives-ouvertes.fr/hal-00598876/fr/

[2] L. Baudouin, M. de Buhan, and S. Ervedoza. Global carleman estimates for waves and applications. *Comm. Partial Differential Equations*, to appear.

[3] L. Baudouin and S. Ervedoza. Convergence of an inverse problem for discrete wave equations. *SIAM J. Control and Optim.*, to appear.

[4] A. L. Bukhgeĭm and M. V. Klibanov. Uniqueness in the large of a class of multidimensional inverse problems. *Dokl. Akad. Nauk SSSR*, 260(2):269–272, 1981.

[5] O. Y. Imanuvilov. On Carleman estimates for hyperbolic equations. *Asymptot. Anal.*, 32(3-4):185–220, 2002.

[6] O. Y. Imanuvilov and M. Yamamoto. Determination of a coefficient in an acoustic equation with a single measurement. *Inverse Problems*, 19(1):157–171, 2003.

[7] M. Yamamoto. Uniqueness and stability in multidimensional hyperbolic inverse problems. *J. Math. Pures Appl. (9)*, 78(1):65–98, 1999.

Improving numerical analysis via data assimilation - The wave equation case

Dominique Chapelle[1], **Nicolae Cîndea**[2], **P. Moireau**[1,*]
[1] Inria Saclay - Ile de France
[2] Université Clermont-Ferrand
*Email: philippe.moireau@inria.fr

Introduction

Data assimilation originally developed for weather forecasting has reached today new applications [4] where various types of measurements can be considered to handle the numerous uncertainties in the modeled system. In this work we focus on a wave system where part of the solution is measured on a subdomain and we demonstrate how the use of a sequential data assimilation strategy through the design of an observer can produce simulations with better global approximation capabilities than classical numerical approximations.

1 Methods

1.1 Observer theory

Let $\mathcal{H}$ be a Hilbert space and $A_0 : \mathcal{D}(A_0) \to \mathcal{H}$ be a self-adjoint, definite positive operator with compact resolvent. We consider the following system

$$\begin{cases} \ddot{w}(t) + A_0 w(t) = 0, & t > 0 \\ w(0) = w_0, \qquad \dot{w}(0) = w_1 \end{cases} \tag{1}$$

which we refer to as a "wave-like system". We rewrite this system in a first order form by denoting $x(t) = \begin{pmatrix} w(t) \\ \dot{w}(t) \end{pmatrix}$ such that

$$\begin{cases} \dot{x}(t) = Ax(t), & t > 0 \\ x(0) = x_0, \end{cases} \tag{2}$$

where $A : \mathcal{D}(A) \to \mathcal{X}$ with $\mathcal{D}(A) = \mathcal{D}(A_0) \times \mathcal{D}(A_0^{\frac{1}{2}})$, $\mathcal{X} = \mathcal{D}(A_0^{\frac{1}{2}}) \times \mathcal{H}$, is given by $A = \begin{pmatrix} 0 & I \\ -A_0 & 0 \end{pmatrix}$, and $x_0 = \begin{pmatrix} w_0 \\ w_1 \end{pmatrix}$. Observation theory is less studied than its dual control theory and consists in using some available measurements on the system

$$z = Hx, \tag{3}$$

with $H \in \mathcal{L}(\mathcal{X}, \mathcal{Z})$ an observation operator, in order to retrieve or filter some initial uncertainties. A new system

$$\begin{cases} \dot{\hat{x}}(t) = A\hat{x}(t) + K(z - H\hat{x}), & t > 0 \\ \hat{x}(0) = \hat{x}_0, \end{cases} \tag{4}$$

called an *observer*, is then built to track the actual system by comparing its outputs to the given observations and correcting the trajectory by use of a *filtering operator* K.

Despite a different objectives, control and observation are closely related, at least when considering linear systems and bounded – observation/control – operators in the sense that they are connected to a stabilization problem – in observation, the stabilization of the errors between the observer and the actual system

$$\begin{cases} \dot{\tilde{x}}(t) = (A - KH)\tilde{x}(t), & t > 0 \\ \tilde{x}(0) = \tilde{x}_0, \end{cases} \tag{5}$$

with $\tilde{x} = x - \hat{x}$. Therefore, some feedback control results can directly lead to the definition of an observer by deriving the adequate operator K. This is typically the case for the wave equation when we assume to measure in time the time-derivative of the variable on a subdomain ω

$$z = \dot{w}_{|\omega} = H_0 \dot{w} \quad \Rightarrow \quad H = (0 \quad H_0).$$

Hence with $K = H^*$, the control and observation problems lead to the same question of stabilizing the wave equation by adding a local dissipation in the subdomain following the stabilization conditions of Bardos-Lebeau-Rauch, meaning for any solution of (1) of initial condition $(w_0, w_1) \in H_0^1(\Omega) \times L^2(\Omega)$

$$\int_0^T \|\dot{w}(.,t)\|^2_{L^2(\omega)} \mathrm{d}t \geq C\big(\|w_0\|^2_{H^1(\Omega)} + \|w_1\|^2_{L^2(\Omega)}\big). \tag{6}$$

This *controllability* condition becomes an *observability* condition for the observation problem which ensures that observing the system on a subdomain gives enough information to estimate its state on the complete domain.

Some differences can however appear between observation and control when no control has been designed to use the prescribed measurements. This is typically the case when we consider observations of the main variable of a wave-like equation instead of its time derivative

$$z = w_{|\omega} = H_0 w \quad \Rightarrow \quad H = (H_0 \quad 0).$$

In that case, using $K = H^*$ for an adequate definition of the adjoint, [4] has proposed an original non-physical observer in the sense that it can only be realized as a virtual numerical system and not a physical one. We write

$$\begin{cases} \dot{\hat{w}}(x,t) = \hat{u}(x,t) + \gamma\, \mathcal{L}_\omega\big(z(t) - \hat{w}(\cdot,t)|_\omega\big), \\ \dot{\hat{u}}(x,t) - \Delta\hat{w}(x,t) = 0, \end{cases} \tag{7}$$

where we define the operator

$$\mathcal{L}_\omega : H^1(\omega) \to H_0^1(\Omega), \qquad \mathcal{L}_\omega\phi = \psi, \tag{8}$$

with ψ the solution of the following elliptic equation

$$\begin{cases} \Delta\psi = 0, & \text{in } \Omega\backslash\omega \\ \psi = 0, & \text{on } \partial\Omega \\ \psi = \phi, & \text{in } \overline{\omega} \end{cases} \tag{9}$$

Indeed, this observer modifies the classical first relation giving the "velocity" variable as the time-derivative of the "main variable" by incorporating a stabilization term. Then in [1], this original observer was demonstrated to exponentially converge to the observed system with an observability condition, here of the form

$$\int_0^T \|w(.,t)\|^2_{H^1(\omega)} \mathrm{d}t \geq C\big(\|w_0\|^2_{H^1(\Omega)} + \|w_1\|^2_{L^2(\Omega)}\big), \tag{10}$$

equivalent to that given by Bardos-Lebeau-Rauch.

1.2 Numerical analysis improvement

In [4], this observer was originally designed to model and numerically simulate systems with uncertain initial conditions or modeling errors. It was in particular applied to a complex mechanical system modeling the heart mechanical contraction observed by medical imaging protocols. However, the benefits of the "closed-loop" observer system over the standard discretization already appear on the classical numerical analysis where the discretization error can be reduced by use of the available measurements. Therefore in [2], we undertake the complete numerical analysis of the observer system for wave-like equations and show that – under some natural observability conditions – we can obtain error estimates that no longer deteriorate with the simulation duration, thereby providing a dramatic improvement over direct discretizations of the original system. This improvement is obtained as far as we can demonstrate that the performance of the continuous observer can be preserved through its discretization. In fact, some spurious high frequencies coming from the discretization are well known to deteriorate the stability constants – and then the convergence properties of the observer – at the discrete level. Following [3], we demonstrate in [2] that specific care in the discretization can ensure a uniform stability with respect to the discretization for the classical observer using time-derivative measurements but also for the original observer introduced in [4]. We therefore obtain an estimation of the type

$$\|\hat{x}_h^n - x(n\Delta t)\|_{\mathcal{X}} \leq C(\hat{x}_0)\max(\varepsilon, \varepsilon^2\, h^{-1}\Delta t),$$

with $\varepsilon = \max\{\Delta t, h^\theta\}$, instead of the classical

$$\|x_h^n - x(n\Delta t)\|_{\mathcal{X}} \leq C(T)(h^\theta + \Delta t^2),$$

for System (1).

Our new error estimates then rely on the classical cornerstones of numerical analysis formed by *stability* and *consistency* to which we add an *observability* condition leading to a new paradigm in numerical analysis.

References

[1] D. Chapelle, N. Cîndea, M. de Buhan, and P. Moireau, *Exponential convergence of an observer based on partial field measurements for the wave equation*, Math. Probl. Eng., vol. 2012, 2012.

[2] D. Chapelle, N. Cîndea, and P. Moireau, *Improving convergence in numerical analysis using observers*
The wave-like equation case, M3AS, 22(12), 2012.

[3] S. Ervedoza and E. Zuazua, *Uniformly exponentially stable approximations for a class of damped systems*, J. Math. Pures Appl. (9), 91(1):20–48, 2009.

[4] P. Moireau, D. Chapelle, and P. Le Tallec, *Filtering for distributed mechanical systems using position measurements: perspectives in medical imaging*, Inverse Problems, 25(3):035010, 25, 2009.

3.4 Control for the wave equation

Minisymposium organized by Belhassen Dehman

Behaviors of the energy of solutions of the wave equation with damping term

M. Daoulatli[1,*]
[1] Faculty of Sciences of Bizerte, University of Carthage and L.A.M.S.I.N, University of Tunis El-Manar
*Email: moez.daoultli@infcom.rnu.tn

Abstract

In this talk we present some results on the behavior of the energy of solutions of the wave equation with damping term in bounded domain or in exterior domain.

1 Wave equation with arbitrary localized damping

Let Ω be a smooth bounded domain in $\mathbb{R}^d$ with boundary $\partial\Omega$. Consider the following wave equation with a nonlinear internal damping:

$$\begin{cases} \partial_t^2 u - \Delta u + a(x)\, g(\partial_t u) = 0 & \mathbb{R}_+ \times \Omega \\ u = 0 & \mathbb{R}_+ \times \partial\Omega \\ (u(0), \partial_t u(0)) = (u_0, u_1) \end{cases} \quad (1)$$

Here Δ denotes the Laplace operator in the space variables. The nonlinear terms satisfy:

- $g : \mathbb{R} \to \mathbb{R}$ is a continuous, monotone increasing function, $g(0) = 0$.

  We assume that g is linearly bounded at infinity

  $$m_0 y^2 \le g(y)\, y \le M_0 y^2, \quad |y| > 1$$

- $a(x)$ is a non negative function in $L^\infty(\Omega)$. $a(x) \ge a_0 > 0$ a.e. in ω, where $\omega \subset\subset \Omega$ an arbitrary non-empty subdomain.

- Energy Functional:

  $$E_u(t) = \frac{1}{2}\int_\Omega \left(|\nabla u(t,x)|^2 + |\partial_t u(t,x)|^2 \right) dx.$$

According to [Lasiecka-Tataru] there exists a concave strictly increasing function and linear at infinity $h_0(s)$ defined for $s \ge 0$, with $h_0(0) = 0$ and

$$h_0(g(y)\, y) \ge \epsilon \left((g(y))^2 + y^2 \right) \quad \text{for} \quad |y| \ll 1.$$

Theorem: $u(t)$ is the solution to the non-linear problem with initial condition $(u_0, u_1) \in X = \left(H_0^1(\Omega) \cap H^2(\Omega)\right) \times H_0^1(\Omega)$. Then we have

$$E_u(t) \le S(t - T), \qquad t \ge T$$

where $S(t)$ is the solution of the following nonlinear ordinary differential equation

$$\frac{dS}{dt} + \frac{1}{T} h^{-1} \circ \psi^{-1}\left(\frac{S}{K}\right) = 0, \qquad S(0) = E_u(0).$$

where $K = C(T, \|(u_0, u_1)\|_X)$,

$$h(s) = s + \mathfrak{m}_a(\Omega_T)\, h_0\left(\frac{s}{\mathfrak{m}_a(\Omega_T)}\right)$$

and $\psi : \mathbb{R}_+ \to \mathbb{R}_+$, strictly increasing function, defined by

$$\psi(s) = \left(\ln\left(\frac{1}{s} + 1\right)\right)^{-2\beta} + s; \ 0 < \beta < 1.$$

2 Wave equation with localized damping and external force

$$\begin{cases} \partial_t^2 u - \mathcal{A}u + a(x)\, g(\partial_t u) = f & \mathbb{R}_+ \times \Omega \\ u = 0 & \mathbb{R}_+ \times \partial\Omega \\ (u(0), \partial_t u(0)) = (u_0, u_1) \end{cases} \quad (2)$$

- $[a_{ij}(x)]_{ij}$ smooth, symmetric $\mathcal{A} = \operatorname{div}[(a_{ij}(x)\, \partial_{x_j})]$.
- Uniform ellipticity. $c > 0$ $\sum_{i,j=1}^d a_{ij}(x)\, \xi_i \xi_j \ge c \sum_{i=1}^d \xi_i^2$
- $g : \mathbb{R} \to \mathbb{R}$: continuous, monotone increasing function, $g(0) = 0$. We assume that g is linearly bounded at infinity.
- $f \in L^2_{loc}\left(\mathbb{R}_+, L^2(\Omega)\right)$.
- Energy Functional: $\nabla_{\mathcal{A}} \equiv \left(\sum_{j=1}^d a_{ij}(x) \partial_{x_j}\right)_i$.

  $$E_u(t) = \frac{1}{2}\int_\Omega \left(|\nabla_{\mathcal{A}} u(t,x)|^2 + |\partial_t u(t,x)|^2 \right) dx.$$

Before introducing our result, we remind the geometric control condition of Bardos- Lebeau and Rauch

GCC (ω, T) geometrically controls Ω, i.e. every generalized geodesic travelling with speed 1 and issued at $t = 0$, enters the set ω in a time $t < T$.

Theorem: We assume that (ω, T) satisfies the assumption (GCC) and

$$\Gamma(t) = \|f(t,.)\|^2_{L^2(\Omega)} + \psi^*\left(\|f(t,.)\|_{L^2(\Omega)}\right) \in L^1_{loc}(\mathbb{R}_+)$$

where ψ^* is the convex conjugate of the function ψ, defined by

$$\psi(s) = \begin{cases} \frac{1}{2T} h^{-1}\left(\frac{s^2}{8C_T e^T}\right) & s \in \mathbb{R}_+ \\ +\infty & s \in \mathbb{R}^*_- \end{cases}$$

Let $u(t)$ is the solution to the non-linear problem (2) with initial condition $(u_0, u_1) \in H^1_0 \times L^2$. Then we have

$$E_u(t) \leq 4e^T \left(S(t-T) + \int_{t-T}^{t} \Gamma(s)\, ds\right), \qquad t \geq T$$

where $S(t)$ is the solution of

$$\frac{dS}{dt} + \frac{1}{4T} h^{-1}\left(\frac{S(t)}{K}\right) = \Gamma(t), \qquad S(0) = E_u(0).$$

3 Wave equation with linear damping in exterior domain

$$\begin{cases} \partial_t^2 u - \Delta u + a(x)\,\partial_t u = 0 & \mathbb{R}_+ \times \Omega \\ u = 0 & \mathbb{R}_+ \times \partial\Omega \\ (u(0), \partial_t u(0)) = (u_0, u_1) \end{cases} \tag{3}$$

- Ω open smooth exterior domain in $\mathbb{R}^d$ $(d \geq 2)$ with boundary $\partial\Omega$.
- $a \in L^\infty(\Omega)$ and $a(x) \geq 0$.
- Space: $\mathcal{H} \equiv H^1_0(\Omega) \times L^2(\Omega)$.

Before introducing our results we shall state several assumptions:

- There exists $L > 0$ such that

$$a(x) > \epsilon_0 > 0 \text{ for } |x| \geq L.$$

- (ω, T) geometrically controls Ω, i.e. every generalized geodesic travelling with speed 1 and issued at $t = 0$, enters the set ω in a time $t < T$.

Theorem: We assume that Hyp A holds and (ω,T) geometrically controls Ω. Then there exists $C_0 > 0$ such that the following estimates

$$E_u(t) \leq C_0 (1+t)^{-1} I_0 \text{ and } \|u(t)\|^2_{L^2} \leq C_0 I_0$$

hold for every solution u of (3) with initial data (u_0, u_1) in $H^1_0(\Omega) \times L^2(\Omega)$, where $I_0 = \|u_0\|^2_{H^1} + \|u_1\|^2_{L^2}$.

4 Wave equation with nonlinear damping in exterior domain

$$\begin{cases} \partial_t^2 u - \Delta u + a(x)\,|\partial_t u|^{r-1}\,\partial_t u = 0 & \text{in } \mathbb{R}_+ \times \Omega, \\ u = 0 & \text{on } \mathbb{R}_+ \times \Gamma, \\ u(0,x) = u_0 \quad \text{and} \quad \partial_t u(0,x) = u_1. \end{cases} \tag{4}$$

- $a \in L^\infty(\Omega)$ and $a(x) \geq 0$.
- $1 < r \leq 1 + \frac{2}{d}$.

Theorem: We assume that Hyp A holds and (ω,T) geometrically controls Ω. Let

$$\begin{array}{ll} \gamma > 0 & \text{if } 1 < r < 1 + \frac{2}{d} \\ 0 < \gamma < \frac{2}{r-1} & \text{if } r = 1 + \frac{2}{d} \end{array}$$

Then there exists $C_0 > 0$ such that the following estimate

$$E_u(t) \leq C_0 (\ln(2+t))^{-\gamma} I(u_0, u_1), \text{ for all } t \geq 0$$

holds for every solution u of (4) with initial data (u_0, u_1) in $H^1_0(\Omega) \cap H^2(\Omega) \times H^1_0(\Omega)$, such that

$$\left\|\left(\ln\left(1+|x|^2\right)\right)^{\frac{\gamma}{2}} \nabla u_0\right\|_{L^2} + \left\|\left(\ln\left(1+|x|^2\right)\right)^{\frac{\gamma}{2}} u_1\right\|_{L^2} <$$

References

[1] M. Daoulatli, I. Lasiecka and D. Toundykov, *Uniform energy decay for a wave equation with partially supported nonlinear boundary dissipation without growth restrictions*, Discrete Contin. Dyn. Syst., Ser. S 2, No. 1. **44** (2009), pp. 67-94 .

[2] M. Daoulatli, *Rates of decay for the wave systems with time dependent damping*, Discrete Contin. Dyn. Syst. 31, No. 2, 407-443 (2011).

[3] M. Daoulatli, *Behaviors of the energy of solutions of the wave equation with damping and external force.*, J. Math. Anal. Appl. 389, No. 1, 205-225 (2012).

[4] M. Daoulatli, *Energy decay rates for solutions of the wave equation with linear damping in exterior domain*, (Arxiv 03/2012).

[5] M. Daoulatli, *Energy decay rates for solutions of the wave equation with superlinear damping in exterior domain*, (Arxiv 07/2012).

Controllability of two coupled wave equations on a compact manifold

B. Dehman[1], J. Le Rousseau[2,*], M. Léautaud[3]
[1] Département de Mathématiques, Faculté des sciences de Tunis, Université de Tunis El Manar
[2] MAPMO, CNRS UMR 6628, Fédération Denis-Poisson, FR CNRS 2964, Université d'Orléans.
[3] IMJ-PRG, UMR CNRS 7586, Universit Paris Diderot - Paris 7. *Email: jlr@univ-orleans.fr

Abstract

We consider the exact controllability problem on a compact manifold Ω for two coupled wave equations, with a control function acting on one of them only. Action on the second wave equation is obtained through a coupling term. We introduce the time $T_{\omega\to\mathcal{O}\to\omega}$ for which all geodesics traveling in Ω go through the control region ω, then through the coupling region $\mathcal{O}$, and finally come back in ω. We prove that the system is controllable if and only if both ω and $\mathcal{O}$ satisfy the Geometric Control Condition and the control time is larger than $T_{\omega\to\mathcal{O}\to\omega}$. Next, we prove that the associated HUM control operator is a pseudodifferential operator.

1 Introduction

Let (Ω, g) be a $\mathscr{C}^\infty$ compact connected n-dimensional Riemannian manifold without boundary. We denote by Δ the (negative) Laplace-Beltrami operator on Ω for the metric g, and $P = \partial_t^2 - \Delta$ denotes the d'Alembert operator (or wave operator) on the manifold $\mathbb{R}\times\Omega$. We take two smooth functions b_ω and $b \geq 0$ on Ω. We consider the controllability problem for the system of coupled wave equations

$$\begin{cases} Pu_1 + b(x)\ u_2 = 0 & \text{in } (0,T)\times\Omega, \\ Pu_2 = b_\omega(x)\ f & \text{in } (0,T)\times\Omega. \end{cases} \tag{1}$$

Here, the state of the system is $(u_1, u_2, \partial_t u_1, \partial_t u_2)$ and f is our control function, with possible action on the set $\omega = \{b_\omega \neq 0\}$. Taking zero initial data, together with a forcing term $f \in L^2((0,T)\times\Omega))$, the associated solution of (1) lies for any time in the space $H^2(\Omega)\times H^1(\Omega)\times H^1(\Omega)\times L^2(\Omega)$ as $u_2 \in L^2(0,T;H^1(\Omega))$. Hence, there is a gain of regularity for the uncontrolled variable u_1 (see [1]).

In this context, the adapted control problem is given by the following definition.

Definition 1.1. We say that System (1) is controllable in time $T > 0$ if for any initial data $(u_1^0, u_2^0, u_1^1, u_2^1) \in H^2(\Omega)\times H^1(\Omega)\times H^1(\Omega)\times L^2(\Omega)$ and any target $(\tilde{u}_1^0, \tilde{u}_2^0, \tilde{u}_1^1, \tilde{u}_2^1) \in H^2(\Omega)\times H^1(\Omega)\times H^1(\Omega)\times L^2(\Omega)$ there exists a control function $f \in L^2((0,T)\times\Omega)$ such that the solution of (1) issued from $(u_1, u_2, \partial_t u_1, \partial_t u_2)|_{t=0} = (u_1^0, u_2^0, u_1^1, u_2^1)$, satisfies $(u_1, u_2, \partial_t u_1, \partial_t u_2)|_{t=T} = (\tilde{u}_1^0, \tilde{u}_2^0, \tilde{u}_1^1, \tilde{u}_2^1)$.

A natural necessary and sufficient condition to obtain controllability for wave equations is to assume that the control set satisfies the Geometric Control Condition (GCC) defined in [7], [2]. For $\omega \subset \Omega$ and $T > 0$, we shall say that (ω, T) satisfies GCC if every geodesic traveling at speed one in Ω meets ω in a time $t < T$. We say that ω satisfies GCC if there exists $T > 0$ such that (ω, T) satisfies GCC. We also set $T_\omega = \inf\{T > 0, (\omega, T) \text{ satisfies GCC}\}$.

Definition 1.2. Given two sets ω and $\mathcal{O}$ both satisfying GCC, we set $T_{\omega\to\mathcal{O}\to\omega}$ to be the infimum of times $T > 0$ for which the following assertion is satisfied:

every geodesic traveling at speed one in Ω meets ω in a time $t_0 < T$, meets $\mathcal{O}$ in a time $t_1 \in (t_0, T)$ and meets ω again in a time $t_2 \in (t_1, T)$.

Note that in general $T_{\omega\to\mathcal{O}\to\omega} \neq T_{\mathcal{O}\to\omega\to\mathcal{O}}$, and that we have the estimate

$$\max(T_\mathcal{O}, T_\omega) \leq T_{\omega\to\mathcal{O}\to\omega} \leq 2T_\omega + T_\mathcal{O}.$$

We can now state our controllability result (in the sense of Definition 1.1).

Theorem 1.3. *Suppose that $b \geq 0$ on Ω, and that both sets $\omega = \{b_\omega \neq 0\}$ and $\mathcal{O} = \{b \neq 0\}$ satisfy GCC. Then, System (1) is controllable if $T > T_{\omega\to\mathcal{O}\to\omega}$ and is not controllable if $T < T_{\omega\to\mathcal{O}\to\omega}$.*

The proof of this result is based on the quantification of the transport of a (vectorial) microlocal defect measure [4], [8] along the bicharacteristic flow. Such measures where first used for this type of results in the work of G. Lebeau [5].

According to the Hilbert Uniqueness Method (HUM) of J.-L. Lions [6], the controllability property of Theorem 1.3 is equivalent to an observability inequality for the adjoint system. More precisely,

System (1) is exactly controllable in time T if and only if the inequality

$$E_{-1}(v_1(0)) + E_0(v_2(0)) \leq C \int_0^T \int_\omega |b_\omega v_2|^2 dx\ dt \quad (2)$$

holds for every $(v_1, v_2) \in \mathscr{C}^0([0,T]; H^{-1}(\Omega) \times L^2(\Omega)) \cap \mathscr{C}^1([0,T]; H^{-2}(\Omega) \times H^{-1}(\Omega))$ solutions of

$$\begin{cases} Pv_1 = 0 & \text{in } (0,T)\times\Omega, \\ Pv_2 = -b(x)\ v_1 & \text{in } (0,T)\times\Omega. \end{cases} \quad (3)$$

In the observability inequality (2), we use the notation

$$E_k(v) = \|v\|^2_{H^k(\Omega)} + \|\partial_t v\|^2_{H^{k-1}(\Omega)}, \quad k \in \mathbb{Z},$$

where the space $H^s(\Omega)$ is endowed with the norm

$$\|v\|_{H^s(\Omega)} = \|(1-\Delta)^{\frac{s}{2}} v\|_{L^2(\Omega)}, \quad s \in \mathbb{R},$$

and the associated inner product.

An important feature of the Hilbert Uniqueness Method, as presented by J.-L. Lions [6], lays in the following two facts: the control one obtains, f_{HUM} minimizes the cost functional $\|f\|^2_{L^2((0,T)\times\Omega)}$ among all $f \in L^2((0,T)\times\Omega)$ realizing a control for System (1); it is the optimal L^2-control. Moreover, it is itself a solution of the adjoint system (3) for appropriate initial data, say W^0.

The Gramian operator $\mathcal{L}$ associated to Systems (1)-(3) is given by

$$\int_0^T \int_\omega |b_\omega v_2|^2 dx\ dt = \langle \mathcal{L}V, V\rangle\,,$$

where v_2 is the solution of (3) associated to the initial data $(v_1, v_2, \partial_t v_1, \partial_t v_2)|_{t=0} = V$. If the observability inequality (2) is satisfied, then, the HUM control operator is the inverse of the mapping $\mathcal{L}$. From the initial data to be controlled, the HUM operator maps the associated initial data W^0 for the adjoint system, giving rise to the control function f_{HUM}.

The second main goal of this article is to give an explicit representation of the HUM operator. We prove the following result

Theorem 1.4. *1. The Gramian operator is a matrix of pseudodifferential operators of order zero. The determinant of its principal symbol takes essentially the following form*

$$\int_0^T \int_0^T (b_\omega^2 \circ \varphi_{t_1})(b_\omega^2 \circ \varphi_{t_2}) \Big(\int_{t_1}^{t_2} b \circ \varphi_\sigma d\sigma \Big)^2 dt_1 dt_2,$$

where φ_σ denotes the geodesic flow on $S^*\Omega$.

2. This operator is elliptic if and only if $T > T_{\omega\to\mathcal{O}\to\omega}$.

3. For $T > T_{\omega\to\mathcal{O}\to\omega}$, the HUM control operator is also a matrix of pseudodifferential operators of order zero.

The proof of this second result orginates in part from the work of B. Dehman and G. Lebeau [3].

References

[1] F. Alabau-Boussouira, *A two-level energy method for indirect boundary observability and controllability of weakly coupled hyperbolic systems*, SIAM J. Control Optim., **42** (2003), pp. 871–906.

[2] C. Bardos, G. Lebeau, and J. Rauch, Sharp sufficient conditions for the observation, control, and stabilization of waves from the boundary, SIAM J. Control Optim., **30** (1992), pp. 1024–1065.

[3] B. Dehman and G. Lebeau, *Analysis of the HUM control operator and exact controllability for semilinear waves in uniform time*, SIAM J. Control Optim., **48** (2009), pp. 521–550.

[4] P. Gérard, *Microlocal defect measures*, Comm. Partial Differential Equations, **16** (1991), pp. 1761–1794.

[5] G. Lebeau, *Équation des ondes amorties*, Algebraic and geometric methods in mathematical physics (Kaciveli, 1993), Math. Phys. Stud., **19**, pp. 73–109, Kluwer Acad. Publ., Dordrecht, 1996.

[6] J.-L. Lions, *Contrôlabilité exacte, perturbations et stabilisation de systèmes distribués. Tome 1*, Recherches en Mathématiques Appliquées, **8**, Masson, Paris, 1988.

[7] J. Rauch and M. Taylor, *Exponential decay of solutions to hyperbolic equations in bounded domains*, Indiana Univ. Math. J., **24** (1974), pp. 79–86.

[8] L. Tartar, *H-measures, a new approach for studying homogenisation, oscillations and concentration effects in partial differential equations*, Proc. Roy. Soc. Edinburgh Sect. A, **115** 1990, pp. 193–230.

Large Time Behaviour of some Damped Equations

M. Khenissi[1,*]
[1] Ecole Supérieure des Sciences et de Technologie
de Hammam Sousse, Tunisie
*Email: Moez.Khenissi@fsg.rnu.tn

Abstract

In this talk, we give a survey of our works on the long-time behavior of some damped equations in exterior domains. As model, we study the wave equation, the elasticity system and the Schrödinger equation. We prove in particular, how the distribution of the resonances depend on the geometry of the domain and the position of the support of the damping terms.

1 Wave equation

Let $\Theta \subset \mathbb{R}^d$ be a compact set with C^∞-smooth boundary Γ. Denote by $\Omega = \mathbb{R}^d \backslash \Theta$ the exterior domain and $a(x) \in C_0^\infty(\Omega, \mathbb{R}_+)$.
For the trapping domains, when no uniform energy decay is hoped, the idea of **stabilization** is to add a **dissipative term** to the equation to **force** the energy of the solution to decrease **uniformly.**

We consider the Cauchy problem for wave equation with an internal damping term

$$\begin{cases} (\partial_t^2 - \Delta + 2a(x)\partial_t)u = 0 & \text{on } \mathbb{R}_+ \times \Omega \\ u(t)_{/\partial\Omega} = 0 & \forall\ t \in \mathbb{R}_+ \\ u(0) = u_0, \partial_t u(0) = u_1 \end{cases} \tag{1.1}$$

For u satisfying (1.1), we define $E_R(u(t))$ the local energy on $\Omega_R = \{|x| < R\} \cap \Omega$,

$$E_R(u(t)) = \int_{\Omega_R} \left[|\nabla u|^2 (t) + |\partial_t u|^2 (t) \right] dx. \tag{1.2}$$

Definition 1.1 (E.G.C.) *[2] We say that the subset ω of Ω satisfies the Exterior Geometric Control (E.G.C.) if any trapped ray*[1] *meets ω.*

Let $\chi \in C_0^\infty(\mathbb{R}^d)$, $\chi = 1$ on B_R and $R_\chi(\lambda) = \chi R(\lambda)\chi$, be the cutoff outgoing resolvent defined as following

$$R_\chi(\lambda) f = \int_0^{+\infty} e^{-i\lambda t} \chi u(t)\, dt, \text{ in } \{\mathrm{Im}\lambda < \mathfrak{o}\}. \tag{1.3}$$

where $u(t)$ is a solution of (1.1) with $(u_0, u_1) = (0, \chi f)$. $R_\chi(\lambda)$ as an operator from $L^2(\Omega)$ to $H_0^1(\Omega)$, which is holomorphic on $\{\mathrm{Im}\lambda < \mathfrak{o}\}$, extends meromorphically to the whole complex plane $\mathbb{C}$ for odd dimensions and to the logarithmic Riemann surface for even dimension.

First, we have to localize the poles of this extension, called resonances ([6], [3]).

Theorem 1.2 *Suppose that $\omega = \{x \in \Omega, a(x) > 0\}$ satisfies the E.G.C., then*

$$\left\| \chi(-\Delta + \lambda^2 + i\lambda a(x))^{-1} \chi \right\|_{L^2(\Omega) \to L^2(\Omega)} \leq \frac{c}{1 + |\lambda|}.$$

We deduce that there exists $c > 0$ such that for all $(u_0, u_1) \in H^1_{comp} \times L^2_{comp}$

$$\begin{aligned} E_R(u(t)) &\leq c e^{-\delta t} E(u(0))) \text{ , if } d \text{ is odd} \\ E_R(u(t)) &\leq \frac{c}{t^d} E(u(0))) \text{ , if } d \text{ is even} \end{aligned}$$

For the elasticity system, we prove in [8] and in odd dimension the same result as the wave equation and in [7] we gives the localisation of the resonances for the elasticity system with boundary dissipative term.

2 Schrödinger equation

As the wave equation, when Ω is a non-trapping, we get for the Schrödinger equation, the uniform decay (polynomial) of the local energy: $\forall f \in L^2_{comp}(\Omega)$

$$E_R(t) := \left\| e^{it(-\Delta_D)} f \right\|_{L^2(\Omega_R)} \leq \frac{c}{t^{d/2}} \|f\|_{L^2}, \quad \forall t > 0$$

We consider the following stabilization problem of the Schrödinger equation [2]

$$\begin{cases} i\partial_t u - \Delta u + ia(x)u = 0 & \text{in } \mathbb{R} \times \Omega \\ u(0, .) = f & \text{in } \Omega \\ u_{/\mathbb{R}\times\partial\Omega} = 0 \end{cases} \tag{2.1}$$

Theorem 2.1 *Suppose that $\omega = \{x \in \Omega, a(x) > 0\}$ satisfies the E.G.C., then $\exists\ \sigma_0$ and C such that for any $|\Im m\tau| < \sigma_0$*

$$\|\chi(-\tau - \Delta + ia)^{-1}\chi\|_{L^2 \to L^2} \leq C.$$

We deduce that there exists $c > 0$ such that for all $u_0 \in L^2_{comp}$

$$\left\| \chi e^{it(-\Delta_D + ia)} u_0 \right\|_{L^2(\Omega)} \leq \frac{c}{t^{d/2}} \|u_0\|_{L^2(\Omega)}$$

[1] A trapped ray is a ray which can not leave B_R.

It is well known that the Schrödinger equation enjoys some smoothing properties. The solutions of (2.1) satisfy the Kato-smoothing effect if and ally if Ω is non trapping. By analogy to the stabilization problem, when Ω is trapping, we introduce the **forced smoothing effect** for Schrödinger equation. It consists **to act** on the equation to produce some smoothing effects.

$$\begin{cases} i\partial_t u - \Delta u + ia(x)(-\Delta)^{\frac{1}{2}}a(x)u = 0 & \text{in} \quad \mathbb{R}\times\Omega, \\ u(0,.) = u_0 & \text{in} \quad \Omega, \\ u|_{\mathbb{R}\times\partial\Omega} = 0, \end{cases} \tag{2.2}$$

In the case of bounded domain, under G.C.C. on the set $w = \{a \neq 0\}$, Aloui [1] proved a **weak** Kato-Smoothing effect:

$$\|u\|_{L^2([\varepsilon,T],H_D^{s+1}(\Omega))} \leq c(\varepsilon)\,\|u_0\|_{H_D^s(\Omega)}\,,$$

where $0 < \varepsilon < T < \infty$. Then by iteration of the last result, C^∞-**smoothing effect** is proved.

Note that these smoothing effects hold away from $t = 0$ and they seem strong compared with the Kato-effect for which the GCC is necessary. Therefore the case when $w = \{a \neq 0\}$ does not control geometrically Ω is very interesting.

We prove that the Geometric control condition is **not necessary** to obtain the forced C^∞- smoothing effect. Let $A_a = -i\Delta_D - a(x)(-\Delta)^{\frac{1}{2}}a(x)$.

Let $O = \cup_{i=1}^N O_i \subset \mathbb{R}^d$ be the union of a finite number of bounded strictly convex bodies, O_i, satisfying the conditions of Ikawa.

Let B be a bounded domain containing O such that $\Omega_0 = O^c \cap B$ is connected, where $O^c = \mathbb{R}^d \setminus O$.

Theorem 2.2 *[5] Assume $a \in C^\infty(\Omega_0)$ is constant near the boundary of B. Then $\exists\ \sigma_0$ and c such that for any $|\Im m\tau| < \sigma_0$*

$$\left\|(-\Delta_D - \tau + ia(x)(-\Delta_D)^{\frac{1}{2}}a(x))^{-1}\right\|_{L^2\to L^2} \leq C\frac{\log^2\langle\tau\rangle}{\langle\tau\rangle^{\frac{1}{2}}},$$

where $\langle\tau\rangle = \sqrt{1+|\tau|^2}$ and let $s \in \mathbb{R}$ then we have
(i) $\forall\ \varepsilon > 0\ \exists\ C > 0\ /\ u(t) = \displaystyle\int_0^t e^{i(t-\tau)A_a} f(\tau)d\tau$ satisfies

$$\|u\|_{L^2_T H^{s+1-\varepsilon}(\Omega_0)} \leq C\,\|f\|_{L^2_T H^s(\Omega_0)} \tag{2.3}$$

(ii) If $u_0 \in H^s(\Omega_0)$ then $e^{itA_a}u_0 \in C^\infty((0,+\infty)\times\Omega_0)$
(iii) there exist $\alpha, c > 0$ such that

$$\|e^{itA_a}u_0\|_{L^2(\Omega_0)} \leq ce^{-\alpha t}\|u_0\|_{L^2(\Omega_0)},\ \forall\ t > 1.$$

Indeed, under the E.G.C. condition, we prove in [4] the Kato-smoothing effect and the **non homogeneous** bound for the regularized Schrödinger equation in exterior domains.

Theorem 2.3 *We suppose that ω satisfies the E.G.C., then for any $\chi \in C_0^\infty(\mathbb{R}^d)$ there exist $c > 0$, λ_0 such that for any $\lambda > \lambda_0$ and $\forall f \in L^2(\Omega)$*

$$\left\|\chi(-iA_a - \lambda)^{-1}\chi f\right\|_{L^2(\Omega)} \leq \frac{c}{|\lambda|^{\frac{1}{2}}}\,\|f\|_{L^2}\,.$$

Moreover, for any $T > 0$ and $s \in]1/2, 1]$ there exist $c > 0$ such that, for all u_0, f in $C_0^\infty(\Omega)$,

$$\left\|\langle x\rangle^{-s}u\right\|_{L^2((0,T);H^{\frac{1}{2}})} \leq C(\|u_0\|_{L^2} + \|\langle x\rangle^s f\|_{L^2((0,T);H^{-\frac{1}{2}})})$$

where $u = e^{itA_a}u_0 + \int_0^t e^{i(t-\tau)A_a}f(\tau)d\tau$.

References

[1] L. Aloui, *Smoothing effect for regularized Schrödinger equation on bounded domains*, Asymptotic Analysis **59** (2008).

[2] L. Aloui & M. Khenissi, *Stabilization of Schrödinger equation in exterior domains*, ESIAM- COCV. Vol. **13**, No 3, (2007).

[3] L. Aloui & M. Khenissi, *Boundary stabilization of the wave and Schrödinger equations in exterior domains*, DCDS-A, Vol. **27**, N.3, (2010)

[4] L. Aloui, M. Khenissi & L. Robbiano, *Kato-smoothing effect for Schrödinger equation in exterior domains*, Preprint, arXiv:1204.1904.

[5] L. Aloui, M. Khenissi & G. Vodev, *Smoothing effect for the regularized Schrödinger equation with non controlled orbits*, Comm.PDE **38**:2 (2013).

[6] M. Khenissi, *Equation des ondes amorties dans un domaine extérieur*, Bull.Soc.Math.France **131** (2003).

[7] M.Khenissi & G. Vodev, On the stabilization of the elasticity system by the boundary. Asymptot. Anal. **58**, (2008).

[8] M. Daoulatli, B. Dehman & M. Khenissi, *Local Energy decay for the elastic system with nonlinear damping in an exterior domain*, SIAM J. Control Optim. **48** (2010).

Slow modulation and large-time asymptotic behavior about periodic traveling waves in general systems of hyperbolic-parabolic composite type.

M.A. Johnson[1], P. Noble[2], L.M. Rodrigues[2,*], K. Zumbrun[3]
[1] Kansas University
[2] Université de Lyon.
[3] Indiana University.
[*]Email: rodrigues@math.univ-lyon1.fr

Abstract

In a joint work with Mathew Johnson, Pascal Noble and Kevin Zumbrun, motivated by fluid dynamics considerations, we tackle the following question:

1. In general systems of hyperbolic-parabolic composite type, in which sense can we obtain asymptotic stability for spectrally stable periodic planar traveling waves ?

2. Is it possible to validate, for large time, formal predictions obtained from a WKB expansion ?

During our talk we will discuss the hardest case of space-dimension one but, for the sake of algebraic simplicity, will restrict the type of the original system. We will see to what extent the answer to the second question is positive even when the reference wave undergoes a non-localized perturbation (allowing for global phase shifts at infinities but not for global changes in wave numbers), thus also provide an answer to the first question. The consideration of non-localized perturbations, requiring an involved modulation process, is made necessary by the fact that in general even initially localized perturbations evolve into non-localized perturbations. Among many other difficulties it should be noted that these scenari exhibit very slow decay in time and poor localization in space.

3.5 Domain decomposition methods

Minisymposium organized by Faker Ben Belgacem

Optimized Schwarz Methods for curl-curl time-harmonic Maxwell's equations

V. Dolean[1,*], **M. J. Gander** [2], **J.-F. Lee** [3], **Z. Peng** [3]
[1] Laboratoire J.A. Dieudonné, Université de Nice-Sophia Antipolis
[2] Section de Mathématiques, Université de Genève
[2] Electro Science Laboratory, Ohio State University
*Email: dolean@unice.fr

Abstract

Like the Helmholtz equation, the high frequency time-harmonic Maxwell's equations are difficult to solve by classical iterative methods. Domain decomposition methods are currently most promising: following the first provably convergent method in [2], various optimized Schwarz methods were developed over the last decade [5], [6], [1], [3], [7], [8], [9], [4]. There are however two basic formulations for Maxwell's equation: the first order formulation, for which complete optimized results are known [3], and the second order, or curl-curl formulation, with partial optimization results [1], [7], [9]. We show in this work that the convergence factors and the optimization process for the two formulations are the same. We then show by numerical experiments that the Fourier analysis predicts very well the behavior of the algorithms for a Yee scheme discretization, which corresponds to Nedelec edge elements on a tensor product mesh, in the curl-curl formulation. When using however mixed type Nedelec elements on an irregular tetrahedral mesh, numerical experiments indicate that transverse magnetic (TM) modes are less well resolved for high frequencies than transverse electric (TE) modes, and a heuristic can then be used to compensate for this in the optimization.

References

[1] Alonso-Rodriguez, A., Gerardo-Giorda, L.: New nonoverlapping domain decomposition methods for the harmonic Maxwell system. SIAM J. Sci. Comput. **28**(1), 102–122 (2006)

[2] Després, B., Joly, P., Roberts, J.: A domain decomposition method for the harmonic Maxwell equations. In: Iterative methods in linear algebra, pp. 475–484. North-Holland, Amsterdam (1992)

[3] Dolean, V., Gerardo-Giorda, L., Gander, M.J.: Optimized Schwarz methods for Maxwell equations, SIAM J. Sci. Comput., **31**(3), 2193–2213 (2009)

[4] El Bouajaji, M., Dolean, V., Gander, M.J., Lanteri, S.: Optimized Schwarz methods for the time-harmonic Maxwell equations with dampimg. SIAM J. Scient. Comp. **34**(4), 2048–2071 (2012)

[5] Gander, M.J., Magoulès, F., Nataf, F.: Optimized Schwarz methods without overlap for the Helmholtz equation. SIAM J. Sci. Comput. **24**(1), 38–60 (2002)

[6] Lee, S.C., Vouvakis, M., Lee, J.F.: A non-overlapping domain decomposition method with non-matching grids for modeling large finite antenna arrays. J. Comput. Phys. **203**(1), 1–21 (2005)

[7] Peng, Z., Lee, J.F.: Non-conformal domain decomposition method with second-order transmission conditions for time-harmonic electromagnetics. J. Comput. Phys. **229**(16), 5615–5629 (2010)

[8] Peng, Z., Rawat, V., Lee, J.F.: One way domain decomposition method with second order transmission conditions for solving electromagnetic wave problems. J. Comput. Phys. **229**(4), 1181–1197 (2010)

[9] Rawat, V., Lee, J.F.: Nonoverlapping domain decomposition with second order transmission condition for the time-harmonic Maxwell's equations. SIAM J. Sci. Comput. **32**(6), 3584–3603 (2010)

Some domain decomposition approaches in scattering and radiation of waves

A. Bendali[1,*]
[1] Université de Toulouse, IMT (UMR 5219), INSA, & CERFACS, Toulouse, France
[*] Email: abendali@insa-toulouse.fr

Abstract

Coupling dissimilar numerical schemes generally enhances the solution process but may lead to specific difficulties. Even more successful, this coupling may be at the basis of the modeling procedure itself. It is first shown here how Domain Decomposition Methods (DDM) can be used to design efficient procedures for solving a radiation problem involving a relatively small heterogeneous material posed on a relatively large impenetrable structure. Typically such a problem is encountered when dealing with the radiation of a complicated antenna in its environment. The next case considered corresponds to a model reduction entering in the determination of the wave reflected by a cavity with walls covered by a thin absorbing material. It is also shown in this context how DDM ideas are at the basis of efficient solving procedures.

Introduction

As said above, the first problem, we deal with, corresponds to the radiation of a time-harmonic wave for the case where some small size heterogenous material is posed on a large scale impenetrable structure (Fig. 1)

$$\begin{cases} \nabla\cdot(\chi\nabla u)+\chi\kappa^2 n^2 u=0 \quad \text{in } \Omega, \\ \chi\partial_{\mathbf{n}}u=-f \text{ on } \Gamma, \\ \lim_{|x|\to\infty}|x|^{1/2}(\partial_{|x|}u-i\kappa u)=0; \end{cases} \tag{1}$$

Ω is the complement of the impenetrable obstacle, $\kappa>0$ is the wave number, χ and n are functions equal to 1 outside the heterogeneous material filling Ω_1 yielding the contrast and the refractive index of the material. The idea here is to use a Boundary Integral Equation (BIE) on the impenetrable part of the structure lying outside and a Finite Element Method (FEM) inside the heterogeneous material. However, straightforward coupling procedures are generally inefficient specially for large size problems where the solution process has to be tackled through an iterative method.

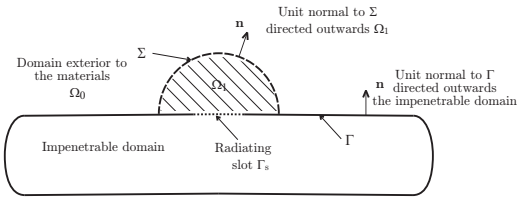

Figure 1: The radiation problem.

The second problem considered is relative to the determination of the wave reflected by a cavity with walls covered by a thin penetrable material (Fig. 2). The problem has a similar setting as (1) except that the Neumann condition is everywhere now 0 on Γ and the radiation condition is set now in terms of an incident plane wave u^{inc}: $\lim_{|x|\to\infty}|x|^{1/2}(\partial_{|x|}-i\kappa)\left(u-u^{\text{inc}}\right)=0$. The challenge is now to solve the corresponding boundary-value problem with a reduced model avoiding the solution of the equations in the interior of the penetrable material.

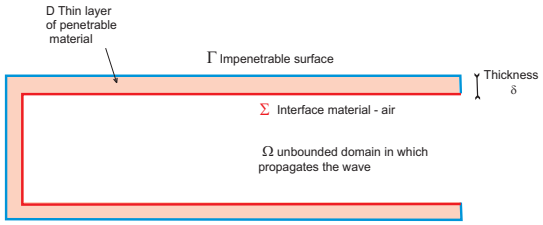

Figure 2: The covered cavity scattering problem.

1 Methods

1.1 An overlaping DDM procedure

We first describe how it is dealt with problem (1). In its basic principle, the method ressembles the one developed by Jami and Lenoir and interpreted later when it is solved through an iterative procedure as a Schwarz overlaping DDM in [1]. In this reference, the whole structure is enclosed in a FE mesh and no BIE is explicitly solved. However, proceeding in this way for the present case results in a too large size problem. Even worse, approximating the propagation of a wave along large distances by a FEM may be very problematic because of the dispersion errors, which can severely damage the accuracy of the final result. Hence, it is only the part Ω_S of the domain which is dealt with a FE mesh as indicated in Fig. 3.

Each iteration is performed by solving a plain BIE

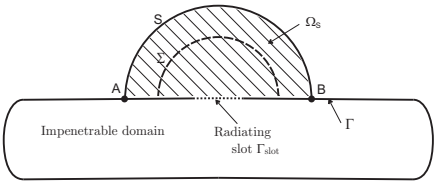

Figure 3: Geometrical setting of the non-overlaping domain decomposition approach.

corresponding to the solution of a transmission equation set in all of the plane and a boundary-value problem set in Ω_S. In the spirit of the method devised in [1], a low-order absorbing condition is added on the fictitious boundary S. Clearly, this solution can be carried out by means of a plain FEM. This study has been carried out in collaboration with Y. Boubendir and N. Zerbib [2].

1.2 A primal domain decomposition approach

Now, we turn our attention to the cavity problem. We first use a usual primal DDM approach for setting the problem to be solved (see Fig. 2 for the notation)

$$
\begin{aligned}
&\text{find } \varphi \text{ and } \chi \text{ resp. def. on } \partial D \text{ and } \partial\Omega \text{ s. t.}\\
&\varphi = \chi \text{ on } \Sigma\\
&\begin{cases} \Delta w + \kappa^2 n^2 w = 0 \text{ in } D \\ w = \varphi \text{ on } \partial D \end{cases}\\
&\begin{cases} \Delta u + \kappa^2 u = 0 \text{ in } \Omega \\ u = \chi \text{ on } \partial D \\ \lim_{|x|\to\infty} |x|^{1/2}(\partial_{|x|} - i\kappa)\left(u - u^{\text{inc}}\right) = 0 \end{cases}\\
&\int_{\partial D} \tfrac{1}{\varepsilon}\partial_{\mathbf{n}} w\varphi' ds - \int_{\partial\Omega} \partial_{\mathbf{n}} u\chi' ds = 0,\\
&\qquad\qquad \forall \varphi', \chi' \text{ such that } \varphi' = \chi' \text{ sur } \Sigma
\end{aligned}
$$

Of course, this equation is not explicit in φ and χ. However, the matrix-vector product relative to the term $\int_{\partial\Omega}\partial_{\mathbf{n}} u\chi' ds$ can be obtained by solving a Burton-Miller BIE. The one corresponding to $\int_{\partial D}\frac{1}{\varepsilon}\partial_{\mathbf{n}} w\varphi' ds$ is completed through a thin layer model. The model used here simply consists in assuming that w is constant along the normal (Fig. 4)

$$
\begin{aligned}
\int_{\partial D}\frac{1}{\varepsilon}\partial_{\mathbf{n}} w\varphi' ds &= \int_D \left(\frac{1}{\varepsilon}\nabla w\cdot\nabla w' - \kappa^2\mu w w'\right) dx\\
&= \underset{\text{thickness}}{\delta}\underbrace{\int_\Sigma \frac{1}{\varepsilon}\partial_s\varphi\partial_s\varphi' - \kappa^2\mu\varphi\varphi' ds}_{\text{Thin layer model}}
\end{aligned}
$$

2 Results

Convergence of the overlaping DDM for radiation problem (1) is mathematically proved in [2]. This

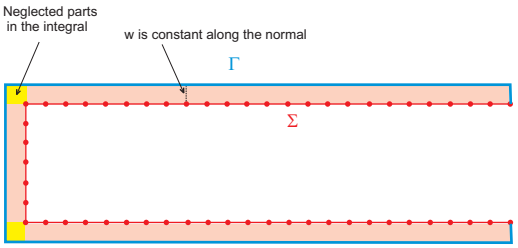

Figure 4: The thin layer model.

study reports also its robustness and that it outperforms usual primal DDMs. The results relative to the cavity problem have not been submitted yet. The plot in Fig. 5 well depictes the accuracy reached by this simple still powerfull method.

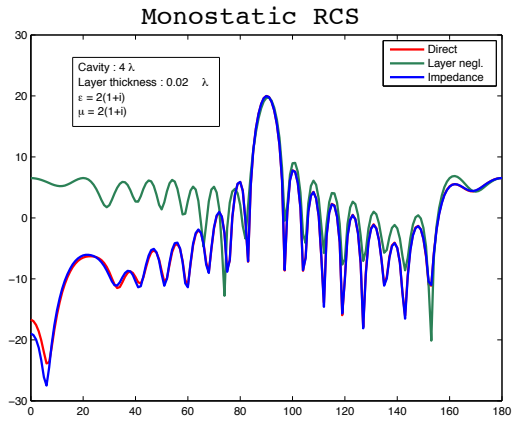

Figure 5: Monostatic calculations by a direct solving and the thin layer model.

References

[1] F. Ben Belgacem, M. Fournier, N. Gmati, and F. Jelassi, *On the Schwarz algorithms for the Elliptic Exterior Boundary Value Problems.*, M2AN, **39** (2006), pp. 693–714.

[2] A. Bendali, Y. Boubendir, and N. Zerbib, *Localized adaptive radiation condition for coupling . . .*, submitted to IMA Numer. Analysis, available at http://hal.archives-ouvertes.fr/hal-00716863.

[3] P. Gosselet, and C. Rey, Non-overlapping Domain Decomposition Methods in Structural Mechanics, Arch. Comput. Meth. Engng. **13** (2006), pp. 515–572.

Domain Decomposition Methods for the interior Helmholtz problem: Spectral Analysis and Numerical Experiments

Martin J. Gander*, **Hui Zhang***
Department of Mathematics, University of Geneva, Switzerland.
*Email: {martin.gander, hui.zhang}@unige.ch

Abstract

In this talk, we review many domain decomposition methods (DDMs) developed for the Helmholtz equation. We focus on the interior Helmholtz problem and show numerical experiments of the DDMs considered on the same set of test models, including the heterogeneous 3-D SEG-SALT model. We also present a spectral analysis of the DDMs in order to get a better understanding of their behavior.

Introduction

The Helmholtz equation is a real challenge for numerical simulations [1]. In addition to the well known pollution effect, the linear algebraic system from the standard discretization of a 3-D problem at mid-frequency is not only too large to be solved by factorization, but also too indefinite for iterative methods to converge well. There has been a lot of interest in the past decades to design (parallel) iterative methods for this equation, which show substantial differences from solving definite problems. In this talk, we focus on DDMs which divide the original problem into smaller problems on subdomains and recover the original solution by iteration. From the literature, special transmission conditions, special coarse problems and the application order of subproblem solves (parallel or serial) appear to be the key components in designing DDMs for the Helmholtz equation.

We consider the Helmholtz equation

$$\mathcal{L}u := \left(-\rho\nabla\cdot(\frac{1}{\rho}\nabla) - \frac{\omega^2}{c^2}\right) u = f, \qquad (1)$$

where $\rho : \Omega \subset \mathbb{R}^3 \to \mathbb{R}^+$ is the density of mass, $c : \Omega \to \mathbb{R}^+$ is the wave speed, $\omega \in \mathbb{R}$ represents the temporary frequency of the corresponding mode $u \cdot \exp(\varsigma\,\mathrm{i}\,\omega t)$ (ς is a constant value equal to one of $\{1, -1\}$ decided upon users' conventions), and $f : \Omega \to \mathbb{R}$ is the source term. We divide the domain into either non-overlapping or overlapping subdomains, which gives rise to internal boundaries called interfaces. We then impose certain boundary conditions on these interfaces to define well-posed subproblems and the correct interface data are sought in an iterative way. There are two different formulations of DDMs, independently of the method being overlapping or not: one is a volume formulation and the other is an interface, or substructured formulation. In the volume formulation, one can use inexact solvers for the subproblems. But if we use exact solvers for subproblems, the spectra (except 0,1) of the two forms are usually the same (or not far from each other), see e.g. [2]. Here, we use the interface formulation, which simplifies the spectral analysis based on Fourier techniques.

1 One-field non-overlapping methods

For non-overlapping subdomains, we note that the Dirichlet and Neumann traces should match across interfaces. If we take one type of common traces as uniquely defined unknowns, and if these unknowns define unique subdomain solutions, taking the other type of traces of subdomain solutions and imposing the matching conditions gives us a system to solve, see e.g. [3]. Unfortunately, the Helmholtz equation in a subdomain can be singular when equipped with Dirichlet or Neumann boundary conditions. This motivated [4] to take Robin conditions $\lambda := \partial_{\mathbf{n}}u + pu$ as unknowns, where $\mathbf{n}$ is a normal direction uniquely defined for each interface (it is outward for a subdomain on one side of the interface and inward for the neighboring subdomain), and $\mathrm{Im}\,p \neq 0$. Although this class of methods has been well studied for definite problems, the results for the Helmholtz equation are still limited, see e.g. [5]. In our talk, we will show spectral results obtained from Fourier analysis on many subdomains or in heterogeneous media.

2 Two-field non-overlapping and overlapping methods

This class of methods take a set of boundary data for every subdomain as unknowns and set up the system by transmission conditions like $\mathcal{B}_i(u_i - u_j) = 0$ on the interfaces $\partial\Omega_i \cap \overline{\Omega_j}$ where $\mathcal{B}_i$ is a boundary operator. All the boundary operators from the literature can be expressed in the form $\mathcal{B}_i := \partial_{\mathbf{n_i}} + \mathcal{T}_i$ with $\mathcal{T}_i$ some tangential, possibly pseudo-differential

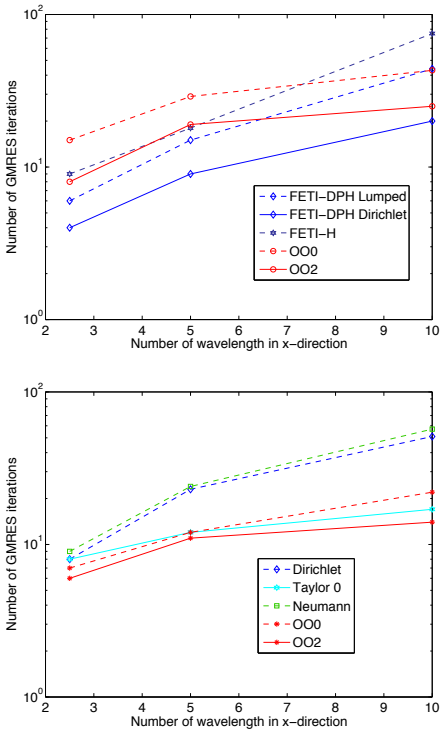

Figure 1: Discretized with $h = \lambda/10$.

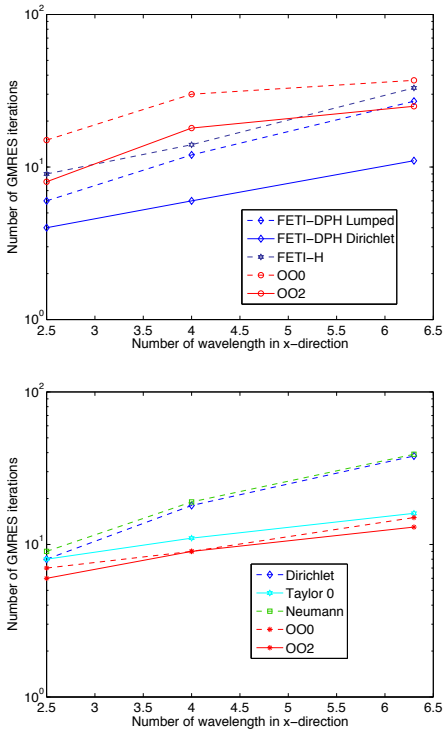

Figure 2: Discretized with $h^2 = C\lambda^3$.

operator. Many DDMs fall into this category, like the D-N alternating method, or optimized Schwarz methods. A significant difference from the one-field non-overlapping methods is the lack of a cheap preconditioner (we can design a preconditioner for the two-field methods but it will not be as cheap as for one-field methods). An advantage are the high-order transmission conditions and/or overlap, as we will illustrate by Fourier analysis.

3 Numerical Experiments

We will also show the actual performance of these DDMs on some test models. Fig. 1 and Fig. 2 depict the scaling of the DDMs on $3\times3\times1$ subdomains augmented with six plane-waves for solving the 3-D SEG-SALT model. The top panel shows non-overlapping methods and the bottom panel overlapping methods. Large scale parallel experiments are in progress.

References

[1] O. G. Ernst and M. J. Gander, *Why it is difficult to solve Helmholtz problems with classical iterative methods*, in Numerical Analysis of Multiscale Problems, Springer Verlag (2012) pp. 325–363.

[2] J. Li and O. B. Widlund, *On the use of inexact subdomain solvers for BDDC algorithms*, Computer methods in applied mechanics and engineering, **196** (2007), pp. 1415–1428.

[3] C. Farhat, P. Avery, R. Tezaur, and J. Li, *FETI-DPH: a dual-primal domain decomposition method for acoustic scattering*, Journal of Computational Acoustics, **13** (2005), pp. 499–524.

[4] C. Farhat, A. Macedo, M. Lesoinne, F. X. Roux, F. Magoulès and A. L.Bourdonnaie, *Two-level domain decomposition methods with Lagrange multipliers for the fast iterative solution of acoustic scattering problems*, Computer methods in applied mechanics and engineering, **184** (2000), pp. 213–239.

[5] J. Li and X. Tu, *Convergence analysis of a balancing domain decomposition method for solving a class of indefinite linear systems*, Numerical Linear Algebra with Applications, **16** (2009), pp. 745–773.

A DDM double sweep preconditioner for the Helmholtz equation with matrix probing of the DtN map

A. Vion[1,*], **R. Bélanger-Rioux**[2], **L. Demanet**[2], **C. Geuzaine**[1]
[1] University of Liège, Belgium.
[2] Massachussets Institute of Technology, USA.
*Email: A.Vion@ulg.ac.be

Abstract

We describe the structure of a fast solver for the Helmholtz equation in the optimized Schwarz framework, based on a preconditioner that leverages impedance-matching boundary conditions on subdomains. In the case of a simple 2D waveguide numerical example, the method requires no more than 4 GMRES iterations, independently of the frequency and the number of subdomains. The challenge remains to make each iteration fast: we give a partial answer to this question by showing how the Dirichlet to Neumann (DtN) map is accurately approximated in a compressed form via the recently introduced notion of matrix probing.

Introduction

Domain Decomposition Methods (DDM) offer a very useful tool for numerically solving PDEs, but require additional ideas to operate optimally in the high-frequency regime [1]. The setting of our proposed method is a reformulation of the problem in terms of a set of unknown sources defined on artificial boundaries inside the domain. These sources must produce the same solution inside the individual subdomains, so a linear system must be solved to find them. It was shown in [2] that a Krylov method for this system can be set up, where the sources are defined from boundary conditions that match impedances of subdomains. The contributions of this paper are twofold: we propose 1) a preconditioner that takes advantage of the particular structure of the iteration matrix in the case of a layered partitioning ; and 2) an efficient computation of the DtN map using matrix probing.

1 Non-overlapping optimized Schwarz DDM

Consider a domain Ω with boundary $\partial\Omega$. We decompose Ω into N non-overlapping slices $\Omega_{i,1\leq i\leq N}$, with artificial boundaries Σ_{ij} between Ω_i and Ω_j. (This is a layered partitioning, not a general 2D partitioning.) The iterative scheme, detailed in [2], uses impedance-matching boundary conditions on Σ_{ij} and recasts the problem in terms of the set of interface data $g = \{g_{ij}, 1 \leq i \neq j \leq N, |i-j| = 1\}$. An iteration amounts to solving all subproblems in parallel:

$$\begin{aligned} -(\Delta + k^2)u_i^{(m+1)} &= 0 && \text{in } \Omega_i \\ (\partial_n + \mathcal{S})u_i^{(m+1)} &= (-\partial_n + \mathcal{S})u_j^{(m)} && \text{on } \Sigma_{ij} \\ &= g_{ij}^{(m)}, \end{aligned} \tag{1}$$

with k the wavenumber and the update:

$$\begin{aligned} g_{ij}^{(m+1)} &= -\partial_n u_j^{(m+1)} + \mathcal{S}u_j^{(m+1)} && \text{on } \Sigma_{ij} \\ &= -g_{ji}^{(m)} + 2\mathcal{S}u_j^{(m+1)}. \end{aligned}$$

Boundary conditions on $\partial\Omega_i \cap \partial\Omega$ are conserved from the original problem. This procedure can be rewritten as a fixed point iteration on the unknowns g:

$$Fg = b, \tag{2}$$

where applying the operator F amounts to solving the subproblems and updating g. The solution of problem (2) can be accelerated using GMRES.

The choice of operator $\mathcal{S}$ is critical for the rate of convergence. It was shown in [3] that the optimum is obtained if $\mathcal{S}$ is the DtN map of the Helmholtz operator on the corresponding interface.

2 Double sweep preconditioner

The matrix of the iteration operator F (never formed in practice, but considered here for the purpose of analysis) consists of blocks arranged near the diagonal, each of which, when applied to a vector, amounts to solving a subproblem where the boundary source is restricted to one side of the domain. Provided that no reflection occurs at the opposite boundary, this matrix is easy to invert. An absence of reflection is hard to achieve in a numerical setting, but can be approached by using a sufficiently good Absorbing Boundary Condition (ABC).

The preconditioning strategy is to neglect those components of the iteration operator that are caused by spurious reflections, and would be zero in the absence of such reflections, to build an approximate inverse $\tilde{F}^{-1}$ of the iteration operator F.

	$N = 10$	20	50	100	200	400
$k = 10\pi$	3	3	4	4	4	4
40π	3	3	3	3	4	4

Table 1: Convergence of the method with double sweep preconditioner and exact DtN map, applied to a rectangular waveguide with increasing number of subdomains N. The iteration count ($||r||_2/||r_0||_2 < 10^{-13}$) is small and independent of N and wavenumber k.

By rearranging the terms of the matrix-vector product $g = \tilde{F}^{-1}r$, one can rewrite the preconditioner as a double sequence (forward and backward) of subproblems solutions, each problem taking into account the contribution of all its predecessors in the sequence. So, considering the forward sequence, the i-th component of g is: $g_i = r_i + H_{f,i}^{-1} g_{i-1}$, with $H_{f,i}^{-1}$ the output of (1) for the i-th problem with impedance data g_i on the left and 0 on the right, and starting with $g_1 = r_1$. Such a sequence of solves is called a sweep over the subdomains, hence the name of double sweep preconditioner.

The idea of sweeping was proposed in [4] for preconditioning the Helmholtz equation. A double sweep strategy was also proposed in [5]. These work use the sweeps to precondition the Helmholtz operator in the original domain, while we use them to precondition the operator F of a Schwarz method. In addition, we precompute the DtN map by matrix probing rather than by using perfectly-matched layers (PML), leading to potential computational savings. Because the complexity of applying a probed DtN map hardly depends on its quality, we can use a better ABC (thicker layer) in our precomputation, hence potentially improved convergence properties for the DDM algorithm.

3 DtN map approximation via probing

We are thus looking for an accurate approximation D to the DtN map $\mathcal{S}$ at some interface Σ. Consider the Helmholtz equation in a (PML) placed next to Σ. The operator D is viewed as a black box that maps Dirichlet data on Σ to the normal derivative, on Σ as well, of the solution to the Helmholtz equation in the PML: $\partial_n \bar{u} = D\bar{u}$. We first precompute the matrix D offline, then apply it to vectors on the fly as needed.

Matrix probing is used to make the precomputation of D tractable. Suppose that we wish to approximate a matrix $D \in \mathbb{R}^{n\times n}$, but we only have access to a handful of products of D with vectors. We assume D can be written as a linear combination of a small number of basis matrices B_j, $D \approx \sum_{j=1}^{p} c_j B_j$ *fixed ahead of time*. Under various assumptions, notably $p \ll n$ (see [6] for details) we can recover the vector c with great accuracy using only a few black box calls. For illustration, it is often advantageous to consider a single random vector z, so that $Dz \approx \sum_{j=1}^{p} c_j B_j z = \Psi_z c$, where the $B_j z$ are columns of Ψ_z. Solving for c now requires the pseudo-inverse of Ψ_z, which can be quickly obtained since this is an $n \times p$ matrix with $p \ll n$.

Hence we need a relatively small set of basis matrices which can accurately approximate the DtN map D. There are different ways to do this: we can use a geometrical optics approximation with oscillations of the form $e^{i\omega\tau(x,y)}$ times a parametrized singular amplitude, see [7] for details, or else we can use the relaxed terms of the Padé expansion proposed in [2], obtained from a few 1D PDE solves. Both methods reproduce the numerical results presented earlier.

Current work focuses on further lowering the complexity of each subdomain solve H^{-1} and each application of D. Preliminary results with a non-homogeneous medium tend to indicate that the behaviour of the method is not fundamentally changed.

References

[1] O. Ernst and M. Gander, *Why it is Difficult to Solve Helmholtz Problems with Classical Iterative Methods*, Numerical Analysis of Multiscale Problems, **83** (2012), pp. 325–363.

[2] Y. Boubendir, X. Antoine and C. Geuzaine, *A quasi-optimal non-overlapping domain decomposition algorithm for the Helmholtz equation*, JCP, **231** (2012), pp. 262–280.

[3] F. Nataf, *Interface Connections in Domain Decomposition Methods*, NATO Science Series II, **75** (2001), pp 323–364.

[4] B. Engquist, L. Ying, *Sweeping Preconditioner for the Helmholtz equation: Moving Perfectly Matched Layers*, SIAM MMS, **9** (2011).

[5] C. Stolk, *A rapidly converging domain decomposition method for the Helmholtz equation*, preprint (2012).

[6] J. Chiu and L. Demanet, *Matrix Probing and its Conditioning*, SIAM J. Numer. Anal., **50** (2012), pp. 171–193.

[7] R. Bélanger-Rioux and L. Demanet, *Compressed absorbing boundary conditions via matrix probing*, preprint (2012).

Riesz potentials and quasi-local transmission condition for optimizing the convergence of iterative non overlapping domain decomposition methods for the Helmholtz equation

F. Collino[1], **P. Joly**[1,*], **M. Lecouvez**[2], **B. Stupfel**[2]
[1] POEMS (UMR 7231 CNRS-INRIA-ENSTA), ENSTA Paristech, Palaiseau, France.
[2] CEA-Cesta, BP 2 - 33114 Le Barp, France. *Email: patrick.joly@inria.fr

The model problem

In the following, Ω denotes a bounded (for simplicity) open set of $\mathbb{R}^d$ (d =2 or 3), $f \in L^2(\Omega)$ and $\omega > 0$ (the frequency) are given and one is interested in $u \in H^1(\Omega)$, the (complex valued) solution of the boundary value problem

$$\begin{cases} -\Delta u - \omega^2 u = f \quad \text{in } \Omega \\ \partial_n u + i\omega u = 0 \quad \text{on } \partial\Omega \end{cases} \tag{1}$$

We assume that Ω can be split into two domains Ω_1

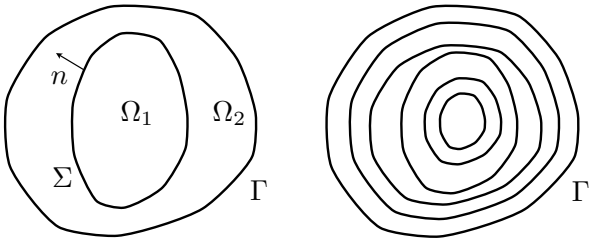

Figure 1: The domain decomposition

and Ω_2 separated by a smooth interface Σ, according to figure 1 and denote u_j the restriction of u to Ω_j. The objective of an iterative domain decomposition method is to construct a sequence

$$(u_1^n, u_2^n) \in H^1(\Omega_1) \times H^1(\Omega_2), \quad n \geq 1$$

such that $(u_1^n, u_2^n) \longrightarrow (u_1, u_2), \quad n \longrightarrow +\infty.$

Obviously, u_j^n solves the Helmholtz equation in Ω_j:

$$\begin{cases} -\Delta u_j^n - \omega^2 u_j^n = f \quad \text{in } \Omega_j, \\ \partial_n u_j^n + i\omega u_j^n = 0 \quad \text{on } \Gamma_j = \partial\Omega \cap \partial\Omega_j \end{cases} \tag{2}$$

The key point is the choice of the boundary conditions on the interface Σ that will link the u_j^n to the previous iterates and are supposed to ensure, after convergence, the correct transmission conditions (n is the unit normal vector oriented from Ω_1 to Ω_2, see figure 1, left picture):

$$u_1 = u_2, \quad \partial_n u_1 = \partial_n u_2, \quad \text{on } \Sigma = \partial\Omega. \tag{3}$$

Remark : What follows is easily generalizable to non constant coefficients and more general boundary conditions in (1). One can also consider more subdomains provided that the interfaces are closed and disjoint manifolds (figure 1, right picture).

Transmission conditions and iterations

Let $T \in \mathcal{L}(H^s(\Sigma), H^{-s}(\Sigma))$ for some $s > 0$ be an operator that we assume to be positive, symmetric and injective operator (the transmission operator). Let $z \neq 0$ be a complex number with $\mathcal{I}m\, z > 0$, we first observe that (3) is equivalent to

$$\begin{cases} B_\lambda u_1 = B_\lambda u_2, \quad \text{for } \lambda = z \text{ and } \lambda = \overline{z}. \\ B_\lambda := \partial_n + \lambda T \end{cases} \tag{4}$$

The missing boundary conditions for (2) are obtained by applying a fixed point algorithm, with relaxation parameter $r \in]0, 1]$, to the transmission conditions (4) so that the resolutions in Ω_1 and Ω_2 are decoupled at each step:

$$\begin{cases} B_z u_1^n = r\, B_z u_2^{n-1} + (1-r)\, B_z u_1^{n-1}, \\ B_{\overline{z}} u_2^n = r\, B_{\overline{z}} u_1^{n-1} + (1-r)\, B_{\overline{z}} u_2^{n-1}, \end{cases} \tag{5}$$

The well-posedness of the local problems (2, 5) is guaranteed as soon as $\mathcal{I}m\, z > 0$.

Let us remark that this general framework contains most of the iterative methods proposed in the literature. For instance, when $z = i\omega$:

- If, $T = I$ ($s = 0$), one recovers the original method proposed by Després [2],
- If T is a second order boundary differential operator ($s = 2$), one gets the conditions of [4],

However, as soon as the operator T is local (i.e. expressed in terms of tangential differential operators), the convergence of the algorithm is at best algebraic (typically in $1/n$). Our goal is to propose new transmission conditions achieving exponential convergence and to optimize the convergence rate.

Convergence issues

We assume that $T = \Lambda\Lambda^*$ where

$$\Lambda \in \mathcal{L}\big(L^2(\Sigma), H^{-s}(\Sigma)\big) \text{ is isomorphic,} \qquad (6)$$

and Λ^* is the adjoint of Λ. Let us consider the errors

$$(e_1^n, e_2^n) = (u_1^n - u_1, u_2^n - u_2), \quad \mathbf{e}^n = (e_1^n, e_2^n)$$

as well as the boundary quantities:

$$x_1^n = \Lambda^{-1}\,\partial_n e_1^n + z\,\Lambda^* e_1^n, \quad x_2^n = \Lambda^{-1}\,\partial_n e_2^n + \overline{z}\,\Lambda^* e_2^n$$

so that $\mathbf{x}^n = (x_1^n, x_2^n) \in L^2(\Sigma)^2$ with norm $\|\cdot\|_\Sigma$.

From the well-posedness of the local problems (2, 5), we deduce that, if $V := H^1(\Omega_1) \times H^1(\Omega_2)$

$$\|\mathbf{e}^n\|_V \leq C\,\|\mathbf{x}^n\|_\Sigma\,.$$

The key point for the convergence of the algorithm is the following identity, that extends a result of [1]:

$$\begin{aligned} \|\mathbf{x}^n\|_\Sigma^2 \;=\; \|\mathbf{x}^{n-1}\|_\Sigma^2 \;&-\; r(1-r)\,\|\mathbf{y}^{n-1}\|_\Sigma^2 \\ &-\; \omega\, r\,\|\mathbf{e}^{n-1}\|_\Gamma^2 \end{aligned} \qquad (7)$$

where $\mathbf{y}^n = (y_1^n, y_2^n) \in L^2(\Sigma)^2$ is defined by

$$y_1^n = \Lambda^{-1}\,\partial_n e_1^n + \overline{z}\,\Lambda^* e_1^n, \quad y_2^n = \Lambda^{-1}\,\partial_n e_2^n + z\,\Lambda^* e_2^n\,.$$

Assume now that

$$(6) \text{ holds with } s = 1/2. \qquad (8)$$

By an abstract functional analytic argument, it is possible to show that there exists $\delta \in]0,1[$ such that

$$\|\mathbf{y}^{n-1}\|_\Sigma \leq \delta\,\|\mathbf{x}^{n-1}\|_\Sigma$$

so that (7) yields

$$\|\mathbf{x}^n\|_\Sigma \leq \tau\,\|\mathbf{x}^{n-1}\|_\Sigma, \quad \tau = \sqrt{1 - r(1-r)\,\delta^2}$$

implying the exponential convergence with rate τ.

However, the condition (8) prevents us from defining T with the help of local operators.

Quasi-local transmission operators

In practice,we need to build an explicit operator satisfying (8). The idea is to use a nonlocal operator of the form $-\mathrm{div}_\Sigma\big(\mathbf{K}\,\nabla_\Sigma\big)$ where $\mathbf{K}$ is an integral operator with kernel $K(x,y)$ that should be a pseudo-differential operator of order -3/2. For this, K must have the correct singularity when $x - y \to 0$ as suggested by Riesz potentials [3]

$$K(x,y) \sim |x-y|^\delta$$

with $\delta = 1/2$ if $d = 2$, $\delta = -1/2$ if $d = 3$. Moreover, to avoid fully nonlocal operators leading to full matrices after space discretization, the idea is to localize K around the diagonal $x = y$. That is why we use a smooth cut-off function $\chi(\rho) : \mathbb{R}^+ \to [0,1]$ such that

$$\text{supp } \chi \subset [0,1], \quad \chi = 1 \quad \text{in } \big[\,0, \frac{1}{2}\,\big]$$

and consider the operator

$$\Lambda = \alpha - \beta\ \mathrm{div}_\Sigma\big(\mathbf{K}_L\,\nabla_\Sigma\big) \qquad (9)$$

where $L > 0, \beta > 0$ and $\alpha \in \mathbb{C}$ are given, and

$$\mathbf{K}_L\varphi(x) = \int_\Sigma \chi\Big(\frac{|x-y|}{L}\Big)\,|x-y|^\delta\,\varphi(y)\,dy \qquad (10)$$

Theorem : As soon as $\mathcal{I}m\,\alpha \neq 0$, the operator Λ defined by (9) satisfies (8).

At the conference, we shall explain how to solve the local problems (2, 5) and investigate, numerically and analytically, how to tune the parameters $(z, \alpha, \beta, \chi, L)$ to optimize the rate of convergence.

References

[1] Collino F., Ghanemi S., Joly P. Domain decomposition method for harmonic wave propagation: a general presentation, CMAME, Vol. 184, 24, 2000, p. 171-211

[2] Després B. Domain decomposition method and the Helmholtz problem (Part II) In Second international conference on mathematical and numerical aspect of wave propagation phenomena, SIAM 1993, p. 197-206

[3] Stein E. Singular Integrals and Differentiability Properties of functions, Princeton Math. Series, Volume 30, Princeton University Press, 1970

[4] Gander, M., Magoulès, F., and Nataf, F. Optimized Schwarz Methods without Overlap for the Helmholtz Equation SIAM Journal on Scientific Computing, 2002, Volume 24:1, Pages 38-60

Domain decomposition for Full-Wave simulation in a tokamak plasma

Takashi Hattori[1,*], **S. Labrunie**[1], **J.R. Roche**[1], **P. Bertrand**[2]
[1] Institut Elie Cartan de Lorraine, Université de Lorraine
[2] Institut Jean Lamour, Université de Lorraine
*Email: takashi.hattori@univ-lorraine.fr

Abstract

The aim of this work is to develop a numerical method for the full-wave simulation of electromagnetic wave propagation in a plasma. The propagation and the absorption of lower hybrid (LH) electromagnetic waves is a powerful method to generate current in tokamaks by Landau wave particle resonance. Full-wave calculations of the LH wave propagation is a challenging issue because of the short wave length with respect to the machine size. We propose a Fourier finite element method for solving the Maxwell equations based on a mixed augmented variational formulation. In order to develop a parallel version of the simulation and consider non homogenous plasma response, a nonoverlapping domain decomposition approach is presented.

Introduction

Let the domain Ω be a torus (tokamak plasma volume) with strong external time-invariant magnetic field $\boldsymbol{B}_{ext}$. We study a second order partial differential equation for the time-harmonic electric field $\boldsymbol{E}$ arising from Maxwell equations:

$$\begin{aligned} \mathbf{curl}\,\mathbf{curl}\,\boldsymbol{E} - \frac{\omega^2}{c^2}\underline{\boldsymbol{K}}\boldsymbol{E} &= \boldsymbol{f} \quad \text{in } \Omega, & (1)\\ \operatorname{div}(\underline{\boldsymbol{K}}\boldsymbol{E}) &= g \quad \text{in } \Omega & (2)\end{aligned}$$

where $\omega > 0$ is the excited wave frequency and c denotes the speed of light in free space. The plasma response is described by the matrix $\underline{\boldsymbol{K}}$, in Stix frame (third coordinate parallel to $\boldsymbol{B}_{ext}$). It includes a cold plasma approximation of the relative dielectric permittivity tensor and Landau damping:

$$\underline{\boldsymbol{K}}(\boldsymbol{x}) = \begin{pmatrix} S(\boldsymbol{x}) & -iD(\boldsymbol{x}) & 0 \\ iD(\boldsymbol{x}) & S(\boldsymbol{x}) & 0 \\ 0 & 0 & P_L(\boldsymbol{x}) \end{pmatrix}$$

Expressions of the entries S, D and P_L involve plasma frequencies, cyclotron frequencies of each species (ion and electron) and also the collision frequency. In general, the matrix $\underline{\boldsymbol{K}}$ is complex-valued and non-hermitian. Let Γ be the boundary of the domain Ω and $\Gamma_A \subset \Gamma$ be an antenna on the tokamak, then several boundary conditions are possible:

$$\begin{aligned} \text{Neumann:} &\quad \mathbf{curl}\,\boldsymbol{E} \times \boldsymbol{n} = i\omega\mu_0 \boldsymbol{j}_s \quad \text{on } \Gamma_A \\ \text{Dirichlet:} &\quad \boldsymbol{E} \times \boldsymbol{n} = \boldsymbol{E}_A \times \boldsymbol{n} \quad \text{on } \Gamma_A. \end{aligned}$$

On the other part of the boundary $\Gamma_C = \Gamma \setminus \Gamma_A$, we assume a perfectly conducting condition:

$$\boldsymbol{E} \times \boldsymbol{n} = \boldsymbol{0} \quad \text{on } \Gamma_C.$$

1 Finite element method

1.1 Variational formulation and well-posedness

Taking the divergence condition (2) as constraint, we use a mixed augmented variational formulation (MAVF) [3], which gives rise to a $\boldsymbol{H}^1$ conforming variational space, $\boldsymbol{X}_N(\underline{\boldsymbol{K}}, \Omega) := \boldsymbol{H}_0(\mathbf{curl}, \Omega) \cap \boldsymbol{H}(\operatorname{div} \underline{\boldsymbol{K}}, \Omega)$. We obtain the following variational formulation of the Dirichlet problem :
Find $(\boldsymbol{E}, p) \in \boldsymbol{X}_N(\underline{\boldsymbol{K}}, \Omega) \times L^2(\Omega)$ such that

$$\begin{aligned} a_s(\boldsymbol{E}, \boldsymbol{F}) + \overline{b(\boldsymbol{F}, p)} &= L_s(\boldsymbol{F}) \quad \forall \boldsymbol{F} \in \boldsymbol{X}_N(\underline{\boldsymbol{K}}, \Omega) \\ b(\boldsymbol{E}, q) &= l(q) \quad \forall q \in L^2(\Omega). \end{aligned}$$

where

$$\begin{aligned} a_s(\boldsymbol{E}, \boldsymbol{F}) &:= (\mathbf{curl}\,\boldsymbol{E} \mid \mathbf{curl}\,\boldsymbol{F}) - \frac{\omega^2}{c^2}(\underline{\boldsymbol{K}}\boldsymbol{E} \mid \boldsymbol{F}) \\ &\quad + s(\operatorname{div} \underline{\boldsymbol{K}}\boldsymbol{E} \mid \operatorname{div} \underline{\boldsymbol{K}}\boldsymbol{F}) \\ L_s(\boldsymbol{F}) &:= (\boldsymbol{f} \mid \boldsymbol{F}) + s(g \mid \operatorname{div} \underline{\boldsymbol{K}}\boldsymbol{F}) \\ b(\boldsymbol{E}, q) &:= (\operatorname{div} \underline{\boldsymbol{K}}\boldsymbol{E} \mid q) \\ l(q) &:= (g \mid q), \end{aligned}$$

with parameter $s \in \mathbb{C}$. Here, $(\cdot \mid \cdot)$ denotes the standard L^2 inner product in Ω.

The well-posedness of the considered formulation follows from the Babuska-Brezzi theorem. Thanks to spectral properties of the dielectric tensor, the sesquilinear form a_s is coercive if $\Re(s) > 0$ and $\Im(s) \leq 0$.

1.2 Dimension reduction and discretization

The 3D problem can be reduced to a series of 2D one by using cylindrical coordinates (R, Z, ϕ) and by

expanding all functions $f(R, Z, \phi)$ as Fourier series in the angular coordinate ϕ

$$f(R, Z, \phi) = \frac{1}{\sqrt{2\pi}} \sum_{\nu \in \mathbb{Z}} f_\nu(R, Z) e^{i\nu\phi}$$

where the coefficients $f_\nu(R, Z)$ are defined on a cross section of Ω [4]. Then the sesquilinear forms of the variational formulation can be written as sum of modal forms

$$a_s(\boldsymbol{u}, \boldsymbol{v}) = \sum_{\nu \in \mathbb{Z}} a_{s,\nu}(\boldsymbol{u}_\nu, \boldsymbol{v}_\nu), \quad b(\boldsymbol{v}, p) = \sum_{\nu \in \mathbb{Z}} b_\nu(\boldsymbol{v}_\nu, p_\nu)$$

The modal variational formulation is then discretized using a Taylor-Hood P_2-iso-P_1 finite element.

1.3 Numerical results

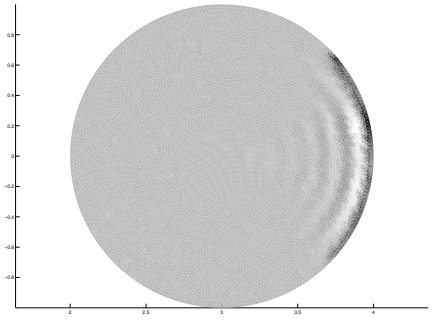

Figure 1: Real part of a component of the electric field for $\omega = \omega_{LH} = 1.3 \times 10^{10}$ rad/s

2 Domain decomposition

Consider a nonoverlapping decomposition $\overline{\Omega} = \bigcup_k \overline{\Omega_k}$. In the domain decomposition method considered here, we solve the original problem in each subdomain Ω_i; the equivalence with the one-domain formulation is obtained by continuity conditions

$$[\boldsymbol{E} \times \boldsymbol{n}]_{\Sigma_{ij}} = 0 \quad \text{and} \quad [\underline{\boldsymbol{K}}\boldsymbol{E} \cdot \boldsymbol{n}]_{\Sigma_{ij}} = 0 \qquad (3)$$

which ensure the $\boldsymbol{X}(\underline{\boldsymbol{K}}, \Omega)$ regularity of the electric field and

$$[\mathbf{curl}\, \boldsymbol{E} \times \boldsymbol{n}]_{\Sigma_{ij}} = 0, \qquad (4)$$

which implies that the one-domain formulation holds in the sense of distributions. We have denoted, as usual, $[f]_{\Sigma_{ij}}$ the jump of a quantity f across the interface $\Sigma_{ij} = \overline{\Omega_i} \cap \overline{\Omega_j}$. The conditions (3) are dualized by introducing the associated Lagrange multipliers $\boldsymbol{\lambda}_{ij} \in \boldsymbol{H}^{1/2}(\Sigma_{ij})$, while (4) is treated as a natural condition. The existence and uniqueness of the solution $(\boldsymbol{E}_i, p_i, \boldsymbol{\lambda}_{ij})$ to the multidomain formulation was proved and :

$$\boldsymbol{E}_i = \boldsymbol{E}_{|\Omega_i} \quad \text{and} \quad p_i = p_{|\Omega_i}$$

where $(\boldsymbol{E}, p)$ is the solution to the one-domain formulation.

The full linear system involving all subdomains (the *outer system*) is a generalized saddle-point problem:

$$\begin{pmatrix} \underline{\boldsymbol{Q}} & \underline{\boldsymbol{G}}^H \\ \underline{\boldsymbol{G}} & 0 \end{pmatrix} = \begin{pmatrix} \boldsymbol{E} \\ \lambda \end{pmatrix} = \begin{pmatrix} \boldsymbol{F} \\ 0 \end{pmatrix} \qquad (5)$$

where $\underline{\boldsymbol{Q}}$ is a block sparse non-hermitian matrix. Each block corresponds to a problem in one subdomain. The sparse matrix $\underline{\boldsymbol{G}}$ expresses the interactions between subdomains. The outer system (5) is solved using a preconditioned GMRES algorithm. The inner problem on each subdomain is also a generalized saddle-point problem, and is solved using a direct method.

References

[1] C. Amrouche et al. : *Vector potentials in three dimensionnal nonsmooth domain.* Mathematical Methods in the Applied Sciences, **21** (1998), pp. 823–864.

[2] F. Assous, J. Segré et E. Sonnendrücker : *A domain decomposition method for parallelization of a three-dimensional Maxwell solver based on a constrained formulation*, Mathematics and Computers in Simulation, **81**, (2011), pp. 2371–2388.

[3] P. Ciarlet Jr : *Augmented formulations for solving Maxwell equations* Comput. Methods Appl. Mech. Engrg. **194**, (2005), pp. 559–586.

[4] P. Ciarlet Jr, S. Labrunie : *Numerical solution of Maxwell's Equations in axisymmetric domains with the Fourier Singular complement method* Differential Equations and Applications **3**, (2011), pp. 113–155.

[5] E. Heintzé : *Résolution des équations de Maxwell tridimensionnelles instationnaires par une méthode d'éléments finis conformes*, PhD Thesis, University of Paris 6, France, 1992.

CONVERGENCE ANALYSIS OF GMRES METHOD FOR EXTERIOR MAXWELL PROBLEM

E. Darrigrand [♭♭], **N. Gmati** [§], **R. Rais** [♭♭,§,*]
[♭♭]Université de Rennes1, IRMAR, France
[§]Université Tunis El Manar, ENIT-LAMSIN, Tunisia.
[*]Email: rania.rais@lamsin.rnu.tn

Abstract

In this paper, we focus on the convergence of the GMRES method for diffraction problems in electromagnetism by a 3D obstacle using the strategy based on coupling of the finite elements and the integral representation. The convergence of the GMRES method has been introduced by I. Moret in a general framework without any additional indicator on the convergence rate. We explain that we have a superlinear convergence of GMRES in our context. The proof is based on the courant-Weyl's min-max principle. Our study is restricted to the case of the perfect conductor problem.

Introduction

We are interested in the resolution of the exterior Maxwell problem. First we introduce an equivalent formulation by adding a regularizing term grad-div in the time-harmonic- Maxwell equation. The aim is to solve an elliptic problem, then it is treated numerically by standard Lagrange finite element instead of edge element. A combination of finite elements and an integral representation reduces the exterior problem to a bounded domain delimited by the surface of the scatterer and an artificial boundary. We derive in this context an analytical proof of a superlinear convergence of GMRES method.

Scattering by a perfect conductor

Let us consider Ω_i a bounded obstacle in $\mathbf{R}^3$ with regular boundary Γ and Ω_e its unbounded complementary. We are concerned with the scattering of a time-harmonic electromagnetic wave by the perfect conductor Ω_i. Our purpose is to determine the total field $\mathbf{E} = \mathbf{E}^s + \mathbf{E}^{inc}$ where $\mathbf{E}^{inc}$ is the incident wave and $\mathbf{E}^s$ is the scattered field. We then consider the following scattering problem:

$$\begin{cases} \textbf{curl curl}\,\mathbf{E} - t^{-1}\nabla(\mathrm{div}\mathbf{E}) - k_s^2\mathbf{E} = 0 \text{ in } \Omega_e, \\ \mathbf{E}\times\mathbf{n}_\gamma = 0, \mathrm{div}\mathbf{E} = 0 \text{ on } \Gamma, \\ \lim\limits_{R\to\infty}\int_{||x||=R} ||\textbf{curl}\,\mathbf{E}^s\times\mathbf{n}_\gamma - ik_s\mathbf{n}_\gamma\times(\mathbf{E}^s\times\mathbf{n}_\gamma)||^2 d\gamma = 0, \\ \lim\limits_{R\to\infty}\int_{||x||=R} |\sqrt{t^{-1}}\mathrm{div}\mathbf{E}^s - ik_s\mathbf{E}^s\cdot\mathbf{n}|^2 d\gamma = 0. \end{cases}$$

$\mathbf{n}_\gamma$ is the exterior unit normal of the domain Ω_i. By the coupling of finite elements and integral representation method introduced for Maxwell equations by C. Hazard and M. Lenoir in [1], we reduce the exterior problem to an equivalent one: find $\mathbf{E}$ such that

$$\begin{cases} \textbf{curl curl}\,\mathbf{E} - t^{-1}\nabla(\mathrm{div}\mathbf{E}) - k_s^2\mathbf{E} = 0 \text{ in } \Omega, \\ \mathbf{E}\times\mathbf{n}_\gamma = 0, \mathrm{div}\mathbf{E} = 0 \text{ on } \Gamma, \\ T_{\nu_1}(\mathbf{E}) = T_{\nu_1}(\mathbf{E}^{inc} - \mathcal{I}_t^{\mathcal{R}}(\Gamma,\mathbf{E})) \text{ on } \Sigma, \\ N_{\nu_2}(\mathbf{E}) = N_{\nu_2}(\mathbf{E}^{inc} - \mathcal{I}_t^{\mathcal{R}}(\Gamma,\mathbf{E})) \text{ sur } \Sigma. \end{cases} \quad (1)$$

where t^{-1} depends on the permittivity and the permeability of air and the regularization parameter. k_s is the wave number, ν_1 and ν_2 are complex numbers which have a strict negative imaginary part .The two operators T_{ν_1} and N_{ν_2} are defined by $T_{\nu_1}\mathbf{E} = \textbf{curl}\,\mathbf{E}\times\mathbf{n}_\sigma + \nu_1(\mathbf{E})_t$ and $N_{\nu_2}\mathbf{U} = \mathrm{div}\mathbf{E} + \nu_2\mathbf{E}\cdot\mathbf{n}_\sigma$. $(\mathbf{E})_t = \mathbf{n}_\sigma\times(\mathbf{E}\times\mathbf{n}_\sigma)$ and $\mathbf{n}_\sigma$ is the exterior unit normal of the domain Ω on Σ. For a sufficiently smooth field $\mathbf{E}$,

$$\mathcal{I}_t^{\mathcal{R}}(\Gamma,\mathbf{E})(x) = -k_s^2\int_\Omega(\mathcal{R}\mathcal{G}_t(x,.)\mathbf{E} + \textbf{rot}\mathcal{R}\mathcal{G}_t(x,.)\textbf{rot}\,\mathbf{E})$$

$$+t^{-1}\int_\Omega \mathrm{div}\mathcal{R}\mathcal{G}_t(x,.)^T\mathrm{div}\mathbf{E} - t^{-1}\int_\Gamma \mathrm{div}\mathcal{G}_t(x,.)^T(\mathbf{E}\cdot\mathbf{n}_\gamma)d\gamma$$

where

$\mathcal{G}_t = G_{k_s}I + \frac{1}{k_s^2}Hess(G_{k_s} - G_{k_p})$, I is the identity matrix in $\mathbf{R}^3$, Hess stands for Hessian operator, $k_p = \sqrt{t}k_s$ and G_k is the fundamental solution of Helmholtz equation. $\mathcal{R}$ is the linear operator that maps every regular function ϕ defined on Γ into a regular function $\mathcal{R}\phi$ defined on Ω that satisfies $\mathcal{R}\phi = \phi$ on Γ and $\mathcal{R}\phi = 0$ on Σ.

Let us introduce $\mathcal{H}_t$ the Hilbert space given by

$\mathcal{H}_t = \big\{\mathbf{E}\in H(\textbf{curl},\Omega)$ such that $\mathrm{div}\mathbf{E}\in L^2(\Omega)$,
$\mathbf{E}\times\mathbf{n}_\gamma = 0, \mathbf{E}\times\mathbf{n}_\sigma\in L^2(\Sigma)^3$ and $\mathbf{E}\cdot\mathbf{n}_\sigma\in L^2(\Sigma)\big\}$

$(.,.)$ denotes the natural scalar product on $\mathcal{H}_t$:

$$(\mathbf{E},\mathbf{E}')_t = \int_\Omega(\mathbf{E}\cdot\mathbf{E}' + \textbf{curl}\,\mathbf{E}\cdot\textbf{curl}\,\mathbf{E}' + |t|^{-1}\mathrm{div}\mathbf{E}\,\mathrm{div}\mathbf{E}')$$

$$+\int_\Sigma((\mathbf{E}\times\mathbf{n}_\sigma)\cdot(\mathbf{E}'\times\mathbf{n}_\sigma) + |t|^{-1}(\mathbf{E}\cdot\mathbf{n}_\sigma)(\mathbf{E}'\cdot\mathbf{n}_\sigma))d\sigma.$$

The reduced problem (1) consists in finding $\mathbf{E}\in\mathcal{H}_t$ such that

$$(\mathcal{A}_t + \mathcal{C}_t)\mathbf{E} = F_t, \quad (2)$$

The operators $\mathcal{A}_t$ and $\mathcal{C}_t : \mathcal{H}_t \to \mathcal{H}_t$ are defined by:

$$(\mathcal{A}_t\mathbf{E},\mathbf{E}')_t = \int_\Omega(\textbf{rot}\,\mathbf{E}\cdot\textbf{rot}\,\mathbf{E}' + t^{-1}\mathrm{div}\mathbf{E}\mathrm{div}\mathbf{E}' + k_s^2\mathbf{E}\cdot\mathbf{E}')$$

$$+\nu_1 \int_\Sigma ((\mathbf{n}_\sigma \wedge \mathbf{E}) \cdot (\mathbf{n}_\sigma \wedge \mathbf{E}') + t^{-1}\nu_2 (\mathbf{n}_\sigma \cdot \mathbf{E})(\mathbf{n}_\sigma \cdot \mathbf{E}'))d\sigma,$$

$$(\mathcal{C}_t \mathbf{E}, \mathbf{E}')_t = -2k_s^2 \int_\Omega \mathbf{E} \cdot \mathbf{E}' + \int_\Sigma T_{\nu_1}(\mathcal{I}_t^{\mathcal{R}}(\Gamma, \mathbf{E})) \cdot \mathbf{E}' d\sigma$$

$$+t^{-1} \int_\Sigma N_{\nu_2}(\mathcal{I}_t^{\mathcal{R}}(\Gamma, \mathbf{E}))(\mathbf{n}_\sigma \cdot \mathbf{E}')d\sigma,$$

and F_t is given by

$$(F_t, \mathbf{E}')_t = \int_\Sigma (T_{\nu_1}\mathbf{E}^{inc} \cdot \mathbf{E}' + t^{-1} N_\nu \mathbf{E}^{inc}(\mathbf{n}_\sigma \cdot \mathbf{E}'))d\sigma$$

The problem (2) is well posed and the operator $\mathcal{A}_t$ is invertible as explained in [1]. If $\mathcal{A}_t$ is chosen as a preconditioner then the problem (2) is formulated as follows $(\mathcal{I}_\Omega + \mathcal{A}_t^{-1}\mathcal{C}_t)\mathbf{E} = \mathcal{A}_t^{-1} F_t$.

1 Convergence analysis for GMRES

There exists a further strategy which consists in solving a problem posed on Σ instead of the problem (2) posed on Ω. We introduce Ψ defined by

$$\Psi = T_{\nu_1}(\mathbf{E}^{inc} - \mathcal{I}_t^{\mathcal{R}}(\Gamma, \mathbf{E})) + t^{-1}\ \mathbf{n}_\sigma N_{\nu_2}(\mathbf{E}^{inc} - \mathcal{I}_t^{\mathcal{R}}(\Gamma, \mathbf{E}))$$

and we consider the operator
$\mathcal{B}_\Gamma^{\mathcal{R}}(\Psi) = T_{\nu_1}(\mathcal{I}_t^{\mathcal{R}}(\Gamma, \mathbf{E})) + t^{-1} N_{\nu_2}(\mathcal{I}_t^{\mathcal{R}}(\Gamma, \mathbf{E}))\mathbf{n}_\sigma$
We get,

$$(\mathcal{I}_\Sigma + \mathcal{B}_\Gamma^{\mathcal{R}})\Psi = \tilde{F}_t \ \text{ on } \ \Sigma. \tag{3}$$

We study the convergence of the resolution for the problem (3). The idea of the proof was initialy introduced by F. Ben Belgacem et al. in [2]. From [1], one can check that $\mathcal{B}_\Gamma^{\mathcal{R}}$ is a compact operator in $(L^2(\Sigma))^3$. Due to the work by I. Moret [4], the GMRES method converges superlinearly to solve the problem (3). In the following part, we present a further proof by verifying the exponentional decaying of each singular value γ_p for $p \geq 0$ of $\mathcal{B}_\Gamma^{\mathcal{R}}$. The first step to prove the convergence of the GMRES method is the construction of an operator $(\mathcal{B}_\Gamma^{\mathcal{R}})_p$ with a rank $\leq p$ which approximates $\mathcal{B}_\Gamma^{\mathcal{R}}$.

Proposition 1 *There exist c and τ two positive constants, such that*

$$\gamma_p \leq c\ \mathrm{e}^{-\tau\sqrt{p}} \ \ \forall\ p \geq 0$$

Proof: The proof is based on the Courant-Weyl min-max principle [3] together with an expansion in term of the Bessel and Hankel funtions and the harmonic spherical functions. In the first step of the proof, we consider the scattering from a perfectly conducting ball with radius R_* and spherical boundary Γ. We suppose that the artificial boundary Σ is the sphere concentric to Γ with radius $R > R_*$. We perform the proof in the case $\nu_1 = \nu_2 = -ik_{s.}$. If the surface of the obstacle is not spherical then we can consider an intermediary spherical surface $\tilde{\Gamma}$ between Γ and the fictitious boundary Σ. Then, the integral representation is written on $\tilde{\Gamma}$ and we can use the same proof.

Proposition 2 *The GMRES method converges superlinearly.*

Proof: We denote r_m the residual at the iteration m Following the theorem 1 of [4] and by the proposition 1 and from Stirling's formula, there exist c and τ two positive constants such that

$$(||\ r_m\ ||_{L^2(\Sigma)^3})^{\frac{1}{m}} \leq \frac{c}{m^\tau};\ \forall m \geq 0.$$

As a future work, we aim to validate this study numerically.

References

[1] **C. Hazard, M. Lenoir**, *On the solution of time-harmonic scattering problems for Maxwell's equations. **S**IAM J. MATH. ANAL. Vol. 27, No. 6, pp. 1597-1630, November 1996.*

[2] **F. Ben Belgacem, N. Gmati, F. Jelassi**, *Convergence bounds of GMRES with Schwarz preconditionner for the scattering problem. International journal for numerical methods in Engineering. 2009; 80:191-209.*

[3] **H. Weyl**, *Das asymptotische Verteilungsgesetz der Eigenwerte linearer partieller Differentialgleichungen (mit einer Anwendung auf die Theorie der Hohlraumstrahlung) (German). Mathematische Annalen 1912; 71:441-479.*

[4] **I. Moret**, *A note on the superlinear convergence of GMRES. SIAM Journal on Numerical Analysis 1997; 34:513-516.*

Shifted Laplace DDM preconditioners for the Helmholtz equation

J. D. Shanks[1,*], **P.N. Childs**[2,†], **I.G. Graham**[1,‡]
[1] University of Bath
[2] Schlumberger Gould Research, Cambridge UK.
*Email: J.D.Shanks@bath.ac.uk †Email: childs4@slb.com ‡Email: I.G.Graham@bath.ac.uk

Abstract

We consider iterative methods for solving the Helmholtz equation with motivation coming from applications in seismic imaging. Once this equation is discretised by finite elements or finite differences (with a suitable boundary condition) the resulting linear system is complex and non-Hermitian. Because of the latter property, conventional iterative methods can fail to converge [2], so it is necessary to precondition the linear system before solving using an iterative method such as GMRES. In this talk we will discuss an optimised Schwarz domain decomposition algorithm for the Helmholtz problem with a complex shift, which can also be used as a preconditioner for the original Helmholtz equation. An analysis of the algorithm will be presented along with numerical examples.

Introduction

When solving the Helmholtz equation on a bounded domain one considers as a model problem the following boundary value problem,

$$\begin{aligned} -\Delta u - k^2 u &= f, \text{ in } \Omega \subset \mathbb{R}^2, \\ (\partial_n + ik)\, u &= 0, \text{ on } \partial\Omega. \end{aligned} \tag{1}$$

Once this is discretised with finite elements we solve the linear system $A\mathbf{U} = f$. Some recent research has focused on preconditioning this system with the discritisation of the following complex shifted problem,

$$\begin{aligned} -\Delta u - \left(k^2 - i\epsilon\right) u &= f, \text{ in } \Omega \subset \mathbb{R}^2, \\ \left(\partial_n + i\sqrt{k^2 - i\epsilon}\right) u &= 0, \text{ on } \partial\Omega. \end{aligned} \tag{2}$$

which we shall call $A_\epsilon \mathbf{U} = f$. This idea was used by Erlangga et. al. [1] where they used solves with the Multigrid method to approximate A_ϵ^{-1}. More recently Kimn and Sarkis [5] used solves with the Restricted Additive Schwarz method to approximate A_ϵ^{-1}. The choice of ϵ so that A_ϵ is a good preconditioner for A and also so that iterative methods for approximating A_ϵ^{-1} work well is a delicate business.

1 Optimised Schwarz methods

We shall use the idea of the optimised Schwarz method without overlap of Gander et. al. [3]. Therefore we take $\Omega = \mathbb{R}^2$ and decomposition it into two equal subdomains $\Omega_1 = (-\infty, 0] \times \mathbb{R}$ and $\Omega_2 = [0, \infty) \times \mathbb{R}$ with an interface $\Gamma = 0 \times \mathbb{R}$. Therefore given u^{m-1} at iterate $m-1$ we solve,

$$\begin{aligned} -\Delta u_1^m - \left(k^2 - i\epsilon\right) u_1^m &= f_1, \text{ in } \Omega_1, \\ (\partial_x + \mathcal{S}_1)\, u_1^m &= (\partial_x - \mathcal{S}_2)\, u_2^{m-1}, \text{ on } \Gamma, \\ -\Delta u_2^{m+1} - \left(k^2 - i\epsilon\right) u_2^{m+1} &= f_2, \text{ in } \Omega_2, \\ (\partial_x + \mathcal{S}_1)\, u_2^{m+1} &= (\partial_x - \mathcal{S}_2)\, u_1^m, \text{ on } \Gamma. \end{aligned} \tag{3}$$

where S_1, S_2 are operators acting tangentially along the subdomain interface Γ, and assumed to be a convolution. By carrying out a Fourier analysis of (3), one can show that the convergence rate of (3) is given by,

$$\rho\left(\sigma, \eta, k, \epsilon\right) = \left(\frac{\sigma_1 - \lambda(\eta, k, \epsilon)}{\sigma_1 + \lambda(\eta, k, \epsilon)}\right)\left(\frac{\sigma_2 - \lambda(\eta, k, \epsilon)}{\sigma_2 + \lambda(\eta, k, \epsilon)}\right), \tag{4}$$

where $\lambda(\eta, k, \epsilon) = \sqrt{\eta^2 - k^2 + i\epsilon}$, (where η comes from performing a Fourier transform tangential to Γ) and σ_1, σ_2 are S_1, S_2 Fourier transformed. We consider parameters σ_i, for $i = 1, 2$, of the form,

$$\sigma_i = \alpha_i(1 + i) + \beta_i(1 + i)\eta^2, \tag{5}$$

and hence,

$$S_i = \alpha_i(1 + i) + \beta_i(1 + i)\partial_{yy}^2. \tag{6}$$

The problem then becomes how to choose σ_1 and σ_2 to ensure that ρ in (4) is as small as possible. This is done by considering the following optimisation problem,

$$\min_{\sigma_1, \sigma_2 \in \mathbb{R}_+} \left(\max_{\eta \in [\eta_{min}, \eta_{max}]} \rho\left(\sigma, \eta, k, \epsilon\right) \right), \tag{7}$$

where we choose $0 < \eta_{min} < \eta_{max}$ for physical reasons.

2 Example

Consider the simplest case $\sigma_1 = \sigma_2 = \alpha(1+i)$ for $\alpha \in \mathbb{R}_+$. This choice is known as *optimised of order zero* ($OO0$). The minimax problem (7) can then be solved analytically under the assumption that $\frac{\epsilon}{k} \to 0$ for large k. The solution is given by,

$$\alpha^* \approx k^{\frac{1}{2}} \epsilon^{\frac{1}{4}}. \tag{8}$$

So that the optimal value of ρ is,

$$\rho^* \approx 1 - \left(\frac{\epsilon}{k}\right)^{\frac{1}{4}} k^{-\frac{1}{4}}. \tag{9}$$

Therefore in this case the number of Schwarz iterations increases like $\left(\frac{\epsilon}{k}\right)^{-\frac{1}{4}} k^{\frac{1}{4}}$. These analytical results will be supported by numerical tests, which show that the number of iterations of the Schwarz algorithm (3) do indeed increase asymptotically like $\left(\frac{\epsilon}{k}\right)^{-\frac{1}{4}} k^{\frac{1}{4}}$. One could consider optimising (7) for a more general choice of parameters α_i and β_i, as was done in [3], [4]. However this can involve numerically solving (7) to observe how the optimised parameters α_i and β_i depend asymptotically on k. This shall be discussed, as will the case of an overlapping decomposition and other choices of ϵ. It is hoped that this method of approximating the solution of (2) by a domain decomposition method using (3), can become an effective preconditioner for solving (1) with convergence nearly independent of k.

References

[1] Y.A. Erlangga, C. Vuik and C.W. Oosterlee, *A novel Multigrid based Preconditioner for Heterogeneous Helmholtz problems*, SIAM J. Sci. Comp, **27** (2006), pp. 1471–1492.

[2] O. G. Ernst and M. J. Gander, *Why it is difficult to solve Helmholtz problems with classical iterative methods*, Numerical Analysis of Multiscale Problems, I.G. Graham, T.Y. Hou, O. Lakkis and R. Scheichl, editors, Proceedings of an LMS Durham Symposium 2010, LNCS 83, Springer Verlag, 2012.

[3] M. Gander, F. Magoules and F. Nataf, *Optimized Schwarz methods without overlap for the Helmholtz equation*, SIAM J. Sci. Comp, **24** (2002), pp. 38–60.

[4] M. Gander, L. Halpern and F.Magoules, *An optimized Schwarz method with two-sided Robin transmission conditions for the Helmholtz equation*, International journal for numerical methods in fluids, **55**, (2007), pp. 163-175.

[5] J-H. Kimn and M. Sarkis, *Shifted Laplacian RAS Solvers for the Helmholtz Equation*, Proceedings of the 20th International Conference on Domain Decomposition Methods, San Diego, U.S.A, 7-11 February 2011, pp. 2047–2078.

3.6 Waves in Industry

Minisymposium organized by Bernard Troclet

Divergence Correction Techniques for the Resolution of the Time-Domain Maxwell's Equations with a Nonconforming Discontinuous Galerkin Method

M. Mounier[1,2,*], **E. Sonnendrücker**[3], **Y. Ventribout**[1]
[1] Nuclétudes, 3 avenue du Hoggar, 91978 Les Ulis, France
[2] IRMA, 7 rue René Descartes, 67084 Strasbourg, France
[3] Max-Plank-Institut für Plasmaphysik, 85748 Garching, Deutschland
*Email: mmounier@nucletudes.com

Abstract

When solving the system of Maxwell's equations, the divergence constraint equations are often neglected. In a simple case, such as when modelling modes, this does not cause an apparent problem. But when a right hand side is added, such as a current term source in the simulations, non physical phenomena related to charge conservation can appear.

We present correction methods that take into account Gauss' law. The novelty of our approach is that we apply these corrections on nonconforming mesh with the help of a Discontinuous Galerkin time domain (DGTD) method.

Introduction

The Maxwell system (1) allows us to determine the evolution of the electromagnetic fields $\mathbf{E}$ and $\mathbf{B}$ from both data charge and current density, ρ and $\mathbf{J}$,

$$\partial_t \mathbf{E} - c^2 \mathbf{rot}\mathbf{B} = -\frac{\mathbf{J}}{\epsilon}, \tag{1a}$$

$$\partial_t \mathbf{B} + \mathbf{rot}\mathbf{E} = 0, \tag{1b}$$

$$\mathrm{div}\mathbf{E} = \frac{\rho}{\epsilon}, \tag{1c}$$

$$\mathrm{div}\mathbf{B} = 0, \tag{1d}$$

where ϵ is the electric permittivity and c is the speed of light. We call equations (1c) and (1d) the divergence constraint equations.

For all times $t \geq 0$, when ρ and $\mathbf{J}$ satisfy the charge conservation equation

$$\partial_t \rho + \mathrm{div}\mathbf{J} = 0. \tag{2}$$

and when the initial $\mathbf{E}$ and $\mathbf{B}$ satisfy (1c) and (1d) the Maxwell system (1a)-(1b) has a unique solution.

Current $\mathbf{J}$ can for example come from an electric-current filament. When data $\mathbf{J}$ is analytically (and consequently ρ), if a numerical method satisfies the conditions of divergence constraint (1c) and (1d) at the initial time, then we can just solve equations (1a)-(1b). In this paper we present the same centered DGTD method as given in [4], which has the property of statisfying the divergence constraint equation only in a weak sense. We show through a numerical test case [3] that a weak sense may not be sufficient and lead to non-physical results. Stock et al. use a correction method to compensate this problem. The originality of our study is to adapt the correction methods on nonconforming mesh such as in Figure 1(b).

1 Centered DGTD on nonconforming mesh

The nonconforming mesh allows us to have hanging nodes, i.e., a mesh can have more than one neighbor in one space dimension. An example of a nonconforming mesh is shown in Figure 1(b).

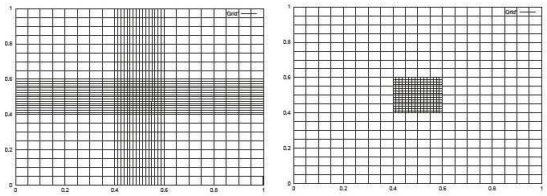

(a) directional refinement mesh (b) nonconforming mesh

Figure 1: refinement mesh

This kind of mesh is useful in modeling highly multi-scale problem, for example when we consider a detail of the order of micrometer in a domain of the order of meter. With a Finite Difference or Finite Element method, a refined mesh is possible only directionally, such as illustrated in Figure 1(a), but it is still hugely computational costly. An interest of the DGTD discretization is to manage nonconforming mesh, Figure 1(b), and so to decrease the computational cost. Indeed, the nonconforming mesh involves an adaptation of interface fluxes, which are managed in DGTD by the local flux matrices.

2 Correction techniques

To satisfy charge conservation, correction techniques consist in adding divergence constraint of Gauss' law to the evolution equation for electrical field $\mathbf{E}$ by a generalized Lagrange multiplier Φ. We solve the following Maxwell system,

$$\partial_t \mathbf{E} - c^2 \mathbf{rot}\mathbf{B} + c^2 \mathbf{grad}\Phi = -\frac{\mathbf{J}}{\epsilon}, \tag{3a}$$

$$\partial_t \mathbf{B} + \mathbf{rot}\mathbf{E} = 0, \tag{3b}$$

$$g(\Phi) + \mathrm{div}\mathbf{E} = \frac{\rho}{\epsilon}, \tag{3c}$$

The new variable Φ defines an additional degree of freedom which respects the following equation

$$\partial_t g(\Phi) - c^2 \Delta \Phi = \frac{1}{\epsilon}(\partial_t \rho + \mathrm{div}\mathbf{J}). \tag{4}$$

We use two choices for the differential operator $g(\Phi)$.

- *Hyperbolic-elliptic formulation :* This formulation corresponds to a Boris' correction [2]. In this approach, we consider in the reformulated Maxwell equations that

  $$g(\Phi) = 0. \tag{5}$$

  This implies, by the equation (3c), that we need to check exactly the Gauss' law. That is why this correction is considered such as the reference correction. But the elliptic correction is costly in computation time because it requires the inversion of a Laplace operator for each time step.

- *Purely hyperbolic approach :* this approach was introduced by Munz et al. [3]. We choose

  $$g(\Phi) = \frac{1}{\chi^2}\partial_t \Phi. \tag{6}$$

  This correction is less expensive but less accurate than the elliptic correction method.

The choice of a non conforming DGTD solver for the Maxwell's equations involved a special adaptation for corrections. It is this adataption that we want to present at the conference in details.

3 Numerical results

Stock et al. in [3] have proven the effectiveness of the hyperbolic correction on a cartesian conforming mesh. We take the test case of their paper to apply on the nonconforming mesh illustrate in Figure 1(b). Figure 3 shows that a correction is needed to keep Gauss' law. Corrections preserve their effectiveness on nonconforming mesh.

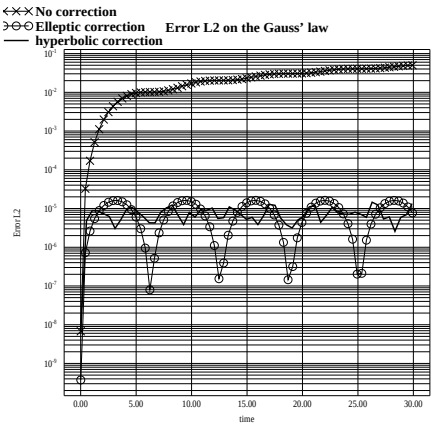

Conclusion

It appears necessary to take into account the divergence constraint of Maxwell's system. Our study shows that the corrections are also robust on conforming or nonconforming mesh. In fututre work we want adapt the correction methods to non conforming mesh for the simulation of plasma with Vlasov-Maxwell equations for which the respect of charge conservation is crucial.

References

[1] C.-D. Munz, P. Omnes, R. Schneider, E. Sonnendrücker and U. Voss, *Divergence Correction Techniques for Maxwell Solvers Based on a Hyperbolic Model*, Journal of Computational Physics , **161** (2000), pp. 484–511.

[2] J.P. Boris, *Relativistic plasma simulations - Optimization of a hybrid code*, Proc. 4th conf. Num. Sim. of Plasma, pp. 3-67, 1970.

[3] A. Stock, J. Neudorfer, R. Schneider, C. Altman and C.-D. Munz, *Investigation of the Purely Hyperbolic Maxwell System for Divergence Cleaning in Discontinuous Galerkin Based Particle-In-Cell Methods*, 4th Conf. on Comp. Meth. for Coupled Problems in Science and Engineering, 2011.

[4] E. Gjonaj, T. Lau and T. Weiland, *Conservation Properties of the Discontinuous Galerkin Method for Maxwell Equations*, Electromagnetics in Advanced Applications, pp. 356-359, 2007.

Defect angular positioning on the wave diffusion through a the Wave Finite Element Method

M. Ichchou[1,*], **M. Kharrat**[1], **O. Bareille**[1]
[1] Ecole Centrale de Lyon, LTDS UMR CNRS 5513
*Email: mohamed.ichchou@ec-lyon.fr

Abstract

This paper provides a numerical investigation concerning the effect of defect angular-position on reflection and transmission coefficients. The spectral method Wave Finite Element has been used to carry out calculation. Results show that the type of incident wave as well as the examined reflected and transmitted waves play an important role in circumferential localization of the defect.

Introduction

A considerable progress has been made over the last few years on the subject of long-range guided wave inspection in pipes [1]. From the numerical pint of view, many useful frequency-domain information, such as wave dispersibility, reflection from damage, interface or boundary, sensitivity of specific mode to various types of damages, mode conversions, etc. can be obtained directly from the eigensolutions in spectral methods, or by the global-local techniques such as hybrid methods [2], [3], [4]. The Wave Finite Element Method (WFEM), which is a spectral method based on the standard finite element (FE) formulation, can be applied to examine the wave interaction with the local defects and the structural features. The hybrid WFE/FE method is one of the hybrid methods for global-local analysis, which is very suitable to the case that wavelength is larger than the axial extension of FE model for complex local defect.

This paper aims to investigate numerically reflection and transmission coefficients from a defined defect in a pipe while varying its angular position at a fixed axial location. The hybrid WFE/FE method has been employed in this study to compute diffusion matrices from the defect, in order to find an approach for the angular localization of the defect.

1 Numerical implementation and results

The principle of the study is to vary the circumferential position of the defect while keeping the axial position constant, and observe the influence of this variation on the reflection and transmission coefficients (see figure 1). The circumference of the pipe is divided into 44 elements. Positions of the defect around the pipe are varied by an increment of 4 elements, that is an angle of about $\Delta\alpha = 32.73°$. Thus, 11 positions were treated in this study as illustrated in figure 2. Three types of incident waves are used: fundamental torsional mode T(0,1), longitudinal mode L(0,2), and flexural mode F(1,2). Let's consider the torsional wave T(0,1). The torsional mode T(0,1) has shown a relevant capability for defect detection in pipes and possesses a lot of advantages in the long range guided waves inspection domain. The first test in our investigation consists of impinging the considered defect by the T(0,1) mode. When T(0,1) is incident, reflection and transmission coefficients of T(0,1), L(0,2) and the three above-mentioned flexural modes are calculated. Several important observations could be taken from the obtained curves. Figure 3 shows the reflection and transmission coefficients of the T(0,1) mode from the considered defect for the 11 positions around the circumference of the pipe. We can note that there is no variation in the obtained

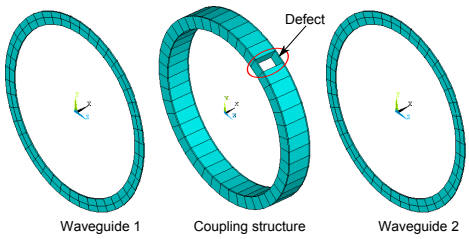

Figure 1: Defect positions around the circumference of the pipe.

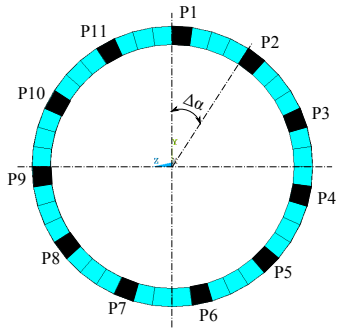

Figure 2: Defect positions around the circumference of the pipe.

curves depending on the circumferential position of the defect. This is obvious regarding the axisymmetry of the T(0,1) mode that makes it insensitive to an angular rotation of the defect.

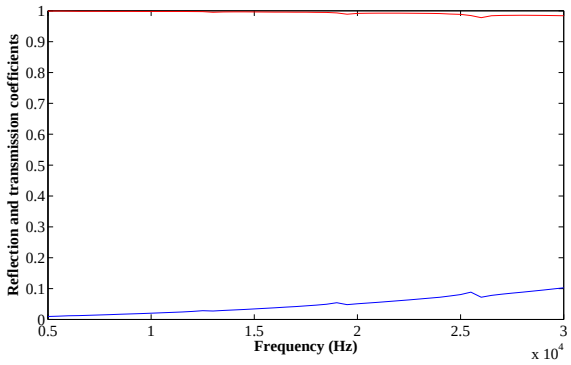

Figure 3: Reflection coefficients (blue line) and transmission coefficients (red line) of T(0,1) from a with a T(0,1) incident mode.

Figures 4 and Figures 5 shows the reflection coefficients of F(1,2) and F(3,2) respectively when T(0,1) is incident. From these figures we can note that for modes F(1,2) and F(3,2) each two positions have the same reflection/transmission coefficient curve except position P9; for example curves of P1 and P6 are confused. That is to say a given reflection/transmission coefficient at a given frequency refers to two possible circumferential positions, which is practically not convenient to localize the circumferential position of the defect. However, the result found in the F(2,2) case shows that each position produces its own reflection/transmission coefficient curve. The F(2,2) mode seems to be more suitable for circumferential localization of the defect when T(0,1) mode is incident. It should be mentioned that these flexural waves, as they are nonaxisymmetric, are sensible to the circumferential position of the defect. Nevertheless, each mode has his own mode shape which impacts on the result.

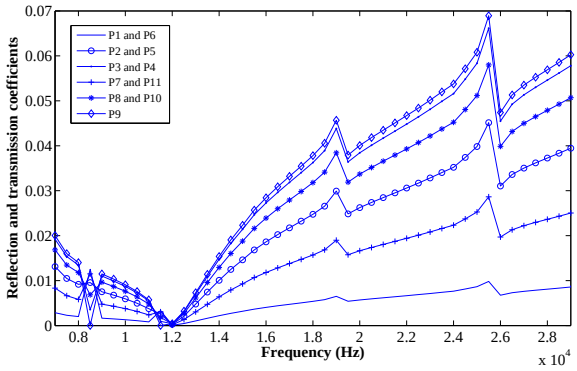

Figure 4: Reflection coefficients of F(1,2) with a T(0,1) incident mode.

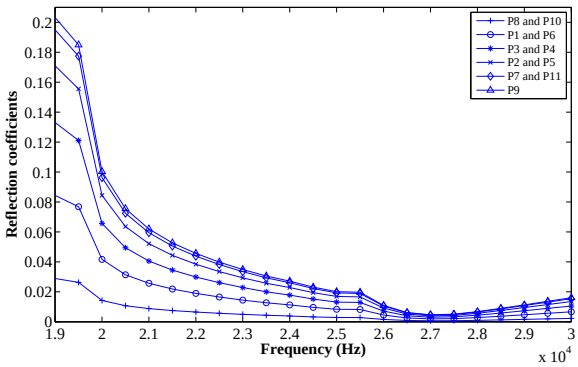

Figure 5: Reflection coefficients of F(3,2) through-thickness defect with a T(0,1) incident mode.

References

[1] D. Alleyne, P. Cawley, The long range detection of corrosion in pipes using lamb waves, Review of Progress in Quantitative NDE 14 (1995) 2073–2080.

[2] M. Ichchou, J. Mencik, W. Zhou, Wave finite elements for low and mid-frequency description of coupled structures with damage, Computer Methods in Applied Mechanics and Engineering 198 (15-16) (2009) 1311–1326.

[3] W. Zhou, M. Ichchou, Wave propagation in mechanical waveguide with curved members using wave finite element solution, Computer Methods in Applied Mechanics and Engineering 199 (33-36) (2010) 2099–2109.

[4] W. Zhou, M. Ichchou, Wave scattering by local defect in structural waveguide through wave finite element method, Structural Health Monitoring 10 (4) (2011) 335–349.

Industrial simulation of electromagnetic wave propagation

Christian BROCHARD.
Astrium Space Transportation.
Email: Christian.Brochard@astrium.eads.net

Abstract

Astrium has been dealing with computational electromagnetics for more than 30 years. Generally speaking, the goal is to predict the electromagnetic behaviour of a body. It can be to calculate the radar cross-section of a target, its "signature", in order for a radar operator to detect and identify it, or to make it as "stealthy" as possible, when designing missiles or atmospheric re-entry vehicles.
Another concrete issue can be the design of an antenna, that can be optimised so that it gives maximum capacity in the environment in which it is used. For such activities, we use various and very performing methods in the harmonic domain, such as boundary element or finite element methods, or analytical asymptotic methods with various direct or iterative solvers and preconditioners or accelerating techniques.

The problem

The problem we are dealing with is to compute the electromagnetic response of a tridimensional structure under an excitation. The physical phenomenas are the same: an incident electromagnetic field creates currents (magnetic and electric) on the surface and inside materials; these currents generate an electromagnetic field in the surrounding space. The general problem is described by Maxwell equations. The numerical methods developed by our teams solve these equations in the frequency domain. There are two main methods (which are called exact in opposition to asymptotic methods).

Methods

Methods We first describe the surfacic methods: they put the unknowns on the boundaries of the solid domains which compose the considered objects and which contain implicitly the boundary limit conditions. Our surfacic method is based on the integral representation of MAXWELL equations (cf.[1]), well known as EFIE (Electric Field Integral Equation) for objects composed with dielectric or perfectly conducting materials:

$$\int_{\Gamma\times\Gamma} [\phi(x).\phi^t(y) - \frac{1}{k^2}\, div\phi(x).div\phi^t(y)].G(x-y).dx.dy = \frac{i}{kZ_0} < E_{inc,\phi^t} >$$

excitation of the problem (incident wave, generator, etc.). For every pair of points (x, y) of Γ (the surface of the body) there is an interaction with an intensity given by the Green kernel G :

$$G(x-y) = \frac{e^{ik|x-y|}}{4\pi|x-y|}$$

Therefore, the complex matrix is a full one. The advantage of these surfacic methods is to transform the initial volumic problem of calculating the electromagnetic field which is scattered in the whole space, into a surfacic equivalent problem acting on electric and magnetic currents J and M on the boundaries. But these methods have an inconvenient: they can take into account only homogeneous and isotropic materials.
The second "exact" methods are volumic ones which calculate inside the volumic domains. They are able to modelize objects with arbitrary physical and geometrical characteristics, but they deal with a great amount of unknowns and they need an explicit boundary condition.
Volumic methods have been developed to calculate electromagnetic behaviour of objects covered by layers of materials, which are no more homogeneous or isotropic without any approximation (cf.[2]). The calculation domain is then parted into 2 areas separated by a coupling surface.

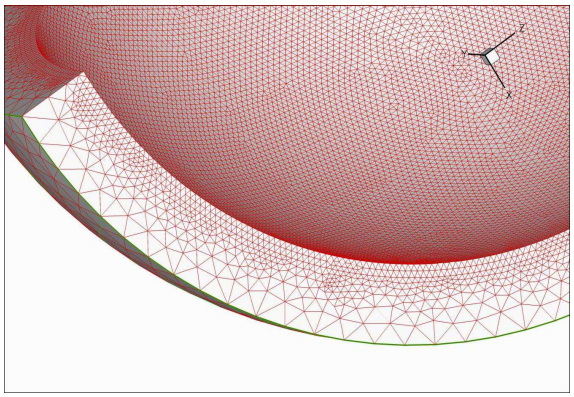

The inner problem is solved by the way of partial derivative equations of the Maxwell system using H(rot) Volumic Finite Elements (cf.[3]), and the external problem is solved using integral equations on the coupling surface.

Direct or iterative solver

A numerical code has been developed since 1989, which is widely used within EADS under the trade name ASERIS-BE.
With the direct solvers, we factorise the matrix which is a very expensive step with a huge number of operations in $O(N^3)$ where N is the number of unknowns.
With iterative solvers we approach the solution step by step using a matrix-vector product which is in $O(N^2)$.
But when N increases, the classical solution of the problem, becomes hugely expensive in CPU duration as well as in storage amount. Therefore, to push the limits, we have developed an iterative solver and a fast matrix-vector product called FMM, for Fast Multipole Method. We are now using it in our daily work for problems with perfectly conducting domains, for dielectric materials with complex coefficients, with wires, antennas, etc...

The FMM (Fast Multipole [Multilevel] Method)

We can give the following description (cf.[4]):

- As a solver, the FMM replaces the standard matrix-vector product by an approximate but fast computation. It works in $O(N\,log\,N)$ time compared to $O(N^2)$ with the usual method,
- From an electromagnetic point of view, FMM cuts scattering body into boxes, and calculates for each of them a radiation function in the far field approximation. These functions are then used to calculate all the interactions between boxes that are sufficiently distant,
- From a matrix point of view, FMM cuts every term $A_{i,j}$ of the matrix A in a sum of terms separating indices i et j which enables a fast computation of the matrix-vector product,
- As an algorithm, FMM travels through a tree which is based on a recursive partition of the scattering body. It is the reason of the asymptotical duration evaluation in $O(N\,log\,N)$.

In order to accelerate the convergence of the solution, we have developed efficient parallel algorithms and preconditioning technics such as SPAI, for Sparse Approximate Inverse Preconditioner.

Work Group

Teams from Astrium, EADS Innovation Works and CEA, met in a work group to exchange on numerical technics used in their own computation codes. A very good agreement was found between numerical results, which confirms the excellence of the codes in the domain of benchmarking. This high level of performance shows the major advantage that can be taken from big computers with a great amount of processors.
"On 2011 May 19., the French Defence Procurement Agency (DGA), awarded its Science & Defence prize to Christian Brochard of Astrium Space Transportation, who had teamed up with Guillaume Sylvand from EADS Innovation Works and with Michel Mandallena and Bruno Stupfel from CEA/CESTA, in recognition of their work on high performance simulation of wave propagation phenomena"

We are now looking forward to solving problems involving hundreds of millions of unknowns such as encountered for radiation in a re-entry plasma or for windmills stealth. In the frame of this FMM work, parallel multilevel H-Matrix methods seem to be a new breakthrough for the years to come.

References

[1] A. Bendali, "Approximation par éléments finis de surface de problèmes de diffraction des ondes électromagnétiques", Thèse de doctorat de l'Université de Paris 6 (1984)

[2] V. Levillain, "Couplage éléments finis - Equations intégrales pour la résolution des équations de Maxwell en milieu hétérogène", Thèse de doctorat de l'Ecole Polytechnique (1991)

[3] J.C. Nédélec, "Mixed elements in R^3", Numer. Math. 35, pp. 315-341 (1980)

[4] G. SYLVAND "La méthode multipôle rapide en électromagnétisme : performance, parallélisation, applications", Thèse de doctorat de l'école nationale des ponts et chaussées (2002)

Ten Industrial Challengesin Wave Propagation Simulation(at EADS)

Eric Duceau
Scientific Director, EADS Innovation Works, BP 76 Suresnes F92152

The presentation deals with the different hurdles that prevent the industrial day-to-day use of Modelling and Simulation activitiesfor the domain of wave propagation. The show stoppers are sorted as follows: **affordability** (the bricks are identified and the limit in usage only depends on time-to-market; software vendors as well as in-house solutions may likely make the step for-ward), **maturity** (the mathematical tools seems identified but the resolution has not yet been demonstrated; short term research can be launched with significant level of confidence) and **understanding** (this means that the modelling phase is not yet available and that fun-damental research should be triggered if the industry wishes to solve the point). I'll be focusing on the 2 last axes to contribute to a potential roadmap in Modelling. I'll just re-mind you with the "starting point" for industrial research labs that can be guessed out of the concerns described in the first axis, which, nevertheless, contains some interesting questions.

1 Affordability as a main driver

Numerical methods have dramatically changed the way of working in engineering of waves thanks to 2 successive revolutions: the FMM breakthrough, end of 90' and, recently, the H-Matrix breakthrough. Even if the mathematical demonstration is not achieved for all formula-tions, engineers have immediately taken the opportunity to pragmatically and systematically test all of them. The result is amazing: performances seem to be improved and accuracy not degraded: the Grail? Not far from ! But remaining industrial hurdles slow down the integration:

- Pre processing is still a nightmare: automatic generation of 100 millions of triangles, without too much distortion or unexpected refinement is a real challenge; and when it comes to mixed surface-volume formulations, mesh generation is too often a show-stopper. (**Challenge 1**)

- Breakthrough in Volume Formulation (Finite Element methods, Galerkine discontinuous etc.) are definitely not at the same level, so couplings between volumic and surfacic formulation suffers from the weaknesses of the 3D part; challenges refer to linear algebra (MUMPS or equivalent libraries for example).(**Challenge 2**)

- Post-processing may represent one of the next "computer science" challenges in the propagation domain for some applications demand a lot of right-hand-sides to be processed (holographic RADAR images being the most representative one). Solutions are currently expected from SVD-like methods; Compress sensing theory could revisit the topic soon...(**Challenge 3**)

Examples will be presented to illustrate the "state-of-the-art" in this perimeter: acoustic propagation of waves in an inhomogeneous flow for the limit we encounter within the coupling approach; Radar Cross Section computation for the last topic.

2 Maturity as a main driver

Unfortunately, the requirements from industry regarding Modelling & Simulation tools have became more demanding and the 2 former breakthroughs do not cover the expectation. The following list gives some typical applications for which a full demonstration has not yet clarify the maturity of the approach:

- Margin analysis is one of the main drivers for simulation in lot of domains. For electromagnetic or acoustic applications, the medium is often consider as well known although the boundary conditions are one of the main sources of uncertainty (just have a look to the inside part of an Aircraft cabin for noise refection/diffusion or wireless installation!). From a mathematical point of view, this problem may lead to modelling a set of deterministic configuration, each of them being a sample of the universe of boundary conditions: not realistic! The worsecase analysis (needed in safety demonstration) cannot be tackled that way too. The corresponding problem can be described as follows: two components are well known (uncertainty propagation in the one hand, a direct solver in the other hand) but we still miss a strategy to couple them in an efficient way (from an industrial point of view) and demonstrate that the results means something valuable...(**Challenge 4**)

- Sensitivity with respect to parameters has been investigated since decades and can be considered as closed from a mathematical point of view in some areas (derivation, Pad? expansions, even topological optimisation, etc). As a matter of facts, only a few software tools exploit such a capability, each time

in a very restricted domain of application. Needs in EADS will be presented with examples: sensitivity to Mach number within acoustic propagation, sensitivity to scaling effects in metamaterials on top of basic sensitivitivity with respect to frequency.(**Challenge 5**)

- Sizing is the main activity in the Design Phase and tools are supposed to speed up that process and give it a better robustness thanks to a better understanding (modelling) and accuracy (margin management). A characteristic requirement in the Design Phase is the need for model reduction methodology. Lots of model reduction algorithms have been published and the buzz is being running well. But a lack of systematic approach prevents industry from efficient usage. Key examples for EADS in Electromagnetic Compatibility are related to "probability to exceed a threshold" or "standard deviation around a mean value" and they do not lead to the same model reduction algorithm as far as propagation effects are concerned.(**Challenge 6**)

3 Understanding as a show stopper

Simultaneously, the requirements from industry regarding Modelling & Simulation tools have became more demanding and the 2 former breakthroughs do not cover the present expectations. The following list gives some typical applications for which a full demonstration has not yet clarify the maturity of the approach:

• Electromagnetic and/or acoustic Wave for periodic materials & metamaterialleads to at least two different problems:

1. Being able to model defects in a periodic structure (see fig. 1) has been investigated[1][2][3] but the models are still not efficient enough to be exploited in an industrial contex. Industrial examples one may

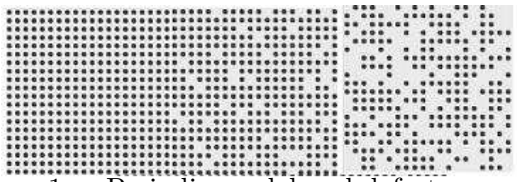

Figure 1: Periodic model and defects, randomly located according to 2 different distributions

think about: an array antenna with broken elements inside; or detection of a defect in a structured material. (**Challenge 7**)

[1]for example Benoit Lizé's presentation at Waves 2013
[2]S. Fliss' PhD thesis
[3]A. Anantharaman -G.Allaire in CMAP internal document

2. being able to model "metamaterial" concepts in a efficient way. Applying domain decomposition techniques seems appropriate and might be accelerated when similarity of geometry is taken into account. Parametric optimisation being the final goal , properties of parametric Dirichlet-to-Neumann operators may be analysed. (**Challenge 8**)

• Elastic and/or Electromagnetic waves in "quasi random" medium (see fig. 2): industrial composite material gives a representative example of the complexity we face today. Very promising approaches have been proposed which are not pure homogenisation techniques and lots of mathematical problems remains open. This material is not periodic, yet

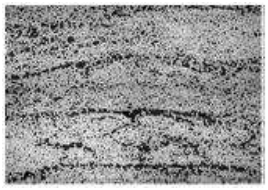

Figure 2: 2D cut of a composite material

there is some kind of underlying periodic arrangement of the fibbers. Taking advantage of the industrial process behind, one can assume that a random perturbation of a regular structure can be a good model to derive homogeneous equivalent parameters.[4] (**Challenge 9**)

• Acoustic wave propagation in a "random" given flow is a major scientific challenge now that the "affordability" for constant or rotational flow is managed: Is stochastic PDE a realistic approach? As in the previous approach, we're trying to find out modelling approaches that cover a locally perturbed propagation phenomenon, the perturbation being of a random nature (or, at least, described by stochastic parameters linked to correlation in space and time for example) (**Challenge** 10)

4 Conclusion:

Challenges for modelling complex propagation effects, as described in this context, refers to various competences. The 3 first ones requires mainly computer science skills. The next 3 ones are well-known mathematical problems and the industrial solutions may emerge in the incoming years. The last four obviously demand a "reinforced" mathematical frame to be tackled. The presentation will develop those examples to help positioning new research axes.

[4]A. Anantharaman -C LeBris in CERMICS internal document

RECENT ADVANCES IN NUMERICAL SIMULATION TO PREDICT INTERIOR NOISE FOR FULL VEHICLE APPLICATIONS

Slaheddine Frikha
ESI France - 99 rue des Solets - Rungis - France
Slaheddine.Frikha@esi-group.com

Abstract

This contribution will give an overview and describes a number of recent advances in the prediction of interior noise with a focus on transport system acoustic comfort. At low frequencies, the response of a system is typically dominated by a small number of modes; standard analysis methods based on finite elements, boundary elements and infinite elements typically provide an accurate description of the response. At high frequencies, the higher order modes of a system tend to be particularly sensitive to small perturbations in the properties of the system. A statistical description of a system becomes essential in order to draw meaningful conclusions about the response. The transition between low and high frequency region so-called the medium frequency ranges is addressed by Hybrid approach which has been demonstrated to be very efficient for structure-born noise analysis.
All these modeling approaches are available in the commercial software VA One which offers a suite of fully coupled solvers in a single plateforme.

Introduction

The perceived quality of a vehicle is strongly influenced by the interior noise that a passenger experiences in the vehicle. In order to model interior noise it is useful to adopt a source-path-receiver model. The sources can be separated into air-borne sources (that inject energy directly into acoustic spaces surrounding the vehicle) and structure-borne sources (that inject energy directly into the body structure). The transmission paths, by which noise and vibration travel to the interior of the vehicle, are also typically different for each source and require low, medium and high frequency dedicated analytical and numerical approches. The paper present recent advance to address air-borne and structure-borne noise in the full frequency range with a focus on mid-frequency range where both structure-borne and airborne contribution to interior noise are significant.

1 FE Models of fully Trimmed vehicle

At low frequencies, Finite Element models provide a good way to describe interior noise. The recent advances in acoustic package design based on porous-elastic material tend to significantly increase the contribution of trimming component to structural damping (resistive effects) and to reduce the acoustic power transmitted by the structural vibrating into adjacent cavity. A number of advances have been made recently in the development of rigorous Finite Element descriptions of bi-phase porous-elastic materials:

$$\begin{cases} div(\dfrac{1}{\omega^2 \tilde{P}_f} grad\,\varphi P - \beta U) + \alpha div\, U + \dfrac{\varphi P}{R} = & 0 \\ \omega^2 \tilde{P}_s U + div(\sigma_{kl} - \alpha\varphi p \delta_{kl}) + \beta grad\,\varphi P = & 0 \end{cases}$$

The trimmed body is described as an assembly of a body, a cavity and an ensemble of trimming component. This substructuring approach developped by prof. M. A. Hamdi leads a plug-in equation:

$$\left[\begin{pmatrix} [\Omega_s^2 - jD - \omega^2 I] & -\tilde{C} \\ -\tilde{C}^T & [\Omega_F^2 - \omega^2 I] \end{pmatrix} - \begin{pmatrix} \tilde{Y}_{ss} & \tilde{Y}_{sc} \\ \tilde{Y}_{cs} & \tilde{Y}_{cc} \end{pmatrix}\right] \begin{Bmatrix} \tilde{W} \\ \tilde{P} \end{Bmatrix} = \begin{Bmatrix} \tilde{F} \\ 0 \end{Bmatrix}$$

Where sound packages impedances are simply added to the body in white impedance. This allows drastically reducing the memory storage and CPU usage to solve the challenging full-FE model of a complete trimmed car in a few hours, using standard computer facilities.

2 SEA models for Interior noise

The use of SEA for airborne interior noise prediction is now a standard part of production modeling for most automotive OEMS and suppliers. Figure 8 shows a typical airborne SEA model.

The model includes the major structural and acoustic components that are important for transmission, along with the sound package, pass-through and leakage paths. While the basic modeling approach for airborne SEA is well established, advances are still being made. Models of poro-elastic materials continue to improve and more detailed descriptions of sound package are now possible.

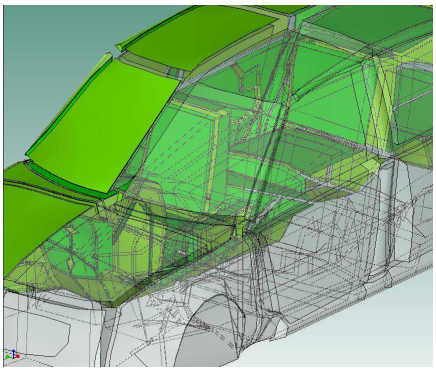

Typical airborne SEA model.

3 The Hybrid FE-SEA Method

A hybrid FE-SEA method ideally combines the low frequency performance of the FE method with the high frequency performance of SEA to produce a robust method that can close the gap where none of the standard FE or SEA approaches applies perfectly.
The main difference to be overcome between FE and SEA approaches lies in the fact that:
- FE is based on dynamic equilibrium while SEA is based on the conservation of energy flow,
- FE is a deterministic method while SEA is inherently random.

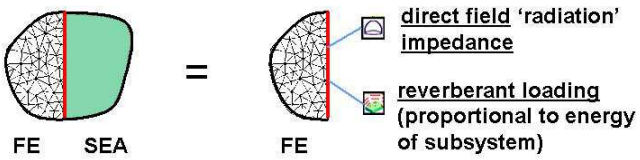

Hybrid approach principle.

In order to express the coupling between deterministic components modeled by finite element method with random components modeled as SEA subsystems, both continuity relationship and flow energy balance have to be verified along the hybrid junctions.
From the point of view of the deterministic subsystem, the SEA random subsystem is perceived as an infinite media that apply to the FE subsystem an added-impedance and a set of uncorrelated and randomly distributed incident waves. These incident waves are representative of the reverberant filed in the SEA subsystem. A similar phenomenon is encountered when modeling the structure excited by a diffuse field in reverberant chamber. Such problem is commonly being represented by a structure coupled to an infinite media and excited by a set of uncorrelated plane waves. The infinite media adds reactive and resistive impedance to the modes of the structure, which can be represented by a complex "modal radiation impedance" matrix. The magnitude of the plane waves loading depends on the energy in the reverberant chamber.

4 Conclusions

All these modeling approaches are available in the commercial software VA One. Detailed theoritical background will presented and some validation results will be shown in the conference.

References

[1] M.A. HAMD and al., An efficient Formulation for the Analysis of Acoustic and Elastic Waves propagation in Porous-Elastic Materials", ISMA 25,, 13-15 septembre 2000, Katholieke Universiteit Leuven, Belgium.

[2] M.A. HAMDI, and al, "An efficient Finite Element Formulation for the Analysis of Acoustic and Elastic Waves propagation in Sound Packages", SAE Noise & Vibration 2001, April 30-May 3, 2001, Traverse City, Michigan, USA.

[3] Ph. Shorter, and R. Langley. "On the reciprocity relationship between direct field radiation and diffuse reverberant loading" JASA 117, 85-95. 2004.

[4] Ph. Shorter, P. and R. Langley, "Vibro-acoustic analysis of complex systems" JSV. 288(3), 669-699, 2005.

Contributed talk abstracts

3.7 Inverse problems

Comparative SVD-analysis of standard L_2 Full Waveform Inversion and its Migration Based Travel Time formulation

G. Chavent[1], K. Gadylshin[2,3,*], V. Tcheverda[3]
[1] Inria-Rocquencourt, Domaine de Voluceau,
BP 105, 78153 Le Chesnay Cedex, France
[2] Novosibirsk State University, Mechanics and Mathematics Department
Pirogova 2, 630090 Novosibirsk, Russia
[3] Institute of Petroleum Geology and Geophysics, SB RAS
Prosp. Akademika Koptyuga 3, 630090 Novosibirsk, Russia
*Email: GadylshinKG@ipgg.sbras.ru

Abstract

The common knowledge now is that standard least squares Full Waveform Inversion is unable to reconstruct macrovelocity for reasonable frequency band of input data but claims unpractically low time frequencies. There are a range of different approaches to overcome this weakness and among them Migration Based Travel Time reformulation of the cost function. Here we compare SVD for linear approximation of standard least squares Full Waveform Inversion with its Migration Based Travel Time reformulation. In order to do that we start with linearization of both nonlinear forward maps with subsequent computations of singular spectra (singular values and right/left singular vectors) for corresponding linear operators. The next step is to construct the two families of linear spans of right singular vectors corresponding to a set of fixed values of the condition number and to analyze their mutual disposition. Our computations demonstrate the reliable reconstruction of the smooth velocity component by full waveform inversion in migration based travel-time formulation.

1 Introduction

Constructing a smooth velocity model (propagator, macro velocity constituent) in the depth domain, which is responsible for correct travel-times of wave propagation is a key element of the up-to-date seismic data processing in areas with complex local geology. Theoretically it could be obtained, along with the subsurface structure, by the Full Waveform Inversion (FWI) technique matching the observed and the synthetic seismograms (Tarantola, 1984). The L_2 norm is usually used for this matching, though other criteria are also considered. To minimize the misfit function and to find the elastic parameters of the subsurface, iterative gradient-based algorithms are usually applied. Such approach to solving seismic inverse problem proposed originally by Tarantola (1984) has been developed and studied in a great number of publications (see Virieux and Operto, 2009, and the references therein).

However, the straightforward application of FWI reconstructs reliably only the reflectivity component of the subsurface but fails to provide a smooth velocity (propagator) component of a model. In order to overcome this trouble G.Chavent with colleagues introduced Full Waveform Inversion in Migration Based Travel-Time formulation (2001). The main idea of this approach is to decompose model space into two orthogonal subspaces - smooth propagator and rough reflector with subsequent reformulation of the cost function.

2 Methods

2.1 Statement

Full Waveform Inversion formally is application of non-linear least squares for seismic inverse problem treated as a nonlinear operator equation

$$\mathcal{F}[m] = d.$$

Here the known right-hand side d is multi-source multi-receivers seismic data, $\mathcal{F}$ is a non-linear operator (forward map) which transforms the current model m to synthetic data. For the sake of simplicity we deal with the Helmholtz equation:

$$\Delta u + \frac{\omega^2}{c(x)^2} u = f(\omega)\delta(x - x_s)$$

with data d being its solution computed at receivers positions.

Instead of regular non-linear least squares formulation of Full Waveform Inversion, when unknown

function $c(x)$ is searched as

$$c_* = \underset{c}{argmin} \|\mathcal{F}(c) - d\|^2, \qquad (1)$$

MBTT introduces the following decomposition of the model space:

$$m = p + r = p + \Pi_r \mathcal{M}(p) < s > .$$

Here $p \in P$ describes smooth macrovelocity, which does not perturb significantly direction of waves propagation, but governs their travel times. In contrast the **depth reflector** r describes rough perturbations of the model, which send seismic energy back to the surface, but do not change travel-times. The key moment here is interrelation $r = \Pi_r \mathcal{M}(p) < s >$ where s is unknown **time reflectivity**, $\mathcal{M}(p)$ - a true amplitude prestack migration operator with linear reweighing W and Π_r is the orthogonal projector onto the space of reflectors (orthogonal to the space of propagators). In more details this operator is written down as

$$\mathcal{M}(p) < s >= W \circ Re \left\{ \left(\frac{\delta \mathcal{F}}{\delta m}(p) \right)^* < s > \right\},$$

where * denotes adjoint operator in application to Frechet derivative of nonlinear forward map $\mathcal{F}$.

In this notations MBTT formulation of FWI with respect to propagator p and time reflectivity s is as follows:

$$(p^*, s^*) = \underset{p,s}{argmin} \|\mathcal{F}(p + \Pi_r \mathcal{M}(p) < s >) - d\| \quad (2)$$

It is worth mentioning that the argument of the cost function in MBTT formulation is linear with respect to the time reflectivity s and is essentially nonlinear with respect to the depth propagator p.

2.2 Linearized inversion

In the linear approximation FWI in standard least squares formulation (1) leads to a linear operator equation of the first kind with respect to the model perturbation:

$$\frac{\delta \mathcal{F}}{\delta m}(m_0) < \delta m >= d - \mathcal{F}(m_0)$$

while in MBTT formulation we have the following linear operator equation with respect to propagator perturbation:

$$\frac{\delta \mathcal{F}}{\delta m}(m_0) \left\langle \delta p + \Pi_r \left(\frac{\partial M}{\partial p}(p_0) < \delta p > \right) < s > \right\rangle$$

$$= d - \mathcal{F}(m_0)$$

3 Illustrations

In Fig.1 one can see the result of the linear Full Waveform Inversion in MBTT formulation for for the simplest model - step-like vertical heterogeneous velocity. Input data are synthesized for Ricker pulse of 25 Hz and frequencies staring 10 Hz are used for inversion. There are two figures - reconstruction of the full model and its smooth macrovelocity component (propagator). One can recognize almost perfect reconstruction of propagator. Some defects in reflector recovery can be explained by the imperfection of the procedure of prestack true amplitude migration. High frequency oscillations can be easy removed by taping time frequency band in use.

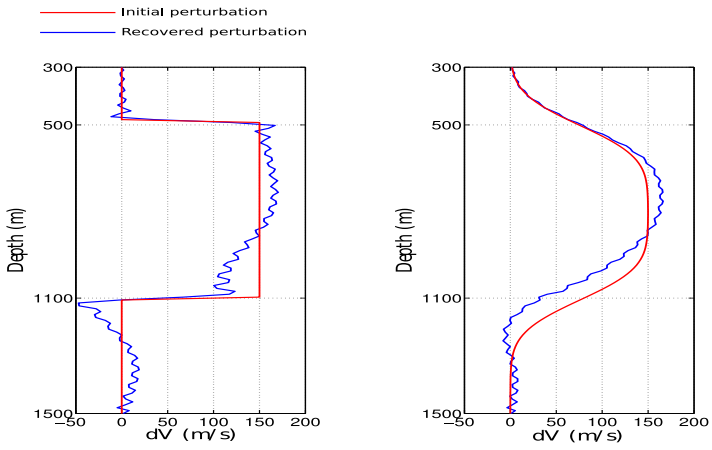

Figure 1: Projections for MBTT formulation. Left - full model, right - macrovelocity component.

Acknowledgements

The research described in this publication is partially supported by RFBR grants 11-05-00947, 12-05-31008, 13-05-00076 and President Grant SP-150.2012.5.

References

[1] F. Clement, G. Chavent and S. Gomez, *Migration-based traveltime waveform inversion of 2-D simple structures: A synthetic example*, Geophysics, **66** (2001), pp. 845–860.

[2] A.Tarantola, *Inversion of seismic reflection data in the acoustic approximation*, Geophysics, **49(8)** (1984), pp. 1259–1266.

[3] J.Virieux, S.Operto *An overview of full-waveform inversion in exploration geophysics*, Geophysics, **74(6)** (2009), WCC1 - WCC26.

Interior point method for time-dependent inverse problems

Loredana Gaudio[1,*], **Marcus J. Grote**[1], **Olaf Schenk**[2]
[1] Department of Mathematics and Computer Science, University of Basel, Basel, Switzerland
[2] Institute of Computational Science, Università della Svizzera italiana, Lugano, Switzerland.
*Email: Loredana.Gaudio@unibas.ch

Abstract

In many inverse problems, box-constraints are used to include some a priori information about the model. We present the numerical solution of a box-constrained inverse problem governed by an acoustic wave equation with unknown coefficients. The identification process is guided by a waveform misfit functional, that is the difference among synthetic and observed measurements at some receivers. Ill-posedness of the problem is tackled through Tikhonov regularization. Finite differences in time and spectral finite elements in space are used for the space-time discretization of both the forward and backward waves associated with the minimization. To also handle inequality constraints, we propose to use an Interior-point Optimization algorithm. Numerical tests illustrate the performance of the suggested optimization method.

Inverse problem

Parameter identification from data measurement is of interest in many engineering applications. The problem is here formulated as a PDE-constrained optimization problem, where the control variable represents the parameter profile we want to identify through minimization.
Let Ω be a bounded domain in $\mathbb{R}^d$, with boundary $\partial\Omega$, and let be $T > 0$ a fixed time. The propagation of an acoustic wave on $\Omega \times [0, T]$ is described by :

$$\begin{cases} \partial_{tt} u(\mathbf{x},t) - \nabla \cdot (c(\mathbf{x})^2 \nabla u(\mathbf{x},t)) = f(\mathbf{x},t) \ \ \Omega \times (0,T), \\ u(\mathbf{x},t) = 0, \ \partial_t u(\mathbf{x},t) = 0 \quad \forall \mathbf{x} \in \Omega, t = 0, \\ \partial_\nu u(\mathbf{x},t) = 0 \quad \forall \mathbf{x} \in \partial\Omega, \forall t \in (0,T). \end{cases} \tag{1}$$

where $\mathbf{x} \in \Omega$, t are the spatial and time coordinate, respectively, $u(\mathbf{x}, t)$ is the pressure wave field, $c = c(\mathbf{x})$ is the velocity profile, f is the source signal and $\partial_\nu(\cdot)$ the co-normal derivative. For each velocity profile $c(x)$, there exists a unique wave field $u \in V$, solution of (1), with V a suitable functional space.
Let $\Omega_o \subset \Omega$ be an observation domain (usually defined as a set of receivers), and u^{obs} observed measurements on $\Omega_o \times [0, T]$. We define the *waveform misfit functional* as follows :

$$J(u,q) = \frac{1}{2} \int_0^T \int_{\Omega_o} (u - u^{obs})^2 \, d\Omega \, dt + \frac{\alpha}{2} \int_\Omega \left(\nabla q\right)^2 d\Omega, \tag{2}$$

with $\alpha > 0$ a fixed penalization parameter. The first term in (2) is the data-fitting error between the simulated wave u and the observed data u^{obs}. The second term corresponds to Tikhonov regularization; it acts on the control variable $q(x) = c(x)^2$ to penalize variations that are invisible to the data.
The inverse problem is: find $(u, q) \in V \times Q^{ad}$ s.t.

$$\begin{cases} \min\limits_{q \in Q_{ad}} J(u,q) \\ \text{where } (u,q) \text{ solution of (1).} \end{cases} \tag{3}$$

The control space Q_{ad} is a bounded convex set defined as $Q_{ad} = \{q(x) \in L^2(\Omega) : q_l \le q_j \le q^u\}$, for fixed lower and upper bounds q_l, $q^u \in L^2(\Omega)$.

Discretize then optimize

To solve (3), we follow the discretize-then-optimize approach: first, we discretize the state equation (1) and the misfit functional (2); then, we apply an optimization method to solve the corresponding discrete minimization problem.

Space-time discretization

We discretize the forward wave equation (1) by Spectral Element Methods (SEM) in space and the Leap-Frog method in time, [1], [2]. Let $Q_\delta^{ad} \subset Q$, $V_\delta \subset V$ be the discretization of Q^{ad} and V, respectively. Given $\mathbf{q} \in Q_\delta^{ad}$, $\mathbf{u} \in V_\delta$ is the discrete solution of (1) if it satisfies:

$$\begin{cases} \mathbf{M} \frac{u^{n+1} - 2u^n + u^{n-1}}{\Delta t^2} + \mathbf{A} u^n = \mathbf{f}^n \quad n = 1, \dots, N_t, \\ \\ u^0 = 0, \quad \frac{2}{\Delta t^2} \mathbf{M} u^1 = \mathbf{f}^0, \end{cases} \tag{4}$$

Δt being a suitable time-step (that satisfies the stability condition, [3]), N_t the number of temporal steps, and A, M the stiffness and mass matrices associated with (1), respectively. The corresponding discrete inverse problem reads: find $(\mathbf{u}, \mathbf{q}) \in V_\delta \times Q_\delta^{ad}$

s.t.

$$\begin{cases} \min\limits_{Q_\delta^{ad}} J(\mathbf{u},\mathbf{q}) \\ (\mathbf{u},\mathbf{q}) \text{ satisfies (4) .} \end{cases} \tag{5}$$

Optimization process

Since for each fixed control $\mathbf{q}$, there is a corresponding unique $\mathbf{u}$, solution of (4), problem (5) is equivalent to minimizing the reduced discrete functional:

$$\hat{J}(\mathbf{q}) = J(\mathbf{u},\mathbf{q})) \tag{6}$$

over Q_δ^{ad}. This is a discrete optimization problem with constraints only on the control variable. To minimize (6), we use an Interior Point Optimizer (Ipopt) algorithm, able to deal with nonlinear programming problems of general nature, [3]. A logarithmic term is added to the reduced misfit functional $\hat{J}(\mathbf{q})$ to handle the inequality constraints; hence for a given parameter $\mu > 0$, we define the auxiliary barrier functional:

$$\hat{J}_\mu(\mathbf{q}) = \hat{J}(\mathbf{q}) - \mu\big(\ln(q - q_l) + \ln(q^u - q)\big). \tag{7}$$

For a decreasing sequence of barrier parameters μ converging to zero, we now solve the unconstrained iterative minimization for $\hat{J}_\mu(\mathbf{q})$. Starting from an initial profile $\mathbf{q}_0$, we perform at the k-th iteration a Gauss-Newton step to find a descent direction $\mathbf{d}^k$; then, the next approximation $\mathbf{q}^{k+1}$ is computed through a line-search approach, $\mathbf{q}^{k+1} = \mathbf{q}^k + \alpha^k \mathbf{d}^k$, where the step-size is determined using a backtracking line-search algorithm $\alpha^k = 2^{-l}\alpha_{\max}^k$, $l = 0, \cdots$, with $\alpha_{\max}^k = \max\{\alpha \in (0,1) : \mathbf{q}_k + \alpha \mathbf{d}_k \geq (1-\tau)\mathbf{q}_k\}$, $\tau = \max\{\tau_{\min}, 1-\mu\}$, $\tau_{min} \in (0,1)$, see [3].

Numerical experiment

We conclude by a numerical test case to illustrate the performance of the proposed algorithm. Let us consider $\Omega = (0,1)$, $T = 1$, Ω_o given by two receivers located at the extrema of the boundary domain. We excite the medium with a high-frequency Ricker Wavelet source function. For the space discretization, we use $K = 25$ spectral elements and a conforming polynomial order $N = 2$ on each subdomain. To construct the observations, we solve the forward problem on a finer mesh using the fixed target profile q_t. In Figure 1, we show the lower and upper profiles q_l, q_u, the initial profile q_0, the target profile q_t and the reconstructed profile q after 20 iterations. In Figure 2, the L^2 norm of $\nabla\hat{J}$ vs the iteration count is plotted. Despite the nonconvexity of the inverse problem and the high variations of the target profile, the algorithm is able to find a good approximation of the target profile.

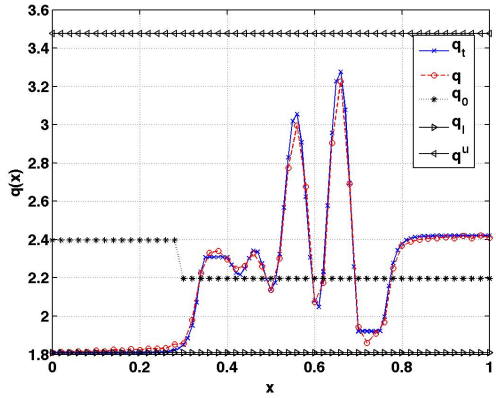

Figure 1: Velocity profile

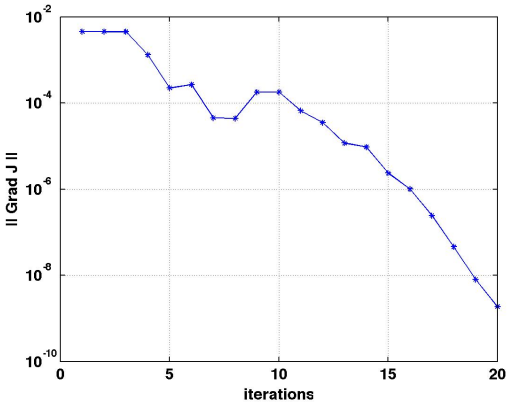

Figure 2: $\|\nabla\hat{J}\|$ vs iterations

References

[1] C. Canuto, M. Y. Hussaini, A. Quarteroni, and T. A. Zang, *Spectral methods: Fundamentals in Single domains.*, Scientific Computation. Springer-Verlag, Berlin, 2006.

[2] E. Zampieri and L. F. Pavarino, *An explicit second order spectral element method for acoustic waves.*, Adv. Comput. Math.,**25** (2006), pp. 381–401.

[3] A. Wächter and L. T. Biegler, *On the implementation of an interior-point filter line-search algorithm for large-scale nonlinear programming*, Math. Program.,**106** (2006), pp. 25-57.

Defects localization applied to the inverse medium problem

Yann Grisel[1,*], **Vincent Mouysset**[2], **Jean-Pierre Raymond**[1]
[1] Institut de Mathématiques de Toulouse, [2] Onera - The French Aerospace Lab
*Email: yann.grisel@iut-tlse3.fr

Abstract

We investigate numerical methods to retrieve a piece-wise constant approximation of an acoustic refraction index from far-field measurements.

We here propose to enhance this reconstruction by coupling it, in two different strategies, with a previously developed defects localization method. Both strategies can be combined and are aimed to reducing the number of computed parameters.

Moreover, our defects localization provides a new (constructive) characterization of an unknown refraction index. We thus investigate the minimization of defects as a new approach to solve the inverse medium problem. Our results are illustrated by numerical experiments.

1 Introduction

In inverse acoustic scattering, one tries to recover information about a scatterer from measurements. The penetrable scatterers we are interested in are also called inhomogeneous media and are characterized by a refraction index $n \in L^\infty(\mathbb{R}^d)$, where $d = 2$ or 3 [1]. We place ourselves in the case of $(n-1)$ having a compact support.

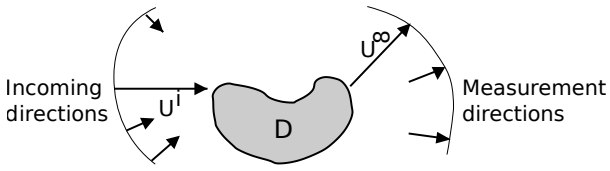

Figure 1: : General setting and notations.

1.1 The direct problem

The acoustic total field $u_n \in L^2_{loc}(\mathbb{R}^d)$ is assumed to satisfy the Helmholtz equation

$$\Delta u_n + k^2 n(x) u_n = 0, \quad x \in \mathbb{R}^d.$$

For practical reasons, we consider plane-wave sources. Hence, the corresponding total field is parameterized by the incidence direction taken in S^{d-1} (see Figure 1). Finally, $u_n^\infty \in \mathcal{C}^\infty(S^{d-1} \times S^{d-1})$ is the associated far-field pattern [1] and $\mathcal{F} : n \mapsto u_n^\infty$ denotes the index-to-far-field mapping.

1.2 The inverse medium problem

With $D = \cup Z_i$, $i = 1 \dots N$, we look for a piece-wise constant approximation $n(x) = \sum \eta_i \mathbf{1}_{Z_i}(x)$ of the actual refraction index, denoted by $n^\star \in L^\infty(\mathbb{R}^d)$, from the corresponding far-field measurements $u_{n^\star}^\infty$. A popular method to approximate $n^\star$, for its ease of implementation and efficiency, is using the iterative Gauss-Newton (G.-N.) method to minimize the following regularized cost function [2]

$$J(n) := \|\mathcal{F}(n) - u_{n^\star}^\infty\|^2_{L^2(S^{d-1}\times S^{d-1})} + \lambda \|n - n_0\|^2_{L^2(D)}.$$

2 Enhancement of piece-wise constant reconstructions through selective focusing

The G.-N. method involves heavy computations in which all parameters η_i are updated at each iteration. However, the initial guess could be exact in some zones Z_i and thus, the corresponding constants should not be updated. Also, during the reconstruction, some constants can reach a satisfactory precision while the other ones still require improvement.

2.1 Defects localization

To address these aspects of the reconstruction, the useful information would thus be a fast localization of the exact (enough) constants. To this end, we have extended the so-called Factorization method (see [3] and references therein) to localize the differences between $n^\star$ and a fixed (known) reference index. We call these differences defects and their localization is achieved *via* a localization function: for each $x \in \mathbb{R}^d$, we have the equivalence between $n(x) \neq n^\star(x)$ and

$$\mathcal{S}_{\{n,n^\star\}}(x) := \left(\sum_j \frac{\left| \langle \overline{u_n(\cdot, x)}, \psi_j \rangle_{L^2(S^{d-1})} \right|^2}{\sigma_j} \right)^{-1} > 0,$$

where (σ_j, ψ_j) is an eigen-system of the self-adjoint operator $W_\# := |W + W^\star| + |W - W^\star|$, where

$$W := (id + \alpha F_n)^\star (F_{n^\star} - F_n),$$

F_n is the classical far-field operator defined by

$$F_n g(\hat{x}) := \langle g, \overline{u_n^\infty(\cdot, \hat{x})} \rangle_{L^2(S^{d-1})},$$

and α is a constant. So, $\mathcal{S}_{\{n,n^\star\}}$ is built only from the measurements $u_{n^\star}^\infty$ and the reference index n.

2.2 Selective reconstruction

First, we consider the case where $n^\star$ is a locally perturbed version of a known initial state, denoted by n_0. These perturbations can now be localized through the function $\mathcal{S}_{\{n_0, n^\star\}}$. So, only the corresponding constants need to be reconstructed, using n_0 as an initial guess. This naturally provides a substantial reduction in computational costs.

2.3 Adaptive refinement

Secondly, we propose an iterative refinement strategy for the reconstruction: starting with $p = 0$,

1. Compute the average value of $\mathcal{S}_{\{n_p, n^\star\}}$ over each zone Z_i.
2. Split the zone corresponding to the highest average value into four and duplicate the corresponding parameter accordingly.
3. Run the G.-N. method on this new set of parameters to compute the approximation n_{p+1}.
4. $p \leftarrow p + 1$ and go to 1.

This leads to an approximation of $n^\star$ with a constrained number of parameters, positioned to fit as much as possible the geometry of this index.

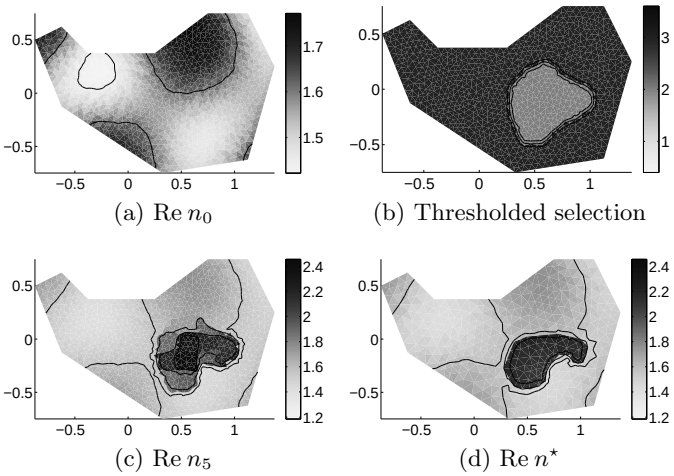

(a) Re n_0 (b) Thresholded selection

(c) Re n_5 (d) Re $n^\star$

Figure 2: : Full reconstruction with 16 parameters.

2.4 Combination of both strategies

Both strategies can be chained. Figure 2a depicts the real part of some unperturbed index n_0. The perturbation is then located by thresholding the values of $\mathcal{S}_{\{n_0, n^\star\}}$ (Figure 2b). Lastly, five iterations of the adaptive refinement process are applied to this selection, starting with a single parameter and ending with only 16. The result is shown on Figure 2c and can be compared to the actual index $n^\star$ on Figure 2d. The final relative error is $\|n_5 - n^\star\| / \|n^\star\| = 0.07$.

3 A new approach to the inverse medium problem

Lastly, the construction of $\mathcal{S}_{\{n, n^\star\}}$ provides a new constructive uniqueness proof for the inverse medium problem that is valid in $\mathbb{R}^3$, but also in $\mathbb{R}^2$, and for any k. Indeed, if $u_n^\infty = u_{n^\star}^\infty$, then $\mathcal{S}_{\{n, n^\star\}} = 0$ and thus, $n = n^\star$. Therefore, we propose a new way to look for $n^\star$ by minimizing

$$J_{\mathcal{S}}(n) := \left\|\mathcal{S}_{\{n, n^\star\}}\right\|^2_{L^2(D)} + \lambda \|n - n_0\|^2_{L^2(D)} .$$

This approach shows encouraging numerical results when compared to the classical cost function J. Also, since the localization function is defined locally, its minimization on any sub-part of D should allow the reconstruction of the unknown index $n^\star$ on this subpart. Thus, in theory, this new method handles domain decomposition straightforwardly, although we have no numerical evidence at this point.

Conclusion and perspectives

The inverse medium problem's numerical resolution has been enhanced in two specific cases by coupling it with a defects localization method. Moreover, this defects localization provides a new reconstruction approach that shows promising results.

Further investigations are performed to extend the localization function and to establish its regularity. That information is needed to develop, in particular, domain decomposition and L^1-norm minimization for our new approach to the inverse medium problem.

References

[1] D. Colton, J. Coyle, and P. Monk. Recent developments in inverse acoustic scattering theory. *SIAM Rev.*, 42(3):369–414 (electronic), 2000.

[2] H.W. Engl, M. Hanke, and A. Neubauer. *Regularization of inverse problems*, volume 375. Springer Netherlands, 1996.

[3] Y. Grisel, V. Mouysset, P-A. Mazet, and J-P. Raymond. Determining the shape of defects in non-absorbing inhomogeneous media from far-field measurements. *Inverse Problems*, 28:055003, 2012.

Reconstruction of the circular Radon transform from partial data

Rim Gouia-Zarrad[1,*] **Gaik Ambartsoumian**[2]
[1] Department of Mathematics and Statistics, American University of Sharjah, UAE
[2]Mathematics Department, University of Texas at Arlington, TX, USA
*rgouia@aus.edu

Abstract*

The representation of a function by its circular Radon transform (CRT) and various related problems arise in many areas of mathematics, physics and imaging science. There has been a substantial spike of interest towards these problems in the last decade mainly due to the connection between the CRT and mathematical models of several emerging medical imaging modalities. This article contains some new results about the existence and uniqueness of the representation of a function by its circular Radon transform with partial data. A new inversion formula is presented in the case of the circular acquisition geometry when the Radon transform is known for only a part of all possible radii. The results are not only interesting as original mathematical discoveries, but can also be useful for applications, e.g. in medical imaging.

Introduction

The circular Radon transform g puts into correspondence to a given function f its integrals along circles

$$g(x_0, y_0, r) = \int_{C(x_0,y_0,r)} f(x, y)\, ds, \qquad (1)$$

where $C(x_0, y_0, r)$ denotes the circle of radius r centered at the point (x_0, y_0).

In circular acquisition geometry there are various inversion formulae when g is known for circles of all possible radii [3], [4], [6], [7], [8], [9]. However, to the best of our knowledge no exact formula is known for the case when g is available for only half of all possible radii.
[1]

1 Uniqueness of reconstruction

In this subsection we consider a smooth function $f(r, \theta)$ supported inside the disc of radius R. We will show that the function can be uniquely recovered from Radon data with only part of all possible radii.

[1]*This article is mainly based on the paper [1]

Theorem 1 *Let $f(r, \theta)$ be an unknown continuous function supported inside the annulus $A(\varepsilon, R) = \{(r, \theta) : r \in (\varepsilon, R), \theta \in [0, 2\pi]\}$, where $0 < \varepsilon < R$. If $g(\rho, \phi)$ is known for $\phi \in [0, 2\pi]$ and $\rho \in [0, R - \varepsilon]$, then $f(r, \theta)$ can be uniquely recovered in $A(\varepsilon, R)$.*

Using an approach similar to Cormack's inversion of the linear Radon transform [2], we can rewrite the Eq (1) by considering the contribution dg to $g(\rho, \phi)$ from two equal elements of arc ds of the circle $C(\rho, \phi)$.

$$dg = \sum_{n=-\infty}^{\infty} [f_n(r)\, e^{in\theta} + f_n(r)\, e^{in(2\phi-\theta)}]\, ds$$

where $0 \le \phi \le \theta \le 2\pi$ and $f_n(r)$ is the Fourier coefficients computed by

$$f_n(r) = \frac{1}{2\pi} \int_0^{2\pi} f(r, \theta)\, e^{-in\theta} d\theta$$

By passing to the basis of complex exponentials we diagonalized the CRT, i.e. the n-th Fourier coefficient of g depends only on n-th Fourier coefficient of f. This is not surprising, due to rotation invariance property of g in the circular geometry. We refer the readers to [1], [5] for further details. As a result our problem breaks down to the following set of one-dimensional integral equations

$$g_n(\rho) = 2 \int_{R-\rho}^{R} \frac{f_n(r)\; r\; T_{|n|}\left(\frac{r^2+R^2-\rho^2}{2rR}\right)}{R\sqrt{1 - \left(\frac{\rho^2+R^2-r^2}{2\rho R}\right)^2}}\, dr, \qquad (2)$$

where $T_k(x)$ is the k-th order Chebyshev polynomial of the first kind. This equation can be written a Volterra integral equation of the first kind with weakly singular kernel

$$g_n(\rho) = \int_0^{\rho} \frac{F_n(u)\, K_n(\rho, u)}{\sqrt{\rho - u}}\, du, \qquad (3)$$

where

$$F_n(u) = f_n(R - u), \qquad (4)$$

$$K_n(\rho,u)=\frac{4\rho\,(R-u)\;T_{|n|}\left[\frac{(R-u)^2+R^2-\rho^2}{2R(R-u)}\right]}{\sqrt{(u+\rho)(2R+\rho-u)(2R-\rho-u)}}. \tag{5}$$

we finally obtain a Volterra equation of second kind

$$G_n(t)=F_n(t)+\int_0^t F_n(u)\,L_n(t,u)\,du, \tag{6}$$

where

$$G_n(t)=\frac{1}{\pi K_n(t,t)}\;\frac{d}{dt}\int_0^t\frac{g_n(\rho)}{\sqrt{t-\rho}}\,d\rho, \tag{7}$$

and

$$L_n(t,u)=\frac{1}{\pi K_n(t,t)}\;\frac{\partial}{\partial t}\int_u^t\frac{K_n(\rho,u)}{\sqrt{\rho-u}\sqrt{t-\rho}}\,d\rho \tag{8}$$

The Volterra equation of the second kind (6) has a unique solution, which finishes the proof of the theorem.

2 Reconstruction formula

Using the Picard's process of successive approximations (e.g. see [10], [11]) for the solution of Volterra equations of second kind one can immediately obtain the following

Corollary 2 *An exact solution of equation (6) is given by the formula*

$$F_n(t)=G_n(t)+\int_0^t H_n(t,u)\,G_n(u)\,du, \tag{9}$$

where the resolvent kernel $H_n(t,u)$ is given by the series of iterated kernels

$$H_n(t,u)=\sum_{i=1}^{\infty}(-1)^i L_{n,i}(t,u), \tag{10}$$

defined by

$$L_{n,1}(t,u)=L_n(t,u), \tag{11}$$

and

$$L_{n,i}(t,u)=\int_u^t L_{n,1}(t,x)\;L_{n,i-1}(x,u)\,dx,\quad\forall\, i\geq 2. \tag{12}$$

This is a new exact formula for inversion of the circular Radon transform in circular acquisition geometry. Its advantage compared to all the other known exact inversion formulas is the fact that only part of the g data is used.

References

[1] Ambartsoumian G, Gouia-Zarrad R, Lewis M 2010, *Inversion of the circular Radon transform on an annulus, Inverse problems* 26 105015.

[2] Cormack A 1963 *Representation of a function by its line integrals, with some radiological applications J. Appl. Phys.* **34** 9, 2722–7.

[3] Finch D, Haltmeier M and Rakesh 2007 *Inversion of spherical means and the wave equation in even dimension SIAM J. Appl. Math* **68** 3 392–412.

[4] Finch D and Rakesh 2007 *The spherical mean value operator with centers on a sphere Inverse Problems* **23** s37–49.

[5] Gouia-Zarrad R and Ambartsoumian G 2012 *Approximate inversion algorithm of the elliptical Radon transform*, 8th International Symposium on Mechatronics and its Applications (ISMA), UAE.

[6] John F 1955 *Plane Waves and Spherical Means, Applied to Partial Differential Equations* (Interscience Publishers).

[7] Kuchment P and Kunyansky L 2008 *A survey in mathematics for industry: mathematics of thermoacoustic tomography European J. Appl. Math.* **19** 2 191–224.

[8] Kunyansky L 2007 *Explicit inversion formulas for the spherical mean Radon transform Inverse Problems* **23** 373–83.

[9] Norton S J 1980 *Reconstruction of a two-dimensional reflecting medium over a circular domain: Exact Solution J. Acoust. Soc. Am.*, **67** 4 1266–73.

[10] Tricomi F 1983 *Integral Equations* (Dover Publications).

[11] Volterra V 2005 *Theory of Functionals and of Integral and Integro-Differential Equations* (New York: Dover Publications).

On the high-frequency behavior of topological sensitivity as an obstacle indicator function

Bojan B. Guzina
Department of Civil Engineering, University of Minnesota, Minneapolis, MN 55455, U.S.A.
Email: guzina@wave.ce.umn.edu

Abstract

This work examines the performance of topological sensitivity as a tool for tackling the inverse scattering of scalar waves in the high-frequency regime, when the wave length of the incident field is small relative to the remaining length scales in the problem. To provide a focus in the study, it is assumed that the obstacle is convex and impenetrable (of either Dirichlet or Neumann type), and that the full-waveform measurements of the scattered field are taken over a sphere whose radius is finite, yet large relative to the size of the sampling region. In this setting, the formula for topological sensitivity is expressed a pair of nested surface integrals – one taken the measurement sphere, and the other over the surface of a hidden obstacle. By way of multipole expansion, the inner integral (over the measurement surface) is reduced to a set of antilinear forms in terms of the Green's function and its gradient. The remaining expression is distilled by evaluating the scattered field on the surface of the obstacle via Kirchhoff (physical optics) approximation, and deploying the method of stationary phase to evaluate the remaining integral. In this way the topological sensitivity is expressed as a sum of the closed-form expressions, signifying the contribution of critical points on the "illuminated" part of the surface of a hidden obstacle. Thus obtained result explicitly demonstrates the localizing nature of the topological sensitivity and, via numerical simulations, helps better understand some of the reconstruction patterns observed in earlier works.

Introduction

Since its inception within the context of shape optimization [1], the notion of topological sensitivity has been generalized and applied to deal with inverse scattering problems in acoustics [2,3], electromagnetism [4], and elastodynamics [5]. In the reconstruction approach the topological sensitivity, which quantifies the perturbation of a given cost functional due to the nucleation of an infinitesimal defect in the (reference) background medium, is used as an effective obstacle indicator through an assembly of sampling points where it attains extreme negative values. Typically, formulas for the topological sensitivity are amenable to an explicit representation in terms of the wavefields computed exclusively for the reference domain, which is the source of computational efficiency of this class of inverse scattering solutions. However, with the exception of the treatment of point-like scatterers [6], the justification for the performance of this class of inverse scattering solutions has been notably lacking. To help bridge the gap, this work aims to expose the essence of the topological sensitivity (TS) indicator in the high-frequency regime, when the scatterer extends many wavelengths of the incident wavefield.

1 Methods

Consider the scattering of time-harmonic scalar waves by a convex impenetrable obstacle $D \subset \mathscr{B}_1 \subset \mathbb{R}^3$ with smooth boundary $S = \partial D$ and outward normal $\boldsymbol{n}$, where $\mathscr{B}_1$ is an open ball of radius R_1 centered at the origin. On denoting by $\tilde{u}$ the scattered field generated by the action of an incident field u^i on D, it is assumed that the total field

$$u(\boldsymbol{\xi}) \;:=\; u^i(\boldsymbol{\xi}) \,+\, \tilde{u}(\boldsymbol{\xi}), \qquad \boldsymbol{\xi} \in \mathbb{R}^3 \backslash \bar{D}$$

is monitored over a closed measurement surface $\Gamma^{\rm obs} = \partial \mathscr{B}_2$, where $\mathscr{B}_2$ is an open ball of radius $R_2 = \alpha^{-1} R_1 \;\; (\alpha \ll 1)$ centered at the origin, see Fig. 1. The reference background medium is assumed to be homogeneous with wave speed c and mass density ρ. Writing the germane time dependence as $e^{{\rm i}\omega t}$ where ω denotes the frequency of excitation, the incident field is for simplicity assumed in the form of a plane wave, $u^i = e^{-{\rm i}k\boldsymbol{\xi}\cdot\boldsymbol{d}}$, where $k = \omega/c$.

On substituting the integral representation of the scattered field over $\Gamma^{\rm obs}$ into the adjoint-field formula [3] for TS and reversing the order of integration over S and $\Gamma^{\rm obs}$, the expression for TS in the case of a sound-soft (Dirichlet) obstacle, taken here

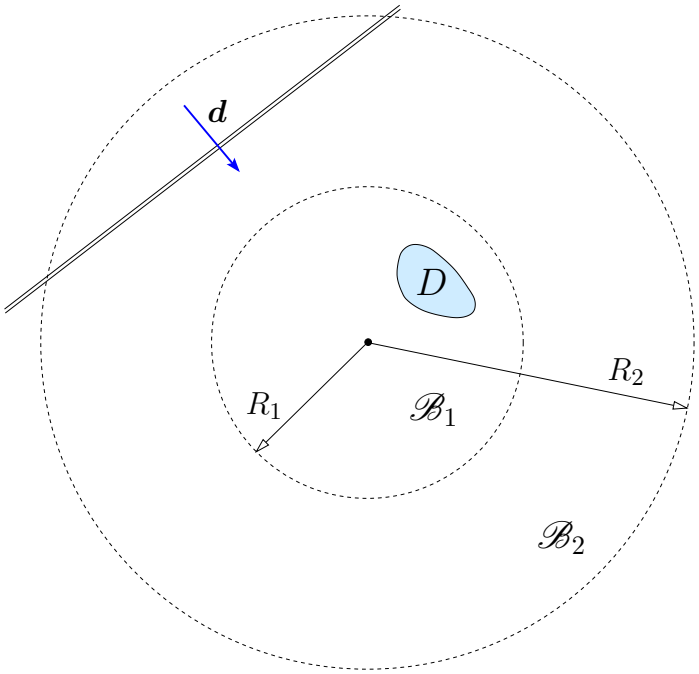

Figure 1: Obstacle $D \in \mathbb{R}^3$ illuminated by plane waves.

as an example, can be written as

$$\begin{aligned}\mathsf{T}(\boldsymbol{x}^\circ,\beta,\gamma) \;=\; 2\mathrm{Re}\Big\{&(1-\beta)\,\nabla u^i(\boldsymbol{x}^\circ)\cdot\boldsymbol{A}\cdot\int_S \overline{u^i_{,n}}(\boldsymbol{\zeta})\\ &\int_{\Gamma^{\rm obs}} \overline{G}(\boldsymbol{\xi},\boldsymbol{\zeta},k)\,\nabla G(\boldsymbol{\xi},\boldsymbol{x}^\circ,k)\,\mathrm{d}\Gamma_\xi\,\mathrm{d}S_\zeta\\ &-(1-\beta\gamma^2)\,k^2\,u^i(\boldsymbol{x}^\circ)\int_{S^{\rm f}}\overline{u^i_{,n}}(\boldsymbol{\zeta})\\ &\int_{\Gamma^{\rm obs}}\overline{G}(\boldsymbol{\xi},\boldsymbol{\zeta},k)\,G(\boldsymbol{\xi},\boldsymbol{x}^\circ,k)\,\mathrm{d}\Gamma_\xi\,\mathrm{d}S_\zeta\Big\},\end{aligned}\quad(1)$$

where G is the fundamental solution of the Helmholtz equation in $\mathbb{R}^3$, while $\beta = \rho/\rho^\star$ and $\gamma = c/c^\star$ denote the material characteristics of a vanishing trial obstacle at $\boldsymbol{x}^\circ$. When the latter is ball-shaped, $\boldsymbol{A} = 2/(3+\beta)\boldsymbol{I}$, where $\boldsymbol{I}$ is the second-order identity tensor.

Representation (1) can further be reduced to a single surface integral with an *explicit* kernel by way of the Helmholtz-Kirchhoff identity

$$\int_{\Gamma^{\rm obs}}\overline{G}(\boldsymbol{\xi},\boldsymbol{\zeta},k)\,G(\boldsymbol{\xi},\boldsymbol{x}^\circ,k)\,\mathrm{d}\Gamma_\xi \;\simeq\; -\frac{1}{k}\,\mathrm{Im}\big(G(\boldsymbol{x}^\circ,\boldsymbol{\zeta},k)\big),\qquad \boldsymbol{x}^\circ,\boldsymbol{\zeta}\in\mathscr{B}_1,\quad \alpha\ll 1,\quad(2)$$

its extension in terms of $\overline{G}\,\nabla G$, and the Kirchhoff (high-frequency) approximation of the scattered field over S which states that

$$u = 0 \quad \text{on} \quad S=\partial D, \qquad u_{,n} = \begin{cases} 2\,u^i_{,n} & \text{on} \quad S^{\rm f} \\ 0 & \text{on} \quad S^{\rm b}\end{cases},\quad(3)$$

when the obstacle is sound-soft. Here $S^{\rm f} = \{\boldsymbol{x}\in S : \boldsymbol{n}(\boldsymbol{x})\cdot\boldsymbol{d} < 0\}$ is the "front" (i.e. illuminated) part of S, and $S^{\rm b} = \{\boldsymbol{x}\in S : \boldsymbol{n}(\boldsymbol{x})\cdot\boldsymbol{d} \geqslant 0\}$ denotes its "back" side.

The remaining surface integral is next evaluated explicitly via the method of stationary phase [7] as a sum of contributions of the kernel in the neighborhood of *critical points* on $S^{\rm f}$, namely those where i) the tangential gradient of the exponential part of the kernel vanishes, and ii) the kernel fails to be differentiable. In this way the TS indicator function is written in terms of the basic transcendental functions combined with their specialized counterparts such as the Airy, Fresnel, and Pearcey integrals.

References

[1] H. A. Eschenauer, V. V. Kobelev, and A. Schumacher, *Bubble method for topology and shape optimization of structures*, Structural Optimization, **8** (1994), pp. 42–51.

[2] G. R. Feijoo, *A new method in inverse scattering based on the topological derivative*, Inverse Problems, **20** (2004), pp. 1819–1840.

[3] B. B. Guzina and M. Bonnet, *Small-inclusion asymptotic of misfit functionals for inverse problems in acoustics*, Inverse Problems, **22** (2006), pp. 1761–1785.

[4] M. Masmoudi, J. Pommier, and B. Samet, *The topological asymptotic expansion for the Maxwell equations and some applications*, Inverse Problems, **21** (2005), 547–564.

[5] B. B. Guzina and M. Bonnet, *Topological derivative for the inverse scattering of elastic waves*, Quart. J. Mech. Appl. Math., **57** (2004), pp. 161–179.

[6] H. Ammari and H. Kang, *Reconstruction of the small inhomogeneities from boundary measurements*, Springer, Berlin, New York, 2004.

[7] J. J. Stamnes, *Waves in Focal Regions: Propagation, Diffraction, and Focusing of Light, Sound, and Water Waves*, Taylor & Francis, New York, 1986.

Selective focusing on unknown scatterers

M. Cassier[†,*], **C. Hazard**[†], **P. Joly**[†]
[†]POEMS (UMR 7231), CNRS-ENSTA-INRIA, ENSTA-ParisTech, Palaiseau, France
[*]Email: maxence.cassier@ensta-paristech.fr

Abstract

We are concerned with focusing effects for time-dependent waves using an array of point-like transducers. We consider a two-dimensional problem which models acoustic wave propagation in a medium which contains several unknown point-like scatterers. Spatial focusing properties have been studied in the frequency domain in the context of the DORT method ("Decomposition of the Time Reversal Operator"). This method consists in doing a Singular Value Decomposition of the scattering operator, that is, the operator which maps the input signals sent to the transducers to the measure of the scattered wave. We show how to construct a wave that focuses in space and time near one of these scatterers, in the form of a superposition of time-harmonic waves related to the singular vectors of the scattering operator. Numerical results will be shown.

Introduction

We consider a reference medium, possibly inhomogeneous, filling the whole plane $\mathbb{R}^2$. We denote by G the time-dependent Green function of the acoustic wave equation, that is the causal solution to

$$\frac{1}{c^2(x)}\frac{\partial^2 G(x,y;t)}{\partial t^2} - \Delta_x G(x,y;t) = \delta(x-y)\otimes\delta(t)$$

where c is the wave speed function of the medium (e.g., $G(x,y;t) = -H(t-|x-y|)/(2\pi(t^2-|x-y|^2))^{\frac{1}{2}}$ for $c\equiv 1$, where H is the Heaviside function). We assume that the reference medium is perturbed by the presence of a family of P point-like scatterers whose positions $s_1,\dots,s_P$ are unknown. Using an array of N point-like transducers located at x_n for $n=1,\dots,N$ (with $N\geq P$), our aim is to generate a wave that focuses in space and time on one of the scatterers. Such a wave is defined by

$$w(x,t) = \sum_{n=1}^{N}\left(G(x,x_n;\cdot)\overset{t}{\star} q_n\right)(t) \qquad (1)$$

where $q_{\rm inp}(t) := (q_1(t),\dots,q_N(t))^\top$ represents the input signals applied to the transducers and $\overset{t}{\star}$ denotes the time convolution. The question is to find signals $q_{\rm inp}(t)$ for which most part of the energy of the wave will be concentrated near one obstacle at a given time. In the present paper, we show how to deduce such signals from the only knowledge of the *scattering operator* $\mathbb{S}: q_{\rm inp}\mapsto q_{\rm mes}$ where $q_{\rm mes}$ represents the measures at points $x_1,\dots,x_N$ of the scattered wave associated with the incident wave (1), that is, the perturbation of this incident wave due to the presence of the unknown scatterers. The idea is to take advantage of the so-called DORT method (see, e.g., [2], [3]) whose spatial focusing properties in the frequency domain are well known.

1 Space focusing in the frequency domain

Let $\widehat{G}$ denote the time-harmonic Green function of the reference medium which is related to the time-dependent Green function G by the Fourier transform:

$$G(x,y;t) = \frac{1}{\pi}\mathrm{Re}\left(\int_0^{+\infty}\widehat{G}(x,y;\omega)\,e^{-i\omega t}\,d\omega\right).$$

At a fixed frequency ω, the array of transducers emits a time-harmonic incident wave defined by

$$\hat{w}(x) = \sum_{n=1}^{N}\hat{q}_n\,\widehat{G}(x,x_n;\omega),$$

for a given $\widehat{q}_{\rm inp} := (\hat{q}_1,\dots,\hat{q}_N)^\top\in\mathbb{C}^N$ (complex amplitudes of the input signals at the N transducers). Then, the array measures the scattered wave $\hat{q}_{mes}$. This yields the time-harmonic scattering operator $\widehat{\mathbb{S}}_\omega : \hat{q}_{\rm inp}\mapsto\hat{q}_{\rm mes}$ which can be written here as a product of three matrices:

$$\widehat{\mathbb{S}}_\omega \quad = \quad \underbrace{\widehat{\mathbb{G}}_\omega^\top}_{\text{back propagation}} \quad \underbrace{\widehat{\Sigma}_\omega}_{\text{reflection}} \quad \underbrace{\widehat{\mathbb{G}}_\omega}_{\text{direct propagation}} \quad ,$$

where $\widehat{\mathbb{G}}_\omega$ is a $P\times N$ matrix defined by $(\widehat{\mathbb{G}}_\omega)_{pn} := \widehat{G}(x_n,s_p;\omega)$ and $\widehat{\Sigma}_\omega$ is a $P\times P$ symmetric matrix ($\widehat{\Sigma}_\omega^\top = \widehat{\Sigma}_\omega$) which represents the reflections on the scatterers. The latter matrix depends on the choice of an asymptotic model for the scatterers. In the simplest case (no interaction between the scatterers),

this is a diagonal matrix composed of the reflection coefficients of the scatterers. The more elaborate Foldy–Lax model [1] takes into account isotropic interactions.

The DORT method consists in a Singular Value Decomposition (SVD) of $\widehat{\mathbb{S}}_\omega$:

$$\widehat{\mathbb{S}}_\omega = \widehat{\mathbb{P}}_\omega \, \widehat{\mathbb{D}}_\omega \, \overline{\widehat{\mathbb{Q}}_\omega}^{\top}, \tag{2}$$

where $\widehat{\mathbb{D}}_\omega$, $\widehat{\mathbb{P}}_\omega$, $\widehat{\mathbb{Q}}_\omega$ are respectively the diagonal matrix of singular values, the matrices of the left and right singular vectors. It is now well understood ([2], [3]) that in a homogeneous medium, for distant enough scatterers, the number of nonzero singular values of $\widehat{\mathbb{S}}_\omega$ coincide with the number of scatterers. Moreover if such a singular value $\lambda_p(\omega)$ is simple, the associated right singular vector $\widehat{q}_p(\omega)$ (pth column of $\widehat{\mathbb{Q}}_\omega$) generates a wave which focuses selectively on one scatterer, say s_p.

2 Space-time focusing

Suppose that in a given frequency band $[\omega_1, \omega_2]$ (imposed by the physical properties of our array), we know a right singular vector $\widehat{q}_p(\omega) \in \mathbb{C}^N$ associated with the pth obstacle. How can one choose a function $A(\omega)$ defined on the frequency band such that the superposition of the time-harmonic input signals:

$$q_p(t) = \mathrm{Re} \int_{\omega_1}^{\omega_2} A(\omega) \, \widehat{q}_p(\omega) \, e^{-\mathrm{i}\omega t} \, \mathrm{d}\omega \tag{3}$$

generates an incident wave which focuses not only in space near s_p, but also in time?

We look for a function A as a product $A(\omega) = \chi(\omega) e^{i\phi(\omega)}$ with χ a given real cutoff function and ϕ an unknown phase. This is a problem of frequency phase synchronization. The phase choice that we propose is based on a particular SVD of the scattering operator related to its symmetry. $\widehat{\mathbb{S}}_\omega$ is a symmetric operator, therefore up to a change of sign, there exists a unique $\phi \in [-\pi, \pi[$ such that

$$\widehat{\mathbb{S}}_\omega \, e^{\mathrm{i}\phi(\omega)} \widehat{q}_p(\omega) = \lambda_p(\omega) \, \overline{e^{\mathrm{i}\phi(\omega)} \widehat{q}_p(\omega)}, \tag{4}$$

$e^{i\phi(\omega)} \widehat{q}_p(\omega)$ is then a right singular vector of a symmetric SVD of $\widehat{\mathbb{S}}_\omega$: $\overline{\mathbb{U}}_\omega \, \mathbb{D}_\omega \, \overline{\mathbb{U}}_\omega^{\top}$. Does this signal yield an *optimal* focusing? We did not succeed in finding a mathematical functional representing the focusing quality which would be maximal for this particular choice. But several arguments are pointing in that direction.

The first one is heuristic. As the time reversal operation $\mathbb{J} : f(t) \mapsto f(-t)$ becomes a complex conjugation in the frequency domain, we see with (4) that at each frequency, the measure of the scattered field is (up to a positive real factor $\lambda_p(\omega)$) the time reversed emitted signal. This temporal symmetry synchronizes the spectral components of the emitted wave at the focusing time $t = 0$. The mathematical counterpart of this property lies in the fact that the input signal q_p is closed (for the L^2 norm) to an eigenfunction of the operator $\mathbb{J}\,\mathbb{S}$ related to a positive eigenvalue.

The second one is related to the well-known time-reversal experiment: a time-reversed wave back-propagates towards the source. In this sense, the time-reversed Green function G emmited at s_p is some kind of optimal space-time focusing wave. We have checked that for high ω, the phases given by (4) become close to those of the frequency components of the measures of the time-reversed Green function.

The last arguments are numerical experiments which confirm these focusing properties. In particular, we have measured the focusing quality of (3) by means of an energy criterion. We compute the ratio of the local acoustic energy contained in a box which surrounds the obstacle s_p by the total energy sent by the transducers during the emission.

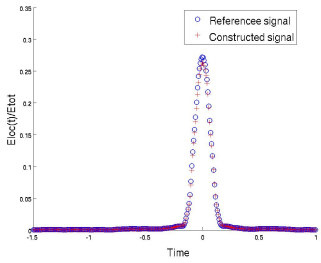

Figure 1: Comparison with a referencee signal built with the obstacle position in the case of two scatterers

References

[1] M.Cassier and C. Hazard, *Multiple scattering of acoustic waves by small sound-soft obstacles in two dimensions: Mathematical justification of the Foldy-Lax model*, Wave Motion , **50** (2013), pp. 18–28.

[2] C. Hazard and K. Ramdani, *Selective acoustic focusing using time-harmonic reversal mirrors*, SIAM J. Appl. Math, **64** (2004), pp. 1057–1076.

[3] C. Prada and M. Fink, *Eigenmodes of time reversal operator: A solution to selective focusing in multiple target media*, Wave Motion , **20** (1994), pp. 151–163.

Shape Identification of Diffraction Gratings from Spectral Data: The TM Case

Dinh-Liem Nguyen*
[1] INRIA/Ecole Polytechnique, Palaiseau, France.
*Email: dnguyen@cmap.polytechnique.fr

1 Abstract

We consider the shape identification problem of diffraction gratings from measured spectral data involving of scattered electromagnetic waves. The model problem that we study here is motivated by the important applications of such structures in optics. Recently, the Factorization method, introduced in [3], has been extended to periodic inverse scattering problems as a tool for imaging. In [1], [2] the authors studied the Factorization method for the imaging problem of impenetrable periodic structures with Dirichlet and impedance boundary conditions. The paper [4] considered imaging of penetrable periodic interfaces between two dielectrics in two dimensions. In the present work, the Factorization method has been studied for identifying shape of diffraction gratings constituted by penetrable periodic dielectrics mounted on a metallic plate. Further, we consider the problem of TM modes instead of TE modes studied in the previous works. We provide a rigorous analysis for the method as well as numerical experiments to examine its performance.

2 Problem Formulation

An important class of diffraction gratings are invariant in one direction and periodic in the orthogonal direction. For these structures, the direct and inverse electromagnetic scattering problems decouple into two scalar problems, if the wave vector of the incident field is orthogonal to the invariant axis of the grating. Here, we consider one of the two scalar reduced problems corresponding to the TM mode,

$$\begin{aligned} \mathrm{div}(a\nabla u) + k^2 u = 0 \quad &\text{in } \mathbb{R}^2_+ = \{(x_1,x_2)^T, x_2 > 0\}, \\ a\partial u/\partial \nu = 0 \quad &\text{on } \Gamma_0, \end{aligned}$$

where $\Gamma_0 := \{(x_1,x_2)^T : x_1 \in (-\pi,\pi), x_2 = 0\}$. The periodic refractive index is $a \in L^\infty(\mathbb{R}^2_+)$, $\Re(a) \geq c > 0$. Further, $a(x_1+2\pi,x_2) = a(x_1,x_2)$ for $(x_1,x_2)^T \in \mathbb{R}^2_+$ and $a = 1$ outside the grating. The wave number is denoted by $k > 0$. For $\alpha \in (-k,k)$ fixed throughout this paper, $n \in \mathbb{Z}$, we denote $\alpha_n = \alpha + n$, and

$$\beta_n := \begin{cases} \sqrt{k^2-\alpha_n^2}, & k^2 \geq \alpha_n^2, \\ i\sqrt{\alpha_n^2-k^2}, & k^2 < \alpha_n^2, \end{cases}$$

Further assume that $k^2 \neq \alpha_n^2$ for all $n \in \mathbb{Z}$ which means $\beta_n \neq 0$. We use plane waves as incident fields,

$$u_n^i = e^{i(\alpha_n x_1 - \beta_j x_2)} + e^{i(\alpha_n x_1 + \beta_n x_2)}, \quad n \in \mathbb{Z}.$$

Those are α-quasiperiodic, i.e.,

$$u_n^i(x_1+2\pi,x_2) = e^{2\pi i\alpha} u_n^i(x_1,x_2),$$

and satisfy the Neumann boundary condition $\partial u_n^i/\partial\nu = 0$ on Γ_0. Further, we require that the scattered fields $u_n^s := u - u_n^i$ are also α-quasiperiodic and satisfy the Rayleigh expansion radiation condition

$$u_n^s(x) = \sum_{j\in\mathbb{Z}} c_{n,j} e^{i\alpha_j x_1 + i\beta_j(x_2-h)} \text{ for } x_2 > h.$$

The numbers $\{c_{n,j}\}_{j\in\mathbb{Z}}$ form the Rayleigh sequence of u_n^s. The differential equation for u_n^s is hence $\mathrm{div}(a\nabla u_n^s) + k^2 u_n^s = -\mathrm{div}(q\nabla u_n^i)$, subject to $a\partial_2 u_n^s = -a\partial_2 u_n^i = 0$ on Γ_0. For a variational formulation, we define the bounded domain $\Omega_h := (-\pi,\pi)\times(0,h)$, $\Gamma_h := (-\pi,\pi)\times\{h\}$. The quasiperiodic Sobolev space $H^1_\alpha(\Omega_h) := \{u \in H^1(\Omega_h) : u = U|_{\Omega_h} \text{ for some } \alpha\text{-quasip. } U \in H^1_{\mathrm{loc}}(\mathbb{R}^2)\}$. Denote by $q := a - 1$ the contrast, the variational problem for the scattered field is to find $u_n^s \in H^1_\alpha(\Omega_h)$ solving the following source problem for the source $f = \sqrt{|q|}\nabla u_n^i \in L^2(\Omega_h)^2$: Find $v \in H^1_\alpha(\Omega_h)$ such that

$$\begin{aligned} &\int_{\Omega_h} (a\nabla v\cdot\nabla\overline{\phi} - k^2 v\overline{\phi})\mathrm{d}x - \int_{\Gamma_h} \overline{\phi}\mathcal{T}(v)\mathrm{d}s \\ &= -\int_{\Omega_h} q/\sqrt{|q|} f\cdot\nabla\overline{\phi}\mathrm{d}x \quad \text{for all } \phi \in H^1_\alpha(\Omega_h). \end{aligned} \tag{1}$$

Here, for $\hat{\phi}_j = \int_0^{2\pi}\phi(t)e^{-i\alpha_j t}\mathrm{d}t$,

$$\mathcal{T} : \phi \mapsto i\sum_{j\in\mathbb{Z}} \beta_j \hat{\phi}_j e^{i\alpha_j x_1}$$

is the Dirichlet-to-Neumann operator on Γ_h. Existence theory for this problem can be derived by Fredholm's alternative. In the sequel, we will assume that (1) is uniquely solvable for any $f \in L^2(\Omega_h)^2$. Then we can define a solution operator

$G : L^2(\Omega_h)^2 \to \ell^2$ which maps f to the Rayleigh sequence $(v_j)_{j\in\mathbb{Z}}$ of $v \in H^1_\alpha(\Omega_h)$, solution to (1).

Due to the linearity of the scattering problem, the scattered field resulting from a linear combination of several incident fields is the corresponding linear combination of the scattered fields. We obtain such linear combination using sequences $(a_n)_{n\in\mathbb{Z}} \in \ell^2$ and define the corresponding operator by

$$H(a_n) = \sqrt{|q|} \sum_{n\in\mathbb{Z}} a_n \nabla u^i_n|_{\Omega_h},$$

In our inverse problem the data operator, due to the near field measurement methodology, is usually referred to as the near field operator, denoted by N. We define $N : \ell^2 \to \ell^2$ to map a sequence (a_n) to the Rayleigh sequence of the scattered field caused by the incident field $H(a_n)$ above. Then

$$N = GH.$$

Our imaging problem is now to reconstruct the support D of the contrast $q = a - 1$ when the near field operator N is given. We solve this problem using the Factorization method that factorizing the near field operator is one of the important steps.

3 Main Results

Denote by $H^* : L^2(\Omega_h)^2 \to \ell^2$ the L^2-adjoint to H.

Theorem 1. *The near field N satisfies $N = H^*TH$, where T involves the solution operator to the variational formulation* (1).

Under the assumption that $\Re(q) \geq c > 0$ and $\Im(q) \leq 0$, the ranges of $H^* : L^2(\Omega_h)^2 \mapsto \ell^2$ and $N_\sharp^{1/2} : \ell^2 \mapsto \ell^2$ coincide. It is moreover a classical result that the sequence

$$(r_n(z)) := e^{-i(\alpha_n z_1 + \sqrt{k^2-\alpha_n^2} z_2)} / \sqrt{k^2 - \alpha_n^2}, \quad n \in \mathbb{Z},$$

belongs to range of H^* if and only if z belongs to D. Finally, the main result is the following.

Theorem 2. *Assume that $\Re(q) \geq c > 0$ and $\Im(q) \leq 0$, and that $(\lambda_j, (\psi_{j,n}))$ is the eigensystem of $N_\sharp$. Then z is in D if and only if*

$$\sum_{j=1}^{\infty} |\langle r_n(z), \psi_{j,n}\rangle|^2 / \lambda_j < \infty.$$

Figures 1 and 2 contain two numercial examples for imaging of sine-profile grating and piecewise linear grating for wave number $k = 3.5$. These numerical examples use data generated by a volume integral equation method [5].

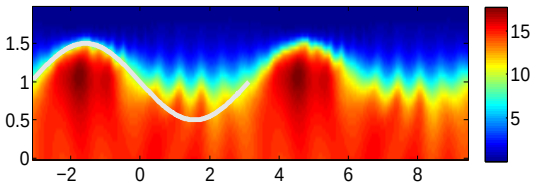

Figure 1: $q = 1.5$, 2% noise

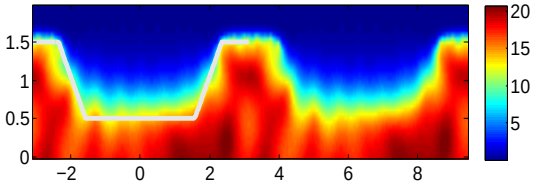

Figure 2: $q = (x_2 + 1)(\sin^2(x_1) + 0.5) - 2i$, 2% noise

References

[1] T. Arens and N. Grinberg *: A complete factorization method in inverse scattering from periodic structures*, Computing, 75:111-132, 2005.

[2] T. Arens and A. Kirsch *: Factorization method for inverse scattering from periodic structures*, Inverse Problems, 19:1195-1211, 2003.

[3] A. Kirsch *: Characterization of the shape of a scattering obstacle using spectral data of the far field operator*, Inverse Problems, 14:1489-1512, 1998.

[4] A. Lechleiter *: Imaging of periodic dielectrics*, BIT Numer. Math., 50:59-83, 2010.

[5] A. Lechleiter and D. L. Nguyen *: A Trigonometric Galerkin Method for Volume Integral Equations Arising in TM Grating Scattering*, Submitted.

Applications of elliptic operator theory to the interior transmission eigenvalue problem

E. Lakshtanov[1], **B. Vainberg**[2,*]
[1] Department of Mathematics, Aveiro University, Portugal.
[2] Department of Mathematics and Statistics, UNC at Charlotte, USA.
*Email: brvainbe@uncc.edu

Introduction

The talk concerns isotropic interior transmission eigenvalue (ITE) problem. This problem is not elliptic, but we show that, using the Dirichlet-to-Neumann map, it can be reduced to an elliptic one. This leads to the discreteness of the spectrum as well as the existence of at most a finite number of eigenvalues inside any closed sector of complex plane that does not contain real positive semi-axis. If the refraction index $n(x)$ is real, we get a result on the existence of infinitely many positive ITEs and lower bounds of the Weyl type on its counting function. All the results are obtained under the assumption that the index of refraction $n(x)-1$ does not vanish at the boundary of the obstacle or it vanishes identically, but its normal derivative does not vanish at the boundary. We consider the classical transmission problem as well as the case when the inhomogeneous medium contains an obstacle. Some results on the discreteness and localization of the spectrum are obtained for complex valued $n(x)$.

Main results

Let us recall that $\lambda \in C$ is called an *interior transmission eigenvalue* (ITE) if the homogeneous problem

$$-\Delta u - \lambda u = 0, \quad x \in \mathcal{O}, \quad u \in H^2(\mathcal{O}), \tag{1}$$

$$-\Delta v - \lambda n(x) v = 0, \quad x \in \mathcal{O}, \quad v \in H^2(\mathcal{O}), \tag{2}$$

$$\begin{array}{l} u - v = 0, \quad x \in \partial\mathcal{O}, \\ \frac{\partial u}{\partial \nu} - \frac{\partial v}{\partial \nu} = 0, \quad x \in \partial\mathcal{O}, \end{array} \tag{3}$$

has a non-trivial solution. Here $\mathcal{O} \subset R^d$ is a bounded domain, $H^2(\mathcal{O})$, $H^s(\partial\mathcal{O})$ are the Sobolev spaces, $n(x) \neq 0$, $x \in \overline{\mathcal{O}}$, and ν is the outward unit normal vector.

Problem (1)-(3) appears naturally when the scattering of plane waves is considered, and the inhomogeneity in R^d is located in $\mathcal{O}$ and is described by the refraction index n. We also consider the case when $\mathcal{O}$ contains a compact obstacle $\mathcal{V} \subset \mathcal{O}$, $\partial V \in C^\infty$. In this case, equation (2) is replaced by

$$\begin{array}{l} -\Delta v - \lambda n(x) v = 0, \quad x \in \mathcal{O}\backslash\mathcal{V}, \quad v \in H^2(\mathcal{O}\backslash\mathcal{V}); \\ v(x) = 0, \quad x \in \partial\mathcal{V}, \end{array}$$

while equation (1) remains valid in $\mathcal{O}$.

There are many results on the discreteness of ITEs, their location, and estimates on positive ITEs under some specific assumptions on $n(x)$. Similar results are obtained in the case of anisotropic media. Recently we showed [1-3] that the proofs of many results on the discreteness and localization of ITEs in the anisotropic case can be simplified and the results can be extended using the parameter-ellipticity of the anisotropic problem. We also suggested a new approach to study the Weyl type estimates on positive ITEs. While the problem in the anisotropic case is elliptic, it is not symmetric, and the existence of positive ITEs and estimates on positive eigenvalues are based on the study of the spectrum of the operator, which is the difference between the Dirichlet-to-Neumann map for equations (1) and the Dirichlet-to-Neumann map for the anisotropic analogue of (2).

The talk will be devoted to the extension of our results to the isotropic problem (1)-(3). The isotropic problem is more complicated since it is neither elliptic, nor symmetric. The properties of its spectrum can not be obtained by soft arguments.

We prove that the set of the ITEs is discrete when n is complex-valued and either

$$n(x) - 1 \neq 0, \quad x \in \partial\mathcal{O}, \tag{4}$$

or

$$n(x) - 1 \equiv 0, \quad \frac{\partial}{\partial \nu} n(x) \neq 0, \quad x \in \partial\mathcal{O}. \tag{5}$$

We show that there are at most finitely many ITEs in any closed sector $\Lambda \in C$ if it does not contain any points of the following set $\mathcal{N}$:

$$\mathcal{N} = \{1\} \cup \left\{ \frac{1}{n(x)}, \ x \in \partial\mathcal{O} \right\}. \tag{6}$$

In the case of real refraction index $n(x), x \in \partial\mathcal{O}$, it means that $\Lambda \bigcap R^+ = \emptyset$.

We also prove the existence of infinitely many real ITEs when $n(x)>0$, $x\in\overline{\mathcal{O}}$, is a real function and

$$\gamma := \sigma\left(Vol(\mathcal{O}) - \int_{\mathcal{O}\setminus\mathcal{V}} n^{d/2}(x)dx\right) > 0,$$

where

$$\sigma = sgn(n(x)-1), \quad x\in\mathcal{O}, \quad \operatorname{dist}(x,\partial\mathcal{O}) \ll 1, \quad (7)$$

is the sign of $n-1$ in a neighborhood of $\partial\Omega$ strictly inside of Ω. The constant σ is well defined due to the conditions imposed on n. Moreover, we obtain the following Weyl type lower bound on the counting function $N_T(\lambda)$ of the positive ITEs:

$$N_T(\lambda) \geq \frac{\omega_d}{(2\pi)^d}\gamma\lambda^{d/2} + O(\lambda^{(d-1)/2}), \quad \lambda\to\infty,$$

where ω_d is the volume of the unit ball in R^d.

Let

$$F(\lambda), F_n(\lambda) : H^{3/2}(\partial\mathcal{O}) \to H^{1/2}(\partial\mathcal{O}) \qquad (8)$$

be the Dirichlet-to-Neumann map for equations (1) and (2), respectively. If $\lambda=\lambda_0$ is not a pole of either $F(\lambda)$ or $F_n(\lambda)$ (i.e., λ_0 is not an eigenvalue of the Dirichlet problem for equation (1) or (2)), then λ_0 is an ITE if and only if operator $F(\lambda_0)-F_n(\lambda_0)$ has a nontrivial kernel. Operators (8) are elliptic pseudo differential operators (p.d.o.) of the first order, but their principal symbols are canceled when the difference is taken. Our approach is based essentially on the fact that operator $F_n(\lambda)-F(\lambda)$ is an elliptic p.d.o. of order -1 or -2 with the principal symbol

$$(1-n(x))\frac{\lambda}{2|\xi|}, \quad \text{if (4) holds,}$$

$$\frac{1}{4}\frac{\partial n(x)}{\partial\nu}\frac{\lambda}{|\xi|^2}, \quad \text{if (5) holds.}$$

Here $x\in\partial\mathcal{O}$, $\xi\in R^{d-1}$.

We also hope to discuss some results on the completeness of eigenfunctions.

References

[1] E.Lakshtanov, B.Vainberg, *Ellipticity in the interior transmission problem in anisotropic media*, SIAM J. Math. Anal., **44**, (2012), pp. 1165-1174.

[2] E.Lakshtanov, B.Vainberg, *Remarks on interior transmission eigenvalues, Weyl formula and branching billiards*, J. Phys. A: Math. Theor. **45**, (2012), 125202.

[3] E.Lakshtanov, B.Vainberg, *Bounds on positive interior transmission eigenvalues*, Inverse Problems **28**, (2012), 105005.

Imaging extended reflectors in a two-dimensional waveguide

C. Tsogka[1,2], **D.A. Mitsoudis**[3,2,*], **S. Papadimitropoulos**[1]
[1] Department of Applied Mathematics, University of Crete, Heraklion, Greece.
[2] Institute of Applied and Computational Mathematics, FORTH, Heraklion, Greece.
[3] Archimedes Center for Modeling, Analysis & Computation (ACMAC),
Department of Applied Mathematics, University of Crete, Heraklion, Greece.
*Email: dmits@tem.uoc.gr

Abstract

We consider the problem of detecting and imaging extended reflectors submerged in a homogeneous two-dimensional waveguide, using acoustic waves produced by an active array. We assume that the available data is the array response matrix for the scattered field. We use the Kirchhoff migration imaging functional and an alternative one, based on the projection of the response matrix on the propagating modes. Our main goal is to examine the behavior of the imaging functionals when selective imaging techniques are used in order to focus in different parts of a single extended scatterer. We present the outcome of some numerical experiments and analyze theoretically the imaging method for a simplified model problem where the scatterer is a vertical one-dimensional perfect reflector. In this case, we derive a relation between the number of significant singular values of the array response matrix and the size of our scatterer.

Introduction

We consider an acoustic waveguide consisting of a single homogeneous water layer confined above by the sea surface and below by the seafloor, both assumed to be horizontal, see Figure 1. Our data for

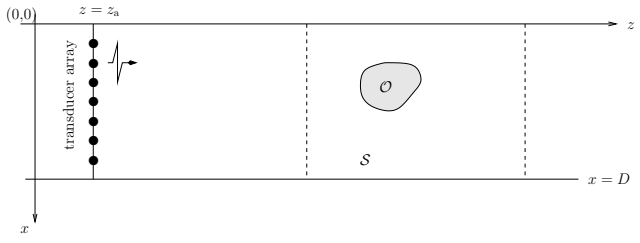

Figure 1: Schematic representation of our waveguide problem and of the array imaging setup.

solving the inverse problem is the array response matrix whose elements, $\Pi(\vec{\boldsymbol{x}}_s, \vec{\boldsymbol{x}}_r, t)$, correspond to the 'scattered' acoustic pressure field recorded as a function of time t at receiver location $\vec{\boldsymbol{x}}_r$ and due to a pulse emitted from a source located at $\vec{\boldsymbol{x}}_s$. The reflector that we wish to image is an acoustically hard scatterer occupying the domain $\mathcal{O}$.

Moreover, we are interested in imaging specific parts of extended reflectors. A way to achieve this is by a *selective imaging* technique called the subspace projection method [1]. This method is based on the singular value decomposition (SVD) of the array response matrix which was originaly used in the DORT method [3] to achieve selective focusing in the case of multiple point (or small) scatterers.

1 Imaging

Here we will specifically consider the *Kirchhoff migration (KM) functional*, see e.g. [2], to create an image, defined for some $\vec{\boldsymbol{y}}^{\,\mathrm{s}} \in \mathcal{S}$ and for a single frequency ω as

$$\mathcal{I}^{\mathrm{KM}}(\vec{\boldsymbol{y}}^{\,\mathrm{s}}, \omega) = \sum_{r=1}^{N} \overline{\hat{G}_0(\vec{\boldsymbol{x}}_r, \vec{\boldsymbol{y}}^{\,\mathrm{s}}, \omega)} \sum_{s=1}^{N} \hat{\Pi}(\vec{\boldsymbol{x}}_r, \vec{\boldsymbol{x}}_s, \omega) \times \times \overline{\hat{G}_0(\vec{\boldsymbol{x}}_s, \vec{\boldsymbol{y}}^{\,\mathrm{s}}, \omega)}, \quad (1)$$

where the bars denote complex conjugation and $\hat{\Pi}(\vec{\boldsymbol{x}}_r, \vec{\boldsymbol{x}}_s, \omega)$ is the Fourier transform of $\Pi(\vec{\boldsymbol{x}}_r, \vec{\boldsymbol{x}}_s, t)$. In (1), $\hat{G}_0$ is a *model* for the Green's function in the propagation medium defined in our case as

$$\hat{G}_0(\vec{\boldsymbol{x}}, \vec{\boldsymbol{x}}_{\mathrm{s}}, \omega) = \frac{\mathrm{i}}{2} \sum_{n=1}^{\infty} \mathrm{e}^{\mathrm{i}\beta_{\mathrm{n}}|\mathrm{z}-\mathrm{z_s}|} X_n(x_{\mathrm{s}}) X_n(x). \quad (2)$$

Here k is the wavenumber, μ_n, X_n are the eigenvalues and corresponding orthonormal eigenfunctions of the operator $-d^2/dx^2$ in $H^2(0,D) \cap H_0^1(0,D)$, $\beta_n = \begin{cases} \sqrt{k^2-\mu_n}, & 1 \le n \le M, \\ \mathrm{i}\sqrt{\mu_n - k^2}, & n \ge M+1, \end{cases}$ are the horizontal wavenumbers, and M is the number of propagating modes. In the case where the array spans the whole depth of the waveguide and the inter-element array distance h is small enough, we introduce an $M \times M$ matrix $\hat{\mathbb{P}}(\omega)$, with entries

$$\hat{\mathbb{P}}_{mn}(\omega) = \beta_m \beta_n \int_0^D \int_0^D \hat{\Pi}(\vec{\boldsymbol{x}}_s, \vec{\boldsymbol{x}}_r, \omega) X_m(x_s) X_n(x_r) dx_s dx_r$$

Then we use for imaging the following functional:

$$\widetilde{\mathcal{I}}^{\mathrm{KM}}(\vec{\boldsymbol{y}}^{\,\mathrm{s}},\omega) = -\frac{1}{4h^2}\sum_{m,n=1}^{M} \mathrm{e}^{-\mathrm{i}(\beta_{\mathrm{m}}+\beta_{\mathrm{n}})|\mathrm{z_a}-\mathrm{z}^{\mathrm{s}}|} \times \\ \times\ X_n(x^{\mathrm{s}})X_m(x^{\mathrm{s}})\hat{\mathbb{P}}_{mn}(\omega). \qquad (3)$$

1.1 *Selective imaging*

The main idea behind selective imaging lies in computing the SVD of the matrix $\hat{\mathbb{P}}(\omega)$ and use a filtered version of it to create the image. If we write the SVD of $\hat{\mathbb{P}}(\omega)$ as a sum of the form: $\hat{\mathbb{P}}(\omega) = \sum_{i=1}^{\rho}\sigma_i U_i V_i^*$, where $\rho = \mathrm{rank}(\hat{\mathbb{P}}(\omega))$, then a filtered version of $\hat{\mathbb{P}}(\omega)$ may be written as $D[\hat{\mathbb{P}}(\omega)] = \sum_{i=1}^{\rho} d_i\sigma_i U_i V_i^*$, where $d_i \in \{0,1\}$ are the filter weights. Then we define

$$\widetilde{\mathcal{I}}^{\mathrm{KM,f}}(\vec{\boldsymbol{y}}^{\,\mathrm{s}},\omega) = -\frac{1}{4h^2}\sum_{m,n=1}^{M} \mathrm{e}^{-\mathrm{i}(\beta_{\mathrm{n}}+\beta_{\mathrm{m}})|\mathrm{z_a}-\mathrm{z}^{\mathrm{s}}|} \times \\ \times\ X_n(y^s)X_m(y^s)\left(D[\hat{\mathbb{P}}(\omega)]\right)_{mn}. \qquad (4)$$

The corresponding multiple-frequency versions of the imaging functionals are obtained by summing over the bandwidth B and then taking the absolute value,

$$\mathcal{I}^{\mathrm{KM}}(\vec{\boldsymbol{y}}^{\,\mathrm{s}}) = \left|\int_B \mathcal{I}^{\mathrm{KM}}(\vec{\boldsymbol{y}}^{\,\mathrm{s}},\omega)d\omega\right|, \qquad (5)$$

$$\widetilde{\mathcal{I}}^{\mathrm{KM}}(\vec{\boldsymbol{y}}^{\,\mathrm{s}}) = \left|\int_B \widetilde{\mathcal{I}}^{\mathrm{KM,f}}(\vec{\boldsymbol{y}}^{\,\mathrm{s}},\omega)d\omega\right|. \qquad (6)$$

2 Numerical results

In Figure 2, we plot the values of the filtered version of (1) (left column) and the values of (6) (right column) for a square shaped scatterer with sidelength $b = 40$ m located 450 m far from the array. Here the central frequency is 75 Hz with corresponding wavelength $\lambda_0 = 20$ m and the bandwidth is $B = 10$ Hz. The depth of the waveguide is $D = 200$ m and the sound speed is $c_0 = 1500$ m/s. Here J indicates the image produced by projecting on the J-th singular vector. We observe that the two functionals behave differently as a function of J. As J increases, $\widetilde{\mathcal{I}}^{\mathrm{KM}}$ focuses at the front edges of the square.

3 Theoretical analysis

We analyze the proposed imaging method for a simplified model of a vertical one-dimensional reflector of width b, and we show that the number of 'significant' singular values of $\hat{\mathbb{P}}(\omega)$ is equal to $[\frac{b}{\lambda/2}]$, that is, the size of the reflector divided by the array resolution $\lambda/2$. This result has been recently proven in free space (cf. [1, §4.5.2]), but, to the best of our knowledge, it is a new result for waveguides. For the example shown in Figure 2 this number is equal to 4.

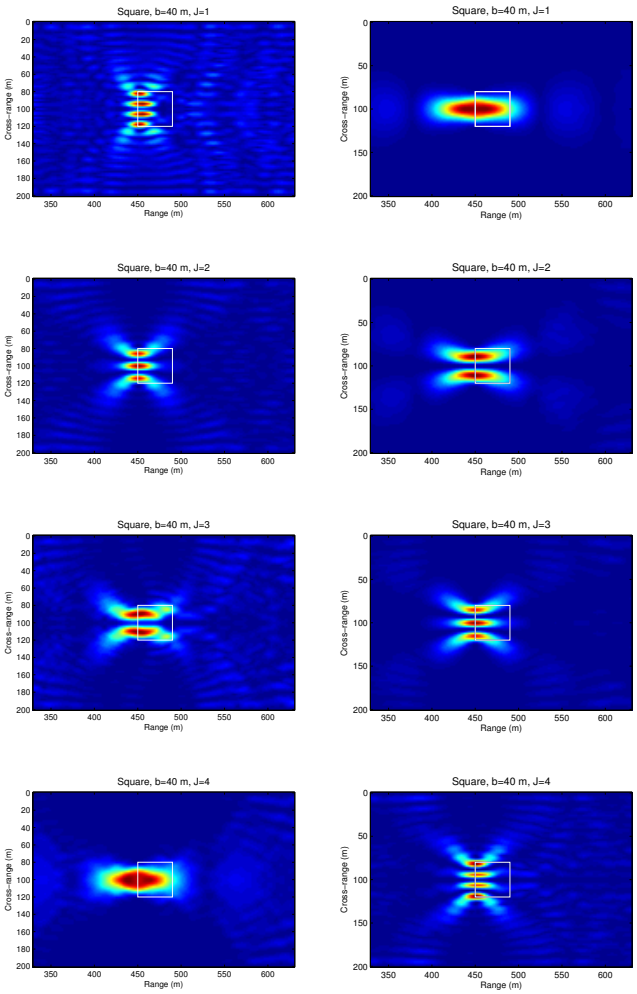

Figure 2: Filtered version of $\mathcal{I}^{\mathrm{KM}}$ (left column) versus $\widetilde{\mathcal{I}}^{\mathrm{KM}}$ (right column) for a square scatterer.

References

[1] L. Borcea, G. Papanicolaou and F. Guevara Vasquez, *Edge illumination and imaging of extended reflectors*, SIAM J. Imaging Sci., **1** (2008) pp. 75–114.

[2] L. Borcea, G. Papanicolaou and C. Tsogka, *Optimal waveform design for array imaging*, Inverse Problems, **23** (2007), pp. 1973–2020.

[3] C. Prada C and M. Fink, *Eigenmodes of the time reversal operator: A solution to selective focusing in multiple-target media*, Wave Motion, **20** (1994), pp. 151–163.

Time-Reversed Absorbing Conditions (*TRAC*): Discrimination between one and two nearby inclusions in the partial aperture case

F. Assous[1,*], M. Grote[2,*], M. Kray[2,*], F. Nataf[3,*]
[1] Ariel University Center, 40700 Ariel, Israel and Bar-Ilan University, 52900 Ramat-Gan, Israel.
[2] Mathematisches Institut, Universität Basel, CH-4051 Basel, Switzerland.
[3] UPMC Université Paris-06, UMR 7598, Laboratoire J.L. Lions, F-75006 Paris, France.
*Email: franckassous@netscape.net, marcus.grote@unibas.ch, marie.kray@unibas.ch, nataf@ann.jussieu.fr

Abstract

The time-reversed absorbing conditions (*TRAC*) method introduced in [2] enables one to "recreate the past" without knowing the source which has emitted the signals that are back-propagated. It has been applied to inverse problems for the reduction of the computational domain size and for the determination of the location and volume of an unknown inclusion from boundary measurements. The method does not rely on any *a priori* knowledge of the physical properties of the inclusion. Here we extend the *TRAC* method to the situation of partial aperture with discrete receivers. In particular, the *TRAC* method is applied to the discrimination between a single inclusion and two nearby inclusions. Our numerical results show that the *TRAC* method is rather insensitive to noise in the data.

Introduction

Since the seminal paper by Fink et al. [3], time reversal has been a subject of active research. The main idea is to take advantage of the reversibility of wave propagation, as it occurs in acoustics, elasticity or electromagnetism in a non-dissipative unknown medium to back-propagate signals to the sources that emitted them.

In [2], we introduce the time-reversed absorbing conditions (*TRAC*) method which enables one to "recreate the past" without knowing the source which has emitted the signals that are back-propagated. It has been applied to inverse problems for the reduction of the computational domain size and for the determination of the location and volume of an unknown inclusion from boundary measurements.

In this paper, we extend the *TRAC* method to the situation of partial aperture with discrete receivers. In particular, the *TRAC* method is applied to the discrimination between a single inclusion and two nearby inclusions, see also [1].

1 Principle of the *TRAC* method

We consider an incident wave u^I impinging on an inclusion D characterized by different physical properties from the homogeneous surrounding medium. The total field u^T can be decomposed into the incident and scattered fields, so $u^T = u^I + u^S$. For simplicity, we consider the problem in two space dimensions and assume that the total field satisfies the linear wave equation:

$$\frac{\partial^2 u^T}{\partial t^2} - c^2 \Delta u^T = 0 \qquad \text{in } \mathbb{R}^2 \tag{1}$$

together with homogeneous initial conditions. The scattered field u^S has a finite energy at any time.

Let Γ_R be a curve that defines a bounded domain Ω and encloses the inclusion D (see Figure 1). After a time T_f, the total field u^T is negligible in Ω. The scattered field u^S is recorded on Γ_R on the time interval $[0, T_f]$. Let $u_R^S := u^S(T_f - t, \vec{x})$ denote the scattered time reversed field which also satisfies (1).

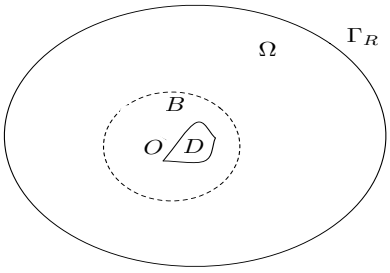

Figure 1: Geometry

Our aim is to reconstruct the time reversed field u_R^S from the measurements on Γ_R. For this purpose, we derive a boundary value problem whose solution is u_R^S in Ω. Yet we know neither the physical properties nor the exact location of the inclusion D, but only the physical properties of the surrounding medium. Therefore, we introduce a subdomain B which encloses the inclusion D. Then, we have to determine

a boundary condition for u_R^S on the boundary ∂B so that the solution to this problem will coincide with u_R^S restricted to $\Omega \setminus B$.

Let us choose B as a ball of radius r. On ∂B, we approximate the radiation condition satisfied by u^S with the first-order Bayliss-Turkel (BT^1) absorbing boundary condition:

$$\text{ABC}(u^S) \;:=\; \frac{\partial u^S}{\partial t} + c\frac{\partial u^S}{\partial r} + c\frac{u^S}{2r} \;=\; 0 \text{ on } \partial B \quad (2)$$

Next we "time reverse" this relation using $u_R^S(t,\cdot) = u^S(T_f - t,\cdot)$. In doing so, we note that $\partial/\partial r = -\partial/\partial n$ on ∂B where n is the outward normal to $\Omega \setminus B$. Hence we obtain:

$$\text{TRAC}(u_R^S) \;:=\; \frac{\partial u_R^S}{\partial t} \;+\; c\frac{\partial u_R^S}{\partial n} \;-\; c\frac{u_R^S}{2r} \;=\; 0\,. \quad (3)$$

Hence the time reversed problem for the scattered field, analogous to (1), reads:

$$\begin{cases} \dfrac{\partial^2 u_R^S}{\partial t^2} - c^2 \Delta u_R^S = 0 \quad \text{in } (0,T_f) \times \Omega \setminus B \\ \text{TRAC}(u_R^S) = 0 \quad \text{on } \partial B \\ u_R^S(t,\vec{x}) = u^S(T_f - t, \vec{x}) \quad \text{on } \Gamma_R \\ \text{homogeneous initial conditions.} \end{cases} \quad (4)$$

Note the "anti-absorbing" term $(-cu_R^S/2r)$ in the TRAC condition.

2 Discrimination between one and two nearby inclusions

Here we consider the partial aperture case with discrete receivers and denote by v_R^S the solution of (4). Hence, v_R^S does not correspond to the time reversal of the scattered field but only to its approximation within the convergence cone defined by the aperture of the source-receivers array.

To quantify the discrimination error, we introduce a criterion from reverse time migration (RTM) techniques. The cross-correlation fonction we use reads:

$$f(\vec{x}) := \int_{t=0}^{t=T_f} v_R^S(T_f - t, \vec{x}) \times u^I(t,\vec{x})\; dt\,. \quad (5)$$

It is used throughout $\Omega \setminus B$ to image the interface of the inclusion which has been highlighted by the incident wave u^I. From 5, we infer the cross-correlation criterion J_{CC}:

$$J_{CC}(B) \;:=\; \frac{\left\| \int_{t=0}^{t=T_f} v_R^S(T_f - t,.) \times u^I(t,.)\; dt \right\|_{L^\infty(\Omega\setminus B)}}{\left\| \int_{t=0}^{t=T_f} |u^I(t,.)|^2\; dt \right\|_{L^\infty(\Omega)}}\,. \quad (6)$$

Figure 2 illustrates the result of the discrimination between one single inclusion (right column) and two a-half-wavelength separated inclusions (left column). Here we compare the result of the *TRAC* method with two connected subdomains B (bottom line) to the classical case (top line), i.e. $B = \emptyset$. The remaining signal on the bottom-left picture is significatively smaller than that on the bottom-right; thus, we enclose correctly all the inclusions on the left, not on the right. However, the BT1 boundary condition shows its limits, because it does not take into account interactions between both inclusions. Therefore, we work on the improvement of the discrimination accuracy by including absorbing boundary conditions for multiple scattering [4] to the *TRAC* method.

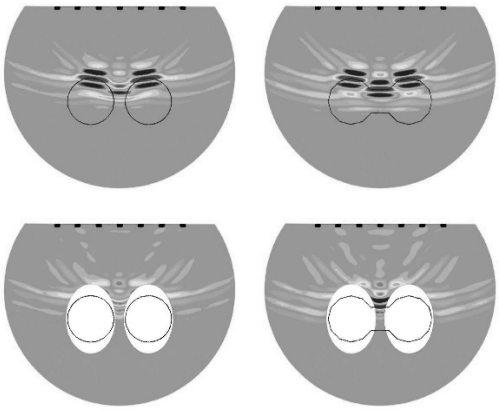

Figure 2: Cross-correlation fonction f. Left: two inclusions; right: single inclusion. Top: classical case; bottom: *TRAC* with two disjoint subdomains B, TRAC condition from BT^1 boundary condition.

References

[1] F. Assous, M. Kray, and F. Nataf. Time reversed absorbing condition in the partial aperture case. *Wave Motion*, 49(7):617–63, 2012.

[2] F. Assous, M. Kray, F. Nataf, and E. Turkel. Time reversed absorbing condition: Application to inverse problem. *Inverse Problems*, 27, 2011.

[3] M. Fink, F. Wu, D. Cassereau, and R. Mallart. Imaging through inhomogeneous media using time reversal mirrors. *Ultrasonic Imaging*, 13(2):199 – 199, 1991.

[4] M. J. Grote and I. Sim. Local nonreflecting boundary condition for time-dependent multiple scattering. *Journal of Computational Physics*, 230(8):3135–3154, 2011.

Convergence in expectation results for phase retrieval problems in x-ray diffraction imaging

T. Hohage[1,*], **F. Werner**[1]
[1] Institut für Numerische und Angewandte Mathematik, Universität Göttingen, Germany
*Email: hohage@math.uni-goettingen.de

Abstract

In coherent x-ray imaging one has to reconstruct the boundary values of a solution to the Helmholtz equation in a half-space from measurements of the squared absolute values g of the solution restricted to a plane. Typically the Fresnel or Fraunhofer approximations to the Helmholtz equation are applicable. Data consist of photon counts, and the distribution of the collected photons is described by a Poisson process with intensity g. For inversion methods it is natural to use the negative log-likelihood as data misfit functional. In expectation this yields the Kullback-Leibler divergence up to an additive constant. Using a concentration inequality for Poisson processes and regularization theory in Banach spaces we show a convergence in expectation result for Newton-type methods as the expected number of collected photons tends to infinity.

1 X-ray diffraction imaging

In coherent x-ray diffraction imaging a sample is illuminated by a coherent x-ray beam with the aim is to retrieve information on the refractive index n of the sample from measurements of the squared absolute values of the field. The Maxwell equations reduce in good approximation to the Helmholtz equation

$$\Delta u + \kappa^2 n^2(x) u = 0\,.$$

We assume a parallel incident beam moving in x_3 direction, a bounded sample contained in the strip $\{x \in \mathbb{R}^3 : x_3 \in (-R, 0)\}$ and measurements of $|u(x', \Gamma)|^2$ for all $x' \in \mathbb{R}^2$ at a distance $\Gamma > 0$. We factor out the rapidly oscillating part of the solution by writing $u(x) = \tilde{u}(x)\exp(i\kappa x_3)$, write down a differential equation for $\tilde{u}$, divide by $2i\kappa$, and neglect all terms that vanish as $\kappa \to \infty$. This yields the so-called *projection approximation* u_{P} of $\tilde{u}$ also used in x-ray tomography: $\frac{\partial u_{\mathrm{P}}}{\partial x_3} = \frac{i\kappa}{2}(n^2(x)-1)u_{\mathrm{P}}$. As the refractive index of matter for x-ray frequencies is very close to 1 and $\Re n \le 1$, it is common to write

$$n(x) = 1 - \delta(x) + i\beta(x), \quad 0 \le \delta, \beta \ll 1$$

Then $n^2 - 1 \approx -2\delta + 2i\beta$, and we obtain the approximation

$$u(x', 0) \approx u_{\mathrm{P}}(x', 0) \tag{1}$$
$$\approx u_{\mathrm{P}}(x', -R)\exp\left(i\kappa \int_{-R}^{0} (\delta(x', x_3) - i\beta(x', x_3))dx_3\right).$$

As $n(x) = 1$ for $x_3 \ge 0$, the Fourier transform $(\mathcal{F}f)(\xi) := \int \exp(-2\pi i x' \cdot \xi) f(x')\,dx'$ with respect to the first two variables yields $(\mathcal{F}u(\cdot, x_3))(\xi) = \exp\left(ix_3\sqrt{\kappa^2 - (2\pi|\xi|)^2}\right)(\mathcal{F}u_0)(\xi)$ for $\xi \in \mathbb{R}^2$, $x_3 > 0$ where $u_0(x') := u(x', 0)$. If $|\xi| \ll \kappa$ for all ξ for which $|\mathcal{F}u_0(\xi)|$ is not neglectible, we can use the Taylor approximation $\sqrt{\kappa^2 - (2\pi|\xi|)^2} \approx \kappa - \frac{(2\pi|\xi|)^2}{2\kappa}$ to obtain the *Fresnel approximation* (also called paraxial or Schrödinger approximation) $u \approx u_{\mathrm{F}}$ defined by

$$u_{\mathrm{F}}(x', x_3) = e^{i\kappa x_3}\mathcal{F}^{-1}\left(e^{-i2\pi^2 \frac{x_3}{\kappa}|\xi|^2} \cdot \mathcal{F}u_0\right)(x')\,. \tag{2}$$

We introduce the chirp functions $\chi_\alpha(x') := \exp\left(i\alpha\pi|x'|^2\right)$ with parameter $\alpha \in \mathbb{C}$ and note that $\mathcal{F}\chi_{i\alpha} = \frac{1}{\alpha}\chi_{i/\alpha}$ for $\Re\alpha \ge 0$, $\alpha \ne 0$. An application of the Fourier convolution theorem (first for $\Im\kappa > 0$ to have an integrable convolution kernel) yields

$$u_{\mathrm{F}}(x', \Gamma) = -\frac{i\kappa}{2\pi\Gamma}e^{i\kappa\Gamma}\int \chi_{\frac{\kappa}{2\pi\Gamma}}(x' - y')u_0(y')\,dy'\,.$$

Expanding the square $|x' - y'|^2$ we obtain

$$|u_{\mathrm{F}}(x', \Gamma)|^2 = \left(\tfrac{\kappa}{2\pi\Gamma}\right)^2\left|\mathcal{F}\left(\chi_{\frac{\kappa}{2\pi\Gamma}}u_0\right)\left(\tfrac{\kappa x'}{2\pi\Gamma}\right)\right|^2 =: (Hu_0)(x')\,.$$

Let us introduce $b := \sup\{|x'| : x' \in \operatorname{supp} u_0\}$ and the dimensionless Fresnel number $\mathfrak{f} := \frac{\kappa b^2}{2\pi\Gamma}$. If $\mathfrak{f} \ll 1$, we have $\chi_{\frac{\kappa}{2\pi\Gamma}}u_0 \approx u_0$, and up to scaling the data are given by the squared modulus of the Fourier transform of u_0 (*Fraunhofer approximation*).

The phase retrieval problem essentially consists in inverting H and requires further infomation on u_0 (see [4] for uniquenss results). For example, we may assume that $\beta = 0$ (phase objects) and define $f(x') := \kappa\int_{-R}^{0}\delta(x', x_3)\,dx_3$ as unknown. Then $u_0 = e^{if}u_{\mathrm{empty}}$ where u_{empty} is the field at $x_3 = 0$ without a sample, and the forward operator is

$$F(f) := H(e^{if}u_{\mathrm{empty}})\,.$$

Let $f^\dagger$ be the exact solution and $g^\dagger := F(f^\dagger)$.

2 Poisson data

The (ideal) observations consist of the positions $x'_1, \dots, x'_N$ of photons in the detector plane $\{x : x_3 = \Gamma\}$ where both the x'_j and N are random. For fundamental physical reasons they are distributed according to a Poisson point process with density $tg^\dagger$ where $t > 0$ can be interpreted as an exposure time. This means in particular that $\mathbf{E}\#\{j : x'_j \in \Omega\} = t \int_\Omega g^\dagger \, dx$ for all measureable $\Omega \subset \mathbb{R}^2$. More generally, writing $G_t := \frac{1}{t} \sum_{j=1}^N \delta_{x'_j}$ we have

$$\mathbf{E} \int \psi dG_t = \int \psi g^\dagger \, dx \quad \mathbf{Var} \int \psi dG_t = \tfrac{1}{t} \int \psi^2 g^\dagger \, dx$$

whenever the integrals on the right hand side exist. The latter identity indicates that $t^{-1/2}$ can be interpreted as a noise level, but there is no pointwise noise level or norm bound. We introduce the data-misfit functional

$$\mathcal{S}(G_t, g) := \int g \, \mathrm{d}x - \int \ln(g + \sigma) \, (\mathrm{d}G_t + \sigma \mathrm{d}x)$$

with $\sigma > 0$ which is the negative log-likelihood functional for $\sigma = 0$. The (deterministic) ideal data misfit functional $\mathcal{T}(g^\dagger, g) := \mathbf{E}\mathcal{S}(G_t, g) - \mathbf{E}\mathcal{S}(G_t, g^\dagger)$ is given by the (shifted) Kullback-Leibler divergence, $\mathcal{T}(g^\dagger, g) = \mathrm{KL}(g^\dagger + \sigma, g + \sigma)$. An essential ingredient of our analysis is a uniform concentration inequality for the error $|\mathcal{S}(G_t, g) - \mathbf{E}\mathcal{S}(G_t, g^\dagger) - \mathcal{T}(g^\dagger, g)|$ based on results in [3], which is only available for $\sigma > 0$.

3 inversion methods and convergence results

We first consider a Tikhonov-type regularization:

$$\widehat{f}_\alpha \in \operatorname{argmin}_{f \in \mathfrak{B}} \left[\mathcal{S}(G_t, F(f)) + \alpha \|f\|_{L^2}^2 \right] \qquad (3)$$

Unfortunately, (3) is a non-convex minimization problem, and no globally convergent algorithms for its solution are known. As an alternative, we consider a Newton-type method: Choose $\alpha_k = \alpha_0 \rho^k$ for some $\rho \in (0, 1)$ and set

$$\widehat{f}_{k+1} \in \operatorname*{argmin}_{f \in \mathfrak{B}} \left[\mathcal{S}\big(G_t, F'[\widehat{f}_k](f - \widehat{f}_k) + F(f_k)\big) + \alpha_k \|f\|_{L^2}^2 \right]$$

In each Newton step the solution to this convex optimization problem is computed using an algorithm proposed in [1].

Theorem 1 *Assume there exists $\beta \in (0, 1]$ and a concave, increasing function $\varphi : [0, \infty) \to \mathbb{R}$ with $\varphi(0) = 0$ such that*

$$\beta \|f - f^\dagger\|^2 \le \|f\|^2 - \|f^\dagger\|^2 + \varphi\left(\mathcal{T}\left(F(f^\dagger), F(f)\right)\right)$$

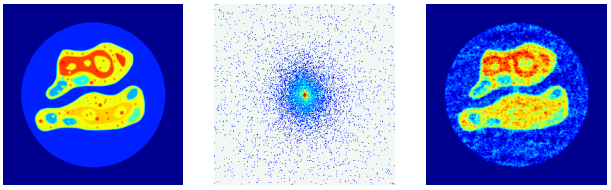

Figure 1: left: simulated phase object $f^\dagger$; middle: data G_t with 10^6 expected photons in Fraunhofer regime; right: Newton reconstruction $\widehat{f}_8$, $\sigma = 10^{-6}$

for all $f \in \mathfrak{B}$ and that $-1/\alpha \in \partial(-\varphi)(t^{-1/2})$. Then

$$\mathbf{E}\|\widehat{f}_\alpha - f^\dagger\|^2 = \mathcal{O}\big(\varphi\big(t^{-1/2}\big)\big), \quad t \to \infty. \qquad (4)$$

For linear operator equations in Hilbert spaces variational formulations of source conditions as in this theorem have been shown to be both necessary and sufficient for certain rates of convergence.

Several extensions of this result are shown in [2], [5]: The regularization parameter α can be chosen adaptively without knowledge of the function φ by a Lepskiĭ rule. For more general nonquadratic convex penalty terms we showed convergence rates with respect to Bregman distances. Finally, similar rates of convergence can also be shown for the Newton-type iteration if an additional assumption concerning the approximation quality of the first order Taylor expansion of F is imposed.

References

[1] A. Chambolle, T. Pock. *A first-order primal-dual algorithm for convex problems with applications to imaging.* J. Math. Imaging Vis **40** (2011), pp. 120–145.

[2] T. Hohage, F. Werner. *Iteratively regularized Newton-type methods for general data misfit functionals and applications to Poisson data.* Numer. Math., published online, 2012.

[3] P. Reynaud-Bouret. *Adapative estimation of the intensity of inhomogeneous Poisson processes via concentration inequalities.* Prob. Theory Rel. **126** (2003), pp. 103–153.

[4] M. V. Klibanov. *On the recovery of a 2-D function from the modulus of its Fourier transform.* J. Math. Anal. Appl. **323** (2006), pp. 818–843.

[5] F. Werner, T. Hohage. *Convergence rates in expectation for Tikhonov-type regularization of inverse problems with Poisson data*, Inverse Problems **28** (2012) 104004 (16p.), 2012.

Qualitative non-destructive testing of concrete-like materials

L. Audibert[1,2,*], **H. Haddar**[2] **and A. Girard**[1]
[1]EDF R&D, STEP Departement
[2]INRIA Saclay Ile de France/Ecole Polytechnique CMAP
*Email: lorenzo.audibert@edf.fr

Abstract

In this paper we explore the capacity of Qualitative Inversion Methods to detect macroscopic cracks or a lattice of small cracks in concrete-like materials. These materials are difficult to probe since the heterogeneities size inside the medium and the wavelength of classically used sensors are of the same order of magnitude. We shall demonstrate how this difficulty can be avoided in the case of macroscopic cracks by using so-called differential measurements and application of the Linear Sampling Method. For a lattice of small cracks we rather propose to construct a macroscopic indicator based on the eigenvalues of a suitable transmission problem.

Introduction

We are interested in using elastic waves to perform complete non destructive testing of concrete-like materials. The main difficulty in controlling concrete is its heterogeneous nature. Concrete is made of cement paste, water and aggregates. After a drying period, this mixture results in a heterogeneous material. As far as waves propagation is concerned, the main characteristics is the difference of celerity between aggregates and cement paste, especially as the wavelength and the size of the aggregates are similar, thus, in what follows, we will model concrete as a biphasic material.This concrete-like material has the following properties: the celerity of pressure wave is $5700ms^{-1}$ in aggregates and $4300ms^{-1}$ in cement paste. Defect

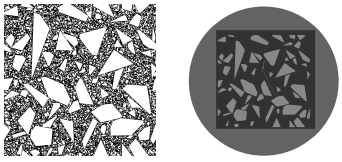

Figure 1: Simulated concrete and numerical set-up for direct and inverse problem

appears in concrete materials mainly in two forms. First a lattice of small cracks which are located at the interface between aggregates and cement paste. When this lattice is too dense, a macroscopic crack which has a length larger than the aggregates appears and grows until it reaches the surface. Those two types of defects are of interest and we will expose our preliminary results on how to detect them. Although waves in concrete are elastic, we start with the simpler case of acoustic waves and postpone the treatment of the elastic one. We therefore assume that the pressure field, u is solution to the well-known Helmholtz equations:

$$\begin{cases} \Delta u + k^2 n u = 0,\ u = u^i + u^s & in \quad \mathbb{R}^2 \backslash \Gamma \\ \lim\limits_{r\to\infty} \sqrt{r}(\frac{\partial u^s}{\partial r} - iku^s) = 0 & \\ \frac{\partial u}{\partial \nu} = 0 & on \quad \Gamma \end{cases}$$

where Γ is the crack(s) inside the medium, ν is a unit normal vector on Γ, n is the relative index with respect to the celerity in the air and u^i is the incident field created by a point source located at the interface air-concrete. For our numerical simulations, in order to simulate the heterogeneities in concrete we used synthetic geometries generated by [4] (See Figure 1, left) and eliminated the aggregates, which have an area smaller than $\frac{\lambda^2}{10^2}$, where $\lambda = \frac{2\pi}{k}$. This results in the medium represented by Figure 1, right. According to the remarks above, the index of the aggregates equals $2,8.10^{-3}$ and of the cement equals $4,8.10^{-3}$.

1 The inverse crack problem

We here investigate the inverse problem of finding cracks in concrete using the framework of the linear sampling method [5]. First we concentrate on the macrocracks and then on the small cracks lattice. We use multistatic measurements with sensor (sources and receivers) located on the interface Σ between air and concrete, namely these measurements are $u^s(x, x_0)$ $x, x_0 \in \Sigma$. In the sequel we introduce the subscript b which indicates the solution of the direct problem without defect and the subscript h which indicates the direct problem without defects and aggregates. The function $\Phi(z, \cdot)$ denotes the fundamental outgoing solution with Dirac source at position z.

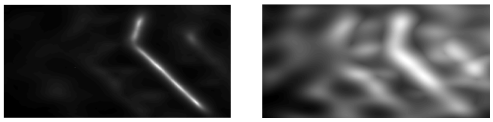

Figure 2: Identification of cracks using Φ_b(left) and Φ_h(right)

1.1 Macroscopic Cracks

We introduce the near field operator for differential-measurements (i.e. measurements of u^s and u_b^s),

$$[\mathcal{N}_b g](\cdot) = \int_\Sigma [u^s(\cdot, x_0) - u_b^s(\cdot, x_0)] g(x_0) ds(x_0)$$

Following the framework of the Linear Sampling Method for cracks developed in [2], one can find the support of the scattering crack, by looking for every z at the value of $\|g_z\|$, where g_z is the (regularized) solution to $[\mathcal{N}_b g_z](\cdot) = \frac{\partial \Phi_b}{\partial \nu(z)}(z, \cdot)$ (We refer to [2] for the details on how one copes with the unknown normal $\nu(z)$). Using this algorithm in our configuration yields to a quite good reconstruction as demonstrated by Figure 2 (left). However, although in practice u_b^s can be known in a differential measurement framework, Φ_b will always be unknown. Considering g_z the solution of $[\mathcal{N}_b g_z](\cdot) = \frac{\partial \Phi_h}{\partial \nu(z)}(z, \cdot)$ shows (Figure 2, right) that the quality of the reconstruction considerably deteriorates, although one can still distinguish the existence of a defect different from aggregates shape. This can be enough for qualitative inspection. We shall explore in the near future how one can improve the reconstruction by optimizing the choice of the background as in [3]. We shall also numerically analyze the feasibility of control with non-differential measurements. Finally, on the theoretical level, sensors at the interface are a realistic set up which is not yet justified for the LSM and we shall seek for a formal justification.

1.2 The case of lattice of microscopic cracks

When the cracks are small and numerous the LSM algorithm would not be able to locate them even in a differential setting. We shall rather use a macroscopic indicator based on the interior transmission eigenvalues which are computable from the measurements using following near field operator:

$$[\mathcal{N}_h g](\cdot) = \int_\Sigma [u^s(\cdot, x_0) - u_h^s(\cdot, x_0)] g(x_0) ds(x_0)$$

With this operator, since it also contains the contribution of the aggregates in the scattering effect, LSM will produce a support that covers almost all the heterogeneous material. It is well known [5] that the LSM fails for some frequencies which are, in our case, the eigenvalues of the following transmission problem:

$$\begin{cases} \Delta v + k^2 v = 0 & in \quad \mathcal{D} \\ \Delta u + nk^2 u = 0 & in \quad \mathcal{D}\backslash\Gamma \\ u = v, \frac{\partial u}{\partial \nu} = \frac{\partial v}{\partial \nu} & on \quad \partial\mathcal{D} \\ \frac{\partial u}{\partial \nu} = 0 & on \quad \Gamma \end{cases}$$

where $\mathcal{D}$ will be the scatterer (including the aggregates convex support and the cracks). Motivated by [1], we shall investigate the evolution of those frequencies with respect to the presence of cracks. In order to ensure that first transmission eigenvalues stay in the frequency range of the sources, we may introduce an artificial contrast in the equation solved by v, (characterized by an index $n_a \neq n$) localized in a region of size comparable to the incident wavelength. We finally recall that our interior transmission problem is still open in terms of existence and evolution of the eigenvalues with respect to Γ.

References

[1] F. Cakoni, A. Cossonnière and H. Haddar, *Transmission eigenvalues for inhomogeneous media containing obstacles*, Inverse Problems and Imaging, 6, no 3, 373-398 (2012).

[2] F. Ben Hassen, Y. Boukari and H. Haddar, *Application of the linear sampling method to identify cracks with impedance boundary conditions*, Inverse Problems in Science and Engineering, pp. 1-25 (2012).

[3] H. Haddar and G. Migliorati, *Numerical analysis of the Factorization Method for EIT with piece wise constant uncertain background*, 2012 (preprint)

[4] J. Escoda and al., *Estimation of local stresses and elastic properties of a mortar sample by FFT computation of fields on a 3D image*,Cement and Concrete Research, 41(5):542556 (2011).

[5] F. Cakoni and D. Colton, *Qualitative Methods in Inverse Scattering Theory*, 1st edition, Springer-Verlag, 2006.

The Point Source Method for Inverse Scattering in Waveguides

Rebecca K. Haunton[1,2], **Simon N. Chandler-Wilde**[1]
[1] Department of Mathematics and Statistics, University of Reading, U.K.
[2]Email: r.k.haunton@pgr.reading.ac.uk

Abstract

In this paper we explore using the point source method [1] to determine the location of a scattering object from measurements of the total acoustic field in a waveguide. The analysis of the method in the 2D case is briefly discussed and sample numerical results are presented.

Introduction

There has been a large development in the last fifteen years of new mathematical algorithms for acoustic inverse problems [1], [2], including applications to problems of scattering in waveguides [3], [4]. Many mathematical techniques for solving the inverse scattering problem require large quantities of initial measured data, in particular this is true for the linear sampling methods of [3], [4]. In contrast to this, the point source method of Potthast [1] only requires measurements of the total field for a single incident field.

In this paper we consider the application of the point source method [1] to inverse scattering in a waveguide. We produce numerical examples for the simplest case, when a sound-soft (Dirichlet) boundary condition holds on the obstacle.

1 An Inverse Waveguide Problem

We consider a 2D sound-hard waveguide of fixed height $L > 0$ (see Figure 1). We assume the incident field, the field in the absence of a scattering object, is time harmonic ($\mathrm{e}^{-\mathrm{i}\omega t}$ time dependence) and due to a point source at z. Perhaps the simplest representation of this incident field is [6]

$$u_k^i(x,z) := \frac{\mathrm{i}}{4}\sum_{m=-\infty}^{\infty} H_0^{(1)}(k|x-z^{(m)}|) + \frac{\mathrm{i}}{4}\sum_{m=-\infty}^{\infty} H_0^{(1)}(k|x-\hat{z}^{(m)}|)$$

with $z^{(m)} = (z_1, z_2 + 2mL)$ and $\hat{z}^{(m)} = (z_1, -z_2 + 2mL)$. This series converges if and only if the wavenumber $k = \omega/c \in \mathbf{R}_L := \mathbf{R} \setminus \{\frac{n\pi}{L} : n \in \mathbf{Z}\}$, and we shall impose this condition on k for the rest of this paper.

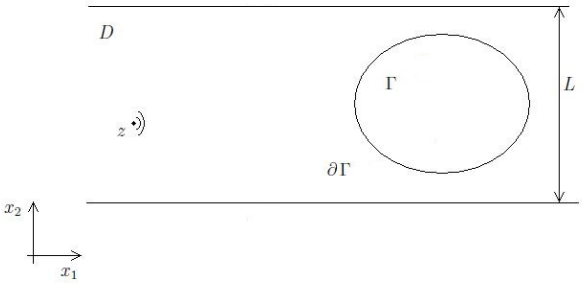

Figure 1: Waveguide setup

The direct scattering problem then entails calculating the total acoustic field $G_k(\cdot, z)$ as the sum of the incident field and some scattered field $u_k^s(\cdot, z) := G_k(\cdot, z) - u_k^i(\cdot, z)$, given the geometry of the scattering object Γ, and a boundary condition on the acoustic field on its boundary, $\partial\Gamma$. We shall assume the Dirichlet condition that the total acoustic field vanishes on $\partial\Gamma$.

The inverse scattering problem we consider is to locate the scattering object Γ based on measurements of the total field.

2 The Point Source Method

Let $m > z_1$ and assume we measure the total acoustic field along the finite vertical line $\gamma = \{(m, x_2) : 0 < x_2 < L\}$. Following [1], [5] we initially construct an approximation $G_k^\alpha(\cdot, z)$ to the total field and then seek the location of the scattering object as a minimum of $|G_k^\alpha(\cdot, z)|$. To eliminate faux results, *i.e.*, minima created by the oscillatory behaviour of the field, we note the merit of a time domain style approach of considering several wavenumbers k and calculating the minimum of

$$\sum_k |G_k^\alpha(\cdot, z)|^2 . \tag{1}$$

We proceed by approximating the total field at a point x^*. For $h > x_1^*$, let Γ_h^* denote the finite vertical line $\Gamma_h^* = \{(h, x_2) : 0 < x_2 < L\}$, and consider the

integral equation

$$\int_\gamma u_k^i(x,y)\phi_{x^*}(y)\ ds(y) = u_k^i(x,x^*),\quad x\in\Gamma_h^*, \quad (2)$$

in operator form $K\phi_* = g$. This integral equation is ill-posed; the inhomogeneous term g does not lie in the range of $K : L^2(\gamma) \to L^2(\Gamma_h^*)$. However, K has dense range and so g lies in the closure of $L^2(\Gamma_h^*)$. Thus we can find a solution $\phi_{x^*}^\alpha \in L^2(\gamma)$ which solves (2) to arbitrary accuracy. Standard results from the theory of Tikhonov regularisation motivate finding $\phi_{x^*}^\alpha$ as the unique solution of

$$\alpha\phi_{x^*}^\alpha + K^*K\phi_{x^*}^\alpha = K^*g \quad (3)$$

where K^* denotes the adjoint of K and $\alpha > 0$ is the regularisation parameter.

Replacing the incident field $u_k^i(x,\cdot)$ with the scattered field $u_k^s(x,\cdot)$ in (2), and using continuous dependence results for the direct problem, we see that, at least whenever Γ_h^* lies to the left of Γ,

$$\int_\gamma u_k^s(z,y)\phi_{x^*}^\alpha(y)\ dS(y) \approx u_k^s(z,x^*). \quad (4)$$

Our method to approximate the total field $G(x^*,z)$ at a point x^* in the domain is to first solve (3) and then, using (4) and reciprocity, approximate the total field by

$$\begin{aligned} G_k^\alpha(x^*,z) &:= u_k^i(z,x^*) + \int_\gamma u_k^s(z,y)\phi_{x^*}^\alpha(y)\ dS(y) \\ &= u_k^i(z,x^*) \\ &+ \int_\gamma \left[G_k(z,y) - u_k^i(z,y)\right]\phi_{x^*}^\alpha(y)\ dS(y). \end{aligned}$$

In this last expression, $G_k(z,y) = G_k(y,z), y\in\gamma$, is the (known) measured data.

3 Numerical results

In the numerical examples we take the height of the waveguide as $L = 3$, locate the point source at $z = (-12.5, 2.1)$, and take $\partial\Gamma$ to be the graph of the function $x_1 = x_2^2/9$, for $0 < x_2 < 3$. The numerical implementation uses a boundary element method to calculate "measurements" of the total field at 15 equally spaced points on the line $x_1 = -11$.

Figure 2 shows, starting from the top, the reconstructed total field $|G_k^\alpha(\cdot,z)|$, in the part of the waveguide $-10 < x_1 < 4$, for $k = 20\pi/11$, $k = 20\sqrt{2}\pi/11$ and $k = 40\pi/11$. The fourth image is (1) for these three wavenumbers and the final plot shows a prediction of the location of $\partial\Gamma$ obtained by plotting, on each horizontal line, the minimum of (1).

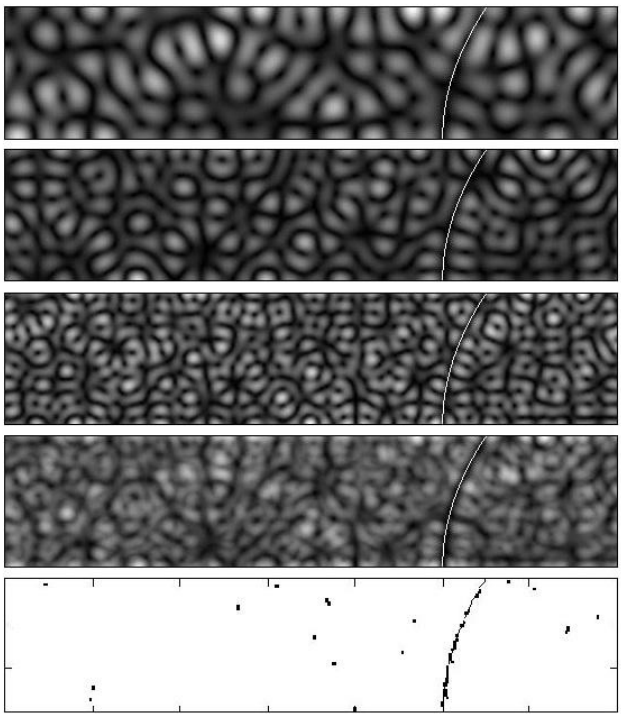

Figure 2: Reconstructions, in $-10 < x_1 < 4$, of the total field and $\partial\Gamma$, from 15 measurements of the total field on the line $x_1 = -11$.

References

[1] R. Potthast, *Point Sources and Multipoles in Inverse Scattering Theory*, Chapman and Hall, 2001.

[2] D. Colton and R. Kress, *Inverse Acoustic and Electromagnetic Scattering Theory*, 3rd Edition, Springer, 2013.

[3] L. Bourgeois and E. Lunéville, *The Linear Sampling Method in a Waveguide: a Modal Formulation*, Inverse Problems, **24** (2008), pp. 1–20.

[4] P. Monk and V. Selgas, *Sampling Type Methods for an Inverse Waveguide Problem*, Inverse Problems and Imaging, **6** (2012), pp. 709–747.

[5] C. D. Lines and S. N. Chandler-Wilde, *A Time Domain Point Source Method for Inverse Scattering by Rough Surfaces*, Computing, **75** (2005), pp. 157–180.

[6] C. M. Linton, *The Green's Function for the Two-Dimensional Helmholtz Equation in Periodic Domains*, Journal of Engineering Mathematics, **33** (1998), pp. 377–402.

On the far field of scattering solutions in a periodic waveguide. Part I : The forward problem

S. Fliss*, **P. Joly**
POEMS (UMR 7231 CNRS-ENSTA-INRIA)
ENSTA Paristech
Palaiseau, France
*Email: sonia.fliss@ensta-paristech.fr

The model problem that we consider in this paper is the propagation of a time harmonic scalar wave in a perfect 2D periodic waveguide. More precisely, we shall assume that the geometry $\Omega = \mathbb{R}\times(0,1)$ as well as the material properties of the medium (typically the refractive index) $n_p \in L^\infty(\Omega)$ - with $n_p \geq c > 0$ - are periodic in one direction (without loss of generality, we will suppose the period equal to 1) :

- $\Omega = \bigcup_{p\in\mathbb{Z}} \mathcal{C} + (p,0)$ where $\mathcal{C} = (-1/2,1/2)\times(0,1)$
- $n_p(x_1+1,x_2) = n_p(x_1,x_2), \quad \forall (x_1,x_2)\in\Omega.$

The Green function of the periodic waveguide, denoted $G(\cdot,y)$ for $y\in\Omega$ is the *outgoing* solution of

$$\begin{cases} -(\triangle + k^2 n_p^2) G(\cdot;y) = \delta_y & \text{in } \Omega \\ \partial_\nu G(\cdot;y) = 0 & \text{on } \partial\Omega \end{cases} \tag{1}$$

In order to define what "outgoing" means in a periodic waveguide, we use the limiting absorption principle and define $G(\cdot,y)$ for $y\in\Omega$ as the limit when ϵ tends to 0^+ of $G_\epsilon(\cdot,y)$, unique solution in $L^2(\Omega)$ of

$$\begin{cases} -(\triangle + (k^2+\imath\epsilon) n_p^2) G_\epsilon(\cdot;y) = \delta_y & \text{in } \Omega \\ \partial_\nu G_\epsilon(\cdot;y) = 0 & \text{on } \partial\Omega \end{cases} \tag{2}$$

Using the Floquet modes of the periodic medium, we are able to give a semi-analytic expression of the "outgoing" Green function. We investigate then the asymptotic behaviour of the Green function, i.e. the radiation condition when x_1 tends to $\pm\infty$. We finally show the uniqueness of the "outgoing" solution of the Helmholtz equation set on a periodic waveguide, satisfying this radiation condition.

1 Limiting absorption principle

Using the Floquet Bloch Transform in the x_1-direction and the well posedness in $L^2(\Omega)$ of problem (2), it is easy to show that $\forall (x,y)\in\mathcal{C}$, $\forall (p,q)\in\mathbb{Z}$,

$$G_\epsilon(x_1+p,x_2;y_1+q,y_2) = \frac{1}{2\pi}\sum_{n\in\mathbb{N}} \int_{-\pi}^{\pi} \frac{\varphi_n(x;\xi)\overline{\varphi_n(y;\xi)}}{\lambda_n(\xi)-(k^2+\imath\epsilon)} e^{\imath(p-q)\xi} d\xi \tag{3}$$

where, for all $\xi\in(-\pi,\pi)$, $\lambda_n(\xi)$ is the n-th eigenvalue and $\varphi_n(\cdot;\xi)$ an associated eigenvector of the self-adjoint and positive operator

$$\left| \begin{array}{l} A(\xi) = -\dfrac{1}{n_p^2}\triangle \\ D(A(\xi)) = \{u\in H^2(\mathcal{C}), \text{ such that } \partial_\nu u|_{\partial\mathcal{C}\cap\partial\Omega} = 0 \\ \qquad \text{and} \left| \begin{array}{l} u(1/2,x_2) = e^{\imath\xi} u(-1/2,x_2) \\ \partial_{x_1} u(1/2,x_2) = e^{\imath\xi}\partial_{x_1} u(-1/2,x_2) \end{array} \right. \}. \end{array} \right.$$

We can easily show that for all $n\in\mathbb{N}$ and $\xi\in(-\pi,\pi)$

$$\lambda_n(\xi) = \lambda_n(-\xi). \tag{4}$$

Let us define the finite sets

$$I(k) = \{n\in\mathbb{N},\ \exists\xi\in(-\pi,\pi),\ \lambda_n(\xi) = k^2\}$$

and for $n\in I(k)$

$$\Xi_n(k) = \{\xi\in(-\pi,\pi),\ \lambda_n(\xi) = k^2\}.$$

Note that if ξ is in $\Xi_n(k)$, $-\xi$ is too.

Using the abstract result of [3], or the more explicit result of [2], the limiting absorption principle can be shown except for a countable set of frequencies

$$\sigma_0 = \left\{ k\in\mathbb{R}^+,\ \exists n\in I(k),\ \exists\xi\in\Xi_n(k),\ \lambda_n'(\xi) = 0 \right\}$$

Theorem 1 *For all $k\notin\sigma_0$, $y\in\Omega$ and $p\in\mathbb{Z}$*

$$\lim_{\epsilon\to 0} \|G(\cdot;y) - G_\epsilon(\cdot;y)\|_{L^2(\mathcal{C}+(p,0))} = 0$$

where $G(\cdot;y)$ is a solution of (1) *and defined by* $\forall (x,y)\in\mathcal{C}$, $\forall (p,q)\in\mathbb{Z}$,

$$\begin{aligned} G(x_1+p,x_2;y_1+q,y_2) = & \\ & \frac{1}{2\pi}\sum_{n\notin I(k)} \int_{-\pi}^{\pi} \frac{\varphi_n(x;\xi)\overline{\varphi_n(y;\xi)}}{\lambda_n(\xi)-k^2} e^{\imath(p-q)\xi} d\xi \\ & + \frac{1}{2\pi}\sum_{n\in I(k)} \Big[p.v. \int_{-\pi}^{\pi} \frac{\varphi_n(x;\xi)\overline{\varphi_n(y;\xi)}}{\lambda_n(\xi)-k^2} e^{\imath(p-q)\xi} d\xi \\ & \qquad + \imath\pi \sum_{\xi\in\Xi_n(k)} \frac{\varphi_n(x;\xi)\overline{\varphi_n(y;\xi)}}{|\lambda_n'(\xi)|} e^{\imath(p-q)\xi} \Big]. \end{aligned} \tag{5}$$

2 Asymptotic behaviour of the Green function

In the following $k \notin \sigma_0$, $y \in \mathcal{C}$ and $q \in \mathbb{Z}$. To prove the asymptotic behaviour of the Green function, the main property is the C^∞-regularity of the eigenvalues $\xi \mapsto \lambda_n(\xi)$ and of the eigenvectors $\xi \mapsto \varphi_n(\xi)$ with respect to ξ for $n \in I(k)$. Using [4], such property holds except for a countable set of frequencies

$$\tilde{\sigma}_0 = \{k \in \mathbb{R}^+,\ \exists n, m \in I(k),\ \exists \xi,\ \lambda_n(\xi) = \lambda_m(\xi)\}.$$

Then the proof relies on

- analyticity arguments to deal with the first sum, denoted $\hat{G}$, in the right hand side of (5). More precisely, one shows that for all $x \in \mathcal{C}$, $p \in \mathbb{Z}$ and $N \in \mathbb{N}$

$$\hat{G}(x_1 + p, x_2; y_1 + q, y_2) = \mathcal{O}_{L^2}\left(p^{-N}\right);$$

- non stationary phase theorem to deal with each principal value, denoted $G_{(n)}$, of the second sum in the right hand side of (5). More precisely, one shows that for all $n \in I(k)$, $x \in \mathcal{C}$, $p \in \mathbb{Z}$ and $N \in \mathbb{N}$

$$G_{(n)}(x_1 + p, x_2; y_1 + q, y_2) = \mathcal{O}_{L^2}\left(p^{-N}\right) + \\ + \imath\pi \mathrm{sign}(p) \sum_{\xi \in \Xi_n(k)} \frac{\varphi_n(x;\xi)\overline{\varphi_n(y;\xi)}}{\lambda_n'(\xi)} e^{\imath(p-q)\xi}$$

Theorem 2 *Suppose in the following $k \notin \sigma_0 \cup \tilde{\sigma}_0$, $y \in \mathcal{C}$ and $q \in \mathbb{Z}$. For all $x \in \mathcal{C}$, $p \in \mathbb{N}$ and $N \in \mathbb{N}$*

$$G(x_1 \pm p, x_2; y_1 + q, y_2) = \mathcal{O}_{L^2}\left(p^{-N}\right) + \\ + \imath \sum_{n \in I(k)} \sum_{\substack{\xi \in \Xi_n(k) \\ \pm\lambda_n'(\xi) > 0}} \frac{\varphi_n(x;\xi)\overline{\varphi_n(y;\xi)}}{|\lambda_n'(\xi)|} e^{\imath(p-q)\xi}$$

For a given y, the Green function $G(x, y)$ behaves when $x \to +\infty$ (resp. $x \to -\infty$) as a linear combination of the Floquet modes $\varphi_n(x, \xi)$ which propagate to the right (resp. to the left) as $\lambda_n'(\xi) > 0$ (resp. $\lambda_n'(\xi) < 0$).

3 Radiation condition and uniqueness of the solution

We use the last result to define a radiation condition and establish, thanks to arguments used in [5], the well-posedness of the Helmholtz equation set in a periodic waveguide.

Definition 3 *We say that u satisfies the outgoing radiation condition if and only if there exist $(u_n^\pm)_n$ such that $\forall x \in \mathcal{C}$, $p \in \mathbb{N}$, $N \in \mathbb{N}$*

$$u(x_1 \pm p, x_2) = \mathcal{O}_{L^2}\left(p^{-N}\right) + \\ + \sum_{n \in I(k)} \sum_{\substack{\xi \in \Xi_n(k) \\ \pm\lambda_n'(\xi) > 0}} u_n^\pm \varphi_n(x;\xi) e^{\imath p \xi}$$

Theorem 4 *Suppose $k \notin \sigma_0$. Let u be a solution of*

$$\begin{cases} -(\triangle + k^2 n_p^2)\, u = 0 & \text{in } \Omega \\ \partial_\nu u = 0 & \text{on } \partial\Omega \end{cases}$$

which satisfies the outgoing radiation condition. Then $u = 0$.

4 Conclusions

This analysis is one of the main tool to solve inverse problems in locally perturbed periodic waveguide when the data are far field measurements of scattering problems (see [1]).

One challenging perspective of this work is to extend these results to periodic problems in free space.

References

[1] L. Bourgeois and S. Fliss, *On the far field of scattering solutions in a periodic waveguide. Part II: the inverse problem*, Proceeding of Waves, June 2013.

[2] S. Fliss, *Etude mathématique et numérique de la propagation des ondes dans des milieux périodiques localement perturbés*, PhD Thesis Ecole Doctorale de Polytechnique,May 2009.

[3] S. Z. Levendorskii, *Acoustic waves in perturbed periodic layer: a limiting absorption principle*, Asymptot. Anal. **16** (1998), no. 1, pp. 15–24.

[4] T. Kato, *Perturbation theory for linear operators*, Springer-Verlag, Classics in Mathematics, Berlin, 1995.

[5] S.A. Nazarov and B.A. Plamenevsky, *Elliptic Problems in Domains with Piecewise Smooth Boundaries*, vol. 13 of de Gruyter Expositions in Mathematics, Berlin, 1994.

On the far field of scattering solutions in a periodic waveguide. Part II : The inverse problem

L. Bourgeois*, **S. Fliss**
Laboratoire POEMS, ENSTA ParisTech, 828, Boulevard des Maréchaux
91762, Palaiseau Cedex, France
*Email: laurent.bourgeois@ensta.fr

Introduction

In this paper, we consider the factorization method to solve the inverse medium problem in a 2D periodic waveguide. Our objective differs from [1] in the following sense: the aim of [1] is to recover the unknown periodic boundary of the waveguide from scattering data, while in the present paper the periodic waveguide is known and our aim is, from the same data, to recover a defect within such periodic waveguide. Our paper can be considered as an extension of [2], in which a homogeneous waveguide is considered. It is based on the analysis conducted in [4] of the far field of the Green function in a periodic waveguide. Such analysis enables us to derive a modal formulation of Kirsch's factorization method [5], in which the incident fields are formed by the Floquet modes.

1 Setting of the problem

In the framework of 2D acoustics, let us consider a periodic waveguide $\Omega = \mathbb{R} \times (0,1)$ of boundary $\Gamma = \partial\Omega$ and for $j \in \mathbb{Z}$, $C_j := \Omega \cap \{x = (x_1, x_2),\ j - 1/2 < x_1 < j + 1/2\}$. The background medium is characterized by a real refractive index $n_p(x) \in L^\infty(\Omega)$ which satisfies $n_p(x) \geq c > 0$ and $n_p(x_1+1, x_2) = n_p(x_1, x_2)$ for all $(x_1, x_2) \in \Omega$. The Green function of the periodic waveguide, denoted $G(\cdot, y)$ for $y \in \Omega$, is the solution of the system

$$\begin{cases} -(\Delta + k^2 n_p^2) G(\cdot, y) = \delta_y & \text{in} \quad \Omega \\ \partial_\nu G(\cdot, y) = 0 & \text{on} \quad \Gamma \\ G(\cdot, y) \text{ satisfies RC} & \text{for} \quad |x_1| \to +\infty, \end{cases}$$

where ν is the outward unit normal to Ω and RC is the radiation condition, which is specified in [4] and is well defined except for $k \in \sigma_0$, where the countable set σ_0 is defined by (4). Now let us consider the forward scattering problem. Assume that a defect lies within the periodic waveguide, in the cell $C_0 := C$ without loss of generality, so that the effective real refractive index $n \in L^\infty(\Omega)$ differs from n_p. More precisely, there exists an open domain D such that $\overline{D} \subset C$ coincides with the support of the contrast $q = n^2 - n_p^2$. For sake of simplicity we assume that $q(x) \geq c > 0$.

For a given incident wave u^i in Ω, that is a field solving $\Delta u^i + k^2 n_p^2 u^i = 0$ in Ω and $\partial_\nu u^i = 0$ on Γ, the scattered field u^s is the solution in Ω of the problem

$$\begin{cases} -(\Delta + k^2 n^2)(u^s + u^i) = 0 & \text{in} \quad \Omega \\ \partial_\nu u^s = 0 & \text{on} \quad \Gamma \\ u^s \text{ satisfies RC} & \text{for} \quad |x_1| \to +\infty. \end{cases} \tag{1}$$

It results from [3] that the problem (1) is well-posed, except for at most a countable set of k. In order to introduce the inverse problem, for all $\xi \in (-\pi, \pi)$ we denote by $\varphi_n(\cdot;\xi)$ and $\lambda_n(\xi)$ the eigenfunctions and eigenvalues of the self-adjoint and positive operator $A(\xi) = -\Delta \cdot / n_p^2$ in $L^2(C, n_p^2\, dx_1 dx_2)$ of domain $D(A(\xi))$ formed by the $H^2(C)$ functions u that satisfy $\partial_\nu u = 0$ on Γ and the pseudo-periodicity conditions $u(1/2, x_2) = e^{i\xi} u(-1/2, x_2)$ and $\partial_{x_1} u(1/2, x_2) = e^{i\xi} \partial_{x_1} u(-1/2, x_2)$ for $x_2 \in (0,1)$. With a correct choice of the φ_n, we have:

$$\lambda_n(-\xi) = \lambda_n(\xi), \quad \varphi_n(\cdot;-\xi) = \overline{\varphi_n(\cdot;\xi)}. \tag{2}$$

Defining the (finite) sets

$$I(k) = \{n \in \mathbb{N},\ \exists \xi \in (-\pi, \pi), \quad \lambda_n(\xi) = k^2\}$$

and for $n \in I(k)$,

$$\Xi_n(k) = \{\xi \in (-\pi, \pi), \quad \lambda_n(\xi) = k^2\},$$

which is symmetric with respect to $\xi = 0$, the Floquet modes $u_n(\cdot;\xi)$ are given for $n \in I(k)$, $\xi \in \Xi_n(k)$, $x \in C$ and $p \in \mathbb{Z}$ by

$$u_n(x_1 + p, x_2; \xi) = \varphi_n(x_1, x_2; \xi) e^{ip\xi},$$

which are particular incident waves. Let us consider the transverse sections S_+ and S_- defined by $x_1 = 1/2 + N$ and $x_1 = -1/2 - M$ for $M, N \in \mathbb{N}$, respectively. The inverse problem is as follows.

The inverse problem (IP). *Assume that we measure on $\hat{S} := S_- \cup S_+$ the scattered fields $u_n^s(\cdot,\xi)$ associated with the incident fields $u^i = u_n(\cdot,\xi)$ for all $n \in I(k)$ and all $\xi \in \Xi_n(k)$. The objective is to find the support D of the defect from those measurements.*

2 The factorization method

In view to solve the inverse problem (IP), we define an intermediate scattering problem based on the scattered fields $u^s(\cdot, y)$ solving (1) for the incident fields $u^i = \overline{G(\cdot, y)}$ for $y \in \hat{S}$. Introducing the near field operator $N : L^2(\hat{S}) \to L^2(\hat{S})$ as

$$(Nh)(x) = \int_{\hat{S}} u^s(x, y) h(y)\, ds(y), \quad x \in L^2(\hat{S}),$$

by adapting the arguments of [5] to our problem, we obtain that for every $z \in \Omega$, we have

$$z \in D \quad \Leftrightarrow \quad G(\cdot, z)|_{\hat{S}} \in R(N_\sharp^{\frac{1}{2}}), \tag{3}$$

where $N_\sharp$ is the self-adjoint and positive operator $|\mathrm{Re}N| + |\mathrm{Im}N|$.
From the analysis of [4] and assuming $k \notin \sigma_0$, where

$$\sigma_0 = \{k,\ \exists n \in I(k),\ \exists \xi \in \Xi_n(k),\ \lambda_n'(\xi) = 0\}, \tag{4}$$

we obtain the following asymptotic behaviour of the Green function G: $\forall x, y \in C$, $\forall q \in \mathbb{Z}$, $G(x_1 \pm p, x_2, y_1 + q, y_2)$ is approximated for large $p \in \mathbb{N}$, up to any power of p, by

$$\tilde{G}(x_1 \pm p, x_2, y_1 + q, y_2) = i \sum_{n \in I(k)} \sum_{\xi \in \Xi_n(k) \lambda_n'(\xi) > 0} \frac{u_n^{\pm}(x_1 \pm p, x_2; \xi) u_n^{\mp}(y_1 + q, y_2; \xi)}{\lambda_n'(\xi)},$$

where $u_n^+(\cdot; \xi)$ denote the Floquet modes $u_n(\cdot, \xi)$ with $\lambda_n'(\xi) > 0$ (they propagate from the left to the right) while by using (2) $u_n^-(\cdot; \xi) := u_n(\cdot, -\xi) = \overline{u_n^+(\cdot, \xi)}$ denote the corresponding Floquet modes with $\lambda_n'(-\xi) < 0$ (they propagate from the right to the left). The scattered field $u^s(\cdot, y)$ is approximated for large $p \in \mathbb{N}$ by the scattered field $\tilde{u}^s(\cdot, y)$ produced by the incident wave $u^i = \overline{\tilde{G}(\cdot, y)}$. By linearity,

$$\tilde{u}^s(x_1 \pm p, x_2, y_1 + q, y_2) = -i \sum_{n \in I(k)} \sum_{\xi \in \Xi_n(k) \lambda_n'(\xi) > 0} \frac{u_n^{s\mp}(x_1 \pm p, x_2; \xi) u_n^{\pm}(y_1 + q, y_2; \xi)}{\lambda_n'(\xi)},$$

where $u_n^{s\pm}$ is the scattered field associated with the incident field $u_n^{\pm}$.
The idea of the modal formulation of the factorization method consists in replacing, in the characterization (3), the test function $G(\cdot, z)|_{\hat{S}}$ by its approximation $\tilde{G}(\cdot, z)|_{\hat{S}}$ and the operator N by the operator $\tilde{N}$ the kernel of which is the scattering field $\tilde{u}^s(\cdot, y)$.

We hence remark that the operator $\tilde{N}$ only depends on the data of our inverse problem (IP). Our method consists in solving equation $\tilde{N}_\sharp^{1/2} h = \tilde{G}(\cdot, z)|_{\hat{S}}$ for all z in a sampling grid of Ω and plotting the function $\psi(z) = 1/||h(z)||_{L^2(\hat{S})}$, which vanishes only outside D. From the practical point of view such equation is projected on a basis of the transverse sections $S_\pm$. With the help of the numerical tools developed in [3], we produce artificial data for the periodic waveguide below, for which the number of Floquet modes is 4. The identification result with our sampling method based on the scattered fields due to those Floquet modes for $(M, N) = (64, 61)$ and without noise is given in the figure below.

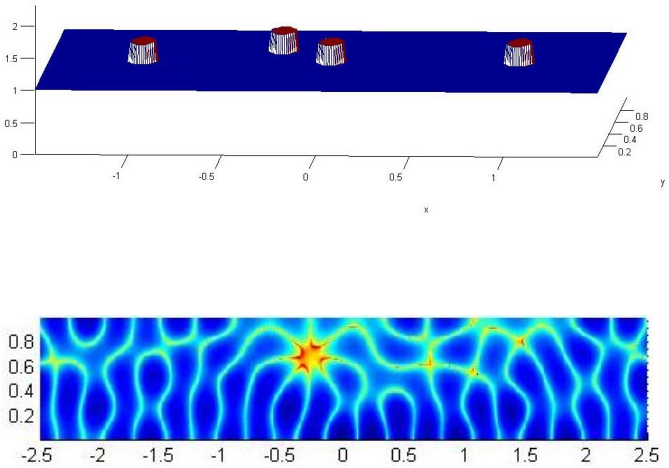

References

[1] T. Arens and A. Kirsch, *The factorization method in inverse scattering from periodic structures*, Inverse Problems, **19** (2003), pp. 1195–1211.

[2] L. Bourgeois and E. Lunéville, *The linear sampling method in a waveguide: a modal formulation*, Inverse Problems, **24** (2008), 015018.

[3] S. Fliss, *Etude mathématique et numérique de la propagation des ondes dans des milieux périodiques localement perturbés*, PhD (2009).

[4] S. Fliss and P. Joly, *On the far field of scattering solutions in a periodic waveguide. Part I : The forward problem*, Proceedings of Waves, (June 2013)

[5] A. Kirsch and N. Grinberg, *The factorization method for inverse problems*, Oxford University Press, Oxford, 2008.

Inverse Source Problem for a One-dimensional Wave Equation Using Observers

S. Asiri [1], **T. Laleg-Kirati**[1,*] **and C. Zayane**[1]
[1] Computer, Electrical and Mathematical Sciences and Engineering, KAUST, Thuwal, KSA.
*Email: taousmeriem.laleg@kaust.edu.sa

Abstract

This paper proposes to use observers to solve an inverse problem for the one-dimensional wave equation where the source is unknown. The problem is first discretized and then an adaptive observer is applied to estimate both the states and the source. Results of simulation are presented.

Introduction

The theory of observers is known since a long time in systems theory for the estimation of the state of dynamical systems from some measurements. However it is recently that the observers have been considered for systems governed by partial differential equations [1]. Observers have been used to solve some inverse problems for PDE [2], [3], [4] [5], including inverse problems for the wave equation to estimate some unknowns. In Ramdani *et al* [2], the initial state of a distributed parameter system has been estimated using two observers, one for the forward time and the second for the backward time. Similarly, Chapouly and Mirrahimi [3] estimated the unknown source term using observers in the minimal observation time. Their observer converged to the real parameter thanks to forth and back iterations approach. Chapelle *et al* [4] sought to estimate the initial conditions using observer based on measurements of the solution in a subset of the domain. Moireau *et al* [5] estimated the states and the parameters using an observer depending on a space discretization for a mechanical system. In addition, they considered partial measurements of the derivative of the solution.

One advantage of using observers to solve inverse problems is that it requires solving only direct problems which are in general well-posed and well studied. Moreover, unlike optimization based methods (including regularization), observers operate recursively which implies their implementation ease and low computational cost especially when it comes to high order systems. We propose in this paper to start with fully discretized version of a one diminsional wave equation and then to apply the adaptive observer presented in [6] for the joint estimation of the states and the source term from partial measurements of the field. Adaptive observers are widely used in control theory for parameter estimation in adaptive control or fault estimation in fault detection and isolation [6].

1 Method

1.1 Problem

We consider the one dimensional wave equation given by,

$$\begin{cases} u_{tt}(x,t) - c^2 u_{xx}(x,t) = f(x) \\ u(0,t) = g_1(t),\ u(L,t) = g_2(t) \\ u(x,0) = r_1(x),\ u_t(x,0) = r_2(x) \end{cases}, \qquad (1)$$

where $x \in [0, L]$ is the space and $t \in [0, T]$ is the time. $g_1(t)$ and $g_2(t)$ are the Dirichlet boundary conditions, and $f(x)$ is the source function that we assume for simplicity independent on time.

We seek to solve the inverse source problem of (1) using an adaptive observer with partial measurements of the field u available. We first propose to rewrite the system in an appropriate form by introducing two auxiliary variables $v(x,t) = u(x,t)$ and $w(x,t) = u_t(x,t)$ and let

$$\xi(x,t) = \left[\ v(x,t), w(x,t)\ \right]^T. \qquad (2)$$

Therefore, system (1) can be written as follows,

$$\begin{cases} \dfrac{\partial \xi(x,t)}{\partial t} = A\xi(x,t) + F, \\ v(0,t) = g_1(t),\ v(L,t) = g_2(t), \\ v(x,0) = r_1(x),\ v_t(x,0) = r_2(x), \\ Y = H\xi(x,t), \end{cases} \qquad (3)$$

where $A = \begin{pmatrix} 0 & I \\ c^2 \frac{\partial^2}{\partial x^2} & 0 \end{pmatrix}$, $F = \begin{pmatrix} 0 \\ f \end{pmatrix}$, Y is the output, and H is the observation operator such that $H = (H_d \ \ 0)$ where $H = \begin{pmatrix} 0 & \cdots & 0 \\ \vdots & I_d & \vdots \\ 0 & \cdots & 0 \end{pmatrix}$ and d refers to the number of measurements. I_d is the identity matrix of dimension d.

System (3) is discretized using implicit Euler scheme in time and central finite difference discretization for space; thus, it can be written as,

$$\begin{cases} \xi^{j+1} = G\xi^j + Bf^j + b, \\ Y^j = H\xi^j, \qquad\qquad j = 1, 2, \cdots, N_k \end{cases} \tag{4}$$

such that

$$G = \begin{pmatrix} kE + I & kI \\ E & I \end{pmatrix};$$

$$E = \frac{c^2 k}{h^2} \begin{pmatrix} -2 & 1 & & \\ 1 & -2 & \ddots & \\ & \ddots & \ddots & 1 \\ & & 1 & -2 \end{pmatrix}; B = \begin{pmatrix} k^2 I \\ kI \end{pmatrix};$$

b is a term that includes the boundary conditions, and N_k is the time grid size. Here h and k refer to space step and time step respectively.

1.2 Observer design

As known in control theory, a state observer is a system that provides an estimate of its internal state, given measurements of the input and the output of the real system. We propose to use an adaptive observer for the joint estimation of the states v and w and the source f. This observer has been proposed in [6], and it has been developed for joint estimation of the state and the parameters for a class of systems. However, we propose to generalize the idea behind this observer to estimate the input considering each spatial sample of the input as an independent parameter. The adaptive observer is given by the following system of equations,

$$\begin{cases} \hat{\xi}^{j+1} = G\hat{\xi}^j + B\hat{F}^j + b + (K + \sigma^j Z^j {Z^j}^T H^T)(Y - \hat{Y}), \\ \hat{F}^{j+1} = \hat{F}^j + \sigma^j {Z^j}^T H^T (Y - \hat{Y}) \\ Z^{j+1} = (G - KH)Z^j + B, \\ \hat{Y} = H\hat{\xi}(x, t), \end{cases} \tag{5}$$

where K is the observer gain matrix, σ^j a scalar gain, and $j = 1, 2, \cdots, N_k$. We point out that it has been shown in [6] that for discrete finite dimensional systems, this observer converges exponentially. The discretization affects the convergence and we are currently studying this effect.

2 Numerical Results

Figure. 1 illustrates the efficiency of this observer to estimate the source where $N_k = 10000$, and the space grid size is $N_h = 199$. Moreover, the state is estimated with relative error 0.09398.

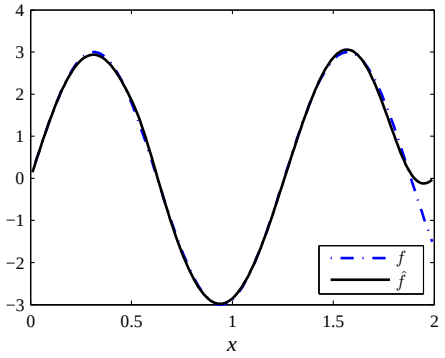

Figure 1: Real source (blue) and Estimated source (red) using partial measurements (74% of the state components taken from the end of the interval)

References

[1] W. Marquadt and H. Auracher *:An Observer-based Solution of Inverse Heat Conduction Problems* ,Int. J. Heat Mass Transfer, **33(7)** (1990), pp. 1545–1562.

[2] K. Ramdani and M. Tucsnak and G. Weissc, *Recovering The Initial State of an Infinite-Dimensional System Using Observers*, Automatica, **46** (2010), pp. 1616–1625.

[3] M. Chapouly and M. Mirrahimi, *Distributed Source Identification for Wave Equations : An Observer-Based Approach*, in Proceedings of the 19th International Symposium on Mathematical Theory of Networks and Systems, (2010), pp. 389–394.

[4] D. Chapelle and N. Cîndea and M. De Buhan and P. Moireau, *Exponential Convergence of An Observer Based on Partial Field Measurements For The Wave Equation*, Mathematical Problems in Engineering, (2012), pp. 1–12.

[5] P. Moireau and D. Chapelle and P. Le Tallec, *Joint state and parameter estimation for distributed mechanical systems*, ELSEVIER, (2008), pp. 659–677.

[6] A. Guyader and Q. Zhang, *Adaptive Observer for Discrete Time Linear Time Varying Systems*. in Proceedings of 13th Symposium on System Identification (SYSID), Rotterdam, (2003), pp. 1743–1748. ,

Modeling of Imaging Method to Localize Targets Inside Buildings

B. Boudamouz, N. Maaref, P. Millot and X. Ferrieres

In this paper, we are interested in a MIMO radar system to localize targets inside buildings. We describe the principle of the method. Then, we show the advantages of a MIMO architecture to localize targets in realistic conditions.

1 Introduction

TTW (Through The Wall) surveillance is of great interest for first-aid workers and security guards in situations like rescue operations or hostages taking. This research topic has been investigated since the last past decade [1]. Today, imaging methods to find targets inside buildings are an important field of theorical research and technological developments [2], [3]. In this application, the key factor is the wall as propagation through it, induces attenuation and distortion on the wave front. Thus, it should be very efficient to take it into account in the modeling process. However, in practice, it is very difficult to introduce real wall effects in the inversion process, because it is not generally well-known, specially for non homogeneous walls as brick or cinder block wall. Another way to mitigate wall effects, is to use spatial diversity by using MIMO concept. This concept in radar consists in using information obtained from several transmitters and several receivers located at differents positions. By this way, propagation effects are averaged all through the set of antennas. The goal of this paper is to show the interest of a MIMO approach to localize targets into a room bounded by concrete brick walls. The paper is split into 3 sections where we present, first, the principle of the imaging methods used and in particular the MIMO approach [4]. Secondly, we present the test case studies and in a third section we give the results obtained and in particular the advantage of applying MIMO approach.

2 Principle of the radar imaging method

Basically, the radar imaging method consists in making an image of the dielectric contrasts existing in a given domain Ω. To obtain this image we take some points source and some points of measurements of the scattered fields induced by the targets localized in the domain Ω considered. The domain Ω is meshed by a set of N_Ω points where signal processings allow to test the existence of a target. Considering a source S_i localized at a point x_i, we assume that the electric fields at a point x for a frequency f is given by $E(f,x) = E_0 e^{-j2\pi f\|x-x_i\|/c}$ where E_0 is the incident amplitude field and c the speed of the light in the domain Ω. When the incident field hits a target, a part of the incident field is backscattered. We assume that this scattered part is represented by a reflectivity R. Then, the received scattered field at a point located at x_j from a source located at x_i and backscattered by a target located at x is given by $E(f,x) = RE_0 e^{-j2\pi f\|x-x_i\|/c} e^{-j2\pi f\|x-x_j\|/c}$. Then, for a set of n_f frequencies f_l, the inverse problem consists in evaluating the N_Ω coefficients R_k at the mesh points of Ω verifying :

$$\min_{R_k} \sum_{l=1}^{n_f} \sum_{i=1}^{n_s} \sum_{j=1}^{n_r} \sum_{k=1}^{N_\Omega} (E_{mes}(f_l, x_j) - G_{k,l,i,j})^2$$

with

$$G_{k,l,i,j} = R_k E_0 e^{-j2\pi f_l\|x_k-x_i\|/c} e^{-j2\pi f_l\|x_k-x_j\|/c}$$

In these expressions, n_i, n_j and E_{mes} define respectively the number of source points, the number of receivers and the electric fields measured at the receivers. This inverse problem can be solved with maximun likelyhood techniques which consists in a linear inversion to obtain the coefficients R_k [5]. Potential targets are localized at the points where the coefficient R_k are non-zero. In terms of source and receiving points spatial distribution, there are different strategies. SISO radars are single transceive and single receive systems. In this case, there is no spatial diversity. Then, SIMO radars generally employs one transmitting antenna and a set of receiving ones. In this approach, spatial diversity is on reception. Finally, MIMO approach consists on having a multitude of transceivers and receivers. And, thus diversity is in this case both on transmission an reception. Transmitting spatial diversity gives robustness againts complex propagation through walls and improves indoor probability detection.

3 Configuration of our test case

The configuration studied here implements a dielectric cylinder ($\sigma = 0.01$, $\varepsilon_r = 50$), located inside a room bounded by walls constituted of concrete slabs with holes (see figure 1). In this example, we also define the joint of cement between the concrete elements. The room heights $h = 2m$ and the dimension of its sides is $L = 4.28m$. The dimensions of the concrete element are $0.5m \times 0.2m.2m$. It is constituted of 6 holes (see figure 2). The height of the cement joint is taken equal to $2cm$. Concerning the dielectric cylinder, its height is equal to $1.8m$ and its radius to $0.15m$. Its location in the $x-y$ axis is $(1.29m, 1.29m)$. Thirty one sensors (receivers and emitters) are located on a cross of center ($x = 2.29m$,$y = -1m$,$z = 1m$). These sensors are located at a distance of $1m$ from the wall. The pulse injected on each sensor is given by $E_z(t) = E_0 e^{-((t-t_0)/T_0)^2} cos(2\pi\, f_0\, t)$ with $E_0 = 377v/m$, $t_0 = 2.6e-9s$, $T_0 = 1.e-9s$ and $f_0 = 2.e9Hz$. This waveform presents a $2GHz$ bandwidth. The simulated data used in the inverse problem are obtained by FDTD.

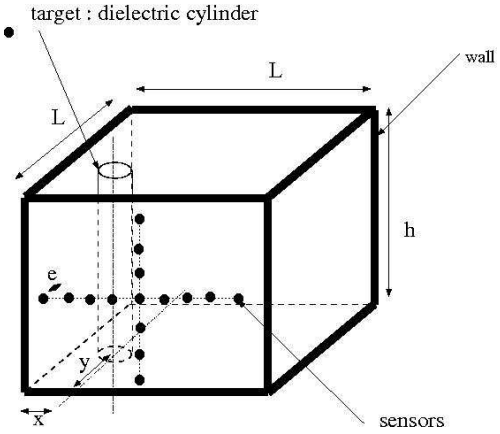

Figure 1: Configuration studied

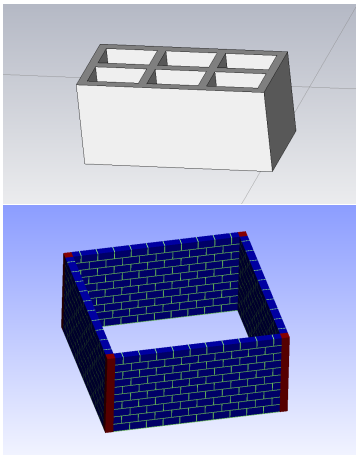

Figure 2: Geometry of a concrete brick.

4 Results

Two radar approaches have been simulated. The first is a SIMO approach and the second a MIMO one. The figure 3 shows the image obtained in the SIMO case (only one emitter placed at $(1.54m, -1m, 1m)$). It is a cut of the room at $z = 1m$. Free space is considered in the inverse process. As one can see, it is difficult to properly localize the cylinder and to find its correct position. Figure 4 shows the same image by considering the MIMO approach. Here all the sources contribute to the image formation. We can see on this image that the cylinder and its position in the room are well identified.

5 Conclusion

In this paper, we described a radar imaging method to detect targets located inside a room with realistic walls. We have studied the advantage of using a MIMO method for this problem, to avoid the perturbations induced by the particular shape of the concrete bricks which constitute the wall. A comparison made with a SIMO approach shows these advantages.

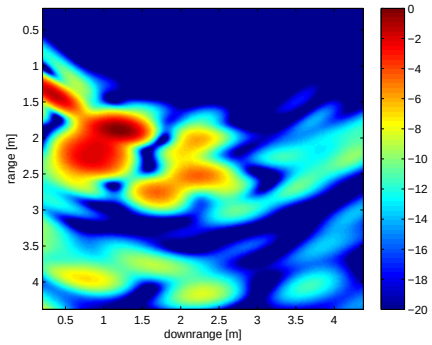

Figure 3: Image obtained by SIMO approach.

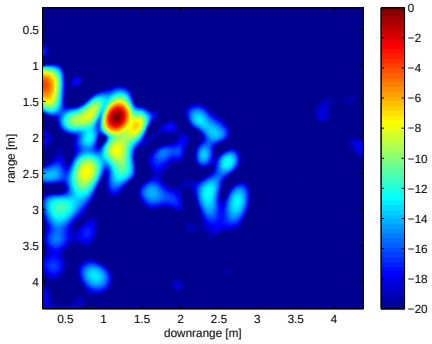

Figure 4: Image obtained by MIMO approach.

References

[1] L.M. Frazier, "Surveillance through walls and other opaque materials", *Aerospace and Electronic Systems Magazine, IEEE, vol.11, no.10, pp6-9, Oct. 1996*

[2] A.R.Hunt, "A wideband imaging radar for through-the-wall surveillance", *Procceings SPIE Sensors, and Command, Control, Communications, and Intelligence (C3I), vol. 5403, pp 590-596,2004*

[3] N.Maaref, P.Millot, P.Pichot, O. Picon, "A study of UWB FMCW Radar for the Detection of Human Beings in Motion Inside a Building", *IEEE Trans. Geoscience and Remote Sensing, vol. 47, no. 5, pp. 1297-1300, May 2009.*

[4] P. Stoica and J. Lee, "MIMO Radar Signal Processing", *Wiley 2008*

[5] N. Bertaux, P. Larzabal, C. Adnet and E. Chaumette, "Parameterized maximum likelyhood method: application to space time radar localization", *Traitement du signal, vol.16, no.3, 1999*

Inversion of Reynolds stresses in the solar interior

D. Fournier[1,*], **T. Hohage**[1], **L. Gizon**[2,3]
[1] Institut für Numerische und Angewandte Mathematik, Göttingen, Germany
[2] Max-Planck-Institut für Sonnensystemforschung, Katlenburg-Lindau, Germany
[3] Institut für Astrophysik, Georg-August-Universität, Göttingen, Germany
[*] Email: d.fournier@math.uni-goettingen.de

Abstract

Local helioseismology aims at recovering the motions (flow velocities) in the solar interior from observations of solar oscillations on the surface of the Sun. In time-distance helioseismology, the basic input data are travel times of waves between pairs of points on the surface. These quantities are linked to the internal properties of the Sun via an integral operator. In previous publications the reconstruction of flow velocities from travel times has been studied by solving an inverse problem. The aim of this paper is to recover directly the Reynolds stresses instead of first recovering the velocities then computing the correlations. This paper is a first attempt in this direction and all the necessary ingredients to perform directly the inversion are presented.

Introduction

Time-distance helioseismology [1] aims at recovering subsurface structure and dynamics of the Sun by the measurement and analysis of travel-times for wave packets moving between two points on the solar surface. Travel-times are obtained thanks to high-resolution Doppler images of the Sun surface given by space and ground-based networks. Once these quantities are known, a forward model has to be derived to link them to internal properties of the Sun. In the upper layers of the Sun, the convective motions are described by a flow field with velocity $\mathbf{v}(\mathbf{x})$, $\mathbf{x} \in \mathbb{R}^3$, which we would like to image using helioseismology. The relation between the travel time τ^a (between two surface points $\mathbf{r}_1$ and $\mathbf{r}_2$) and the flow velocity $\mathbf{v}(\mathbf{x})$ can be expressed as:

$$\tau_a(\mathbf{r}_1, \mathbf{r}_2) = \int_V \mathbf{K}^a(\mathbf{r} - \mathbf{r}_1, \mathbf{r}_2, z) \cdot \mathbf{v}(\mathbf{r}, z) d^2\mathbf{r} dz + n^a(\mathbf{r}_1, \mathbf{r}_2) \qquad (1)$$

where the integration is performed over a volume $V = S \times [0, z_{min}]$ formed by the product of a surface S in the $(x, y)-$plane (supposed planar) by a small depth interval $[0, z_{min}]$ under the Sun's surface. The superscript a denotes the type of travel time, $\mathbf{K}^a$ is the sensitivity kernel and n^a the noise generated by the stochastic excitation of the waves by the smallest scales of convection (granulation). The position vector $\mathbf{x}$ is written as $\mathbf{x} = (\mathbf{r}, z)$ where $\mathbf{r} = (x, y)$ are the horizontal coordinates and z points up.

To recover internal properties of the Sun, the inverse problem corresponding to (1) has to be solved. A good knowledge of the sensitivity kernel and of the noise model is required to perform the inversion reliably. A methodology to construct the kernels is presented in [2], [3] and in [4] for the noise model. If one wants to recover another quantity related to velocities like the Reynolds stresses one could first compute the velocities and then deduce the Reynolds stresses. However, this method is time-consuming and not very accurate. This paper presents a first attempt to compute directly the Reynolds stresses from the travel times spatial correlations. In a first part, inversion methods for travel times are presented, then we show that the velocity correlations can also be linked to travel times via an integral operator and so deduced by inversion methods.

1 Inversion for velocities

Two methods are traditionally used to invert (1): the Regularized Least Square (RLS) method (equivalent to the Tikhonov method in the mathematical literature) and the Optimally Localized Averages (OLA) (equivalent to the approximate inverse). A modified version of the latter has been recently used [5] in order to invert (1) in the Fourier space instead of the real space. It is of great interest as the different modes are not correlated in the Fourier space so a lot of small matrices ($\approx 300 \times 300$) have to be inverted instead of a large one. The small size of the matrices makes possible the calculation of its singular value and thus, to perform the inversion by singular value decomposition (SVD). This method is particularly efficient for our problem. As the problem is severely ill-posed, a lot of eigenvalues are close to 0 so only few ones are kept for most of the modes.

2 Inversion for velocity correlations

Using Reynolds's decomposition, the i^{th} composant of the flow velocity vector can be written as $v_i = V_i + v_i'$ where V_i is the deterministic mean part of the flow velocity and v_i' the small scale (random) part. The Reynolds stresses R_{ij} are then defined as:

$$\mathbf{R}_{ij}(\mathbf{x}, \mathbf{x}') = \langle v_i'(\mathbf{x}), v_j'(\mathbf{x}') \rangle \tag{2}$$

If we assume that the correlations of the fluctuating part of the flow are horizontally homogeneous, $\mathbf{R}_{ij}$ depends only on the distance $\boldsymbol{\delta} = \mathbf{r}' - \mathbf{r}$, z and z':

$$\mathbf{R}_{ij}(\boldsymbol{\delta}, z, z') = \langle v_i'(\mathbf{r}, z), v_j'(\mathbf{r} + \boldsymbol{\delta}, z') \rangle \tag{3}$$

Multiplying $\tau^a(\mathbf{r_1}, \mathbf{r_2})$ and $\tau^b(\mathbf{r_1}', \mathbf{r_2}')$ (using (1)) and supposing for the sake of clarity that $V_i = 0$, one can link Reynolds stresses and measured travel times:

$$\langle \tau^a(\mathbf{r_1}, \mathbf{r_2}), \tau^b(\mathbf{r_1}', \mathbf{r_2}') \rangle = \mathbf{\Lambda}^{ab}(\mathbf{x_1}, \mathbf{x_2}, \mathbf{x_1}', \mathbf{x_2}') + \int_{\odot'} \int_z K_{ij}^{ab}(\mathbf{r}', z, z'; \mathbf{r_1}, \mathbf{r_2}, \mathbf{r_1}', \mathbf{r_2}') \times \mathbf{R}_{ij}(\mathbf{r}', z, z') dz d^2\mathbf{r}' dz' \tag{4}$$

where $K_{ij}^{ab}(\mathbf{r}', z, z'; \mathbf{r_1}, \mathbf{r_2}, \mathbf{r_1}', \mathbf{r_2}') =$

$$\int_{\mathbf{r}} \mathbf{K}_i^a(\mathbf{r} - \mathbf{r_1}, \mathbf{r_2}, z) \mathbf{K}_j^b(\mathbf{r} + \mathbf{r}' - \mathbf{r_1}', \mathbf{r_2}', z') d^2\mathbf{r} \tag{5}$$

with $\mathbf{K}_i^a$ the i^{th} component of $\mathbf{K}^a$ and $\mathbf{\Lambda}^{ab}$ defined in [4] the noise covariance matrix for travel times.

Eq. (4) gives a relation between the Reynolds stresses and the travel times correlations via an integral operator. It turns out that the kernels are known as they are a correlation between two kernels for travel times. They can even be computed efficiently by Fast Fourier Transform (FFT):

$$K_{ij}^{ab} = \mathcal{F}^{-1} \left\{ \mathcal{F}\left(\overline{\mathbf{K}_i^a}\right) \mathcal{F}\left(\mathbf{K}_j^b\right) \right\} \tag{6}$$

where $\overline{\mathbf{K}_i^a}(\mathbf{r}) = \mathbf{K}_i^a(-\mathbf{r})$, $\mathcal{F}$ and $\mathcal{F}^{-1}$ represent the Fourier and inverse Fourier transform.

A 2D case used for kernel computations is presented in Figure 1. The kernels are computed between a one-way wave packet traveling west-east from the point $(-10\text{Mm}, 0)$ to $(10\text{Mm}, 0)$ and a south-north one traveling from $(0, -10\text{Mm})$ to $(0, 10\text{Mm})$. The kernel representing the cross-correlation for the Reynolds stresses is shown in Figure 1. Once the kernels are known, a noise model for Reynolds stresses is required. This can be done following the ideas of

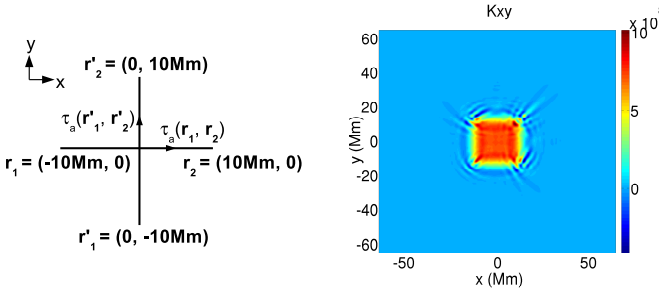

Figure 1: Test case for kernels computations (left); $K_{xy}^{aa}(x, y, \mathbf{r_1}, \mathbf{r_2}, \mathbf{r_1}', \mathbf{r_2}')$, a refers to a f-mode measure between pairs separated by 20Mm (right)

[4]. Computations are unfortunately way more complicated. In [4] it was necessary to compute the expected value of a product of four complex random Gaussian variables. Here, the moments of order six and eight are required which lead to about one hundred terms to estimate. However an exact formula can be derived for this purpose. Knowing the kernels and a noise model, (4) can be inverted for example by using a singular value decomposition.

This approach is significantly more efficient both concerning memory storage and computation time. In this direct approach, computations are made with mean values instead of maps on the whole domain if one wants to first compute the velocities then deduce the Reynolds stresses. So the size of the matrix to invert is much smaller. This approach will be validated using a model for flow velocities and travel times.

References

[1] T. L. Duvall Jr et al. Time-distance helioseismology. *Letters to Nature*, 362:430–432, 1993.

[2] L. Gizon and A. C. Birch. Time-distance helioseismology: the forward problem for random distributed sources. *The Astrophysical Journal*, 571:966–986, 2002.

[3] A. C. Birch and L. Gizon. Linear sensitivity of helioseismic travel times to local flows. *Astronomical Notes*, 328(3/4):228–233, 2007.

[4] L. Gizon and A. C. Birch. Time-distance helioseismology: Noise estimation. *The Astrophysical Journal*, 614:472–489, 2004.

[5] J. Jackiewicz et al. Multichannel three-dimensional SOLA inversion for local helioseismology. *Sol. Phys.*, 276:19–33, 2012.

An Inverse Algorithm for Reconstructing an Initial Tsunami Waveform

T. Voronina[1,*]
[1] The Institute of Computational Mathematics and Mathematical Geophysics SB RAS,Russia
*Email: tanvor@bk.ru

Abstract

This paper outlines an approach to reconstructing an initial tsunami waveform in a tsunami source area based on the inversion of remote measurements of water-level data. Tsunami wave propagation is considered within the scope of the linear shallow-water theory. Numerical simulation is based on the finite difference algorithm and the method of splitting. The ill-posed inverse problem at hand is regularized by means of the least square inversion using the truncated SVD approach. In this method the inverse operator is replaced by its restriction to a subspace spanned by a finite number of the first right singular vectors [1]. The so-called **r**-solution [2] is produced by a numerical process. One of the main advantages of this method is that it does not require a priori assumption on the fault plane solution, actually, this method is completely independent of any particular source model. By analyzing characteristics of a given tide gauges network, the proposed method allows one to control numerical instability of the solution and therefore to obtain an acceptable result in spite of the ill-posedness of the problem. The algorithm was verified by numerical simulating with real bathymetry of the Peru subduction zone and synthetic data.

Introduction

Recently, devastating tsunamis have acutely put forward the problem for their timely warning. In case of near field tsunamis that are generated by sources located at short distances of less than 300 km and that are the most devastating, the disaster management has a little time for decision-making. Mathematical modeling of tsunamis is to provide tsunami-resilient communities with reliable information of inundation heights and arrival times for the purpose to immediate protective measures. There are two important aspects of the assessment of tsunami risk in the coastal areas: the initial waves generated at the source area and provided further distractive strength of tsunami impact and the subsequent propagation. It is known that only after a certain time after the event, having analyzed the various seismic, tidal and other data, it appears possible to estimate basic characteristics of triggering mechanisms and simulating them in more realistic level. The sea level data inversion could be used to make appropriate conclusions about the static deformation in the source area, i.e. about the initial condition for real-time tsunami simulation.

1 Methods

The inverse problem in question is treated as an ill-posed problem of the hydrodynamic inversion with tsunami tide gauge records, so it imposes some restrictions on the use of mathematical techniques. Another words, any attempt to solve this inverse problem numerically must be followed by a regularization procedure. The proposed method is based on singular value decomposition (SVD) and r-solution technique. The unknown function of water surface displacement $\varphi(x,y)$ in the source area (rectangular $[l_1 \times l_2]$) can be represented as a series of spatial harmonics

$$\varphi(x,y) = \sum_{m=1}^{M}\sum_{n=1}^{N} c_{mn} \sin\frac{m\pi}{l_1}x \cdot \sin\frac{n\pi}{l_2}y$$

for $x \in [0,l_1]$, $y \in [0,l_2]$, with unknown coefficients $\vec{c} = \{c_{mn}\}$. In our case the inverse problem data are water level oscillations ($marigrams$) $\vec{\eta} = (\eta_{11},\eta_{12},\ldots,\eta_{1N_t},\eta_{21},\ldots,\eta_{2N_t},\eta_{P1},\ldots,\eta_{PN_t})^T$, $\eta_{pj} = \eta(x_p,y_p,t_j)$ at the set of points (x_p,y_p), $p = 1,\ldots,P$ and time moments t_j, $j = 1,\ldots,N_t$. Then $\vec{\eta}$ can be expressed as follows:

$$\vec{\eta} = \mathbf{A}\vec{c}, \qquad (1)$$

where to obtain the matrix $\mathbf{A}$, one has to solve numerically a series of direct problems with every spatial harmonics used as a source. Coefficients α_k of decomposition of $\vec{c}$ into right singular vectors $\vec{c} = \sum_{j=1}^{MN}\alpha_j\vec{v}_j$ are expressed as follows $\alpha_j = \frac{(\vec{\eta},\vec{u}_j)}{s_j}$, where $\vec{u}_j$ and $\vec{v}_j$ are left and right singular vectors of the matrix $\mathbf{A}$ and s_j are its singular values. Then the r-solution is $\vec{c}^{[r]} = \sum\limits_{j=1}^{r}\alpha_j\vec{v}_j$ and, finally, our solution $\varphi^{[r]}(x,y) = \sum\limits_{j=1}^{r}\alpha_j\sum\limits_{m=1}^{M}\sum\limits_{n=1}^{N}\beta_{mn}^{j}\varphi_{mn}(x,y)$

where $\vec{v}_j = (\beta^j_{11}, \beta^j_{12} \ldots, \beta^j_{MN})^T$. The obtained solution is stable for any fixed $\mathbf{r}$ with respect to perturbations of the right-hand side and operator itself (see [2]). The dependance of $\mathbf{r}$ and the condition number *cond* of matrix $\mathbf{A}$ can be expressed as $\mathbf{r} = \max\{k : s_k/s_1 \geq 1/cond\}$. The value of $\mathbf{r}$ is determined by the singular spectrum of the matrix $\mathbf{A}$ and noise level of the signals observed. A sharp decrease in the singular values, when their number increases, is typical for all calculations, due to the ill-posedness of the problem. In Figure 1.(a) typical graphs of singular values of matrix $\mathbf{A}$ on a common log scale with respect to their numbers are presented. The parameter $\mathbf{r}$ should be taken only from the first interval, where the common logarithms of singular values are slightly sloping. As one can notice, increasing of $\mathbf{r}$ leads to increasing of *cond* and, therefore, to the lower stability. On the other hand, $\mathbf{r}$ should be large enough to provide a suitable spatial approximation of $\varphi(x, y)$. In our numerical experiments the most reasonable choice is $\mathbf{r} \geq 70$. It is clear that properties of the matrix $\mathbf{A}$ and, consequently, the quality of the obtained solution are determined by the location and extent of the tsunamigenic area, configuration of the observation system and temporal extent of the signal. A series of calculations with

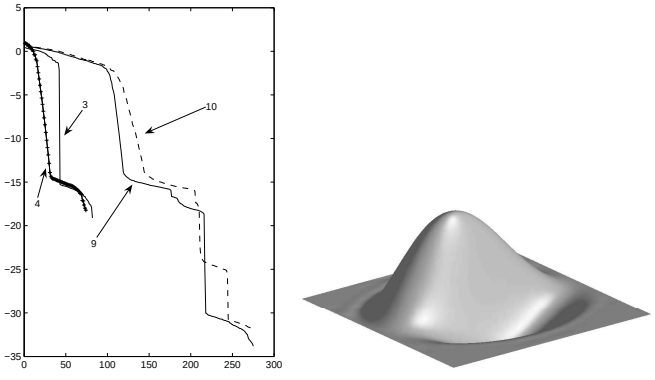

a) b)

Figure 1: a) The typical graphs of singular values of the matrix $\mathbf{A}$ on a common log scale with respect to their numbers. Markers $3, 4, 9, 10$ correspond to the number of *marigrams* used in certain variants of reconstruction; b) Model tsunami source: $\varphi_{\max} = 1.959m;\ \varphi_{\min} = -0.67m$.

synthetic data and real bathymetry of Peru subduction zone [3] was carried out by the proposed method to investigate the influence of certain characteristics of the observation system on the reconstructing process. First, the purpose was to obtain acceptable results of the recovering using the minimum number of *marigrams*. As a model of initial water displacement the function $\varphi(x, y)$ represented in Figure 1.(b) was used. Two variants of the reconstructed tsunami waveforms are presented in Figure 2.(a)-(b). The values in parentheses are extreme values of the reconstructed waveforms after smoothing, *err* is the relative error (in the L_2 -norm).

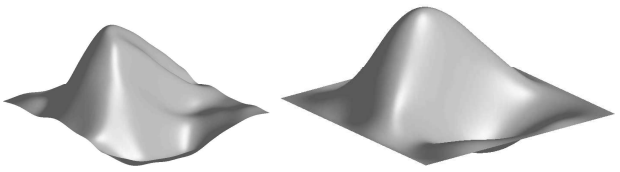

a) b)

Figure 2: a) Tsunami source reconstructed with three *marigrams*: $\varphi_{\max} = 1.213m;\ \varphi_{\min} = -0.738m; r = 41; err. = 0.717$; b) Tsunami source reconstructed with seven *marigrams*: $\varphi_{\max} = 1.835(1.5138)m;\ \varphi_{\min} = -0.7016(-0.5484)m; err = 0.262; r = 103; lg(cond) = 6$.

2 Acknowledgements

This work was supported by the Russian Foundation for Basic Research under grant No 12-07-00406, by the Siberian Branch of the RAS (Project 117) and the Far-Eastern Branch of the RAS (Project 37), by the Ministry of Education and Science of Russian Federation (No. 14.B37.21.0643).

References

[1] Voronina, T. A., Tcheverda,V. A., *Reconstruction of tsunami initial form via level oscillation* , in Bull.Nov.Comp.Center,Math.Model.in Geoph., **4** (1998), pp.127-136.

[2] V. A. Cheverda, V. I. Kostin, *r-pseudoinverse for compact operators in Hilbert space: existence and stability*, in J. Inverse and Ill-Posed Problems, **3** (1995), pp. 131-148.

[3] T.Voronina, *Reconstruction of Initial Tsunami Waveforms by a Trancated SVD Method* , in J. Inverse and Ill-posed Problems, **19** (2011), pp.615-629.

Prediction of Long-Crested Wind Waves from Inaccurate Input

A. P. Wijaya[1,2,*], **E. van Groesen**[1,2]
[1] LabMath-Indonesia, Bandung, Indonesia.
[2] Department of Applied Mathematics, University of Twente, Netherlands.
*a.parama@labmath-indonesia.org

Abstract

This research is motivated by the real problem to predict short-crested waves in the ocean from sequences of radar images, i.e. prediction of waves from inaccurate wave input. Avoiding the commonly used 3DFFT-method, improved radar images will be used as sequential input for the dynamic model. Errors in the radar images, mainly caused by the shadowing effect, lead to errors in the prediction. We propose methods to reconstruct the missing information and to average several inputs in order to improve the accuracy. A nonlinear dynamic model with exact dispersion will be used to calculate the waves at downstream positions. Instead of using real radar images, we use long-crested synthetic data to construct shadowed images and to qualify the performance of the reconstruction and averaging methods.

Introduction

With ever increasing human activities in the coastal zone, seas and oceans, research to predict properties of waves travelling towards a ship or offshore structure has been initiated in the past years, see for instance ([1], [2], [3]). Using radar observations and 3DFFT- analysis tools, statistical wave properties such as period, wave directionality and (with more problems) significant wave height are calculated. For various operational activities, the main challenge remains to use the inaccurate radar images to predict the incoming waves in real time, i.e. a deterministic, phase-resolved, prediction of the wave field.

Instead of trying to adjust the 3DFFT-methods, we proposed in [4] the use of a deterministic dynamic model and to apply an averaging method for the inaccurate images to improve the prediction. In this contribution we will report about the method for initial value problems. To that end, we will improve radar information to more accurate input data. Synthetic data are used as obtained by evolving a signal from measurements of experiments in a wave tank at Maritime Research Institute Netherlands (Marin).

1 Inaccurate Input and Reconstruction

Starting with elevation profiles from the synthetic data, the shadowing effect is taken into account to produce inaccurate input that resembles somewhat real radar images (although a physical attenuation by distance from the radar is absent). The shadowing effect results when waves are hidden by higher waves closer to the radar that prevent them to be detectable by the radar. As an illustration, the shadowed areas are indicated by the characteristic function (zero elevation when shadowed) in Figure 1 for a typical irregular wave profile with significant wave height of 3m as observed by an ideal radar of height 30m at position $x = 2500$.

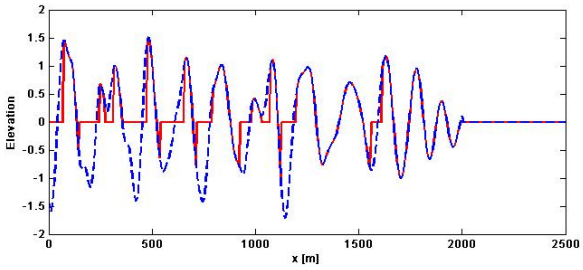

Figure 1: The full profile (dashed blue) and the shadow (solid red line) for the situation that the radar with height 30 m is located at $x = 2500$ m.

Analysis of radar images is a difficult subject. Young et al [5] proposed a 3D-FFT method to get the directional wave component. This method is still the common tool; see for instance Naaijen and Blondel [6] who applied the method to filter the radar images and force the frequency components to satisfy the exact dispersion relation.

We propose another approach to avoid the cumbersome justification of such methods and the requirement to have temporal information over a substantial time interval. The new approach consists of two main ingredients. One is to reconstruct as good as possible the original profile from the information given by the shadowed wave by 'filling the holes'. Since a reconstruction of irregular waves may still have substantial errors, the second ingredient is to reduce the input

errors, for which we apply an averaging method that is discussed in the next section.

2 Averaging Methods

Consider a spatial domain $x \in [0, A]$ in which two or more reconstructed profiles $f_0(x)$ and $f_1(x)$ of the shadowed waves $f_0^{sha}(x)$ and $f_1^{sha}(x)$ at time t_0 and t_1 respectively are available. Let B, with $B > A$, be the position of the radar where we want to calculate the elevation resulting from f_0 or f_1. Since the profiles will contain (substantial) errors, to obtain a reduced error at B, we proposed a new averaging method in [4]. A somewhat improved averaging process can be described, for 2 profiles for simplicity, as follows. Starting at time t_0, the profile f_0 is evolved until time t_1. At that time, we calculate the averaged profile as follows. We average the two profiles, i.e. the evolution of f_0 (denoted as $\mathcal{E}(f_0)$) and the profile f_1, with the same factor only at the shadowed areas of f_1^{sha} and we simply keep the full profile of f_1 at the visible areas. Therefore, the averaged profile can be written as

$$av(x) = \left(\frac{\mathcal{E}(f_0)(x) + f_1(x)}{2}\right)(1 - \chi(x)) + f_1(x)\chi(x) \tag{1}$$

where χ is the characteristic function which describes the visible areas of the shadowed profile f_1^{sha}. Using such averaged profiles as sequential updates, we will show by comparison with the exact synthetic data that the wave prediction at the radar position B is improved considerably.

3 Governing Equation

For uni-directional wave propagation to the right (positive x-axis direction), we use the so-called second-order AB equation [7]. This equation with Hamiltonian structure, has exact dispersion properties in first and second order, and is given by

$$\begin{aligned}\partial_t \eta &= -\mathcal{C}\partial_x \Big[\eta + \frac{g}{4}(\mathcal{C}^{-1}\eta)^2 + \frac{g}{2}\mathcal{C}^{-1}(\eta\mathcal{C}^{-1}\eta) \\ &\quad -\frac{1}{4g}(\mathcal{C}\partial_x\eta)^2 + \frac{1}{2g}\mathcal{C}\partial_x(\eta\mathcal{C}\partial_x\eta)\Big] \end{aligned} \tag{2}$$

where $\mathcal{C}$ is the phase velocity (pseudo-differential) operator related to the exact dispersion relation. A pseudo-spectral implementation is used for the wave advancing.

Acknowledgment

The motivation for this study was stimulated by some of the challenge in the IOP (Industrial Research Project) entitled "Prediction of wave induces motions and forces in ship, offshore and dredging operation", funded by Agency NL, a department of the Dutch Ministry of Economic Affairs, Agriculture and Innovation and co-funded by Delft University of Technology, University of Twente, Maritime Research Institute Netherlands, OceanWaves GMBH, Allseas, Heerema Marine Contractors and IHC Merwede.

References

[1] G.F. Clauss, D. Testa, S. Kosleck, and R. Stuck, *Forecast of Critical Wave Groups from Surface Elevation Snapshots*, in Proceedings of OMAE 2007, San Diego, USA, 10-15 June 2007.

[2] G.F. Clauss, D. Testa, S. Kosleck, and K. Hessner, *Forecast of Critical Situations in Short-Crested Seas*, in Proceedings of OMAE 2008, Estoril, Portugal, 15-20 June 2008.

[3] S. Hassanaliaragh, *Radar Data Assimilation and Forecast of Evolving Nonlinear Wave Fields*, PhD Thesis, Univeristy of Michigan, 2009.

[4] A.P. Wijaya and E. van Groesen, *Simulation of Waves with Highly Inaccurate Input*, 2nd ICPCO, Bandung, Indonesia, 12-13 November 2012.

[5] I.R. Young, W. Rosenthal and F. Ziemer, *A Three-dimensional Analysis of Marine Radar Images for The Determination of Ocean Waves Directionality and Surface Currents*, Journal of Geophysical Research, **90** (1985), pp. 1049–1059.

[6] P. Naaijen and E. Blondel, *Reconstruction and Prediction of Short-Crested Seas Based on The Application of A 3D-FFT on Synthetic Waves Part1: Reconstruction*, in Proceedings of the ASME 2012, Rio de Janeiro, Brazil, 1-6 July 2012.

[7] E. van Groesen and Andonowati, *Variational Derivation of KdV-type Models for Surface Water Waves*, Physics Letters A, **366** (2007),pp. 195–201.

Eddy Current Tomography of Deposits in Steam Generators

M. El-Guedri[1], H. Haddar[2], Z. Jiang[2,*], A. Lechleiter[2,3]
[1] Departement STEP, EDF R&D, Chatou, France.
[2] Team DÉFI, INRIA Saclay – CMAP Ecole Polytechnique, Palaiseau, France.
[3] Center for Industrial Mathematics, Universitaet Bremen, Bremen, German.
*Email: zixian.jiang@polytechnique.edu

Abstract

Eddy current testing (ECT) is widely practiced in the inspection of steam generators (SG) in nuclear power plants. In this talk, we consider the deposit shape reconstruction problem using ECT signals. For an axisymmetric case, we build a PDE-based direct model with appropriate Dirichlet-to-Neumann boundary operators in order to truncate the computational domain. Then we propose and numerically validate a regularized shape optimization method for the deposit reconstruction.

1 Industrial background

Conductive magnetic deposits on the shell side of SG tubes can affect the power production and the structure safety. In ECT, we introduce in the tube a probe composed by two coils, each one connected to a current generator and a voltmeter. The generator coil creates an electromagnetic field which in turn induces a current flow in the conductive material nearby. The deposits distort the flow and change the current in the receiver coil, which is measured as ECT signals ([1]), from which we will estimate the shape of deposits with known physical parameters.

2 Axisymmetric eddy current model

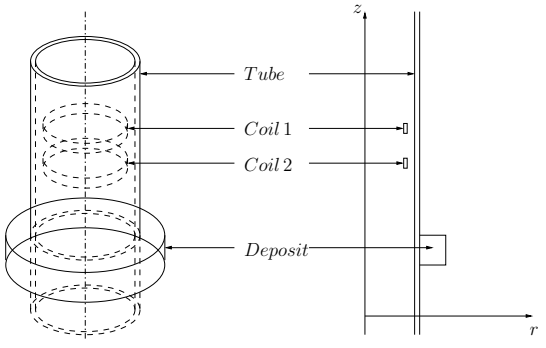

Figure 1: : 3-D and 2-D geometrical representations

Maxwell's equations with the Eddy current hypothesis $\epsilon \ll \sigma/\omega$ yield the second order equation for the azimuthal part of the electric field u in a cylindric coordinate system (see Figure 1):

$$\begin{cases} -\operatorname{div}\left(\dfrac{1}{\mu r}\nabla(ru)\right) - \mathrm{i}\omega\sigma u = \mathrm{i}\omega J \quad \text{in } \mathbb{R}^2_+, \\ u|_{r=0} = 0, \end{cases} \tag{1}$$

with the condition that u is bounded at infinity. In order to bound the compuational domain, we introduce first a domain truncation in the r direction by imposing a Neumann condition at $r = r_0$. Then, for the z direction, we explicitly express the D-t-N operators on $\Gamma_\pm$ (see Figure 2), in the form

$$\mathcal{T}_\pm = \sum_{j=1}^{m} \sqrt{\nu_{0j}} Q_{0j} + \sum_{k>n} \sqrt{\nu_k} Q_k. \tag{2}$$

$\{\nu_{0j}, \nu_k\}, \{Q_{0j}, Q_k\}$ are eigenvalues and eigenprojections of a perturbed self-adjoint boundary operator from the problem (1) (see [2]). The variational prob-

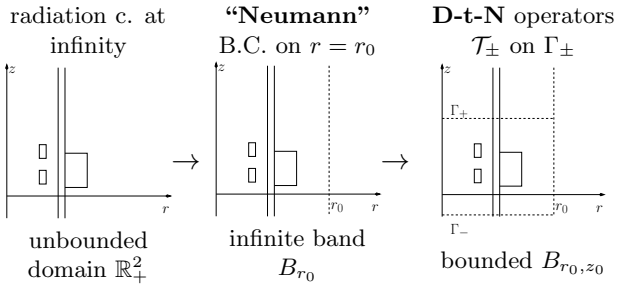

Figure 2: : Domain truncation

lem for the truncated domain can be written as

$$\int_{B_{r_0,z_0}} \left(\frac{1}{\mu r}\nabla(ru)\cdot\nabla(r\bar{v}) - \mathrm{i}\omega\sigma u\bar{v}r\right) \mathrm{d}r\,\mathrm{d}z + \int_{\Gamma_\pm} \frac{1}{\mu}\mathcal{T}_\pm(u|_{\Gamma_\pm})\bar{v}r\,\mathrm{d}s = \int_{B_{r_0,z_0}} \mathrm{i}\omega J\bar{v}r\,\mathrm{d}r\,\mathrm{d}z \tag{3}$$

for all $v \in H := \{v : \sqrt{r}v, \frac{1}{\sqrt{r}}\partial_r(rv), \sqrt{r}\partial_z v \in L^2(B_{r_0,z_0})\}$. This problem is well posed and we shall discuss in the talk some issues related to approximations using standard Lagrange finite elements as well as the efficiency of the domain truncation startegy in increasing the speed of the numerical resolution. This is an important issue for our inversion algorithm.

3 Inverse problem

From [3, (10a)], a deposit with permeability μ, conductivity σ and the shape Ω_D leads to a change of impedance measurements for the coil k in the electromagnetic field induced by the coil l:

$$\triangle Z_{kl} = \triangle Z_l(u_k) = -\frac{2\pi}{I^2}\int_{\Omega_D}\Big((\sigma-\sigma^0)u_k u_l^0 r + \frac{1}{\mathrm{i}\omega}\frac{\mu-\mu^0}{\mu\mu^0 r}\nabla(ru_k)\cdot\nabla(ru_l^0)\Big)\,\mathrm{d}r\,\mathrm{d}z, \tag{4}$$

where u_l^0 is the electric field induced by the coil l in the deposit free case with μ^0, σ^0 for vacuum. The ECT signal Z on a probe position ζ is a linear combination of $\triangle Z_{kl}(k,l=1,2)$, depending on the measurement mode. We set $Z = Z(\Omega_D;\zeta)$. To approximate the real deposit shape Ω_D^* using ECT signals on $\zeta \in [z_{\min}, z_{\max}]$ is to minimize the cost functional

$$\mathcal{J}(\Omega_D) = \int_{z_{\min}}^{z_{\max}} |Z(\Omega_D;\zeta) - Z(\Omega_D^*;\zeta)|^2\,\mathrm{d}\zeta.$$

We shall use a steepest descent method based on evaluation of the derivative of the cost functional using the adjoint state technique. More precisely, if the original deposit domain Ω_D^0 is deformed by a shape perturbation $\boldsymbol{\theta}$: $\Omega_D = (\mathrm{Id}+\boldsymbol{\theta})\Omega_D^0$, then we prove (see [4]) that $\mathcal{J}(\Omega_D)$ is differentiable at $\boldsymbol{\theta}=0$ and the derivative, denoted by $\mathcal{J}'(\Omega_D^0)(\boldsymbol{\theta})$, writes

$$\mathcal{J}'(\Omega_D^0)(\boldsymbol{\theta}) = \int_{\partial\Omega_D^0} g(u,p)(\boldsymbol{\theta}\cdot\boldsymbol{n})\,\mathrm{d}s,$$

where g is a functional of the solution u to the direct problem (3) and p is the adjoint state. Then $\boldsymbol{\theta}$ such that $\boldsymbol{\theta}|_{\partial\Omega_D^0} = g(u,p)\boldsymbol{n}$ is a descent direction. For the numerical algoritm we regularize $\boldsymbol{\theta}$ using H^1 boundary regularization by solving for $\boldsymbol{\lambda}$

$$\boldsymbol{\lambda} - \alpha\triangle_{\partial\Omega_D^0}\boldsymbol{\lambda} = \boldsymbol{\theta} \quad \text{on } \partial\Omega_D^0, \tag{5}$$

where $\triangle_{\partial\Omega_D^0}$ is the Laplace-Beltrami operator, $\alpha>0$ is a regularization parameter. $\boldsymbol{\lambda}$ is also a descent direction and is more regular than $\boldsymbol{\theta}$.

4 Numerical results

We consider deposits with low conductivity ($\sigma = 1\times10^4 S/m$) and constant permeability ($\mu_r = 1$). In Figure 3 the real deposit shape is a rectangle. The inversion algorithm without boundary regularization is blocked due to singularities (Figure 3b). The regularized algorithm ends after 60 steps with a good estimate (Figure 3c). In Figure 4 we show the reconstruction of a semi-disc issued from different initial shapes (Figures 4a and 4c). The corresponding results shown in Figure 4b (52 steps) and in Figure 4d (39 steps) are satisfying.

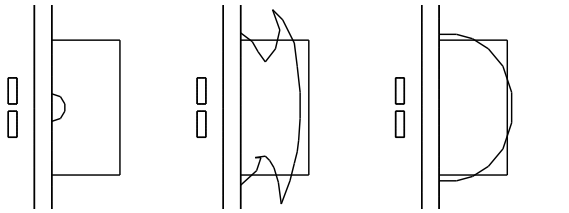

(a) initialization with small semi-disc (b) without regularization: algorithm diverges (c) with regularization

Figure 3: : Reconstruct a rectangle

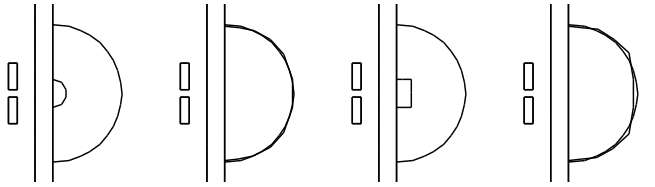

(a) initial. (b) reconstr. (c) initial. (d) reconstr.

Figure 4: : Reconstruction of a semi-disc

References

[1] A. Trillon, A. Girard, J. Idier, Y. Goussard, F. Sirois, S. Dubost, N. Paul, *Eddy Current Tomography Based on a Finite Difference Forward Model with Additive Regularization*, AIP Conference Proceedings, **1211** (2010), pp. 782–789.

[2] T. Kato, *Perturbation theory for linear operators*, Springer-Verlag Berlin, 1995.

[3] B. A. Auld, J. C. Moulder, *Review of Advances in Quantitative Eddy Current Nondestructive Evaluation*, Journal of Nondestructive Evaluation, **18, Issue 1**, (1999), pp. 3–36.

[4] M. El-Guedri, H. Haddar, Z. Jiang, A. Lechleiter, *Identification of magnetit deposits on steam generator tubes*, in preparation.

Inverse scattering problem in perturbed half-plane

L. Chorfi[1,*], **B. Berhail**[2]
[1,2] LMA, Badji Mokhtar University, Annaba, Algeria.
*Email: l_chorfi@hotmail.com

Abstract

We consider in this work an inverse problem in scattering theory. We construct an arc γ of the boundary from the far field pattern u_∞ of the scattered wave at fixed energy. This leads to the direct scattering problem for the Helmholtz equation in a perturbed half-plane with Dirichlet condition on the boundary. We first show that the direct problem is well posed and characterize the forward operator $\mathcal{F} : \gamma \to u_\infty$ which act between two Hilbert spaces. The aim of this article is to solve the ill-posed non linear equation $\mathcal{F}(\gamma) = u_\infty^\delta$ (δ is a noise in data), . For this we use Newton method developed by Kress [3] with a strategy of regularization. We also show some numerical results to illustrate the method.

Introduction

Regularized Newton iteration methods have been analyzed and successfully applied for the approximate solution of inverse obstacle scattering problems for time-harmonic waves in the case of smooth closed boundary curves in R^2 [3], in the case of smooth open arcs (see [5]) and recently for locally perturbed half- plane in [4]. In the previous paper [4] the authors consider a particular perturbation such that the problem is reformulated as an exterior obstacle problem for a symmetric domain. Our aim is to generalize this article for perturbation where it is not possible to use the symmetry.

1 Direct scattering problem

A perturbed half-plane is the open set $\Omega = \{x = (x_1, x_2) \in \mathrm{R}^2; x_2 > f(x_1)\}$ where f is C^2 function such that $f(t) = 0$ for $|t| > a > 0$. The boundary split into $\Gamma = \Gamma_- \cup \gamma \cup \Gamma_+$ with $\Gamma_\pm = \{(x_1, 0); (\pm)x_1 > a\}$ and $\gamma = \{(x_1, f(x_1)); -a < x_1 < a\}$. We consider the following direct scattering problem: given an incident field $u^i = e^{ikd\cdot x}$, find the total field $u = u^i + u^r + u^s$ as a solution of the Helmholtz equation:

$$\begin{array}{cc} \Delta u + k^2 u = 0 & \text{in } \Omega \\ u = 0 & \text{on } \Gamma \\ \lim\limits_{r\to\infty} \sqrt{r}\left(\dfrac{\partial u^s}{\partial r} - iku^s\right) = 0, \quad r = |x| & \end{array} \tag{1}$$

To construct the solution we use the double layer potential

$$u^s(x) = \int_\gamma \frac{\partial G(x,y)}{\partial n(y)} \varphi(y) ds(y), \quad x \in \Omega \tag{2}$$

where the density φ satisfy a boundary integral equation on γ. We prove that there exists a unique solution $u^s \in H^1_{loc}(\Omega)$ which depend continuously on $g = u^i + u^r$, $u^r = -e^{ikd'\cdot x}$, $d' = (d_1, -d_2)$. The Green function is $G(x, y) = \phi(x, y) - \phi(x, y')$ with $\phi(x, y) = \frac{i}{4} H_0^{(1)}(k|x - y|)$. The scattered field u^s has the asymptotic behavior

$$u^s(x) = \frac{e^{ikr}}{\sqrt{r}} \left(u_\infty(\hat{x}) + O(\frac{1}{r}) \right), \quad r = |x| \to \infty \tag{3}$$

uniformly in all directions $\hat{x} = \frac{x}{r} = (\cos\phi, \sin\phi)$ with the far field pattern defined on the interval $[0, \pi]$ by

$$u_\infty(\phi) = c \int_\gamma \frac{\partial G_\infty(\phi, y)}{\partial n(y)} \varphi(y) ds(y), \ (c = \frac{e^{i\pi/4}}{\sqrt{8\pi k}}) \tag{4}$$

with $G_\infty(\phi, y) = e^{ik\hat{x}\cdot y} - e^{ik\hat{x}\cdot y'}$ and φ is the density, solution of a Fredholm integral equation of type $\varphi + K\varphi = -2g$ on γ.

2 Inverse problem

The inverse scattering problem we consider is: given the far-field pattern u_∞ for one incident wave u^i determine the arc γ. A sound-soft crack in two dimensions is uniquely determined from the knowledge of the far field pattern for all $(\theta, \phi) \in [0, 2\pi]$ with fixed wave number k, see [1]. Using the point source technique we prove the same uniqueness result for γ. For the construction, we fix an incident wave and formulate the inverse problem into a nonlinear and ill posed integral equation $\mathcal{F}(f) = u_\infty^\delta$ where $\mathcal{F} : D(\mathcal{F}) \to L^2(0, \pi)$, $f \in D(\mathcal{F}) = H_0^1(-a, a) \cap H^2(-a, a)$ is the parametrization of γ and u_∞^δ is the measured far-field data, which is solved by a Newton method. This approach was developed by Kress ([4], [3]) for an obstacle inverse problem.

2.1 Algorithm

We suggest an iterative method $f_{n+1} = f_n + h_n$ where h solves the linearized equation

$$\mathcal{F}'(f_n)h_n = u_\infty^\delta - \mathcal{F}(f_n) \quad (\Leftrightarrow Ax = b) \qquad (5)$$

The computation of the the derivative $\mathcal{F}'(f;h)$ is not obvious as F is a composition of several operators. $\mathcal{F}(f)$ is a compact, then equation (5) is ill posed. Therefore we look for the least square solution by solving the normal equation $A^*Ax = A^*b$. This is done with conjugate gradient method as a regularizer (see [2]). In practice we chose a parametrization of f with basic functions as polynomials, trigonometric polynomials or Gaussian's. The iteration is stopped according to the discrepancy principle: at the first $n = n(\delta)$ for which the residue $\|\mathcal{F}(f_n) - u_\infty^\delta\| \leq \delta$, δ is the noise of the data.

2.2 Numerical examples

For the first example, we consider the parabolic arc given by $f(t) = 1 - t^2$, $t \in [-1, 1]$. In the direct problem we solve integral equation by Nyström method. We simulate the forward problem with the following parameters: $k = 1$, angle of incidence $\theta = \frac{\pi}{6}$, $n = 32$ points for $t \in [-1, 1]$, $p = 18$ points for $\phi \in [0, \pi]$. In the inversion we use $M = 4$ basic functions in the parametrization. For initial guess $f_0 = 0.1f$ and after 4 iterations we obtain the profile in figure 1.
In the second example we consider the arc with the equation $f(t) = \sin(\pi t) + 0.5\cos(0.5 * \pi t)$, $t \in [-1, 1]$. For the reconstruction we use the basic functions

$$\begin{aligned} q_1(t) &= 1 - 2\tfrac{t}{\pi} + \tfrac{t^2}{\pi^2} \\ q_2(t) &= 1 - 2\tfrac{\pi - t}{\pi} + \tfrac{(\pi - t)^2}{\pi^2} \\ q_i(t) &= \cos((i-2)t) * \sin(t), \quad i = 3, 4 \end{aligned} \qquad (6)$$

After 4 iterations we obtain the profile in the figure 2. This algorithm suffer from two defaults. Once, f_0 is chosen proportional to f, indeed if we set $f_0 = 0$ the algorithm diverges. Two, we remark that the reconstruction is good for grazing incident wave ($\theta_{inc} \leq \frac{\pi}{6}$), but is bad for normal incidence.

Remark: In the paper [4] we avoid the case when the perturbation is tangential to the line at the end points $(\pm a, 0)$, since the symmetric domain becames singular (with cuspidal point). This difficulty is due to the method. But in our case if f is C^2 the solution of (1) has no singularity near the corners as in the tip of a crack ([5]).

2.3 Illustrations and References

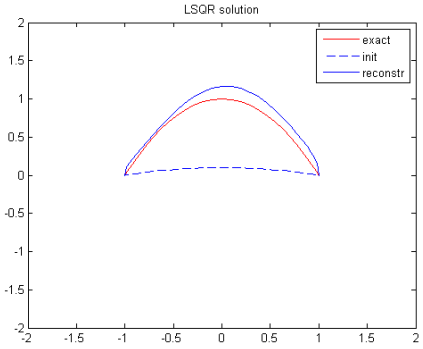

Figure 1: reconstruction of γ with $\theta_i = \frac{\pi}{6}$, after 4 iterations

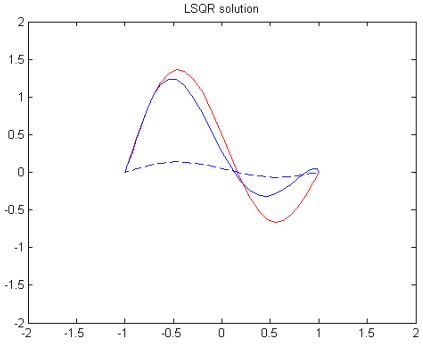

Figure 2: reconstruction of γ after 4 iterations with $\theta_i = \frac{\pi}{6}$

References

[1] F. Cakoni and D. Colton, *Qualitative Methods in Inverse Scattering Theory* , IMM, Springer-Verlag , 2006.

[2] M. Hanke, *Regularizing properties of a truncated Newton CG algorithm for nonlinear inverse problems*, Numer. Funct. Anal. Optim. 18 (1997), p.p. 971-93

[3] R. Kress, *Newtons method for inverse obstacle scattering meets the method of least squares*, Inverse Problems , **19** (2003), pp. 19–104.

[4] R. Kress, T. Tran, *Inverse scattering for a locally perturbed half-plane*, Inverse Problems **16** (2000) p.p. 1541-1559.

[5] L. Mönch L, *On the inverse acoustic scattering problem from an open arc: the sound-hard case*, Inverse Problems **13** (1997), p.p 1379-92

Numerical method for an inverse obstacle scattering problem based on the logarithmic differential of indicator function in the enclosure method

Takashi Ohe[1,*], **Masaru Ikehata**[2]
[1] Department of Applied Mathematics, Okayama University of Science, Okayama, JAPAN
[2] Department of Mathematics, Gunma University, Kiryu, JAPAN.
*Email: ohe@xmath.ous.ac.jp

Abstract

We consider an inverse scattering problem to extract information about unknown obstacles from scattering wave field. For this problem, we apply the enclosure method proposed by Ikehata, specifically, reconstruction formula for vertexes of polygonal obstacle using the logarithmic differential of the indicator function. Since the formula is based on the asymptotic behaviour of the indicator function, it is difficult to implement this formula directly as a numerical procedure. To avoid this difficulty, we propose a method to approximate the formula without computing the asymptotic behaviour directly. Our numerical method is examined by some numerical experiments.

1 Introduction

An inverse scattering problem is a mathematical model of many problems in science and engineering, e.g. nondestructive evaluation in mechanical engineering, and acoustic diagnostics in medical science[1]. In this paper, we consider a problem to extract information of unknown obstacles from observations of scattering wave field governed by the Helmholtz equation.

Let $D \subset \mathbb{R}^2$ be an unknown polygonal domain, and $u(x) = u_{\rm i}(x) + u_{\rm s}(x)$ denotes the total wave field that satisfies

$$\Delta u + k^2 u = 0 \text{ in } \mathbb{R}^2 \backslash \overline{D}, \tag{1}$$

$$\frac{\partial u}{\partial \nu} = 0 \text{ on } \partial D, \tag{2}$$

$$\lim_{r\to\infty} \sqrt{r}\left(\frac{\partial u_{\rm s}}{\partial r} - iku_{\rm s}\right) = 0, \tag{3}$$

where $u_{\rm i}(x) = e^{ikx\cdot d}$ denotes the incident plain wave, $k > 0$ the wave number, $d \in S^1$ the direction of the incident wave, ν the outward unit normal relative to $\mathbb{R}^2\backslash\overline{D}$, and $r = |x|$. The boundary condition (2) describes the sound-hard scattering on the boundary of D, and the condition (3) shows that the scattering wave $u_{\rm s}$ satisfies the Sommerfeld radiation condition.

Let B_R be an open disc with radius R centered at the origin satisfying $\overline{D} \subset B_R$, and we assume that the total field u and its normal derivative $\frac{\partial u}{\partial \nu}$ are observed on ∂B_R. Then, our problem becomes to extract information about the unknown domain D from observations u and $\frac{\partial u}{\partial \nu}$ on ∂B_R.

For $\omega \in S^1$, let us define the *support function* of D by $h_D(\omega) = \sup_{x\in D} x\cdot\omega$. We say that ω is regular with respect to D if the set $\partial D \cap \{x \in \mathbb{R}^2 \,|\, x\cdot\omega = h_D(\omega)\}$ consists of only one point.

For $\tau > 0$, let

$$v_\tau(x;\omega,k) = \exp\left(x\cdot\left(\tau\omega + i\sqrt{\tau^2+k^2}\omega^\perp\right)\right), \tag{4}$$

where $\omega^\perp \in S^1$ is perpendicular to ω, and define the *indicator function* by

$$I(\tau;\omega,d,k) = \int_{\partial B_R}\left(\frac{\partial u}{\partial \nu}v_\tau - \frac{\partial v_\tau}{\partial \nu}u\right)dS. \tag{5}$$

Using the indicator function $I(\tau;\omega,d,k)$, Ikehata established the following formula that extracts information about the locations of vertexes of the convex hull of the polygon D [2]:

Theorem 1 *Let ω be regular with respect to D. Let $x_0 \in \partial D$ be the point with $x_0\cdot\omega = h_D(\omega)$. Then, there exists $\tau_0 > 0$ such that $|I(\tau;\omega,d,k)| > 0$ for all $\tau \geq \tau_0$, and the logarithmic differential of the indicator function $I(\tau;\omega,d,k)$ satisfies*

$$\lim_{\tau\to\infty}\frac{I'(\tau;\omega,d,k)}{I(\tau;\omega,d,k)} = h_D(\omega) + ix_0\cdot\omega^\perp. \tag{6}$$

In this paper, we propose a numerical method to extract information about unknown obstacles based on the reconstruction formula (6). We also discuss the effectiveness of the method by some numerical experiments.

2 Numerical Method

Since the reconstruction formula (6) is based on the asymptotic behaviour of the indicator function

as $\tau \to \infty$, it is difficult to implement this formula directly as a numerical procedure . Therefore, we discuss a method to approximate the formula (6) with some numerical experiments.

Figure 1 shows a typical behaviour of numerical estimates of the logarithmic differential of $I(\tau;\omega,d,k)$. The logarithmic differential of $I(\tau;\omega,d,k)$ behaves as a constant in a finite interval (in Figure 1, $10 \leq \tau \leq 25$), and varies violently for large τ caused by the error in the numerical evaluation of the indicator function. From this numerical result, we propose the following procedure to approximate the formula (6):

Step 1. Choose $\widetilde{\tau}$ in the interval in which the logarithmic differential of the indicator function behaves as a constant.

Step 2. Using this $\widetilde{\tau}$, approximate the formula (6) by

$$h_D(\omega) + ix_0 \cdot \omega^{\perp} \simeq \frac{I'(\widetilde{\tau};\omega,d,k)}{I(\widetilde{\tau};\omega,d,k)}. \qquad (7)$$

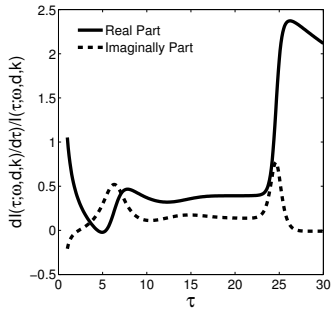

Figure 1: A typical behaviour of numerical estimates of $I'(\widetilde{\tau};\omega,d,k)/I(\widetilde{\tau};\omega,d,k)$.

3 Numerical Experiments

We present numerical experiments for our proposed method. We consider the case where a kite-shape obstacle is placed in B_1 as shown in Figure 2, and we set $k = 5.0$ and $d = (\cos\pi/5, \sin\pi/5)$. Observations of u and $\frac{\partial u}{\partial \nu}$ are given at 64 points on ∂B_1. To consider the effect of noises in observations, we use observations without noise (case (a)), and with 0.5% noise (case (b)). For the approximation formula (7), we choose $\widetilde{\tau} = 22.0$ for case (a), and $\widetilde{\tau} = 7.0$ for case (b). The points $h_D(\omega) + ix_0 \cdot \omega^{\perp}$ are estimated for 32 directions of ω.

Small circles in Figure 2 show the identified results of the points $h_D(\omega) + ix_0 \cdot \omega^{\perp}$ for various ω. From Figure 2, one can see that the vertexes of unknown obstacle are identified well for case (a), and the identification result becomes rather bad for case (b). However, we may consider that the shape of unknown obstacle is reconstructed successfully in both cases.

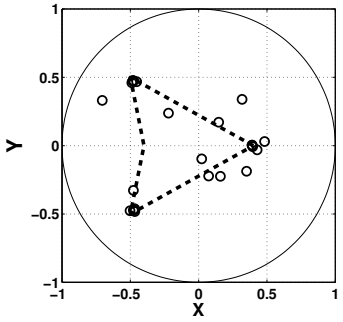

case (a): without noise

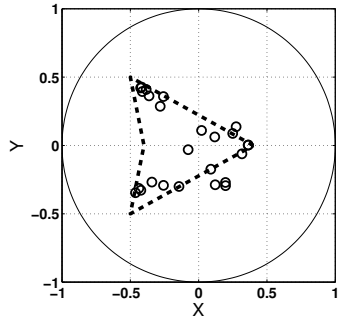

case (b): with 0.5% noise

Figure 2: Identification results of vertexes of unknown obstacle.

Acknowledgement

TO was partially supported by Grand-in-Aid for Scientific Research (C) (no. 23540173), and MI was partially supported by Grand-in-Aid for Scientific Research (C) (no. 21540162) of Japan Society for the Promotion of Science.

References

[1] D. Colton and R. Kress, *Inverse Acoustic and Electromagnetic Scattering Theory*, 3rd edition, Springer, New York, 2012,

[2] M. Ikehata, *Inverse obstacle scattering problems with a single incident wave and the logarithmic differential of the indicator function in the enclosure method*, Inverse Problems, **27** (2011), 085006 (23pp).

Inverse Source Problem for a Space Fractional Advection-Dispersion Equation

A. Aldoghaither[1,*], **T.M. Laleg-Kirati**[1,**]
[1] Applied Mathematics and Computational Science, KAUST, Thuwal, KSA
*Email: abeer.aldoghaither@kaust.edu.sa
**Email: taousmeriem.laleg@kaust.edu.sa

Abstract

This paper deals with an inverse source problem for a fractional advection-dispersion equation on a finite domain where the unknown source term is to be determined from a final observation. The problem is first discretized using finite difference scheme based on the shifted Grunwald formula. Then, the Tikhonov regularization is used to determine the source term in presence of noise.

Introduction

Fractional derivatives have proven their efficiency and accuracy in modeling and solving equations in many scientific fields [1], such as physics, chemistry, biology, mechanical engineering, signal processing and systems identification, control theory and finance,etc... [1],[3]. Thanks to their memory effect and non-locality properties [1],[4], fractional derivatives are very useful in describing anomalous diffusion, such as contaminants transport in the soil, oil flow in porous media, groundwater flow and turbulence [5],[6]. Recently, many studies have been interested in modeling with fractional partial differential equations and their analysis. However, few studies considered the inverse problem for such equations [3],[7]. In this paper, we are interested in an inverse problem for the fractional advection-dispersion equation that can be used for example for modeling groundwater transport in heterogeneous porous media [6].

Recently, the inverse problem of the space fractional advection-dispersion equation have been considered by Chi *et al* [7] where they have solved the inverse problem numerically in presence and in absence of a noise using an optimal perturbation regularization algorithm. However, the stability of the proposed method depends on the initial guess and the choice of some base functions. Moreover, Zhang and Li *et al* [8] have solved this inverse problem using the same optimal perturbation regularization algorithm when the fractional order, the diffusion coefficient and the average velocity are unknown . In this paper, we propose to analyze this inverse problem. We propose first to discretize the problem. Then, because of the ill-posedness of the problem, a regularization strategy is needed. For this purpose, we use a Tikhonov regularization to recover the source term from a final observation, when the velocity and the dispersion coefficient are known.

1 Methods

We consider a space fractional advection-dispersion equation with the following initial and Dirichlet boundary conditions:

$$\begin{cases} \frac{\partial u(x,t)}{\partial t} = -v\frac{\partial u(x,t)}{\partial x} + d\frac{\partial^\alpha u(x,t)}{\partial x^\alpha} + f(x), \\ u(x,0) = u_0(x), \\ u(0,t) = h_1(t), \\ u(L,t) = h_2(t), \end{cases} \tag{1}$$

where $t \geq 0, 0 \leq x \leq L$. v is the velocity, u is the concentration, d is the dispersion coefficient, and α is the derivative order with $1 < \alpha \leq 2$. Moreover, the fractional derivative is a left-sided Riemann-Liouville fractional derivative over the x domain.

For the direct problem, we will use a finite difference scheme based on the shifted Grunwald formula [2], [5]. Then, the discretization form of equation (1) is given by:

$$\begin{aligned} &(1 - d\Delta t\delta_{\alpha,x})u_i^{j+1} = -\tfrac{\Delta t}{\Delta x}v(u_{i+1}^j - u_i^j) + f_i\Delta t, \\ &i = 1, \ldots, N-1 \text{ and } j = 1, 2, \ldots \end{aligned} \tag{2}$$

where

$$\delta_{\alpha,x}u_i^j = \frac{1}{(\Delta x)^\alpha}\sum_{k=0}^{i+1} g_k u_{i-k+1}^j,$$

and

$$g_k = \frac{\Gamma(k-\alpha)}{\Gamma(-\alpha)\Gamma(k+1)},$$

with $t_j = j\Delta t$, $x_i = i\Delta x$, $u_i^j = u(x_i, t_j)$, $f_i = f(x_i)$, $u_0^j = h_1(t_j)$, and $u_N^j = h_2(t_j)$.

Thus, the matrix form of the implicit finite difference scheme is given by:

$$(I - M)U^{j+1} = CU^j + F, \tag{3}$$

for $n = 1, 2, ...N + 1$ and $m = 1, 2, ..., N + 1$,

$$M_{m\times n} = \frac{d(\Delta t)}{(\Delta x)^\alpha} \begin{cases} 0 & m = 1, N+1 \\ g_{m-n+1} & n \le m-1, 2 \le m \le N \\ g_1 & n = m, 2 \le m \le N \\ g_0 & n = m+1, 2 \le m \le N \end{cases}, \tag{4}$$

$$C_{m\times n} = \frac{-vd(\Delta t)}{(\Delta x)^\alpha} \begin{cases} -1 & n = m, \quad n, m \ne 1, N+1 \\ 1 & m = n-1, \quad n \ne N+1 \\ 0 & o.w \end{cases}, \tag{5}$$

$$F = \Delta t \times [f_0, f_1, ..., f_{N-1}, f_N]^T,$$
$$U^{j+1} = [u_0^{j+1}, u_1^{j+1}, ..., u_N^{j+1}]^T.$$

If we assume that the final observation is known then, we can rewrite (3) in the following form: $Y = KF$, where $K_{(N+1)\times(N+1)} = A(I - A)^{-1}(I - A^{N+1})$ and $Y = U^{N+1} - (AC)^{N+1}U^0$ with $A = (I - M)^{-1}$, and U^{N+1} the final observation.
In order to estimate the unknown source, we propose to minimize the following cost function with a Tikhonov regularization:

$$J = \| d - KF \|_2^2 + \lambda \| F \|_2^2, \tag{6}$$

where d denotes the observation of Y. The solution of $argmin_F J$ is given by: $\hat{F} = (K^*K + \lambda I)^{-1}KY$. The regularization parameter λ is determined using the L-curve. Results of simulation are shown in Figure 1 for different levels of noise.

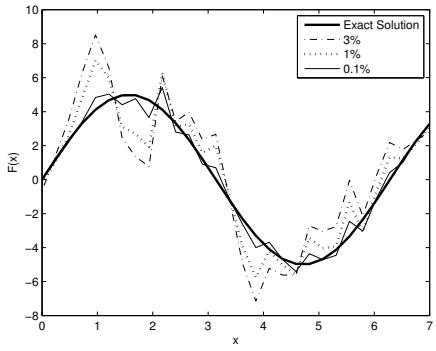

Figure 1: The exact and the regularized solution when $f(x) = 5\sin(x)$, with different noise levels.

2 Conclusion

In this paper, we have discussed the inverse source problem of a space fractional advection-dispersion equation on a finite domain. The problem is ill-posed then, the Tikhonov regularization has been used. It produces slightly larger errors than the perturbation regularization algorithm introduced by Chi *et al* [7]. However, in the latter, the stability and the accuracy of the perturbation regularization algorithm depends on the choice of the initial guess and the basis functions. It is not obvious if the properties of the source term are unknown.

References

[1] I. Podlubny, *Fractional Differential Equations*, Academic Press, San Diego, 1999.

[2] M. M.Meerschaert and C. Tadjeran, *Finite Difference Approximations for Fractional Advection-Dispersion Flow Equations* , Journal of Computational and Applied Mathematics, **172** (2004), pp. 65–77.

[3] X. Xiong and Q. Zhou and Y.C. Hon, *An Inverse Problem for Fractional Diffusion Equation in 2-Dimensional Case: Stability Analysis and Regularization*, Journal of Mathematical Analysis and Applications, **393** (2012), pp. 185–199.

[4] E. D. Giuseppe and M. Moroni andM. Caputo, *Flux in Porous Media With Memory: Models and Experiments*, Transport in Porous Media, (2010), pp.479 –500.

[5] H. Wei and W. Chen and H. Sun and X. Li, *A Coupled Method for Inverse Source Problem of Spatial Fractional Anomalous Diffusion Equations*, Inverse Problems in Science and Engineering, **81** (2010), pp. 945–956.

[6] R. Schumer and M. M. Meerschaert and B. Baeumer, *Fractional Advection-Dispersion Equations for Modeling Transport at the Earth Surface*, Journal of Geophysical Research, **114** (2009), F00A07.

[7] G. Chi and G. Li and X. Jia, *Numerical Inversions of a Source Term in the FADE with a Dirichlet Boundary Condition Using Final Observations*, Computers and Mathematics with Applications, **62** (2011), pp.1619–1626.

[8] D. Zhang and G. Li and G. Chi and X. Jia and H. Li, *Numerical Identification of Multi-parameters in the Space Fractional Advection-Dispersion Equation by Final Observations*, Journal of Applied Mathematics, **2012** (2012).

Characterizing Non-Scatterering of Electromagnetic Waves

Tilo Arens[1,*], **John Sylvester**[2]
[1] Institut für Algebra und Geometrie, Karlsruhe Institute of Technology, Germany
[2] Department of Mathematics, University of Washington, USA
*Email: tilo.arens@kit.edu

Abstract

In this talk, we consider the propagation of electromagnetic waves in an anisotropic medium. An important case is when the medium is non-scattering. Through testing by plane waves, we derive an equation characterizing corresponding permitivities and permeabilities. We construct some specific cases of non-scattering media from this characterization.

1 Introduction

We consider a solution pair (E, H) to the inhomogeneous Maxwell Equations

$$\begin{aligned} \nabla \times E - \mathrm{i}\, k\, \mu\, H &= 0\,, \\ \nabla \times H + \mathrm{i}\, k\, \varepsilon\, E &= 0\,. \end{aligned} \tag{1}$$

Here k denotes the circular frequency and ε and μ the space dependent permitivity and permeability, respectively, with values in $\mathbb{C}^{3\times 3}$. We will assume that both ε and μ are equal to the identity matrix outside some ball B and that they are symmetric in B.

It is the goal in this paper to characterize families of such ε, μ, so that no scattered field arises. The subject has recently obtained considerable attention in the context of *cloaking*, i.e. the hiding of scattering objects behind a non-scattering coat. It is well-known that non-scattering ε, μ can be constructed from appropriate coordinate transforms. It is an open question whether there are other possibilities to explicitely construct suitable cloaks and how to do this.

We will consider the problem under the assumption of weak scattering, i.e. the Born approximation. We will explicitely derive conditions on the Fourier transforms of ε, μ that lead to non-scattering. From these we will be able to construct such media.

2 A Characterizing Equation

In addition to (E, H), consider a pair (E^0, H^0) of entire solutions to the homogeneous Maxwell system

$$\begin{aligned} \nabla \times E^0 - \mathrm{i}\, k\, H^0 &= 0\,, \\ \nabla \times H^0 + \mathrm{i}\, k\, E^0 &= 0\,. \end{aligned} \tag{2}$$

We multiply the equations in (1) by E^0 and H^0, respectively, add them and integrate over B. After a after partial integration, we obtain

$$\begin{aligned} \frac{1}{\mathrm{i}\, k} \int_{\partial B} (E \times H^0 + H \times E^0) \cdot \nu \,\mathrm{d}s(x) \\ = \int_B \left[E^0 \cdot \delta\varepsilon\, E - H^0 \cdot \delta\mu\, H \right] \mathrm{d}x\,. \end{aligned} \tag{3}$$

Here ν denotes the outward drawn unit normal to ∂B and we have set $\delta\varepsilon = \varepsilon - I_3$, $\delta\mu = \mu - I_3$.

Assume now, that (E, H) is the total field of a scattering problem

$$E = E_2^0 + E_2^s\,, \qquad H = H_2^0 + H_2^s\,,$$

where (E_2^0, H_2^0) is an entire solution to (2) (the incident field) and (E_2^s, H_2^s) is the corresponding scattered field satisfying the Silver-Müller radiation condition. Note that (3) remains valid for (E, H) replaced by (E_2^0, H_2^0) and $\delta\varepsilon = \delta\mu = I_3$, so that we conclude

$$\int_{\partial B} (E_2^0 \times H^0 + H_2^0 \times E^0) \cdot \nu \,\mathrm{d}s(x) = 0\,.$$

A careful asymptotic analysis yields the following lemma:

Lemma 1 *Suppose that the far field asymptotics of (E_2^s, H_2^s) are given by*

$$\begin{aligned} E_2^s(x) &= \frac{\mathrm{e}^{\mathrm{i}k|x|}}{|x|} \left(l_2^s(\hat{x}) + \mathrm{O}\left(\frac{1}{|x|}\right)\right), \\ H_2^s(x) &= \frac{\mathrm{e}^{\mathrm{i}k|x|}}{|x|} \left(\hat{x} \times l_2^s(\hat{x}) + \mathrm{O}\left(\frac{1}{|x|}\right)\right), \end{aligned}$$

for $|x| \to \infty$ and that (E^0, H^0) denotes the plane wave given by

$$E^0(x) = l^0\, \mathrm{e}^{\mathrm{i}k\,\hat{\theta}\cdot x}\,, \qquad H^0(x) = \hat{\theta} \times l^0\, \mathrm{e}^{\mathrm{i}k\,\hat{\theta}\cdot x}\,.$$

Then for $B_R(0) = \{x \in \mathbb{R}^3 : |x| < R\}$ there holds

$$\begin{aligned} \lim_{R\to\infty} \int_{\partial B_R(0)} (E_2^s \times H^0 + H_2^s \times E^0) \cdot \nu \,\mathrm{d}s(x) \\ = -\frac{4\pi\,\mathrm{i}}{k}\, l_2^s(-\hat{\theta})^\top l^0\,. \end{aligned}$$

Applying Lemma 1 to equation (3) for some R large enough so that $B \subseteq B_R(0)$, we obtain

$$-\frac{4\pi}{k^2}\, l_2^s(-\hat\theta)^\top l^0 = \int_B \big[E^0\cdot\delta\varepsilon\,(E_2^0+E_2^s) - H^0\cdot\delta\mu\,(H_2^0+H_2^s)\big]\,\mathrm{d}x\,. \quad (4)$$

We now use the Born approximation that

$$E_2^0+E_2^s\approx E_2^0\,,\qquad H_2^0+H_2^s\approx H_2^0$$

in B, and also assume that (E_2^0, H_2^0) is a plane wave,

$$E_2^0(x) = l_2^0\,\mathrm{e}^{\mathrm{i}k\,\hat\psi\cdot x}\,,$$
$$H_2^0(x) = \hat\psi\times l_2^0\,\mathrm{e}^{\mathrm{i}k\,\hat\psi\cdot x}\,.$$

Denote by $\mathcal{B}_{\hat\psi}$ the linear operator mapping l_2^0 (where ${l_2^0}^\top\hat\psi = 0$) onto the far field pattern of the corresponding scattered field in Born approximation. Then from (4), we conclude

$$-\frac{4\pi}{k^2}\,{l^0}^\top\mathbf{B}(\hat\theta,\hat\psi)\,l_2^0 = \int_B \big[E^0\cdot\delta\varepsilon\,E_2^0 - H^0\cdot\delta\mu\,H_2^0\big]\,\mathrm{d}x\,. \quad (5)$$

Suppose now that ε, μ are non scattering. Then the left hand side of (5) vanishes. The right hand side can easily be rewritten as a Fourier transform. Denoting by $\widehat{\delta\varepsilon}$ and $\widehat{\delta\mu}$ denoted the Fourier transform of $\delta\varepsilon$ and $\delta\mu$ evaluated at $\hat\psi+\hat\theta$, respectively, we obtain the characterizing equation

$$0 = {l^0}^\top\widehat{\delta\varepsilon}\,l_2^0 - (\hat\theta\times l^0)^\top\widehat{\delta\mu}\,(\hat\psi\times l_2^0) \quad (6)$$

for all $\hat\theta$, $\hat\psi\in\mathbb{S}^2$ and l^0, $l_2^0\in\mathbb{C}^3$ such that ${l^0}^\top\hat\theta = 0$, ${l_2^0}^\top\hat\psi = 0$.

3 Representations of $\widehat{\delta\varepsilon}$, $\widehat{\delta\mu}$ and Consequences

Set $\hat s = \widehat{\delta\varepsilon}+\widehat{\delta\mu}$, $\hat d = \widehat{\delta\varepsilon}-\widehat{\delta\mu}$. These matrices have particular representations.

Theorem 2 *If $\hat\theta$ and $\hat\psi$ are linearly independent, then there exists an orthogonal matrix M and numbers s_1, s_2, s_3, $d\in\mathbb{C}$ such that*

$$M^\top\hat s M = \begin{pmatrix} s_1 & s_2 & s_3\\ s_2 & -s_1 & 0\\ s_3 & 0 & -s_1\end{pmatrix}$$

and

$$M^\top\hat d M = d\left[I+\begin{pmatrix} r_+^2 & 0 & 0\\ 0 & -r_+^2 & 0\\ 0 & 0 & -r_+^2\end{pmatrix}\right].$$

Here $r_+ = |\hat\theta+\hat\psi|/2$.

An immediate consequence is the following proposition that a non-scattering medium cannot be obtained by perturbing either only ε or only μ:

Corollary 3 *There holds $\delta\varepsilon = 0$ iff $\delta\mu = 0$.*

It also possible to use the representations of $\hat s$ and $\hat d$ to construct specific examples of non-scattering media. For example, the case $\hat d = 0$ leads to the representation

$$\widehat{\delta\varepsilon}(\xi) = \hat w(\xi)\,\xi^\top + \xi\,\hat w(\xi)^\top - \mathrm{tr}(\xi\,\hat w(\xi)^\top)\,I \quad (7)$$

for $\xi\in\mathbb{R}^3$, $0<|\xi|<2$ and some vector field $\hat w$. This representation can be seen to hold whenever scattering by a non-scattering inhomogeneity obtained by a diffeomorphism which is a local perturbation of the identity is studied in Born approximation. Thus the case $\hat d = 0$ corresponds to the non-scattering media obtained in transformation optics. Other cases will be discussed in the conference presentation.

Numerical computation of non-scattering boundary deformations of a 2D acoustic waveguide

A.S. Bonnet-Ben Dhia[1,*], **E. Lunéville**[1], **S. Nazarov**[2]
[1] POEMS (UMR 7231 CNRS-ENSTA-INRIA),
Palaiseau, France.
[2] Institute of Mechanical Engineering Problems,
Saint-Petersburg, Russia.
*Email: bonnet@ensta.fr

Abstract

In [1] is proved theoretically the existence of small perturbations of the rigid boundary of a 2D acoustic waveguide which are invisible at some given frequencies, in the sense that they do not perturb propagative modes in the far field. This communication concerns the numerical computations of such deformations.

Introduction

The practical realization of invisibility cloaks is a topic which gives currently rise to a very intensive research activity in optics. Here we want to achieve invisibility only at one given frequency (or at a finite number of given frequencies). The specificity is that we consider propagation in a waveguide, and not in the free space. Following [1] (where the approach of [2] is used) the deformation of the boundary is searched as a linear combination of known (compactly supported) functions. The coefficients of the linear combination are solution of a contractant fixed point equation, expressed thanks to the scattering coefficients of the deformation. These scattering coefficients can be computed numerically. To avoid remeshing at each iteration of the fixed point algorithm, we use a multimodal method written in the straight waveguide as in [3].

1 Setting of the problem

We consider a 2D acoustic waveguide defined as follows:

$$B_h^\varepsilon = \{(x,y) \text{ such that } 0 < y < 1 + \varepsilon h(x)\}$$

where ε is a small positive parameter and h a smooth function compactly supported in $[-1,1]$. The time harmonic pressure field u satisfies the following boundary value problem:

$$\left\{ \begin{array}{ll} \Delta u + k^2 u = 0 & (B_h^\varepsilon), \\ \dfrac{\partial u}{\partial n} = 0 & (\partial B_h^\varepsilon), \end{array} \right. \tag{1}$$

where $k > 0$ is the wavenumber.

For the sake of simplicity, we consider here the monomode case where $k < 1$ so that the only propagative mode is the plane mode $e^{\pm ikx}$. Suppose this plane mode is incident from the left, then the diffraction problem consists in finding u solution of (1) such that

$$u(x,y) =$$
$$e^{ikx} + Re^{-ikx} + \sum_{n\geq 1} u_n^- e^{\sqrt{n^2\pi^2-k^2}x}\cos(n\pi y) \quad x < -1$$
$$Te^{ikx} + \sum_{n\geq 1} u_n^+ e^{-\sqrt{n^2\pi^2-k^2}x}\cos(n\pi y) \quad x > 1,$$

where R, T and the $u_n^\pm$ are complex coefficients. We look for a non-trivial perturbation h such that the reflection coefficient R vanishes. Then, we deduce from

$$|R|^2 + |T|^2 = 1$$

that $|T| = 1$. If this occurs, it means that the field reflected by the perturbation is purely evanescent, so that the presence of the perturbation is not observable in the far-field. Concerning the transmitted field, a phase shift can be observed (since we ensure $|T| = 1$ but not necessarily $T = 1$). Moreover, it is easy to check that the same conclusion holds for an incident wave coming from the right.

2 The theoretical results

We look for a deformation h of the form

$$h = h_0 + \tau_1 h_1 + \tau_2 h_2$$

where τ_1 and τ_2 are real parameters to be determined, and h_0, h_1 and h_2 are given functions satisfying the following requirements:

$$\int_{-1}^{1} \cos(2kx) h_j(x) = \delta_{j1} \text{ and } \int_{-1}^{1} \sin(2kx) h_j(x) = \delta_{j2}$$

Then it can be proved by an asymptotic analysis that

$$T = 1 + \varepsilon^2 \widetilde{T}_\varepsilon(\tau)$$

and

$$R = ik\varepsilon\tau + \varepsilon^2 \widetilde{R}_\varepsilon(\tau)$$

where $\tau = \tau_1 + i\tau_2$, with the estimates:

$$|\widetilde{T}_\varepsilon(\tau)| + |\widetilde{R}_\varepsilon(\tau)| \leq C$$

for some constant C independent of ε and τ, for τ bounded. Finally the invisibility condition $R = 0$ is written as a fixed point equation in τ:

$$\tau = F_\varepsilon(\tau)$$

where

$$F_\varepsilon(\tau) = \frac{i\varepsilon}{k}\widetilde{R}_\varepsilon(\tau).$$

This fixed-point equation is proved to be contractant for small ε.

3 The numerical algorithm

For the numerical computations, we solve for a given ε the above fixed point equation by the classical fixed point algorithm

$$\tau^{(n+1)} = F_\varepsilon(\tau^n).$$

For the evaluation of $F_\varepsilon(\tau)$, we use the multimodal method presented in section 3.3 of [3], which has already been used for optimum design purposes. Contrary to a 2D finite elements method, the multimodal approach avoids remeshing at each iteration (remember that the deformation $h(x)$ depends on the parameter τ).

On the one hand, we use the change of variables

$$\mathcal{H} : (x, y) \in B_h^\varepsilon \to \left(X = x, Y = \frac{y}{1 + \varepsilon h(x)} \right) \in B,$$

to set the initial problem in a straight waveguide $B =]-1, 1[\times]0, 1[$. On the other hand, exact transparent boundary conditions are imposed on the artificial boundaries $x = \pm 1$. This leads finally to the following variational problem :

$$\begin{aligned} &\text{Find } U \in H^1(B) \text{ such that } \forall V \in H^1(B) \\ &\int_B (\mathbb{H}\nabla U) \cdot \nabla V - k^2(1 + \varepsilon h(x))UV \\ &- \langle \mathbb{T}(-1)U, V\rangle - \langle \mathbb{T}(1)U, V\rangle = V(-1) \end{aligned}$$

where $\mathbb{H}$ is the matrix

$$\mathbb{H} = \begin{bmatrix} 1 + \varepsilon h(X) & -Y\varepsilon h'(X) \\ -Y\varepsilon h'(X) & \dfrac{1 + \varepsilon^2 Y^2 h'(X)^2}{1 + \varepsilon h(X)} \end{bmatrix}$$

and $\mathbb{T}$ is the Dirichlet-to-Neumann operator defined by:

$$\langle \mathbb{T}(\pm 1)U, V\rangle = ikU_0(\pm 1)V_0(\pm 1) - \sum_{n>0} \sqrt{n^2\pi^2 - k^2} U_n(\pm 1)V_n(\pm 1)$$

where

$$U_n(X) = \frac{\int_0^1 U(X, Y)\cos(n\pi Y)dY}{\int_0^1 \cos(n\pi Y)^2 dY}.$$

Finally, the problem is discretized by using a Galerkin approximation, replacing $H^1(B)$ by the finite-dimensional space of functions of the form

$$U(X, Y) = \sum_{0\leq n\leq N} \sum_{0\leq p\leq P} w_p(X)\cos(n\pi Y)$$

where the $w_p(X)$ form a finite element basis. In other words, we use a modal decomposition in Y and finite elements in X.

4 Extensions

The proposed algorithm can be directly extended to other cases described in [1]. For instance, one can find a deformation which is invisible at several frequencies $k_1, k_2 \cdots k_M$ below the cut-off π, using $2M + 1$ design functions h_j. Also invisibility in the first interval of the spectrum $]\pi, 2\pi[$ can be investigated.

References

[1] A.-S. Bonnet-Ben Dhia and S. Nazarov, *Obstacles in acoustic waveguides becoming "invisible" at given frenquencies*, Preprint.

[2] S. Nazarov, *Asymptotic expansions of eigenvalues in the continuous spectrum of a regularly perturbed quantum waveguide*, Theoretical and Mathematical Physics, 167 (2), pp. 606–627, 2011.

[3] C. Hazard and E. Lunéville, *An improved multimodal approach for non uniform acoustic waveguides*, IMA Journal of Applied Math., 73 (4), pp. 668–690, 2008.

Conductive Material Distribution Optimization for Ultrawideband Antennas

E. Hassan[1], E. Wadbro[1], and M. Berggren[1,*]
[1] Department of Computing Science, Umeå University, Umeå, Sweden.
*Email: martin.berggren@cs.umu.se

Abstract

An Ultrawideband (UWB) planar monopole antenna is designed using the material distribution approach to topology optimization. The design variables are the local conductivity values in a 75×75 mm area where the radiating element can be located. The antenna is optimized for maximum reception, in an attached coaxial cable, of incoming plane waves. The wave propagation is modeled using the time domain 3D Maxwell equations discretized using FDTD, and the optimization is carried out using a gradient-based optimization method, in which the derivatives are supplied through solving corresponding adjoint equations. The outer dimensions of the optimized antenna is 75×60 mm, and its reflection coefficient $|S_{11}|$, with respect to a feeding signal in the coaxial cable, stays below -10 dB throughout the frequency band 1.2–9.7 GHz.

Introduction

A well established method for computational design optimization of load-carrying elastic structures is *the material distribution approach to topology optimization*, in which a function indicating local density of material is the decision variable subject to optimization [1]. The method has been generalized to the design of devices that interact with acoustic as well as electromagnetic waves. However, the method has not much been used to design metallic antennas through optimization of the local conductivity. To the best of our knowledge, the only contribution that uses a large design space is by Erentok & Sigmund [2]. These authors, who have an extensive experience from applying topology optimization to a wide class of problems, report that this problem is unusually sensitive to various parameters in the optimization.

There are no ohmic losses in a material with vanishing or infinite values of the conductivity, but any in-between value leads to energy losses. A gradient-based optimization algorithm, however, needs to operate on the continuum between insulator and conductor, and cannot avoid intermediate lossy values. Thus, when such an algorithm is used to maximize transmission, any intermediate conductivity value will quickly be forced to one of the extreme values in order to minimize energy losses: the problem is "self penalizing" to extreme values of the conductivity. Moreover, it will be difficult to change a vanishing or very large (infinite) conductivity value to its opposite, since it needs to pass through a "barrier" of intermediate lossy values. Thus, a gradient-based optimization algorithm for transmission optimization of metallic antennas will quickly be trapped in a local optimum with bad performance if no precaution is taken. Among material distribution problems for devices in the context of wave propagation, this complication is rather unique and does not occur when optimizing, for instance, the distribution of sound-hard material for acoustics problems [5] or the distribution of material for dielectric resonator antennas [3]. We believe that the difficulty of handling lossy intermediate values of the conductivity is the reason for the lack of progress up to recently in the application of topology optimization techniques to the design of metallic antennas.

Problem statement

As a reference configuration, we consider a rectangular monopole antenna, occupying area Γ_{m}, mounted perpendicularly and close to an infinite ground plane. For the optimization, we consider the antenna in its receiving mode. The objective function is the energy picked up in a coaxial cable mounted in the middle of the edge facing the ground plane,

$$E_c(\sigma) = \frac{1}{2Z_{\mathrm{c}}} \int_0^T (V - Z_{\mathrm{c}} I)^2 \, dt, \qquad (1)$$

where V and I are the voltage and the current at a point in the cable, Z_{c} its characteristic impedance, and $V - Z_{\mathrm{c}} I$ is the characteristic variable associated with the receiving signal. The optimization problem is to maximize E_c over all $\sigma \in L^\infty(\Gamma_{\mathrm{m}})$, $0 \le \sigma(\boldsymbol{x}) \le \sigma_{\max}$. The state equation is the 3D Maxwell equations with a variable conductivity in Γ_{m}. No feeding signal is provided through the coaxial cable, which means that the associated characteristic variable vanishes: $V(t) + Z_{\mathrm{c}} I(t) = 0$. The coupling between the voltage and current in the coaxial cable

and the electromagnetic fields in the domain is accomplished through boundary conditions on the annular, dielectric cross section Γ_{coax} of the cable.

Results

The aim is to design an Ultrawideband (UWB) antenna in the GHz region. The 3D Maxwell equations are numerically solved in time domain using the classical Yee scheme (FDTD) with a Perfectly Matched Layer (PML) to absorb outgoing waves and with an attached 50 Ω coaxial cable. The potential antenna area Γ_{m} is 75×75 mm and is discretized by 100×100 Yee cell faces. The conductivity at each edge in Γ_{m} is subject to design, which yields a total of 20200 design variables. The Method of Moving Asymptotes (MMA) [4] is used to solve the optimization problem, and the required gradients are computed using the associated adjoint equations, derived in the fully discrete case. In order to create a rich source of waves for the antenna, we expose it to circularly polarized waves from all 4 sides. The wave amplitude is a truncated sinc pulse covering the frequency band 1–10 GHz.

We address the issue of self penalization discussed above by a continuation approach and *enforce* intermediate values of the conductivity, and therefore a certain amount of losses, from the start of the optimization iterations. We then successively reduce the losses as the iterations proceed. To enforce intermediate values, the conductivity σ used in the Maxwell equations is obtained by a local averaging (filtering) of the design variables $\tilde{\sigma}$ that are actually updated by the optimization algorithm: $\sigma = K_R * \tilde{\sigma}$, where the kernel of the integral operator K_R has support in a disk of radius R. (Such a filter is commonly used also for topology optimization of elastic structures, but for other reasons, namely to regularize an ill-posed problem [1].) The filter leads to a "blurring" of the design variables $\tilde{\sigma}$, which imposes a certain amount of ohmic losses.

We start with an initial filter radius R_0 and successively reduce the radius by setting $R_{n+1} = \gamma R_n$, where $\gamma < 1$, while performing a number of iterations of the optimization algorithm for each filter radius. In the numerical experiments, $R_0 = 1.5$ cm, $\gamma = 0.7$, and, for each filter radius, we iterate until a selected convergence criterion based on the first-order necessary conditions is met, which typically requires 10–20 iterations. The algorithm thus progresses through a succession of less and less lossy designs until, for small values of the filter radius, the radiating element

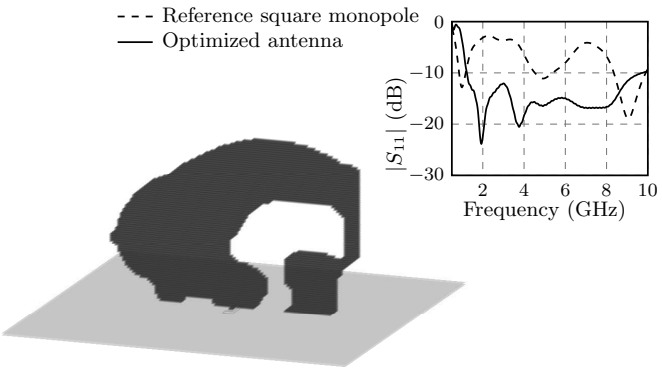

Figure 1: The reference and optimized antenna and their reflection coefficients $|S_{11}|$.

will almost entirely consist of elements with σ being either 0 or $\sigma_{\max}$, due to the self-penalizing nature of the problem.

The MMA algorithm required a total of 126 iterations to converge to the final design shown in figure 1. Performance is measured, by reciprocity, in terms of the reflection coefficient S_{11} with the antenna as a transmitter. Overall, the performance of the optimized antenna is superior to the reference, and the reflection coefficient, $|S_{11}|$, of the optimized antenna stays below -10 dB for the frequency band 1.2–9.7 GHz.

References

[1] M. P. Bendsoe and O. Sigmund. *Topology Optimization. Theory, Methods, and Applications.* Springer, 2003.

[2] A. Erentok and O. Sigmund. Topology optimization of sub-wavelength antennas. *IEEE Trans. Antennas and Propagation*, 59(1):58–69, 2011.

[3] T. Nomura, K. Sato, K. Taguchi, T. Kashiwa, and S. Nishiwaki. Structural topology optimization for the design of broadband dielectric resonator antennas using the finite difference time domain technique. *Internat. J. Numer. Methods Engrg.*, 71:1261–1296, 2007.

[4] K. Svanberg. The method of moving asymptotes—a new method for structural optimization. *Internat. J. Numer. Methods Engrg.*, 24:359–373, 1987.

[5] E. Wadbro and M. Berggren. Topology optimization of an acoustic horn. *Comput. Methods Appl. Mech. Engrg.*, 196:420–436, 2006.

Analytical Algorithms for the Inverse Source Problem in a Sphere

N. L. Tsitsas[1,*], **P. A. Martin**[2]
[1] Department of Informatics, Aristotle University of Thessaloniki, Thessaloniki, Greece
[2] Department of Applied Mathematics and Statistics, Colorado School of Mines, Golden, USA.
*Email: ntsitsas@csd.auth.gr

Abstract

A homogeneous sphere is excited by a point source lying inside the sphere. Analytical inversion algorithms are established concerning the determination of the physical characteristics of the sphere as well as the location and strength of the source. The basic quantity utilized in these algorithms is the total field on the sphere which is assumed to be known. The investigation of the above described problem is motivated by various applications in medical imaging.

Introduction

A point source inside a homogeneous spherical conductor constitutes a simplified yet realistic model for investigating a variety of applications in brain imaging [1], [2]. Locating point sources using surface measurements is an example of an *inverse source problem* [3].

We consider the basic static problem consisting of Laplace's equation in a ball V_i with boundary ∂V. The goal is to identify a point source lying in V_i from Cauchy data on ∂V. There are fields both inside and outside the sphere, with appropriate interface conditions on the sphere. The inverse problem is to determine the location and strength of the source knowing the total field on the sphere. The internal conductivity is also to be found.

We obtain exact and complete results by developing analytical inversion algorithms utilizing the moments obtained by integrating the product of the total field on the spherical interface with spherical harmonic functions. All the information about the primary source and the ball's physical characteristics is encoded in these moments. The presented method is simple, explicit and exact (given exact data). Other analytic inversion algorithms for determining static point dipoles as well as acoustic point sources inside a homogeneous sphere are presented in [4].

1 Mathematical Formulation

Consider a homogeneous spherical object of radius a, surrounded by an infinite homogeneous medium. Denote the exterior by V_e and the interior by V_i. A point source lies inside the sphere at an unknown location $\mathbf{r}_1 \in V_\mathrm{i}$. We will determine the source, using information on the spherical interface.

Denote the field outside the sphere by u_e and the total field inside by u_i. Then, $u_\mathrm{i} = u^\mathrm{pr} + u^\mathrm{sec}$, where u^pr is the primary field due to the source (u^pr is singular at $\mathbf{r}_1$) and u^sec is the secondary (regular) field. The field u_e is regular and satisfies an appropriate far-field condition. The fields u_e and u_i are related by transmission conditions on the sphere.

For the primary field, we choose a point source,

$$u^\mathrm{pr}(\mathbf{r};\mathbf{r}_1) = \frac{A}{|\mathbf{r}-\mathbf{r}_1|}, \qquad \mathbf{r} \in \mathbb{R}^3 \backslash \{\mathbf{r}_1\}, \qquad (1)$$

where A is a real constant.

Introduce spherical polar coordinates (r,θ,ϕ) for the point at $\mathbf{r}$ so that the source is at (r_1,θ_1,ϕ_1) with $r_1 = |\mathbf{r}_1| < a$. Then, the transmission conditions are

$$u_\mathrm{e} = u_\mathrm{i} \quad \text{and} \quad \frac{1}{\rho_\mathrm{e}}\frac{\partial u_\mathrm{e}}{\partial r} = \frac{1}{\rho_\mathrm{i}}\frac{\partial u_\mathrm{i}}{\partial r} \quad \text{at } r = a, \qquad (2)$$

where ρ_e and ρ_i are constants.

Since we deal with a static problem, both u_e and u^sec are governed by Laplace's equation. The field u_e decays to zero at infinity. In the context of electrostatics, ρ_e and ρ_i are inverse conductivities.

2 Inverse Source Problem

A static point source lies at $\mathbf{r}_1$ and generates the field u^pr. Near the sphere ($r_1 < r < a$), separation of variables gives the expansion

$$u^\mathrm{pr}(\mathbf{r};\mathbf{r}_1) = \sum_{n=0}^{\infty}\sum_{m=-n}^{n} f_n^m(\mathbf{r}_1)(a/r)^{n+1}Y_n^m(\hat{\mathbf{r}}),$$

where $\hat{\mathbf{r}} = \mathbf{r}/|\mathbf{r}|$ and $Y_n^m(\hat{\mathbf{r}}) = Y_n^m(\theta,\phi)$ is a spherical harmonic (see [5, §3.2]), and the quantities f_n^m

characterizing the source, are given by

$$f_n^m(\mathbf{r}_1) = \frac{4\pi A}{a}\frac{(-1)^m}{2n+1}(r_1/a)^n Y_n^{-m}(\hat{\mathbf{r}}_1)\,. \qquad (3)$$

The secondary field inside the sphere is

$$u^{\rm sec}(\mathbf{r}) = \sum_{n=0}^{\infty}\sum_{m=-n}^{n} \alpha_n f_n^m(\mathbf{r}_1)(r/a)^n Y_n^m(\hat{\mathbf{r}}),\ 0 \le r < a$$

whereas the field outside is given by

$$u_{\rm e}(\mathbf{r}) = \sum_{n=0}^{\infty}\sum_{m=-n}^{n} \beta_n f_n^m(\mathbf{r}_1)(a/r)^{n+1} Y_n^m(\hat{\mathbf{r}}), \quad r > a$$

The transmission conditions at $r = a$, (2), give

$$\alpha_n = \frac{(1-\varrho)(n+1)}{n+\varrho(n+1)}, \quad \beta_n = \frac{2n+1}{n+\varrho(n+1)}, \qquad (4)$$

where $\varrho = \rho_{\rm i}/\rho_{\rm e}$. Note that α_n and β_n do not depend on any characteristics of the source.

The field on the sphere is

$$u_{\rm surf}(\theta,\phi) = \sum_{n=0}^{\infty}\sum_{m=-n}^{n} \frac{2n+1}{n+\varrho(n+1)} f_n^m(\mathbf{r}_1) Y_n^m(\theta,\phi).$$

It is this quantity that we shall use to find the source.

The spherical harmonics are orthonormal,

$$\int_\Omega Y_n^m \overline{Y_\nu^\mu}\,{\rm d}\Omega = \int_0^\pi \int_{-\pi}^{\pi} Y_n^m(\theta,\phi)\overline{Y_\nu^\mu(\theta,\phi)}\sin\theta\,{\rm d}\phi\,{\rm d}\theta = \delta_{n\nu}\delta_{m\mu},$$

where Ω is the unit sphere and the overbar denotes complex conjugation. Hence, the moments

$$M_n^m \equiv \frac{1}{\sqrt{4\pi}}\int_\Omega u_{\rm surf}\overline{Y_n^m}\,{\rm d}\Omega = \frac{1}{\sqrt{4\pi}}\frac{2n+1}{n+\varrho(n+1)} f_n^m(\mathbf{r}_1), \qquad (5)$$

are known, in principle, if u is known on $r = a$; the double integral over Ω could be approximated using a suitable quadrature rule and corresponding point evaluations of $u_{\rm surf}$. The problem now is to determine properties of the source and the interior material (namely, $\rho_{\rm i} = \rho_{\rm e}\varrho$) from M_n^m.

For a point source, (3) and (5) give

$$M_n^m = (-1)^m \frac{\tilde{A}\tilde{r}_1^n\sqrt{4\pi}}{n+\varrho(n+1)} Y_n^{-m}(\theta_1,\phi_1), \qquad (6)$$

with $\tilde{A} = \frac{A}{a}$ and $\tilde{r}_1 = \frac{r_1}{a}$. Thus, there are five unknowns, $\tilde{A}$, ϱ, $\tilde{r}_1$, θ_1 and ϕ_1.

As $Y_0^0 = (4\pi)^{-1/2}$, we obtain

$$M_0^0 = \tilde{A}/\varrho.$$

This ratio is all that can be recovered if the source is at the sphere's centre ($r_1 = \tilde{r}_1 = 0$). So, let us assume now that $\tilde{r}_1 \neq 0$.

For $n = 1$, we can use the expressions of Y_1^0, Y_1^1, and Y_1^{-1} (see e.g. [5, eqn (8.28)]) to obtain

$$M_1^0 = \tilde{A}\,\frac{\tilde{r}_1\sqrt{3}}{1+2\varrho}\,\cos\theta_1,$$

$$M_1^{\pm 1} = \mp\tilde{A}\,\frac{\tilde{r}_1\sqrt{3/2}}{1+2\varrho}\,{\rm e}^{\mp{\rm i}\phi_1}\sin\theta_1.$$

If $M_1^{\pm 1} = 0$, then $\theta_1 = 0$ or π (the source is on the z-axis and so ϕ_1 is irrelevant); to decide which, note that the sign of $M_0^0 M_1^0$ is the sign of $\cos\theta_1$. If $M_1^{\pm 1} \neq 0$, ϕ_1 is determined by noting that the complex number $M_0^0 M_1^{-1}$ has argument ϕ_1.

If $M_1^0 = 0$, then $\theta_1 = \pi/2$. If $M_1^0 \neq 0$, $\sqrt{2}\,M_1^{-1}/M_1^0 = {\rm e}^{{\rm i}\phi_1}\tan\theta_1$ determines θ_1. Also

$$(1+2\varrho)^2\{(M_1^0)^2 - 2M_1^1 M_1^{-1}\} = 3(\tilde{A}\tilde{r}_1)^2. \qquad (7)$$

To conclude, we take a measurement with $n = 2$

$$\varrho(2+3\varrho)M_0^0 M_2^m = (\tilde{A}\tilde{r}_1)^2(-1)^m\sqrt{4\pi}Y_2^{-m}(\theta_1,\phi_1). \qquad (8)$$

Choosing m such that $Y_2^{-m}(\theta_1,\phi_1) \neq 0$ (namely take $m = 0$ unless $P_2(\cos\theta_1) = 0$), we eliminate $(\tilde{A}\tilde{r}_1)^2$ between (7) and (8) to give a quadratic equation for ϱ (which is real and positive). Then, $\tilde{A} = A/a = M_0^0\varrho$ and $\tilde{r}_1 = r_1/a$ follows from M_1^m or from (7).

References

[1] G. Dassios, *Electric and magnetic activity of the brain in spherical and ellipsoidal geometry*, Lecture Notes in Math. **1983** (2009), pp. 133–202.

[2] H. Ammari, *An Introduction to Mathematics of Emerging Biomedical Imaging*, Springer, Berlin, 2008.

[3] V. Isakov, *Inverse Source Problems*, American Mathematical Society, Providence, 1990.

[4] N. L. Tsitsas and P. A. Martin, *Finding a source inside a sphere*, Inverse Problems **28** (2012), 015003.

[5] P. A. Martin *Multiple Scattering*, Cambridge University Press, Cambridge, 2006.

Silent electrical sources in a sphere

L. Baratchart[1], M.Clerc[2], J. Leblond[1,*]
[1] Team APICS, INRIA, Sophia-Antipolis, France
[2] Team ATHENA, INRIA, Sophia-Antipolis, France
[*] Email: juliette.leblond@inria.fr

Abstract

We discuss uniqueness properties for the inverse current source recovery problem of electroencephalography, from boundary values of the associated electrical potential.

Introduction

The inverse EEG (electroencephalography) problem consists in recovering a current distribution within the brain from measurements of the generated electric potential taken by electrodes on the scalp. From Maxwell's equation in their quasi-static approximation, it is modelled by a conductivity elliptic partial differential equations (PDE).

Physical applications come from medical imaging and engineering, neurosciences, for both therapeutic and functional brain analysis, but are related to many other non-destructive testing issues.

Such inverse source problems from partial boundary data are severely ill-posed when they concern elliptic PDE (this in known since Hadamard), due to the lack of uniqueness of solutions or of their stability properties. One of these strong ill-posedness phenomena is the case of silent sources, that correspond to non-unique solutions.

We look for a caracterization of silent electrical sources within a volume Ω of $\mathbb{R}^3$: what are the electrical currents localized inside Ω that generate an electrical potential vanishing identically outside Ω?

1 Problem, model

A classical EEG setup is that of a spherical head Ω (a ball) composed of 3 nested spherical layers, each of constant conductivity value, for the brain Ω_0, the skull Ω_1 and the scalp Ω_2, see [3]: $\Omega = \overline{\Omega_0} \cup \overline{\Omega_1} \cup \Omega_2$.

The (real-valued) electrical potential u satisfies

$$\nabla \,.\, (\sigma \nabla u) = \nabla \,.\, J^p \text{ in } \Omega\,,$$

where the current source (primary cerebral current) J^p is supported in Ω_0 (as a distribution on $\mathbb{R}^3$, thus with compact support). Hence, u is harmonic in Ω_1, Ω_2:

$$\Delta u = 0 \text{ in } \Omega_1\,,\ \Omega_2\,, \tag{1}$$

and in the innermost layer (the brain), modelled by a ball, say $\Omega_0 = \mathbb{B}$, it satisfies the Poisson equation (in the distributional sense):

$$\Delta u = \nabla \,.\, J^p \text{ in } \mathbb{B}\,, \tag{2}$$

where the transmission conditions at interfaces imply that, for $i = 1, 2$,

$$u\,,\ \sigma\, \partial_n u \text{ are continuous on } \partial\Omega_{i-1} \cap \partial\Omega_i\,. \tag{3}$$

The inverse EEG problem then consists in the following Cauchy-type issue:

being given (partial, overdetermined) boundary data, namely a set of measured pointwise values of the potential u on a subset of the boundary $\partial\Omega$, together with the assumption that the current flux $\partial_n u = 0$ on $\partial\Omega$, find the current source J^p associated to these data through (1), (2), (3).

It is a typical ill-posed problem (in view of Hadamard), whose solution may not be unique and, even in situations where uniqueness holds, may possess an unstable behaviour with respect to the boundary data (practically furnished by electrodes measurements). Well-posedness however can be granted provided suitable assumptions are satisfied by the current source J^p. Namely, a classical model in EEG consists in modelling J^p by a finite number of pointwise dipolar sources within $\mathbb{B}$:

$$J^p = \sum_{k=1}^{K} p_k\, \delta_{C_k}\,,$$

with an integer K, moments $p_k \in \mathbb{R}^3$, sources locations $C_k \in \mathbb{B}$. For such (unknown) pointwise dipolar source J^p, uniqueness properties hold [5] from values of u on an open subset of $\partial\Omega$ (which can be built from the given pointwise measures, in a robust manner). In particular, pointwise dipolar sources are never silent. In such situations, efficient source localization scheme are furnished by constructive best quadratic rational approximation techniques in planar sections [2]. Figure 1 provides an illustration

of this recovery procedure, using the software FindSources3D [6] (matlab); there, pointwise data are (numerically) given at 128 electrodes locations on the outermost upper hemisphere of $\partial\Omega_2$, from which the quantity $K = 2$, the sources locations C_k and associated moments p_k are estimated.

It raises however the uniqueness issue, for other important models of sources, like those distributed on surfaces, and motivates the (inverse) silent source problem:

find those source distributions J^p with support in (the closed ball) $\bar{\mathbb{B}}$ such that the associated potential u through (2) has its support contained in $\bar{\mathbb{B}}$.

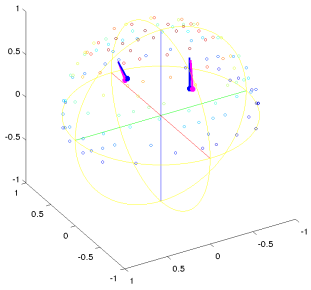

Figure 1: Pointwise dipolar sources estimation

2 Solutions

A characterization of such silent sources will be explained, which is obtained using a Helmholtz-Hodge decomposition formula, Green formula, together with properties of the Poisson kernel of the ball and of harmonic functions there. It asserts that silent sources J^p coincides with gradients of functions that belong to the Sobolev space $W_0^{1,2}(\mathbb{B})$ of functions with vanishing trace on the boundary and $L^2(\mathbb{B})$ derivative (or of their distributional derivatives), up to the addition of a divergence free term. In particular, $W^{1,2}(\mathbb{B})$ functions with support strictly contained in $\mathbb{B}$ belong to $W_0^{1,2}(\mathbb{B})$. A sketch of the proof will be proposed. Examples of such silent sources will be provided as well, some of which being also magnetically silent (generating a magnetic field that vanishes outside $\mathbb{B}$), which are of practical interest for magnetoencephalography (MEG) experiments.

Note that similar uniqueness issues are in order for inverse magnetization problems [1], where the magnetization of some material (like martian rocks) is to be recovered from magnetic measurements (by SQUID microscopy). They also appear to be raised by many physical issues modelled by Maxwell's or Newton's equations (geophysics).

3 Illustrations and References

References

[1] L. Baratchart, D. Hardin, E.A. Lima, E.B. Saff, B.P. Weiss, *Characterizing kernels of operators related to thin-plate magnetizations via generalizations of Hodge decompositions*, Inverse Problems, **29** (2013), to appear.

[2] L. Baratchart, J. Leblond and J.-P. Marmorat, *Inverse source problem in a 3D ball from best meromorphic approximation on 2D slices*, Elec. Trans. Numerical Analysis (ETNA), **25** (2006), pp. 41–53.

[3] M. Clerc, J. Leblond, J.-P. Marmorat and T. Papadopoulo, *Source localization in EEG using rational approximation on plane sections*, Inverse Problems, **28** (2012), 055018.

[4] R. Dautray and J.-L. Lions, *Mathematical Analysis and Numerical Methods for Science and Technology*, Vol. 2, Springer, 2000.

[5] T.H. Duong and A. El Badia, *An inverse source problem in potential analysis Inverse Problems*, **16** (2000), pp. 651-663.

[6] FindSources3D, http://www-sop.inria.fr/apics/FindSources3D/

Numerical analysis of the Factorization Method for Electrical Impedance Tomography in uncertain background

H. Haddar[1], **G. Migliorati**[1,2,*]
[1] INRIA Saclay Ile de France and Ecole Polytechnique (CMAP) Palaiseau, France.
[2] Dipartimento di Matematica - Politecnico di Milano, Italy.
*Email: giovanni.migliorati@gmail.com

Introduction

We address the Factorization Method (FM) as introduced in [1] applied to the Continuous Model of Electrical Impedance Tomography (EIT). Most of the works on the FM in the literature treat the case of homogeneous background. Our works [2], [3] are mostly related to numerical issues associated with EIT in inhomogeneous and uncertain background.

To begin with, we propose a numerical scheme to solve the dipole-like Neumann boundary-value problem when the background conductivity coefficient is inhomogeneous and deterministic, and use this scheme to design an efficient implementation of the FM algorithm for inhomogeneous but deterministic background.

We then discuss the case where the background conductivity coefficient is piecewise constant with known spatial distribution but unknown parameter values. We propose three variants of the FM to cope with this configuration. In the first algorithm we simultaneously recover the background parameters and the location of the inclusion, by means of an optimization scheme motivated by the structure of the sampling operator and the outcome of the FM. This algorithm is well suited for low dimensional configurations of the parameter space. In addition, a second approach is proposed, where the optimization scheme is replaced by a weighting of the FM indicator function with a misfit indicator for the background. This procedure requires an extensive sampling of the parameter space which would be very expensive. However, in the case where many independent realizations of the measurement operator are available, we describe how this strategy can be made efficient. The third algorithm deals with the case where paired measurements are available, namely measurements for the inclusion free background and measurements for the medium with inclusion. In this case, a uniform weight for the FM associated with random sampling of the parameter spaces provides an effective indicator function.

Overview of the results

We consider backgrounds that are piecewise constant in r regions $\{R_i\}_{i=1}^r$ that are a partition of the computational domain $B = \bigcup_{i=1}^r R_i$, see *e.g.* Fig. 1. Denote by $\mathbf{m}$ the r-dimensional vector of positive numbers that specifies the coefficient value in each region R_i of the domain B. The background conductivity coefficient σ_B is defined as

$$\sigma_B(\mathbf{x}) = \sum_{i=1}^{r} m_i \, \mathbb{I}_{R_i}(\mathbf{x}), \qquad \mathbf{x} \in B, \tag{1}$$

where $\mathbb{I}_X(\mathbf{x})$ denotes the indicator function of the subdomain $X \subseteq B$. If $\boldsymbol{m} = (1, 1, \ldots, 1)^\top$ then we obtain a homogeneous deterministic coefficient, and Fig. 2 shows the reconstructions obtained with the geometries shown in Fig. 1. Fig. 3 shows the reconstructions obtained when the background coefficient σ_B is given by (1), with the vector $\mathbf{m}$ chosen such that the coefficient jumps by two orders of magnitude across different regions.

More general deterministic inhomogeneous coefficients σ_B, nonlinearly depending on $\mathbf{x}$, have been analysed in [2]. The effect of artificial noise has been analysed in [2] as well. In Fig. 4-left we report (from [2]) the reconstruction of ten small obstacles, obtained with the following background conductivity coefficient, with $\pm 50\%$ variation,

$$\sigma_B(\mathbf{x}) = 1 + 0.25\Big(\sin(5x_1) + \cos(5x_2)\Big). \tag{2}$$

In Fig. 4-right the reconstruction is obtained after the measurements have been contaminated by noise.

To model the background in the uncertain case, we parametrize σ_B with the exponential model

$$\sigma_B(\mathbf{x}, \mathbf{y}) = \sum_{i=1}^{r} 10^{y_i} \, \mathbb{I}_{R_i}(\mathbf{x}), \quad \mathbf{x} \in B, \quad \mathbf{y} \in \Gamma, \tag{3}$$

where $\Gamma = [-1, 1]^r$. The parameter $\mathbf{y}$ is a realization of the random variable $\mathbf{Y} \sim \mathcal{U}(\Gamma)$ uniformly distributed over Γ. Again, the coefficient jumps up to

two orders of magnitude in each one of the r regions. The corresponding reconstructions are reported in Fig. 5-left, in the case of arbitrary measurements, and Fig. 5-right in the case of paired measurements.

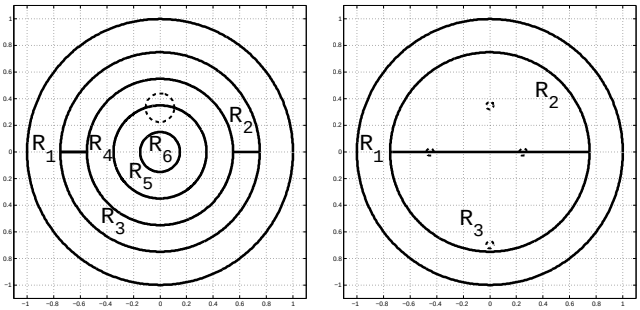

Figure 1: Two geometries of the background and of the inclusions (displayed in dashed lines). Left: six regions and one circular inclusion. Right: three regions and four small circular inclusions. Notice: the inclusion can fall on the interface between different regions.

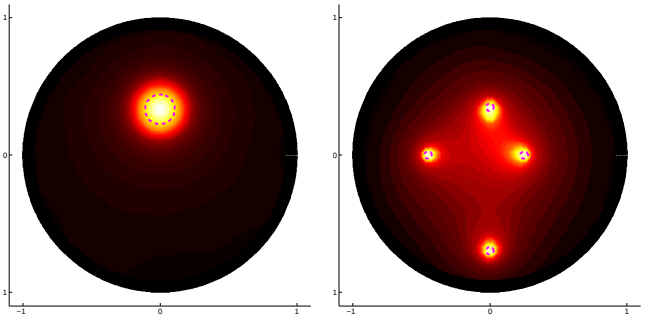

Figure 2: Reconstructions obtained in the case of homogeneous background, *i.e.* $\sigma_B \equiv 1$. No artificial noise.

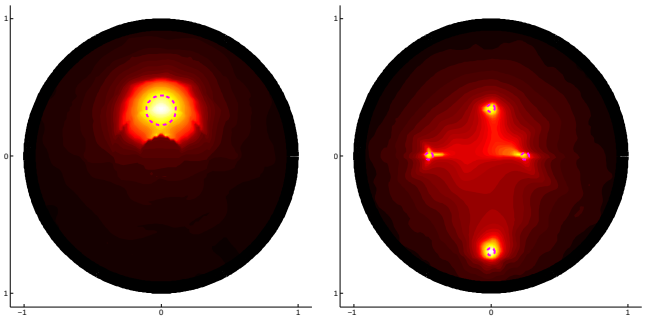

Figure 3: Reconstructions obtained in the case of inhomogeneous but deterministic background, with σ_B given by (1) and two orders of magnitude jumps between different regions. No artificial noise.

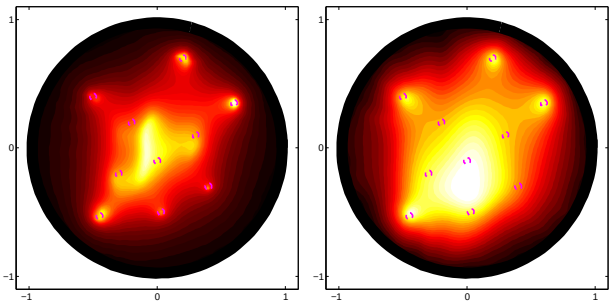

Figure 4: Reconstructions obtained in the case of inhomogeneous deterministic background (2). Left no artificial noise. Right 0.1% artificial noise.

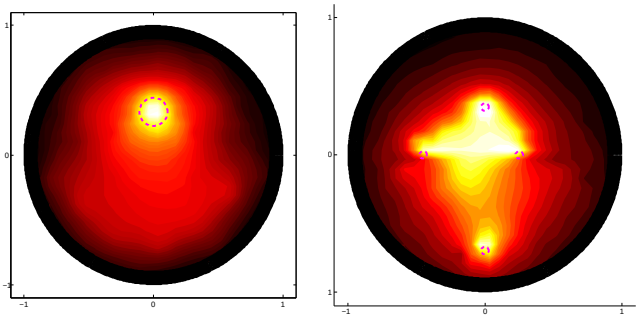

Figure 5: Reconstructions obtained in the case of uncertain background (3). Left: case of arbitrary measurements, no artificial noise. Right: case of paired measurements, no artificial noise.

References

[1] A. Kirsch and N. Grinberg, *The Factorization Method for inverse problems*, Oxford University Press, 2008.

[2] H. Haddar and G. Migliorati, *Numerical analysis of the Factorization Method for Electrical Impedance Tomography in inhomogeneous isotropic medium*, INRIA RR-7801, 2011.

[3] H. Haddar and G. Migliorati, *Numerical analysis of the Factorization Method for EIT with piecewise constant uncertain background* , submitted.

Reconstruction of piecewise constant Robin parameter in two or three dimensional case

S. Chaabane[1,*], **I. Feki**[1], **N. Mars**[1]
[1]Laboratory of Mathematics LAMHA-LR 11ES52, Department of Mathematics, Faculty of Sciences of Sfax, Sfax University, BP 1171, Sfax 3000, Tunisia.
[*]Email: slim.chaabane@fsm.rnu.tn

Abstract

We are concerned with the inverse problem of identification of an unknown piecewise constant Robin parameter arising in the corrosion detection by electrostatic boundary measurements in both two and three dimensional cases.

Introduction

In this paper, we are interested in the reconstruction of an unknown piecewise constant Robin parameter $\overline{q}$ by boundary measurements.

Several numerical methods have been proposed for the identification of the Robin inverse problem in some admissible sets of regular functions [2], [4], [6]. These methods do not apply in the reconstruction of discontinuous parameters.

In the case of piecewise constant Robin parameter, a new variational formulation using a regularization technique based on Modica-Mortola functional, has been recently proposed by B. Jin and J. Zou [5]. This method has the advantage of being robust to noise as it was shown through the numerical tests presented in [5]. However, the regularization of the class of admissible parameters by H^1 functions naturally involves a large number of parameters especially when the unknown Robin parameter has a limited number of singularities surfaces.

We present in this paper a numerical method for the identification of a singular piecewise Robin parameter $\overline{q}$ by making use of the Kohn-Vogelius cost function J. We prove differentiability of J with respect to the singularities surfaces of the Robin parameter in two or three dimensional cases.

1 The Kohn-Vogelius function

Let Ω be a simply connected bounded domain of $\mathbb{R}^2$ or $\mathbb{R}^3$ with $\mathcal{C}^{1,\alpha}$ boundary $\partial\Omega$; $\alpha \in]0,1[$. We designate by Γ_u and Γ_d two $\mathcal{C}^{1,\alpha}$ nonempty connected disjoint open parts of $\partial\Omega$ such that $\partial\Omega = \overline{\Gamma}_u \cup \overline{\Gamma}_d$.

Let $n \in \mathbb{N}^*$ and $m > 0$. We denote by $\mathcal{T}$ the set of all nonempty connected open subsets of Γ_u with Lipschitz boundary, by $\mathcal{V}_{ad}^n$ the set of admissible singularities surfaces:

$$\mathcal{V}_{ad}^n = \left\{ \begin{array}{c} (\vartheta_i)_{i=0,\dots,n} \ / \ \vartheta_i \in \mathcal{T} \ ; \ \vartheta_i \cap \vartheta_j = \emptyset \text{ if } i \neq j \\ \text{and} \quad \bigcup_{i=0}^n \overline{\vartheta}_i = \overline{\Gamma}_u \end{array} \right\}$$

and by $\mathbf{Q}_{ad}^n$ the set of admissible Robin parameters:

$$\mathbf{Q}_{ad}^n = \left\{ \begin{array}{l} q = \displaystyle\sum_{i=0}^{n} c_i \chi_{\vartheta_i} \ /(\vartheta_i) \in \mathcal{V}_{ad}^n, \ / \ c_i > 0, \text{ and} \\ |c_i - c_j| \geq m \ / \text{if } (i \neq j \text{ and } \ \overline{\vartheta}_i \cap \overline{\vartheta}_j \ \neq \ \emptyset) \end{array} \right.$$

Let $\Phi \in \ L^2(\Gamma_d)$ denotes the imposed current flux; $\phi \ \not\equiv 0$ and f be the potential measurement.

For $q \in \mathbf{Q}_{ad}^n$, we denote by $u_{q,N}$ the solution of the following Neumann-Robin problem $(\mathcal{N}.\mathcal{R})$:

$$(\mathcal{N}.\mathcal{R}) \left\{ \begin{array}{lll} \triangle u = 0 & \text{in} & \Omega, \\ \partial_n u = \Phi & \text{on} & \Gamma_d, \\ \partial_n u + qu = 0 & \text{on} & \Gamma_u, \end{array} \right.$$

and by $u_{q,D}$ the solution of the following problem:

$$(\mathcal{D}.\mathcal{R}) \left\{ \begin{array}{lll} \triangle u = 0 & \text{in} & \Omega, \\ u = f & \text{on} & \Gamma_d, \\ \partial_n u + \ q \ u = 0 & \text{on} & \Gamma_u. \end{array} \right.$$

The inverse problem, subject of our present study is the following:

$$(\mathcal{I}.\mathcal{P}) \left\{ \begin{array}{l} \text{Given} \ \ (\phi, f) \text{ on } \Gamma_d, \\ \text{recover} \ \ q \in \mathbf{Q}_{ad}^n, \text{ such that } u_{q,N} \ = f \text{ on } \Gamma_d \end{array} \right.$$

Referring to [1], [3], the inverse problem $(\mathcal{I}.\mathcal{P})$ has only one solution denoted by $\overline{q}$ which is the unique minimum of the Kohn-Vogelius cost function J:

$$J(q) = \int_\Omega |\nabla u_{q,N} - \nabla u_{q,D}|^2 + \int_{\Gamma_u} q|u_{q,N} - u_{q,D}|^2.$$

Moreover, the derivative of J w.r.t. c_i is given by:

$$\partial_{c_i} J(q) \ = \ \int_{\vartheta_i} (u_{q,D}^2 - u_{q,N}^2).$$

2 Differentiability of J with respect to the singularities surfaces of q

In this section, we prove the differentiability of J with respect to the singularities surfaces of q in both two and three dimensional cases despite the fact that the states $u_{q,N}$ and $u_{q,D}$ are not differentiable.

2.1 Derivative in the two-dimensional case

In this part, we suppose that the curve Γ_u is parameterized by a $\mathcal{C}^{1,\alpha}$ function $\psi : [0,1] \longmapsto \mathbb{R}^2$.

Let $q = \sum_{i=0}^{n} c_i \chi_{\vartheta_i} \in \mathbf{Q}_{ad}^n$, where $\vartheta_i = \psi([\ \alpha_i, \alpha_{i+1}[)$ and $m_i = \psi(\alpha_i)$. Then we have:

$$\partial_{m_i} J(q) = (c_{i-1} - c_i)\ \left(u_{q,D}^2(m_i) - u_{q,N}^2(m_i)\right) |\psi'(\alpha_i)|.$$

2.2 Derivative in the three-dimensional case

In this section, Γ_u is assumed to be a surface parameterized by a $\mathcal{C}^{1,\alpha}$ function $\Psi : [0,1]\times[0,1] \longrightarrow \mathbb{R}^3$ for some $\alpha \in]0,1[$ and $\mathcal{F}$ be the set of $\mathcal{C}^{1,\alpha}$ functions $\varphi : [0,1] \to [0,1]$.

For every $\varphi \in \mathcal{F}$, we denote by $\mathcal{C}_\varphi$ the graph of φ and by:

$$D_1^\varphi = \{(x,y) \in [0,1] \times [0,1] \ / \ y \leq \varphi(x)\}$$

$$D_2^\varphi = \{(x,y) \in [0,1] \times [0,1] \ / \ y \geq \varphi(x)\}.$$

For $i = 1, 2$, we denote by: $V_i^\varphi = \psi(D_i^\varphi)$. and we suppose that the set of admissible Robin parameter $\mathbf{Q}_{ad}$ is defined by:

$$\mathbf{Q}_{ad} = \left\{ q = c_1 \chi_{V_1^\varphi} + c_2 \chi_{V_2^\varphi};\ \varphi \in \mathcal{F};\ c_1 \neq c_2;\ q > 0 \right\}.$$

Let $h > 0$, $g \in \mathcal{F}$ and $D_{1,h} = \{(x,y) \in [0,1]^2; \varphi(x) \leq y \leq \varphi(x) + h.g(x)\}$. For $q \in \mathbf{Q}_{ad}$, we denote by:

$$q_h = q_h(X) = \begin{cases} c_1 & \text{if} \quad X \in V_{1,h} := \Psi(D_{1,h}) \\ q(X) & \text{else.} \end{cases}$$

a small perturbation of q. Then, we have:

$$\lim_{h \to 0^+} \frac{J(q_h) - J(q)}{h} = (c_1 - c_2) \int_0^1 g(x)\eta(x)dx, \text{ where}$$

$$\eta(x) = \left\| (\tfrac{\partial \Psi}{\partial x} \wedge \tfrac{\partial \Psi}{\partial y})(x, \varphi(x)) \right\| \left[(u_{q,D}^2 - u_{q,N}^2)(\Psi(x, \varphi(x))) \right].$$

3 Numerical results

In this section, we present some numerical results in two or three dimensional cases using an algorithm of gradient type. The potential measurements have been simulated by synthetic data obtained by means of numerical computations solving the forward problem $(\mathcal{N}.\mathcal{R})$.

Figures 1 and 2 represent the curves of $\overline{q}$ (in red), the initialization q_0 (in green) and the reconstructed parameter q (in blue) where Ω is the unit disk and $\Gamma_u = \{e^{i\theta}\ ;\ 0 \leq \theta \leq \pi\}$ in the case of 2D and Ω is the unit cube where $\Gamma_u = [0, 1 \times [0,1] \times \{1\}$ in 3D.

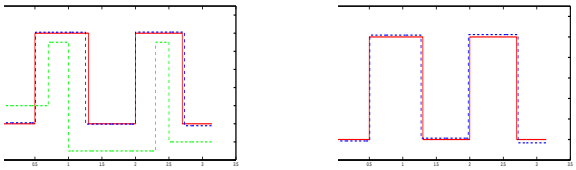

0% of noise 5% of noise

Figure 1: Reconstruction of $\overline{q}$ in 2D.

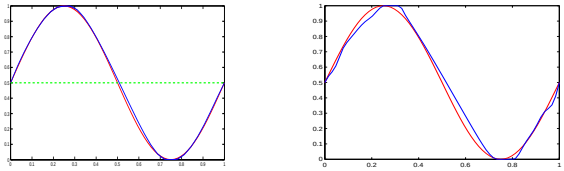

0% of noise 5% of noise

Figure 2: Reconstruction of the discontinuity curve $\overline{\mathcal{C}}$ of $\overline{q}$ in 3D.

References

[1] S. Chaabane and M. Jaoua, *Identification of Robin coefficients by the means of boundary measurements*, Inverse Problems, **15** (1999), pp. 1425–1438.

[2] S. Chaabane, C. Elhechmi and M. Jaoua, *A stable recovery algorithm for the Robin inverse problem*, Mathematics and computers in simulation, **66** (2004), pp. 367–383.

[3] S. Chaabane, J. Ferchichi and K. Kunisch, *Differentiability properties of the L^1-tracking functional and application to the Robin inverse problem*, Inverse problems **20** (2004), pp. 1083–1097.

[4] D. Fasino and G. Inglese, *An inverse Robin problem for Laplace equation: theoretical results and numerical methods*, Inverse Problems, **15** (1999), pp. 41–8.

[5] B. Jin and J. Zou, *Numerical estimation of piecewise constant Robin coefficient*, SIAM Journal on control and optimization, **48 (3)** (2009), pp. 1977–2002.

[6] B. Jin and J. Zou, *Numerical estimation of the Robin coefficient in a stationary diffusion equation*, IMA Journal of Numerical Analysis, **30 (3)** (2010), pp. 677–701.

3.8 Numerical methods for time dependent wave problems

Transient BEM-FEM coupling for symmetric hyperbolic Friedrichs systems on unbounded domains

T. Abboud[1], P. Joly[2], J. Rodríguez[3,*]
[1] CMAP Ecole Polytechnique, 91128 Palaiseau, France
[2] POEMS project, INRIA Rocquencourt, Domaine de Voluceau, B.P. 105, 78153 Le Chesnay, France
[3] Departamento de Matemática Aplicada, USC, Santiago de Compostela, A Coruña, Spain
*Email: jeronimo.rodriguez@usc.es

Abstract
We are interested in the numerical simulation of wave propagation phenomena modeled by Friedrichs hyperbolic systems of the form (1) on unbounded domains containing heterogeneities. To do so we propose a hybrid algorithm based on the retarded potential method combined with a discontinuous Galerkin (DG) approximation with upwind fluxes and finite differences in time. The numerical procedure is stable by construction when the CFL in the interior domain is satisfied.

1 Symmetric hyperbolic Friedrichs systems

Our goal is to numerically solve the following PDE that, for our purposes, it is useful to write as a transmission problem between two non-overlapping subdomains Ω_e (unbounded and homogeneous) and Ω_i (bounded and eventually heterogeneous) with the common boundary Γ

$$\left|\begin{array}{rcll} \boldsymbol{M}\dfrac{\partial \boldsymbol{u}_i}{\partial t} + \displaystyle\sum_{j=1}^{d} \boldsymbol{A}_j \dfrac{\partial \boldsymbol{u}_i}{\partial x_j} & = & \boldsymbol{f}_i, & \text{in } \Omega_i, \\ \boldsymbol{u}_i(t=0) & = & \boldsymbol{u}_0, & \text{in } \Omega_i, \\ \boldsymbol{M}\dfrac{\partial \boldsymbol{u}_e}{\partial t} + \displaystyle\sum_{j=1}^{d} \boldsymbol{A}_j \dfrac{\partial \boldsymbol{u}_e}{\partial x_j} & = & \boldsymbol{0}, & \text{in } \Omega_e, \\ \boldsymbol{u}_e(t=0) & = & \boldsymbol{0}, & \text{in } \Omega_e, \\ [\![\boldsymbol{A}(\boldsymbol{n})\boldsymbol{u}]\!]_\Gamma & = & \boldsymbol{0}, & \text{on } \Gamma. \end{array}\right. \tag{1}$$

In the previous system $\boldsymbol{A}_j,\ j \in \{1,\dots,d\}$ and $\boldsymbol{M}$ are $n \times n$ symmetric matrices (the latter is also positive definite). Additionally $\boldsymbol{n}$ is the normal unit vector outward to Ω_i, $\boldsymbol{A}(\boldsymbol{n}) = \sum_{j=1}^{d} \boldsymbol{n}_j \boldsymbol{A}_j$ and $[\![\boldsymbol{A}(\boldsymbol{n})\boldsymbol{u}]\!]_\Gamma = \boldsymbol{A}(\boldsymbol{n})\boldsymbol{u}_e - \boldsymbol{A}(\boldsymbol{n})\boldsymbol{u}_i$.

2 The integral equation in Ω_e

To derive an integral equation equivalent to the equations in Ω_e we start by introducing the following auxiliary problem (for which we assume that the coefficients in the equations are homogeneous not only in Ω_e but also in Ω_i even if we use the same notation)

$$\left|\begin{array}{rcll} \boldsymbol{M}\dfrac{\partial \boldsymbol{u}_{\boldsymbol{\varphi}}}{\partial t} + \displaystyle\sum_{j=1}^{d} \boldsymbol{A}_j \dfrac{\partial \boldsymbol{u}_{\boldsymbol{\varphi}}}{\partial x_j} & = & \boldsymbol{0}, & \text{in } \Omega_i \cup \Omega_e, \\ \boldsymbol{u}_{\boldsymbol{\varphi}}(t=0) & = & \boldsymbol{0}, & \text{in } \Omega_i \cup \Omega_e, \\ [\![\boldsymbol{A}(\boldsymbol{n})\ \boldsymbol{u}_{\boldsymbol{\varphi}}]\!]_\Gamma & = & \boldsymbol{A}(\boldsymbol{n})\ \boldsymbol{\varphi}, & \text{on } \Gamma, \end{array}\right. \tag{2}$$

where the datum $\boldsymbol{\varphi}$ is a function defined in $\Gamma \times [0,T]$. We define the integral operator $\mathcal{X}_\Gamma(\cdot)$ by

$$\mathcal{X}_\Gamma\ \boldsymbol{\varphi} = \frac{1}{2}\Big(\boldsymbol{A}(\boldsymbol{n})(\boldsymbol{u}_{\boldsymbol{\varphi}})_e + \boldsymbol{A}(\boldsymbol{n})(\boldsymbol{u}_{\boldsymbol{\varphi}})_i\Big). \tag{3}$$

Defining the function $\boldsymbol{w}$ as the extension by $\boldsymbol{0}$ of exterior solution $\boldsymbol{u}_e$ we realize that $\boldsymbol{w} = \boldsymbol{u}_{\boldsymbol{\varphi}}$ for $\boldsymbol{\varphi} = \mathcal{P}_{\mathrm{Im}\boldsymbol{A}(\boldsymbol{n})}(\boldsymbol{u}_e)$ (where $\mathcal{P}_Y(\cdot)$ is the projection from $\mathbb{R}^n$ into Y). In consequence we have (the function γ is supposed to be strictly positive)

$$\mathcal{X}_\Gamma\ \boldsymbol{\varphi} + \gamma\ \mathcal{P}_{\mathrm{Ker}\boldsymbol{A}(\boldsymbol{n})}\ \boldsymbol{\varphi} = \frac{1}{2}\ \boldsymbol{A}(\boldsymbol{n})\ \boldsymbol{\varphi}. \tag{4}$$

Multiplying by a test function and integrating in $\Gamma \times [0,T]$ we get the following variational formulation

$$\overbrace{\int_0^T \int_\Gamma \Big(\mathcal{X}_\Gamma\ \boldsymbol{\varphi} + \gamma\ \mathcal{P}_{\mathrm{Ker}\boldsymbol{A}(\boldsymbol{n})\boldsymbol{\varphi}}\Big) \cdot \boldsymbol{\psi}\ \mathrm{d}\gamma\ \mathrm{d}t}^{b_T(\boldsymbol{\varphi},\boldsymbol{\psi})} = \frac{1}{2}\int_0^T \int_\Gamma \boldsymbol{A}(\boldsymbol{n})\ \boldsymbol{u}_i \cdot \boldsymbol{\psi}\ \mathrm{d}\gamma\ \mathrm{d}t, \tag{5}$$

where we have used the transmission condition to couple with the interior. It can be shown that

$$b_T(\boldsymbol{\varphi},\boldsymbol{\varphi}) = \frac{1}{2}\int_{\Omega_i \cup \Omega_e} \boldsymbol{M}\boldsymbol{u}_{\boldsymbol{\varphi}}(T) \cdot \boldsymbol{u}_{\boldsymbol{\varphi}}(T)\ \mathrm{d}x + \int_0^T \int_\Gamma \gamma\ |\mathcal{P}_{\mathrm{Ker}\boldsymbol{A}(\boldsymbol{n})}\boldsymbol{\varphi}|^2\ \mathrm{d}\gamma\ \mathrm{d}t > 0,$$

which provides the positivity of the $b_T(\cdot,\cdot)$ (a weak coercivity property for short time can be also shown).

3 A DG variational formulation in Ω_i

To derive a DG formulation of the interior equations we introduce $\mathcal{T}_h$ a mesh of Ω_i. Let $\mathcal{F}_h$ be the set of internal faces of the mesh. Standard techniques [2] provide the following variational formulation

$$\begin{aligned}
&\sum_{K\in\mathcal{T}_h}\frac{\mathrm{d}}{\mathrm{d}t}\int_K \boldsymbol{M}\boldsymbol{u}_i\cdot\boldsymbol{w}\ \mathrm{d}x\\
&+\sum_{K\in\mathcal{T}_h}\sum_{j=1}^{d}\int_K\Big(\boldsymbol{A}_j\frac{\partial\boldsymbol{u}_i}{\partial x_j}\cdot\boldsymbol{w}\ -\ \boldsymbol{A}_j\frac{\partial\boldsymbol{w}}{\partial x_j}\cdot\boldsymbol{u}_i\Big)\ \mathrm{d}x\\
&+\frac{1}{4}\sum_{F\in\mathcal{F}_h}\int_F\Big(\,[\![\boldsymbol{A}(\boldsymbol{n})\ \boldsymbol{u}_i]\!]\cdot[\![\boldsymbol{w}]\!]-[\![\boldsymbol{A}(\boldsymbol{n})\ \boldsymbol{w}]\!]\cdot[\![\boldsymbol{u}_i]\!]\Big)\ \mathrm{d}\gamma\\
&+\frac{1}{2}\sum_{F\in\mathcal{F}_h}\int_F\alpha|\boldsymbol{A}(\boldsymbol{n})|\,[\![\boldsymbol{u}_i]\!]\cdot[\![\boldsymbol{w}]\!]\ \mathrm{d}\gamma\\
&-\frac{1}{2}\sum_{K\in\mathcal{T}_h}\int_K\mathrm{div}\ \boldsymbol{A}\ \boldsymbol{u}_i\cdot\boldsymbol{w}\ \mathrm{d}x\\
&+\frac{1}{2}\int_\Gamma\boldsymbol{A}(\boldsymbol{n})\ \boldsymbol{\varphi}\cdot\boldsymbol{w}\ \mathrm{d}\gamma\ =\ \sum_{K\in\mathcal{T}_h}\int_K\boldsymbol{f}_i\cdot\boldsymbol{w}\ \mathrm{d}x,
\end{aligned}\tag{6}$$

where the matrix $\mathrm{div}\ \boldsymbol{A}\ =\ \sum_{j=1}^{d}\partial\boldsymbol{A}_j/\partial x_j$ is assumed to be positive and where we have selected the following numerical fluxes for the internal boundaries of the element K ($\alpha\in[0,1]$)

$$F_K(\boldsymbol{u}_K,\boldsymbol{u}_{\widetilde{K}})\ =\ \boldsymbol{A}(\boldsymbol{n})\frac{\boldsymbol{u}_K+\boldsymbol{u}_{\widetilde{K}}}{2}+\frac{\alpha}{2}|\boldsymbol{A}(\boldsymbol{n})|(\boldsymbol{u}_K-\boldsymbol{u}_{\widetilde{K}}).$$

The bilinear forms involved in (6) have the following properties: i) the one in the first line is symmetric and positive definite, ii) the one composed by the second and third lines is skew, iii) those in the fourth and fifth lines (including the minus sign) are symmetric and positive, v) the one in the sixth line accounts for the coupling.

In consequence the coupled problem is given by equations (5) and (6). From both equations we can get the following energy decay (in absence of volume forces)

$$\begin{aligned}
&\sum_{l\in\{i,e\}}\frac{1}{2}\int_{\Omega_l}\boldsymbol{M}\boldsymbol{u}_l(T)\cdot\boldsymbol{u}_l(T)\ \mathrm{d}x-\frac{1}{2}\int_{\Omega_i}\boldsymbol{M}\boldsymbol{u}_0\cdot\boldsymbol{u}_0\ \mathrm{d}x\\
&\qquad=\ \frac{1}{2}\int_0^T\int_{\Omega_i}\sum_{j=1}^{d}\frac{\partial\boldsymbol{A}_j}{\partial x_j}\ \boldsymbol{u}_i\cdot\boldsymbol{u}_i\ \mathrm{d}x\ \mathrm{d}t.
\end{aligned}$$

4 Discretization for the coupled problem

The discretization of the coupled problem is based on the following ideas: i) the left hand side of (5) is approximated through a space-time Galerkin procedure (see [1] for the details in the acoustic case), ii) all the terms in (6) not involved in the coupling are discretized with a DG standard approximation in space combined with explicit finite differences in time (an extension of the leap frog scheme allowing to include dissipative terms), iii) following the ideas introduced in [1], the coupling terms are specially design to satisfy a discrete energy estimate. This leads to the following matrix formulation of the discrete problem

$$\left|\begin{aligned}
&\mathbb{M}\ \frac{\boldsymbol{U}_i^{n+\frac{3}{2}}-\boldsymbol{U}_i^{n-\frac{1}{2}}}{2\Delta t}\ +\ \mathbb{A}\ \boldsymbol{U}_i^{n+\frac{1}{2}}\ +\ \mathbb{S}_\alpha\ \boldsymbol{U}_i^{n-\frac{1}{2}}\ -\\
&\qquad\mathbb{D}\ \frac{\boldsymbol{U}_i^{n+\frac{3}{2}}\ +\ \boldsymbol{U}_i^{n-\frac{1}{2}}}{2}\ +\ \mathbb{C}\ \boldsymbol{U}_e^{n+\frac{1}{2}}\ =\ \boldsymbol{F}_i^{n+\frac{1}{2}},\\
&\sum_{m=0}^{n}\mathbb{B}_{n-m}\ \boldsymbol{U}_e^{m+\frac{1}{2}}\ +\ \mathbb{P}_\gamma\ \boldsymbol{U}_e^{n+\frac{1}{2}}\ \Delta t\ -\\
&\qquad\mathbb{C}^t\ \frac{\boldsymbol{U}_i^{n+\frac{3}{2}}\ +\ \boldsymbol{U}_i^{n-\frac{1}{2}}}{2}\ \Delta t\ =\ 0.
\end{aligned}\right.\tag{7}$$

Assuming $\boldsymbol{F}_i^{n+\frac{1}{2}}\ =\ \boldsymbol{0}$, the discrete solution can be shown to satisfy the following discrete energy decay (the matrix $\mathbb{S}_\alpha-\mathbb{D}$ is symmetric and positive)

$$\begin{aligned}
&\mathcal{E}_{i,\alpha}^n\ +\ \overbrace{\sum_{l=0}^{n}\sum_{m=0}^{n}\mathbb{B}_{n-m}\ \boldsymbol{U}_e^{m+\frac{1}{2}}\cdot\boldsymbol{U}_e^{l+\frac{1}{2}}}^{>0}\ =\ \mathcal{E}_{i,\alpha}^0\ -\\
&\Delta t\sum_{m=0}^{n}\mathbb{P}_\gamma\ \boldsymbol{U}_e^{m+\frac{1}{2}}\cdot\boldsymbol{U}_e^{m+\frac{1}{2}}\ +\\
&\Delta t\sum_{l=1}^{n-1}(\mathbb{D}\ -\ \mathbb{S}_\alpha)\frac{\boldsymbol{U}_i^{l+\frac{3}{2}}\ +\ \boldsymbol{U}_i^{l-\frac{1}{2}}}{2}\cdot\frac{\boldsymbol{U}_i^{l+\frac{3}{2}}\ +\ \boldsymbol{U}_i^{l-\frac{1}{2}}}{2},
\end{aligned}$$

where ($\mathbb{M}_\alpha\ =\ \mathbb{M}-\Delta t\ \mathbb{S}_\alpha$)

$$\begin{aligned}
\mathcal{E}_{i,\alpha}^n\ =\ \frac{1}{4}\Big[&\mathbb{M}_\alpha\boldsymbol{U}_i^{n+\frac{1}{2}}\cdot\boldsymbol{U}_i^{n+\frac{1}{2}}\ +\ \mathbb{M}_\alpha\boldsymbol{U}_i^{n-\frac{1}{2}}\cdot\boldsymbol{U}_i^{n-\frac{1}{2}}\\
&-2\Delta t\ \mathbb{A}\boldsymbol{U}_i^{n+\frac{1}{2}}\cdot\boldsymbol{U}_i^{n-\frac{1}{2}}\Big],
\end{aligned}$$

is a positive discrete energy when the usual CFL condition on the interior domain is satisfied. This provides a robust BEM-FEM transient coupling.

References

[1] T. Abboud et al. Coupling DG methods and RP for transient wave propagation on unbounded domains. *JCP*, 230 (2011), 5877–5907.

[2] J. S. Hesthaven, T. Warburton: Nodal DG methods, Texts in Applied Mathamatics, vol. 54, Springer, New York, 2008.

Energetic BEM-FEM coupling for wave propagation in unbounded domains

A. Aimi[1,*], **M. Diligenti**[1], **A. Frangi**[2], **C. Guardasoni**[1]
[1] Dept. of Mathematics and Computer Science, University of Parma, Italy
[2] Dept. of Structural Engineering, Polytechnic of Milan, Italy.
*Email: alessandra.aimi@unipr.it

Abstract

Starting from a recently developed energetic space-time weak formulation of boundary integral equations related to wave propagation problems defined on single and multi domains, a coupling algorithm is presented, which allows a flexible use of finite and boundary element methods as local discretization techniques, in order to efficiently treat unbounded media. Partial differential equations associated to boundary integral equations will be weakly reformulated by the energetic approach too, and a particular emphasis will be given to the stability analysis of the proposed method. Several numerical results on wave propagation model problems will be presented and discussed.

Introduction

Even if the Finite Element Method (FEM) has obviously a dominant status in the field of computational techniques in physics and engineering, mostly because of its great flexibility and wide range of applicability, discretization approaches based on integral equations are superior for certain classes of problems. For instance, the numerical study of wave propagation in unbounded media in two or three dimension still represents a challenging issue for domain methods. In this context, time-dependent problems modeled by hyperbolic partial differential equations (PDEs) can be dealt with the boundary integral equations (BIEs) method. For the discretization phase, Boundary Element Methods (BEMs) are successfully applied in seismology, in particular for the study of the soil-structure interaction, in acoustics and in the analysis of the electromagnetic scattering, taking advantage of dimensionality reduction and of the implicit enforcement of radiation conditions at infinity.

When one deals with regions having different material properties (e.g. layered soils) or even different physics (e.g. in solid-fluid coupling or wave-soil-structure interaction) domain decomposition is needed. In this framework, there are advantages in combining finite and boundary element techniques. BEM, also when formulated directly in the space-time domain, has attracted particular interest for its high accuracy, the simplicity of imposing the interface conditions in problems defined on multi domains, the implicit fulfillment of radiation conditions at infinity, the low cost of discretization when problems are defined over unbounded domains. The use of BIEs and BEMs, however, is complex and not particularly efficient in presence of non-linearities localized in small parts of the domain. In this case, the classical differential models and related numerical techniques, such as the finite difference method (FDM) and FEM, help to efficiently deal with the nonlinear part of the problem, but require, in general, a fine discretization of the entire domain with a significant increase in computational cost.

To summarize, BEM and FEM methods for the approximation of systems of BIEs and PDEs are nowadays understood to be complementary rather than concurrent and a suitable coupling of these two techniques can take advantage of what both offer.

In the last decades, contributions to BEM-FEM coupling, in the context of hyperbolic problems, started to appear, especially analyzing stability issues (see e.g. [1]). In this work, we propose an energetic BEM-FEM coupling procedure, based on recently obtained results [2]-[5]. In particular, taking advantage of the theoretical stability analysis of the coupling technique proposed in [6], where simple one dimensional benchmarks were discussed, here the focus is the extension of the energetic BEM-FEM procedure for the approximate resolution of wave propagation model problems in higher dimension.

1 Model problem

Let Ω be an open bounded set in $\mathbb{R}^n$, $n = 2, 3$ with sufficiently smooth boundary Γ_N. Let us consider the decomposition $\mathbb{R}^n \setminus \Omega = \Omega_1 \cup \Omega_2$, with $\Omega_1 \cap \Omega_2 = \emptyset$ and $\bar{\Omega}_1 \cap \bar{\Omega}_2 = \Gamma$. The two non-overlapping subdomains can be constituted by different materials with typical constants μ_1, μ_2, and Ω_1, differently from Ω_2, is unbounded, as depicted in Figure 1.

Having set c_i the propagation velocity of a perturba-

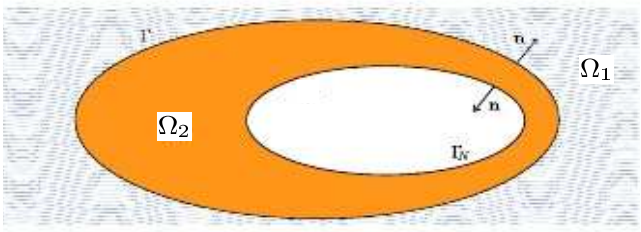

Figure 1: Space domain of the model problem.

tion in the i-th subdomain, the model problem which will be taken into account is the following: for $i = 1, 2$

$$\begin{cases} \Delta u_i(x,t) - \frac{1}{c_i^2}\ddot{u}_i(x,t) = f_i(x,t), & x \in \Omega_i,\ t \in [0,T] \\ u_i(x,0) = \dot{u}_i(x,0) = 0, & x \in \Omega_i \end{cases}$$

with Neumann boundary condition $p_2(x,t) := \mu_2 \frac{\partial u_2}{\partial n_x}(x,t) = \bar{p}(x,t)$ on $\Sigma_N := \Gamma_N \times [0,T]$ and with standard continuity and equilibrium conditions between the two materials, i.e. $u_1(x,t) = u_2(x,t)$, $p_1(x,t) = -p_2(x,t)$ on $\Sigma := \Gamma \times [0,T]$. The forcing term f_1 is trivial and suitably connected to f_2.
After a boundary integral reformulation of the differential problem in the subdomain Ω_1 which involves the classical boundary integral operator quartet V, K, K^*, D depending on the fundamental solution of the wave operator, the energetic weak formulation of the coupled problem reads:

$$\begin{cases} \frac{1}{\mu_1} < (V\dot{p}_1), q_1 > - < (K\dot{u}_{2|\Gamma}), q_1 > -\frac{1}{2} < \dot{u}_{2|\Gamma}, q_1 >= 0 \\ -\frac{1}{2} < p_1, \dot{v}_{2|\Gamma} > - < K^* p_1, \dot{v}_{2|\Gamma} > + \mu_1 < Du_{2|\Gamma}, \dot{v}_{2|\Gamma} > \\ \qquad -\mu_2 \mathcal{A}(v_2, u_2) = \mu_2 \mathcal{F}(v_2) - << \dot{v}_{2|\Gamma_N}, \bar{p} >>, \end{cases}$$

with $< \cdot, \cdot >=< \cdot, \cdot >_{L^2(\Sigma)}$, $<< \cdot, \cdot >=< \cdot, \cdot >>_{L^2(\Sigma_N)}$, $\mathcal{A}(v_2, u_2) := \int_0^T \int_{\Omega_2} \left[\nabla \dot{v}_2 \cdot \nabla u_2 + \frac{1}{c_2^2}\, \dot{v}_2\, \ddot{u}_2\right] dx\, dt$ and $\mathcal{F}(v_2) := \int_0^T \int_{\Omega_2} \dot{v}_2\, f_2\, dx\, dt$.

2 Space-time Galerkin discretization

For time discretization we consider a uniform decomposition of the time interval $[0,T]$ with time step $\Delta t = T/N_{\Delta t}, N_{\Delta t} \in \mathbb{N}^+$, generated by the $N_{\Delta t} + 1$ time-knots $t_k = k\,\Delta t, \quad k = 0, \cdots, N_{\Delta t}$, and we choose temporally piecewise constant shape functions for the approximation of p_1 and piecewise linear shape functions for the approximation of u_2, although higher degree shape functions can be used. Double integrals in time have been performed analytically.

For the space discretization, we consider the bounded subdomain Ω_2 (suitably approximated by a domain) of polygonal/polyhedral type and a mesh $\mathcal{T}_h = \{e_1, \cdots, e_{M_h}\}$, constituted by M_h triangles/tetrahedra with $diam(e_i) \le h$, $e_i \cap e_j = \emptyset$ if $i \neq j$ and such that $\bigcup_{i=1}^{M_h} \bar{e}_i = \overline{\Omega}_2$. The mesh $\mathcal{T}_{\Gamma,h}$ on the interface will be the restriction of $\mathcal{T}_h$ to Γ. We choose piece-wise constant basis functions related to $\mathcal{T}_{\Gamma,h}$ for the approximation of p_1 over the interface and piece-wise linear continuous functions related to $\mathcal{T}_h$ for the approximation of u_2 in Ω_2. Double integrals over the interface Γ have been performed as described in [4].
Several results coming from the related energetic time-marching procedure will be presented and discussed.

References

[1] T. Abboud, P. Joly, J. Rodriguez and I. Terrasse, *Coupling discontinuous Galerkin methods and retarded potentials for transient wave propagation on unbounded domains*, J. Comput. Physics, **230** N.15 (2011), pp. 5877–5907.

[2] A. Aimi and M. Diligenti, *A new space-time energetic formulation for wave propagation analysis in layered media by BEMs*, Int. J. Numer. Meth. Engrg., **75** (2008), pp. 1102–1132.

[3] A. Aimi, S.Gazzola and C.Guardasoni, *Energetic Boundary Element Method analysis of wave propagation in 2D multilayered media*, Math. Methods Appl. Sciences, **35** (2012), pp. 1140–1160.

[4] A. Aimi, M. Diligenti, A. Frangi and C.Guardasoni, *A stable 3D energetic Galerkin BEM approach for wave propagation interior problems*, Engineering Analysis with Boundary Elements, **36** (2012), pp. 1756–1765.

[5] A. Aimi, M. Diligenti, A. Frangi and C.Guardasoni, *Neumann exterior wave propagation problems: computational aspects of 3D energetic Galerkin BEM*, Comp. Mech., DOI: 10.1007/s00466-012-0796-5 (2012), in press.

[6] A. Aimi, M. Diligenti, C.Guardasoni and S. Panizzi, *Energetic BEM-FEM coupling for wave propagation in layered media*, Communications in Applied and Industrial Mathematics, (2013), in press.

Discontinuous Galerkin Time-Domain method for nanophotonics

S. Lanteri[1], C. Scheid[1,2], J. Viquerat[1,*]
[1] Inria Sophia Antipolis, Nachos project-team
[2] Nice-Sophia Antipolis University, J. A. Dieudonné Lab.
*Email: jonathan.viquerat@inria.fr

Abstract

The numerical study of electromagnetic wave propagation in nanophotonic devices requires among others the integration of various types of dispersion models, such as the Drude one, in numerical methodologies. Appropriate approaches have been extensively developed in the context of the Finite Differences Time-Domain (FDTD) method, such as in [1] for example. For the discontinuous Galerkin time-domain (DGTD), stability and convergence studies have been recently realized for some dispersion models, such as the Debye model [2]. The present study focuses on a DGTD formulation for the solution of Maxwell's equations coupled to (i) a Drude model and (ii) a generalized dispersive model. Stability and convergence have been proved in case (i), and are under study in case (ii). Numerical experiments have been made on classical situations, such as (i) plane wave diffraction by a gold sphere and (ii) plane wave reflection by a silver slab.

1 Drude model

The Drude model describes the response of certain dispersive media to an electromagnetic wave propagating in a certain range of frequencies. The considered model permits to establish a dependency between the permittivity of the material and the angular frequency of the electromagnetic wave in the following form:

$$\varepsilon_{r,d}(\omega) = \varepsilon_\infty - \frac{\omega_d^2}{\omega^2 + i\omega\gamma_d},$$

where ω_d, γ_d and ω are respectively the plasma frequency and the damping constant of the medium, and the angular frequency. Adding a Drude dispersion model therefore implies a coupling, in the time domain, between the electric field $\mathbf{E}$ and an additional field, the dipolar current ($\mathbf{J}_p$), through an ODE whose solution we choose is here approximated in a DG framework. A centered fluxes DG method has been chosen to develop a numerical approximation of the problem, given the geometry and the inhomogeneous media to be considered. It is associated with a second-order Leap-Frog scheme in time, therefore inducing a non-dissipative scheme. A theoretical study of the latter has been made, demonstrating an error convergence in $O\left(h^{\min(s,p)} + \Delta t^2\right)$, where p is the spatial order of approximation, and s is related to the regularity assumptions made on the electromagnetic field.

2 Generalized dispersive model

Recently, several arbitrary dispersive models have been proposed, such as the Critical Points (CP) [3] and the Complex-Conjugate Pole-Residue Pairs (CCPRP) [1]. Here, another formulation is considered: in accordance with the fundamental theorem of algebra, the permittivity function is written as a decomposition of a constant, one zero-order pole (ZOP), a set of first-order generalized poles (FOGP), and a set of second-order generalized poles (SOGP). This leads to the following expression in the frequency domain:

$$\varepsilon_{r,g}(\omega) = \varepsilon_\infty - \frac{\sigma}{j\omega} - \sum_{l\in L_1} \frac{a_l}{j\omega - b_l} - \sum_{l\in L_2} \frac{c_l - j\omega d_l}{\omega^2 - e_l + j\omega f_l}.$$

This general writing allows an important flexibility for two reasons: (i) it unifies most of the common dispersion models in a single formulation (such as Drude, Drude-Lorentz and Debye media for example), and (ii) it permits to fit any experimental data set in a reasonable number of poles (and thus a reasonable number of coefficients). The stability and convergence properties of the resulting DG formulation seem at first glance to be a feasible extension of the Drude case, and are currently under investigation.

3 Numerical validations

First, a simple validation case has been set up in order to verify that the orders of convergence theoretically obtained for the Drude model based DGTD method were achieved. A unitary PEC cavity with dispersive properties defined by a Drude model is defined. A forced source current has been added to the

set of equations in order to obtain an analytical solution to compare with. The calculated convergence orders match the theoretical prediction, as presented in table 1.

Then, a more physical case is considered: a gold nanosphere of radius 20 nm, whose properties are described by a Drude model, is illuminated by a plane wave, the latter being modulated in time by a gaussian function. The discrete Fourier transform of the field is processed along the computation, and is in the end compared with the Mie solution[1] of the problem, which is taken as a reference solution. A good adequation has been found between the reference and the numerical solution, which is displayed on figure 1. Further accuracy and performance assessment will be performed on this fondamental case, then paving the way to situations of high interest in the nanophotonic domain.

Table 1: **Convergence orders with $\mathbb{P}_1$ and $\mathbb{P}_2$ approximations** for the PEC cavity case.

(a) Convergence rate, $\mathbb{P}_1$

Refinement	Convergence rate
$\frac{1}{50}$	–
$\frac{1}{75}$	1.2575
$\frac{1}{100}$	1.1197
$\frac{1}{125}$	1.1000
$\frac{1}{150}$	1.0614

(b) Convergence rate, $\mathbb{P}_2$

Refinement	Convergence rate
$\frac{1}{25}$	–
$\frac{1}{50}$	2.2004
$\frac{1}{75}$	2.0826
$\frac{1}{100}$	2.0366
$\frac{1}{125}$	2.0432

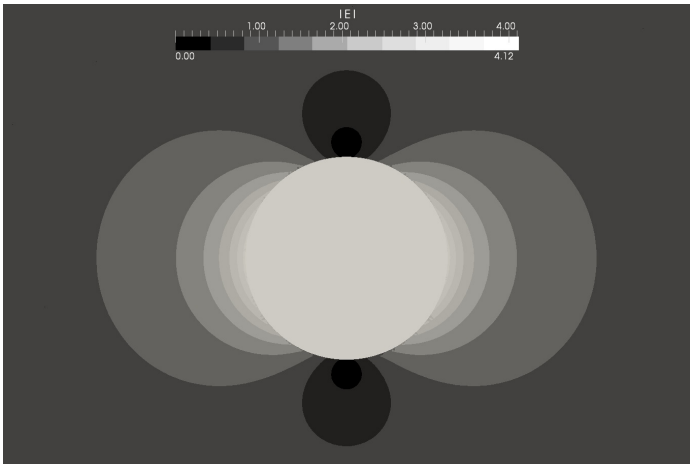

Figure 1: **E field magnitude in the frequency domain calculated by the DGTD method in the vicinity of the gold nanosphere.** The view is a $z = 0$ slice.

References

[1] M. Han, R. W. Dutton, and S. Fan. Model dispersive media in FDTD method with complex-conjugate pole-residue pairs. *IEEE Microwave and Wireless Components Letters*, 16:119 – 121, 2006.

[2] Stéphane Lanteri and Claire Scheid. Convergence of a discontinuous Galerkin scheme for the mixed time domain Maxwell's equations in dispersive media. *IMA Journal of Numerical Analysis*, 2012.

[3] A. Vial, T. Laroche, M. Dridi, and L. Le Cunff. A new model of dispersion for metals leading to a more accurate modeling of plasmonic structures using the FDTD method. *Applied Physics A*, 103:849 – 853, 2011.

[1] The Mie theory provides an analytical solution to diffraction problems in the case of spherical obstacles.

Runge-Kutta type Explicit Local Time-Stepping Methods

Marcus J. Grote[1], **Michaela Mehlin**[1,*], **Teodora Mitkova**[2]
[1] Department of Mathematics and Computer Science, University of Basel, Basel, Switzerland
[2]Department of Mathematics, University of Fribourg, Fribourg, Switzerland.
*Email: michaela.mehlin@unibas.ch

Abstract

We propose explicit local time-stepping (LTS) schemes of high order based either on classical or low-storage Runge-Kutta schemes for the simulation of wave phenomena. By using smaller time steps precisely where smaller elements in the mesh are located, these methods overcome the bottleneck caused by local mesh refinement in explicit time integrators.

FE Discretization of damped wave equations

As a model problem we consider the (damped) wave equation

$$\begin{aligned} u_{tt} + \sigma u_t - \nabla \cdot (c^2 \nabla u) &= f \ \text{ in } \ \Omega \times (0,T)\,, \\ u(\cdot,t) &= 0 \ \text{ on } \ \partial\Omega \times (0,T)\,, \\ u(\cdot,0) = u_0\,,\ u_t(\cdot,0) &= v_0 \text{ in } \Omega\,, \end{aligned} \tag{1}$$

where Ω is a bounded domain in $\mathbb{R}^d$. Here, $f \in L^2(0,T;L^2(\Omega))$ is a (known) source term, while $u_0 \in H_0^1(\Omega)$ and $v_0 \in L^2(\Omega)$ are prescribed initial conditions. At the boundary, $\partial\Omega$, we impose a homogeneous Dirichlet boundary condition, for simplicity. The damping coefficient, $\sigma = \sigma(x)$, is assumed nonnegative ($\sigma \geq 0$) whereas the speed of propagation, $c = c(x)$, is piecewise smooth and strictly positive ($c(x) \geq c_0 > 0$). Spatial discretization of (1) with continuous finite elements (with mass lumping [1]) or a nodal discontinuous Galerkin (DG) method [2] leads to a system of ordinary differential equations

$$\mathbf{M}\,\frac{d^2\mathbf{U}}{dt^2}(t) + \mathbf{M}_\sigma\,\frac{d\mathbf{U}}{dt}(t) + \mathbf{K}\,\mathbf{U}(t) = \mathbf{R}(t)\ , \tag{2}$$

or

$$\mathbf{M}\frac{d\mathbf{Q}}{dt}(t) + \mathbf{M}_\sigma\,\mathbf{Q}(t) + \mathbf{C}\,\mathbf{Q}(t) = \mathbf{R}(t)\,, \tag{3}$$

respectively, with an essentially diagonal mass matrix $\mathbf{M}$. Thus, when combined with explicit time integration, the resulting fully discrete scheme of (1) will be truly explicit.

Runge-Kutta based LTS

Locally refined meshes impose severe stability constraints on explicit time-stepping methods for the numerical solution of (1). LTS methods overcome that bottleneck by using smaller time-steps precisely where the smallest elements in the mesh are located. In [3], [4], explicit second-order LTS integrators for transient wave motion were developed, which are based on the standard leap-frog scheme. In the absence of damping, i.e. $\sigma = 0$, these time-stepping schemes, when combined with the modified equation approach, yield methods of arbitrarily high (even) order. To achieve arbitrarily high accuracy in the presence of damping, while remaining fully explicit, explicit LTS methods for the scalar damped wave equation based on Adams-Bashforth multi-step schemes were derived in [5].

Here we propose explicit LTS methods of high accuracy based either on explicit classical or low-storage Runge-Kutta (RK) schemes. In contrast to Adams-Bashforth methods, RK methods are one-step methods; hence, they do not require a starting procedure and easily accommodate adaptive time-step selection. Although RK methods do require several further evaluations per time-step, that additional work is compensated by a less stringent CFL stability condition.

In order to derive RK based LTS methods, we rewrite both (2) and (3) as a first-order system

$$\mathbf{y}'(t) = \mathbf{B}\mathbf{y}(t) + \mathbf{F}(t) \tag{4}$$

and split the vectors

$$\begin{aligned} \mathbf{y}(t) &= (\mathbf{I}-\mathbf{P})\mathbf{y}(t) + \mathbf{P}\mathbf{y}(t) = \mathbf{y}^{[\mathrm{c}]}(t) + \mathbf{y}^{[\mathrm{f}]}(t), \\ \mathbf{F}(t) &= (\mathbf{I}-\mathbf{P})\mathbf{F}(t) + \mathbf{P}\mathbf{F}(t) = \mathbf{F}^{[\mathrm{c}]}(t) + \mathbf{F}^{[\mathrm{f}]}(t), \end{aligned} \tag{5}$$

where the entries of the diagonal matrix $\mathbf{P}$, equal to zero or one, identify the unknowns associated with the locally refined regions, $\mathbf{y}^{[\mathrm{f}]}$. Hence the exact solution of (4) is

$$\begin{aligned} \mathbf{y}(t_n+\xi\Delta t) = \mathbf{y}(t_n) &+ \int_{t_n}^{t_n+\xi\Delta t} \mathbf{B}\mathbf{y}^{[\mathrm{c}]}(t) + \mathbf{F}^{[\mathrm{c}]}(t)\,dt \\ &+ \int_{t_n}^{t_n+\xi\Delta t} \mathbf{B}\mathbf{y}^{[\mathrm{f}]}(t) + \mathbf{F}^{[\mathrm{f}]}(t)\,dt\,. \end{aligned} \tag{6}$$

To derive LTS methods that overcome the stringent stability conditions dictated by the smallest elements in the mesh, $\mathbf{y}^{[f]}$, we shall treat those elements differently from the remaining coarser elements, $\mathbf{y}^{[c]}$. In doing so, we approximate the first integral in (6) by a sufficiently accurate quadrature formula, where the (unknown) values of $\mathbf{y}^{[c]}$ at the quadrature points are approximated by Taylor expansion. Differentiation of the resulting expression then leads to a modified differential equation, which is solved numerically from t_n to $t_n + \Delta t$ by using a RK method with $\Delta\tau = \Delta t/p$ in the locally refined region; here p denotes the coarse to fine aspect ratio. The resulting LTS-RK schemes have the same high rate of convergence as the original classical or low-storage RK methods.

Numerical Experiments

To illustrate the versatility of our approach, we consider the scalar damped wave equation

$$u_{tt} + \sigma u_t - \nabla \cdot (c^2 \nabla u) = f \qquad \text{in } \Omega \times (0,T)\,, \quad (7)$$

in a rectangular domain of size $[0,2] \times [0,1]$ with two rectangular barriers inside forming a narrow gap. Here $f(x,t)$ is a (known) source term, whereas the damping coefficient $\sigma(x) \geq 0$ and the speed of propagation $c(x) > 0$ are piecewise smooth. We use continuous P^2 elements on a triangular mesh, which is highly refined in the vicinity of the gap, as shown in Fig. 1. For the time discretization, we choose an LTS method based on an explicit third-order low-storage Runge-Kutta scheme. Since the typical mesh size inside the refined region is about $p = 7$ times smaller than that in the surrounding coarser region, we take p local time steps of size $\Delta\tau = \Delta t/p$ for every time step Δt. Thus, the numerical method is third-order accurate both in space and time with respect to the L^2-norm. In Fig. 2, a vertical Gaussian pulse initiates two plane waves (with Gaussian amplitude) propagating in opposite directions. The right-moving wave proceeds until it impinges on the obstacle.

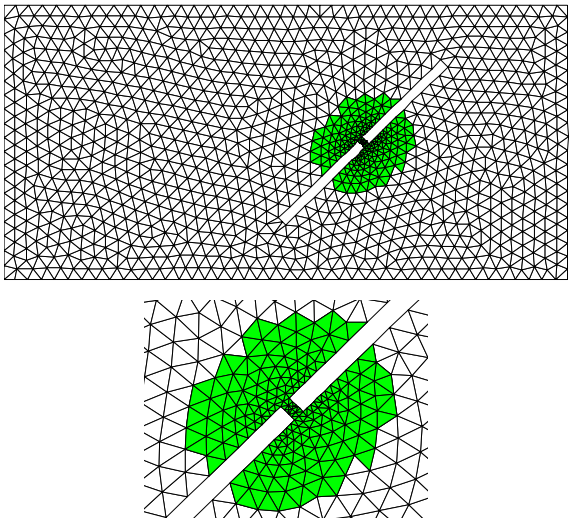

Figure 1: The initial triangular mesh (top); zoom on the "fine" mesh indicated by the darker (green) triangles (bottom).

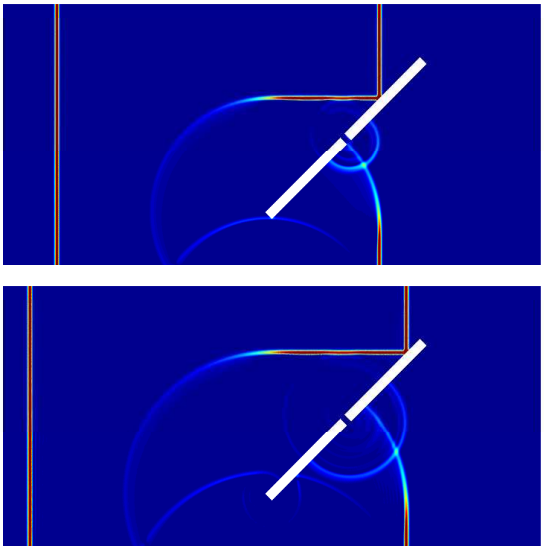

Figure 2: The solution at times t =0.6 and 0.7.

References

[1] G. Cohen, *High-order numerical methods for transient wave equations*, Springer, 2002.

[2] J.S. Hesthaven and T.Warburton, *Nodal Discontinuous Galerkin Methods*, Springer, 2008.

[3] J. Diaz and M.J. Grote, *Energy conserving explicit local time-stepping for second-order wave equations*, SIAM J. Sci. Comput., **31** (2009), pp. 1985–2014.

[4] M.J. Grote and T. Mitkova, *Explicit local time-stepping for Maxwell's equations*, J. Comput. Appl. Math., **234** (2010), pp. 3283–3302.

[5] M.J. Grote and T. Mitkova, *High-order explicit local time-stepping methods for damped wave equations*, J. Comput. Appl. Math., **239** (2013), pp. 270–289.

A Time-domain BIEM for Wave Equation accelerated by Fast Multipole Method using Interpolation

Toru Takahashi[1,*]
[1] Dept. Mech. Sci. and Eng., Grad. Sch. Eng., Nagoya Univ., Nagoya, Japan
*Email: ttaka@nuem.nagoya-u.ac.jp

Abstract

This study proposes a fast time-domain boundary integral equation method (TDBIEM) for wave equation. The present method resorts to interpolate the fundamental solution to construct a fast algorithm in the fashion of the fast multipole method (FMM) [1].

1 Introduction

The application of the FMM to the TDBIEM has not been investigated well in contrast to the frequency-domain BIEM [2]. As of now, the plane wave time domain (PWTD) algorithm, which is a time-domain version of the FMM, is promising for wave problems in acoustics, electromagnetics [3], and elastodynamics [4].

Meanwhile, Tausch developed an FMM-like algorithm for the heat equation [5]. He exploited Lagrange/Chebyshev interpolation to represent the time-dependent fundamental solution in the form of separation-of-variables, which enables to formulate an FMM. It is to be noted that such interpolation-based FMMs were studied in other problems, e.g., the black-box FMM [6] and the references therein.

Being motivated by Tausch's paper [5], the present study aims at establishing an interpolation-based fast multipole TDBIEM for the scalar wave equation in three dimensions, as an alternative of the PWTD algorithm.

2 Formulation

2.1 TDBIEM for wave equation

We solve $u(\boldsymbol{x},t)$ ($\boldsymbol{x}\in D\subset\mathbb{R}^3$, $t>0$) from the wave equation $c^2\Delta u(\boldsymbol{x},t)=\ddot{u}(\boldsymbol{x},t)$ subject to given initial and boundary conditions, where c denotes the wave velocity. This problem is reduced to solve the following BIE:

$$\frac{1}{2}u(\boldsymbol{x},t)=\int_0^t\int_{\partial D}\Bigg(\Gamma(\boldsymbol{x}-\boldsymbol{y},t-s)\frac{\partial u}{\partial n_y}(\boldsymbol{y},s) - \frac{\partial\Gamma}{\partial n_y}(\boldsymbol{x},\boldsymbol{y},t-s)u(\boldsymbol{y},s)\Bigg)\mathrm{d}s\mathrm{d}S_y\ \ \boldsymbol{x}\in\partial D,\ t>0,\ (1)$$

where $\Gamma(\boldsymbol{r},t):=\frac{\delta(t-|\boldsymbol{r}|/c)}{4\pi|\boldsymbol{r}|}$ is the fundamental solution.

We apply the collocation method to solve the BIE (1). The boundary ∂D is discretised with N_s piecewise-constant elements E_i ($i=1,\dots,N_\mathrm{s}$) and their centres are chosen as the spacial collocation points, denoted by $\boldsymbol{x}_i$. Meanwhile, we use the piecewise-linear basis for time and let $t_\alpha:=\alpha\Delta_\mathrm{t}$ ($\alpha=0,...,N_\mathrm{t}$) be the temporal collocation points, with Δ_t being a time step length.

Owing to the expensive computation of the layer potential in (1), the computational complexity of the naïve TDBIEM results in $\mathcal{O}(N_\mathrm{s}^2N_\mathrm{t})$.

Hence, it is necessary to construct a fast method to evaluate the layer potential in (1). To show the main idea of the method, we now focus on the interaction between two 'well-separated' clusters in space-time, say a source cluster $S\times J$ and observation cluster $O\times I$ (Fig. 1). For these clusters, the layer potential is represented as

$$\frac{1}{4\pi c\Delta_\mathrm{t}}\sum_{t_\beta\in J}\sum_{E_j\in S}\Bigg(\sigma_j^\beta\int_{E_j}\boldsymbol{W}(\boldsymbol{x}_i,\boldsymbol{y},t_\alpha,t_{\beta-1})\cdot\boldsymbol{n}(\boldsymbol{y})\,\mathrm{d}S_y - \tau_j^\beta\int_{E_j}U(\boldsymbol{x}_i,\boldsymbol{y},t_\alpha,t_{\beta-1})\,\mathrm{d}S_y\Bigg)\ \ \boldsymbol{x}_i\in O,\ t_\alpha\in I,\ (2)$$

where the time integral was already performed analytically. Also, σ_j^β and τ_j^β represent the boundary values that are already known at the passed time t_β on E_j. The single- and double-layer kernels U and $\boldsymbol{W}$ are defined as

$$U(\boldsymbol{x},\boldsymbol{y},t,s):=\frac{(c(t-s)-|\boldsymbol{x}-\boldsymbol{y}|)_+}{|\boldsymbol{x}-\boldsymbol{y}|},$$

$$\boldsymbol{W}(\boldsymbol{x},\boldsymbol{y},t,s):=\frac{c(t-s)(\boldsymbol{x}-\boldsymbol{y})}{|\boldsymbol{x}-\boldsymbol{y}|^3}H(c(t-s)-|\boldsymbol{x}-\boldsymbol{y}|).$$

2.2 Approximation of U and $\boldsymbol{W}$ with interpolation

Following the papers [5][6], we approximate the kernels U and $\boldsymbol{W}$ with certain interpolation functions. We denote the approximated function of a given function $f(x)$ on $[-1,1]$ by $\sum_{i<p}f(\omega_i^p)\ell_i(x)$, where $\ell_i(x)$ are interpolants and ω_i^p are nodes where f is sampled. To apply this interpolation scheme to U and $\boldsymbol{W}$ in (2), we let O and S be cubes with the edge length $2h_\mathrm{s}$ and centres of $\bar{O}$ and $\bar{S}$, respectively. Similarly, we let I and J be time-intervals of length $2h_\mathrm{t}$ and centres of $\bar{I}$ and $\bar{J}$, respectively. Then, with the given numbers p_s and p_t, we can expand U as

$$U(\boldsymbol{x},\boldsymbol{y},t,s)\approx\sum_{a<p_\mathrm{s}}\sum_{b<p_\mathrm{s}}\sum_{m<p_\mathrm{t}}\sum_{n<p_\mathrm{t}}U_{a,b,m,n}(O,S,I,J) \times\ell_a\left(\frac{\boldsymbol{x}-\bar{O}}{h_\mathrm{s}}\right)\ell_b\left(\frac{\boldsymbol{y}-\bar{S}}{h_\mathrm{s}}\right)\ell_m\left(\frac{t-\bar{I}}{h_\mathrm{t}}\right)\ell_n\left(\frac{s-\bar{J}}{h_\mathrm{t}}\right),$$

where $\boldsymbol{\omega}_v^{p_\mathrm{s}} := (\omega_{v_1}^{p_\mathrm{s}}, \omega_{v_2}^{p_\mathrm{s}}, \omega_{v_3}^{p_\mathrm{s}})$, $U_{a,b,m,n}(O,S,I,J) := U(\bar{O} + h_\mathrm{s}\boldsymbol{\omega}_a^{p_\mathrm{s}}, \bar{S} + h_\mathrm{s}\boldsymbol{\omega}_b^{p_\mathrm{s}}, \bar{I} + h_\mathrm{t}\omega_m^{p_\mathrm{t}}, \bar{J} + h_\mathrm{t}\omega_n^{p_\mathrm{t}})$, and

$$\sum_{v<p_\mathrm{s}} \ell_v(\boldsymbol{z}) := \sum_{v_1<p_\mathrm{s}} \sum_{v_2<p_\mathrm{s}} \sum_{v_3<p_\mathrm{s}} \ell_{v_1}(z_1)\ell_{v_2}(z_2)\ell_{v_3}(z_3)$$

for $v = a, b$ and $\boldsymbol{z} := (z_1, z_2, z_3) \in [-1,1]^3$. Meanwhile, we can approximate $\boldsymbol{W}$ by differentiating ℓ_b because $\boldsymbol{W} = \nabla_y U$ holds. Note that the *discontinuity* of $\boldsymbol{W}$ on the sphere $|\boldsymbol{x} - \boldsymbol{y}| = c(t-s)$ in $\mathbb{R}^3$ (or wavefront) causes a certain approximation error.

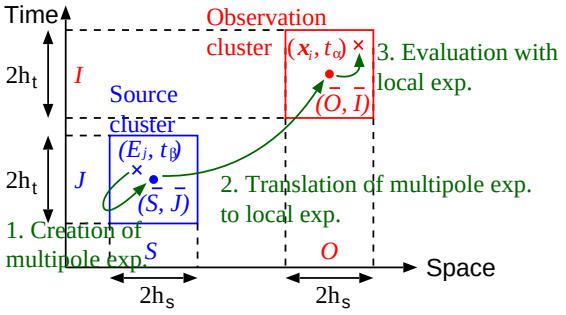

Figure 1: Schematic illustration to evaluate Eq.(2) through the three FMM-steps formulated in Section 2.3.

2.3 *FMM-expression of layer potential in Eq.(2)*

With the help of the interpolated kernels, we can express (2) in the following FMM-like fashion:

$$\approx \sum_{a<p_\mathrm{s}} \sum_{m<p_\mathrm{t}} \ell_a\left(\frac{\boldsymbol{x}_i - \bar{O}}{h_\mathrm{s}}\right) \ell_m\left(\frac{t_\alpha - \bar{I}}{h_\mathrm{t}}\right) L_{a,m}(O,I). \tag{3}$$

Here, $L_{a,m}$ is the local expansion computed from the so-called M2L formula:

$$L_{a,m}(O,I) := \sum_{b<p_\mathrm{s}} \sum_{n<p_\mathrm{t}} U_{a,b,m,n}(O,S,I,J) M_{b,n}(S,J),$$

where $M_{b,n}$ denotes the multipole expansion:

$$M_{b,n}(S,J) := \frac{1}{4\pi c \Delta_\mathrm{t}} \sum_{E_j \in S} \sum_{t_\beta \in J} \ell_n\left(\frac{t_{\beta-1} - \bar{J}}{h_\mathrm{t}}\right)$$

$$\times \int_{E_j} \left(\sigma_j^\beta \nabla \ell_b\left(\frac{\boldsymbol{y} - \bar{S}}{h_\mathrm{s}}\right) \cdot \boldsymbol{n}(\boldsymbol{y}) - \tau_j^\beta \ell_b\left(\frac{\boldsymbol{y} - \bar{S}}{h_\mathrm{s}}\right)\right) \mathrm{d}S_y.$$

As in ordinary FMM, the so-called M2M and L2L formulae can be obtained with the help of interpolation [5].

2.4 *Algorithm and computational complexity*

Using the previous formulae, we can construct a fast algorithm to solve the BIE (1) in the similar fashion to the multi-level PWTD algorithm [3]. We can show that computational complexity of the present FMM is $\mathcal{O}(N_\mathrm{s}^{4/3} N_\mathrm{t})$. Here, p_t and p_s are to be constants, meaning we basically consider low frequency regime.

3 Numerical validation (in progress)

The present FMM code was tested through an external scattering analysis, where a hard sphere is irradiated with a plane pulse. The sphere is discretised with 5120 elements and 400 time steps were calculated. The cubic Hermite interpolation was used with $p_\mathrm{s} = p_\mathrm{t} = 8$.

Fig. 2 compares the fast TDBIEM with the conventional one for u at the front (irradiated) and back sides of the sphere. The fast TDBIEM exhibits over/under shoots as well as a larger diffraction (around $t = 2.7$ for the front side) but the discrepancy from the conventional method is not enormous. In this tentative result, the fast and conventional TDBIEMs took 1269 and 2134 sec., respectively.

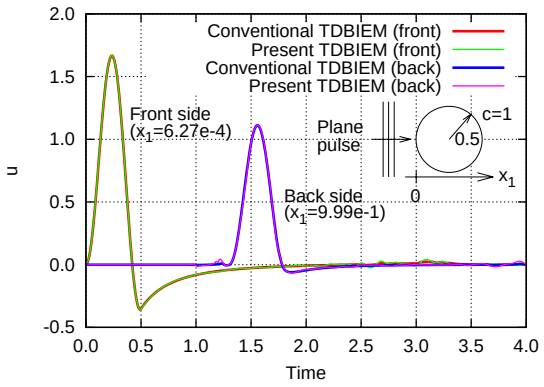

Figure 2: Comparison of the numerical solutions.

4 Conclusion

An FMM-accelerated TDBIEM for wave equation was presented together with the tentative numerical result.

References

[1] L. Greengard, V. Rokhlin: A Fast Algorithm for Particle Simulations, J. Comp. Phys., 73, 325–348, 1987.

[2] Y.J. Liu, et al: Recent Advances and Emerging Applications of the Boundary Element Method, Appl. Mech. Rev., 64, 2011, DOI: 10.1115/1.400549.

[3] W.C. Chew, J.M. Jin, E. Michielssen (Eds.): Fast and Efficient Algorithms in Computational Electromagnetics, Artech House, Chapter 18, 2001.

[4] T. Takahashi, et al: A Fast BIEM for Three-dimensional Elastodynamics in Time Domain, Eng. Anal. Boundary Elem., 27, 91–506, 2003.

[5] J. Tausch: A Fast Method for Solving the Heat Equation by Layer Potentials, J. Comp. Phys., 224, 956–969, 2007.

[6] W. Fong, E. Darve: The Black-box Fast Multipole Method, J. Comp. Phys., 228, 8712–8725, 2009.

Acknowledgement: This work is supported by JSPS KAKENHI Grant Number 24656072.

BEM-FEM coupling for the one-dimensional Klein-Gordon equation

A. Aimi[1], **C. Guardasoni**[1], **S. Panizzi**[1,*]
[1]Dept. of Mathematics and Computer Science, University of Parma,
Parco Area delle Scienze, 53/A, 43124 Parma, Italy
*Email: stefano.panizzi@unipr.it

Abstract

The one-dimensional Klein-Gordon equation defined on a bi-domain will be numerically solved by a BEM-FEM coupling procedure. Stability and convergence of the proposed technique, based on energy arguments, will be presented, together with several numerical results, including the extension to the dissipative case.

Introduction

We present a BEM-FEM numerical scheme for the approximation of solutions $u = u(x,t)$ to the one-dimensional linear Klein-Gordon equation in a half-line $x > 0$:

$$\frac{\partial^2 u}{\partial t^2} - \frac{\partial}{\partial x}\left(c(x)^2 \frac{\partial u}{\partial x}\right) + m(x)^2 u = f(x,t), \qquad (1)$$

with Neumann boundary condition at the endpoint $x = 0$ and vanishing initial conditions $u(x,0) = u_t(x,0) = 0$, $x > 0$. The functions $c(x) > 0$ and $m(x) \geq 0$ take the constant values c_i, $i = 1,2$ and m_i, $i = 1,2$, in the two sub-intervals $(0,L)$ and $(L,+\infty)$ respectively. The source term $f(x,t)$ is assumed to vanish for $x > L$.

Equivalently, the problem can be set as a coupled bi-doman initial-boundary value problem with transmission conditions at the interface point $x = L$: $u(L^-,t) = u(L^+,t)$, $c_1^2 u_x(L^-,t) = c_2^2 u_x(L^+,t)$.

Equation (1) arises in mathematical physics in several different contexts: in relativistic quantum mechanics as a model for a free particle, in which case it is actually known as Klein-Gordon equation; in continuum mechanics as a linear model for either transversal or longitudinal vibrations of a one-dimensional string/bar subject to a restoring force $m(x)$ per unit length; in propagation of electric waves in wire lines where it is known as the Telegraph equation (actually in this case, an additional dissipative term u_t appears in the equation).

In addition to the interest that the equation (1) has in applications, it is also important from the mathematical point of view, being the simplest hyperbolic equation with a non trivial dispersion relation. This fact makes the problem stimulating to be studied and, at the same time, simple enough to make possible a complete mathematical justification of the BEM-FEM numerical approximation.

1 Analysis and discretization

The continuous problem is set in a space-time weak formulation which couples the initial-boundary value problem for the PDE in the bounded interval $(0,L)$ with two retarded integro-differential equations at the interface point $x = L$, whose unknowns are $u^L(t) = u(L,t)$ and $p^L(t) = -c_2^2 u_x(L,t)$:

$$u^L(t) = (Vp^L)(t), \qquad p^L(t) = (-Du^L)(t). \qquad (2)$$

The integro-differential operators V and D are defined as follows (in the following J_0 and J_1 are the Bessel functions of order 0 and 1 respectively):

$$(Vp^L)(t) := \frac{1}{c_2}\int_0^t J_0(m_2(t-\tau))p^L(\tau)\,d\tau,$$

$$-(Du^L)(t) := c_2\dot{u}^L(t) + m_2 c_2 \int_0^t \frac{J_1(m_2(t-\tau))}{t-\tau} u^L(\tau) d\tau.$$

The basic idea underlying the proposed numerical scheme is to preserve the symmetry properties and the energy estimates valid for the continuous weak formulation. The essential elements of our numerical scheme are: 1) finite elements for space discretization and an implicit Newmark finite differences scheme for time discretization in the FEM interval $(0,L)$; 2) collocation technique for the first equation in (2) and time-Galerkin method for the second one (which in this case plays the role of the hyper-singular equation).

We will show stability and convergence of the method essentially by discrete energy estimates (see [1], [4], [7], [8] for related results), the crucial remark being the well-known relation:

$$\mathcal{E}_{BEM}(t,u) = \int_0^t p^L(\tau)\dot{u}^L(\tau)\,d\tau = \int_0^t (V\dot{p}^L)(\tau)p^L(\tau)\,d\tau$$
$$= -\int_0^t (Du^L)(\tau)\dot{u}^L(\tau)\,d\tau \geq 0. \qquad (3)$$

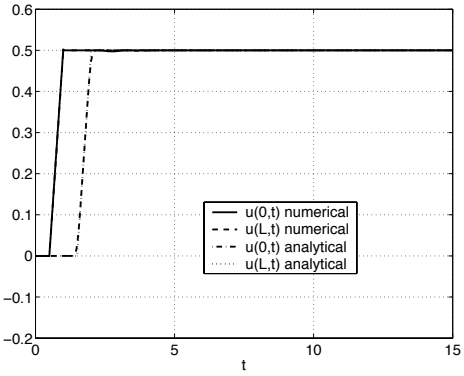

Figure 1: $m_1 = m_2 = 0$

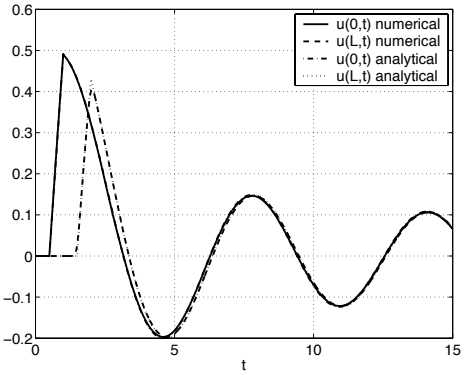

Figure 2: $m_1 = m_2 = 1$

Here $\mathcal{E}_{BEM}(t,u)$ represents the energy in the BEM sub-interval. In the present work we actually strengthen the simple inequality (3), and as a consequence, we prove optimal stability estimates for the BEM unknowns p^L and $\dot{u}^L$ and convergence of the BEM-FEM approximations in energy norm (see [2], [3] and the seminal papers [5], [6] for related results).

2 Numerical results

Let us consider the spatial domain $\Omega = (0, +\infty)$ decomposed in $\Omega_1 = (0, L)$ and $\Omega_2 = (L, +\infty)$, with $c_1 = c_2 = 1$ and trivial forcing term $f(x,t) = 0$. The Neumann condition in $x = 0$ is the rectangular impulse $H(t-0.5) - H(t-1)$. In Figures 1-3 we show the obtained numerical results in $x = 0$ and $x = L$ compared with the analytical solution, which is known for this simple benchmark, for different values of m_1, m_2. The agreement is very good.

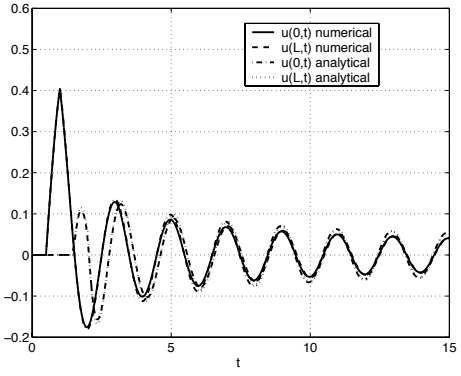

Figure 3: $m_1 = m_2 = \sqrt{10}$

References

[1] T. Abboud, P. Joly, J. Rodriguez and I. Terasse, *Coupling discontinuous Galerkin methods and retarded potentials for transient wave propagation on unbounded domains*, J. Comput. Phys., **230** (2011), 5877-5907.

[2] A. Aimi, M. Diligenti and S. Panizzi, *Energetic Galerkin BEM for wave propagation Neumann exterior problems*, CMES Comput. Model. Eng. Sci., **58** N.2 (2010), 185-219

[3] A. Aimi, M. Diligenti, C. Guardasoni, I. Mazzieri and S. Panizzi, *An energy approach to space-time Galerkin BEM for wave propagation problems*, Internat. J. Numer. Methods Engrg., **80** (2009), 1196-1240.

[4] A. Bachelot, L. Bounhoure and A. Pujols, *Couplage éléments finis–potentiels retardés pour la diffraction électromagnétique par un obstacle hétérogène*, Numer. Math., **89** (2001), 257-306.

[5] A. Bamberger and T. Ha Duong, *Formulation variationnelle espace-temps pour le calcul par potentiel retardé de la diffraction d'une onde acoustique I*, Math. Methods Appl. Sci., **8** (1986), 405-435.

[6] A. Bamberger and T. Ha Duong, *Formulation variationnelle pour le calcul de la diffraction d'une onde acoustique par une surface rigide*, Math. Methods Appl. Sci., **8** (1986), 598-608.

[7] P. Grob and P. Joly, *Conservative coupling between finite elements and retarded potentials. Application to vibroacoustics*, SIAM J. Sci. Comp., **29** (2007), 1127-1159.

[8] H. Houde and Z. Zhang, *An analysis of the finite-difference method for one-dimensional Klein-Gordon equation on unbounded domain*, Appl. Num. Math., **59** (2009), 1568-1583.

Full discretization of wave equations on evolving surfaces

Dhia Mansour
Universität Tübingen, Germany
Email: mansour@na.uni-tuebingen.de

Abstract

A linear wave equation on a moving surface is discretized in space by evolving surface finite elements and in time by the implicit midpoint rule. We study stability and convergence of the fully discrete scheme in the natural time-dependent norms. Under suitable assumptions we prove optimal-order error estimates.

Keywords. Wave equation, evolving surface finite elements, implicit midpoint rule, error analysis.

1 Introduction

The numerical study of partial differential equations on moving surfaces has attracted considerable attention over the last years.

In [1], the authors considered a wave equation on a moving surface, which is derived from Hamilton's principle, and presented a fully discrete variational integrator that is stable under a CFL condition. To overcome the time step restriction due to the CFL condition, we investigate in this paper the implicit midpoint rule for the time discretization. We prove the unconditional stability of the fully discrete scheme. Furthermore, under suitable regularity conditions, we show second order of the error measured in the L^2 norm over the time-dependent surface for displacements and their material derivatives, and first order for the L^2 norm of the error in the surface gradient of the displacements, uniformly on bounded time intervals.

2 The wave equation on evolving surfaces

Let $\Gamma(t)$, $t \in [0,T]$, be a smoothly evolving family of smooth m-dimensional compact closed hypersurfaces in $\mathbb{R}^{m+1}$ without boundary, with unit outward pointing normal ν. We let $v(x(t),t)$ denote the given *velocity* of the surface $\Gamma(t)$, i.e., $\dot{x}(t) = v(x(t),t)$.

We consider the linear wave equation on evolving surfaces (c.f [1])

$$\partial^\bullet \partial^\bullet u + \partial^\bullet u \; \nabla_\Gamma \cdot v - \Delta_\Gamma u = 0 \qquad (1)$$

with given initial data $u(0) \in H^2(\Gamma_0)$ and $\partial^\bullet u(0) \in H^1(\Gamma_0)$.

We let $\partial^\bullet u$ denote the *material derivative* $\partial^\bullet u = \frac{\partial u}{\partial t} + v \cdot \nabla u$. The tangential gradient is given by $\nabla_\Gamma u = \nabla u - \nabla u \cdot \nu \, \nu$. The Laplace-Beltrami operator is the tangential divergence of the tangential gradient $\Delta_\Gamma u = \nabla_\Gamma \cdot \nabla_\Gamma u = \sum_{j=1}^{d+1} (\nabla_\Gamma)_j (\nabla_\Gamma)_j u$.

2.1 Weak formulation

A weak form of (1) reads:

$$\frac{d}{dt} \int_\Gamma \partial^\bullet u \varphi + \int_\Gamma \nabla_\Gamma u \cdot \nabla_\Gamma \varphi = \int_\Gamma \partial^\bullet u \partial^\bullet \varphi \qquad (2)$$

for all smooth $\varphi : \bigcup_{t\in[0,T]} \Gamma(t) \times \{t\} \to \mathbb{R}$.

2.2 The evolving surface finite element method

Following [2], the smooth surface $\Gamma(t)$ is interpolated at nodes $a_i(t) \in \Gamma(t)$ $(i = 1, \dots, m)$ by a discrete polygonal surface $\Gamma_h(t)$, where h denotes the grid size. These nodes move with velocity $da_i(t)/dt = v(a_i(t),t)$. The discrete surface $\Gamma_h(t) = \bigcup_{E(t)\in\mathcal{T}_h(t)} E(t)$ is the union of d-dimensional simplices $E(t)$ that is assumed to form an admissible triangulation $\mathcal{T}_h(t)$; see [2] for details. We define for each $t \in [0,T]$ the finite element space $S_h(t) = \{\phi_h \in C^0(\Gamma_h(t)) \; : \; \phi_h|_E \text{ linear affine for each } E \in \mathcal{T}_h(t)\}$. The moving nodal basis $\{\chi_i\}_{i=1}^m$ of $S_h(t)$ are determined by $\chi_i(a_j(t),t) = \delta_{ij}$ for all j, so we have

$$S_h(t) = \operatorname{span}\{\chi_1(\cdot,t), \dots, \chi_m(\cdot,t)\}.$$

The discrete velocity V_h of the discrete surface $\Gamma_h(t)$ is the piecewise linear interpolant of v: $V_h(x,t) = \sum_{j=1}^N v(a_j(t),t)\chi_j(x,t), \quad x \in \Gamma_h(t)$. Then the discrete material derivative on $\Gamma_h(t)$ is given by $\partial_h^\bullet \phi_h = \frac{\partial \phi_h}{\partial t} + V_h \cdot \nabla \phi_h$. The construction is such that

$$\partial_h^\bullet \chi_j = 0. \qquad (3)$$

The discrete surface gradient is defined piecewise as $\nabla_{\Gamma_h} g = \nabla g - \nabla g \cdot \nu_h \nu_h$, where ν_h denotes the normal to the discrete surface.

2.3 The spatial semi-discretization

The spatial semi-discretization of the wave equation reads as follows: Find $u_h(\cdot,t) \in S_h(t)$ such that for all temporally smooth ϕ_h with $\phi_h(\cdot,t) \in S_h(t)$ and for all $t \in [0,T]$,

$$\frac{d}{dt} \int_{\Gamma_h} \partial_h^\bullet U_h \, \phi_h + \int_{\Gamma_h} \nabla_{\Gamma_h} U_h \cdot \nabla_{\Gamma_h} \phi_h = \int_{\Gamma_h} \partial_h^\bullet U_h \partial_h^\bullet \phi_h. \qquad (4)$$

2.4 The Hamiltonian ODE system

We denote the discrete solution $U_h(\cdot,t) = \sum_{j=1}^m q_j(t)\chi_j(\cdot,t) \in S_h(t)$ and define $q(t) \in \mathbb{R}^m$ as the nodal vector with entries $q_j(t) = U_h(a_j(t),t)$. Then by the transport property (3), we have $\partial_h^\bullet U_h(\cdot,t) = \sum_{j=1}^m \dot{q}_j(t)\chi_j(\cdot,t) \in S_h(t)$. The evolving mass matrix $M(t)$ and the stiffness matrix $A(t)$ are defined by $M(t)_{ij} = \int_{\Gamma_h(t)} \chi_i(t)\chi_j(t)$, $A(t)_{ij} = \int_{\Gamma_h(t)} \nabla_{\Gamma_h(t)}\chi_i(t) \cdot \nabla_{\Gamma_h(t)}\chi_j(t)$. The mass matrix is symmetric and positive definite. The stiffness matrix is symmetric and only positive semidefinite. Then (4) can be written as

$$\frac{d}{dt}\left(M(t)\dot{q}(t)\right) + A(t)q(t) = 0. \tag{5}$$

By introducing the conjugate *momenta* $p(t) = M(t)\dot{q}(t)$, we reformulate (5) in the variable $y(t) = (p(t),q(t))^{\mathsf{T}}$ as *Hamilton's equations* ($\dot{} = \frac{d}{dt}$)

$$\dot{y}(t) = J^{-1}H(t)y(t), \tag{6}$$

with

$$J = \begin{pmatrix} 0 & I \\ -I & 0 \end{pmatrix}, \quad H(t) = \begin{pmatrix} M(t)^{-1} & 0 \\ 0 & A(t) \end{pmatrix}.$$

3 The implicit midpoint rule

For the numerical integration of the above Hamilton's equations (6) we consider the implicit midpoint rule with time step size $\tau > 0$ given by

$$Y_{n+\frac{1}{2}} = y_n + \frac{\tau}{2}J^{-1}H_{n+\frac{1}{2}}Y_{n+\frac{1}{2}} \tag{7a}$$

$$y_{n+1} = y_n + \tau J^{-1}H_{n+\frac{1}{2}}Y_{n+\frac{1}{2}} \tag{7b}$$

3.1 Defects and errors

Let $\widetilde{y}_n$ and $\widetilde{Y}_{n+\frac{1}{2}}$ be reference values that we want to compare with y_n and $Y_{n+\frac{1}{2}}$ respectively. Inserted into (7) they yield defects in

$$\widetilde{Y}_{n+\frac{1}{2}} = \widetilde{y}_n + \frac{\tau}{2}J^{-1}H_{n+\frac{1}{2}}\widetilde{Y}_{n+\frac{1}{2}} + \Delta_{n+\frac{1}{2}} \tag{8a}$$

$$\widetilde{y}_{n+1} = \widetilde{y}_n + \tau J^{-1}H_{n+\frac{1}{2}}\widetilde{Y}_{n+\frac{1}{2}} + \delta_{n+1} \tag{8b}$$

3.2 Stability

We define the symmetric positive definite matrix $\hat{H}(t)$ as

$$\hat{H}(t) = \begin{pmatrix} M(t)^{-1} & 0 \\ 0 & A(t)+M(t) \end{pmatrix},$$

and therewith the time-dependent energy norm:

$$\|y\|_t^2 = \left\langle y \,\middle|\, \hat{H}(t) \,\middle|\, y \right\rangle = y^{\mathsf{T}}\hat{H}(t)y. \tag{9}$$

Lemma 3.1 *The error is bounded for $0 \le t_n \le T$ by*

$$\|y_n - \widetilde{y}_n\|_{t_n} \le C\left\|\Delta_{\frac{1}{2}}\right\|_{t_0} + C\left\|\delta_n - \Delta_{n-\frac{1}{2}}\right\|_{t_n} + C\sum_{j=1}^{n-1}\left\|\delta_j + \Delta_{j+\frac{1}{2}} - \Delta_{j-\frac{1}{2}}\right\|_{t_j}.$$

The constant C is independent of h, τ and n.

4 Error bound for the full discretization

For $U_h : \Gamma_h \to \mathbb{R}$ we define the extension or the lift onto Γ by $U_h^l(a(x)) = U_h(x)$, where $a(x) \in \Gamma$ is the orthogonal projection of $x \in \Gamma_h$. We consider the lifts of the fully discrete numerical solution and its numerical material derivative given by $u_h^n := (U_h^n)^l = \sum_{j=1}^m q_j^n \chi_j^l(t_n)$, $\partial_h^\bullet u_h^n := (\partial_h^\bullet U_h^n)^l = \sum_{j=1}^m \left(M(t_n)^{-1}p_n\right)_j \chi_j^l(t_n)$, which are lifted finite element functions defined on the surface $\Gamma(t_n)$. This will be compared with the solution $u(t_n)$ of the wave equation (1) and its material derivative $\partial^\bullet u(t_n)$.

We rewrite the error by subtracting and adding the Ritz map applied to the exact solution,

$$u_h^n - u(t_n) = u_h^n - \mathcal{P}_h(t_n)u(t_n) + \mathcal{P}_h(t_n)u(t_n) - u(t_n),$$

where $\mathcal{P}_h(t)$ is the Ritz map defined in [1]. Then we are able to prove our main result:

Theorem 4.1 *Let u be a sufficiently smooth solution of the wave equation* (1) *and assume that the discrete initial data satisfy*

$$\left\|u_h^0 - (\mathcal{P}_h u)(0)\right\|_{L^2(\Gamma_0)} + \left\|\nabla_{\Gamma_0}u_h^0 - \nabla_{\Gamma_0}(\mathcal{P}_h u)(0)\right\|_{L^2(\Gamma_0)} + \left\|\partial_h^\bullet u_h^0 - \partial_h^\bullet(\mathcal{P}_h u)(0)\right\|_{L^2(\Gamma_0)} \le C_0 h^2.$$

Then, there exist $h_0 > 0$ and $\tau_0 > 0$ such that for $h \le h_0$ and $\tau \le \tau_0$, the following error bound holds for $0 \le t_n = n\tau \le T$:

$$\|u_h^n - u(t_n)\|_{L^2(\Gamma_n)} + h\,\|\nabla_{\Gamma_n}u_h^n - \nabla_{\Gamma_n}u(t_n)\|_{L^2(\Gamma_n)} + \|\partial_h^\bullet u_h^n - \partial^\bullet u(t_n)\|_{L^2(\Gamma_n)} \le C\big(h^2+\tau^2\big).$$

The constant C is independent of h, τ, and n subject to the stated conditions.

References

[1] C. Lubich, and D. Mansour. Variational discretization of linear wave equations on evolving surfaces. Submitted, http://na.uni-tuebingen.de/pub/mansour/papers/varsurf.pdf

[2] G. Dziuk and C.M. Elliott. Finite elements on evolving surfaces. *IMA Journal of Numerical Analysis*, 27:262–292, 2007.

Stable and High Order Accurate Difference Methods for the Elastic Wave Equation in Discontinuous Media

K. Duru[1,*], **K. Virta**[2]
[1] Department of Geophysics, Stanford University, Stanford, CA.
[2] Division of Scientific Computing, Uppsala University, Sweden.
*Email: kduru@stanford.edu

Abstract

A stable and systematic procedure for numerical treatment of elastic waves in layered media is presented. We discretize in space using high order finite difference schemes that satisfy the summation by parts (SBP) rule. Conditions at layer interfaces are imposed weakly using penalties. By deriving lower bounds of the penalty strength and constructing discrete energy estimates we prove strict stability. Numerical experiments in discontinuous media are presented confirming high order accuracy and strict stability.

1 Introduction

Elastic media are in general heterogeneous or discontinuous. For example applications arising in geophysics, ultrasonics and geological prospecting can be composed of layers of rock, air, water and possibly oil. To enable efficient treatments, numerical schemes must be designed to couple discontinuous material interfaces in a stable and accurate manner.

Consider elastic waves propagating in two isotropic half-planes [1]. The half-planes are in welded contact at $y = 0$. The displacement field $\mathbf{u} = (u_1, u_2)^T$ in the half-plane $y > 0$ and $\mathbf{v} = (v_1, v_2)^T$ in the half-plane $y < 0$ are governed by:

$$\rho \frac{\partial^2 \mathbf{u}}{\partial t^2} = \frac{\partial}{\partial x}\left(A\frac{\partial \mathbf{u}}{\partial x} + C\frac{\partial \mathbf{u}}{\partial y}\right) + \frac{\partial}{\partial y}\left(B\frac{\partial \mathbf{u}}{\partial y} + C^T\frac{\partial \mathbf{u}}{\partial x}\right)$$
$$\rho' \frac{\partial^2 \mathbf{v}}{\partial t^2} = \frac{\partial}{\partial x}\left(A'\frac{\partial \mathbf{v}}{\partial x} + C'\frac{\partial \mathbf{v}}{\partial y}\right) + \frac{\partial}{\partial y}\left(B'\frac{\partial \mathbf{v}}{\partial y} + C'^T\frac{\partial \mathbf{v}}{\partial x}\right) \quad (1)$$

where

$$A = \begin{pmatrix} 2\mu+\lambda & 0 \\ 0 & \mu \end{pmatrix}, B = \begin{pmatrix} \mu & 0 \\ 0 & 2\mu+\lambda \end{pmatrix}, C = \begin{pmatrix} 0 & \lambda \\ \mu & 0 \end{pmatrix}.$$

Here $\rho, \mu, \lambda > 0, \rho', \mu', \lambda' > 0$ are densities and Lame parameters of the upper ($y > 0$) and lower ($y < 0$) half-planes respectively. Note that by replacing μ, λ with μ', λ' in the matrices above we obtain expressions for A', B', C'. At the interface $y = 0$, we enforce the continuity of normal stresses and displacements,

$$B\frac{\partial \mathbf{u}}{\partial y} + C^T\frac{\partial \mathbf{u}}{\partial x} = B'\frac{\partial \mathbf{v}}{\partial y} + C'^T\frac{\partial \mathbf{v}}{\partial x}, \quad \mathbf{u} = \mathbf{v}. \quad (2)$$

We will discretize each half-plane problem in (1) independently using high order accurate SBP operators, see [2]. The two discrete half-planes problems are then patched together by (2) to the global domain using penalties. The crucial step in the scheme is choosing penalties and ensuring numerical stability. It is important to mention that a similar approach has been suggested for the scalar wave equation [3]. However, the penalties derived in [3] can not be used for general systems such as the elastic wave equation.

2 Numerical approximation

We discretize in space using a uniform spatial step h in both x and y axes. Introduce the 2-D difference operators

$$\mathbf{D}_{xx} = I_y \otimes \mathrm{D}_{2x}, \quad \mathbf{D}_{yy} = \mathrm{D}_{2y} \otimes I_x, \quad \mathbf{D}_{yx} = \mathrm{D}_{1y} \otimes \mathrm{D}_{1x},$$
$$\mathcal{P} = A \otimes \mathbf{D}_{xx} + B \otimes \mathbf{D}_{yy} + C \otimes \mathbf{D}_{yx} + C^T \otimes \mathbf{D}_{yx},$$

where $\otimes$ denotes the Kronecker product and $\mathrm{D}_{2x}, \mathrm{D}_{2y}$ $\mathrm{D}_{1x}, \mathrm{D}_{1y}$ are one dimensional SBP operators with the corresponding norms $\mathrm{H}_x, \mathrm{H}_y$, see [2] for more details. In advance we define the following: $E_{Ry} = \mathrm{diag}(0, 0, \ldots, 1), E_{Ly} = \mathrm{diag}(1, 0, \ldots, 0)$, S_y a one-sided difference operator approximating the first derivative, identity matrices I_2, I_x, I_y and

$$\mathrm{T}_y = \left(B \otimes (E_{Ry} - E_{Ly})\, \mathrm{S}_y \otimes I_x\right) + \left(C^T \otimes I_y \otimes \mathrm{D}_{1x}\right),$$
$$\mathbf{H}_{xy} = I_2 \otimes \mathrm{H}_y \otimes \mathrm{H}_x, \quad \widetilde{\mathbf{H}} = \begin{pmatrix} \mathbf{H}_{xy} & \mathbf{0} \\ \mathbf{0} & \mathbf{H}_{xy} \end{pmatrix},$$
$$S_b = \left(B \otimes \mathrm{S}_y \otimes I_x\right), \quad D_c = \left(C^T \otimes I_y \otimes \mathrm{D}_{1x}\right),$$
$$\widetilde{B} = I_2 \otimes \begin{pmatrix} \mathbf{0} & & \mathbf{0} \\ & \widetilde{P} & \\ \mathbf{0} & & \mathbf{0} \end{pmatrix} \otimes I_x, \widetilde{P} = \begin{pmatrix} 1 & -1 \\ -1 & 1 \end{pmatrix},$$
$$\widetilde{\mathcal{P}} = \begin{pmatrix} \mathcal{P} & \mathbf{0} \\ \mathbf{0} & \mathcal{P}' \end{pmatrix}, \widehat{B} = I_2 \otimes \begin{pmatrix} \mathbf{0} & & \mathbf{0} \\ & \widehat{P} & \\ \mathbf{0} & & \mathbf{0} \end{pmatrix} \otimes I_x, \mathbf{w} = \begin{pmatrix} \mathbf{u} \\ \mathbf{v} \end{pmatrix},$$

$$\widehat{P} = \begin{pmatrix} 1 & 1 \\ -1 & -1 \end{pmatrix}, S_{By} = \begin{pmatrix} S_b & \mathbf{0} \\ \mathbf{0} & S_{b'} \end{pmatrix}, D_{Cy} = \begin{pmatrix} D_c & \mathbf{0} \\ \mathbf{0} & D_{c'} \end{pmatrix}.$$

A semi-discrete approximation of the system (1) with a weak enforcement of the interface condition (2) is

$$\begin{aligned} \frac{\mathrm{d}^2\mathbf{w}}{\mathrm{dt}^2} &= \widetilde{\mathcal{P}}\mathbf{w} - \tau_N \widetilde{\mathbf{H}}^{-1}\widetilde{B}\tilde{\mathrm{T}}_x\mathbf{w} - \gamma_N \widetilde{\mathbf{H}}^{-1} S_{By}^T \widehat{B}^T \mathbf{w} \\ &\quad - \gamma_N \widetilde{\mathbf{H}}^{-1} D_{Cy}^T \widehat{B}^T \mathbf{w} - \tau_0^{(p)} \widetilde{\mathbf{H}}^{-1} \widetilde{B}\mathbf{w}. \end{aligned} \tag{3}$$

Here $\tau_N, \tau_0^{(p)}, \gamma_N$ are penalties, and the superscript (p) denotes the order of accuracy of the SBP operator. The second term in the RHS of (3) enforces the continuity of the stress field while the last three terms enforce the continuity of the displacement field. We can rewrite the semi-discrete problem (3) as

$$\frac{\mathrm{d}^2\mathbf{w}}{\mathrm{dt}^2} = -\widetilde{\mathbf{H}}^{-1}\widetilde{\mathcal{D}}\mathbf{w}, \tag{4}$$

where $\widetilde{\mathcal{D}}$ is symmetric. In addition we can choose penalties $\tau_N, \tau_0^{(p)}, \gamma_N$ such that $\widetilde{\mathcal{D}}$ is positive semi-definite. Consider $\bar{\lambda} = \max(\lambda, \lambda')$, $\bar{\mu} = \max(\mu, \mu')$. We can prove that if $\tau_N = \frac{1}{2}$, $\gamma_N = -\frac{1}{2}$ and $\tau_0^{(p)} \geq (\alpha_{02}^{(p)}\sqrt{\bar{\mu}\bar{\lambda}} + \alpha_{01}^{(p)}\left(2\bar{\mu} + \bar{\lambda}\right))/h$ (with $\alpha_{01}^{(2)} = 2, \alpha_{01}^{(4)} = 4.5, \alpha_{01}^{(6)} = 5.6$ and $\alpha_{02}^{(2)} = 1, \alpha_{02}^{(4)} = 1.4, \alpha_{02}^{(6)} = 1.6$) then $\widetilde{\mathcal{D}} = \widetilde{\mathcal{D}}^T \geq 0$ and we have $E_{\mathbf{w}}(t) = E_{\mathbf{w}}(0)$ where

$$E_{\mathbf{w}}(t) = \left\| \frac{\mathrm{d}\mathbf{w}}{\mathrm{dt}} \right\|_{\widetilde{H}}^2 + \mathbf{w}^T \widetilde{\mathcal{D}}\mathbf{w}. \tag{5}$$

3 Numerical experiment: Reflection and refraction of a plane wave

Consider a compressional plane wave of unit amplitude propagating with angle θ_1 and temporal frequency $\frac{\omega}{2\pi}$ in the negative y-direction, with displacement

$$\begin{aligned} &\mathbf{u}_P^{(\mathrm{in})} = \begin{pmatrix} \xi_1 \\ -\eta_1 \end{pmatrix} e^{i(\gamma_1\xi_1 x - \gamma_1\eta_1 y - \omega t)}, \\ &x \in (-\infty, \infty), y \in [0, \infty), \\ &\theta_1 \in (0, \tfrac{\pi}{2}), \xi_1 = \sin(\theta_1), \eta_1 = \cos(\theta_1), \gamma_1 = \tfrac{\omega}{\sqrt{\lambda+2\mu}}. \end{aligned}$$

If this wave encounters an interface between two different materials in welded contact it will be split into reflected, compressional and shear waves,

$$\begin{aligned} &\mathbf{u} = \mathbf{u}^{(\mathrm{in})} + \mathbf{u}_P^{(\mathrm{refl})} + \mathbf{u}_S^{(\mathrm{refl})}, x \in (-\infty, \infty), y \in (\infty, 0], \\ &\mathbf{u}_P^{(\mathrm{refl})} = A_{\mathrm{refl}} \begin{pmatrix} \xi_1 \\ \eta_1 \end{pmatrix} e^{i(\gamma_1\xi_1 x + \gamma\eta_1 y - \omega t)}, \\ &\mathbf{u}_S^{(\mathrm{refl})} = B_{\mathrm{refl}} \begin{pmatrix} \gamma_2\eta_2 \\ \gamma_1\xi_1 \end{pmatrix} e^{i(\gamma_1\xi_1 x + \gamma_2\eta_2 y - \omega t)}, \\ &\eta_2 = \cos(\theta_2), \sin(\theta_2) = \tfrac{\gamma_1}{\gamma_2}\xi_1, \gamma_2 = \tfrac{\omega}{\sqrt{\mu}}. \end{aligned}$$

and refracted compressional and shear waves,

$$\begin{aligned} &\mathbf{v} = \mathbf{u}_P^{(\mathrm{refr})} + \mathbf{u}_S^{(\mathrm{refr})}, x \in (-\infty, \infty), y \in (-\infty, 0], \\ &\mathbf{u}_P^{(\mathrm{refr})} = A_{\mathrm{refr}} \begin{pmatrix} \gamma_1\xi_1 \\ \gamma_3\eta_3 \end{pmatrix} e^{i(\gamma_1\xi_1 x - \gamma_3\eta_3 y - \omega t)}, \\ &\mathbf{u}_S^{(\mathrm{refr})} = B_{\mathrm{refr}} \begin{pmatrix} -\gamma_4\eta_4 \\ \gamma_1\xi_1 \end{pmatrix} e^{i(\gamma_1\xi_1 x - \gamma_4\eta_4 y - \omega t)}, \\ &\eta_3 = \cos(\theta_3), \sin(\theta_3) = \tfrac{\gamma_1}{\gamma_3}\xi_1, \gamma_3 = \tfrac{\omega}{\sqrt{\lambda'+2\mu'}}, \\ &\eta_4 = \cos(\theta_4), \sin(\theta_4) = \tfrac{\gamma_1}{\gamma_4}\xi_1, \gamma_4 = \tfrac{\omega}{\sqrt{\mu'}}. \end{aligned}$$

The constants $A_{\mathrm{refl}}, B_{\mathrm{refl}}, A_{\mathrm{refr}}, B_{\mathrm{refr}}$ are obtained by inserting $\mathbf{u}$ and $\mathbf{v}$ into the conditions (2) and solving the resulting linear system. For a more detailed discussion see [4]. We choose $\theta_1 = \frac{\pi}{4}$, $\omega = 2\pi$, $\lambda = \mu = 1$, $\lambda' = 0.3, \mu' = 0.1$ and computational domain $(x, y) \in [-2\frac{2\pi}{\gamma_1\xi_1}, 2\frac{2\pi}{\gamma_1\xi_1}] \times [-2\frac{2\pi}{\gamma_3\eta_3}, 2\frac{2\pi}{\gamma_4\eta_4}]$. Initial data for the numerical scheme is taken as the real part of the analytic solution at time $t = 0$ and exact data is imposed at the outer boundaries. The solution is computed for 10 periods until $T = 10$ and the discrete l_2 error is measured. We use $2N \times N$ grid points. In Table 1 we display accuracy and convergence results obtained with using 4th and 6th order SBP operators.

N	$\log_{10}(e_4)$	p_4	$\log_{10}(e_6)$	p_6
21	-0.99	-	-1.73	-
41	-2.18	3.96	-3.64	6.33
81	-3.38	3.99	-5.53	6.29
161	-5.59	4.00	-7.33	5.98

Table 1: l_2 error and the rate of convergence.

References

[1] L. Cagniard, E. A. Flinn, C. H. Dix, Reflection and refraction of progressive seismic waves, McGraw–Hill Book Company Inc., (1962).

[2] K. Duru, G. Kreiss, K. Mattsson, *Accurate and Stable Boundary Treatments for Elastic Wave Equations in Second Order Formulation*, submitted manuscript, (2012).

[3] K. Mattsson, F. Ham, G. Iaccarin, *Stable and accurate wave propagation in discontinuous media*, J. Comp. Phys, **218** (2006) pp. 8753–8767

[4] K.F.Graff, *Wave Motion In Elastic Solids*, Dover Publications.

Platonic Solids, Restrictions Matrices and Space-Time Energetic Galerkin BEM

A. Aimi[1], **M. Diligenti**[1], **C. Guardasoni**[1,*]
[1] Dept. of Mathematics and Computer Science, University of Parma, Italy.
*Email: chiara.guardasoni@unipr.it

Abstract

In this paper we consider 3D exterior wave propagation Neumann problems reformulated in terms of a space-time hypersingular boundary integral equation with retarded potential. This latter is set in the so-called energetic weak form and then approximated by Galerkin Boundary Element Method. We illustrate a technique for exploiting (partial) symmetry in the time-marching procedure used to solve the final discretization linear system, if the problem is invariant under a finite group $\mathcal{G}$ of congruences of $\mathbb{R}^3$. The proposed procedure is based on the construction of suitable restriction matrices recently introduced in the context of symmetric wave propagation problems.

Introduction

Time-dependent problems that are frequently modeled by hyperbolic partial differential equations can be dealt with the boundary integral equations (BIEs) method. The transformation of the problem to a BIE follows the same well-known method for elliptic boundary value problems. For the discretization phase Boundary Element Methods (BEMs) are successfully applied for instance in seismology, in particular for the study of the soil-structure interaction, in acoustics and in the analysis of the electromagnetic scattering, taking advantage of dimensionality reduction and of the implicit enforcement of radiation conditions at infinity.

Recently, a direct space-time Galerkin BEM for the discretization of retarded potential boundary integral equations related to 3D wave propagation problems has been introduced [2] and compared with the classical space-time discretization approach due to Bamberger and Ha-Duong ([3], [4]).

The main drawback is that in the adopted time-marching scheme we have to solve at every time step a discretization linear system with symmetric, non-singular and fully populated matrix. The aim of this paper is to illustrate a technique to reduce the computational cost and memory storage of this time-marching procedure, in terms of both generation and numerical solution of the linear system. This technique can be applied if the problem and its discretization present complete or partial invariance with respect to a finite group $\mathcal{G}$ of congruences of $\mathbb{R}^3$. At every time step the global solution is obtained from superposition of the partial results.

Here we consider three dimensional geometries which are invariant under finite groups of distance preserving transformations, i.e. rotations and reflections. For instance, the so called Platonic solids provide nice examples of this kind of symmetry. In order to exploit the symmetry in a structured way, we can use information of the underlying transformations group acting on the physical as well as on the discretized geometry.

There is, of course, a strong connection between symmetry and group theory, and a main purpose of this paper is to present a technique for exploiting symmetry in the numerical treatment of boundary value problems, based upon suitable *restriction matrices* strictly related to a system of irreducible matrix representations of a finite group of congruences of $\mathbb{R}^3$ and to the mesh defined in the problem domain. Restriction matrices have a block structure and any block can be obtained from an *elementary restriction matrix*. Using these restriction matrices we can decompose an invariant discrete problem into independent problems with reduced dimension with respect to the original one. In fact, for the discretization with Galerkin BEM, one has to construct suitable basis functions for each problem. This can be done with restriction matrices which, applied to the vector of basis functions for the discrete complete problem, generate a basis for each finite-dimensional subproblem. This decomposition can also be obtained using Generalized Fourier Transform generated by an arbitrary finite group of permutations [6] . In literature, restriction matrices have been widely used in the context of parallel multigrid algorithms and domain decomposition reduction methods for the numerical solution of elliptic boundary value problems [5].

Also in the discrete case the geometry of the mesh, in addition to its shape, may further limit the group

of symmetries. In fact, we note that an important prerequisite to be satisfied in the mesh generation is that the mesh should be symmetry respecting. This property can also be used to reduce the storage of the mesh. Note, however, that meshes of this kind can always be constructed and this requirement does not limit the application of this technique to any continuous symmetries.
Further, restriction matrices can also be applied under the weaker assumption of partial geometrical symmetry, where the domain boundary has disconnected components, one of which at least is invariant. In fact, in many applications the operator equation presents approximate symmetries in the geometrical shape. In this case equivariant preconditioners for iterative solvers can be constructed to drastically improve convergence, in particular for equations with bad conditioning.
Various numerical simulations using restriction matrices in 3D Energetic Galerkin BEM will be presented and discussed.

1 Main result

The time-marching procedure of the Energetic Galerkin BEM is equivalent to the solution, at every discretization time step $t_\ell = (\ell+1)\,\Delta t$, $\ell = 0, \cdots, N_{\Delta t}-1$, of a linear system of order N (N is related to the discretization of the spatial domain) of the type:

$$\mathcal{A}^{(0)}\alpha^{(\ell)} = \tilde{\beta}^{(\ell)} \tag{1}$$

where $\tilde{\beta}^{(\ell)} = \beta^{(\ell)} - (\mathcal{A}^{(1)}\alpha^{(\ell-1)} + \cdots + \mathcal{A}^{(\ell)}\alpha^{(0)})$ and $\alpha^{(\ell)} = \left(\alpha_k^{(\ell)}\right)$, $\beta^{(\ell)} = \left(\beta_k^{(\ell)}\right)$, $k = 1, \cdots, N$ are, respectively, the vector collecting the unknowns at the ℓ-time step and the known vector coming from the problem data. The symmetric, non singular matrix $\mathcal{A}^{(0)}$ is the coefficient block which remains fixed, while all the other square blocks $\mathcal{A}^{(\ell)}$ of order N are used to update at every time step the right-hand side. All matrices $\mathcal{A}^{(\ell)}$ are dense and they can be of considerable dimension. Hence, if the boundary Γ of the spatial domain of the wave propagation problem satisfies some (even partial) symmetry properties, it would be useful to exploit them to increase the computational gain in the construction of blocks $\mathcal{A}^{(\ell)}$ and in the numerical solution of (1) at every time step. Now, we indicate with $\mathcal{R}_1, \cdots, \mathcal{R}_M$, M suitable restriction matrices constructed in relation to the symmetry properties of the problem at hand, where $\mathcal{R}_j$ has N_j rows, and $N = \sum_{j=1}^{M} N_j$. The following result holds [1]:

Theorem. *Matrix $\mathcal{A}^{(0)}$ verifies conditions*

$$\mathcal{R}_i\mathcal{A}^{(0)}\mathcal{R}_j^H = 0 \qquad i \neq j, \quad i,\, j = 1, \cdots, M, \tag{2}$$

and system (1) *can be decomposed in M independent subsystems:*

$$\mathcal{A}_j^{(0)}\,\alpha_j^{(\ell)} = \tilde{\beta}_j^{(\ell)} \qquad j = 1, \cdots, M, \tag{3}$$

with $\mathcal{A}_j^{(0)} = \mathcal{R}_j\mathcal{A}^{(0)}\mathcal{R}_j^H$ non-singular matrix of order N_j and $\tilde{\beta}_j^{(\ell)} = \mathcal{R}_j\tilde{\beta}^{(\ell)}$. The solution $\alpha^{(\ell)}$ of (1) *is obtained by $\alpha^{(\ell)} = \sum_{j=1}^{M}\mathcal{R}_j^H\alpha_j^{(\ell)}$, where $\alpha_j^{(\ell)} = \mathcal{R}_j\alpha^{(\ell)}$ is the solution of* (3).

Of course, this results can be equivalently interpreted as a block diagonalization of system (1).

References

[1] A. Aimi and M. Diligenti, *Restriction matrices for numerically exploiting symmetry*, Adv. Comput. Math., **28** (2008), pp. 201–235.

[2] A. Aimi, M. Diligenti, A. Frangi and C. Guardasoni, *A stable 3D energetic Galerkin BEM approach for wave propagation interior problems*, Engineering Analysis with Boundary Elements, **36** (2012), pp. 1756–1765.

[3] A. Bamberger and T. Ha Duong, *Formulation variationnelle espace-temps pour le calcul par potentiel retardé de la diffraction d'une onde acoustique. I*, Math. Methods Appl. Sci., **8** (1986), pp. 405–435.

[4] A. Bamberger and T. Ha Duong, *Formulation variationnelle pour le calcul de la diffraction d'une onde acoustique par une surface rigide*, Math. Methods Appl. Sci., **8** (1986), pp. 598–608.

[5] C.C. Douglas and B.F. Smith, *Using symmetries and antisymmetries to analyze a parallel multigrid algorithm: The elliptic boundary value problem case*, SIAM J. Numer. Anal., **26** (1989), pp. 1439–1461.

[6] J. Tausch, *A generalization of the discrete Fourier transform in Exploiting Symmetry*, in: Applied and Numerical Analysis, E.L. Allgower, K. Georg and R. Miranda (Eds.), Lectures in Applied Mathematcs **29**, Providence, RI, AMS, 1993, pp. 405–412.

Stable and accurate wave simulations in complex geometries and discontinuous media

K. Mattsson[1,*], **M. Almquist**[1], **S. Engblom**[1]
[1] Division of Scientific Computing, Department of Information Technology, Uppsala University.
*Email: ken.mattsson@it.uu.se

Abstract

A stable and high order accurate Cartesian grid-discretization is derived for hyperbolic equations, with focus on the compressible Euler equations and the second order wave equation. Physical boundaries and interfaces are treated by interpolating from the neighboring Cartesian grid-points. The Summation-By-Parts property (SBP) [1] is extended to cases where the physical boundary and interfaces do not coincide with the Cartesian grid-points. Combined with a penalty (SAT) method [2] for imposing boundary and interface conditions we obtain a stable and fully explicit time integration scheme. We present higher order (higher than third order) accurate finite difference approximations. The analysis is verified by numerical simulations in two space dimensions.

Introduction

The focus in the present study is to derive a Cartesian grid method to solve the compressible Euler equations and the second order wave equation in complex geometries and discontinuous media. Traditionally, there have been essentially two approaches of handling the discontinuity, sometimes referred to as the heterogeneous and the homogeneous formulations. In the heterogeneous approach (see for example [3]), the discontinuity is treated by taking an average "smoothing" of the spatially varying coefficients to recover stability. The benefit with this technique is that irregular shaped discontinuous interfaces are handled with no special treatment. However, the formal order of accuracy reduces to first-order (see for example [2]). In [4] a globally second-order accurate finite difference method for the acoustic wave equation on second-order form is constructed, where the discontinuity and complex geometry are handled by embedding the domain into a Cartesian grid, making use of ghost-points and Lagrange interpolation to impose the boundary and interface conditions. It is unclear if that embedded boundary method can be extended to system of equations and more general boundary conditions.

In the present study we will treat the boundaries and interfaces using a heterogeneous approach that leads to high-order accurate and stable approximations also for hyperbolic systems. The present method, referred to as *the immersed SBP-SAT method*, does not introduce stiffness and we use the explicit fourth order Runge-Kutta method for time integration. The physical boundaries and the media discontinuity are treated with SBP operators, where the boundary and interface conditions are imposed weakly using the SAT method in combination with interpolation.

1 The immersed SBP-SAT method

The SBP operators are 1-D operators and each spatial dimension is treated separately. The computational domain is split into a sum of 1-D lines, where the numerical boundaries at each line (left and right) are located at $\tilde{x}_l$ and $\tilde{x}_r$ respectively. The physical boundaries are located at $x_l = \tilde{x}_l - h\,\alpha_l$ and $x_r = \tilde{x}_r + h\,\alpha_r$ where $-1/2 \le \alpha^{l,r} < 1/2$. $\alpha^{l,r} = 0$ corresponds to the case where the physical and numerical boundaries intersect. Here h denotes the Cartesian grid-spacing. We introduce qth order accurate interpolations at the left and right boundaries,

$$v_l = \sum_{k=0,\dots q} \beta_k^l v_k \ , v_r = \sum_{k=0,\dots q} \beta_k^r v_{N-k} \ ,$$

where $v^T = [v_0, v_1, \dots, v_N]$ is the discrete solution vector. This means that $v_l \simeq u(x_l, t)$, $v_r \simeq u(x_r, t)$. To simplify notation we introduce the following vectors

$$\begin{aligned} e_l &= [\beta_0^l, \dots, \beta_q^l, 0, \dots, 0]^T \\ e_r &= [0, \dots, 0, \beta_q^r, \dots, \beta_q^r]^T \ , \end{aligned} \tag{1}$$

i.e, $v_l = e_l^T v$, $v_r = e_r^T v$.

We are now ready to introduce the immersed SBP property (here presented only for the first derivative),

Definition 1.1 *A difference operator* $D_1^{(\alpha)} = H_\alpha^{-1}(\tilde{Q} - e_l^T e_l + e_r^T e_r)$ *approximating* $\partial/\partial x$, *using a pth-order accurate stencil, is said to be a pth-order accurate immersed first-derivative SBP operator if* $H_\alpha = H_\alpha^T > 0$ *and* $\tilde{Q} = -\tilde{Q}^T$.

To motivate the strength and usefulness of the new immersed SBP operators we consider the advection

N	$\log l_2^{triangle}$	q	$\log l_2^{circle}$	q
41^2	-5.19	0.00	-5.23	0.00
81^2	-6.51	4.38	-6.57	4.44
161^2	-7.82	4.35	-7.78	4.03
321^2	-9.01	3.97	-9.03	4.15

Table 1: $log(l_2 - errors)$ and convergence rates for an immersed triangle and an immersed circle.

equation,

$$u_t + u_x = 0, \quad x_l \le x \le x_r, \quad t \ge 0 \, , u(x,0) = f(x)$$
$$u(x_l, t) = g_l(t) \, . \tag{2}$$

The energy method applied to (2) leads to

$$\frac{d}{dt}\|u\|^2 = + g_l^2 - u(x_r,t)^2 \, . \tag{3}$$

The computational grid is between $\tilde{x}_l = x_l + \alpha_l h \le x \le x_r - \alpha_r h = \tilde{x}_r$. The discrete approximation of (2) using the SAT method for the boundary condition leads to

$$v_t + D_1^\alpha v = -\tau_l H_\alpha^{-1} e_l \left\{ v_l - g_l(t) \right\} \, , \quad v(0) = f \, , \tag{4}$$

where e_l and e_r are defined in (1).

The energy method applied to (4) leads to

$$\frac{d}{dt}\|v\|_H^2 = \frac{\tau^2}{2\tau - 1} g_l^2 - v_r^2 - (2\tau_l - 1)\left(v_l - \frac{\tau_l}{2\tau - 1} g_l \right)^2 \, .$$

An energy estimate exist for $\tau > 1/2$. The choice $\tau_l = 1$, yields

$$\frac{d}{dt}\|v\|_H^2 = g_l^2 - v_r^2 - (v_l - g_l)^2 \, . \tag{5}$$

2 Computations

A convergence study is presented for the 2-D compressible Euler equations with the present immersed SBP-SAT technique. A triangle is embedded into the Cartesian grid (see Figure 1). To verify accuracy and stability we perform simulations where an analytic Euler vortex is imposed at the surface of a triangle and a circle. A convergence study is found in Table 1.

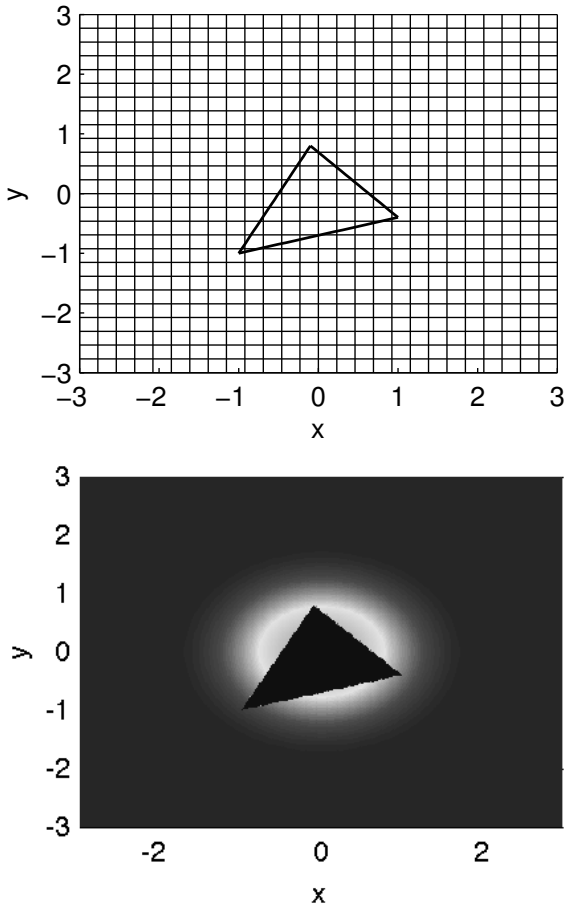

Figure 1: A triangle embedded in the underlying Cartesian grid. Here simulating an Euler vortex.

References

[1] K. Mattsson and J. Nordstrom. "Summation by parts operators for finite difference approximations of second derivatives". *J. Comp. Phys.*, Vol. **199(2)**, 503–540, 2004.

[2] K. Mattsson. "Summation by parts operators for finite difference approximations of second-derivatives with variable coefficients". *J. Sci. Comp.*, Vol. **51(3)**, 650–682 2012.

[3] G. Cohen and P. Joly. "Construction and analysis of fourth-order finite difference schemes for the acoustic wave equation in nonhomogeneous media". *SIAM J. Num. Anal.*, Vol. **33(4)**, 1266–1302, 1996.

[4] H.-O. Kreiss and N.A. Petersson. "An embedded boundary method for the wave equation with discontinuous coefficients". *SIAM J. Sci. Comput.*, Vol. **28**, 2054–2074, 2006.

Dispersion analysis of improved time discretization for simply supported prestressed Timoshenko systems. Application to the stiff piano string.

J. Chabassier[1,*], **S. Imperiale**[2]
[1] Magique3d, Inria Sud Ouest, Talence, France.
[2] Department of Applied Physics and Applied Mathematics, Columbia University, New York, USA.
*Email: juliette.chabassier@inria.fr

Abstract

We study the implicit time discretization of Timoshenko prestressed beams. This model features two types of waves: flexural and shear waves, that propagate with very different velocities. We present a novel implicit time discretization adapted to the physical phenomena occuring at the continuous level. After analyzing the continuous system and the two branches of eigenfrequencies associated with the standing modes, the classical θ-scheme is studied. A dispersion analysis recalls that $\theta = 1/12$ reduces the numerical dispersion, but yields a severely constrained stability condition for our application. Therefore we propose a new θ-like scheme based on two parameters adapted to each wave velocity, which reduces the numerical dispersion while relaxing this stability condition. Numerical experiments successfully illustrate the theoretical results on the specific cas of a realistic piano string. This motivates the extension of the proposed approach for more challenging physics.

Introduction

Piano strings can be modeled as simply supported Timoshenko prestressed beams. This model introduced in [2] accounts for inharmonicity of the transversal displacement, via a coupling with a shear angle resulting in the propagation of flexural and shear waves with very different speeds. Our concern in this work is to develop a new implicit time discretization, which will be associated with finite element methods in space, in order to reduce the numerical dispersion of flexural waves while allowing the use of a large time step in spite of the high shear velocity (compared to the maximal time step allowed with the explicit leap-frog scheme).

1 Continuous system

The prestressed Timoshenko model considers two unknowns (u, φ) which stand respectively for the transversal displacement and the shear angle of the cross section of the the string. We assume that the physical parameters (see [1] for definition) are positive and that $ES > T_0$ (which is true in practice for piano strings). We consider "simply supported" boundary conditions (zero displacement and zero torque). It reads:
Find (u, φ) such that $\forall\, x \in]0, L[, \quad \forall\, t > 0$,

$$\begin{cases} \rho S \dfrac{\partial^2 u}{\partial t^2} - T_0 \dfrac{\partial^2 u}{\partial x^2} + SG\kappa \dfrac{\partial}{\partial x}\big(\varphi - \dfrac{\partial u}{\partial x}\big) = \sigma, \\ \rho I \dfrac{\partial^2 \varphi}{\partial t^2} - EI \dfrac{\partial^2 \varphi}{\partial x^2} + SG\kappa\big(\varphi - \dfrac{\partial u}{\partial x}\big) = 0, \end{cases} \tag{1}$$

with boundary conditions

$$\begin{aligned} u(x=0,t) = 0, \qquad & u(x=L,t) = 0, \\ \partial_x \varphi(x=0,t) = 0, \quad & \partial_x \varphi(x=L,t) = 0, \end{aligned} \tag{2}$$

where σ stands for a source term. Standard energy techniques for systems of wave equations can be used to show a priori estimates on this system thanks to the following energy identity:

$$\frac{d\mathcal{E}}{dt} = \int_0^L \rho S\, \sigma \cdot \partial_t u, \quad \text{with} \tag{3}$$

$$\mathcal{E}(t) = \frac{1}{2}\int_0^L \rho\, S\, |\partial_t u|^2 + \frac{1}{2}\int_0^L \rho\, I\, |\partial_t \varphi|^2 + \frac{1}{2}\int_0^L T_0\, |\partial_x u| + \frac{1}{2}\int_0^L EI\, |\partial_x \varphi|^2 + \frac{1}{2}\int_0^L SG\kappa\, |\varphi - \partial_x u|^2 . \tag{4}$$

If we seek a solution of the form ${}^t(u, \varphi)(x, t) = V(x) e^{-2i\pi f\, t}$, then there exists (see [3]) ℓ such that $f = f_\ell^{\pm}$, where

$$\begin{cases} f_\ell^- = \ell f_0^- \left(1 + \epsilon\, \ell^2\right) + \mathcal{O}(\ell^5), & \text{(5a)} \\ \text{where } \ f_0^- = \dfrac{1}{2L}\sqrt{\dfrac{T_0}{\rho S}},\ \epsilon = \dfrac{\pi^2}{2L^2}\dfrac{EI}{T_0}\Big[1 - \dfrac{T_0}{ES}\Big]. \\ f_\ell^+ = f_0^+ \left(1 + \eta\, \ell^2\right) + \mathcal{O}(\ell^4), & \text{(5b)} \\ \text{where } \ f_0^+ = \dfrac{1}{2\pi}\sqrt{\dfrac{SG\kappa}{\rho I}},\ \eta = \dfrac{\pi^2}{2L^2}\dfrac{EI + IG\kappa}{SG\kappa}. \end{cases}$$

2 Discretisation

Space discretisation is done with high order finite elements on a mesh of size h. After this process, we

get the following equation:

$$\frac{d^2}{dt^2} M_h U_h + K_h U_h = M_h \mathbf{\Sigma}_h \tag{6}$$

where M_h is symmetric positive definite and K_h is positive semi-definite.

2.1 Time discretisation with a classical θ-scheme

Using a classical θ-scheme leads to :

$$M_h \frac{U_h^{n+1} - 2U_h^n + U_h^{n-1}}{\Delta t^2} + K_h \left(\theta U_h^{n+1} + (1-2\theta) U_h^n + \theta U_h^{n-1}\right) = M_h \mathbf{\Sigma}_h \tag{7}$$

Stability of this numerical scheme and a priori estimates can be shown with energy techniques. First, any numerical solution is shown to satisfy an energy identity. If $\theta \geq 1/4$, this discrete energy is always positive, while if $\theta < 1/4$, the time step Δt must be lower than a maximal value Δt^θ. Then, the scheme is shown to be stable if the energy is positive. Orignial proofs of stability are proposed in [1].

We also remind that if we seek a solution of the form $U_h^n = V_h^0 e^{2i\pi f_h n\Delta t}$, then there exists ℓ such that $f_h = f_{h,\ell}$, where

$$f_{h,\ell} = f_\ell + \frac{f_\ell^3}{2}\left(\frac{1}{12} - \theta\right)\Delta t^2 + \mathcal{O}(\Delta t^4 + h^4) \tag{8}$$

where $f_\ell = f_\ell^\pm$ is one of the eigenfrequencies of the continuous problem given in (5). Choosing $\theta = 1/12$ reaches fourth order of accuracy. This value being lower than $1/4$, it leads to a conditionally stable scheme. This condition will be very severe, because of the large velocity of the shear waves of the system of a realistic piano string.

Our goal is to construct a numerical scheme with a small numerical dispersion on the flexural wave, without undergoing the time step restriction coming from the shear waves.

2.2 Time discretisation with a new θ-scheme.

The idea is to separate the matrix K_h into the sum of two matrices $\overline{K}_h$ and $\underline{K}_h$, respectively inducing the energy terms $T_0 |\partial_x u|^2$ and $EI |\partial_x \varphi|^2 + SG\kappa |\varphi - \partial_x u|^2$. We consider the following scheme, with $(\theta, \overline{\theta}) \in [0,\ 1/2]^2$:

$$M_h \frac{\mathbf{U}_h^{n+1} - 2\mathbf{U}_h^n + \mathbf{U}_h^{n-1}}{\Delta t^2} + \underline{K}_h \{\mathbf{U}_h\}_\theta^n + \overline{K}_h \{\mathbf{U}_h\}_{\overline{\theta}}^n = M_h \mathbf{\Sigma}_h^n \tag{9}$$

where the θ-approximation of $\mathbf{U}_h(t^n)$ is the weighted average on three time steps:

$$\{\mathbf{U}_h\}_\theta^n = \theta\, \mathbf{U}_h^{n+1} + (1-2\theta)\, \mathbf{U}_h^n + \theta\, \mathbf{U}_h^{n-1}, \tag{10}$$

Stability of this scheme and a priori estimates can be shown via energy techniques. Sufficient conditions of stability can be given according to the values of $(\theta, \overline{\theta})$ (see [1]).

We show that if we seek a solution of the form $U_h^n = V_h^0 e^{2i\pi f_h n\Delta t}$, then there exists ℓ such that $f_h = f_{h,\ell}$, where

$$\begin{cases} f_{h,\ell}^- = \ell\, f_0^- \left(1 + \epsilon_{\Delta t}\, \ell^2\right) + \mathcal{O}(\ell^5 + \Delta t^4 + h^4), & \text{(11a)} \\ f_{h,\ell}^+ = f_{0,\Delta t}^+ \left(1 + \eta_{\Delta t}\, \ell^2\right) + \mathcal{O}(\ell^3 + \Delta t^4 + h^4), & \text{(11b)} \end{cases}$$

with (f_0^-, f_0^+, ϵ and η were defined in (5))

$$\begin{cases} \epsilon_{\Delta t} = \epsilon + 2\pi^2\, \Delta t^2 \left(\frac{1}{12} - \overline{\theta}\right) \left(f_0^-\right)^2, & \text{(12a)} \\ f_{0,\Delta t}^+ = f_0^+ \left[1 + (2\pi f_0^+)^2 \left(\frac{1}{12} - \theta\right) \Delta t^2\right], & \text{(12b)} \\ \eta_{\Delta t} = \eta + \frac{\pi^2 (E + G\kappa)}{2\rho L^2} \left(\theta - \frac{1}{12}\right) \Delta t^2. & \text{(12c)} \end{cases}$$

We note that the value $\overline{\theta} = 1/12$ provides fourth order accuracy for the approximation $f_{h,\ell}^-$ of the flexural eigenfrequencies given by (5a), for small ℓ.

The main interest of this scheme is to choose, for the slow wave, a value of $\overline{\theta}$ that diminishes numerical dispersion, and for the fast wave, a value of θ that ensures stability under acceptable conditions, typically $(\overline{\theta}, \theta) = (1/12, 1/4)$.

Numerical illustrations that show the interest of this scheme for piano strings will be displayed.

References

[1] J. Chabassier and S. Imperiale Stability and dispersion analysis of improved time discretisation for prestressed Timoshenko systems. Application to the stiff piano string. *Wave Motion*, to appear, doi : 10.1016/j.wavemoti.2012.11.002..

[2] S Timoshenko. On the correction for shear of the differential equation for transverse vibrations of bars of uniform cross-section. *Philosophical Magazine*, vol 41, pp 744–746, 1921.

[3] N. F. J van Rensburg and A. J van der Merwe. Natural frequencies and modes of a Timoshenko beam. *Wave Motion*, 44(1):58–69, 2006.

Hybrid parallel algorithm for numerical simulation of seismic waves propagation in complex 3D models: anisotropy, attenuation, small-scale heterogeneity

V. Kostin[1], V. Lisitsa[2,*], G. Reshetova[3], V. Tcheverda[2], D. Vishnevsky[2]
[2] ZAO Intel A/O, Novosibirsk, Russia.
[2] Institute of Petroleum Geology and Geophysics SB RAS, Novosibirsk, Russia.
[3] Institute of Computational Mathematics and Mathematical Geophysics SB RAS, Novosibirsk, Russia.
*Email: lisitsavv@ipgg.sbras.ru

Abstract

This paper presents an algorithm oriented on the simulation of seismic wave propagation in models containing geological formations with complex properties such as anisotropy, attenuation and small-scale inhomogeneities. These formations are typically relatively small (about 25 % of the model), however all counted features require special treatment and use of problem-oriented numerical methods which are computationally more intense than that for ideally elastic isotropic models. We suggest use of these methods locally and couple them with standard staggered grid scheme used in the major part of the model. In this paper we discuss both mathematical aspects of algorithm and peculiarities of its parallel implementation.

Introduction

Nowadays numerical simulation of wave propagation in realistic 3D isotropic elastic media have became common part of seismic data processing and interpretation. Typically these simulations are performed by finite-difference (FD) schemes and in particular by standard staggered grid scheme (SSGS) [1]. However, if anisotropy, attenuation or small-scale inhomogeneities present in the model one needs to apply more computationally intense techniques, such as generalized standard linear solid (GSLS) model [2] for attenuation, Lebedev scheme (LS) [3] for anisotropy, or fine grids for small-scale objects. Meanwhile, these complex structures take relatively small part of the model - up to 25%. To improve the efficiency of such simulation we suggest using named approaches locally. As the result the problem of coupling of several different numerical techniques is arisen.

1 The algorithm

1.1 Local time-space mesh refinement

In order to take into account fine structure of the model fine grids are used in the vicinity of clusters of small-scale objects which are coupled with a coarse grid applied for discretization of the main part of computational domain. Coupling of the different grids is based on original procedure of mesh refinement which has the following peculiarities:

- refinement of spatial and temporal steps are performed separately; i.e. at different interfaces, to ensure stability;
- refinement of temporal grid steps is based on approximation of elastic wave equation (both first and second order formulations) and free from interpolation, to ensure second order of convergence and low artificial reflections;
- 2D FFT based interpolation is used for spatial steps refinement, to minimize amount of data to exchange between processor groups;
- independent domain decomposition is applied for fine and coarse grid regions with allocation of different groups of processors, to ensure high level of processor balancing.

As the result the algorithm is stable, low-reflecting, well-balanced and allows the fine-gridded region to be placed in arbitrary position within computational domain.

1.2 Anisotropy

The principal difference between isotropic and anisotropic models is the structure of the stiffness tensor, which has block-diagonal form for isotropic media and no special structure in case of anisotropy. As the result the SSGS [1] used for isotropic models can not be applied for general anisotropy, where we suggest using the Lebedev scheme (LS) [3]. However, the LS requires four times mode RAM and floating point operations per grid cell than the SSGS. As the result a coupling of these two schemes was implemented, so that the LS is used only in subdomains containing anisotropic formations. The LS has a set of 9 spurious modes which propagate along their own

characteristics. So, the coupling of the SSGS and the LS is based on the requirement that the true wave should pass the artificial interface with as low reflections and artificial transmissions as possible, while the spurious modes of the LS should not penetrate to the SSGS region.

1.3 Viscoelasticity

Seismic attenuation is introduced into a model by a convolution-like operator mapping strains into stresses. In order to localize the operator in time a rational approximation in frequency space is applied after that the additional memory variables are used in time space. As the result the size of the model (number of variables and equations) doubles in comparison with ideally elastic model. At the same time stating the memory variables being equal to zero one gets the ideally elastic material. Moreover, the conjugation conditions at the interfaces for elastic and viscoelastic wave equation are the same; i.e. there is no conditions for the memory variables. Thus the simplest way to improve the performance of the numerical algorithm for simulation of wave propagation in models containing viscoelastic formations is to allocate RAM for the memory variables and solve corresponding equations only locally.

On the other hand if domain decomposition technique is applied for parallel implementation one have to solve a PU balancing problem. Moreover, algorithm based on finite-difference approximation of the first order equations has two types of synchronization points. The first one is after velocity being updated which assumes equal amount of computational work per grid cell for both models. The second one is after stresses being updated where the computational work is different. Thus some of PU will be waiting regardless to the particular sizes of the elementary subdomains. So, we suggest to construct domain decomposition to minimize total computational time (core-hours) of the algorithm. It was proved theoretically and confirmed numerically that the optimal ratio of the elementary subdomains volumes for elastic and viscoelastic parts of the model should be equal to 3.1.

2 Numerical experiment

Designed algorithm was implemented to study wave propagation in fractured reservoir embedded in complex model of buried channel which was viscoelastic, see fig. 1. Zero off-set seismic data is provided in fig. 2, illustrating presence of scattered waves associated with fractured reservoir.

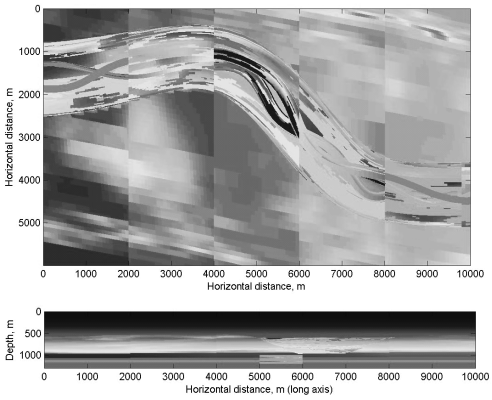

Figure 1: The buried channel model.

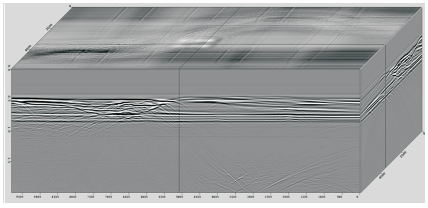

Figure 2: Zero off-set seismogram.

3 Acknowledgements

This research was supported by RFBR grants no. 12-05-31008, 13-05-00076, 11-05-00947, grant MK-77.2013.5 and fellowship SP-150.2012.5 of President of Russian Federation, and Integration projects SB RAS 127 and 130.

References

[1] J. Virieux, *P-SV wave propagation in heterogeneous media: Velocity-stress finite-difference method*, Geophysics, **51** (1986), pp. 889–901.

[2] J.O. Blanch, A. Robertson, W.W. Symes, *Modeling of a constant Q: Methodology and algorithm for an efficient and optimally inexpensive viscoelastic technique*, Geophysics, **60** (1995), pp. 176–184.

[3] V. I. Lebedev, *Difference analogies of orthogonal decompositions of basic differential operators and some boundary value problems*, Soviet Comput. Math. Math. Physics., **4** (1964), pp. 449–456.

Numerical modeling of nonlinear acoustic waves with fractional derivatives

B. Lombard[1], **J. F. Mercier**[2,*]
[1] LMA, CNRS UPR 7051, Marseille, France
[2] POEMS, CNRS-INRIA-ENSTA UMR 7231, Palaiseau, France
*Email: jean-francois.mercier@ensta.fr

Abstract

Wave propagation in a 1-D guide with an array of Helmholtz resonators is considered, with large amplitude waves and viscous boundary layers. A numerical strategy is proposed to get efficient simulations: conservative schemes for hyperbolic conservation laws, diffusive representation for the fractional derivatives and integrals, and splitting to couple both aspects.

Introduction

Wave propagation in lattices is the object of many theoretical and experimental works. Floquet-Bloch band gaps are exhibited in ordered lattices, whereas localization occurs in disordered cases. Usually, linear conservation laws are assumed, and nonlinearities (if present) are incorporated punctually [1].

Figure 1: Guide with an array of Helmholtz resonators (courtesy given by O. Richoux).

The case of large amplitude waves in a 1-D array of Helmholtz resonators is addressed theoretically in [2], where the evolution equations are put in the form

$$\left\{ \begin{array}{l} \dfrac{\partial u}{\partial t} + \dfrac{\partial}{\partial x}\left(a u + b \dfrac{u^2}{2} \right) = c \dfrac{\partial^{-1/2}}{\partial t^{-1/2}} \dfrac{\partial u}{\partial x} + d \dfrac{\partial^2 u}{\partial x^2} - e \dfrac{\partial p}{\partial t}, \\ \dfrac{\partial^2 p}{\partial t^2} + f \dfrac{\partial^{3/2} p}{\partial t^{3/2}} + g p = h u. \end{array} \right. \tag{1}$$

The variables are the horizontal acoustic velocity u and the acoustic pressure p in the throat of Helmholtz resonators. The physical parameters are positive and constant: a for advection; b for Burgers; c and f for the dissipation in the viscous boundary layer of the guide and resonators; d for the diffusivity of sound; g for the oscillation in the resonators. Lastly, e and h couple the evolution of u and p.

Depending on the initial conditions and the parameters in (1), an equilibrium between steepening effects of nonlinearity and smoothing effects of dissipation may be reached, leading to acoustic solitary waves [2]. Our aim is to investigate numerically their properties and as a first approach we propose here simulations in the uncoupled case $e = 0 = h$.

1 Numerical methods

A uniform grid with spatial mesh size Δx and time step Δt is used. The nonlinear acoustic equations with diffusion (parameters a, b and d) are integrated by standard explicit TVD scheme with MC-limiter:

$$\begin{array}{rcl} u_i^{n+1} & = & u_i^n - \dfrac{\Delta t}{\Delta x} \left(f_{i+1/2} - f_{i-1/2} \right) \\ & + & \dfrac{d\,\Delta t}{\Delta x^2} \left(u_{i+1}^n - 2\,u_i^n + u_{i-1}^n \right), \end{array} \tag{2}$$

where $f_{i\pm1/2}$ is the numerical flux [3]. The condition of stability is

$$\Delta t \leq \min \left(\left(\frac{2\,d}{\Delta x^2} + \frac{c_{\max}}{\Delta x} \right)^{-1}, \frac{\Delta x}{c_{\max}} + \frac{2\,d}{c_{\max}^2} \right), \tag{3}$$

where $c_{\max} = a + b \max(u)$. The fractional derivatives in (1) are non-local in time. To avoid storing past values of the solution, we use a diffusive representation [4]. For instance, the fractional integral of order 1/2 is replaced by a sum of memory variables

$$\frac{\partial^{-1/2}}{\partial t^{-1/2}} \frac{\partial u}{\partial x} = \int_0^{+\infty} \phi(\theta, t)\, d\theta \approx \sum_{\ell=1}^{N} \kappa_l\, \phi(\theta_\ell, t),$$

where local-in-time $\phi_\ell(t) \equiv \phi(\theta_\ell, t)$ are defined by

$$\left\{ \begin{array}{l} \dfrac{d\phi_\ell}{dt} = -\theta_\ell^2\, \phi_\ell + \dfrac{2}{\pi} \dfrac{\partial u}{\partial x}, \\ \phi_\ell(0) = 0. \end{array} \right.$$

The weights κ_ℓ and the nodes θ_ℓ are based on Gauss-Laguerre orthogonal polynomials [5]. Strang splitting is used to couple nonlinear acoustic equations (a, b and d) with the boundary layer effects in the tube (c): doing so is easy and does not modify the condition of stability (3). Lastly, a diffusive approach is also applied for the fractional oscillatons of p in (1); time integration is performed by a unconditionnally stable Newmark scheme.

2 Numerical experiments

The first test is a validation of the algorithms for nonlinear advection. The physical parameters are $a = 300$ m/s, $b = 1$, whereas all the other parameters are null. Consequently, no coupling between u and p is considered, and no fractional derivatives are introduced. A 5-m long domain is discretized on 1000 grid nodes. The CFL number is 0.9. The initial solution is a door function: $u_0(x) = 200\ (H(x-0.5) - H(x-1))$, where H is the Heaviside function. Figure 2 shows the solution at $t = 0$ and a comparison between numerical and exact solutions at various times. After 400 time steps, the right part of the rarefaction fan has not still reached the right-going shock; at 800 time steps, the rarefaction fan interacts with the shock. One observes a very good agreement between the two solutions: good description of the corners on the rarefaction wave, accurate location of the shock, and almost no smearing or oscillations at the discontinuity.

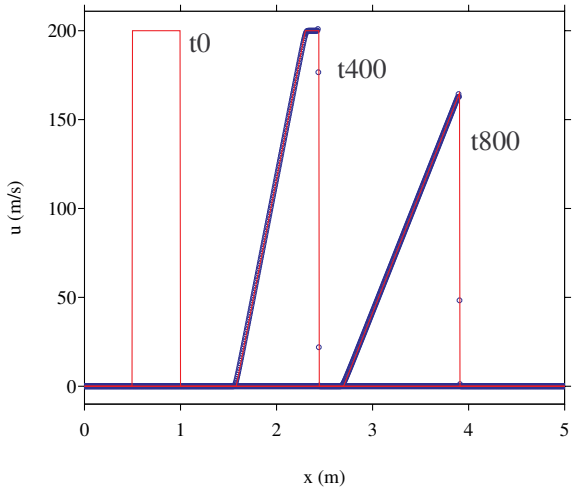

Figure 2: nonlinear acoustics. Initial solution (green line); comparison between TVD solution (blue circles) and exact solution (red line).

The second test focuses on the homogeneous fractional oscillator of order 3/2 in (1), with nonnull coefficients $f = 0.5$ and $g = 1$. The initial conditions are $p(0) = 1$ and $\frac{\partial p}{\partial t}(0) = 0$. The numerical solution is computed on 50 Laguerre nodes. The exact solution is computed by a power series [4]. Comparison between the solutions is given in Figure 3.

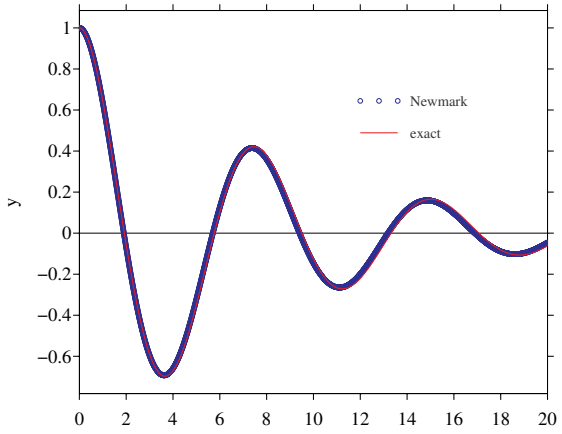

Figure 3: fractional oscillator of order 3/2.

Acknowledgements. This study has been initiated with Agnès Maurel (ESPCI, France), Olivier Richoux and Vincent Pagneux (LAUM, France), and is supported by the ANR ProCoMedia. Pierre Haldenwang (AMU, France) is thanked for the exact solution in Figure 2.

References

[1] O. Richoux, V. Tournat, T. Le Van Suu *Acoustic wave dispersion in a one-dimensional lattice of nonlinear resonant scatterers*, Phys. Rev. E, **75(2)** (2007), 026615.

[2] N. Sugimoto, *Propagation of nonlinear acoustic waves in a tunnel with an array of Helmholtz resonators*, J. Fluid. Mech., **244** (1992), 55–78.

[3] R. J. LeVeque, *Numerical methods for conservation laws*, 2nd edition, Birkhäuser-Verlag, 1992.

[4] J. F. Deü, D. Matignon, *Simulation of fractionnaly damped mechanical systems by means of a Newmark-diffusive scheme*, Comput. Math. App., **59** (2010), 1745–1753.

[5] C. Birk, C. Song, *An improved non-classical method for the solution of fractional differential equations*, Comput. Mech., **46** (2010), 721-734.

A Predictor-Corrector Algorithm for Animating Nonlinear Water Waves

F. Benkhaldoun[1], **S. Sari**[1,*], **M. Seaid**[2]
[1] LAGA, Université Paris 13, 99 Av J.B. Clement, 93430 Villetaneuse, France
[2] School of Engineering and Computing Sciences, University of Durham, South Road, Durham DH1 3LE, UK.
*Email: sari@math.univ-paris13.fr

Abstract

Nonlinear shallow water equations are used to model the dynamics of water waves over non-flat beds. To approximate numerical solutions to this class of hyperbolic systems of conservation laws we propose a simple and accurate finite volume solver. The method consists of a predictor stage to reconstruct the numerical fluxes using the method of characteristics, while a corrector stage is used to discretize the conservative system in a finite volume framework. Numerical results are presented for animating water waves in a closed domain with gradually varying bed.

1 Introduction

In the conservative form, the nonlinear shallow water equations can be reformulated in a compact form as

$$\partial_t \mathbf{W} + \partial_x \mathbf{F}(\mathbf{W}) + \partial_y \mathbf{G}(\mathbf{W}) = \mathbf{S}(\mathbf{W}), \qquad (1)$$

where

$$\mathbf{W} = \begin{pmatrix} h \\ hu \\ hv \end{pmatrix}, \quad \mathbf{S} = \begin{pmatrix} 0 \\ -gh\partial_x Z \\ -gh\partial_y Z \end{pmatrix},$$

$$\mathbf{F} = \begin{pmatrix} hu \\ hu^2 + \frac{1}{2}gh^2 \\ huv \end{pmatrix}, \quad \mathbf{G} = \begin{pmatrix} hv \\ huv \\ hv^2 + \frac{1}{2}gh^2 \end{pmatrix}.$$

The equations (1) can also be reformulated in an advective compact form as

$$D_t \mathbf{U} + \mathbf{Q}(\mathbf{U}) = \mathbf{0}, \qquad (2)$$

where $D_t = \partial_t + u\partial_x + v\partial_y$ is the total derivative and

$$\mathbf{U} = \begin{pmatrix} h \\ u \\ v \end{pmatrix}, \quad \mathbf{Q} = \begin{pmatrix} h\left(\partial_x h + \partial_y v\right) \\ g\partial_x\left(h + Z\right) \\ g\partial_y\left(h + Z\right) \end{pmatrix}.$$

2 Characteristic Finite Volume Method

we cover the spatial domain with rectangular cells $\mathcal{C}_{i,j} = [x_{i-\frac{1}{2}}, x_{i+\frac{1}{2}}] \times [y_{j-\frac{1}{2}}, y_{j+\frac{1}{2}}]$ of uniform sizes Δx and Δy for simplicity. The finite volume discretization of (1) is

$$\begin{aligned} W_{i,j}^{n+1} &= W_{i,j}^n - \frac{\Delta t}{\Delta x}\left(F_{i+1/2,j}^n - F_{i-1/2,j}^n\right) \\ &\quad - \frac{\Delta t}{\Delta y}\left(G_{i,j+1/2}^n - G_{i,j-1/2}^n\right) + \Delta t S_{i,j}^n, \end{aligned}$$

where $F_{i\pm1/2,j}^n$ and $G_{i,j\pm1/2}^n$ are the numerical fluxes.

2.1 Predictor stage

Step 1. *Compute the departure points* $\mathbf{X}_{i+1/2,j}(t_n)$ *and* $\mathbf{Y}_{i,j+1/2}(t_n)$ *using an iterative procedure*

$$\mathbf{X}_{i+1/2,j}(t_n) = \mathbf{x}_{i+1/2,j} - \int_{t_n}^{t_n+\alpha\Delta t} \mathbf{V}\left(\tau, \mathbf{X}_{i+1/2,j}(\tau)\right)$$

where $\mathbf{V}$ *is the advective vector and* α *is a parameter between 0 and 1.*

Step 2. *Calculate the interpolated solutions* $\widetilde{\mathbf{U}}_{i+1/2,j}$ *and* $\widetilde{\mathbf{U}}_{i,j+1/2}$ *e.g.,*

$$\widetilde{\mathbf{U}}_{i+1/2,j} = \mathcal{P}\Big(\mathbf{U}\left(t_n, X_{i+1/2}, Y_j\right)\Big),$$

where $\mathcal{P}$ *is an interpolating polynomial.*

Step 3. *Construct the intermediate solution* $\mathbf{U}_{i+1/2,j}$ *and* $\mathbf{U}_{i,j+1/2}$ *using a first-order scheme for the SWE in the advective form e.g.,*

$$\mathbf{U}_{i+1/2,j}^{n+1} = \widetilde{\mathbf{U}}_{i+1/2,j}^n - \Delta t\, \mathbf{Q}\left(\widetilde{\mathbf{U}}_{i+1/2,j}^n\right).$$

2.2 Predictor stage

Step 4. *Cover the conservative variables* $\mathbf{W}_{i+1/2,j}$ *and* $\mathbf{W}_{i,j+1/2}$ *from the advective variables* $\mathbf{U}_{i+1/2,j}$ *and* $\mathbf{U}_{i,j+1/2}$.

Step 5. *Update the solution using the simple first-order scheme with respect to the C-property*

$$\begin{aligned} \mathbf{W}_{i,j}^{n+1} &= \mathbf{W}_{i,j}^n - \frac{\Delta t}{\Delta x}\left(\mathbf{F}(\mathbf{W}_{i+1/2,j}^n) - \mathbf{F}(\mathbf{W}_{i-1/2,j}^n)\right) \\ &- \frac{\Delta t}{\Delta y}\left(\mathbf{G}(\mathbf{W}_{i,j+1/2}^n) - \mathbf{G}(\mathbf{W}_{i,j-1/2}^n)\right) + \Delta t \mathbf{S}(\bar{\mathbf{V}} \end{aligned}$$

3 Numerical Results

3.1 Geostrophic adjustment simulation on a flat bottom

We consider a test proposed in [4] corresponding to the following initial condition:

$$h(x,y,0) = 1+\frac{1}{4}\left[1-\tanh\left[10\left[\sqrt{2.5x^2+0.4y^2}-1\right]\right]\right],$$
$$(hu)(x,y,0)=0, \qquad (hv)(x,y,0)=0.$$

We consider a quadrilateral 200×200 mesh for the domain $[-10,10]\times[-10,10]$ and the CFL number is fixed to 0.5. Figure 1 shows the numerical results obtained with the first order proposed scheme. The initial elliptical mass imbalance evolves in an axisymmetric way. Shock waves propagate leaving behind an elevation which is slowly spinning clockwise.

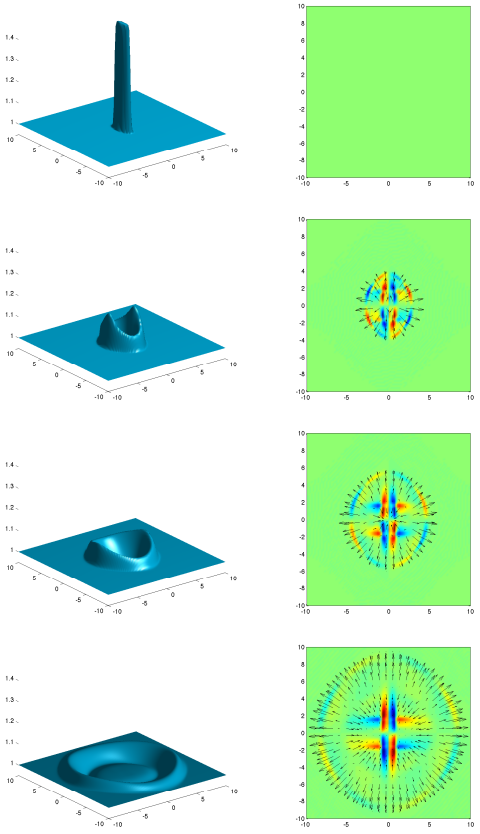

Figure 1: Evolution of the free surface (left) and the velocity field (right) on a flat bottom at different simulation times. From top to bottom $t = 0, 0.5, 1$ and 2 s

3.2 Geostrophic adjustment simulation on a non flat bottom

We consider the same initial conditions for the water height and the discharge as the example treated in the section above. We add a topography having the following form

$$z(x,y)=\begin{cases}0, & \text{if} \quad x<0,\\ 0.3\,(1.0+\tanh(1.5x))\,, & \text{otherwise.}\end{cases}$$

Unlike the previous test, Figure 2 shows a flow evolving in a nonaxisymmetric way.

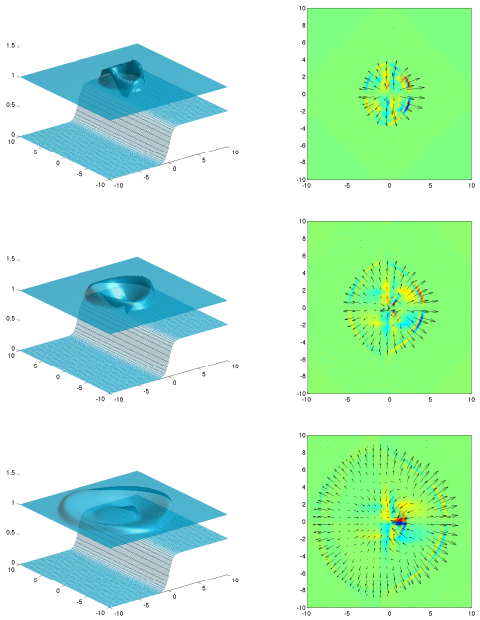

Figure 2: Evolution of the free surface (left) and the velocity field (right) on a non-flat bottom at different simulation times. From top to bottom $t = 0.5, 1$ and 2 s

References

[1] J. LeVeque Randall, *Numerical Methods for Conservation Laws*, Lectures in Mathematics ETH Bürich, (1992).

[2] F. Benkhaldoun and M. Seaïd, *Combined characteristics and finite volume methods for sediment transport and bed morphology in surface water flows*, Mathematics and Computers in Simulation. **81**, 2073-2086 (2011).

[3] F. Benkhaldoun and M. Seaïd, *A simple finite volume method for the shallow water equations*, J. Comp. Applied Math. **234**, 58–72 (2010).

[4] A. C. Kuo, L. M. Polvani, *Nonlinear geostrophic adjustment, cyclone/anticyclone asymmetry, and potential vorticity rearrangement*, Phys. of Fluids. **12** 1087–1100 (2000).

The Transient Motion of a Floating Rigid or Elastic Body

M. H. Meylan[1,*],
[1] School of Mathematical and Physical Sciences, The University of Newcastle, Callaghan 2308, NSW, Australia
*Email: mike.meylan@newcastle.edu.au

Abstract

We consider the time dependent motion of a floating body, either rigid or elastic, which is subject to some initial displacement and which subsequently evolves freely. We show how the solution can be calculated using a Laplace/Fourier transform. We also show that this is solution method is equivalent to the Cummins, or memory effect, method. We also show how the Laplace/Fourier transform solution can be coupled with an expansion over resonances to give the singularity expansion method.

Introduction

We are concerned here with the time-dependent motion of a floating body which is given an initial displacement and then allowed to evolve freely. A strong connection between the frequency domain and time domain solution exists and this is the basis of the generalized eigenfunction solution method [1], [2], [3], the *Cummins* method [4] and also the Laplace/Fourier transform solution [5].

The *singularity expansion method* is a method to approximate the time-dependent response of a wave scattering problem using *resonances*, *resonance poles* or *scattering frequencies*. They have been investigated for the rigid-body case [6], for floating bodies [7] and for hydroelastic bodies [8]. The presentation here generality is new as are the formula and identities.

1 General Equations for a Floating Body in the Time Domain

The fluid motion is assumed to be irrotational so that it may be described by a velocity potential $\Phi(\mathbf{x}, z, t)$, where $\mathbf{x} = (x, y)$ are the horizontal coordinates and z is the vertical coordinate pointing vertically up-wards with the free-surface is at $z = 0$. The velocity potential satisfies the following equations

$$\Delta\Phi = 0, \ (\mathbf{x}, z) \in \Omega, \tag{1a}$$

$$\partial_z\Phi = 0, \ z = -h, \tag{1b}$$

$$\partial_z\Phi + \frac{1}{g}\,\partial_t^2\Phi, \ \mathbf{x} \in \partial\Omega_F, \tag{1c}$$

where Ω is the fluid volume, g is the acceleration due to gravity, and $\partial\Omega_F$ is the free-surface.

We expand the body motion modes and we define the motion coefficient $\zeta_p(t)$ as the motion of the pth mode. Therefore, on the structure, the normal fluid velocity must match that of the structure so that

$$\partial_n\Phi = \sum_p \partial_t\zeta_p(t)n_p, \ \ \mathbf{x} \in \partial\Omega_B, \tag{2}$$

where n_p is the normal associated with the pth mode and $\partial\Omega_B$ is the wetted surface of the body. The decomposition is entirely identical to that for a rigid body. The motion is subject to the initial conditions that the fluid is at rest and that initial body motion is prescribed.

The equations of motion for the elastic body are found by coupling the elastic body equations with the forcing due to the fluid and we obtain

$$\sum_q M_{pq}\partial_t^2\zeta_q + \sum_q K_{pq}\zeta_q = -\rho\iint_{\partial\Omega_B}\partial_t\Phi\, n_p \ \mathrm{d}S - \sum_q C_{pq}\zeta_q = 0. \tag{3}$$

Here M_{pq} are the elements of the mass matrix, K_{pq} are the elements of the stiffness matrix and C_{pq} are the elements of the restoring force matrix. The integral term of (3) is the hydrodynamic force arising from the fluid motion. The only difference for the elastic and rigid body is the inclusion of the K_{pq} terms.

2 Expression for the Solution via the Fourier/Laplace Transform

We will calculate the solution to equation (3) by the Fourier/Laplace transform. We define the Fourier/Laplace transform as

$$\hat{\zeta_p}(s) = \int_0^\infty \zeta_p(t)\mathrm{e}^{\mathrm{i}st}\,\mathrm{d}t,$$

and

$$\hat{\Phi}(s) = \int_0^\infty \Phi(t)\mathrm{e}^{\mathrm{i}st}\,\mathrm{d}t.$$

Note that there is a strong connection between the frequency domain variable ω and the s variable but we distinguish these here.

We assume that at $t = 0$ the fluid is at rest and the body is given only an initial displacement. The Fourier/Laplace transform of (2) and (3) gives

$$\mathbf{M}\left(-s^2\hat{\boldsymbol{\xi}} + \mathrm{i}s\boldsymbol{\xi}(0)\right) + \mathbf{K}\hat{\boldsymbol{\xi}} + \mathbf{C}\hat{\boldsymbol{\xi}} + \left(\mathbf{A}(s) + \frac{\mathrm{i}}{s}\mathbf{B}(s)\right)\left(-s^2\hat{\boldsymbol{\xi}} + \mathrm{i}s\boldsymbol{\xi}(0)\right) = 0 \quad (4)$$

where $\mathbf{A}$ and $\mathbf{B}$ are the added mass and damping [4]. The exact solution in the time domain is given by

$$\boldsymbol{\xi}(t) = \frac{1}{2\pi}\int_{-\infty}^{\infty}\left(-s^2\mathbf{M} + \mathbf{K} + \mathbf{C} - s^2\mathbf{A}(s) - \mathrm{i}s\mathbf{B}(s)\right)^{-1} \times \left(-\mathbf{M} - \mathbf{A}(s) - \frac{\mathrm{i}}{s}\mathbf{B}(s)\right)\mathrm{i}s\boldsymbol{\xi}(0)\mathrm{e}^{-\mathrm{i}st}\,\mathrm{d}s. \quad (5)$$

The following expression is easier to calculate numerically,

$$\boldsymbol{\xi}(t) = \frac{1}{\pi}\int_{0}^{\infty}\mathrm{Re}\left\{\left(-s^2\mathbf{M} + \mathbf{K} + \mathbf{C} - s^2\mathbf{A}(s) - \mathrm{i}s\mathbf{B}(s)\right)^{-1} \times \left(-\mathbf{M} - \mathbf{A}(s) - \frac{\mathrm{i}}{s}\mathbf{B}(s)\right)\mathrm{i}s\boldsymbol{\xi}(0)\right\}\cos(st)\,\mathrm{d}s, \quad (6)$$

since the real part decays rapidly at $s \to \infty$.

Note that this implies that

$$\mathbf{I} = \frac{1}{\pi}\int_{0}^{\infty}\mathrm{Re}\left\{\left(-s^2\mathbf{M} + \mathbf{K} + \mathbf{C} - s^2\mathbf{A}(s) - \mathrm{i}s\mathbf{B}(s)\right)^{-1} \times \left(-\mathbf{M} - \mathbf{A}(s) - \frac{\mathrm{i}}{s}\mathbf{B}(s)\right)\mathrm{i}s\right\}\,\mathrm{d}s, \quad (7)$$

3 Complex Resonances

We can approximate the solution to equation (5) using the *singularity expansion method*. In this method the solution is approximated as a sum over the complex resonances. We define

$$\boldsymbol{\Phi}(s) = -s^2\mathbf{A}(s) - \mathrm{i}s\mathbf{B}(s).$$

The equation for a complex resonance at ω_m is

$$\left(\mathbf{K} - \omega_m^2\mathbf{M} + \mathbf{C} + \boldsymbol{\Phi}(\omega_m)\right)\mathbf{u}_m = 0. \quad (8)$$

and $\mathbf{u}_m$ is the resonance vector.

Near the complex resonance at position ω_m with associated resonance vector $\mathbf{u}_m$ with the solution can be approximated by

$$\hat{\boldsymbol{\xi}}(s) = \mathbf{u}_m\frac{\mathbf{u}_m\cdot\left(-\mathbf{M} - \mathbf{A}(s) - \frac{\mathrm{i}}{s}\mathbf{B}(s)\right)}{(s-\omega_m)\bar{\mathbf{u}}_m\cdot\left(\mathbf{M} - \boldsymbol{\Phi}'\right)\mathbf{u}_m}, \quad (9)$$

We substitute our approximation for $\hat{\boldsymbol{\xi}}$ (9) into (5) and obtain

$$\boldsymbol{\xi}(t) \approx \mathrm{Re}\left\{\sum_m \mathbf{u}_m\frac{\mathbf{u}_m\cdot\left(-\mathbf{M} - \mathbf{A}(\omega_n) - \frac{\mathrm{i}}{\omega_n}\mathbf{B}(\omega_n)\right)\mathrm{i}\omega_n\boldsymbol{\xi}(0)}{\mathbf{u}_m\cdot\left(\mathbf{M} - \boldsymbol{\Phi}'\right)\mathbf{u}_m}\mathrm{e}^{-\mathrm{i}}\right.$$

4 Conclusions

We have presented the general solution for a time-dependent motion of a floating body which is subject to some initial displacement and then allowed to evolve freely. The solution is derived using the Fourier/Laplace transform and we show that this solution can be approximated using complex resonances by applying the singularity expansion method.

References

[1] M. H Meylan. Spectral solution of time dependent shallow water hydroelasticity. *J. Fluid Mech.*, 454:387 – 402, 2002.

[2] C. Hazard and M. H Meylan. Spectral theory for a two-dimensional elastic thin plate floating on water of finite depth. *SIAM J. Appl. Math.*, 68(3):629–647, 2007.

[3] C. Fitzgerald and M. H Meylan. Generalized eigenfunction method for floating bodies. *J. Fluid Mech.*, 677:544–554, 2011.

[4] W. E. Cummins. The impulse response function and ship motions. *Schiffstechnik*, 9:101–109, 1962.

[5] F. Ursell. The decay of the free motion of a floating body. *J. Fluid Mech.*, 19:303–319, 1964.

[6] M. H. Meylan and R. Eatock Taylor. Time-dependent water-wave scattering by arrays of cylinders and the approximation of near trapping. *J. Fluid Mech.*, 631:103–125, 2009.

[7] S.J. Maskell and F. Ursell. The transient motion of a foating body. *J. Fluid Mech.*, 44:303–313, 1970.

[8] C. Hazard and F. Loret. Generalized eigenfunction expansions for scattering problems with an application to water waves. *Proc. R. Soc. Edin. A*, 137:995–1035, 2007.

Stable and accurate simulation of phenomena in relativistic quantum mechanics

M. Almquist[1,*], **K. Mattsson**[1], **T. Edvinsson**[2]
[1] Department of Information Technology, Uppsala University, Uppsala, Sweden.
[2] Department of Chemistry, Uppsala University, Uppsala, Sweden.
*Email: martin.almquist@it.uu.se

Abstract

We present studies of phenomena in relativistic quantum mechanics, with focus on Klein tunneling (also known as the Klein paradox) which occurs in single- and bi-layer graphene [3]. The underlying model is the time-dependent Dirac equation, which we solve in two and three spatial dimensions. By using Summation-By-Parts (SBP) operators [2] and a penalty (SAT) approach [1] to impose boundary and interface conditions, we obtain stable and fully explicit high-order finite difference schemes. The analysis is verified by convergence studies against analytical solutions.

Introduction

The aim in the present study is to study time-dependent phenomena in relativistic quantum mechanics. We focus on electrons tunneling through potential barriers. According to non-relativistic quantum mechanics, the tunneling probability decays exponentially with the barrier height. In the relativistic case however, the tunneling probability tends to a non-zero limit as the barrier height goes to infinity. This phenomenon is known as Klein tunneling. In this setting, the fundamental model is the time-dependent Dirac equation, which incorporates both relativity and particle spin. The more studied Schrödinger equation can be shown to be the non-relativistic approximation of the Dirac equation without spin. In a coming study, we hope to compare the two models and investigate the importance of spin and relativity in relevant applications.

1 The Dirac equation

The Dirac equation for a spin $\frac{1}{2}$ particle is of the form

$$i\hbar\boldsymbol{\psi}_t = \boldsymbol{H}\boldsymbol{\psi}, \tag{1}$$

where $\boldsymbol{H}$ is the Hamiltonian operator. In three spatial dimensions, the equation can be written as

$$\boldsymbol{\psi}_t = \boldsymbol{A}\boldsymbol{\psi}_x + \boldsymbol{B}\boldsymbol{\psi}_y + \boldsymbol{C}\boldsymbol{\psi}_z + \boldsymbol{D}\boldsymbol{\psi}, \tag{2}$$

where the matrices $\boldsymbol{A}$, $\boldsymbol{B}$ and $\boldsymbol{C}$ are Hermitian, while $\boldsymbol{D}$ is skew-Hermitian. $\boldsymbol{A}$, $\boldsymbol{B}$ and $\boldsymbol{C}$ can be diagonalized,

$$\boldsymbol{A} = \boldsymbol{T}_A\boldsymbol{\Lambda}_A\boldsymbol{T}_A^*,\ \boldsymbol{B} = \boldsymbol{T}_B\boldsymbol{\Lambda}_B\boldsymbol{T}_B^*,\ \boldsymbol{C} = \boldsymbol{T}_C\boldsymbol{\Lambda}_C\boldsymbol{T}_C^*,$$

where the diagonal matrices $\boldsymbol{\Lambda}_{A,B,C}$ hold the eigenvalues of $\boldsymbol{A}$, $\boldsymbol{B}$ and $\boldsymbol{C}$, respectively. In the simple case of a free particle, we have analytical solutions of the form

$$\boldsymbol{\psi}(\vec{r},t) = \boldsymbol{u}_{\vec{p}}\, e^{\frac{i}{\hbar}(\vec{r}\cdot\vec{p}-E_p t)}, \tag{3}$$

where $E_p = \pm\sqrt{p^2c^2 + m^2c^4}$.

1.1 The continuous problem

Consider the 1-D Dirac equation with Dirichlet boundary conditions,

$$\begin{cases} \boldsymbol{\psi}_t = \boldsymbol{A}\boldsymbol{\psi}_x + \boldsymbol{D}\boldsymbol{\psi}, & 0 < x < 1, & t \le 0, \\ \boldsymbol{\psi} = \boldsymbol{g}_l, & x = 0, & t > 0, \\ \boldsymbol{\psi} = \boldsymbol{g}_r, & x = 1, & t > 0, \\ \boldsymbol{\psi} = \boldsymbol{f}, & 0 \le x \le 1, & t = 0. \end{cases} \tag{4}$$

We split $\boldsymbol{A}$ into a positive and negative part, $\boldsymbol{A} = \boldsymbol{A}_+ + \boldsymbol{A}_-$, using *Steger-Warming* flux-splitting,

$$\boldsymbol{A}_\pm = \boldsymbol{T}_A\left(\frac{\boldsymbol{\Lambda}_A \pm |\boldsymbol{\Lambda}_A|}{2}\right)\boldsymbol{T}_A^*. \tag{5}$$

We impose the boundary conditions on the ingoing characteristic variables. That is, we apply the *Steger-Warming* flux-splitting at the boundaries and specify $\boldsymbol{A}_-\boldsymbol{\psi}$ and $\boldsymbol{A}_+\boldsymbol{\psi}$ at the left and right boundaries, respectively. Applying the energy method to (4) yields

$$\begin{aligned} \frac{d}{dt}||\boldsymbol{\psi}||^2 = {} & \boldsymbol{g}_r^*\boldsymbol{A}_+\boldsymbol{g}_r + \boldsymbol{\psi}^*\boldsymbol{A}_-\boldsymbol{\psi}|_{x=1} \\ & - \boldsymbol{g}_l^*\boldsymbol{A}_-\boldsymbol{g}_l - \boldsymbol{\psi}^*\boldsymbol{A}_+\boldsymbol{\psi}|_{x=0}. \end{aligned} \tag{6}$$

1.2 The semi-discrete problem

To simplify the notation we define E_0 and E_N as matrices that pick out the values at the left and right boundaries, respectively. Applying the SBP-SAT method to (4) with a first derivative SBP operator D_x and a corresponding norm H_x leads to the semi-discrete problem

$$\begin{aligned} \psi_t = {} & AD_x\psi + D\psi + \tau_l H_x^{-1}E_0A_-(\psi_0 - g_l) \\ & + \tau_r H_x^{-1}E_N A_+(\psi_N - g_r). \end{aligned} \tag{7}$$

N	$\log l_2{}^{(4th)}$	$q^{(4th)}$	$\log l_2{}^{(6th)}$	$q^{(6th)}$
31^3	-1.39	0.00	-1.26	0.00
61^3	-2.07	2.24	-2.11	2.80
121^3	-2.83	2.55	-3.07	3.20
241^3	-3.76	3.09	-4.28	4.01

Table 1: $log(l_2-errors)$ and convergence rates using diagonal-norm operators.

N	$\log l_2{}^{(8th)}$	$q^{(8th)}$	$\log l_2{}^{(10th)}$	$q^{(10th)}$
31^3	-1.06	0.00	-0.70	0.00
61^3	-2.12	3.54	-1.90	4.00
121^3	-3.32	3.98	-3.42	5.06
241^3	-4.72	4.64	-5.17	5.80

Table 2: $log(l_2-errors)$ and convergence rates using diagonal-norm operators.

Multiplying by $\psi^* H_x$, adding the transpose and choosing $\tau_l = 1$, $\tau_r = -1$, we obtain (for diagonal-norm operators)

$$\begin{aligned}\frac{d}{dt}(\psi^* H_x \psi) = {} & g_r^* A_+ g_r + \psi_N^* A_- \psi_N \\ & - g_l^* A_- g_l - \psi_0^* A_+ \psi_0 \\ & + (\psi_0 - g_l)^* A_- (\psi_0 - g_l) \\ & - (\psi_N - g_r)^* A_+ (\psi_N - g_r).\end{aligned} \tag{8}$$

We note that the semi-discrete energy estimate (8) exactly mimics the continuous estimate (6) with the addition of the two last terms, which are small damping terms.

Extending the technique to two and three dimensions is straightforward.

2 Computations

A convergence study for a free particle in 3-D is presented. The analytical solution (3) is imposed at the boundaries. Tables 1 and 2 show the results obtained with diagonal-norm SBP operators. Tables 3 and 4 show the results for block-norm operators. The operators are here denoted by the order of accuracy of the interior stencil.

To simulate Klein tunneling, we introduce a potential barrier and let a wave packet collide with the barrier. Figure 1 shows the probability density in the x-y plane, as the wave packet interacts with the barrier at $x = 0.5$ pm. The discontinuity at the potential step is handled with a multi-block technique. The continuity of the solution across the interface is imposed weakly using the SAT technique.

N	$\log l_2{}^{(4th)}$	$q^{(4th)}$	$\log l_2{}^{(6th)}$	$q^{(6th)}$
31^3	-1.60	0.00	-1.93	0.00
61^3	-2.60	3.33	-3.61	5.59
121^3	-3.77	3.88	-5.38	5.86
241^3	-4.98	4.03	-7.20	6.07

Table 3: $log(l_2-errors)$ and convergence rates using block-norm operators.

N	$\log l_2{}^{(8th)}$	$q^{(8th)}$	$\log l_2{}^{(10th)}$	$q^{(10th)}$
31^3	-2.14	0.00	-2.18	0.00
61^3	-4.55	7.99	-4.91	9.06
121^3	-6.86	7.69	-7.59	8.90
241^3	-9.27	8.00	-10.08	8.27

Table 4: $log(l_2-errors)$ and convergence rates using block-norm operators.

References

[1] M. H. Carpenter and D. Gottlieb and S. Abarbanel, *Time-stable boundary conditions for finite-difference schemes solving hyperbolic systems: Methodology and application to high- order compact schemes* , J. Comp. Phys., **111** (1994), pp. 220–236.

[2] K. Mattsson and M. Svärd and M. Shoeybi, *Stable and accurate schemes for the compressible Navier-Stokes equations* , J. Comp. Phys., **227** (2008), pp. 2293–2316.

[3] M. I. Katsnelson and K. S. Novoselov and A. K. Geim, *Chiral tunneling and the Klein paradox in graphene* , Nature Physics, **2** (2006), pp. 620–625.

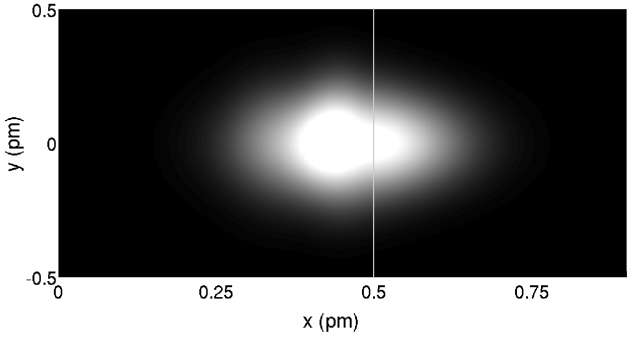

Figure 1: Wave packet tunneling through a potential barrier.

3.9 Random and periodic media

On the Müller formulation for periodic electromagnetic wave scattering problems

Kazuki Niino[1], **Naoshi Nishimura**[1,*]
[1] Graduate school of Informatics, Kyoto University
*Email: nchml@i.kyoto-u.ac.jp

Abstract

We investigate a boundary element method with Müller's formulation for dielectric scattering problems in periodic domains. In this method, the iteration number of iterative methods is expected to be small since the operators in Müller's formulation are essentially identical with the unit operator to within a compact operator. We use the Nyström method for the discretisation so that we do not need to use any basis functions. We make several numerical experiments to see the accuracy and the efficiency of this method.

1 Introduction

For analysing periodic optical structures numerically, the combination of boundary element methods(BEM) and periodic fast multipole methods(FMM) is considered to provide an effective solver. In periodic problems, the computational time can be larger since the iteration number increases sharply around Wood's anomaly[1], which is a peculiar phenomenon of periodic problems. It is, therefore, important to decrease the iteration number in the periodic FMM.

To develop a fast solution method for periodic problems, we consider BEM for the Müller formulation with Nyström's method in this paper in order to avoid difficulties related to basis functions[2]. Müller's formulation is one of resonance-free formulations of boundary integral equations for transmission problems. The iteration number of iterative methods for this formulation is expected to be small even with no preconditioning[3] since the integral operators in this formulation are essentially identical with the unit operator to within a compact operator.

2 Müller's formulation for periodic boundary value problems

For simplicity, we solve problems which have one scatterer in the unit domain(unit of periodicity). We define $\Omega = (-\infty, \infty) \times (-L/2, L/2) \times (-L/2, L/2)$ as the unit domain. We denote a simply connected domain in Ω by Ω^-, and also define Ω^+ to be $\Omega \backslash \overline{\Omega^-}$. The electric field $\boldsymbol{E}$ and the magnetic field $\boldsymbol{H}$ satisfy Maxwell's equations: $\nabla \times \boldsymbol{E} = \mathrm{i}\omega\mu^{\pm}\boldsymbol{H}$, $\nabla \times \boldsymbol{H} = -\mathrm{i}\omega\varepsilon^{\pm}\boldsymbol{E}$ in $\Omega^{\pm}$. They also satisfy the boundary conditions: $\boldsymbol{m} := \boldsymbol{E}^+ \times \boldsymbol{n} = \boldsymbol{E}^- \times \boldsymbol{n}$, $\boldsymbol{j} := \boldsymbol{n} \times \boldsymbol{H}^+ = \boldsymbol{n} \times \boldsymbol{H}^-$ on the boundary $\Gamma = \overline{\Omega^+} \cap \overline{\Omega^-}$, and satisfy the periodic boundary condition:

$$\begin{aligned}
\boldsymbol{E}(x_1, L/2, x_3) &= \mathrm{e}^{\mathrm{i}\beta_2}\boldsymbol{E}(x_1, -L/2, x_3),\\
\boldsymbol{E}(x_1, x_2, L/2) &= \mathrm{e}^{\mathrm{i}\beta_3}\boldsymbol{E}(x_1, x_2, -L/2),\\
\boldsymbol{H}(x_1, L/2, x_3) &= \mathrm{e}^{\mathrm{i}\beta_2}\boldsymbol{H}(x_1, -L/2, x_3),\\
\boldsymbol{H}(x_1, x_2, L/2) &= \mathrm{e}^{\mathrm{i}\beta_3}\boldsymbol{H}(x_1, x_2, -L/2),
\end{aligned}$$

where $\boldsymbol{n}$ is the unit normal vector which is outward from Ω^-, $\boldsymbol{E}^{\pm}$ and $\boldsymbol{H}^{\pm}$ are the limit values of $\boldsymbol{E}$ and $\boldsymbol{H}$ from the domain $\Omega^{\pm}$, $\varepsilon^{\pm}$ and $\mu^{\pm}$ are the permittivity and the permeability in the domain $\Omega^{\pm}$ and β_2 and $\beta_3 \in \mathbb{R}$ are phase differences along x_2 and x_3 directions, respectively. We solve the Maxwell's equations under these conditions and the radiation condition for the scattered waves $\boldsymbol{E}^{\mathrm{sca}}$ and $\boldsymbol{H}^{\mathrm{sca}}$ at infinity, where $\boldsymbol{E}^{\mathrm{sca}} := \boldsymbol{E} - \boldsymbol{E}^{\mathrm{inc}}$, $\boldsymbol{H}^{\mathrm{sca}} := \boldsymbol{H} - \boldsymbol{H}^{\mathrm{inc}}$ and $\boldsymbol{E}^{\mathrm{inc}}$ and $\boldsymbol{H}^{\mathrm{inc}}$ are the electric and magnetic fields of the incident wave, respectively.

To solve this problem, we use boundary element methods with Müller's formulation. The boundary integral equations corresponding to this problem are given as follows:

$$\begin{aligned}
&\mathrm{i}\omega\varepsilon^+\boldsymbol{E}^{\mathrm{inc}} \times \boldsymbol{n} = \mathrm{i}\omega\frac{\varepsilon^+ + \varepsilon^-}{2}\boldsymbol{m} +\\
&\boldsymbol{n} \times \int_\Gamma \Big\{ -\mathrm{i}\omega(\varepsilon^+\nabla G^{p+} - \varepsilon^-\nabla G^-) \times \boldsymbol{m} -\\
&(k^{+2}G^{p+} - k^{-2}G^-)\boldsymbol{j} - (\nabla\nabla G^{p+} - \nabla\nabla G^-)\boldsymbol{j} \Big\} \mathrm{d}S_y,
\end{aligned} \tag{1}$$

$$\begin{aligned}
&\mathrm{i}\omega\mu^+\boldsymbol{n} \times \boldsymbol{H}^{\mathrm{inc}} = \mathrm{i}\omega\frac{\mu^+ + \mu^-}{2}\boldsymbol{j} +\\
&\boldsymbol{n} \times \int_\Gamma \Big\{ -\mathrm{i}\omega(\mu^+\nabla G^{p+} - \mu^-\nabla G^-) \times \boldsymbol{j} +\\
&(k^{+2}G^{p+} - k^{-2}G^-)\boldsymbol{m} + (\nabla\nabla G^{p+} - \nabla\nabla G^-)\boldsymbol{m} \Big\} \mathrm{d}S_y,
\end{aligned} \tag{2}$$

where G^{p+} is the periodic Green function for Helmholtz' equation in Ω^+ defined by $G^{p+}(\boldsymbol{x}) =$

$\sum_{\boldsymbol{\omega}\in\mathcal{L}} G^+(\boldsymbol{x}-\boldsymbol{\omega})\mathrm{e}^{\mathrm{i}\boldsymbol{\beta}\cdot\boldsymbol{\omega}}$, $G^\pm(\boldsymbol{x}) = \mathrm{e}^{\mathrm{i}k^\pm|\boldsymbol{x}|}/(4\pi|\boldsymbol{x}|)$, $\boldsymbol{\beta} = (0,\beta_2,\beta_3)$ and $\mathcal{L} = \{(0,\omega_2,\omega_3)|\omega_2 = pL, \omega_3 = qL,\ p,q\in\mathbb{Z}\}$.

We can rewrite the equations (1) and (2) into the following form:

$$\left\{\begin{pmatrix}\mathrm{i}\omega\frac{\varepsilon^+ +\varepsilon^-}{2}\mathcal{I} & 0\\ 0 & \mathrm{i}\omega\frac{\mu^+ +\mu^-}{2}\mathcal{I}\end{pmatrix} + \begin{pmatrix}\mathcal{K}_{11} & \mathcal{K}_{12}\\ \mathcal{K}_{21} & \mathcal{K}_{22}\end{pmatrix}\right\}\begin{pmatrix}\boldsymbol{m}\\ \boldsymbol{j}\end{pmatrix} = \begin{pmatrix}\mathrm{i}\omega\varepsilon^+\boldsymbol{E}^{\mathrm{inc}}\times\boldsymbol{n}\\ \mathrm{i}\omega\mu^+\boldsymbol{n}\times\boldsymbol{H}^{\mathrm{inc}}\end{pmatrix}, \quad (3)$$

where $\mathcal{K}_{ij}\,(i,j=1,2)$ are the integral operators which appear in the right-hand sides of equations (1) and (2) and $\mathcal{I}$ is the unit operator. Taking into account the fact that an integral operator is compact if the integral kernel of the operator is integrable, we see that the operators $\mathcal{K}_{ij}\,(i,j=1,2)$ are compact operators. Hence, the accumulation points of the eigenvalues of the operator on the LHS of equation (3) are $\mathrm{i}\omega(\varepsilon^+ +\varepsilon^-)/2$ and $\mathrm{i}\omega(\mu^+ +\mu^-)/2$. It is, therefore, probable that almost all the eigenvalues of the coefficient matrix obtained by discretising equations (1) and (2) are also close to these points. From this fact, we expect that iterative solvers for this equation converge fast without any preconditioning.

We use Nyström's method for discretisation with Gauss's integral formulae as a quadrature method. The collocation points of Nyström's method are thus the integral points of the Gaussian quadrature.

3 Numerical example

We solve a periodic problem by using both the proposed method and our previous method, i.e., the PMCHWT formulation with the matrix of the directly computed part in periodic FMM as a right preconditioner[4]. The scatterer consists of spheres which are arranged periodically along both x_2 and x_3 axes. The radii of the spheres are 0.35. We set $L_2 = L_3 = 1$, $\varepsilon^+ = 1$, $\varepsilon^- = 2.56$ and $\mu^\pm = 1$. The incident wave is a planar wave given as $\boldsymbol{E}^{\mathrm{inc}} = \boldsymbol{E}_c\mathrm{e}^{\mathrm{i}k_1x_3}$, $\boldsymbol{H}^{\mathrm{inc}} = \boldsymbol{H}_c\mathrm{e}^{\mathrm{i}k_1x_3}$ where $\boldsymbol{E}_c = (0,1,0)$ and $\boldsymbol{H}_c = (0,0,1)$, hence $\beta_2 = \beta_3 = 0$. The spherical scatterer is discretised with 5780 triangles. We use the Galerkin method with RWG basis[5] for discretising the PMCHWT integral equation. For solving linear equations, we use GMRES with the error tolerance of $\varepsilon = 10^{-3}$ for Müller's formulation and FGMRES with $\varepsilon = 10^{-3}$ for the PMCHWT formulation. For inverting the preconditioner in the PMCHWT formulation, we use GMRES with $\varepsilon = 10^{-1}$. We did not use restart in GMRES or FGMRES.

The iteration numbers of the iterative methods in the Müller and the PMCHWT formulations are shown in Figure 1. The iteration number of Müller's formulation is smaller than that of the PMCHWT formulation for any of the frequencies considered. We also confirm that Müller's formulation with the Nyström method is faster than the PMCHWT formulation with the Galerkin method in terms of computational time.

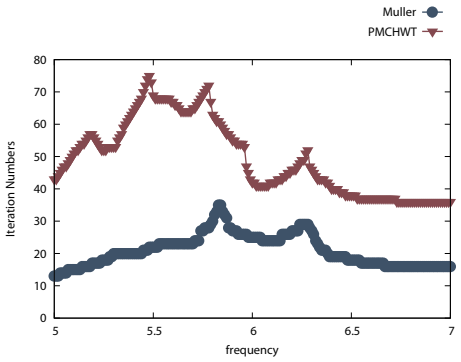

Figure 1: Iteration numbers.

4 Conclusion

We developed a solution method for periodic boundary value problems with Müller's formulation. We found that the iterative method with Müller's formulation converges faster than that with PMCHWT formulation with the matrix of directly computed part in FMM algorithm as the right preconditioner.

References

[1] R. Petit and L.C. Botten. *Electromagnetic Theory of Gratings*. Springer-Verlag, Berlin, 1980.

[2] K. Niino and N. Nishimura. *International Journal of Numerical Modelling: Electronic Networks, Devices and Fields*, Vol. 25, pp. 558–572, 2012.

[3] Y. Saad. *Iterative Methods for Sparse Linear Systems*. Society for Industrial and Applied Mathematics, Philadelphia, PA, USA, 2003.

[4] Y. Otani and N. Nishimura. *Journal of Computational Physics*, Vol. 227, No. 9, pp. 4630–4652, 2008.

[5] S. Rao, D. Wilton, and A. Glisson. *IEEE Transactions on Antennas and Propagation*, Vol. 30, No. 3, pp. 409–418, 1982.

An efficient integral equation solver for two-dimensional simulations in nanoplasmonics

H. Kurkcu[1,2,*], **F. Reitich**[3] **and A. Ortan**[3],
[1] TOBB Economy and Technology University, Sögütözü, Ankara 06560, Turkey
[2] Gulf University for Science and Technology, Mishref, Kuwait
[3] School of Mathematics, University of Minnesota, Minneapolis, Mn 55455, USA
*Email: kurkcu@math.umn.edu

Abstract

Nanoplasmonics forms a major part of the field of nanophotonics, which explores how electromagnetic fields can be confined over dimensions on the order of or smaller than the wavelength. Here, we present an integral-equation formulation of the mathematical model that delivers accurate solutions in small computational times for surface plasmons coupled by periodic corrugations of flat surfaces.

1 Introduction

Nanoplasmonics forms a major part of the field of nanophotonics, which explores how electromagnetic fields can be confined over dimensions on the order of or smaller than the wavelength. Initiated in 1902 by R.W. Wood [1] with the discovery of grating anomalies, this phenomenon has attracted significant attention over the last hundred years [2], [3], [4]. Mie in 1908 gave a mathematical description of light scattering from spherical particles of sizes comparable to the wavelength [3], describing an effect that would come to be known as localized surface plasmons in the context of nanoplasmonics. It is based on interaction processes between electromagnetic radiation and conduction electrons at metallic interfaces or in small metallic nanostructures, leading to an enhanced optical near-field at sub-wavelength dimension. In 1899, Sommerfeld had described surface waves (waves propagating at the surface of metals) mathematically, and in 1902 Wood observed anomalous drops in the intensity of light reflected by a metallic grating [3]. But theory and observation would not be linked until 1941, by Fano [5]. Further experimental validation came in 1968, when Kretschmann and Raether used prism coupling to excite surface waves with visible light [5]. Other forms of coupling to surface plasmons have been thoroughly investigated since then. All of the phenomena mentioned above are based entirely on classical electromagnetics, and thus can be mathematically described by Maxwells equations. In this paper, an integral-equations formulation is given for an infinitely periodic metal surface whose period d is on the nanometer scale. The metal is assumed to extend infinitely below this surface, while a dielectric material extends infinitely above the surface. Some details of the numerical implementation and the results of a few numerical experiments are also given in Sec. 2 and 3.

2 Formulation and Algorithm

In this section, a system of integral equations for the total exterior field u ($u = E_z$ in Transverse Electric –TE– and $u = H_z$ in Transverse Magnetic –TM– polarizations) and its normal derivative $\frac{\partial u}{\partial n}$ on the surface ∂D are given. The metal surface ∂D is infinitely thick and periodic and satisfies

$$f(x + d, y) = f(x, y).$$

These fields $[u, \frac{\partial u}{\partial n}]$ satisfy [7];

$$u^i(r) = \int_P G_i(r, r') \frac{\partial u^i(r')}{\partial n(r')} - \frac{\partial G_i}{\partial n(r')}(r, r') u^i(r') ds(r'),$$
$$u^e(r) = \int_P u^e(r') \frac{\partial G_e}{\partial n(r')}(r, r') - G_e(r, r') \frac{\partial u^e(r')}{\partial n(r')} ds(r'),$$

for $x \in D$, and for $x \in D^c$, respectively where n is the unit normal to ∂D directed into the exterior of D and P is a single period of the surface ∂D. Here, $G(r, r')$ is the quasi-periodic Green's function [8] given by

$$G_Q(r, r') = \sum_{n=-\infty}^{\infty} G_0(r, r') = \frac{i}{4} \sum_{n=-\infty}^{\infty} e^{i\alpha n d} H_0^{(1)}(k r_n)$$

where $G_0(r, r') = \frac{i}{4} H_0^{(1)}(kr)$ is the free-space Green's function for the Helmholtz equation and $\alpha = k \sin(\theta)$ where θ is incidence angle.

As $x \to \partial D$ and using the boundary conditions,

the surface integral equations become

$$u^{\text{inc}}(r) = \psi(r) + \int_P \frac{\partial(G_i - G_e)}{\partial n(r')}(r,r')\psi(r')dr' - \int_P (\nu G_i - G_e)(r,r')\frac{\partial \psi(r')}{\partial n(r')}dr',$$

$$\frac{\partial u^{\text{inc}}(r)}{\partial n(r)} = \frac{\nu+1}{2}\frac{\partial \psi(r)}{\partial n(r)} + \int_P \frac{\partial^2(G_i - G_e)}{\partial n(r)\partial n(r')}(r,r')\psi(r')dr' - \int_P \frac{\partial(\nu G_i - G_e)}{\partial n(r)}(r,r')\frac{\partial \psi(r')}{\partial n(r')}dr',$$

for $r \in \partial D$ with the unknowns $\psi(r) = u_e(r) + u^{\text{inc}}(r)$ and $\partial\psi(r)/\partial n(r)$. Here $u^{\text{inc}}(r)$ denotes the incoming incident wave and $\nu = 1$ for TE polarization and $\nu = k_i/k_e$ for TM polarization.

Our numerical algorithm depends on seeking the unknowns on the surface of the grating, and the matrix elements are evaluated through the derivation of a careful decomposition that allows for explicit evaluation of the singular and non-singular parts of the kernels [9].

3 Numerical Results

In this section, we provide numerical experiments for the algorithm described above implemented in MATLAB. The test cases in the simulations that follow correspond to ("two-dimensional") infinitely periodic metal gratings that invariant in the z direction. To investigate the existence of plasmonic resonances, we concentrate on the analysis at length scales where these do appear, namely

$$h << \lambda \sim d.$$

where d is the period, h is the height of the rough surface and λ is the wavelength.

The first grating profile is given by

$$f(x) = \frac{h}{2}\sin(x)$$

where $h = 48$nm, $d = 300$nm $\lambda = 226$nm, $\theta = 29^o$ and the metal is silver. Note that $h/\lambda \approx 0.2$ and $\lambda/d \approx 0.75$ (See Figures 1-3).

Our second example, on the other hand, correspond to a more complex profile consisting of a (Fejér-smoothed) approximation to a semi-elliptical profile represented with 51 Fourier modes (See Figure 4). The "linewidth" (size of the major axis of the ellipse) is 400 nm, and the period is $d = 630$nm. Here we present results of the integral solver for heights

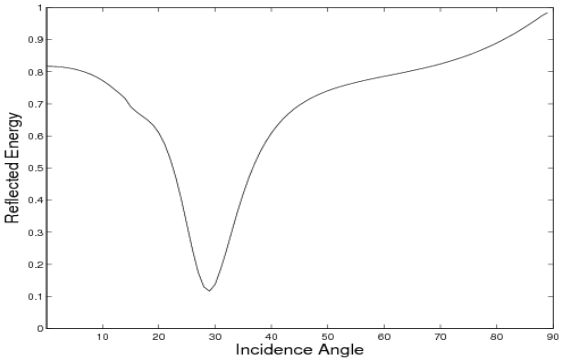

Figure 1: Reflectivity vs incidence angle map for the sinusoidal grating.

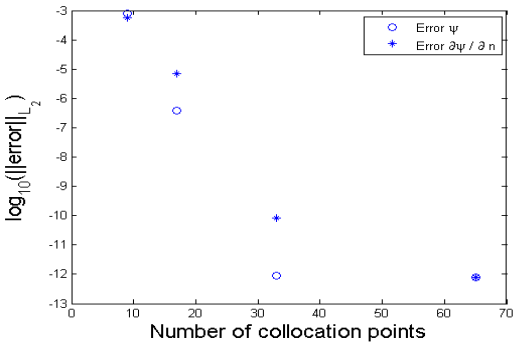

Figure 2: The error in the total field and its normal derivative as a function of the number of collocation points for the sinusoidal grating. The error is shown on a logarithmic scale for where a plasmon is generated.

$h = 20$nm and $h = 30$nm, and display a specific verification against the high-order perturbation method introduced in [10], [11] (See Figures 5 and 6).

References

[1] R. W. Wood, *On a remarkable case of uneven distribution of light in a diffraction grating spectrum*, Philos. Mag. 4, 396-402 (1902).

[2] Lord Rayleigh, *On the dynamical theory of gratings*, Proc. Royal Society (London) 79, 399-416 (1907).

[3] G. Mie, *Contributions to the optics of turbid media, particularly of colloidal metal solutions,* 25, vol. 3, no. Annalen der Physik, pp. 377445, 1908.

[4] M. I. Stockman, *Nanoplasmonics: The physics behind the applications,* Physics Today, vol. 64, no. 2, pp. 3944, 2011.

[5] Fano U., *The theory of anomalous diffraction*

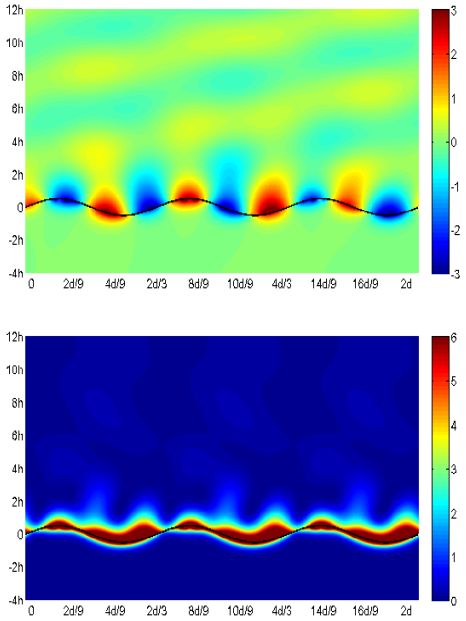

Figure 3: The real part (top) and intensity (bottom) of the field above and below the surface of the sinusoidal grating for an angle of incidence of $\theta = 29^o$.

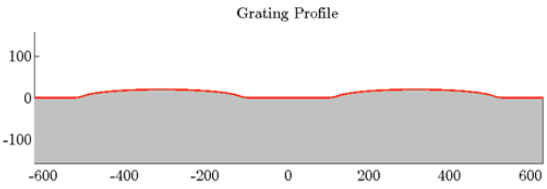

Figure 4: A semi-elliptical grating.

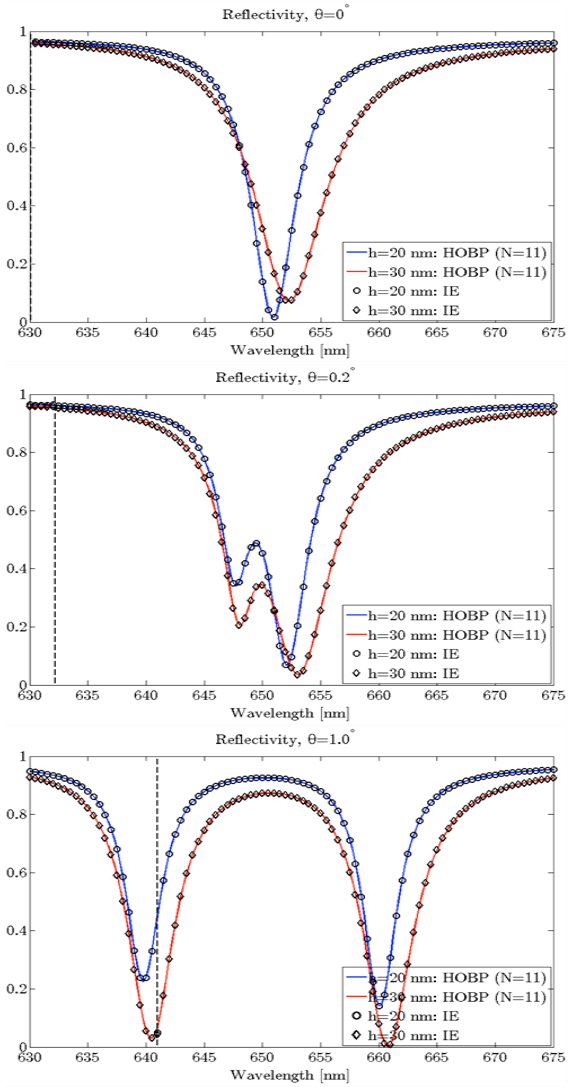

Figure 5: Comparison of integral equation solver and High Order Perturbation Method of [10,11] for the profile in Figure 4. Results for incident angles $\theta = 0^o, 0.1^o$ and 0.2^o and heights of $h = 20$nm and $h = 30$nm.

gratings and of quasi-stationary waves on metallic surfaces (Sommerfeld's waves), Journal of the Optical Society of America 31, 213-222 1941.

[6] C.H. Palmer Jr., *Parallel diffraction grating anomalies,* J. Opt. Soc. Amer. 42, 269-276, 1952.

[7] David Colton and Kress Rainer, *Inverse Acoustic and Electromagnetic Scattering Theory*, Springer-Verlag, 1992.

[8] Kurkcu H. and Reitich F., *Stable and efficient evaluation of periodized Green's functions for the Helmholtz equation at high frequencies*, in Journal of Comp. Physics, 228, 2009 pp. 75-95.

[9] Kurkcu H., *An efficient algorithm for the solution of high-frequency scattering by infinite rough surfaces*, PhD Thesis 2008.

[10] Reitich F., Johnson T., Oh S., and Meyer G., *A fast and high-order accurate boundary perturbation method for nanoplasmonic simulations: basic concepts, analytic continuation and applications*, submit..

[11] Reitich F., Johnson T., Oh S., and Meyer G., *A fast and high-order accurate boundary perturbation method for nanoplasmonic simulations: adaptivity, comparison and verifcation*, submit..

Effective boundary conditions for thin periodic coatings

M. Chamaillard[†,*], **H. Haddar**[‡], **P. Joly**[†]
[‡] DEFI, CMAP, Ecole Polytechnique, Route de Saclay, 91128 Palaiseau Cedex, France .
[†] POEMS (UMR 7231 CNRS-ENSTA-INRIA) , 828, Boulevard des Marchaux, 91762 Palaiseau
*Email: mathieu.chamaillard@inria.fr

1 Setting of the problem

We consider wave propagation in a domain $\Omega \subset \mathbb{R}^d$, with smooth boundary Γ, whose complement can be written as ($\delta > 0$ denoting a small length)

$$\mathbb{R}^3 \setminus \Omega = \overline{\mathcal{O}^\delta} \cup \overline{C^\delta}$$

where $\mathcal{O}_\delta = \{x \in \mathbb{R}^3 \,/\, d(x, \overline{\Omega}) > \delta\}$ is a perfectly reflecting object and $\mathcal{C}_\delta = \{x \in \mathbb{R}^3 \,/\, 0 < d(x, \overline{\Omega}) < \delta\}$ is a thin penetrable coating (see figure 1). We assume that this coating is "periodic" and strongly varying (see section 2), which means, roughly speaking, that its physical characteristics are highly oscillating, at scale δ, in the directions tangential to Γ. The goal of this work is to find, for numerical purpose, "equivalent" boundary conditions on Γ for replacing the presence of C^δ. This is achieved by means of a multiscale asymptotic analysis when δ tends to 0.

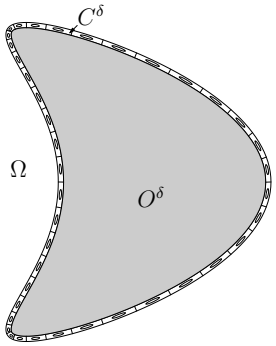

Figure 1: The geometry of the problem

2 Definition of periodic function in C^δ

Except in the case of a flat or cylindrical surface Γ, giving a precise mathematical meaning to the notion, however intuitive, of periodic coating is not a trivial modelization issue. We have chosen to see a periodic coating as resulting from a deformation of a plane coating. This refers to a parametric representation of the surface Γ that should correspond to the manufacturing of the coating. We assume the existence of a smooth and injective transformation:

$$\begin{array}{rccc} \Phi_\Gamma : & \Gamma_r \equiv \mathbb{R}^2 & \mapsto & \mathbb{R}^3 \\ & x_r \in \Gamma_r & \mapsto & x_\Gamma = \Phi_\Gamma(x_r) \end{array}$$

where Γ_r denotes the reference plane, such that the deformed surface Γ is the image of Γ_r by Φ_Γ:

$$\Gamma = \big\{x = \Phi_\Gamma(x_r), x_r \in \Gamma_r\big\}.$$

Most important geometrical objects can be defined from the differential of Φ_Γ, $D\Phi_\Gamma(x_r) \in \mathcal{L}(\mathbb{R}^2, \mathbb{R}^3)$ and its adjoint in $\mathcal{L}(\mathbb{R}^3, \mathbb{R}^2)$. At the point $x_\Gamma = \Phi_\Gamma(x_r)$,

- $\Pi(x_\Gamma) = \mathrm{Im}\ D\Phi_\Gamma(x_r)$ is the tangent plane to Γ,
- $n(x_\Gamma) \perp \Pi(x_\Gamma)$ is the normal vector to Γ,
- $g(x_\Gamma) \equiv g(x_r) = D\Phi_\Gamma(x_r)^*\, D\Phi_\Gamma(x_r) \in \mathcal{L}(\mathbb{R}^2)$ is the metric matrix of Γ.

The vector $n(x_\Gamma)$ is oriented in such a way that

$$C^\delta = \big\{x = x_\Gamma + \nu\, n(x_\Gamma),\ \nu \in]-\delta, 0], x_\Gamma \in \Gamma\ \big\}$$

Moreover, for δ small enough, (x_Γ, ν) define local coordinates in C^δ. Let C_r be the flat normalized layer:

$$C_r = \Gamma_r \times]-1, 0[\quad \text{with current point } \hat{x} = (\hat{x}_r, \hat{\nu}).$$

A periodic function f^δ in C^δ with period δ will be define from a x_r-periodic reference function, with period 1, $\hat{f}$ defined in the reference layer C_r, namely:

$$f^\delta(x) = f^\delta(x_\Gamma, \nu) = \hat{f}\Big(\frac{x_r}{\delta}, \frac{\nu}{\delta}\Big), \text{ if } x_\Gamma = \Phi_\Gamma(x_r) \quad (1)$$

where $\hat{f}(\hat{x}_r + (m,n), \hat{\nu}) = \hat{f}(\hat{x}_r, \hat{\nu}), \quad \forall\, (m,n) \in \mathbb{Z}^2$.

3 The model problem

We consider a (family) of scalar propagation problems with variable coefficients: the solution u^δ is defined in the "exterior" to the unpenetrable object

$$\Omega^\delta = \mathbb{R}^3 \setminus \mathcal{O}^\delta \quad (\Longrightarrow \quad \overline{\Omega^\delta} = \overline{\Omega} \cap \overline{C^\delta}\ )$$

and is subject, in addition to a radiation condition we shall ignore here, to a Neumann boundary condition:

$$\begin{cases} \mathrm{div}\big(\rho^\delta\, \nabla u^\delta\big) + \omega^2 \mu^\delta\, u^\delta = f, & \text{in } \Omega^\delta \\ \partial_\nu u_\delta = 0 & \text{on } \partial\Omega_\delta \end{cases} \quad (2)$$

where f denotes a compactly supported source term and where the positive and bounded functions ρ^δ and μ^δ are such that the medium is homogeneous in Ω :

$$\rho^\delta(x) = \rho^\infty, \quad \mu^\delta(x) = \mu^\infty \quad \text{in } \Omega,$$

and δ-periodic inside C^δ, i. e. ρ^δ and μ^δ are periodic (see (1)) with reference functions $\hat\rho(\hat x_r, \hat\nu)$ and $\hat\mu(\hat x_r, \hat\nu)$, extended to $\hat\nu > 0$ by ρ^∞ and μ^∞ (for (7)).

4 A third order effective boundary condition

The purpose of this work is to build a "simple" problem for computing an approximation u^δ_{app} solution in the exterior domain Ω, with the help of a generalized impedance boundary of the form:

$$\partial_\nu u^\delta_{app} + T_\delta\, u^\delta_{app} = 0, \quad \text{on } \Gamma. \tag{3}$$

The impedance operator T_δ should be a local and represent the thin coating C^δ. To construct T_δ, we search a formal power series asymptotic expansion in δ of the exact solution u^δ on the exterior domain Ω:

$$u^\delta = u^0 + \delta\, u^1 + \delta^2\, u^2 + \cdots \quad \text{in } \Omega$$

which is valid, in fact, outside a small neighborhood of Γ. In a first step, to construt inductively on k, the terms u^k of the expansion. This uses the method of matched asymptotic expansions that relies on another asymptotic expansion of u^δ, of multi-scale nature (involving homogenization and boundary layer ansatz), in a neighborhood of the coating C^δ (see [2] for more details). Then, in a second step, we look for a boundary condition "approximately satisfied" by the same expansion truncated at a given order. Doing so, our third order condition (constructed with u_0, u_1 and u_2) is obtained with the operator:

$$T_\delta = \delta\, T_1 + \delta^2\, T_2 \tag{4}$$

For simplicity, we shall give the expression of T_1 is T_2 when the coating has some symmetry properties:

$$\hat\rho(-\hat x_r, \hat\nu) = \hat\rho(\hat x_r, \hat\nu), \;\; \hat\mu(-\hat x_r, \hat\nu) = \hat\mu(\hat x_r, -\hat\nu).$$

In the general case, their expressions are similar but more involved. Let $Y^a_r = [0,1]^2 \times [-1, a]$. First, we introduce particular mean values $\overline{\rho_0}$ and $\overline{\rho_1}$ (resp. $\overline{\mu_0}$ and $\overline{\mu_1}$) of $\hat\rho$ (resp. μ):

$$\overline{\rho}_0 = \int_{Y_r} \hat\rho(\hat x)\, d\hat x, \quad \overline{\rho}_1 = \int_{Y_r} 2\,\hat\nu\,\hat\rho(\hat x)\, d\hat x, \tag{5}$$

Next, let us set, $\mathcal{L}_s(\mathbb{R}^3)$ being the space of symmetric 3×3 matrices,

$$\mathcal{T}(x_\Gamma) := \big\{ A \in \mathcal{L}_s(\mathbb{R}^3) \;/\; A\, n(x_\Gamma) = 0 \big\} \equiv \mathcal{L}_s\big(\Pi(x_\Gamma)\big)$$

the space of symmetric linear maps in $\Pi(x_\Gamma)$. Let $R(x_\Gamma) \in \mathcal{T}(x_\Gamma)$, be the curvature tensor of Γ at x_Γ (see [1]), with trace $2H(x_\Gamma)$, where by definition $H(x_\Gamma)$ is the mean curvature of Γ at x_Γ. Now, we define, for each $x_\Gamma \in \Gamma$, the two profile functions:

$$w^1(\cdot, x_\Gamma), w^2(\cdot, x_\Gamma) : Y^\infty_r \to \mathbb{R}, \tag{6}$$

as the (unique) solutions of the elliptic problems

$$\begin{cases} \operatorname{div}\big(\hat\rho^{-1}\, g(x_r)^{-1}\, \nabla w^j(\cdot, x_\Gamma)\big) = \partial_{\hat x_j}\hat\rho \text{ in } Y^\infty_r \\ \\ w^j(\cdot, x_\Gamma) \text{ is 1-periodic in } \hat x_r, \text{ bounded at } \infty \\ \\ \partial_{\hat\nu} w^j(\hat x_r, 0) = 0, \quad \int_{Y^0_r} w^j(\cdot, x_\Gamma)\, d\hat x = 0 \end{cases} \tag{7}$$

from which we define the 2×2 symmetric matrices

$$a(\hat x, x_\Gamma) \text{ such that } a_{ij}(\hat x, x_\Gamma) = \rho(\hat x)\, \frac{\partial w^j}{\partial \hat x^i}(\hat x, x_\Gamma).$$

Next, for each $(\hat x, x_\Gamma = \Phi_\Gamma(x_r))$, we define the positive symmetric positive operators $m(\hat x, x_\Gamma) \in \mathcal{T}(x_\Gamma)$ through their bilinear form on $\Pi(x_\Gamma) = \operatorname{Im} D\Phi_\Gamma(x_r)$:

$$\big(m(\hat x, x_\Gamma)\, D\Phi_\Gamma(x_r)u, D\Phi_\Gamma(x_r)v\big)_{\mathbb{R}^3} = \\ = \rho(\hat x)\, \big(a(\hat x, x_\Gamma)u, v\big)_{\mathbb{R}^3}$$

Finally, we set $M(x_\Gamma) = \displaystyle\int_{Y^0_r} m(\hat x, x_\Gamma)\, d\hat x \quad \in \mathcal{T}(x_\Gamma).$

Then, the operators T_1 and T_2 appearing in (4) are

$$T_1 := \overline{\rho}_0\, \Delta_\Gamma + \operatorname{div}_\Gamma\big(M(x_\Gamma)\nabla_\Gamma\big) + \overline{\mu}_0\, \omega^2,$$

$$T_2 := \overline{\rho}_1\, \operatorname{div}_\Gamma\big[\big(H(x_\Gamma) - R(x_\Gamma)\big)\, \nabla_\Gamma\big] + \overline{\mu}_1\, H(x_\Gamma)\, \omega^2$$

When $\hat\rho$ and $\hat\mu$ are constant, one recovers well-known thin layer conditions for homogeneous coatings [1].

In the talk, we shall give insights on the analysis of the condition (3, 4) and its numerical validation.

References

[1] A. Bendali and K. Lemrabet. The effect of a thin coating on the scattering of a time-harmonic wave for the helmholtz equation. *SIAM J. Appl. Math.*, 56:1664–1693, December 1996.

[2] B. Delourme, H. Haddar, and P. Joly. Approximate Models for Wave Propagation Across Thin Periodic Interfaces. *Jounal de mathématiques pures et appliquées*, 98(1):28–71, 2012.

Reflection of Pulses by Heterogeneous Media

E. Barnwell[1,*], **D. Abrahams**[1], **W. Parnell**[1]
[1] School of Mathematics, University of Manchester
*Email: ellis.barnwell@gmail.com

Abstract

This talk will discuss the reflection of pulses from heterogeneous media. In particular, I will be focusing on a solution technique for a semi-infinite set of beads. The reflection coefficient can be found exactly and used to reconstruct a pulse using Fourier transforms. Related work includes the analogous 2-D problems of membranes and plates. We also make comments on the reflection coefficient calculated assuming the heterogeneous media can be treated as an effective medium. It becomes clear that this is not a reasonable assumption as the reflection and transmission within the beaded region has significant effect on the waves which are reflected.

Introduction

The problem of waves travelling in heterogeneous media has been studied extensively. It is of great interest in engineering, covers a broad range of topics and holds many rich and interesting problems. There are numerous different methods to be used to describe heterogeneous media, including asymptotic homogenisation [1], Bloch-Floquet theory [2] and direct numerical evaluation of the heterogenities. The majority of these techniques rely on finding some effective properties such that we average out the microstructure and find a homogeneous medium which holds the same properties.

Each method has its own merits and is useful for certain problems. Asymptotic homogenisation for example, gives a good description of the averaged properties when the microstructure is very small compared to the wavelengths of the propagating wave. This method however does not give any insight into the stop and pass band structure of the material. Bloch-Floquet theory on the other hand gives us good insight into the stop and pass band structure of the material but does not offer an obvious way to model pulses.

In this talk we will be interested in the problem of an incoming pulse impinging a heterogeneous medium. To keep the analysis simple we consider the case of periodically spaced point masses attached to one half of an infinite string. We can find the effective wave number of the string and the reflection coefficient at a specific frequency. We then reconstruct the solution using Fourier integrals over the entire frequency range.

1 The problem set up

For the time being we shall consider the simple case of waves on an infinite string. On one half of the infinite string we will place an infinite number of masses at periodic spacings as pictured in figure 1.

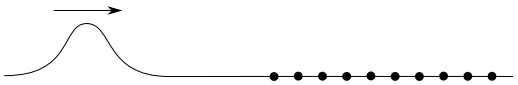

Figure 1: A pulse on a string encountering a series of periodic point masses.

We choose to introduce the parameter

$$\epsilon = \frac{\omega l}{c_0} \tag{1}$$

where ω is the frequency, l is the bead spacing and c_0 is the wave speed in the homogeneous string. This parameter acts as the nondimensional frequency.

2 Solution approach

The solution technique is to picture the pulse as being made up of an infinite number of harmonic waves, each with a different frequency as in [4]. We are then able to treat each frequency separately to find what the reflected portion of that harmonic wave is, subsequently allowing us to reconstruct the reflected pulse. This method relies on the Fourier transform, which is defined as

$$\mathcal{F}(f(t)) = F(\epsilon) = \int_{-\infty}^{\infty} f(t)e^{-i\epsilon t}dt. \tag{2}$$

If our input to the problem is given by

$$u(x, t=0) = \begin{cases} h(x) & \text{if } x < 0 \\ 0 & \text{if } x > 0. \end{cases} \tag{3}$$

then we first take the Fourier transform of this, which we shall call $H(\epsilon)$ to get the frequency spectrum of

the input. Assuming we know the reflection coefficient, denoted by $R(\epsilon)$, we can reconstruct the problem in the homogeneous string by using the Inverse Fourier transform

$$u_R(x+ct) = \frac{1}{2\pi}\int_{-\infty}^{\infty} R(\epsilon)H(\epsilon)e^{i\epsilon(x/c_0+t)}d\epsilon \qquad (4)$$

The reflection coefficient for the semi-infinite set of beads on a string can be found exactly as derived in [3]. It is found to be

$$R(\epsilon) = \frac{e^{-i\epsilon}\sin(\epsilon(1-\gamma)/2)}{\sin(\epsilon(1+\gamma)/2)} \qquad (5)$$

where γ is the nondimensional effective wavenumber in the beaded string, and is given by

$$\cos\gamma\epsilon = \cos\epsilon - \frac{M\epsilon}{2}\sin\epsilon \qquad (6)$$

We may compare this reflection coefficient with the one found if the beaded string can be thought of as an effective medium with wavenumber γ. The reflection coefficient in this case is found to be

$$R_{\text{eff}}(\epsilon) = \frac{1-\gamma}{1+\gamma}. \qquad (7)$$

We can see by expanding (5) for small ϵ that these two reflection coefficients match up in the homogenisation limit ($\epsilon \ll 1$). For larger ϵ the two reflection coefficients differ. It can be seen in figure 2 by how much these two differ, even for relatively small ϵ. This is worrying as it means we are unable to use the concept of an effective medium in reflection and transmission problems when we don't know the exact coefficients. A typical example of when the exact reflection coefficient is unavailable is the commonly studied layered composite.

In order to investigate the solution given by (4) we look at the singularity structure in the complex plane. Provided that our input is entire, then the fourier transform of this, $H(\epsilon)$ is entire. Thus, the only singularities in the problem come from the reflection coefficient. It may not be immediately clear what singularities this function has. We may find them by rearranging $R(\epsilon)$ into the form

$$R(\epsilon) = \frac{2}{M\epsilon}\left(\sin(\epsilon)\sqrt{1-\left(\frac{M\epsilon}{2}\right)^2 + \frac{M\epsilon}{\tan(\epsilon)}} - \sin(\epsilon) - \frac{M\epsilon}{2}\cos(\epsilon)\right) \qquad (8)$$

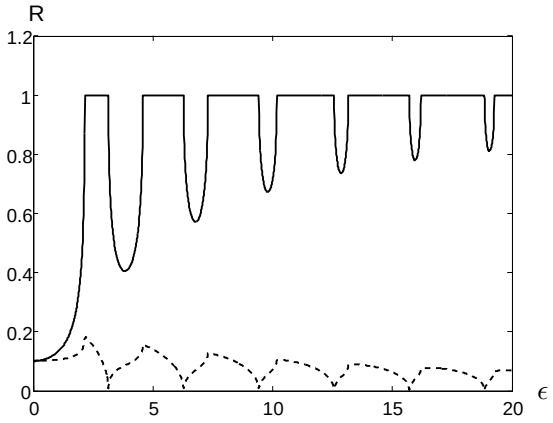

Figure 2: The exact reflection coefficient (solid line) compared to the effective medium reflection coefficient (dashed line).

We can now see that the only singularities are given by the branch cuts which occur from the square root. These all lie on the real line and due to the $\tan(\epsilon)$ there are an infinite number of them. We may now convert the integral given by (4) into a sum of integrals around each cut, being much easier to handle numerically.

3 Further work

We will then discuss areas where these types of problems are heading. The possibility of obtaining some effective reflection coefficient for the periodic layered medium will be discussed. The extension of these problems into two dimensions is also of interest.

References

[1] Bakhvalov, N and Panasenko, G, *Homogenisation: Averaging Processes in Periodic Media*, Kluwer, 1989.

[2] Andrianov, I, Bolshakov, V and Danishevs'kyy, V, *Higher Order Asymptotic Homogenization and Wave Propagation in Periodic Composite Materials*, Proceedings of the Royal Society A, **464** (2008), pp. 1181-1201.

[3] Abrahams, D, *Advanced Analytical Methods for Continuum Modelling: Complex Variable Methods, the Wiener-Hopf Technique and 1-D Dynamic Homogenization*, Magical books for industry lecture series, 2012

[4] A. Bedford and D. Drumheller, *Introduction to Elastic Wave Propagation*, Wiley, 1994

On Born approximation for scattering by rough surfaces

T. Arnold[1,*], **A. Rathsfeld**[1]
[1] Weierstrass Institut, Berlin, Germany
*Email: thomas.arnold@wias-berlin.de

Abstract

In many modern industrial processes, diffractive optical elements employ light with small wavelengths. The current technological progress is based on the steady decrease in wavelengths (e.g. EUV light). For such wavelengths, the effect of random surface roughness of gratings has an increasingly high impact on the behaviour of the scattered wave. Consequently, the roughness should be included into the modelling of the scattering and, maybe, into the numerical solution process of inverse problems. Since the solution for the full Maxwell system for rough surfaces is extremely difficult, many authors employ simplified models. One way to do so is proposed by Stearns and is based on the Born approximation of the Maxwell equations. We will discuss mathematically strict assumptions which allow the use of the manipulations in Stearns' approach. Under these assumptions, we give a rigorous definition of an approximate solution and derive the corresponding formulas for the scattered far field.

Introduction

It is the goal of this paper to obtain an approximate solution in the sense of the limiting absorption principle for the far-field, when a homogeneous X-ray plane wave is being scattered by a non-ideal interface between two dielectric media. The interface, described by the graph of a function f, separates two materials with the dielectric constants ϵ_0 and ϵ_0' and the globally constant magnetic permeability μ_0. We assume that the interface is illuminated by a plane wave $\vec{E}^0(\vec{x})\,e^{-i\omega t}$, with $\vec{E}^0(\vec{x}) := \vec{e}^{\,0}e^{i\vec{k}\cdot\vec{x}}$, $\vec{x} := (x,y,z)^\top$ and a real valued wave vector $\vec{k} := (k_x,k_y,k_z)^\top$, from above. Furthermore, we assume that the material above the interface has a real valued refractive index and thus is non-absorbing. Stearns [1] provides the far-field formula

$$\vec{E}^r(R\vec{m}) \sim -i\frac{[\epsilon_0-\epsilon_0']k^2}{4\pi\epsilon_0}\,\frac{\hat{g}(k\vec{m}-\vec{k})}{km_z-k_z}\,\vec{e}^{\,0}\,\frac{e^{ikR}}{R},$$

for $R\to\infty$. Here, $\hat{g}$ is the Fourier transform of the function $g(\vec{x}) := \delta(z-f(x,y))$. We will present a class of functions f and a sufficient condition for f such that a generalised Stearns' formula (cf. the subsequent (1)) can be justified.

1 The vector Helmholtz equation

In both, the sense of the limiting absorption principle and the first order Born approximation, the problem is described by an inhomogeneous vector Helmholtz equation

$$\left(\nabla^2+k_\tau^2\right)\vec{D}^{sc}(\vec{x}) = -\nabla\times\left[\nabla\times\left(\alpha(\vec{x})\vec{E}^0(\vec{x})\right)\right],$$

where $k_\tau := \sqrt{\mu_0\epsilon_\tau}\omega$, ϵ_τ results from ϵ_0 by introducing a small imaginary part and $\alpha(\vec{x}) := 0$ for $z > f(x,y)$ and $\alpha(\vec{x}) := -\Delta := \epsilon_0'-\epsilon_\tau$ for $z < f(x,y)$. The same equation also holds when considering the difference $\vec{D}^d$ between the desired scattered field $\vec{D}^{sc}$ and the approximated solution $\vec{D}^{sc}_{\mathcal{Q}}$ for an ideal interface $f_{\mathcal{Q}}\equiv 0$ with $\alpha_d(\vec{x}) := \alpha(\vec{x})-\alpha_{\mathcal{Q}}(\vec{x})$

$$\left(\nabla^2+k_\tau^2\right)\vec{D}^{d}(\vec{x}) = -\nabla\times\left[\nabla\times\left(\alpha_d(\vec{x})\vec{E}^0(\vec{x})\right)\right].$$

Note, that for $\vec{D}^{sc}_{\mathcal{Q}}$ the exact solution can be used by employing Fresnel's formula.

To solve this equation we apply the generalised Fourier transform in the dual of the Schwartz space $\mathcal{S}(\mathbb{R}^3)$ to both sides of the equation. We then resolve the resulting equation w.r.t. the Fourier transform of $\vec{D}^d$ and use the generalised inverse Fourier transform to get an integral representation of $\vec{D}^d$

$$\begin{aligned}&\left\langle\vec{D}^d(\vec{x}),\varphi(\vec{x})\right\rangle\\ &=\int_{\mathbb{R}^3}\alpha_d(\vec{\eta})\,e^{i\vec{k}_\tau\cdot\vec{\eta}}\int_{\mathbb{R}^3}\frac{\left[\left(\vec{s}\times\vec{e}^{\,0}\right)\times\vec{s}\right]}{\|\vec{s}\|^2-k_\tau^2}\;\check{(\bar{\varphi})}(\vec{s})\,e^{-i\vec{\eta}\cdot\vec{s}}\,\mathrm{d}\vec{s}\,\mathrm{d}\vec{\eta},\end{aligned}$$

for all $\varphi\in\mathcal{S}(\mathbb{R}^3)$. We can easily show that these transformations are well defined for all $f\in\mathrm{L}^\infty(\mathbb{R}^2)$ and $\tau\neq 0$.

2 The near-field formula

To prove the existence of the limit $\mathrm{Im}\,\epsilon_\tau\to 0$, resulting from the limiting absorption principle, we have restrict the class of interface functions to the set of

all real valued functions in $\mathrm{L}^\infty(\mathbb{R}^2)$ of the form

$$f(\eta') = \sum_{\ell=0}^{3} \left[\frac{1}{\sqrt{1+|\eta'|^2}^{\ell}} \sum_{j\in\mathbb{Z}} \lambda_{\ell,j}\, e^{i\omega'_{\ell,j}\cdot\eta'} \right] + g(\eta'),$$

where $\lambda_{\ell,j} \in \mathbb{C}$, $\lambda_{\ell,j} \in \mathbb{C}$, $\|f\|_{\mathcal{A}_1} < \infty$. This norm is defined as $\sum_{\ell=0}^{3}\sum_{j\in\mathbb{Z}} |\lambda_{\ell,j}| + \|g\|_{1,1}$, with $\|g(\eta')\|_{1,1} := \|\,(1+|\eta'|)\,g(\eta')\|_{L^1(\mathbb{R}^2)}$. We have restricted the set of interface functions to these, since it necessary that the set is a Banach algebra and that the corresponding functions have an explicit Fourier transform. Furthermore, the set should contain almost periodic functions, which have already been used by Stover [2]. Moreover, combinations of Fourier modes play an important role for stochastic processes (cf. e.g. Yaglom [3, Equ. (2.61) in Sect. 8]), as well.

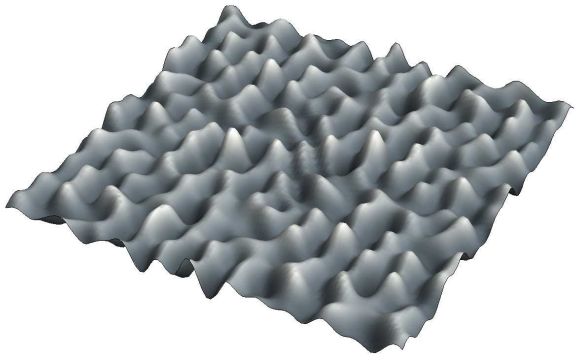

Figure 1: Example of an interface f from $\mathcal{A}_1$

Using the properties of this set of interface functions and considering the integrals in $\left\langle \vec{D}^d(\vec{x}), \varphi(\vec{x}) \right\rangle$ as Cauchy principle value integrals at infinity, we can show that the limit $\mathrm{Im}\,\epsilon_\tau \to 0$ exists and evaluates as a classical function of the form

$$\vec{D}^d(\vec{x}) = \sum_{n=0}^{\infty}\sum_{j\in\mathbb{Z}} C_{j,n} \left[\left(\vec{\omega}_z^j \times \vec{e}^{\,0}\right) \times \vec{\omega}_z^j \right] \frac{\mathrm{sgn}\, z}{\left(\omega_z^j\right)^{1-n}}\, e^{i\vec{\omega}_z^j\cdot\vec{x}} + \sum_{\ell=1}^{4}\sum_{n=0}^{\infty}\sum_{j\in\mathbb{Z}} \int_{\mathbb{R}^2} h_{\ell,j}^n(s') \left[\left(\vec{s}_{\xi_z} \times \vec{e}^{\,0}\right) \times \vec{s}_{\xi_z} \right] e^{i\vec{s}_{\xi_z}\cdot\vec{x}}\, \mathrm{d}s',$$

for $|z| > 2\|f\|_{\mathrm{L}^\infty}$, where the vector $\vec{\omega}_z^j$ is defined as $(k' + \tilde{\omega}'_{0,j}, \omega_z^j)^\top$, $\omega_z^j := \mathrm{sgn}\, z \sqrt{k^2 - |k' + \tilde{\omega}'_{0,j}|^2}$, $\tilde{\omega}'_{0,j} := \sum_{j\in\mathbb{Z}} m_j \omega'_{0,j}$ for all $(m_j) \in \ell^1(\mathbb{N}_0)$, $h_{\ell,j}^n(s')$ is an at most weakly singular function, $\vec{s}_{\xi_z} := (s', \xi_z)^\top$ and $\xi_z := \sqrt{k^2 - |s'|^2}$. Note that the condition $\omega_z^j \neq 0$ is necessary for all $j \in \mathbb{Z}$. This holds if

$$k \notin \mathrm{cl}\left\{ \left| k' + \sum_{j\in\mathbb{Z}} m_j \omega'_{0,j} \right| :\ (m_j)_{j\in\mathbb{Z}} \in \ell^1(\mathbb{N}_0) \right\}.$$

3 The far-field formula

In a very lengthy process we have obtained the far-field asymptotics $R := \|\vec{x}\| \to \infty$ of the formula for $\vec{D}^d(\vec{x})$ above. The proof mostly consists of splitting off terms of the integrals w.r.t. s' for which we can show their asymptotic behaviour. This is largely compromised of integrations by parts using specially chosen coordinate systems. Finally, e.g. for the reflected field ($Rm_z = z > 2\max\{\|f\|_{\mathcal{A}_1}, \|f\|_{\mathrm{L}^\infty}\}$), we have reached a formula of the form

$$\vec{E}^r(R\vec{m}) = \sum_{n=0}^{\infty}\sum_{j\in\mathbb{Z}} C_{j,n} \frac{\left[\left(\vec{\omega}_z^j \times \vec{e}^{\,0}\right) \times \vec{\omega}_z^j\right]}{\left(\omega_z^j\right)^{1-n}}\, e^{iR\vec{\omega}_z^j\cdot\vec{m}} + r_1(f,\vec{m},\vec{e}^{\,0})\frac{e^{ikR}}{ikR} + r_2(f,\vec{m},\vec{e}^{\,0})\frac{1}{ikR} + r_3(f,\vec{m},\vec{e}^{\,0})\frac{e^{ikR}}{i\sqrt{kR}} + \frac{1}{\epsilon_0}\,\vec{D}_{\mathcal{Q}}^{sc}(R\vec{m}), \quad (1)$$

where $\vec{E}^r = \vec{D}^r/\epsilon_0$ and $\vec{D}^r = \vec{D}^d + \vec{D}_{\mathcal{Q}}^{sc}$ for $m_z > 0$.

References

[1] D.G. Stearns, *The scattering of x rays from nonideal multilayer structures*, J. Appl. Phys., *65* (1989), pp. 491–506

[2] J.C. Stover, *Roughness characterization of smooth machined surfaces by light scattering*, Appl. Optics, *Vol 14 (8)* 1975, pp. 1796–1802

[3] A.M. Yaglom *Correlation theory of stationary and related random functions*, Springer Series in Statistics, Springer Verlag Inc., New York, 1987

Acoustic Wave Propagation in Quasiperiodic Media

S. R. Voisey[1,*], **I. D. Abrahams**[1], **W. J. Parnell**[1]
[1]School of Mathematics, University of Manchester, Manchester, UK
*Email: ruth.voisey@postgrad.manchester.ac.uk

Abstract

Understanding and predicting wave propagation and scattering by non-periodic media is much more difficult than that of periodic, but still very important. Very few existing structures are actually exactly periodic, thus it is crucial to gain a better, more accurate understanding of nearly periodic, quasiperiodic and random structures.

In this talk I will present methods to determine the acoustic wave scattering properties of quasiperiodic structures, where by quasiperiodic we mean non-periodic in the sense that the structure is non-repeating, but also non-random in the sense that the distribution is deterministic. Quasiperiodic structures are simpler to work with than fully random structures due to this deterministic nature, but are still of great importance as such structures do exist and can be used in engineering applications.

We consider two dimensional quasiperiodic structures with sound-soft, circular, cylindrical scatterers. We will then find periodic structures which give similar scattering properties to the quasiperiodic structures, in order to find effective homogeneous materials that give good approximations.

1 Motivation

With such influential papers as those by Anderson [1] and Foldy [2], people are under the impression that random microstructure within a material can cause acoustic wave localisation/decay. Anderson showed how the interference of coherent, multiple scattered waves from the randomly positioned inclusions can cause wave transmission to completely stop. Whilst Foldy's use of ensemble averaging and the closure condition results in a complex effective wave number, i.e. exponential decay in the wave field.

In an attempt to understand this phenomenon, whilst fully appreciating the work of Anderson and Foldy, we want to try to find an alternative way to fully understand wave propagation in random media, from the basics.

In this talk we will introduce work with quasiperiodic distributions. These have an 'air' of randomness as they are aperiodic, although they do have a deterministic distribution. Working with such distributions will allow us to see how the transition from a periodic structure to a quasiperiodic structure alters the amount of transmitted wave field allowed, and will thus could provide insight into how introducing 'randomness' to a structure effects the wave propagation.

On a side note, quasicrystalline coatings are being widely used on a multitude of objects due to their hardness, low thermal and electrical conductivity, low friction and high corrosion resistivity. Therefore, a material with inclusions distributed the same as the atomic structure of a quasicrystal may also have similar characteristics and thus applications, making it an extremely interesting and exciting structure to look at.

Due to this link with quasicrystals [3] and because of a high interest in the 'phononics' of quasicrystals, the main inclusion distribution we will look at is the 2D Penrose tiling. We will also mention a 1D quasiperiodic structure similar to this called the Fibonacci chain, and propose ideas to extend to the 3D analogue of the Penrose tiling.

2 The Problem

The governing equation for acoustic wave propagation in 2D with one sound-soft cylindrical inclusion of radius a at the origin is

$$(\nabla^2 + k^2)u(r,\theta) = 0, \quad u = 0 \text{ on } r = a, \qquad (1)$$

where we have assumed the wave is time harmonic, $U = \mathrm{Re}(ue^{-i\omega t})$, and we have factored out the time dependence. Here r and θ are the distance and angle of the observation point from the origin and $k = \omega/c$ is the wavenumber.

We have an incident plane wave of the form

$$u_{inc} = e^{ikr\cos(\theta-\alpha)}, \qquad (2)$$

at angle α from the horizontal. We will position circular, cylindrical inclusions at the lattice nodes of our quasiperiodic distributions.

Our main focus is on the distribution of the scatterers, therefore, to make our scattering modelling more

simple we will assume we have cylinders with small radii, i.e. $0 < ka \ll 1$.

3 Methods

Numerous techniques and approaches are useful in looking at the multiple scattering and at the quasiperiodic structures which we want to discuss. In this talk we will present the multipole method [4] as one technique for modelling the wave behaviour through a finite lattice, and the projection method to construct our quasiperiodic lattice at which we will position our inclusions.

3.1 The Multipole Method

We know that the solution to the governing equation (1) gives us a scattered field of the form

$$u_{sc} = \sum_{n=-\infty}^{\infty} i^n B_n H_n^{(1)}(kr) e^{in(\theta-\alpha)}, \qquad (3)$$

where the coefficients $B_n = -J_n(ka)/H_n^{(1)}(ka)$ are dependent on the boundary conditions. The total field is defined by $u(r,\theta) = u_{inc}(r,\theta) + u_{sc}(r,\theta)$.
By considering limiting forms of the Bessel and Hankel functions for small arguments we find that, for small cylinder radius (i.e. as $ka \to 0$), our scattered field will look like

$$u_{sc} = -\frac{1}{1 + \frac{2i}{\pi}(\gamma - \ln 2 + \ln(ka))} H_0^{(1)}(kr), \qquad (4)$$

thus showing that the cylinder acts as a monopole source.
To extend to a finite number of scatterers we simply express the scattered field as a sum of the monopole sources at the centre of each circle (monopole and dipole for sound-hard, and multipoles for large scatterers),

$$u_{sc} = \sum_{i=1}^{N} C_i H_0^{(1)}(kr_i), \qquad (5)$$

where $r_i = |\mathbf{r}_i|$ is the distance from the ith cylinder to the observation point.

If we evaluate the boundary conditions at each cylinder boundary we will get a matrix equation of the form $\mathbf{HC} = -\mathbf{I}$, where

$$\mathbf{H}_{ij} = \begin{cases} 1 + \frac{2i}{\pi}(\gamma - \ln 2 + \ln(ka)), & i = j \\ H_0^{(1)}(kb_{ij}) = H_0^{(1)}(kb_{ji}), & i \neq j, \end{cases} \qquad (6)$$

$$\mathbf{C} = \begin{pmatrix} C_1 \\ \vdots \\ C_N \end{pmatrix}, \quad \mathbf{I} = \begin{pmatrix} 1 \\ \vdots \\ 1 \end{pmatrix}. \qquad (7)$$

Our total field is again just the sum of the incident and scattered fields.
Once we know the coordinates of the distribution we can very easily use this matrix equation to see the behaviour of the wave field through this finite distribution.

3.2 The Projection Method

The Penrose tiling is a 2D aperiodic tiling of the plane that uses only two tiles, 'fat' and 'thin' rhombi [5]. We want to place a scatterer on every corner of each rhomb, giving us a Penrose lattice. One method for constructing such a lattice is via projection from higher dimension. In this method one takes some slice/window W of a five dimensional hypercubic lattice and projects on to a plane at a certain irrational slope, giving us lattice points

$$PT = \left\{ \frac{2}{5} \begin{pmatrix} \sum_{j=1}^{4} m_j(\cos(2\pi j/5) - 1) - p \\ \sum_{j=1}^{4} m_j \sin(2\pi j/5) \end{pmatrix} \right\}, \qquad (8)$$

where $1 \leq p \leq 4$ and the $\vec{m} = (m_1, ..., m_4)$ are to be found using an algorithm. If time allows I will discuss the algorithm we have constructed in more detail.
We will also discuss how the projection method can be adapted to give a periodic lattice which scatters the waves in a similar manner. We can do this via the projection of the window W at some oblique angle, or an alternative is to consider rational slopes, giving us a rational approximant with the same two tiles.

References

[1] P. W. Anderson, *Absence of Diffusion in Certain Random Lattices*, Phys. Rev., **109** (1958), pp. 1492–1505.

[2] L. L. Foldy, *The Multiple Scattering of Waves. I. General Theory of Isotropic Scattering by Randomly Distributed Scatterers*, Phys. Rev., **67** (1945), pp. 107–119.

[3] M. Senechal, *Quasicrystals and Geometry*, Cambridge University Press, Cambridge, 1996.

[4] P. A. Martin, *Multiple Scattering: Interaction of Time-Harmonic Waves with N Obstacles*, Volume 10, Cambridge University Press, Cambridge, 2006.

[5] B. Grunbaum and G. C. Shephard, *Tilings and Patterns*, W. H. Freeman & Co., New York, 1986.

An efficient calculation of photonic crystal band structures using Taylor expansions

D. Klindworth[1,*], **K. Schmidt**[1]
[1] MATHEON, TU Berlin, Berlin, Germany.
*Email: klindworth@math.tu-berlin.de

Abstract

This work deals with the computation of the group velocity of photonic crystal (PhC) modes and higher derivatives of their dispersion curves. We employ these derivatives in a Taylor expansion of the band structure, which reduces the computational costs significantly. The presented results can be transferred to the computation of guided modes in PhC waveguides using the supercell approach or Dirichlet-to-Neumann (DtN) maps.

1 Introduction

We consider the problem of finding *Bloch modes* $U(\mathbf{x};k)$ with *transverse magnetic* (TM) polarization and their associated eigenvalues $\omega^2(k) \in \mathbb{R}^+$ that satisfy

$$-\Delta U(\mathbf{x}) - \omega^2 \varepsilon(\mathbf{x}) U(\mathbf{x}) = 0$$

in the unit cell $C \subset \mathbb{R}^2$ of the PhC, see Fig. 1, with quasi-periodic boundary conditions

$$U(\cdot\,;k)|_{\Gamma_\mathrm{R}} = \mathrm{e}^{\mathrm{i}k|\mathbf{a}_1|} U(\cdot\,;k)|_{\Gamma_\mathrm{L}},$$
$$\partial_\mathbf{n} U(\cdot\,;k)|_{\Gamma_\mathrm{R}} = -\mathrm{e}^{\mathrm{i}k|\mathbf{a}_1|} \partial_\mathbf{n} U(\cdot\,;k)|_{\Gamma_\mathrm{L}},$$

in dependence on the quasi-momentum $k \in B$ in the one-dimensional Brillouin zone $B = [-\pi/|\mathbf{a}_1|, \pi/|\mathbf{a}_1|]$. Here, ε denotes the relative permittivity and the operator $\partial_\mathbf{n}$ is given by $\partial_\mathbf{n} = \nabla \cdot \mathbf{n}$ with the unit normal vector $\mathbf{n}$ outward to the unit cell C.

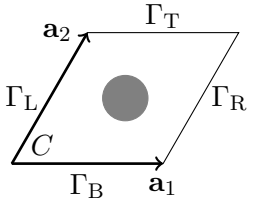

Figure 1: The computational domain C.

At the top and bottom boundaries Γ_T and Γ_B we impose (a) quasi-periodic boundary conditions with quasi-momentum $k_2 \in [-\pi/|\mathbf{a}_2|, \pi/|\mathbf{a}_2|]$ in the direction of $\mathbf{a}_2$, (b) periodic boundary conditions (as used in the supercell method for the approximation of guided modes in PhC wave-guides, or (c) transparent boundary conditions (*e. g.* DtN maps as used in [1] for the exact computation of guided modes in PhC wave-guides). For simplicity, we shall focus on periodic boundary conditions in this work, but the results can also be applied to problems with DtN transparent boundary conditions.

Moreover, we restrict our considerations to the TM-mode, but the results can directly be transferred to the TE-mode.

By substituting $u(\mathbf{x}) = U(\mathbf{x})\mathrm{e}^{-\mathrm{i}k\mathbf{a}_1\cdot\mathbf{x}}$, we arrive at a periodic problem that we express in variational sense using the space of periodic H^1-functions in C denoted by $H^1_\mathrm{p}(C)$. For any $k \in B$ we seek modes $u(\cdot\,;k) \in H^1_\mathrm{p}(C)$ and eigenvalues $\omega^2(k) \in \mathbb{R}^+$ such that

$$\int_C (\nabla + \mathrm{i}k\mathbf{a}_1)u \cdot (\nabla - \mathrm{i}k\mathbf{a}_1)\overline{v} - \omega^2 \varepsilon(\mathbf{x}) u\overline{v}\,\mathrm{d}\mathbf{x} = 0 \quad (1)$$

for all $v \in H^1_\mathrm{p}(C)$.

Proposition 1. *(see [2]) For any $k \in B$, there exists an ordering of the eigenvalues $\omega^2_m(k) \in \mathbb{R}^+$, $1 \le m \le M(k)$, of the eigenvalue problem (1) such that the functions $\omega_m : k \mapsto \omega_m(k)$ — the so-called* dispersion curves *— are continuously differentiable to any order.*

2 Group velocity and higher derivatives of the dispersion curves

Thanks to this ordering of the eigenvalues $\omega^2_m(k)$ of (1), the group velocity $\frac{\partial\omega_m}{\partial k}(k)$ and any higher derivative of $\omega_m(k)$ with respect to k are well defined.

This implies that we can take the derivative of Eq. (1) with respect to k and obtain

$$\int_C (\nabla + \mathrm{i}k\mathbf{a}_1)\frac{\partial u}{\partial k} \cdot (\nabla - \mathrm{i}k\mathbf{a}_1)\overline{v} - \omega^2\varepsilon\frac{\partial u}{\partial k}\overline{v}\,\mathrm{d}\mathbf{x} = f_1(v) \quad (2)$$

for all $v \in H^1_\mathrm{p}(C)$, where the linear form f_1 reads

$$f_1(v) = \omega\frac{\partial\omega}{\partial k}\int_C \varepsilon u\overline{v}\,\mathrm{d}\mathbf{x} - 2k|\mathbf{a}_1|^2\int_C u\overline{v}\,\mathrm{d}\mathbf{x} - \mathrm{i}|\mathbf{a}_1|\int_C u(\partial_1\overline{v}) - (\partial_1 u)\overline{v}\,\mathrm{d}\mathbf{x}.$$

The solution $\frac{\partial u}{\partial k}(\cdot\,;k) \in H^1_\mathrm{p}(C)$ of (2) is not unique since by assumption there exists at least one mode

$u \in H^1_{\mathrm{p}}(C)$ that solves (1) with zero right hand side and hence, any of these modes u can be added to the solution $\frac{\partial u}{\partial k}$ of (2) and the equation will still be satisfied. However, taking $v = u$ as test function in Eq. (2), the left hand side — including all terms containing $\frac{\partial u}{\partial k}$ — vanishes since $(-k)$ is an eigenvalue with associated eigenmode $\overline{u}$ [1]. Thus, the group velocity reads

$$\frac{\partial \omega}{\partial k} = \frac{k|\mathbf{a}_1|^2 \int_C |u|^2 \,\mathrm{d}\mathbf{x} - |\mathbf{a}_1| \,\mathrm{Im}\big(\int_C u \partial_1 \overline{u} \,\mathrm{d}\mathbf{x}\big)}{\omega \int_C \varepsilon |u|^2 \,\mathrm{d}\mathbf{x}}$$

and is real-valued.

Since the group velocity $\frac{\partial \omega}{\partial k}$ is now known, we can — applying the Fredholm-Schauder theory — compute a particular solution $\frac{\partial u}{\partial k}$ of (2) by additionally requiring $H^1(C)$-orthogonality of $\frac{\partial u}{\partial k}$ and any eigenmode $u(\cdot\,; k)$ of the eigenvalue problem (1) with associated eigenvalue $\omega^2(k)$.

Consecutively repeating the above considerations, we can write the n-th derivative of Eq. (1) with respect to k in the form

$$\int_C (\nabla + \mathrm{i}k\mathbf{a}_1)\frac{\partial^n u}{\partial k^n} \cdot (\nabla - \mathrm{i}k\mathbf{a}_1)\overline{v} - \omega^2 \varepsilon \frac{\partial^n u}{\partial k^n}\overline{v} \,\mathrm{d}\mathbf{x} = f_n(v) \quad (3)$$

for all $v \in H^1_{\mathrm{p}}(C)$, where the linear form f_n depends on $\frac{\partial^1 u}{\partial k^1}, \ldots, \frac{\partial^{n-1} u}{\partial k^{n-1}}$. Testing with $v = u$ we again arrive at $f_n(u) = 0$ from which we deduce the n-th derivative of $\omega(k)$.

Analogously to above we can then compute the particular solution $\frac{\partial^n u}{\partial k^n} \in H^1_{\mathrm{p}}(C)$ of (3) that is $H^1(C)$-orthogonal to any eigenmode $u(\cdot\,; k)$ of the eigenvalue problem (1) with associated eigenvalue $\omega^2(k)$.

3 Taylor expansion of the dispersion curves

Since the dispersion curves $\omega_m(k)$ are continuously differentiable to any order we can apply the Taylor's theorem, and hence, for any $k_0 \in B$ and $n \in \mathbb{N}$

$$\omega(k) = \sum_{n'=1}^{n} \frac{(k-k_0)^{n'}}{n'!} \frac{\partial^{n'} \omega}{\partial k^{n'}}(k_0) + R_n(k),$$

with the remainder

$$R_n(k) = \frac{1}{n!} \int_{k_0}^{k} (k-\kappa)^n \frac{\partial^{n+1} \omega}{\partial k^{n+1}}(\kappa) \,\mathrm{d}\kappa.$$

In Fig. 2 we present numerical results of the Taylor expansion. As computational domain we choose the unit square $[0,1]^2$ with a hole of radius 0.4 and permittivity $\varepsilon = 1$ surrounded by dispersive material of permittivity $\varepsilon = 3$. We study the TM-mode in the whole reduced Brillouin zone $[0, \pi]$ and compare the eigenvalues $\omega(k)$ of (1) at 40 values of k with the results of the Taylor expansion of order $n = 5$ around the centre $k_0 = \frac{\pi}{2}$ of the reduced Brillouin zone. For the computation we choose finite elements on curved cells with polynomial degree $p = 5$ using the C++ library *Concepts*.

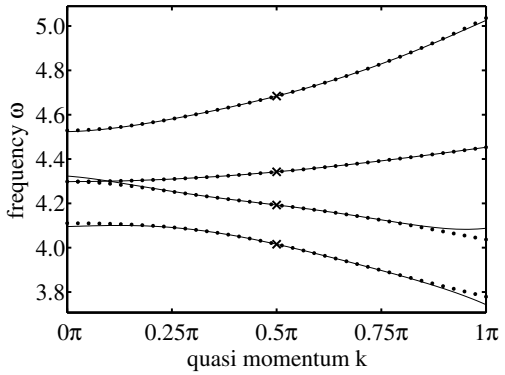

Figure 2: Comparison of dispersion curves (dots) with their Taylor expansion (solid lines) around $k_0 = \frac{\pi}{2}$ (crosses).

The time saving of the Taylor expansion is enormous: We only need to solve the eigenvalue problem (1) once, compute the group velocity $\frac{\partial \omega}{\partial k}(k_0)$ for all eigenmodes, which is a simple matrix vector multiplication, and subsequently compute $\frac{\partial^n u}{\partial k^n}(\cdot\,; k_0)$ and $\frac{\partial^{n+1} \omega}{\partial k^{n+1}}(k_0)$, where the computation of $\frac{\partial^n u}{\partial k^n}(\cdot\,; k_0)$ can be done very efficiently since (1) – (3) are of the same form with varying right hand side.

The error of the Taylor expansion increases with the distance to k_0. However, increasing the order n might not always be appropriate to improve accuracy since the derivatives $|\frac{\partial^n \omega}{\partial k^n}(k_0)|$ might grow faster with n then the factorial. In this case, a decomposition of the Taylor expansion in subintervals is necessary.

References

[1] D. Klindworth, K. Schmidt, and S. Fliss, *Numerical realization of Dirichlet-to-Neumann transparent boundary conditions for photonic crystal wave-guides*, accepted for publication in Comput. Math. Appl., 2013.

[2] T. Katō, *Perturbation theory for linear operators*, Grundlehren der mathematischen Wissenschaften, Springer, Berlin & Heidelberg, Germany, 1995.

Finite Element Heterogeneous Multiscale Method for the Wave Equation: Long-Time Effects

Assyr Abdulle[1], **Marcus J. Grote**[2], **Christian M. Stohrer**[2,*]
[1] ANMC, Section of Mathematics, EPFL, Lausanne, Switzerland
[2] Department of Mathematics and Computer Science, University of Basel, Basel, Switzerland
*Email: christian.stohrer@unibas.ch

Abstract

For limited time the propagation of waves in a highly oscillatory medium is well-described by the non-dispersive homogenized wave equation. With increasing time, however, the true solution deviates from the classical homogenization limit, as a large secondary wave train develops unexpectedly. Here, we propose a new finite element heterogeneous multiscale method (FE-HMM), which captures not only the short-time macroscale behavior of the wave field but also those secondary long-time dispersive effects.

1 Long-Time Wave Propagation

Let $\Omega \subset \mathbb{R}^d$ be a domain and $T > 0$. We consider the wave equation

$$\begin{cases} \partial_{tt} u^\varepsilon - \nabla \cdot (a^\varepsilon \nabla u^\varepsilon) = F & \text{in } \Omega \times (0,T), \\ u^\varepsilon(x,0) = f(x) & \text{in } \Omega, \\ \partial_t u^\varepsilon(x,0) = g(x) & \text{in } \Omega, \end{cases} \tag{1}$$

where $a^\varepsilon(x) \in (L^\infty(\Omega))^{d\times d}$ is symmetric, uniformly elliptic, and bounded. Here $\varepsilon > 0$ represents a small scale in the problem, which characterizes the multiscale nature of the tensor $a^\varepsilon(x)$. We set either homogeneous Dirichlet or periodic boundary conditions to uniquely determine the solution for every $\varepsilon > 0$.

1.1 Classical homogenization

According to classical homogenization theory, u^ε converges to the solution u^0 of the "homogenized" wave equation as $\varepsilon \to 0$,

$$\partial_{tt} u^0 - \nabla \cdot (a^0 \nabla u^0) = F,$$

where the homogenized tensor (or squared velocity field) a^0 can only rarely be computed explicitly. Thus, u^0 approximates u^ε but only for short times. For longer times $T \sim \varepsilon^{-2}$, the homogenized solution becomes increasingly inadequate, since it neglects microscopic dispersive effects that accumulate over time, as shown in Figure 1. Here we consider (1) in $\Omega = (-1,1)$ with periodic boundary conditions, let $u(x,0)$ be a Gaussian pulse with zero initial velocity

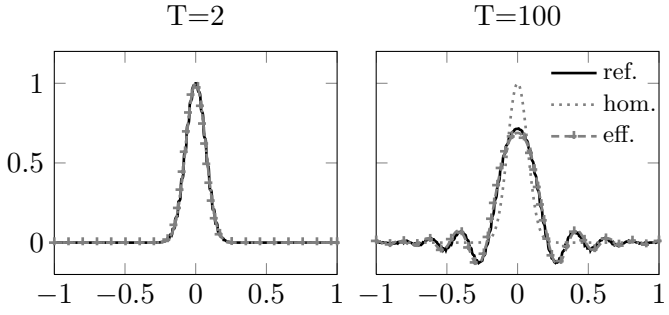

Figure 1: Reference (ref.), homogenized (hom.) and effective (eff.) solution: short-time (left) and long-time (right).

and set

$$a^\varepsilon = \sqrt{2} + \sin\Big(2\pi \frac{x}{\varepsilon}\Big) \text{ with } \varepsilon = \frac{1}{50}. \tag{2}$$

The reference solution of (1)–(2) corresponds to a direct numerical simulation (DNS), where the microscale is fully resolved. After one revolution ($T = 2$), the homogenized and the DNS solution coincide. After fifty revolutions ($T = 100$), however, the DNS displays dispersive effects, which the homogenized solution fails to capture.

1.2 Effective dispersive equation

Various formal asymptotic arguments were derived to elucidate that peculiar inherently dispersive long-time behavior of waves propagating through a strongly heterogeneous periodic medium [1]. An effective equation that captures those dispersive effects was recently derived in [2] for the one-dimensional case when a^ε is ε-periodic:

$$\partial_{tt}(u^{\text{eff}} - \varepsilon^2 b \partial_{xx} u^{\text{eff}}) - a^0 \partial_{xx} u^{\text{eff}} = F. \tag{3}$$

Again, a^0 denotes the homogenized effective coefficient from classical homogenization theory and $b > 0$. As shown in Figure 1, u^ε and u^{eff} essentially coincide both at early and later times.

2 FE Heterogeneous Multiscale Method

In [3], the FE-HMM for elliptic [4] was extended to the time dependent wave equation. It was shown to

converge to u^0 at finite times, yet it failed to capture long-time dispersive effects in the true solution. To incorporate those dispersive effects, we not only need an effective bilinear form but we add a correction to the L^2 inner product, akin to the weak formulation of (3). Similarly to the computation of the bilinear form, the correction relies on numerical solutions of micro problems on sampling domains K_δ of size δ proportional to ε. An alternative HMM scheme, based on the finite difference approximation of an effective flux, was proposed in [5].

We now give a description of the algorithm: First, we generate a macro triangulation $\mathcal{T}_H$ and choose an appropriate macro FE space $S(\Omega, \mathcal{T}_H)$. By macro we mean that $H \gg \varepsilon$ is allowed. Within each macro element $K \in \mathcal{T}_H$ we choose a quadrature formula $\{x_{K,j}, \omega_{K,j}\}$. The FE-HMM solution u_H is given by the following variational problem:

$$\begin{cases} \text{Find } u_H : [0,T] \to S(\Omega, \mathcal{T}_H) \text{ such that} \\ (\partial_{tt} u_H, v_H)_Q + B_H(u_H, v_H) = (F, v_H) \\ \text{for all } v_H \in S(\Omega, \mathcal{T}_H) \text{ and,} \\ \quad u_H(0) = f_H,\ \partial_t u_H(0) = g_H \text{ in } \Omega, \end{cases} \tag{4}$$

where the initial data f_H and g_h are suitable approximations of f and g in $S(\Omega, \mathcal{T}_H)$. The effective bilinear form B_H and $(\cdot,\cdot)_Q$ are defined as follows:

$$B_H(v_H, w_H) = \sum_{K,j} \frac{\omega_{K,j}}{|K_\delta|} \int_{K_\delta} a^\varepsilon(x) \nabla v_h(x) \cdot \nabla w_h(x) dx,$$

and

$$(v_H, w_H)_Q = (v_H, w_H) + \sum_{K,j} \frac{\omega_{K,j}}{|K_\delta|} \int_{K_\delta} (v_h(x) - v_{H,\mathrm{lin}}(x))(w_h(x) - w_{H,\mathrm{lin}}(x)) dx.$$

In the above, the micro solution v_h (resp. w_h) is given by

$$\begin{cases} \text{Find } v_h \text{ such that } (v_h - v_{H,\mathrm{lin}}) \in S(K_\delta, \mathcal{T}_h) \text{ and} \\ \qquad \displaystyle\int_{K_\delta} a^\varepsilon(x) \nabla v_h(x) \cdot \nabla z_h(x) dx = 0, \\ \text{for all } z_h \in S(K_\delta, \mathcal{T}_h). \end{cases}$$

Here $S(K_\delta, \mathcal{T}_h)$ is a micro FE space on the sampling domain K_δ with micro triangulation $\mathcal{T}_h$, and $v_{H,\mathrm{lin}}$ denotes the linearization of v_H at the quadrature point $x_{K,j}$, Since B_H is elliptic and bounded and $(\cdot,\cdot)_Q$ is a true inner product, the FE-HMM is well-defined for all $H, h > 0$. It can be shown that the correction of the L^2 inner product is of order ε^2 in agreement with (3).

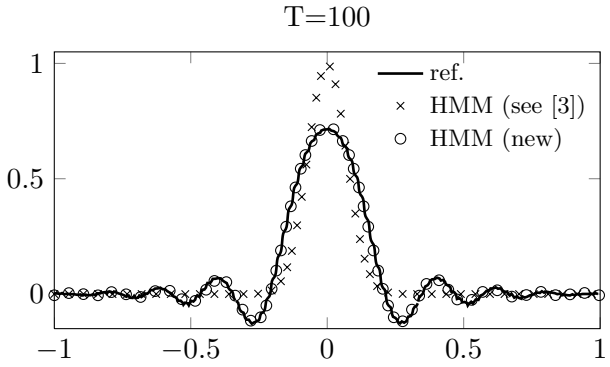

Figure 2: Reference solution (ref.), FE-HMM from [3] and new FE-HMM.

3 Numerical Experiments

We again apply our FE-HMM, defined in (4), to (1)–(2) as in Figure 1. We use cubic FE at the macro- and the micro-scale, with mesh sizes $H = 1/75$ and $h = \varepsilon/20 = 1/1000$. Note that linear or quadratic finite elements could also be used. For time-stepping we use a standard Leap-Frog scheme, with $\Delta t = H/10$. As shown in Figure 2, the new FE-HMM succeeds in capturing, the long-time effects in the true solution. In contrast, the solution of the FE-HMM of [3] without correction is unable to capture those dispersive effects, since this solution was proven to converge to the homogenized solution, u^0, as $\varepsilon \to 0$.

References

[1] F. Santosa and W. W. Symes, *A Dispersive Effective Medium for Wave Propagation in Periodic Composites*, SIAM J. Appl. Math., **51**, pp. 984–1005.

[2] A. Lamacz, *Dispersive Effective Models for Waves in Heterogeneous Media*, Math. Models Methods Appl. Sci., **21** (2011), pp. 1871–1899.

[3] A. Abdulle and M. J. Grote, *Finite Element Heterogeneous Multiscale Method for the Wave Equation*, Multiscale Model. Simul., **9** (2011), pp. 766–7921.

[4] A. Abdulle, *The Finite Element Heterogeneous Multiscale Method: a computational strategy for multiscale PDEs*, GAKUTO Internat. Seri. Math. Sci. Appl., **31** (2009), pp. 133–182.

[5] B. Engquist, H. Holst and O. Runborg , *Multiscale methods for wave propagation in heterogeneous media*, Comm. Math. Sci., **9** (2011), pp. 33–56.

A Super-Algebraic Convergent Solver for Scattering by Biperiodic Gratings

Thomas Rösch[1,*], **Tilo Arens**[1]
[1] Institut für Algebra und Geometrie, Karlsruhe Institute of Technology, Germany
*Email: thomas.roesch@kit.edu

Abstract

We present a numeric solver for scattering by biperiodic layered media. The solver has super-algebraic convergence rate provided the interfaces between the layers are smooth enough. The method is derived as a variant of the method of Bruno and Kunyanski [3–5]. From a theoretical point of view, we present the basic ideas – ending up with the formulation of the main convergence theorem. The performance of the solver can be verified from the presented numerical examples.

1 Problem Setting

We consider scattering of a plane acoustic wave u^i with wave number $k > 0$ and direction of incidence $d = (d_1, d_2, d_3)^\top \in S^2$ with $d_3 < 0$ by a layered medium periodic in the x_1 and x_2-directions. More precisely, given the periods $L_j > 0$, $j = 1, 2$, a number $A > 0$, and setting

$$Q = (0, L_1) \times (0, L_2)\,, \qquad D = Q \times (0, A)\,,$$

we consider interfaces Γ_j given as graphs of Q-periodic functions f_j,

$$\Gamma_j = \{x = (x_1, x_2, x_3)^\top \in D : x_3 = f_j(x_1, x_2)\}\,, \quad j = 0, \dots, N,$$

as well as the domains D_j located between Γ_j and Γ_{j+1}, $j = 0, \dots, N-1$. Additionally define $\Gamma^+ = \{x \in \partial D : x_3 = A\}$ and D_N the domain between Γ_N and Γ^+.

The problem under consideration is the scattering problem

$$\begin{aligned} \Delta u + q_j\, k^2\, u = 0 \qquad & \text{in } D_j\,,\ j = 0, \dots, N\,, \\ [u] = 0\,, \quad \left[\frac{\partial u}{\partial n}\right] = 0 \qquad & \text{on } \Gamma_j\,,\ j = 1, \dots, N\,, \\ u = 0 \qquad & \text{on } \Gamma_0\,, \\ u - u^i \text{ is propagating upward in } & Q \times (A, \infty)\,. \end{aligned}$$

Here q_j denote indices of refraction for the medium layers, satisfying $\operatorname{Im} q_j \geq 0$, $j = 0, \dots, N$. In addition, we require quasi-periodicity of the total field u, i.e. that

$$\begin{aligned} u(L_1, x_2, x_3) &= \mathrm{e}^{\mathrm{i}\, k d_1\, L_1}\, u(0, x_2, x_3)\,, \\ u(x_1, L_2, x_3) &= \mathrm{e}^{\mathrm{i}\, k d_2\, L_2}\, u(x_1, 0, x_3)\,. \end{aligned}$$

The condition that the scattered field $u - u^i$ be upward propagating in $Q \times (A, \infty)$ can be recast in the form that the Fourier expansion of $u - u^i$ on Γ^+ contains only upward propagating or evanescent terms.

Unique solvability of the above scattering problem is studied in [1]. There, a variational formulation in Sobolev spaces of periodic functions is given. Uniqueness of solution is a special feature due to the Dirichlet boundary condition of Γ_0 and also requires that the interfaces Γ_j are sufficiently smooth.

2 Integral Equations

The problem described in 1 can be reformulated as a system of Q-periodic integral equations. This requires the quasi-biperiodic Green's function $G(\cdot, \cdot)$ for the Helmholtz equation [1, 2]. Within each subdomain D_j, the total field can then be expressed as suitable combinations of single and double layer potentials defined on Γ_j and Γ_{j+1}, respectively. Of course, in D_N the incident field needs to be taken into account as well.

Once expressions for the field in each subdomain have been obtained, passing to the interfaces Γ_j reduces the problem to a system of periodic integral equations on Q,

$$\varphi_j - \sum_{m=1}^{2N+1} K_{j,m} \varphi_m = \psi_j \quad \text{on } Q, \tag{1}$$

for $j = 1, \dots, 2N+1$ with unknown densities φ_j sought for in some Sobolev space H^s_Q of Q-periodic functions. All integral operators $K_{j,m}$ turn out to be weakly singular so that Fredholm theory is applicable. Under suitable conditions on regularity of the interfaces, a unique solution to the system of integral equations can be shown to exist.

3 Numerical Solution

To solve the system of integral equations numerically, a variant of the method of Bruno and Kunyan-

ski [3–5] is employed. A convergence analysis of this variant of the method was first given in [1].

Our method is best described as a quasi-collocation method. First of all, the weak singularities are taken care of by local isolation using a smooth cut-off function. The weakly singular integrals are then transformed to polar coordinates around the singularity thus removing it. In order to carry out a convergence analysis, a first approximation comes into play consisting of a manipulation of the integrand by an orthogonal projection and an interpolation with respect to polar coordinates. Thus, the term *quasi* refers to this additional approximation – done, before the usual collocation method is applied: Looking for approximate solutions in a space V_p of trigonometric polynomials on Q of degree at most p by considering the equations only in the collocation points

$$t_\mu = \left(\frac{\mu_1 L_1}{2p}, \frac{\mu_2 L_2}{2p} \right)^\top, \quad \mu_j = 0, \ldots, 2p-1,\ j = 1, 2.$$

To obtain a discrete system from the derived semi-discrete system, a last approximation of certain integrals has to be introduced.

Considering the product space (endowed with the sum-norm)

$$\mathcal{H}_Q^s := \underbrace{H_Q^s \times H_Q^s \times \ldots H_Q^s}_{M \text{ times}},$$

where $M := 2N + 1$, denoting by K the continuous matrix integral operator

$$K = \begin{pmatrix} I - K_{1,1} & -K_{1,2} & \ldots & -K_{1,M} \\ -K_{2,1} & I - K_{2,2} & \ldots & -K_{2,M} \\ \vdots & \vdots & \ddots & \vdots \\ -K_{M,1} & -K_{M,2} & \ldots & I - K_{M,M} \end{pmatrix},$$

setting

$$\varphi := (\varphi_1, \ldots, \varphi_M)^\top \quad \text{and} \quad \psi := (\psi_1, \ldots, \psi_M)^\top,$$

and writing K_p, φ_p and ψ_p for its discrete counterparts, we can state the following theorem.

Theorem 1 *Suppose that $f_j \in C^\infty(\mathbb{R}^2)$ for $j = 0, \ldots, N$. Then for the solutions to $K\varphi = \psi$ and $K_p \varphi_p = \psi_p$, there holds for all $s \geq 0$*

$$\|\varphi - \varphi_p\|_{\mathcal{H}_Q^0} \leq C\, p^{-s}\, \|\varphi\|_{\mathcal{H}_Q^s}.$$

References

[1] T. Arens, *Scattering by Biperiodic Layered Media: The Integral Equation Approach,* Habilitation Thesis, Karlsruhe Institute of Technology, 2010, `http://digbib.ubka.uni-karlsruhe.de/volltexte/1000016241`.

[2] Tilo Arens, Kai Sandfort, Susanne Schmitt and Armin Lechleiter, *Analysing Ewalds method for the evaluation of Greens functions for periodic media*, IMA J. Appl. Math. (2011) `doi:10.1093/imamat/hxr057`.

[3] O.P. Bruno, V. Domínguez, and F.J. Sayas, *Convergence analysis of a high-order Nyström integral-equation method for surface scattering problems*, to appear in Numerische Mathematik.

[4] O.P. Bruno and L.A. Kunyanski, *A fast high order algorithm for the solution of surface scattering problems: Basic implementation, tests and applications*, J. Comp. Phys. **169** (2001), pp. 80–110.

[5] O.P. Bruno and L.A. Kunyanski, *Surface scattering in three dimensions: an accelerated high-order solver*, Proc. R. Soc. Lond. A **457** (2001), pp. 2921–2934.

Acoustic Wave Scattering from Periodic Arrays of Non-Spherical Scatterers by the Boundary Element Method

V. Andrew[1,*], **I. D. Abrahams**[1], **W. J. Parnell**[1]
[1] The School of Mathematics, University of Manchester, Manchester, UK
*Email: victoria.andrew@manchester.ac.uk

Abstract

The problem of reflection and transmission of an incoming plane acoustic wave by an array of periodically distributed non-spherical axi-symmetric scatterers in a compressible fluid is considered. The governing equation is expressed as a singular integral equation for each Fourier decomposed mode. Taking advantage of the geometrical periodicity, the integral over an infinite number of scatterers can be reduced to a single integral over the cross section of a reference scatterer. The integral equation for each mode has been solved by the boundary element method. The reflection and transmission coefficients are plotted for values of $ka \sim O(1)$ and the resulting plots show rapid variations at the cut on frequencies for higher order modes.

1 Problem Statement

A plane wave $\phi^{in} = e^{ik\sin\phi_0 x_1 + ik\cos\phi_0 x_3} e^{-i\omega t}$ is incident on a doubly periodic array of axi-symmetric scatterers in an acoustic medium. The cavities are of characteristic length scale a and their centres are located in the x_1, x_2 plane at positions $x_1 = nd_1$, $x_2 = md_2$ where $m, n = 0, \pm1, \pm2 \ldots$. The geometry is as shown in figure 1.

The velocity potential is of the form $\phi(\mathbf{x})$ and satisfies

$$\nabla^2\phi(\mathbf{x}) + k^2\phi(\mathbf{x}) = 0 \tag{1}$$

in the acoustic medium. The scatterers are sound hard and so we apply

$$\frac{\partial\phi(\mathbf{x})}{\partial n} = 0 \quad \text{on} \quad S^{mn} \tag{2}$$

where S^{mn} defines the surface of scatterer mn.

2 The Boundary Integral Equation

For a point $\mathbf{x} \in S^{mn}$, we apply Green's Theorem to the region exterior to the scatterers and obtain an integral representation for the problem:

$$\frac{1}{2}\phi(\mathbf{x}) = \phi^{in}(\mathbf{x}) + \sum_{m=-\infty}^{\infty}\sum_{n=-\infty}^{\infty} \barint_{S^{mn}} \phi(\mathbf{x}) \frac{\partial G(\boldsymbol{\xi}, \mathbf{x})}{\partial n(\boldsymbol{\xi})}\, dA, \tag{3}$$

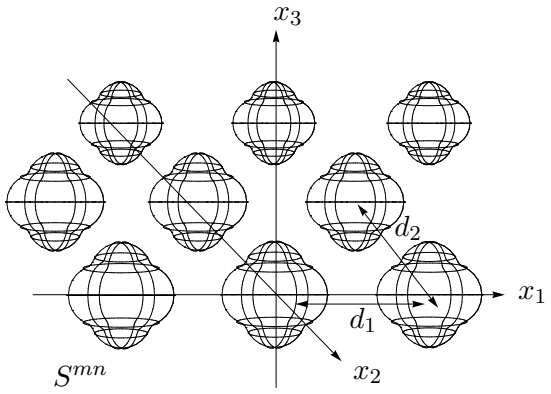

Figure 1: Array of bodies of revolution with centres located in the (x_1, x_2) plane.

where the dash on the integral sign indicates that the integral is a Cauchy Principle value. If we define a cell A^{pq} by $-d_1/2 + pd_1 \le x_1 \le d_1/2 + pd_1$, $-d_2/2 + qd_1 \le x_2 \le d_2/2 + qd_2$, $-\infty < x_3 < \infty$, then for a point $\mathbf{x^0} \in A^{00}$ we have the relations

$$x_1 = x_1^0 + pd_1, \qquad x_2^0 = qd_2, \qquad x_3 = x_3^0. \tag{4}$$

These expressions combined with the form of the incident plane wave suggest the following form for the total velocity potential

$$\phi(\mathbf{x}) = \phi(\mathbf{x^0}) e^{ikpd_1\sin\phi_0}. \tag{5}$$

Using expressions (4)-(5), the integral term in the boundary integral equation can be written as a single integral over the surface S^{00} in the reference cell A^{00}:

$$\frac{1}{2}\phi(\mathbf{x^0}) = \phi^{in}(\mathbf{x^0}) + \barint_{S^{mn}} \phi(\mathbf{x^0}) \frac{\partial G^P(\boldsymbol{\xi^0}, \mathbf{x^0})}{\partial n(\boldsymbol{\xi^0})}\, dA, \tag{6}$$

where $\boldsymbol{\xi^0} \in A^{00}$ and $G^P(\boldsymbol{\xi^0}, \mathbf{x^0})$ is the periodic Green's function

$$G^P(\boldsymbol{\xi^0}, \mathbf{x^0}) = \sum_{m=-\infty}^{\infty}\sum_{n=-\infty}^{\infty} e^{ikmd_1\sin\phi_0} G(\boldsymbol{\xi^0}, \mathbf{x^0}; m, n). \tag{7}$$

Since the scatterers are bodies of revolution, the surface integral in equation (6) can be written as a

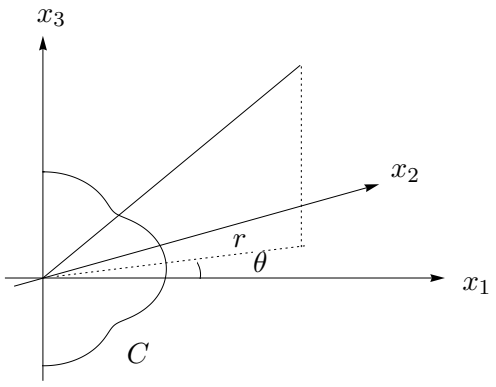

Figure 2: Generating shape C of axisymmetric scatterers.

double integral over the generating shape, C, of the scatterer, and the polar angle θ, as shown in figure 2

$$\int_C \int_{-\pi/2}^{\pi/2} \phi(\mathbf{x^0}) \frac{\partial G^P(\boldsymbol{\xi^0}, \mathbf{x^0})}{\partial n(\boldsymbol{\xi^0})} r \, d\theta dl. \tag{8}$$

We now assume that the total field ϕ can be written as a Fourier series expansion

$$\phi(\mathbf{x}) = \sum_{n=-\infty}^{\infty} \phi_n(r_1, x_3) e^{in\theta_1}, \tag{9}$$

and both the incident wave and the normal derivative of the Green's function can be expressed as a Fourier series expansions

$$\phi^{in}(\mathbf{x}) = \sum_{n=-\infty}^{\infty} I_n(r_1, \phi_0, x_3) e^{in(\theta_1 - \theta_0)}, \tag{10}$$

$$\frac{\partial G}{\partial n} = \sum_{n=-\infty}^{\infty} A_n(r, r_1, x_3, \xi_3) e^{in(\theta - \theta_1)}. \tag{11}$$

Substituting equations (9), (10) and (11) into the governing integral equation, multiplying each term by $e^{-im\theta}$ and integrating from $\theta = 0$ to 2π, we obtain a system of integral equations for each Fourier mode:

$$\frac{1}{2}\phi_m(r_1, x_3) = I_m(r_1, x_3, \phi_0) e^{-im\theta_0} + \int_C \phi_m(r, \xi_3) A_{-m}(r, \xi_3, r_1, x_3) r dl, \tag{12}$$

where A_{-m} is the known Fourier coefficient.

3 The Boundary Element Method

The contour C is divided into N segments $C = \sum_{j=1}^{N} \Gamma_j$, with each having a node at either end and in the centre. We are assuming isoparametric quadratic elements, and so both the shape of the element and the variation in the unknown ϕ can be expressed in terms of the quadratic shape functions $\Psi^1(\nu) = \frac{1}{2}\nu(\nu - 1)$, $\Psi^2(\nu) = (\nu + 1)(1 - \nu)$, $\Psi^3(\nu) = \frac{1}{2}\nu(\nu + 1)$, where ν is a local homogeneous coordinate. The field point $\mathbf{x}$ is placed at each node in turn to generate a system of equations

$$\frac{1}{2}\phi_i = \phi_i^{in} + \sum_{\substack{j=1 \\ j \text{ odd}}}^{2N} \phi_j \left(h^1_{i\frac{(j+1)}{2}} + h^3_{i\frac{(j-1)}{2}} \right) + \sum_{\substack{j=1 \\ j \text{ even}}}^{2N} \phi_j h^2_{i(\frac{j}{2})} \tag{13}$$

where

$$h^k_{ij} = \int_{\nu=-1}^{1} \psi^k(\nu) \frac{\partial G_i(\nu)}{\partial n} |J| \, d\nu. \tag{14}$$

4 Results

The direction of propagation of the incident wave is in the x_1, x_3 plane, the scattered field can be expressed as

$$\phi^{sc}(\mathbf{x}) = \hat{\phi}^{sc}(\mathbf{x}) e^{ikx_1 \sin\phi_0}, \tag{15}$$

and the geometry of array suggests that

$$\hat{\phi}^{sc}(x_1, x_2, x_3) = \hat{\phi}^{sc}(x_1 + md_1, x_2 + md_2, x_3). \tag{16}$$

The periodic form of the scattered field can be represented as a Fourier series

$$\phi^{sc}(\mathbf{x}) = \sum\sum \Phi^{pq}_{\pm} e^{i(\alpha_p x_1 + \beta_q x_2 + \gamma_{pq} x_3)}, \tag{17}$$

where $\alpha_p = k \sin\phi_0 + 2\pi p/d_1$, $\beta_q = 2q\pi/d_2$ and $\gamma^2_{pq} = k^2 - \alpha^2_p - \beta^2_q$. The terms of equation (17) represent individual wave modes. Initially only the zeroth order mode is propagating, but each higher order mode has a cut on frequency that can be calculated. We define the reflection and transmission coefficients for each mode n by

$$T_0 = 1 + \Phi^0_+, \quad T_n = \Phi^n_+, \quad R_n = \Phi^n_-. \tag{18}$$

References

[1] J.D. Achenbach, Y.C. Lu and M. Kitahara, *3-D Reflection and Transmission of Sound by an Array of Rods*, Journal of Sound and Vibration, **125** (1988), pp. 463–476.

Electromagnetic scattering by biperiodic multilayer gratings: A recursive integral equations approach

B. Bugert[1,2,*], **G. Schmidt**[1]
[1] Weierstrass Institute for Applied Analysis and Stochastics, Berlin, Germany
[2] Berlin Mathematical School, Technical University Berlin, Berlin, Germany
*Email: bugert@wias-berlin.de

Abstract

We propose a recursive integral equation algorithm for the study of electromagnetic scattering by a biperiodic multilayer grating structure. The combined use of a Stratton-Chu integral representation and an electric potential ansatz yields a singular integral equation on each interface. These equations arise from each other via recursion from the bottom to the top interface leading to a recursive algorithm. We investigate the analytic properties of the derived algorithm such as existence and uniqueness of solutions resulting from it and show that these coincide with the solutions of the original scattering problem.

Introduction

Scattering theory has numerous applications in micro-optics like the construction of holographic films, optical storage disks and antireflective coatings. Many of these optical devices are implemented by a multilayered structure. We study the special case of electromagnetic scattering by biperiodic multilayered structures and in particular derive a recursive integral equation algorithm. This generalizes the results from [1] where the equivalent problem for oneperiodic structures was treated.

1 The electromagnetic scattering problem

Let Σ_j, $j = 0, \dots, N$, be smooth non-selfintersecting surfaces which are 2π-periodic in both x_1- and in x_2-direction and separate the regions $G_j \subset \mathbb{R}^3$ filled with materials of constant electric permittivity ϵ_j and magnetic permeability μ_j. The scattering of a time-harmonic plane wave $\mathbf{E}^{\mathrm{i}}$ (with wave vector $\alpha = (\alpha_1, \alpha_2, -\alpha_3)^{\mathrm{T}}$) incident on the top layer Σ_0 of the multilayered structure from G_0 is computed by solving

$$\mathbf{curl}\,\mathbf{curl}\,\mathbf{E}_j - \kappa_j^2 \mathbf{E}_j = 0 \quad \text{in } G_{j\in J_0^N}, \tag{1}$$

$$\mathbf{n}_0 \times \left(\mathbf{E}_1 - \left(\mathbf{E}_0 - \mathbf{E}^{\mathrm{i}}\right)\right) = 0 \quad \text{on } \Sigma_0, \tag{2}$$

$$\mathbf{n}_0 \times \left(\mu_1^{-1}\mathbf{E}_1 - \mu_0^{-1}\left(\mathbf{E}_0 + \mathbf{E}^{\mathrm{i}}\right)\right) = 0 \quad \text{on } \Sigma_0, \tag{3}$$

$$\mathbf{n}_j \times (\mathbf{E}_{j+1} - \mathbf{E}_j) = 0 \quad \text{on } \Sigma_{j\in J} \tag{4}$$

$$\mathbf{n}_j \times \left(\mu_{j+1}^{-1}\mathbf{E}_{j+1} - \mu_j^{-1}\mathbf{E}_j\right) = 0 \quad \text{on } \Sigma_{j\in J}, \tag{5}$$

where $J = \{1, \dots, N-1\}$, $J_0^N = J \cup \{0, N\}$, and, the outgoing wave condition at infinity is satisfied:

$$\mathbf{E}_0 - \mathbf{E}^{\mathrm{i}} = \sum_{n\in\mathbb{Z}^2} \mathbf{E}_n^0 e^{\mathrm{i}\left(\alpha_0^{(n)}\cdot\tilde{x} + \beta_0^{(n)} x_3\right)}, \tag{6}$$

$$\mathbf{E}_N = \sum_{n\in\mathbb{Z}^2} \mathbf{E}_n^N e^{\mathrm{i}\left(\alpha_N^{(n)}\cdot\tilde{x} - \beta_N^{(n)} x_3\right)}. \tag{7}$$

Here, $\mathbf{n}_j$ is the unit normal vector on Γ_j, $\mathbf{E}_j = \mathbf{E}|_{G_j}$,

$$\alpha_j^{(n)} = \begin{pmatrix}\alpha_1 + n_1 \\ \alpha_2 + n_2\end{pmatrix}, \quad \beta_j^{(n)} = \sqrt{\kappa_j^2 - |\alpha_j^{(n)}|^2}, \tag{8}$$

and, $\kappa_j = \omega\sqrt{\epsilon_j\mu_j}$, $j = 1, \dots, N$. Note, that the tilde over a three-dimensional vector indicates its orthogonal projection to the (x_1, x_2)-plane. The solutions $\mathbf{E}_j$, $j = 1, \dots, N$, of (1)-(7) shall possess locally finite energy, i.e.

$$\mathbf{E}_j, \mathbf{curl}\,\mathbf{E}_j \in \left(L^2_{\mathrm{loc}}(\mathbb{R}^3)\right)^3. \tag{9}$$

The $\tilde{\alpha}$-quasiperiodicity of the incident waves motivates the fields above to be $\tilde{\alpha}$-quasiperiodic themselves, i.e. they shall satisfy the relation $\mathbf{u}(\tilde{x} + 2\pi \cdot m) = e^{\mathrm{i}2\pi\tilde{\alpha}\cdot m}\mathbf{u}(x)$ for all $m \in \mathbb{Z}^2$. In the following, we assume $0 \le \arg\epsilon_j, \arg\mu_j \le \pi$, such that $\arg\epsilon_j + \arg\mu_j < 2\pi$.

2 Integral equation method

In order to solve the electromagnetic scattering problem, we derive an equivalent system of integral equations from potential representations of $\mathbf{E}_j$ in G_j. For this, we combine a direct with an indirect method, meaning that we are using the $\tilde{\alpha}$-quasiperiodic version of the Stratton-Chu integral representation and an electric potential ansatz. As it is common when working with periodic structures, we restrict our calculations to one period of the multilayered structure. For this, we use the notation $\Gamma_j = \{x \in \Sigma_j \mid -\pi \le x_1, x_2 < \pi\}$ to refer to one period of the interface Σ_j, $j = 0, \dots, N$. The one-sided limits from G_j and G_{j+1} will be denoted by Γ_j^+ and Γ_j^-, respectively.

2.1 Potential operators

The potentials providing $\tilde{\alpha}$-quasiperiodic solutions of (1)-(7) are based on the $\tilde{\alpha}$-quasiperiodic fundamental solution

$$G_{\kappa_j,\tilde{\alpha}}(x) = \frac{\mathrm{i}}{8\pi^2} \sum_{n\in\mathbb{Z}^2} \frac{e^{\mathrm{i}\left(\alpha_j^{(n)}\cdot\tilde{x}+\beta_j^{(n)}|x_3|\right)}}{\beta_j^{(n)}}. \tag{10}$$

The single layer potential $\mathbf{S}^{\tilde{\alpha}}_{j,k}$ on Γ_j is then given by

$$\mathbf{S}^{\tilde{\alpha}}_{j,k}\mathbf{j}(x) = \int_{\Gamma_k} G_{\kappa_j,\tilde{\alpha}}(x-y)\mathbf{j}(y)\, d\sigma(y), \tag{11}$$

for $x \in \mathbb{R}^3 \setminus \Gamma_j$. We define the electric potential $\Psi^{\tilde{\alpha}}_{E_{\kappa_j},k}$ and the magnetic potential $\Psi^{\tilde{\alpha}}_{M_{\kappa_j},k}$ generated by $\mathbf{j} \in \mathbf{H}^{-\frac{1}{2}}_{\tilde{\alpha}}(\mathrm{div}_{\Gamma_k},\Gamma_k)$ as

$$\Psi^{\tilde{\alpha}}_{E_{\kappa_j},k}\mathbf{j} = \kappa_j^{-1}\,\mathbf{curl}\,\mathbf{curl}\,\mathbf{S}^{\tilde{\alpha}}_{j,k}\mathbf{j}, \quad \text{and,} \tag{12}$$

$$\Psi^{\tilde{\alpha}}_{M_{\kappa_j},k}\mathbf{j} = \mathbf{curl}\,\mathbf{S}^{\tilde{\alpha}}_{j,k}\mathbf{j}, \tag{13}$$

respectively. Moreover, we will need the operators

$$\mathbf{C}^{\tilde{\alpha},(m)}_{jk}\mathbf{j}(x) = \{\gamma_{\mathrm{D},k}\}\Psi^{\tilde{\alpha}}_{\mathrm{E}_{\kappa_j},k}\mathbf{j}(x), \quad x\in\Gamma_m, \tag{14}$$

$$\mathbf{M}^{\tilde{\alpha},(m)}_{jk}\mathbf{j}(x) = \{\gamma_{\mathrm{D},k}\}\Psi^{\tilde{\alpha}}_{\mathrm{M}_{\kappa_j},k}\mathbf{j}(x), \quad x\in\Gamma_m, \tag{15}$$

where $\{\gamma_{\mathrm{D},k}\} = -\frac{1}{2}\left(\gamma^-_{\mathrm{D},k} + \gamma^+_{\mathrm{D},k}\right)$ with the Dirichlet trace $\gamma^\pm_{\mathrm{D},k}\mathbf{u} = (\mathbf{n}_k \times \mathbf{u})\,|_{\Gamma^\pm_k}$. We will also make use of the Neumann trace $\gamma^\pm_{\mathrm{N}_{\kappa_j},k}\mathbf{u} = \kappa_j^{-1}\,(\mathbf{n}_k \times \mathrm{curl}\,\mathbf{u})\,|_{\Gamma^\pm_k}$.

2.2 Formulation of the recursive algorithm

With the potential ansatz

$$\mathbf{E}_0 = \Psi^{\tilde{\alpha}}_{\mathrm{E}_{\kappa_0},0}\gamma^+_{\mathrm{N}_{\kappa_0},0}\mathbf{E}_0 + \Psi^{\tilde{\alpha}}_{\mathrm{M}_{\kappa_0},0}\gamma^+_{\mathrm{D},0}\mathbf{E}_0 \text{ in } G_0, \tag{16}$$

$$\mathbf{E}_j = \Psi^{\tilde{\alpha}}_{\mathrm{E}_{\kappa_j},j}\gamma^+_{\mathrm{N}_{\kappa_j},j}\mathbf{E}_j + \Psi^{\tilde{\alpha}}_{\mathrm{M}_{\kappa_j},j}\gamma^+_{\mathrm{D},j}\mathbf{E}_j + \Psi^{\tilde{\alpha}}_{\mathrm{E}_{\kappa_j},j-1}\varphi_{j-1} \text{ in } G_j, \tag{17}$$

$$\mathbf{E}_N = \Psi^{\tilde{\alpha}}_{\mathrm{E}_{\kappa_N},N-1}\varphi_{N-1} \text{ in } G_N, \tag{18}$$

for solutions $\mathbf{E}_{j\in J_0^N}$ of (1)-(7), our algorithm leads to the unknown densities $\varphi_j \in \mathbf{H}^{-\frac{1}{2}}_{\tilde{\alpha}}(\mathrm{div}_{\Gamma_j},\Gamma_j)$ by the recursive relation

$$\varphi_j = \mathcal{Q}_{j-1}\varphi_{j-1}, \quad j\in J. \tag{19}$$

The idea for this ansatz is taken from [2]. The operators $\mathcal{Q}_{j-1}$ are determined by solving the integral operator equation

$$\mathcal{C}_j\mathcal{Q}_{j-1} = -\mathbf{C}^{\tilde{\alpha},(j)}_{jj-1}, \tag{20}$$

where $\mathcal{C}_j = \left[\left(\mathbf{M}^{\tilde{\alpha},(j)}_{jj} + \frac{1}{2}\mathbb{I}\right)\mathcal{A}_j + \rho_{j+1}\mathbf{C}^{\tilde{\alpha},(j)}_{jj}\mathcal{B}_j\right]$. The initial values are given as

$$\begin{aligned}\mathcal{A}_{N-1} &= -\mathbf{C}^{\tilde{\alpha},(N)}_{N-1N-1},\\ \mathcal{B}_{N-1} &= -\left(\mathbf{M}^{\tilde{\alpha},(N)}_{N-1N-1} + \frac{1}{2}\mathbb{I}\right),\end{aligned} \tag{21}$$

and, the subsequent terms are obtained by

$$\begin{aligned}\mathcal{A}_{j-1} = &-\mathbf{C}^{\tilde{\alpha},(j)}_{j-1j-1}\\ &-\left(\rho_{j+1}\mathbf{C}^{\tilde{\alpha},(j)}_{j-1j}\mathcal{B}_j + \mathbf{M}^{\tilde{\alpha},(j)}_{j-1j}\mathcal{A}_j\right)\mathcal{Q}_{j-1},\end{aligned} \tag{22}$$

$$\begin{aligned}\mathcal{B}_{j-1} = &-\left(\mathbf{M}^{\tilde{\alpha},(j)}_{j-1j-1} + \frac{1}{2}\mathbb{I}\right)\\ &-\left(\rho_{j+1}\mathbf{M}^{\tilde{\alpha},(j)}_{j-1j}\mathcal{B}_j + \mathbf{C}^{\tilde{\alpha},(j)}_{j-1j}\mathcal{A}_j\right)\mathcal{Q}_{j-1}.\end{aligned} \tag{23}$$

Then, the initial value φ_0 of (19) is a solution of

$$\left[\left(\mathbf{M}^{\tilde{\alpha},(0)}_{00} + \frac{1}{2}\mathbb{I}\right)\mathcal{A}_0 + \rho_1\mathbf{C}^{\tilde{\alpha},(0)}_{00}\mathcal{B}_0\right]\varphi_0 = \mathbf{E}^{\mathrm{i}}. \tag{24}$$

3 Analysis of the recursive algorithm

In our study, we establish necessary and sufficient conditions such that the existence of solutions of (20) and (24) implies that the electromagnetic scattering problem (1)-(7) is solvable. This result follows from the Fredholm properties of $\mathcal{C}_j$ which can be established using the results in [2] and the techniques in [3]. Following [4], it is also possible to find conditions ensuring the uniqueness of solutions of (1)-(7).

Acknowledgement

The research of B. Bugert is funded by the Berlin Mathematical School at the Technical University Berlin.

References

[1] G. Schmidt, *Conical diffraction by multilayer gratings: A recursive integral equations approach*, Preprint of the Weierstrass Institute, **1601** (2011).

[2] M. Costabel and F. Le Louër, *On the Kleinman-Martin integral equation method for electromagnetic scattering by a dielectric body*, SIAM J. Appl. Math., **71** (2011), pp. 635–656.

[3] T. Arens, *Scattering by biperiodic layered media: the integral equation approach*, Habilitation thesis, KIT, Karlsruhe, 2010.

[4] G. Schmidt, *Integral methods for conical diffraction*, Preprint of the Weierstrass Institute, **1435** (2009).

2D-Rapidly convergent quasi-periodic Green function for the scattering of acoustic waves from rough surfaces throughout the spectrum–including Wood Anomalies.

O.P. Bruno [1], **B.Delourme**[2,*]
[1] Computing and Mathematical Sciences, Caltech, Pasadena, USA
[2] LAGA, Université Paris 13, Sorbonne Paris Cité, CNRS, UMR 7539, Villetaneuse, France
*Email: delourme@math.univ-paris13.fr

Abstract
This work deals with the scattering of acoustic waves from one dimensional rough surfaces. Based on a periodic green function that quickly converges both at and away from Wood anomalies, we build a second kind integral equation valid throughout the spectrum. Discretizing this integral equation by the Nyström method, we obtain an efficient numerical method to solve scattering problems by periodic gratings.

1 Setting of the problem

We consider the problem of scattering of a plane wave by a perfectly reflecting periodic surface

$$\Gamma = \{(x, f(x)), x \in \mathbb{R}\},$$

where $f : \mathbb{R} \mapsto \mathbb{R}$ is an L-periodic r-times continuously differentiable function with $r \geq 2$. The incident and scattered waves propagate throughout the domain

$$\Omega = \{(x, y) \in \mathbb{R}^2, \text{such that } y > f(x)\}.$$

Letting $k \in \mathbb{R}^+$, $\theta \in (-\pi/2, \pi/2)$, $\alpha = k\sin(\theta)$ and $\beta = k\cos(\theta)$ (where θ is the angle between the direction of propagation of the incident field, measured counterclockwise from the negative y-axis), we assume the periodic surface is illuminated by the incident plane wave

$$u^{\text{inc}}(x, y) = e^{i(\alpha x - \beta y)}.$$

The scattered field $u^s \in H^1_{\text{loc}}(\Omega)$ satisfies the partial differential equation

$$\Delta u^s + k^2 u^s = 0 \quad \text{in } \Omega$$

as well as the quasi-periodicity condition

$$u^s(x + L, y) = u^s(x, y)e^{i\alpha L}$$

together with either the Dirichlet boundary conditions or Neumann boundary conditions

$$u^s = -u^{\text{inc}} \quad \text{or} \quad \frac{\partial u^s}{\partial \nu} = -\frac{\partial u^{\text{inc}}}{\partial \nu} \quad \text{on } \Gamma.$$

where ν is the unit normal. To close the problem we impose u^s to be *outgoing*, that is, for $y > \max_{x\in[0,L]} f(x)$, u^s is given by a Rayleigh expansion of the form

$$u^s(x, y) = \sum_{n\in\mathbb{N}} a_n e^{i(\alpha_n x + \beta_n y)},$$

where

$$\alpha_n = \alpha + \frac{nL}{k}, \quad \beta_n = \begin{cases} \sqrt{k^2 - \alpha_n^2} & \text{if } k^2 \geq n^2, \\ i\sqrt{\alpha_n^2 - k^2} & \text{otherwise.} \end{cases}$$

Remark 1.1 *In the case where there exists $n \in \mathbb{Z}$ such that $\alpha_n^2 = k^2$ we have a* Wood Anomaly frequency.

Away from Wood anomalies, as is well known, the scattering problems previously described can be reduced to second kind integral equations (cf. for instance [1], [2]). For instance, for the Dirichlet problem, we can solve the second kind integral equation

$$\int_{\Gamma_\#} \partial_{\nu(x')} G^{\text{q}}\left(x - x', f(x) - f(x')\right) \mu(x')\, ds(x') + \frac{1}{2}\mu(x') = -u^{\text{inc}}{}_{|\Gamma_\#}, \quad (1)$$

the diffracted field being deduced by a post-processing step using a representation formula. In the previous formula G^{q} denotes the quasi-periodic Green function (see [3]) which is defined by the following converging series, except in the Wood anomaly case:

$$G^{\text{q}}(X, Y) = \frac{i}{4} \sum_{n\in\mathbb{Z}} e^{-i\alpha nL} H_0^1(k\sqrt{(X + nL)^2 + Y^2}).$$

The objective of our talk is to build an integral equation that works at an around the Wood anomalies.

2 New, rapidly convergent quasi-periodic Green functions series valid at and around Wood anomalies

Based on a finite difference approach (see [4]), we construct a family of periodic Green functions as follows: for $j \in \mathbb{N}$, let

$$G_j^{\mathrm{q}}(X,Y) := \frac{i}{4} \sum_{n\in\mathbb{Z}} e^{-i\alpha nL} \sum_{m=0}^{j} C_j^m (-1)^m H_0^1\left(k\sqrt{(X+nL)^2+(Y-m\,h\,j)^2}\right), \quad (2)$$

where h is a real parameter satisfying $h > \max(f) - \min(f)$. For $j \in \mathbb{N}^*$, G_j^{q} is defined for any frequency k. Indeed, the general term of the series behaves linke $n^{-j/2-1/2}$ if j is even and $n^{-j/2-1}$ if j is odd. As a result of this fast decay, the truncated sum of the infinite series

$$G_{j,N}^{\mathrm{q}}(X,Y) := \frac{i}{4} \sum_{n=-N}^{N} e^{-i\alpha nL} \sum_{m=0}^{j} C_j^m (-1)^m H_0^1\left(k\sqrt{(X+nL)^2+(Y-m\,h\,j)^2}\right),$$

converges more rapidly than does a corresponding truncation of the classical quasi-periodic Green function (see Figure 1).

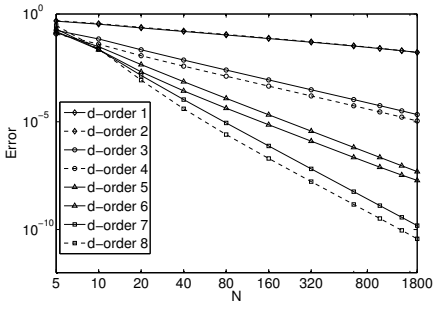

Figure 1: Absolute approximation error arising from the rapidly convergent Green function as a function of the truncation parameter N for various differencing orders j at the Wood anomaly frequency $k = 1$.

Replacing the quasi-periodic Green function by G_j^{q} in Equation (1), we obtain an integral equation that can be solved at and away from Wood Anomalies.

Remark 2.1 *In fact, our proposed rapidly convergent quasi-periodic Green function series results from a slight but important modification of* G_j^{q}.

3 Numerical results

Our numerical method incorporates the shifting methodology developped in Section 2 together with a suitable modified version of a well known Nyström approach (see [5]) for high-order evaluation of basic integral operators.

To demonstrate the beneficial effect of our new method, we consider the problem of scattering by the surface $f(x) = \frac{\pi}{10}\cos x$. In figure 2, we plot the evolution of the error on the energy (see [1]) with respect to the frequency k for the classical quasi-periodic Green function and for the 9th order shifted one. As expected our new method also works at the Wood anomalies ($k = 1$ and $k = 2$), although the classical fails.

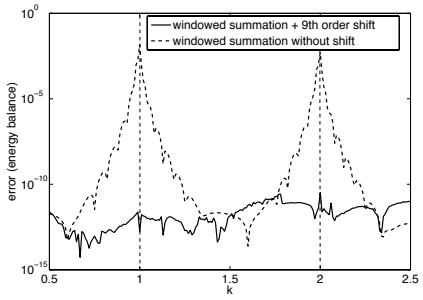

Figure 2: Energy balance with respect to the frequency

References

[1] R. Petit, editor. *Electromagnetic Theory of gratings*, volume 22 of *Topics in Current Physics*, Springer-Verlag, Berlin, 1980.

[2] A. Kirsch. *Diffraction by periodic structures*, Inverse problems in mathematical physics, vol. 422 of *Lecture Notes in Phys.*, p. 87-102, Springer, Berlin, 1993.

[3] C.M. Linton, *The Green's function for the two-dimensional Helmoltz equation in periodic domains*, J. Engrg. Math., 33(4), p. 377-402, 1998.

[4] S.N. Chandler-Wilde and C.R. Ross. *Scattering by rough surfaces: The Dirichlet problem for the Helmholtz equation in a non-locally perturbed half-plane.*, Math. Methods. Appl. Sci., 19(12), p. 959-976, 1996.

[5] D. Colton and R. Kress. *Inverse Acoustic and Electromagnetic Scattering Theory*, vol. 93 of Applied Mathematical Sciences, Springer-Verlag, Berlin, second edition, 1998.

3.10 Theoretical issues in time harmonic scattering

Is the Helmholtz equation really sign-indefinite?

A. Moiola[1], **E. A. Spence**[2,*]
[1] Department of Mathematics and Statistics, University of Reading
[2] Department of Mathematical Sciences, University of Bath
*Email: E.A.Spence@bath.ac.uk

Abstract

We introduce a new *sign-definite* (also called *coercive* or *elliptic*) formulation of the Helmholtz equation posed in the interior of a star-shaped domain with impedance boundary conditions. Like the standard variational formulation, this new formulation arises just by multiplying the Helmholtz equation by a particular test function and integrating by parts.

Introduction

The usual variational (or weak) formulations of the Helmholtz equation are sign-indefinite in the sense that the sesquilinear forms cannot be bounded below by a positive multiple of the appropriate norm squared. This is often for a good reason, since in bounded domains under certain boundary conditions the solution of the Helmholtz equation is not unique at certain wavenumbers (those that correspond to eigenvalues of the Laplacian), and thus the variational problem cannot be sign-definite. However, even in cases where the solution is unique for all wavenumbers, the standard variational formulations of the Helmholtz equation are still indefinite when the wavenumber is large.

Indeed consider the *interior impedance problem* for the Helmholtz equation. That is, given a bounded Lipschitz domain $\Omega \subset \mathbb{R}^d$, $f \in L^2(\Omega)$, $g \in L^2(\partial\Omega)$, and $k > 0$, find u such that

$$\mathcal{L}u := \Delta u + k^2 u = -f \quad \text{in } \Omega, \tag{1a}$$

$$\frac{\partial u}{\partial n} - \mathrm{i}ku = g \quad \text{on } \partial\Omega. \tag{1b}$$

This problem can be put in weak (or variational) form by multiplying by the complex conjugate of a test function v and integrating by parts, i.e. using Green's identity

$$\overline{v}\mathcal{L}u = \nabla \cdot [\overline{v}\nabla u] - \nabla u \cdot \overline{\nabla v} + k^2 u\overline{v}. \tag{2}$$

The result is that the boundary value problem (BVP) (1) can be reformulated as:

$$\text{Find } u \in \mathcal{V} \text{ such that } a(u,v) = F(v) \text{ for all } v \in \mathcal{V}. \tag{3}$$

with $\mathcal{V}$ the Hilbert space $H^1(\Omega)$ equipped with norm

$$\|v\|^2_{1,k,\Omega} := \|\nabla v\|^2_{L^2(\Omega)} + k^2 \|v\|^2_{L^2(\Omega)},$$

the sesquilinear form $a(\cdot,\cdot) : \mathcal{V} \times \mathcal{V} \to \mathbb{C}$ given by

$$a(u,v) := \int_\Omega \left(\nabla u \cdot \overline{\nabla v} - k^2 u\overline{v}\right) \mathrm{d}\mathbf{x} - \mathrm{i}k \int_{\partial\Omega} u\overline{v}\, \mathrm{d}s, \tag{4}$$

and the antilinear functional $F : \mathcal{V} \to \mathbb{C}$ given by

$$F(v) := \int_\Omega f\overline{v}\, \mathrm{d}\mathbf{x} + \int_{\partial\Omega} g\overline{v}\, \mathrm{d}s, \tag{5}$$

Given a variational problem of the form (3), ideally one would like to prove that there exist constants $C_c, \alpha > 0$ such that

$$|a(u,v)| \le C_c \|u\|_{\mathcal{V}} \|v\|_{\mathcal{V}} \text{ for all } u,v \in \mathcal{V}, \text{(continuity)},$$
$$|a(v,v)| \ge \alpha \|u\|^2_{\mathcal{V}} \text{ for all } v \in \mathcal{V}, \text{(coercivity)}.$$

"Sign-definite" is used as a synonym for "coercive" (thus a variational problem is sign-indefinite if and only if it is not coercive).

If continuity and coercivity can be established then there are three important consequences (i) existence and uniqueness of the solution to (3) via the Lax–Milgram theorem, (ii) quasi-optimality of the Galerkin method applied to (3) for *any* finite dimensional subspace of V, and (iii) sign-definiteness of the finite dimensional matrix of the Galerkin method.

Returning to the variational formulation of the interior impedance problem (4) and (5), one can show that if $k^2 \ge \lambda_1$ (the smallest eigenvalue of the negative Laplacian with Dirichlet boundary conditions) then there exists a $v \in V$ such that $a(v,v) = 0$; thus $a(\cdot,\cdot)$ is not coercive. This indefiniteness has implications for both the analysis and the practical implementation of finite element methods based on the variational formulation.

A new sign-definite variational formulation of the Helmholtz equation

Consider the Hilbert space

$$V := \left\{ v : v \in H^1(\Omega),\ \Delta v \in L^2(\Omega),\ \nabla v \in \left(L^2(\partial\Omega)\right)^d \right\} \tag{6}$$

with norm

$$\|v\|_V^2 := k^2\|v\|_{L^2(\Omega)}^2 + \|\nabla v\|_{L^2(\Omega)}^2 + k^{-2}\|\Delta v\|_{L^2(\Omega)}^2 + L\left(k^2\|v\|_{L^2(\partial\Omega)}^2 + \|\nabla v\|_{L^2(\partial\Omega)}^2\right),$$

and obvious inner product, where L is the diameter (or some other characteristic length scale) of the domain Ω. (Note that if $v \in V$, then the restriction of v to $\partial\Omega$ is in $L^2(\partial\Omega)$ by standard trace results.)

Define the sesquilinear form $b : V \times V \to \mathbb{C}$ by

$$b(u,v) := \int_\Omega \left(\nabla u \cdot \overline{\nabla v} + k^2 u\overline{v} + \left(\mathcal{M}u + \frac{1}{3k^2}\mathcal{L}u\right)\overline{\mathcal{L}v}\right)\mathrm{d}\mathbf{x} - \int_{\partial\Omega}\left(\mathrm{i}ku\,\overline{\mathcal{M}v} + \left(\mathbf{x}\cdot\nabla_{\partial\Omega}u - \mathrm{i}k\beta u + \frac{d-1}{2}u\right)\overline{\frac{\partial v}{\partial n}} + (\mathbf{x}\cdot\mathbf{n})\left(k^2 u\overline{v} - \nabla_{\partial\Omega}u\cdot\overline{\nabla_{\partial\Omega}v}\right)\right)\mathrm{d}s,$$

and antilinear functional $G : V \to \mathbb{C}$ by

$$G(v) := \int_\Omega \left(\overline{\mathcal{M}v} - \frac{1}{3k^2}\overline{\mathcal{L}v}\right) f\,\mathrm{d}\mathbf{x} + \int_{\partial\Omega}\overline{\mathcal{M}v}\,g\,\mathrm{d}s,$$

where β is an arbitrary real constant, d is the spatial dimension,

$$\mathcal{L}u := \Delta u + k^2 u, \quad \mathcal{M}u := \mathbf{x}\cdot\nabla u - \mathrm{i}k\beta u + \frac{d-1}{2}u,$$

and $\nabla_{\partial\Omega}$ is the surface gradient on $\partial\Omega$.

With the Hilbert space V, sesquilinear form $b(\cdot,\cdot)$, and functional $G(\cdot)$ defined as above, if u is the solution to the BVP (1) then $u \in V$ and

$$b(u,v) = G(v) \quad \text{for all } v \in V \tag{7}$$

(this is not immediately obvious, see [1, Proposition 3.2]).

Using the Cauchy–Schwarz inequality it is straightforward to show that the sesquilinear form $b(\cdot,\cdot)$ is continuous on V. In particular, if β is independent of k (as we choose it to be below), then the continuity constant $C_c \sim k$ as $k \to \infty$.

The main novelty of $b(\cdot,\cdot)$ is that, for some domains, it is coercive on V:

Theorem 1. ***[1, Theorem 3.4]*** *Let Ω be a Lipschitz domain with diameter L that is star-shaped with respect to a ball, i.e. there exists a $\gamma > 0$ such that*

$$\mathbf{x}\cdot\mathbf{n}(\mathbf{x}) \geq \gamma L$$

for all $\mathbf{x} \in \partial\Omega$ such that $\mathbf{n}(\mathbf{x})$ exists. If the arbitrary constant β is chosen such that

$$\beta \geq \frac{L}{2}\left(1 + \frac{4}{\gamma} + \frac{\gamma}{2}\right)$$

then, for any $k > 0$,

$$\Re b(v,v) \geq \frac{\gamma}{4}\|v\|_V^2 \quad \text{for all } v \in V,$$

i.e. $b(\cdot,\cdot)$ is coercive on V with constant $\gamma/4$.

The idea behind the new formulation

As we saw in above, the standard variational formulation of the interior impedance problem (1) is based on integrating over Ω Green's identity for the Helmholtz equation (2).

The new variational formulation (7) comes from integrating the following identity over Ω

$$\begin{aligned}&\overline{\mathcal{M}_1 v}\mathcal{L}u + \mathcal{M}_2 u\overline{\mathcal{L}v}\\ &= \nabla\cdot\left[\overline{\mathcal{M}_1 v}\,\nabla u + \mathcal{M}_2 u\,\overline{\nabla v} + \mathbf{x}(k^2 u\overline{v} - \nabla u\cdot\overline{\nabla v})\right]\\ &\quad + \big(d - 2 - \alpha_1 - \alpha_2 - \mathrm{i}k(\beta_1 - \beta_2)\big)\nabla u\cdot\overline{\nabla v}\\ &\quad + \big(\alpha_1 + \alpha_2 - d + \mathrm{i}k(\beta_1 - \beta_2)\big)k^2 u\overline{v}.\end{aligned}$$

where the multipliers $\mathcal{M}_j$ are defined by

$$\mathcal{M}_j v := \mathbf{x}\cdot\nabla v - \mathrm{i}k\beta_j v + \alpha_j v, \quad j = 1, 2,$$

and the real numbers β_j, α_j are chosen so as to ensure coercivity of the resulting sesquilinear form.

The idea of multiplying the Helmholtz operator, $\mathcal{L}$, by the multiplier $\mathcal{M}_j$ goes back to Morawetz and Ludwig [3] and was then extensively used by Morawetz in her famous work on the wave equation [2].

References

[1] A. Moiola and E. A. Spence, *Is the Helmholtz equation really sign-indefinite?*, preprint, (2012).

[2] C. S. Morawetz, *Decay for solutions of the exterior problem for the wave equation*, Communications on Pure and Applied Mathematics, 28 (1975), pp. 229–264.

[3] C. S. Morawetz and D. Ludwig, *An inequality for the reduced wave operator and the justification of geometrical optics*, Communications on Pure and Applied Mathematics, 21 (1968), pp. 187–203.

Theoretical features of the hybrid resonance for time harmonic Maxwell's equations

B. Després[1,*], R. Weder[2] and L.M. Imbert-Gérard[1]
[1] Laboratory Jacques Louis Lions, University Pierre et Marie Curie, 75252 Paris Cedex 05, France
[2] Departamento de Física Matemática, Instituto de Investigaciones en Matemáticas Aplicadas y en Sistemas, Universidad Nacional Autónoma de México, Apartado Postal 20-726, DF 01000, México
*Email: despres@ann.jussieu.fr

Abstract

The starting point is Maxwell's equations for the propagation of a wave in a strongly magnetized plasma. It can be modeled by the so called cold plasma dielectric tensor. In this context we construct and analyze a mathematical solution of the time harmonic Maxwell's equations with a hybrid resonance in slab (planar) geometry. We use the limit absorption principle to construct the relevant solutions. This is related to an original singular integral equation which is attached to the Fourier solution.

Introduction

In slab geometry the equations for the transverse electric (TE) mode, $E = (E_x, E_y, 0)$, and E_x, E_y independent of z, are

$$\left\{\begin{array}{rrrl} W & +\partial_y E_x & -\partial_x E_y & = 0, \\ \partial_y W & -\alpha\frac{\omega^2}{c^2}E_x & -i\delta\frac{\omega^2}{c^2}E_y & = 0, \\ -\partial_x W & +i\delta\frac{\omega^2}{c^2}E_x & -\alpha\frac{\omega^2}{c^2}E_y & = 0, \end{array}\right. \qquad (1)$$

where the coefficients are

$$\alpha = 1 - \frac{\omega_p^2}{\omega^2 - \omega_c^2} \qquad \delta = \frac{\omega_c\omega_p^2}{\omega\left(\omega^2 - \omega_c^2\right)},$$

and W is the vorticity (also equal to B_z). The plasma parameter are the cyclotron frequency $\omega_c = \frac{eB_0}{m_e}$ which can taken as constant in first approximation and the plasma frequency $\omega_p = \sqrt{\frac{e^2N_e}{\varepsilon_0 m_e}}$ which depends on the electronic density N_e. The geometry and the coefficients are described in figures 1 and 2.

1 The Budden problem

In the case where the solution is independent of y, what for the plane waves corresponds to normal incidence, the system (1) is called the Budden problem [2]

$$\left\{\begin{array}{ll} W - E_y' & = 0, \\ -\alpha E_x - i\delta E_y & = 0, \\ -W' + i\delta E_x - \alpha E_y & = 0. \end{array}\right.$$

It is instructive to design an analytical solution.

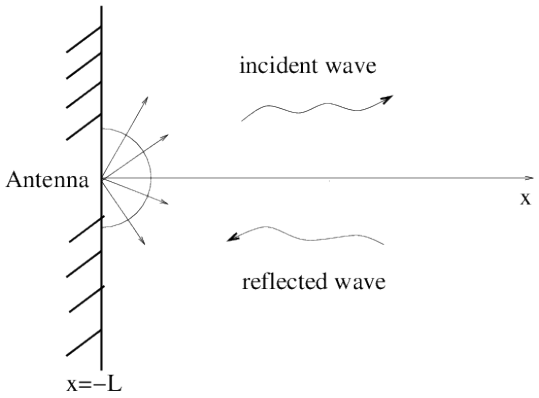

Figure 1: X-mode in slab geometry. The medium is filled with a plasma.

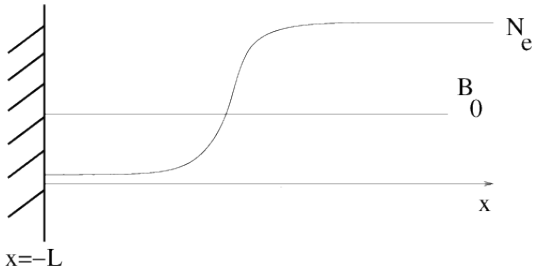

Figure 2: The electronic density $x \mapsto N_e(x)$ is low at the boundary, and increases towards a plateau. The background magnetic field B_0 is constant.

After elimination of E_x and W we obtain that, $-E_y'' + \left(\frac{\delta^2}{\alpha} - \alpha\right)E_y = 0$. Let us consider that $\alpha = -x$ and δ is solution of $\frac{\delta^2}{x} - x = -\frac{1}{4} + \frac{1}{x}$. The positive solution is $\delta(x) = \sqrt{x^2 - \frac{x}{4} + 1} > 0$. The y-component of the electric field is solution of

$$E_y'' + \left(-\frac{1}{4} + \frac{1}{x}\right)E_y = 0. \qquad (2)$$

This equation is of Whittaker type. It is a particular case of the confluent hypergeometric equation, and can also be rewritten under the Kummer form. The general theory shows that the first fundamental solution is regular $v(x) = e^{-\frac{x}{2}}x$. Let us consider a

second solution w with linear independence with respect to the first one. The linear independence can be characterized by the normalized Wronskian relation $v(x)w'(x) - v'(x)w(x) = 1$. Seeking for a representation $w = vz$, one gets that

$$v^2 z' = 1 \Rightarrow z = \int \frac{dx}{v^2} \Rightarrow w = v \int \frac{dx}{v^2} = x\, e^{-x/2} \int \frac{e^x}{x^2}.$$

Moreover $\int \frac{e^x}{x^2} = -\frac{e^x}{x} + \int \frac{e^x}{x} = -\frac{e^x}{x} + E_i(x)$ where $E_i(x)$ is the Exponential-integral function. It follows that $w(x) = -e^{x/2} + x\, e^{-x/2}\, E_i(x)$. Furthermore $E_i(x) = \ln|x| + |\sum_{j=1}^{\infty} \frac{x^j}{j \cdot j!}$. It follows that,

$$w(x) = -1 + x\, \ln|x| + O(|x|), \quad |x| \to 0. \qquad (3)$$

We notice that the second function w is bounded, but non regular at origin. The y component of the electric field of the Budden problem is a bounded function: $E_y = av + bw \Rightarrow E_y \in L^\infty]-\varepsilon, \varepsilon[$. The general form of the x component of the electric field is a linear combination $E_x = -ia\delta \frac{v}{\alpha} - ib\delta \frac{w}{\alpha}$ where $\frac{v}{\alpha}$ is a bounded function and $\frac{w}{\alpha}$ is not a bounded function. Since $E_x^w \notin L^2]-\varepsilon, \varepsilon[$, we notice that the electric field is not a square integrable function in general.

This singularity is the mathematical manifestation of the resonance. We notice however that $\frac{w}{\alpha}$ can be defined as a singular value.

2 Analysis

We solve the system (1) first using a Fourier reduction in the vertical direction, and second with a specific singular integral equation obtained after elimination of E_y and W. The structure of the singular equation is as follows ($U = E_x$)

$$xU(x) + \int_0^x K(x,y)U(y)dy = f(x)$$

where the kernel K and the right hand side are functions of the parameters of the problem. They are bounded. However the singularity $x = 0$ makes this integral equation highly singular. It is actually a third kind integral equation [6], [1] for which the Fredholm theory does not hold.

Very fortunately the friction of the particles in a plasma generates a damping phenomenon which yields the regularized integral equation

$$(x + i\nu)U_\nu(x) + \int_0^x K_\nu(x,y)U_\nu(y)dy = f_\nu(x).$$

Here $\nu > 0$ is a very small positive number which comes from the friction of particles inside the plasma: K_ν and f_ν are some regularizations of K and f. It means that one can invoke the **limit absorption principle** to give a meaning to the limit solution. This mechanism is the fundamental tool which allows to construct a physically and mathematically sound solution to the system (1).

Our main result [3] can be summarized as follows.

Proposition 1 *Under some natural hypotheses [3], for every $g \in L^2(\mathbb{R})$ with $\widehat{g}$ of compact support there exists a solution in the sense of distributions of (1) with non homogeneous boundary condition*

$$W + i\lambda n_x E_y = g \text{ on the left boundary } x = -L,$$

and that goes to zero at infinity (in the horizontal direction). Moreover, unless the source term g is identically zero, the electric field E_x does not belong to $L^1_{\rm loc}((-L,\infty)\times(-\infty,\infty))$. The other components E_y and W are more regular, they belong to $L^2((-L,\infty)\times(-\infty,\infty))$.

References

[1] G.R. Bart and R.L. Warnock, *Linear integral equations of the third kind*, Siam J. of Math. Anal, 4, 609-622, 1973.

[2] F.F. Chen and R.B. White. *Amplification and Absorption of Electromagnetic Waves in Overdense Plasmas*, Plasma Phys. (1974), ed. by C. Yamanaka, Phys. Soc. Japan, 1984.

[3] B. Després, L.-M. Imbert-Gérard, R. Weder, *Hybrid resonance of Maxwell's equations in slab geometry*, online http://arxiv.org/abs/1210.0779, 2012.

[4] P. Monk, *Finite element for Maxwell's equations*, Clarendon Press, Oxford, 2003.

[5] L.-M. Imbert-Gérard, and B. Després, *About numerical approximation of Maxwells equations with singular solutions*, submitted to Waves 2013.

[6] E. Picard, *Sur les équations intégrales de troisième espèce*, Annales scientifiques de l'ENS, 28, 459-472, 1911.

[7] R. Weder, *A Rigorous Analysis of High-Order Electromagnetic Invisibility Cloaks*, J.o Phys. A: Mathematical and Theoretical, **41** (2008) 065207.

Coercive modifications of the double-layer potential on Lipschitz domains

S. N. Chandler-Wilde[1,*], **E. A. Spence**[2]
[1] Department of Mathematics and Statistics, University of Reading
[2] Department of Mathematical Sciences, University of Bath
*Email: S.N.Chandler-Wilde@reading.ac.uk

Abstract

A popular way of solving boundary value problems for the Helmholtz equation $\Delta u + k^2 u = 0$, with k a real constant, is to convert them into integral equations posed on the boundary of the domain. Although the numerical analysis of boundary integral equations for the Helmholtz equation has been investigated by many researchers over the years, the following important result remains open: it has not yet been proved that the Galerkin method converges when applied to the standard second-kind integral equation formulation of the Helmholtz exterior Dirichlet problem posed on a general Lipschitz domain. This result could be obtained by proving that the Laplace double-layer potential satisfies a Gårding inequality on $L^2(\Gamma)$, where Γ denotes the boundary of a general Lipschitz domain, but this result remains open. In this paper we should that if the Laplace double-layer potential is modified in a certain way, then the stronger result of coercivity (a.k.a. $L^2(\Gamma)$-ellipticity) can be obtained for a general Lipschitz domain. This then implies that an analogously modified operator for the Helmholtz equation satisfies a Gårding inequality.

Introduction

Let Ω_- be a bounded Lipschitz open set in 3-d, such that the open complement $\Omega_+ := \mathbb{R}^3 \setminus \Omega_-$ is connected (and thus Ω_+ is a Lipschitz domain). Let $\Gamma := \partial\Omega_+$. We consider the exterior Dirichlet problem for the Helmholtz equation; namely, given $k > 0$ and $h \in H^1(\Gamma)$, find $u \in C^2(\Omega_+) \cap H^1_{\rm loc}(\Omega_+)$ such that

$$\Delta u + k^2 u = 0 \text{ in } \Omega_+, \tag{1a}$$

$$\gamma^+ u = h \text{ on } \Gamma, \text{ and} \tag{1b}$$

$$\frac{\partial u}{\partial r} - {\rm i}ku = o(r^{-1}) \text{ as } r := |\mathbf{x}| \to \infty, \tag{1c}$$

where γ^+ denotes the (exterior) trace on Γ.

Note that one usually assumes $h \in H^{1/2}(\Gamma)$, but here we assume that $h \in H^1(\Gamma)$; this will be the case, for example, if u is the scattered field arising from plane-wave incidence, in which case h is given in terms of the trace of the incident field on Γ – see, e.g., [1, Theorem 2.12].

From Green's integral representation we can obtain two integral equations for the unknown Neumann boundary value $\partial_n^+ u$:

$$S_k \partial_n^+ u = \left(-\frac{1}{2} I + D_k\right) h, \tag{2}$$

$$\left(\frac{1}{2} I + D_k'\right) \partial_n^+ u = H_k h, \tag{3}$$

where S_k is the single-layer potential, D_k the double-layer potential, D_k' the adjoint double-layer potential, and H_k the hypersingular operator (see, e.g., [1, §2.3, §2.5]).

Since both integral equations (2) and (3) fail to be uniquely solvable for certain values of k the standard way to resolve this difficulty is to take a linear combination of the two equations. This yields the integral equation

$$A'_{k,\eta} \partial_n^+ u = f \tag{4}$$

where

$$A'_{k,\eta} := \frac{1}{2} I + D_k' - {\rm i}\eta S_k \tag{5}$$

is the standard combined potential operator, with $\eta \in \mathbb{C}$ the so-called coupling parameter, and f given in terms of the right-hand sides of (2) and (3).

It can be shown that if $\Re\eta \neq 0$, then $A'_{k,\eta}$ is a bounded and invertible operator as a mapping from $H^s(\Gamma)$ to itself for $s \in [-1, 0]$ [1, Theorem 2.27].

When Ω_+ a Lipschitz domain and $h \in H^1(\Gamma)$ the regularity result of Nečas [1, Theorem A.5] implies that $\partial_n u \in L^2(\Gamma)$, and mapping properties of D_k and H_k imply that $f \in L^2(\Gamma)$; thus we can consider the integral equation (4) as an equation in $H^s(\Gamma)$ for any $s \in [-1, 0]$

The question now arises: what space should we pick? If we seek to solve (4) with the Galerkin method, then the variational formulation of (4) in the space $H^s(\Gamma)$ involves the $H^s(\Gamma)$ inner product. Whereas this is simple to implement when $s = 0$, it is cumbersome when $s \neq 0$; thus we would ideally like

to consider (4) as an integral equation in $L^2(\Gamma)$. The standard way to prove that the Galerkin method for (4) converges in $L^2(\Gamma)$ would be to show that $A'_{k,\eta}$ is coercive up to a compact perturbation (a.k.a. satisfies a Gårding inequality), i.e. there exists a compact operator $T : L^2(\Gamma) \to L^2(\Gamma)$ and an $\alpha > 0$ such that

$$((A'_{k,\eta} + T)\phi, \phi)_{L^2(\Gamma)} \geq \alpha \|\phi\|^2_{L^2(\Gamma)} \text{ for all } \phi \in L^2(\Gamma), \tag{6}$$

Since both S_k and $D'_k - D'_0$ are compact operators on $L^2(\Gamma)$ one only needs to prove that (6) holds with $A'_{k,\eta}$ replaced by $\frac{1}{2}I + D'_0$, but it is not yet known whether this is true or not. (Note that the corresponding result for (4) in $H^{-1/2}(\Gamma)$ was proved independently in[3, Appendix A] and [4, Theorem 3.2] (see [1, p.145], [2, Theorem 1]).

The main result

The following results were obtained through attempts to prove that $A'_{k,\eta}$ satisfies a Gårding inequality in $L^2(\Gamma)$ (i.e. that (6) holds).

Given a vector field $\mathbf{Z} \in (L^\infty(\Gamma))^d$, and $\eta \in \mathbb{C}$, define the operator $A'_{k,\eta,\mathbf{Z}}$ by

$$A'_{k,\eta,\mathbf{Z}} := (\mathbf{Z} \cdot \mathbf{n}) \left(\frac{1}{2}I + D'_k\right) + \mathbf{Z} \cdot \nabla_\Gamma S_k - \mathrm{i}\eta S_k$$

where ∇_Γ is the surface gradient on Γ (see, e.g., [1, Equation (A.14)]). If $\mathbf{Z} = \mathbf{n}$, the outward-pointing normal vector to Ω_-, then $A'_{k,\eta,\mathbf{Z}} = A'_{k,\eta}$. If u satisfies the exterior Dirichlet problem (1) one can show that $A'_{k,\eta,\mathbf{Z}}\partial_n^+ u = g$, for some $g \in L^2(\Gamma)$ given in terms of $\mathbf{Z}, \eta$, and h [1, Theorem 2.36].

The novelty of $A'_{k,\eta,\mathbf{Z}}$ is that, for certain $\mathbf{Z}$, it satisfies a Gårding inequality on $L^2(\Gamma)$:

Theorem 1. *If $\eta \in \mathbb{C}$, $\mathbf{Z} \in (C^{0,1}(\Gamma))^d$ is real-valued and*

$$\text{there exists } c > 0 \text{ such that } \mathbf{Z}\cdot\mathbf{n} \geq c > 0 \text{ for a.e. } \mathbf{x} \in \Gamma \tag{7}$$

then the operator $A'_{k,\eta,\mathbf{Z}} : L^2(\Gamma) \to L^2(\Gamma)$ is the sum of a coercive operator and a compact operator.

Theorem 1 is obtained as a corollary of the following theorem:

Theorem 2. *If $\mathbf{Z} \in (C^{0,1}(\Gamma))^d$ is real-valued and satisfies (7), then there exists a real constant β (depending on $\mathbf{Z}$) such that the operator*

$$(\mathbf{Z} \cdot \mathbf{n}) \left(\frac{1}{2}I + D'_0\right) + \mathbf{Z} \cdot \nabla_\Gamma S_0 + \beta S_0$$

is coercive on $L^2(\Gamma)$.

Although $A'_{k,\eta,\mathbf{Z}}$ satisfies a Gårding equality, to prove that the Galerkin method converges we also need that $A'_{k,\eta,\mathbf{Z}}$ is injective. It is not yet known whether this holds in general, but if Ω_- is star-shaped (so that the vector field $\mathbf{x}$ satisfies (7)) then $A'_{k,\eta,\mathbf{x}}$ is injective if η is suitably chosen; see [1, Theorems 2.3.7 and 5.2.6].

References

[1] S. N. CHANDLER-WILDE, I. G. GRAHAM, S. LANGDON, AND E. A. SPENCE, *Numerical-asymptotic boundary integral methods in high-frequency acoustic scattering*, Acta Numerica, 21 (2012), pp. 89–305.

[2] M. COSTABEL, *Some historical remarks on the positivity of boundary integral operators*, in Boundary element analysis: mathematical aspects and applications, O. S. M. Schanz, ed., Lecture notes in Applied and Computational Mechanics, Springer, 2007, pp. 1–27.

[3] J. ELSCHNER, *The double layer potential operator over polyhedral domains I: Solvability in weighted Sobolev spaces*, Applicable Analysis, 45 (1992), pp. 117–134.

[4] O. STEINBACH AND W. L. WENDLAND, *On C. Neumann's method for second-order elliptic systems in domains with non-smooth boundaries*, J. Math. Anal. Appl., 262 (2001), pp. 733–748.

Aeroacoustics in a waveguide with a shear flow

J.-F. Mercier[1,*], **F. Millot**[2]
[1] POEMS (UMR 7231 CNRS-INRIA-ENSTA), ENSTA Paristech, 828, boulevard des Marchaux, 91762 Palaiseau Cedex
[2] CERFACS, 42, Avenue Gaspard Coriolis, 31057 Toulouse Cedex 01, France.
*Email: jean-francois.mercier@ensta.fr

Abstract

We study the acoustic radiation of a source in a 2D waveguide in time harmonic regime and in presence of a shear flow. The main difficulty is the coupling between acoustic waves and vortices convected by the flow. To describe this coupling, the Goldstein equations [1] are chosen. It is a vectorial model whose interest is to reduce to a scalar model in the uniform flow parts. Theoretically in the dissipative regime we prove that the radiation problem is well-posed. Moreover for low Mach flows we derive a simpler model which is accurate up to a small error, varying like the square of the Mach. Introducing PMLs to bound the calculation domain, a Finite Element methods coupling Lagrange and Discontinuous Galerkin elements is used to highlight the accuracy of the Low Mach Approximation.

1 The Goldstein equations in a waveguide

A 2D waveguide $\Omega_\infty = \mathbb{R}\times]0,h[$ is filled with a compressible fluid with a velocity $\boldsymbol{v}_0 = v_0(y)\boldsymbol{e}_x$. In time harmonic regime $e^{-i\omega t}$ and in presence of a source term $f(\boldsymbol{x})$ compactly supported in Ω_∞, the perturbations satisfy the Goldstein equations:

$$\begin{aligned} \mathrm{D}^2\varphi &= \operatorname{div}(\boldsymbol{\nabla}\varphi+\boldsymbol{\xi}) + f \qquad (\Omega_\infty),\\ \mathrm{D}\boldsymbol{\xi} &= M'\left[-\left(\frac{\partial\varphi}{\partial y}+\xi_y\right), \frac{\partial\varphi}{\partial x}\right]^T \qquad (\Omega_\infty),\\ \frac{\partial\varphi}{\partial y}+\xi_y &= 0 \qquad (\partial\Omega_\infty). \end{aligned} \tag{1}$$

φ is the velocity potential and $\boldsymbol{\xi}$ is the hydrodynamic unknown such that $\boldsymbol{v} = \boldsymbol{\nabla}\varphi + \boldsymbol{\xi}$ is the perturbation velocity. $\mathrm{D} = M(y)\partial/\partial x - ik$ is the convective operator where $M(y) = v_0(y)/c_0$ is the Mach number and $k = \omega/c_0$ the acoustic frequency with c_0 the sound speed. Compared to other linearized aeroacoustics systems like Euler's equations [2] or Galbrun's equation [3], Goldstein's equations have the main advantage to be essentially scalar, the vectorial unknown $\boldsymbol{\xi}$ just living in the shear areas, where $M' \neq 0$.

2 Theory in the dissipative regime

k is replaced by $k_\varepsilon = k + i\varepsilon$ and thanks to the dissipation $\varepsilon > 0$ we are authorized to look for a solution with finite energy $\varphi \in H^1(\Omega)$ and $\boldsymbol{\xi} \in L^2(\Omega)$ (which stands for the radiation condition). M is supposed positive in this section.

2.1 The hydrodynamic equation

The second equation of (1) admits a unique solution $\boldsymbol{\xi} = \boldsymbol{A}^\varepsilon\varphi = (A_x^\varepsilon\varphi, A_y^\varepsilon\varphi)^T$ where

$$A_x^\varepsilon\varphi = G_\varepsilon * \left(-M'\frac{\partial\varphi}{\partial y}\right) + \tilde{G}_\varepsilon * \left(-M'^2\frac{\partial\varphi}{\partial x}\right),$$

and $A_y^\varepsilon\varphi = G_\varepsilon * M'\partial\varphi/\partial x$ with the Green functions $MG_\varepsilon(x,y) = Y(x)e^{ik_\varepsilon x/M}$ and $M^2\tilde{G}_\varepsilon(x,y) = Y(x)xe^{ik_\varepsilon x/M}$. Moreover using the inequality $||G * h||_{L^2(\Omega)} \leq ||G||_{L^1(\Omega)}||h||_{L^2(\Omega)}$ we proved that $\boldsymbol{A}^\varepsilon$ is continuous from $H^1(\Omega)$ onto $L^2(\Omega)^2$ with the constant $\gamma_\varepsilon = \sqrt{2}(s_1/\varepsilon)\left[1+(s_1/\varepsilon)\right]$, where $s_1 = \max_{y\in[0,h]}|M'(y)|$.

2.2 Well-posedness of the acoustic problem

The first equation of (1), after injection of the expression of $\boldsymbol{\xi}$, leads to the following variational formulation:

$$\begin{cases} \text{Find } \varphi \in H^1(\Omega) \text{ such that } \forall\psi \in H^1(\Omega),\\ a_\varepsilon(\varphi,\psi) = b_\varepsilon(\varphi,\psi) + c_\varepsilon(\varphi,\psi) = \int_\Omega f\overline{\psi}, \end{cases} \tag{2}$$

with

$$\begin{aligned} b_\varepsilon(\varphi,\psi) &= \int_\Omega \boldsymbol{\nabla}\overline{\varphi}\cdot\boldsymbol{\nabla}\overline{\psi} - \mathrm{D}_\varepsilon\varphi\overline{\mathrm{D}_\varepsilon\psi},\\ c_\varepsilon(\varphi,\psi) &= \int_\Omega (\boldsymbol{A}^\varepsilon\varphi)\cdot\boldsymbol{\nabla}\overline{\psi}. \end{aligned}$$

This problem has good mathematical properties: for instance the Lax-Milgram theorem applies if the flow is subsonic and enough dissipation is introduced.

Theorem 1 *The variational problem* (2) *is well-posed for* $s_0 = \max_{y\in[0,h]}|M(y)| < 1$ *and* ε *large enough.*

Indeed using $|b_\varepsilon(\varphi,\varphi)| \geq |k_\varepsilon|\Im m\left(-b_\varepsilon(\varphi,\varphi)/k_\varepsilon\right)$ is found that $b_\varepsilon(\varphi,\psi)$ is coercive with the constant $C_\varepsilon^c = \min\left(\varepsilon(1-s_0^2)/|k_\varepsilon|, \varepsilon|k_\varepsilon|\right)$ and we deduce that $a_\varepsilon(\varphi,\psi)$ is coercive with the constant $\sigma_\varepsilon = C_\varepsilon^c - \gamma_\varepsilon$. Since $\lim_{\varepsilon\to\infty}\sigma_\varepsilon = 1 - s_0^2 > 0$, $a_\varepsilon(\varphi,\psi)$ is coercive for ε large enough, such that the introduced dissipation compensate the growing of hydrodynamic instabilities whose strength is proportional to s_1.

$\boldsymbol{A}^\varepsilon$ is defined by integrals highly oscillating when M is small. For instance the expression of A_y^ε is:

$$A_y^\varepsilon\varphi = \frac{M'(y)}{M(y)}\int_{-\infty}^{x} e^{i\frac{k_\varepsilon}{M(y)}(x-s)}\frac{\partial\varphi}{\partial x}(s,y)ds.$$

In fact an integration by parts leads to (non-stationary phase theorem):

$$A_y^\varepsilon\varphi = \frac{iM'(y)}{k_\varepsilon}\left(\frac{\partial\varphi}{\partial x} - \int_{-\infty}^{x} e^{i\frac{k_\varepsilon}{M(y)}(x-s)}\frac{\partial^2\varphi}{\partial x^2}(s,y)ds\right), \tag{3}$$

and A_y^ε has a well-defined limit when $M\to 0$ (the integral term vanishes). More generally by considering only the first term in the previous expression we can derive for small M an alternative model.

2.3 Low Mach Approximation

We consider the general flow $M(y) = Mm(y)$ with M now a constant and $\max_{0\le y\le h}|m(y)| < 1$. We suppose that ε is fixed, we note $\boldsymbol{A}^M$ instead of $\boldsymbol{A}^\varepsilon$ the hydrodynamic operator and φ_M the solution. We look for an approximation $\tilde\varphi_M$ of φ_M at low Mach numbers such that the calculation of $\tilde\varphi_M$ does not require the evaluation of oscillating integrals [4]. $\boldsymbol{A}^M\varphi$ is approximated by:

$$\tilde{\boldsymbol{A}}^M\varphi = \frac{iM}{k_\varepsilon}m'(y)\left(-\frac{\partial\varphi}{\partial y}, \frac{\partial\varphi}{\partial x}\right)^T.$$

$\tilde\varphi_M$ is a good approximation of φ_M in the sense:

Theorem 2 *$\exists M_0 \in]0,1[$ and $C > 0$ such that $\forall\, 0 \le M \le M_0$:*

$$||\varphi_M - \tilde\varphi_M||_{H^1(\Omega)} \le CM^2.$$

When comparing to the no flow case we get only $||\varphi_M - \varphi_0||_{H^1(\Omega)} \le CM$ and $||\tilde\varphi_M - \varphi_0||_{H^1(\Omega)} \le CM$, which proves the quality of the Low Mach Approximation. The idea of the proof is to show that $\left|\left|\boldsymbol{A}^M\varphi_M - \tilde{\boldsymbol{A}}^M\tilde\varphi_M\right|\right|_{L^2(\Omega)^2}$ is bounded by M^2 and this is mainly due to the integration by parts (3) which leads to:

$$\left(A_y^M - \tilde A_y^M\right)\varphi_0 = -M^2 G_\varepsilon * \frac{im'(y)m(y)}{k_\varepsilon}\frac{\partial^2\varphi_0}{\partial x^2}.$$

3 Problem with PML and numerical results

For the numerical results we take $\varepsilon = 0$ and we introduce PMLs $\Omega_\pm^L$ of length L to bound the calculation domain $\Omega_b = [0,d]\times[0,1]$:

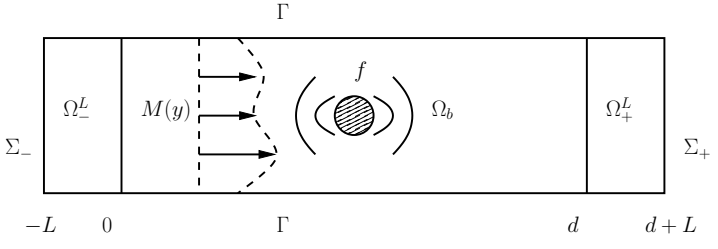

The Goldstein equations become:

$$\begin{cases} \mathrm{D}_\alpha^2\varphi - \mathrm{div}_\alpha\left(\nabla_\alpha\varphi + \boldsymbol{A}^\alpha\varphi\right) &= f \quad (\Omega),\\ \dfrac{\partial\varphi}{\partial y} + A_y^\alpha\varphi &= 0 \quad (\partial\Omega),\\ \dfrac{\partial\varphi}{\partial x} &= 0 \quad (\Sigma_\pm), \end{cases}$$

where $\Omega = \Omega_b\cup\Omega_\pm^L$, $\mathrm{D}_\alpha = M(y)\tilde\alpha\dfrac{\partial}{\partial x} - ik$ with $\tilde\alpha = 1$ in Ω_b and $\tilde\alpha = \alpha$ in $\Omega_\pm^L$ where α is the complex PML parameter. For a source $f = 1$ in the disc of center $(1, 0.5)$ and of radius 0.1, a profile with the strongest shear located at $y_c = 0.5$, namely $M(y) = 0.5\left\{(M_{max} - M_{min})\tanh\left[\kappa(y-y_c)\right] + M_{max} + M_{min}\right\}$ with $M_{min} = 0$, $M_{max} = 0.1$, $\kappa = 10$, $k = 5$, $d = 3$, $L = 0.5$ and $\alpha = 0.3(1-i)$, the obtained vertical velocities $v_y = \partial\varphi/\partial y + \xi_y$ in the domain Ω_b are:

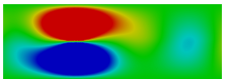
$\Re e(v_y)$ Low Mach

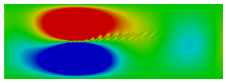
$\Re e(v_y)$ exact

The vertical velocities are not exactly the same due to the Low Mach Approximation: patterns highly oscillating, located at $y = y_c$ and associated to the large wave number $k/M(y_c) = 100$ (wavelength $\lambda = 6.10^{-2}$) are clearly cancelled by the Low Mach Approximation. However the pressure, which is the most important quantity since it corresponds to the heard sound, is nearly the same (error of 1.6% in L^2-norm):

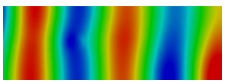
$p = -D\varphi$ Low Mach

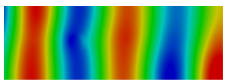
$p = -D\varphi$ exact

References

[1] M. E. Goldstein, Unsteady vortical and entropic distortions of potential flows round arbitrary obstacles, *Journal of Fluid Mechanics* **89**(3), 433-468 (1978)

[2] Y. Ozyoruk, E. Alpman, V. Ahuja and L. N. Longs, Frequency-domain prediction of turbofan noise radiation, *Journal of sound and vibration* **270**(4-5), 933-950 (2004)

[3] A.-S. Bonnet-Ben Dhia, J.-F. Mercier, F. Millot, S. Pernet and E. Peynaud, Time-Harmonic Acoustic Scattering in a Complex Flow: a Full Coupling Between Acoustics and Hydrodynamics, *Commun. Comput. Phys.* **11**(2) 555-572 (2012)

[4] A.-S. Bonnet-Ben Dhia, J.-F. Mercier, F. Millot and S. Pernet, A low Mach model for time harmonic acoustics in arbitrary flows, *J. of Comp. and App. Math.* **234**(6), 1868-1875 (2010)

WAVENUMBER-EXPLICIT COERCIVITY ESTIMATES IN SCATTERING BY SCREENS

D. P. Hewett[1,*], **S. N. Chandler-Wilde**[1]
[1] Department of Mathematics and Statistics, University of Reading, Berkshire, UK
*Email: d.p.hewett@reading.ac.uk

Abstract

We consider time-harmonic acoustic scattering by flat sound soft and sound hard screens occupying an arbitrary bounded open set in the plane. We propose mathematical models for such problems, and show that these are well-posed, by proving the coercivity of the single-layer and hypersingular integral operators arising in the boundary integral equation reformulations of the problems. We also tease out the explicit wavenumber dependence of the norms and coercivity constants of these integral operators, this in part extending previous results of Ha Duong.

Introduction

This paper is concerned with the mathematical analysis of classical time-harmonic acoustic scattering problems, modelled by the Helmholtz equation

$$\Delta u + k^2 u = 0, \tag{1}$$

where $k > 0$ is the *wavenumber*. The scatterer is assumed to be a thin flat screen, occupying some bounded and relatively open set $\Gamma \subset \Gamma_\infty := \{x = (x_1, ..., x_d) \in \mathbb{R}^d : x_d = 0\}$ ($d = 2$ or 3), with (1) assumed to hold in $D := \mathbb{R}^d \setminus \overline{\Gamma}$. We suppose the screen is *sound soft*, in which case $u = 0$ on Γ, or *sound hard*, when the normal derivative $\partial u/\partial \mathbf{n} = 0$ on Γ.

This is a well-studied problem, both theoretically and in applications. However, all previous studies assume that $\Gamma \subset \Gamma_\infty$ is at least a Lipschitz relatively open set (in the sense of [2]), and most that Γ is substantially smoother. The focus of the present paper is: (i) to formulate these problems correctly when Γ is an arbitrary bounded relatively open set; (ii) to get wavenumber-explicit estimates on the associated boundary integral operators. For full details see [1].

1 Preliminaries

Our analysis is in the context of Sobolev spaces, for which we follow the notation in [2], except we use wavenumber dependent norms (equivalent to the usual norms). Explicitly, on the Bessel potential space $H^s(\mathbb{R}^{d-1})$, $s \in \mathbb{R}$, we define

$$\|u\|^2_{H^s_k(\mathbb{R}^{d-1})} := \int_{\mathbb{R}^{d-1}} (k^2 + |\boldsymbol{\xi}|^2)^s \, |\hat{u}(\boldsymbol{\xi})|^2 \, \mathrm{d}\boldsymbol{\xi},$$

where $\widehat{\ }$ represents the Fourier transform in $\mathbb{R}^{d-1}$.

Let $H^s(\Gamma) := \{U|_\Gamma : U \in H^s(\mathbb{R}^{d-1})\}$, where $|_\Omega$ denotes the restriction to Γ, and let $\tilde{H}^s(\Gamma)$ denote the closure of $C_0^\infty(\Gamma)$ in the space $H^s(\mathbb{R}^{d-1})$. Then $H^s(\Gamma)$ is the dual space of $\tilde{H}^{-s}(\Gamma)$; we denote by $\langle \cdot, \cdot \rangle_{\Gamma,s}$ the duality pairing on $H^s(\Gamma) \times \tilde{H}^{-s}(\Gamma)$. Let $H^s_{\overline{\Gamma}} := \{u \in H^s(\mathbb{R}^{d-1}) : \operatorname{supp} u \subset \overline{\Gamma}\}$. Clearly $\tilde{H}^s(\Gamma) \subset H^s_{\overline{\Gamma}}$, and when Γ is C^0 (so certainly if Γ is Lipschitz), it holds that $\tilde{H}^s(\Gamma) = H^s_{\overline{\Gamma}}$ [2, Theorem 3.29], but in general these spaces are not equal.

2 Boundary value problems

Definition 2.1 (Problem D). *Given $g_\mathsf{D} \in H^{1/2}(\Gamma)$, find $u \in C^2(D) \cap W^1_{\mathrm{loc}}(D)$ such that*

$$\Delta u + k^2 u = 0, \quad \text{in } D, \tag{2a}$$
$$u = g_\mathsf{D}, \quad \text{on } \Gamma, \tag{2b}$$
$$[u] = 0, \tag{2c}$$
$$[\partial u/\partial \mathbf{n}] \in \tilde{H}^{-1/2}(\Gamma), \tag{2d}$$

and u satisfies the Sommerfeld radiation condition. Here $[f] = f^+ - f^-$ represents the jump of f across Γ (interpreted in the sense of traces).

Conditions (2c)-(2d) ensure well-posedness for an arbitrary relatively open subset Γ. In interpreting (2c)-(2d) we remark that, a priori, $[u] \in H^{1/2}_{\overline{\Gamma}}$ and $[\partial u/\partial \mathbf{n}] \in H^{-1/2}_{\overline{\Gamma}}$, and, while $[u]|_\Gamma = 0$ (from (2b)), it could hold that $[u] \neq 0$ with $\operatorname{supp}(u) \subset \partial\Gamma$. We note that (2c)-(2d) are automatically satisfied when Γ is Lipschitz, because then $\partial\Gamma$ cannot support non-zero elements of $H^{1/2}(\mathbb{R}^{d-1})$, and also $\tilde{H}^{-1/2}(\Gamma) = H^{-1/2}_{\overline{\Gamma}}$.

Definition 2.2 (Problem N). *Given $g_\mathsf{N} \in H^{-1/2}(\Gamma)$, find $u \in C^2(D) \cap W^1_{\mathrm{loc}}(D)$ such that*

$$\Delta u + k^2 u = 0, \quad \text{in } D, \tag{3a}$$
$$\frac{\partial u}{\partial \mathbf{n}} = g_\mathsf{N}, \quad \text{on } \Gamma, \tag{3b}$$
$$[\partial u/\partial \mathbf{n}] = 0, \tag{3c}$$
$$[u] \in \tilde{H}^{1/2}(\Gamma), \tag{3d}$$

and u satisfies the Sommerfeld radiation condition.

Again, (3c)-(3d) automatically hold if Γ is Lipschitz.

Example 2.3. *In the scattering by Γ of an incident plane wave $u^i(\mathbf{x}) := \mathrm{e}^{\mathrm{i}k\mathbf{x}\cdot\mathbf{d}}$, $\mathbf{x}\in\mathbb{R}^d$, where $\mathbf{d}\in\mathbb{R}^d$ is a unit direction vector, a 'sound soft' and a 'sound hard' screen are modelled respectively by problems* D *(with $g_{\mathsf{D}}=-u^i|_\Gamma$) and* N *(with $g_{\mathsf{N}}=-\partial u^i/\partial\mathbf{n}|_\Gamma$), with u representing the scattered field.*

3 Boundary integral equations

We introduce the standard single- and double-layer potentials $\mathcal{S}_k : \tilde{H}^{-1/2}(\Gamma) \to C^2(D)\cap W^1_{loc}(D)$ and $\mathcal{D}_k : \tilde{H}^{1/2}(\Gamma) \to C^2(D)\cap W^1_{loc}(D)$, and single-layer and hypersingular operators $S_k : \tilde{H}^{-1/2}(\Gamma)\to H^{1/2}(\Gamma)$ and $T_k : \tilde{H}^{1/2}(\Gamma) \to H^{-1/2}(\Gamma)$. For $\phi\in C_0^\infty(\Gamma)$ the latter two have the integral representations

$$S_k\phi(\mathbf{x}) = \int_\Gamma \Phi(\mathbf{x},\mathbf{y})\phi(\mathbf{y})\,\mathrm{d}s(\mathbf{y}), \qquad \mathbf{x}\in\Gamma,$$

$$T_k\phi(\mathbf{x}) = \frac{\partial}{\partial\mathbf{n}(\mathbf{x})}\int_\Gamma \frac{\partial\Phi(\mathbf{x},\mathbf{y})}{\partial\mathbf{n}(\mathbf{y})}\phi(\mathbf{y})\,\mathrm{d}s(\mathbf{y}), \quad \mathbf{x}\in\Gamma,$$

where Φ is the fundamental solution of (1). Problems D and N are equivalent to certain integral equations involving S_k and T_k, as the following theorems show.

Theorem 3.1. *Suppose that u is a solution of problem* D*. Then Green's representation formula*

$$u(\mathbf{x}) = -\mathcal{S}_k\left[\partial u/\partial\mathbf{n}\right](\mathbf{x}), \qquad \mathbf{x}\in D,$$

holds, and $\phi := [\partial u/\partial\mathbf{n}]\in\tilde{H}^{-1/2}(\Gamma)$ satisfies

$$-S_k\phi = g_{\mathsf{D}}. \tag{4}$$

Conversely, suppose that $\phi\in\tilde{H}^{-1/2}(\Gamma)$ satisfies (4). Then $u := -\mathcal{S}_k\phi$ satisfies problem D*, and $[\partial u/\partial\mathbf{n}]=\phi$.*

Theorem 3.2. *Suppose that u is a solution of problem* N*. Then Green's representation formula*

$$u(\mathbf{x}) = \mathcal{D}_k[u](\mathbf{x}), \qquad \mathbf{x}\in D,$$

holds, and $\psi := [u]\in\tilde{H}^{1/2}(\Gamma)$ satisfies

$$T_k\psi = g_{\mathsf{N}}. \tag{5}$$

Conversely, suppose that $\psi\in\tilde{H}^{1/2}(\Gamma)$ satisfies (5). Then $u := \mathcal{D}_k\psi$ satisfies problem N*, and $[u]=\psi$.*

Because the screen is flat we have Fourier representations for S_k and T_k. For $\phi\in C_0^\infty(\Gamma)$ and $\tilde{\mathbf{x}}\in\tilde{\Gamma} := \{\tilde{\mathbf{x}}\in\mathbb{R}^{d-1} : (\tilde{\mathbf{x}},0)\in\Gamma\}\subset\mathbb{R}^{d-1}$,

$$S_k\phi(\tilde{\mathbf{x}},0) = \frac{\mathrm{i}}{2(2\pi)^{(d-1)/2}}\int_{\mathbb{R}^{d-1}}\frac{\mathrm{e}^{\mathrm{i}\boldsymbol{\xi}\cdot\tilde{\mathbf{x}}}}{Z(\boldsymbol{\xi})}\widehat{\phi}(\boldsymbol{\xi})\,\mathrm{d}\boldsymbol{\xi},$$

$$T_k\phi(\tilde{\mathbf{x}},0) = \frac{\mathrm{i}}{2(2\pi)^{(d-1)/2}}\int_{\mathbb{R}^{d-1}} Z(\boldsymbol{\xi})\mathrm{e}^{\mathrm{i}\boldsymbol{\xi}\cdot\tilde{\mathbf{x}}}\widehat{\phi}(\boldsymbol{\xi})\,\mathrm{d}\boldsymbol{\xi},$$

where

$$Z(\boldsymbol{\xi}) := \begin{cases}\sqrt{k^2-|\boldsymbol{\xi}|^2}, & |\boldsymbol{\xi}|\le k\\ \mathrm{i}\sqrt{|\boldsymbol{\xi}|^2-k^2}, & |\boldsymbol{\xi}|>k,\end{cases} \qquad \boldsymbol{\xi}\in\mathbb{R}^{d-1}.$$

These representations allow us to prove the following k-explicit continuity and coercivity estimates, which improve on those in [3], [4].

Theorem 3.3. *For any $s\in\mathbb{R}$, the single-layer operator $S_k : \tilde{H}^s(\Gamma)\to H^{s+1}(\Gamma)$ is bounded, and $\exists C>0$, independent of k and Γ, such that, for all $0\ne\phi\in\tilde{H}^s(\tilde{\Gamma})$ and $k>0$, and with $A := \operatorname{diam}\Gamma$,*

$$\frac{\|S_k\phi\|_{H^{s+1}_k(\Gamma)}}{\|\phi\|_{\tilde{H}^s_k(\Gamma)}} \le \begin{cases} C(1+\sqrt{kA}), & d=3,\\ C\log\left(2+(kA)^{-1}\right)(1+\sqrt{kA}), & d=2.\end{cases}$$

Theorem 3.4. *$S_k : \tilde{H}^{-1/2}\to H^{1/2}(\Gamma)$ satisfies*

$$\langle S_k\phi,\psi\rangle_{\Gamma,1/2} \ge \frac{1}{2\sqrt{2}}\|\phi\|^2_{\tilde{H}_k^{-1/2}(\Gamma)}, \quad \phi\in\tilde{H}^{-1/2}(\Gamma),\ k>0$$

Theorem 3.5. *For any $s\in\mathbb{R}$, the hypersingular operator $T_k : \tilde{H}^s(\Gamma)\to H^{s-1}(\Gamma)$ is bounded, and*

$$\|T_k\phi\|_{H^{s-1}_k(\Gamma)} \le \frac{1}{2}\|\phi\|_{\tilde{H}^s_k(\Gamma)}, \quad \phi\in\tilde{H}^s(\Gamma),\ k>0.$$

Theorem 3.6. *$T_k : \tilde{H}^{1/2}(\Gamma)\to H^{-1/2}(\Gamma)$ satisfies, for any $k_0>0$, and $k\ge k_0$,*

$$\langle T_k\phi,\psi\rangle_{\Gamma,-1/2} \ge C(kA)^\beta\|\phi\|^2_{\tilde{H}^{1/2}_k(\Gamma)}, \quad \phi\in\tilde{H}^{1/2}(\Gamma),$$

where $C>0$ is a constant depending only on k_0A, and $\beta=-2/3$ for $d=3$ and $\beta=-1/2$ for $d=2$.

The Lax-Milgram Lemma then implies:

Theorem 3.7. *Equation (4), and hence also problem* D*, has a unique solution for all $g_{\mathsf{D}}\in H^{1/2}(\Gamma)$.*

Theorem 3.8. *Equation (5), and hence also problem* N*, has a unique solution for all $g_{\mathsf{N}}\in H^{-1/2}(\Gamma)$.*

References

[1] S. N. Chandler-Wilde and D. P. Hewett, *Frequency-explicit coercivity estimates in high frequency scattering by screens and apertures*, under review.

[2] W. McLean, *Strongly Elliptic Systems and Boundary Integral Equations*, CUP, 2000.

[3] Tuong Ha-Duong, *On the transient acoustic scattering by a flat object*, Jpn J. Ind. Appl. Math., **7** (1990), pp. 489–513.

[4] ——, *On the boundary integral equations for the crack opening displacement of flat cracks*, Integr. Equat. Oper. Th., **15** (1992), pp. 427–453.

A rigorous approach to the propagation of electromagnetic waves in co-axial cables

G. Beck[1], **S. Imperiale**[1], **P. Joly**[1]
[1] POEMS (UMR 7231 CNRS-INRIA-ENSTA), ENSTA Paristech, Palaiseau, France.
*Email: patrick.joly@inria.fr

Abstract

We investigate the question of the electromagnetic propagation in thin electric cables from a mathematical point of view via an asymptotic analysis with respect to the (small) transverse dimension of the cable: as it has been done in the past in mechanics for the beam theory from 3D elasticity, we use such an approach for deriving simplified effective 1D models from 3D Maxwell's equations.

Position of the problem

Denoting $\delta > 0$ a small parameter, we consider a family of (thin) domains $\Omega^\delta = \mathcal{G}_\delta(\Omega)$ where

$$\mathcal{G}_\delta : (x_1, x_2, x_3) \longrightarrow (\delta x_1, \delta x_2, x_3).$$

and Ω is a normalized cylinder of axis x_3 and variable cross section(see Figure 1, left picture)

$$\Omega = \bigcup_{z\in\mathbb{R}} S_z, \quad S_z = \mathcal{O}_z \setminus \overline{T_z}$$

where $\mathcal{O}_z$ and T_z (the hole) are simply connected, Lipschitz, open sets included in the plane $x_3 = z$, so that ∂S_z has two connected components ∂S_z^+ (exterior) and ∂S_z^- (interior). We are interested in

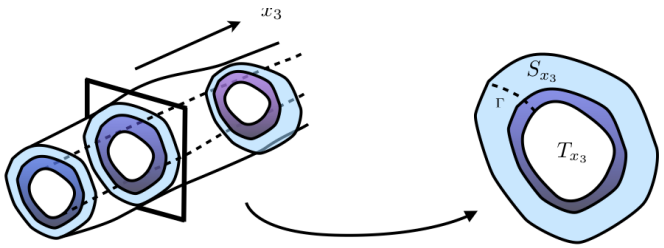

Figure 1: The structure of the co-axial cable

the electromagnetic field (E^δ, H^δ) solution of the 3D Maxwell's equation in Ω^δ :

$$\begin{cases} \varepsilon^\delta\, \partial_t E^\delta + \sigma_e^\delta\, E^\delta - \mathbf{curl}\ H^\delta = \mathbf{j}^\delta, \\ \mu^\delta\, \partial_t H^\delta + \sigma_m^\delta\, H^\delta + \mathbf{curl}\ E^\delta = \mathbf{0}, \end{cases} \tag{1}$$

where the permittivity ε^δ, the permeability μ^δ, the electric and magnetic conductivities σ_e^δ and σ_m^δ, as well as the source term $\mathbf{j}^\delta$ are obtained by a scaling in the transverse variable $\mathbf{x}_T = (x_1, x_2)$ of fixed distributions in the reference domain Ω :

$$\varepsilon^\delta(\mathbf{x}_T, x_3) = \varepsilon(\mathbf{x}_T/\delta, x_3), \cdots$$

We are interested in the behaviour of the solution for small δ.

The main result

Under usual non degeneracy assumptions about the geometry of Ω and the coefficients in (1), one proves, by mean of formal asymptotics, that (∇ holds for the 2D transverse gradient in $\mathbf{x}_T$, that can be identified to a 3D vector with third component 0)

$$\begin{cases} E^\delta(\mathbf{x}_T, x_3, t) \sim V(x_3, t)\ \nabla\varphi_s^\infty(\mathbf{x}_T/\delta, x_3) \\ \qquad + \displaystyle\int_0^t V(x_3, s)\ \nabla\varphi_r(\mathbf{x}_T/\delta, x_3, t-s)\ ds, \\ H^\delta(\mathbf{x}_T, x_3, t) \sim I(x_3, t)\ \nabla\psi_s^\infty(\mathbf{x}_T/\delta, x_3) \\ \qquad + \displaystyle\int_0^t I(x_3, s)\ \nabla\psi_r(\mathbf{x}_T/\delta, x_3, t-s)\ ds, \end{cases} \tag{2}$$

where

- The scalar potentials $\varphi_s^\infty(\cdot, x_3)$ and $\psi_s^\infty(\cdot, x_3)$ are solutions of specific 2D "elliptic" problems in each cross section S_{x_3}. For instance, for $\varphi_s^\infty(\cdot, x_3)$ (see [1] for $\psi_s^\infty(\cdot, x_3)$)

$$\begin{cases} \mathrm{div}\left(\, \varepsilon(\cdot, x_3)\, \nabla\, \varphi_s^\infty(\cdot, x_3)\, \right) = 0, \quad \text{in } S_{x_3}, \\ \varphi_s^\infty(\cdot, x_3) = 0 \quad \text{on } \partial S_{x_3}^+, \ \ = 1 \quad \text{on } \partial S_{x_3}^-. \end{cases} \tag{3}$$

- The scalar functions $(\varphi_r(\cdot, x_3, t), \psi_r(\cdot, x_3, t)) \in H_0^1(S_{x_3})^2$ are solutions of non standard 2D evolution problems in each cross section S_{x_3}. For intance, for $\varphi_r(\cdot, x_3, t)$ (see [1] for $\psi_r(\cdot, x_3, t)$)

$$\begin{cases} \partial_t \left[\mathrm{div}\left(\, \varepsilon\, \nabla\varphi_r\right)\right] + \ \mathrm{div}\left(\sigma_e\, \nabla\varphi_{r,0}\right) = 0 \\ \varphi_r(\cdot, x_3, 0) = \varphi_{r,0}(\cdot, x_3) \end{cases} \tag{4}$$

where the initial data $\varphi_{r,0}(\cdot, x_3)$ is defined by

$$\begin{cases} \text{div}\left(\varepsilon\,\nabla\varphi_{r,0}\right) = -\,\text{div}\left(\sigma_e\,\nabla\varphi_s^\infty\right), \\ \varphi_{r,0} = 0\,, \quad \text{on } \partial S_{x_3}, \end{cases} \tag{5}$$

- The functions $V(x_3,t)$ and $I(x_3,t)$, respectively called the electric potential and the electric current, are new 1D unknowns.

$V(x_3,t)$ and $I(x_3,t)$ are governed by the generalized telegraphist's equations :

$$\begin{cases} C^\infty(x_3)\,\dfrac{\partial V}{\partial t} + G^\infty(x_3)\,V + \dfrac{\partial I}{\partial x_3}(x_3,t) \\ \qquad\qquad + k_e(x_3,\cdot) * V(x_3,\cdot) = j, \\ L^\infty(x_3)\,\dfrac{\partial I}{\partial t} + R^\infty(x_3)\,I + \dfrac{\partial V}{\partial x_3}(x_3,t) \\ \qquad\qquad + k_m(x_3,\cdot) * I(x_3,\cdot) = 0, \end{cases} \tag{6}$$

where $*$ holds for time convolution. In (6), $j(x_3,t)$ is an effective source term given by:

$$\begin{aligned} j(x_3,t) &= \int_{S_{x_3}} \mathbf{j}_T(x_3,\cdot,t)\cdot\nabla\varphi_s^\infty(x_3,\cdot) \\ &+ \int_0^t \int_{S_{x_3}} \mathbf{j}_T(x_3,\cdot,t-s)\cdot\nabla\varphi_r(x_3,\cdot,s)\,ds, \end{aligned} \tag{7}$$

the capacity $C^\infty(x_3)$, the inductance $L^\infty(x_3)$, the resistance $R^\infty(x_3)$ and the conductance $G^\infty(x_3)$ are given by:

$$\begin{aligned} C^\infty(x_3) &\equiv \int_{S_{x_3}} \varepsilon(\cdot,x_3)\,\left|\nabla\varphi_s^\infty(\cdot,x_3)\right|^2 d\mathbf{x}_T, \\ L^\infty(x_3) &\equiv \int_{S_{x_3}} \mu(\cdot,x_3)\,\left|\nabla\psi_s^\infty(\cdot,x_3)\right|^2 d\mathbf{x}_T, \\ G^\infty(x_3) &\equiv \int_{S_{x_3}} \sigma_e(\cdot,x_3)\,\left|\nabla\varphi_s^\infty(\cdot,x_3)\right|^2 d\mathbf{x}_T, \\ R^\infty(x_3) &\equiv \int_{S_{x_3}} \sigma_m(\cdot,x_3)\,\left|\nabla\psi_s^\infty(\cdot,x_3)\right|^2 d\mathbf{x}_T, \end{aligned} \tag{8}$$

and the convolution kernels $k_e(x_3,\cdot)$ and $k_m(x_3,\cdot)$ by

$$\begin{cases} k_e(x_3,t) = \displaystyle\int_{S_{x_3}} \sigma_e(\cdot,x_3)\,\nabla\varphi_r(\cdot,x_3,t)\cdot\nabla\varphi_s^\infty(\cdot,x_3), \\ k_m(x_3,t) = \displaystyle\int_{S_{x_3}} \sigma_m(\cdot,x_3)\,\nabla\psi_r(\cdot,x_3,t)\cdot\nabla\psi_s^\infty(\cdot,x_3). \end{cases} \tag{9}$$

Miscillaneous results

Formula (2) shows that, in the limit $\delta \to 0$, the electromagnetic field is transversely polarized. It also exhibits a 1D structure for the limit solution, via a "quasi" separation of variables in $\mathbf{x}_T$ and x_3. Moreover, the kernels k_e and k_m are such that

$$k_e(\cdot,t) \neq 0 \Longleftrightarrow \tfrac{\sigma_e(.x_3)}{\varepsilon(.,x_3)} \text{ is not constant in } S_{x_3}$$

$$k_m(\cdot,t) \neq 0 \Longleftrightarrow \tfrac{\sigma_m(.x_3)}{\mu(.,x_3)} \text{ is not constant in } S_{x_3}$$

In other words, the presence of the convolution terms results from the presence of losses conjugated with the heterogeneity of the cross sections.

We have been able to justify our model rigorously by means of error estimates which show that, in cylindrical geometry, our model is second order accurate for the transverse fields and first order for the longitudinal fields (see [2]). It is easy to propose a first order corrector for the longitudinal fields in order to restore the global second order accuracy.

We have implemented a code for the simultion of wave propagation in a thin cable using our 1D model. Numerical simulations will be presented at the conference. The computation is made in two steps:

- Pre-processing : one computes all the coefficients appearing in (6) by solving 2D auxiliary problems - in particular (3),(4),(5) - in each cross section (in order to determine $\varphi_s^\infty, \varphi_r, \psi_s^\infty, \psi_r$) and applying formulas (7), (8) and (9).
- Calculation : one solves the 1D evolution problem (6).

We are currently working on higher order models, which leads, in the loss less case, to introduce the concept of non local capacitance and inductance operators $\mathbf{C}^\delta$ and $\mathbf{L}^\delta$. This work is in progress.

References

[1] S. Imperiale, P. Joly *The mathematical modelling of electromagnetic waves in heterogeneous lossy coaxial cables with variable cross section*, in Applied Numerical Mathematics (To appear)

[2] S. Imperiale, P. Joly *Error estimates for 1D asynptotic models in coaxial cables with heterogeneous cross section*, in Advances in Applied Mathematics and Mechanics, Vol. 4, No. 6, pp. 647-664 (2012)

On the essential spectrum in the diffraction theory of electromagnetic waves

M. Costabel[1], **E. Darrigrand**[1], **H. Sakly**[1,*]
[1] IRMAR UMR CNRS 6625, Université de Rennes 1, Rennes, France.
*Email: hamdi.sakly@univ-rennes1.fr

Abstract

We study the essential spectrum of strongly singular volume integral operators arising in the scattering of time harmonic electromagnetic waves. We will first treat the case of piecewise constant constitutives parameters like the electric permittivity ε and the magnetic permeability μ. We will recall the known results for the dielectric operator and will show that the magnetic one has the same essential spectrum in the case of a smooth boundary Γ which is the set $\{0, \frac{1}{2}, 1\}$ and that the situation for a Lipschitz one is quite different. Then we will explain how such results give necessary and sufficient criteria for the Fredholmness of the total operator for both regular and Lipschitz interfaces. For non constant parameters, the spectrum is shown to be contained in the set corresponding to constant case multiplied by contrast parameters for the dielectric and the magnetic problem.

Introduction

We consider the scattering of time-harmonic electromagnetic waves by a penetrable object. The mathematical model is given by the Maxwell equations involving the wave number $k \in \mathbf{R}$, the electric permittivity ε and the magnetic permeability μ. We consider here that ε and μ are constant outside a bounded domain Ω such that the scattering problem is equivalently described by the Lippmann-Schwinger integral equation on Ω [1]. This equation, sometimes simply called "volume integral equation" (VIE) of electromagnetic scattering has been intensively used by physicists for numerical calculations. However, a complete mathematical study of the (VIE) when the parameters ε and μ are discontiuous on the surface Γ of the scatterer Ω does not yet seem to be available in the literature. Partial results have been obtained in [2], [3], [4], [5], [6].
Let Ω be a bounded Lipschitz domain. Let ε and μ be such that

$$\varepsilon = \varepsilon_0 > 0, \mu = \mu_0 > 0 \text{ in } \mathbf{R}^3 \setminus \Omega;$$

$$\varepsilon = \varepsilon_r \varepsilon_0, \mu = \mu_r \mu_0 \text{ in } \Omega;\ \varepsilon_r, \mu_r \in L^\infty(\Omega)$$

Define the electric and the magnetic contrast

$$\eta = 1 - \varepsilon_r,\ \nu = 1 - \frac{1}{\mu_r};$$

The (VIE) can then be written as:

$$\text{Find } u \text{ such that } u - A_k^\eta u - B_k^\nu u = u^0.$$

where the integral operators A_k^η and B_k^ν are given, for $x \in \Omega$ by

$$A_k^\eta u(x) = (-\nabla\nabla. - k^2) \int_\Omega g_k(x-y)\, \eta(y)\, u(y)\, dy,$$

$$B_k^\nu u(x) = \nabla \times \int_\Omega g_k(x-y)\, \nu(y)\, \nabla \times u(y)\, dy;$$

and where g_k is the fundamental solution of the Helmholtz equation and u^0 is a data.
In this talk, we will first consider the case where ε and μ are constant on Ω. Furthermore, we will give here a complete spectral analysis of the operators involved in the (VIE) for a regular or Lipschitz domain Ω, namely the operators $A_k := A_k^1$, $B_k := B_k^1$ and the operator $\eta A_k + \nu B_k$.
This approach helps us to approximate the essential spectrum of the operators A_k^η and B_k^ν in a more general case where ε and μ are not constant, at least of class C^1 with discontinuity across Γ.

1 The case of piecewise constant constitutive parameters:

We denote by $\Sigma = \sigma_{ess}(\frac{1}{2}I + K')$ where $\frac{1}{2}I + K'$ is the normal derivative of the single layer potential in the interior domain.

1.1 Motivation: Results for the dielectric scattering equation($\nu = 0$):

First, we remember that the operator A_k can be extended from $H(\nabla\times, \Omega)$ to $L^2(\Omega)$ as a bounded operator and that $A_k - A_0$ is a compact operator defined on $L^2(\Omega)$ [3]. For the determination of the essential spectrum of the operator A_0, we have these results already shown in [2]:

- If Γ is smooth, then

$$\sigma_{ess}(A_k) = \{0, \frac{1}{2}, 1\}$$

- If Γ is Lipschitz, then

$$\sigma_{ess}(A_k) = \{0\} \cup \{1\} \cup (\Sigma)$$

We will give a more elegant proof of the last two statements also based on the orthogonal decomposition:

$$L^2(\Omega) = \nabla H_0^1(\Omega) \oplus H_0(div0, \Omega) \oplus W$$

with $W = \nabla H^1(\Omega) \cap H(div0, \Omega)$ the space of gradients of harmonic H^1 vector fields.

1.2 Results for the magnetic problem($\eta = 0$):

For the operator B_k, we will demonstrate via the analysis of the boundary transmission conditions that it cannot be extended to $L^2(\Omega)$. This result can also be checked using integrations by parts. Its essential spectrum is then given in $H(\nabla\times, \Omega)$ by

- If Γ is smooth, then

$$\sigma_{ess}(B_k) = \{0, \frac{1}{2}, 1\}$$

- If Γ is Lipschitz, then

$$\sigma_{ess}(B_k) = \{0\} \cup \{1\} \cup (1 - \Sigma)$$

The proof is also based on an orthogonal decomposition of the space $H(\nabla\times, \Omega)$ in addition to a classical result from the theory of linear operators which states:
Let X and Y be two vector spaces, $P : Y \to X$ and $Q : X \to Y$ two linear operators then we have:

$$\sigma_{ess}(QP) \setminus \{0\} = \sigma_{ess}(PQ) \setminus \{0\}$$

1.3 Results for the electromagnetic configuration:

For a smooth boundary Γ, we use the same orthogonal decomposition as for B_k. We then do some integrations by parts to decompose the operator $\eta A_k + \nu B_k$ like the operator B_k and finish by applying the same method done for the last one to find that:

$$\sigma_{ess}(\eta A_k + \nu B_k) = \{0, \frac{\eta}{2}, \frac{\nu}{2}, \eta, \nu\}$$

If Γ is Lipschitz, we use the classical lemma given in paragraph 1.2 to obtain this inclusion of spectrum:

$$\sigma_{ess}(\eta A_k + \nu B_k) \subset \{0, \eta, \nu\} \cup (\eta\Sigma) \cup (\nu - \nu\Sigma)$$

2 Some further results for piecewise regular parameters:

Let $\eta, \nu \in C^1(\bar{\Omega})$. In order to determine the essential spectrum of the two operators A_k^η and B_k^ν, we reduce them modulo compact operators such that $A_k^\eta \sim \eta A_0$ in $L^2(\Omega)$ and $B_k^\nu \sim \nu B_0$ in $H(\nabla\times, \Omega)$. Via some elementary tools from the Fredholm theory, we will show that if Ω is a star-shaped Lipschitz domain then

$$\sigma_{ess}(A_k^\eta) \subset \eta\sigma_{ess}(A_k) = \{\eta(x)\lambda | x \in \bar{\Omega},\ \lambda \in \sigma_{ess}(A_k)\}$$

$$\sigma_{ess}(B_k^\nu) \subset \nu\sigma_{ess}(B_k) = \{\nu(x)\lambda | x \in \bar{\Omega},\ \lambda \in \sigma_{ess}(B_k)\}$$

References

[1] D. Colton and R. Kress. *Inverse acoustic and electromagnetic scattering theory*, volume 93 of *Applied Mathematical Sciences*. Springer-Verlag, Berlin, second edition, 1998.

[2] Mark J. Friedman and Joseph E. Pasciak. Spectral properties for the magnetization integral operator. *Math. Comp.*, 43(168):447–453, 1984.

[3] M. Costabel, E. Darrigrand, and E. H. Koné. Volume and surface integral equations for electromagnetic scattering by a dielectric body. *J. Comput. Appl. Math.*, 234(6):1817–1825, 2010.

[4] A. Kirsch. An integral equation approach and the interior transmission problem for Maxwell's equations. *Inverse Probl. Imaging*, 1(1):159–179, 2007.

[5] A. Kirsch and A. Lechleiter. The operator equations of Lippmann-Schwinger type for acoustic and electromagnetic scattering problems in L^2. *Appl. Anal.*, 88(6):807–830, 2009.

[6] M. Costabel, E. Darrigrand, and H. Sakly. The essential spectrum of the volume integral operator in electromagnetic scattering by a homogeneous body. *Comptes Rendus Mathematique*, 350(34):193–197, February 2012.

A curious instability phenomenon for a rounded corner in presence of a negative material

L. Chesnel[1,*], **X. Claeys**[2], **S.A. Nazarov**[3]
[1] Department of Mathematics and Systems Analysis, Aalto University, Finland
[2] Laboratoire Jacques-Louis Lions, Université Pierre et Marie Curie, Paris VI, France
[3] Laboratory of Mathematical Methods in Mechanics of Materials, IPME RAS, St. Petersburg, Russia
*Email: lucas.chesnel@aalto.fi

Abstract

We study a 2D transmission problem between a positive material and a negative material. In electromagnetism, this negative material can be a metal at optical frequencies or a negative metamaterial. We highlight an unusual instability phenomenon for this problem in some configurations: when the interface between the two materials presents a rounded corner, it can happen that the solution depends critically on the value of the rounding parameter.

1 Numerical observations

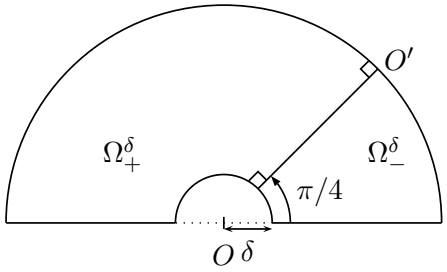

Figure 1: Domain Ω^δ.

Let us denote (r, θ) the polar coordinates centered at the origin O. Consider $\delta \in (0; 1)$ and define (see Figure 1) the domains:

$$\begin{aligned}\Omega_+^\delta &:= \{(r\cos\theta, r\sin\theta)\,|\,\delta < r < 1,\ \pi/4 < \theta < \pi\};\\ \Omega_-^\delta &:= \{(r\cos\theta, r\sin\theta)\,|\,\delta < r < 1,\ \ 0 < \theta < \pi/4\};\\ \Omega^\delta &:= \{(r\cos\theta, r\sin\theta)\,|\,\delta < r < 1,\ \ 0 < \theta < \pi\}.\end{aligned}$$

We define the function $\sigma^\delta : \Omega^\delta \to \mathbb{R}$ by $\sigma^\delta = \sigma_\pm$ in $\Omega_\pm^\delta$, where $\sigma_+ > 0$ and $\sigma_- < 0$ are constants. We shall focus on the problem:

$$\left|\begin{array}{l}\text{Find } u^\delta \in \mathrm{H}_0^1(\Omega^\delta) \quad \text{such that}\\ -\mathrm{div}(\sigma^\delta \nabla u^\delta) = f,\end{array}\right. \tag{1}$$

where $\mathrm{H}_0^1(\Omega^\delta) := \{v \in \mathrm{H}^1(\Omega^\delta) \text{ s.t. } v|_{\partial\Omega^\delta} = 0\}$. We choose a source term $f \in \mathrm{L}^2(\Omega^\delta)$ whose support does not meet O and we try to approximate the solution of problem (1), assuming it is uniquely defined, by a classical finite element method. We call u_h^δ the numerical solution and we make δ tends to zero. The results are displayed on Figure 2. For a contrast $\kappa_\sigma := \sigma_-/\sigma_+ = -1.0001$, the sequence $(\|u_h^\delta\|_{\mathrm{H}_0^1(\Omega^\delta)})_\delta$ is relatively stable with respect to δ, for δ small enough. For $\kappa_\sigma := \sigma_-/\sigma_+ = -0.9999$, it looks that there exists of sequence of values of δ, which accumulates in zero, such that problem (1) is not well-posed. In other words, it seems that the solution of problem (1) is not stable with respect to δ when δ tends to zero. The goal of the present document is to understand these two observations.

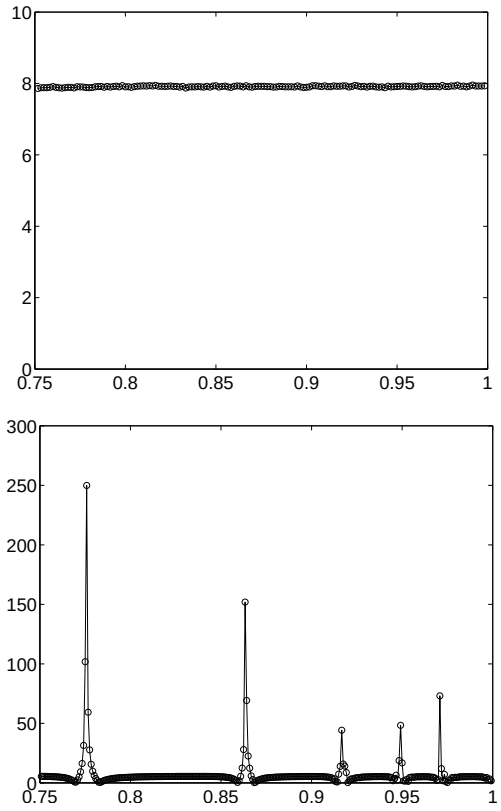

Figure 2: Evolution of $\|u_h^\delta\|_{\mathrm{H}_0^1(\Omega^\delta)}$ w.r.t. $1 - \delta$. Above, we take $\sigma_+ = 1$ and $\sigma_- = -1.0001$. Below, we take $\sigma_+ = 1$ and $\sigma_- = -0.9999$.

2 Properties of the problem for $\delta = 0$

We associate with problem (1) the continuous linear operator $\mathcal{A}^\delta : \mathrm{H}_0^1(\Omega^\delta) \to \mathrm{H}^{-1}(\Omega^\delta)$ defined by $\langle \mathcal{A}^\delta u, v\rangle_{\Omega^\delta} = (\sigma^\delta \nabla u, \nabla v)_{\Omega^\delta}$, $\forall u, v \in \mathrm{H}_0^1(\Omega^\delta)$. As it

is known from [1], $\mathcal{A}^\delta$ is a Fredholm operator of index 0 if and only if $\kappa_\sigma := \sigma_-/\sigma_+ \neq -1$, as the interface $\Sigma^\delta := \overline{\Omega}^\delta_+ \cap \overline{\Omega}^\delta_-$ is smooth and meets $\partial\Omega^\delta$ orthogonally.

Now, for $\delta = 0$, the interface no longer meets $\partial\Omega^\delta$ perpendicularly. In the sequel, we denote $\mathcal{A}$, Ω and σ instead of $\mathcal{A}^0$, Ω^0 and σ^0. As shown in [1], there exist values of the contrasts $\kappa_\sigma = \sigma_-/\sigma_+$ for which the operator $\mathcal{A}$ fails to be of Fredholm type. More precisely, for the chosen configuration, $\mathcal{A}$ is a Fredholm operator (and actually, an isomorphism) if and only if, $\kappa_\sigma < 0$ does not belong to the *critical interval* $[-1; -1/3]$. Here, the value 3 comes from the ratio of the two apertures: $3 = (\pi - \pi/4)/(\pi/4)$.

$\star$ When $\kappa_\sigma = -1.0001 \notin [-1; -1/3]$, $\mathcal{A}$ is an isomorphism (c.f. [1]). In this case, we can prove that $\mathcal{A}^\delta$ is an isomorphism for δ small enough. Moreover, defining $u^\delta = (\mathcal{A}^\delta)^{-1} f$ and $u = \mathcal{A}^{-1} f$, we can show that the sequence (u^δ) converges to u for the H^1 norm. This explains the first curve of Figure 2.

$\star$ When $\kappa_\sigma = -0.9999 \in [-1; -1/3]$, $\mathcal{A}$ is not of Fredholm type (c.f. [1]). In this configuration, there is a qualitative difference between problem (1) for $\delta > 0$, and problem (1) for $\delta = 0$. In [2], we define a new functional framework to restore Fredholmness for the limit problem. More precisely, we prove that, for $\kappa_\sigma \in (-1; -1/3)$ the operator $\mathcal{A}^+ : \mathrm{V}^+_\beta \to \mathrm{V}^1_\beta(\Omega)^*$ defined by $\langle \mathcal{A}^+ u, v\rangle_\Omega = (\sigma\nabla u, \nabla v)_\Omega$, $\forall u \in \mathrm{V}^+_\beta$, $v \in \mathscr{C}^\infty_0(\Omega)$, is an isomorphism for all $\beta \in (0; 2)$. In this notation, $\mathrm{V}^+_\beta := \mathrm{span}\{s^+\} \oplus \mathrm{V}^1_{-\beta}(\Omega)$, where $s^+ \in \mathrm{L}^2(\Omega) \setminus \mathrm{H}^1(\Omega)$ is a singular function at O and $\mathrm{V}^1_{-\beta}(\Omega)$ is the completion of $\mathscr{C}^\infty_0(\Omega)$ for the weighted norm $\|\cdot\|_{\mathrm{V}^1_{-\beta}(\Omega)} = (\|r^{-\beta}\nabla\cdot\|^2_{\mathrm{L}^2(\Omega)} + \|r^{-\beta-1}\cdot\|^2_{\mathrm{L}^2(\Omega)})^{1/2}$.

3 Asymptotic expansion of the solution inside the critical interval

For a contrast inside the critical interval, the exotic functional framework introduced for the limit problem leads to two surprising phenomena in the asymptotic expansion of the solution of problem (1). First, when we proceed to a usual matched asymptotic expansion method, we observe that we can define an asymptotic expansion of the solution u^δ only for

$$\delta \in \mathscr{S}_{\mathrm{adm}} := (0; 1) \setminus \mathscr{S}_{\mathrm{forb}} \quad \text{with } \mathscr{S}_{\mathrm{forb}} := \bigcup_{k\in\mathbb{N}} \delta_\star^k \delta_0,$$

$\delta_\star, \delta_0$ being two numbers of $(0; 1)$. Notice that 0 is an accumulation point for $\mathscr{S}_{\mathrm{forb}}$. For $\alpha \in (0; 1/2)$, we define $I(\alpha) := \bigcup_{k\in\mathbb{N}} [\delta_\star^{k+1-\alpha}\delta_0; \delta_\star^{k+\alpha}\delta_0] \subset \mathscr{S}_{\mathrm{adm}}$. In [3], we prove the following result:

Proposition 1. *Let $\beta \in (0; 2)$ and $f \in \mathrm{V}^1_\beta(\Omega)^*$. There exists δ_0 such that problem (1) is uniquely solvable for all $\delta \in (0; \delta_0) \cap \mathrm{I}(\alpha)$, with $\alpha \in (0; 1/2)$. Moreover, we can build an approximation $\hat{u}^\delta \in \mathrm{H}^1_0(\Omega^\delta)$ of u^δ such that, for all ε in $(0; \beta)$, $\forall \delta \in (0; \delta_0) \cap \mathrm{I}(\alpha)$, there holds*

$$\|u^\delta - \hat{u}^\delta\|_{\mathrm{H}^1_0(\Omega^\delta)} \leq \; c\, \delta^{\beta-\varepsilon} \|f\|_{\mathrm{V}^1_\beta(\Omega)^*},$$

where $c > 0$ is a constant independent of δ and f.

The second original phenomenon in this asymptotic expansion concerns the approximation $\hat{u}^\delta$ introduced in Proposition 1. The function $\hat{u}^\delta$ depends on δ and its far field does not converge to the far field of $(\mathcal{A}^+)^{-1} f$ when $\delta \to 0$, even for the L^2 norm . This proves that the solution of problem (1), when it is well-defined, is unstable with respect to δ.

4 Discussion

In this document, we have considered a special geometry for Ω^δ because it simplifies the numerical calculations of the first paragraph. However, we observe exactly the same curiosities for a rounded corner: when the contrast lies inside the critical interval, the solution of problem (1), which is defined except for a sequence of values of δ which tends to 0, depends critically on the rounding parameter. From a physical point of view, one may wonder what happens in a neighbourhood of the corner...

References

[1] A.-S. Bonnet-Ben Dhia, L. Chesnel and P. Ciarlet Jr., *T-coercivity for scalar interface problems between dielectrics and metamaterials*, Math. Mod. Num. Anal., 46:1363–1387, 2012.

[2] A.-S. Bonnet-Ben Dhia, L. Chesnel and X. Claeys, *Radiation condition for a non-smooth interface between a dielectric and a metamaterial*, to appear in Math. Models Meth. App. Sci., 2012.

[3] L. Chesnel, X. Claeys and S.A. Nazarov, *A curious instability phenomenon for a rounded corner in presence of a negative material*, preprint.

3.11 Numerical methods for time harmonic wave problems

$\mathcal{H}$-Matrix vs. FMM : Fast Methods applied to BEM Solvers

B. Lizé[1], **G. Sylvand**[1]
[1] EADS Innovation Works, France. Email: benoit.lize@eads.net, guillaume.sylvand@eads.net.

Abstract

For the numerical simulation of wave propagation in accoustics and electromagnetism, EADS Innovation Works relies on integral equations solved with the Boundary Elements Method, leading to the need to solve dense linear systems. In this presentation, we intend to present two famillies of fast solvers (Fast Multipole Method and $\mathcal{H}$-Matrix method) that can be used on these systems. We propose to underline their similarities, their connections and their differences, to present their complementarity in future high performance solvers and to illustrate their performances on industrial class applications.

1 Context

EADS Innovation Works is EADS research center, dedicated to upstream research applied to all Business Units (Airbus, Eurocopter, Astrium, Cassidian). The applied mathematics team has developped over the years a family of software called Aseris destined to solve various physical problems (acoustics, electromagnetism, electrostatics, etc.) using integral equations and boundary elements methods. This software suite is used in design and research departement to work on noise reduction, stealthiness, antenna sitting, etc.

The advantages of integral equations and BEM solver are well known: mainly accuracy, and simpler (surfacic) mesh. The main drawback is the need to cope with a dense matrix whose size can be quite large for wave propagation problems, where the mesh step is governed by the wavelength of the physical problem treated (in frequency domain).

Since the late 90's, fast methods have been introduced to deal with these limitations. First, the Fast Multipole Method (FMM) allowed to compute fast matrix-vector products (in $\mathcal{O}(n\log^2(n))$ instead of $\mathcal{O}(n^2)$ for the standard algorithm), and hence to design fast solvers using *iterative* methods. Lately, $\mathcal{H}$-Matrix methods have gained wide acceptance by introducing fast *direct* solvers, allowing to solve systems in $\mathcal{O}(n\log^2(n))$ – or less – without the hassle of using iterative solvers (unknown convergence rate and difficulty to find a good preconditionner).

2 Fast Multipole Methods

The initial FMM was introduced in the late 80's for particle simulation [1]. Basically, the idea is to gather the particle in clusters and to compute all the interactions not point-to-point, but cluster-to-cluster, using approximations adapted to the considered kernel. A hierarchical approach for bulding the clusters leads to a multi-level algorithm, which we refer to as "the" FMM. The introduction of FMM for Helmholtz kernel [2] paved the way to a very broad use of FMM in the field of wave propagation, mainly in electromagnetism, but also (at EADS) in acoustics [3].

Since then, new FMM formulations have been introduced. The directional FMM [4] extends the black box FMM to all oscillatory kernels, for instance for 2D applications. The advantage of this "black box" approach is that it only relies on kernel evaluations, and not on an analytical decomposition of this kernel. In [5], the authors deal with a numerical breakdown that prevents the classical FMM for Helmholtz to handle low-frequency problems. Recently, this method has been improved and simplified [6], leading to a new FMM scheme for Helmholtz stable at all frequencies.

3 $\mathcal{H}$-Matrix

$\mathcal{H}$-Matrix [7] is a lossy, hierarchical storage scheme for matrices that, along with an associated arithmetic, provides a rich enough set of approximate operations to perform the matrix addition, multiplication, factorization (*e.g.* LU or LDL^T) and inversion. It relies on two core ideas : (a) nested clustering of the degrees of freedom, and of their products; and (b) adaptative compression of these clusters. Several choices exist in the literature for these two ingredients, the most common being *Binary Space Partitioning* for the clustering and *Adaptative Cross Approximation* for the compression.

The first step yields a tree-like matrix structure as shown in the figure 1, that is "filled" in a second step with low-rank approximations of the corresponding matrix blocks, representing the interaction of two clusters. The algorithms then perform the operations on this structure, using adaptative recompression to avoid inflating the matrix as the algorithm

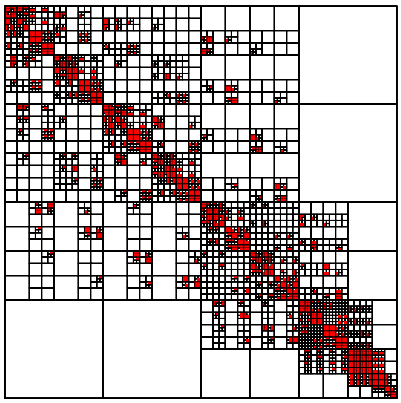

Figure 1: $\mathcal{H}$-Matrix structure. Grey blocks will not be compressed, white ones will.

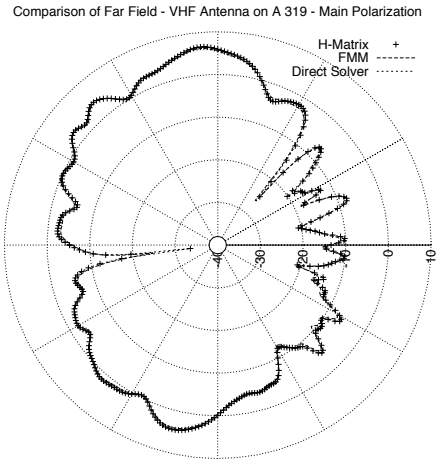

Figure 2: VHF antenna on an A319. The scale is logarithmic.

progresses.

Together, they allow for the construction of a fast direct solver with complexity $\mathcal{O}(n \log^2(n))$ in some cases [8], which is especially important for BEM applications as it gracefully handles a large number of Right-Hand Sides (RHS). They also provide a kernel-independent fast solver, allowing one to use the method for the several physics addressed by ASERIS in short order.

EADS has recently implemented the $\mathcal{H}$-Matrix arithmetic and successfully applied it to a wide range of industrial applications in electromagnetism and acoustics. Furthermore, these algorithms are hard to efficiently parallelize, as the very scarce literature on the subject shows [9]. We developed a parallel solver that goes beyond the aforementioned reference, using innovative techniques on top of a state-of-the-art runtime system. This enables the solving of very large problems, with a very good efficiency. In this presentation, we show some results on the accuracy of the this method on several challenging applications, and its fast solving time and efficient use of resources.

The figure 2 shows an antenna diagram for a VHF antenna (127MHz) on an A319 with 290.000 unknowns. The results show a very good agreement between the three solvers, with a slightly better result for the $\mathcal{H}$-Matrix solver. Computation time was 25 hours on 64 cores for the direct solver, 33 minutes and 17 minutes for the FMM and $\mathcal{H}$-Matrix solvers on 12 cores.

References

[1] L. Greengard, V. Rokhlin, *A fast algorithm for particle simulations*, J. Comp. Phys. 73 (2) (1987).

[2] *The Fast Multipole Method I: Error Analysis and Asymptotic Complexity* Darve, E. SIAM Journal on Numerical Analysis 2000 38:1.

[3] *La méthode multipôle rapide en électromagnétisme. Performances, parallélisation, applications*, Sylvand G., PhD Ecole des Ponts ParisTech (2002)

[4] M. Messner, M. Schanz, E. Darve, *Fast directional multilevel summation for oscillatory kernels based on Chebyshev interpolation*, J.C.P., Volume 231, Issue 4, 20 (2012).

[5] E. Darve, P. Havé, *Efficient fast multipole method for low-frequency scattering*, J.C.P., Volume 197, Issue 1 (2004).

[6] F. Collino, *Analyse théorique d'une méthodes multipôles stable à toutes échelles pour le noyau d'Hemholtz* , Technical Report CERFACS (2013, in preparation).

[7] W. Hackbusch, *A Sparse Matrix Arithmetic Based on H-Matrices. Part I: Introduction to H-Matrices*, Computing, Volume 62, Issue 2 (1999)..

[8] L. Grasedyck, W. Hackbusch, *Construction and Arithmetics of H-Matrices*, Computing, Volume 70, Issue 4 (2003).

[9] R. Kriemann, *Parallel $\mathcal{H}$-Matrix Arithmetics on Shared Memory Systems*, Computing, Volume 74, Issue 3 (2005).

An Active Noise Control Method based on Stochastic Finite Element Models

T. Airaksinen[1], **J. Toivanen**[1,2,*]
[1] Department of Mathematical Information Technology, University of Jyväskylä, Jyväskylä, Finland
[2] Department of Aeronautics and Astronautics, Stanford University, Stanford, CA, USA
*Email: toivanen@stanford.edu

Abstract

A new optimal feed-forward local active noise control (ANC) method is proposed for stochastic environments. The method is based on frequency domain finite element acoustical models. Stochastic domains and noise sources are considered. Measurements from an array of microphones are mapped to secondary loudspeakers, by an offline optimized linear mapping minimizing the expected value of a noise functional. The presented ANC method gives robust and efficient noise attenuation. A numerical study demonstrates it in a passenger car cabin.

Introduction

The basic idea of ANC is to produce secondary, opposite-phase sound to cancel the noise. Typically it is particularly effective at low frequencies. A novel feed-forward ANC method is introduced for enclosed cavities [2]. This is an extension of the earlier study [1]. The expected value of a noise measure is computed in a stochastic environment by integrating the noise over the underlying probability space. The feed-forward map from the measurements to the secondary sources is computed offline by solving a quadratic programming problem.

1 Acoustic model

The time harmonic sound propagation in an enclosed domain Ω is modeled by the Helmholtz equation

$$-\nabla \cdot \frac{1}{\rho}\nabla p - \frac{\omega^2}{c^2\rho}p = 0 \quad \text{in} \quad \Omega,$$

where ρ is the density of air, and c is the speed of sound. The complex-valued solution p defines the amplitude and the phase of the sound pressure. A partially absorbing wall material is described by the impedance boundary conditions

$$\frac{\partial p}{\partial \mathbf{n}} = \frac{i\eta\omega}{c}p + f \quad \text{on } \partial\Omega,$$

where η is the absorption coefficient and f is the sound source which is nonzero on a part of the boundary $\partial\Omega$. An approximate solution for the above model is obtained using a finite element method.

2 Noise control problem

The acoustical model is posed in a stochastic domain $\Omega(\mathbf{r})$, where $\mathbf{r}$ is a stochastic variable with the PDF (probability density function) $F_{\mathbf{r}}(\mathbf{r})$. The total pressure field is

$$p(\mathbf{x},\mathbf{r},\mathbf{s},\boldsymbol{\gamma}) = p_0(\mathbf{x},\mathbf{r},\mathbf{s}) + \boldsymbol{\gamma}^T\mathbf{p}(\mathbf{x},\mathbf{r}),$$

where $p_0(\mathbf{x},\mathbf{r},\mathbf{s})$ is the sound pressure originating from a stochastic noise source governed by a stochastic variable $\mathbf{s}$ with the PDF $F_{\mathbf{s}}(\mathbf{s})$. The vector $\mathbf{p}(\mathbf{x},\mathbf{r}) = (p_1(\mathbf{x},\mathbf{r}),\ldots,p_{n_a}(\mathbf{x},\mathbf{r}))^T$ gives the sound pressures originating from unit secondary sources. The amplitudes and phases of the secondary sources are defined by $\boldsymbol{\gamma} \in \mathbb{C}^{n_a}$.

The aim is to minimize the noise measure

$$N(\mathbf{r},\mathbf{s},\boldsymbol{\gamma}) = \int\limits_{V_C(\mathbf{r})} |p(\mathbf{x},\mathbf{r},\mathbf{s},\boldsymbol{\gamma})|^2 \, d\mathbf{x},$$

where $V_C(\mathbf{r}) \subset \Omega(\mathbf{r})$ is a control volume. Its expected value is given by

$$E\left[N(\mathbf{r},\mathbf{s},\boldsymbol{\gamma})\right] = \int\limits_{\mathbf{r}}\int\limits_{\mathbf{s}} N\left(\mathbf{r},\mathbf{s},\boldsymbol{\gamma}\right) F_{\mathbf{s}}\left(\mathbf{s}\right) d\mathbf{s}\, F_{\mathbf{r}}\left(\mathbf{r}\right) d\mathbf{r}.$$

To find the optimal $\boldsymbol{\gamma}$ for the secondary sources, an optimal linear form defined by a matrix $\mathbf{C}$ is sought between the measurements $\mathbf{m}(\mathbf{r},\mathbf{s}) = \left(p_0(\mathbf{x}^1,\mathbf{r},\mathbf{s}),\ldots,p_0(\mathbf{x}^{n_m},\mathbf{r},\mathbf{s})\right)^T$ and the secondary sources in the form

$$\boldsymbol{\gamma} = \mathbf{C}\mathbf{m}(\mathbf{r},\mathbf{s}).$$

The minimization of the expected value of the noise measure leads to the optimization problem

$$\min_{\mathbf{C}} E\left[N(\mathbf{r},\mathbf{s},\mathbf{C}\mathbf{m}(\mathbf{r},\mathbf{s}))\right].$$

This problem can be formulated as a quadratic programming problem. Without any constraints, $\mathbf{C}$ can be computed by solving a system of linear equations describing the optimality conditions.

3 Numerical example

The proposed ANC method is demonstrated in BMW 330i car interior shown in Figure 1. The computational domain is the cabin excluding the driver. Variations on the posture of the driver define a stochastic domain $\Omega(\mathbf{r})$. The posture is controlled by a three-dimensional stochastic vector $\mathbf{r}$. The objective is to minimize noise at the ears of the driver. Thus, the control volume $V_C(\mathbf{r})$ is a set of two points defined by the left and right ear. These points can be seen as virtual error microphones. A stochastic source is modeled as a vibrating rectangular surface behind the leg room and it is controlled by a four-dimensional stochastic vector $\mathbf{s}$.

The frequency range 10–1000 Hz is considered with 10 Hz steps. Thus, 100 frequencies are sampled. The domain is sampled by 125 postures of the driver. The maximum number of the measurement points is 16. By employing the reciprocity principle, it is sufficient to perform one acoustic simulation for each measurement point and both ears for each posture and frequency. Thus, the total number of offline finite element simulations is $18 \times 125 \times 100 = 225000$.

The number of secondary sound sources is chosen to be 6; see Figure 1. Once the simulations have been performed the optimal matrices $\mathbf{C}$ for each frequency can be computed offline by solving a small linear system. The online controller only needs to perform Fourier transformations between time and frequency domains, and matrix-vector multiplications by the precomputed $\mathbf{C}$.

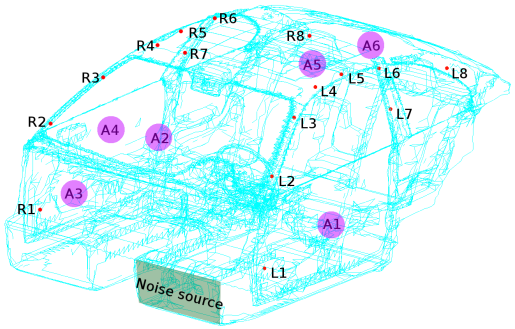

Figure 1: The interior of the car, the locations of the noise source, the measurement points L1...L8, R1...R8, and the secondary sources A1...A6.

Figure 2 shows the expected noise reduction over the considered frequency range. At the frequencies below 100 Hz the reduction is 20–30 dB while around 500 Hz the reduction is 10–20 dB. Increasing the number of measurement points improves the reduction. Figure 2 shows the same plot when the measurement error is 4 %. All results are based on a more robust formulation including terms for measurement errors. For details, see [2]. With these errors the effectiveness of ANC is reduced by 0–10 dB. Also increasing the number of measurements is less beneficial in this case.

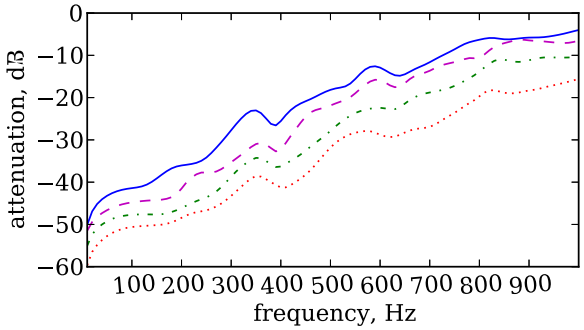

Figure 2: The expected noise attenuation based on 2, 4, 8, and 16 measurement points (lines from top to bottom respectively) without measurement error.

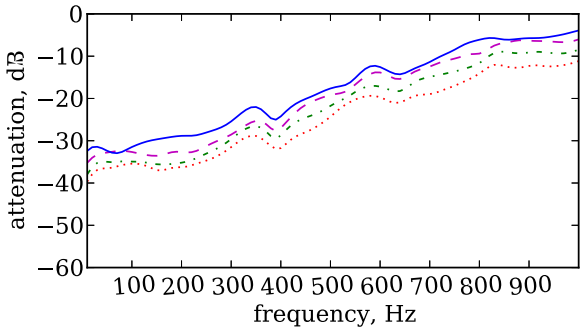

Figure 3: The expected noise attenuation based on 2, 4, 8, and 16 measurement points (lines from top to bottom respectively) with 4% measurement error.

References

[1] T. Airaksinen, E. Heikkola and J. Toivanen, *Local Control of Sound in Stochastic Domains Based on Finite Element Models*, Journal of Computational Acoustics, **19** (2011), pp. 205–219.

[2] T. Airaksinen and J. Toivanen, *An Optimal Feed-forward Local Active Noise Control Method based on Stochastic Finite Element Models*, submitted, URL: http://urn.fi/URN:NBN:fi:jyu-201211203036

Combining Analytic Preconditioner and Fast Multipole Method for the 3-D Helmholtz equation[†]

M. Darbas[1,*], **E. Darrigrand**[2], **Y. Lafranche**[2]
[1] LAMFA UMR CNRS 7352, Université de Picardie, Amiens, France
[2] IRMAR UMR CNRS 6625, Université de Rennes 1, Rennes, France.
[†]This work was funded in part by the project ANR MicroWave
[*]Email: marion.darbas@u-picardie.fr

Abstract

We present a detailed numerical study of an iterative solution to 3-D sound-hard acoustic scattering problems at high frequency considering Combined Field Integral Equations. We propose a combination of an OSRC preconditioning technique and a Fast Multipole Method which leads to a fast and efficient algorithm independently of both a frequency increase and a mesh refinement. To validate its effectiveness, we apply the resolution algorithm to various and significant test-cases using a GMRES solver.

1 The problem setting

Let us consider a bounded domain $\Omega^- \subset \mathbb{R}^3$ representing an impenetrable body with Lipschitz continuous boundary $\Gamma := \partial\Omega^-$. We denote by $\Omega^+ := \mathbb{R}^3 \setminus \overline{\Omega^-}$ the exterior domain of propagation. We are concerned with the scattering of an incident time-harmonic acoustic wave $u^{\rm inc}$, characterized by the wavenumber k, by the obstacle Ω^-. The scattered field u^+ satisfies the Helmholtz exterior boundary-value problem

$$\begin{cases} \Delta u^+ + k^2 u^+ = 0, & \text{in } \mathcal{D}'(\Omega^+), \\ \partial_{\boldsymbol{n}} u^+_{|\Gamma} = g = -\partial_{\boldsymbol{n}} u^{\rm inc}_{|\Gamma}, & \text{in } H^{-1/2}(\Gamma), \\ \lim\limits_{|x|\to+\infty} |x| \left(\nabla u^+ \cdot \dfrac{x}{|x|} - iku^+ \right) = 0. \end{cases} \tag{1}$$

Several integral equations have been derived for solving this scattering problem (see for instance [3]). We consider the following CFIE (Combined Field Integral Equation): Find $\varphi = -(u^+_{|\Gamma} + u^{\rm inc}_{|\Gamma}) \in H^{1/2}(\Gamma)$ solution to

$$\left(\frac{I}{2} + M - \eta D \right) \varphi = -u^{\rm inc}_{|\Gamma} + \eta \partial_{\boldsymbol{n}} u^{\rm inc}_{|\Gamma}, \quad \text{on } \Gamma, \tag{2}$$

where η is a complex coupling parameter. The operator I is the identity operator, and M and D the first and second traces of the double-layer potential respectively. The CFIE (2) is uniquely solvable in $H^{1/2}(\Gamma)$ for all frequency $k > 0$. This equation is a first-kind integral equation and does not provide an interesting spectral behavior. It involves the first-order, strongly singular and non-compact operator D. To obtain better spectral properties, a strategy consists in introducing an efficient approximation $\widetilde{V}$ of the exact Neumann-to-Dirichlet map in order to precondition the EFIE operator D before combining it with the MFIE operator $(I/2 + M)$ [1]. The operator $\widetilde{V}$ is derived from On-Surface Radiation Condition (OSRC) methods

$$\widetilde{V} = \frac{1}{ik} \left(1 + \frac{\Delta_\Gamma}{k_\varepsilon^2} \right)^{-1/2}. \tag{3}$$

The operator Δ_Γ is the Laplace-Beltrami operator over the surface Γ and the parameter $k_\varepsilon = k + i\varepsilon$ is complex-valued ($\varepsilon \in \mathbb{R}^*$). The analytical preconditioner $\widetilde{V}$ has a sparse structure, is very easy to implement and implies a low additional computational cost. This choice leads to the well-posed second-kind Fredholm integral equation

$$\left(\frac{I}{2} + M - \widetilde{V} D \right) \varphi = -u^{\rm inc}_{|\Gamma} + \widetilde{V} \partial_{\boldsymbol{n}} u^{\rm inc}_{|\Gamma}, \quad \text{on } \Gamma. \tag{4}$$

The following relation holds

$$\frac{I}{2} + M - \widetilde{V} D = \left(\frac{1}{2} + \frac{k_\varepsilon}{2k} \right) I + C, \tag{5}$$

where C is a compact operator [1].

2 Numerical results

2.1 Spectral analysis

A thorough study of the eigenvalues behavior of the integral operators involved in (2) and (4) is realized in order to illustrate the impact of the OSRC-preconditioning technique on the spectrum of the CFIE operator. First, let us say few words about discretization: we consider a classical $\mathbb{P}_1$ boundary finite element discretization. We denote by n_λ the density of discretization points per wavelength. Concerning

the preconditioner $\widetilde{V}$, the localization of the square-root operator is efficiently realized by only solving N_p Helmholtz-type sparse linear systems thanks to a Padé paraxial approximation of order N_p with a rotating branch-cut technique. The single-level Fast Multipole Method is applied to the calculation involving the integral operators D and M.

When the scatterer is the unit sphere, explicit expressions of the eigenvalues of the CFIE operators are known. In Fig. 1, we can observe that the numerical eigenvalues of the OSRC-preconditioned operator are well clustered at a point near to $(1, 0)$ which is the accumulation point of the analytical ones according to (5). This is not the case of the CFIE. We observe a dispersion of the eigenvalues in the elliptic part.

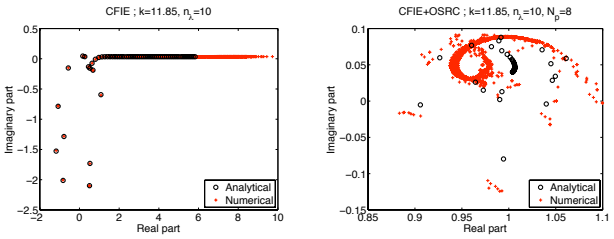

Figure 1: Unit sphere: distribution of the eigenvalues, $k = 11.85$, $n_\lambda = 10$

Now, let us consider a 3-D trapping domain and a submarine.

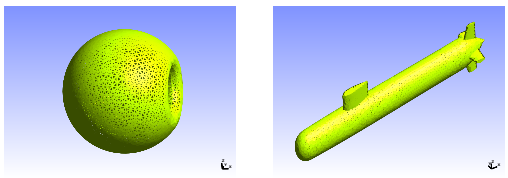

Figure 2: Scatterers: Sphere with cavity, Submarine

In the case of the sphere with cavity, Fig. 3 shows a dispersion in the elliptic part and eigenvalues in a neighborhood of zero in the hyperbolic zone for the CFIE; clustering around a point near to $(1, 0)$ for the OSRC-preconditioned CFIE. Same conclusions hold for the submarine. Consequently, the condition number of the CFIE depends on both a frequency increase and a mesh refinement. The OSRC-preconditioner $\widetilde{V}$ avoids these dependencies.

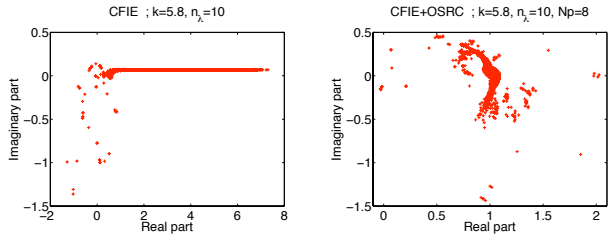

Figure 3: Sphere with cavity: distribution of the eigenvalues, $k = 8$, $n_\lambda = 9.6$, $N_p = 8$

2.2 Convergence results

The convergence of the GMRES, with respect to both physical and mesh parameters, corroborates the spectral analysis. The speed of convergence is strongly improved by the OSRC preconditioning and the application of FMM does not disturb this benefit. Consequently, only a few GMRES iterations are required to obtain the same accuracy as the CFIE with no preconditioning when we increase the frequency or the mesh density (cf. Fig. 4 for the sphere with cavity). Moreover, the algorithm complexity is essentially governed by the FMM due to the low computation cost of the preconditioner. The details on this work can be found in [2].

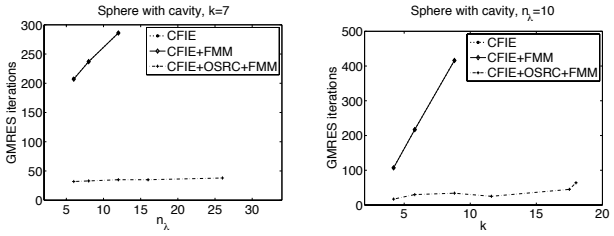

GMRES iterations vs n_λ GMRES iterations vs k

Figure 4: Convergence of GMRES, $N_p = 8$

References

[1] X. Antoine, M. Darbas, *Generalized combined field integral equations for the iterative solution of the Helmholtz equation in three dimensions*, M2AN, **41**(1) (2007), pp. 147-167.

[2] M. Darbas, E. Darrigrand, Y. Lafranche, *Combining Analytic Preconditioner and Fast Multipole Method for the 3-D Helmholtz equation*, J. Comput. Phys., **236** (2013), pp. 289-316.

[3] W. McLean, *Strongly Elliptic Systems and Boundary Integral Equations*, Cambridge University Press, Cambridge, UK , 2000.

A high-order Nyström scheme for acoustic scattering by inhomogeneous penetrable media in two dimensions

Akash Anand[1], **Ambuj Pandey**[1,*], **Jagabandhu Paul**[1]
[1] Indian Institute of Technology Kanpur, India
*Email: ambuj@iitk.ac.in

Abstract

A high-order Nyström method to solve the integral equation formulation of volumetric scattering problem in two dimensions is proposed in the text. To achieve desired approximations, this scheme relies on analytic resolution of singularities present in the integral operator via changes of parametric variables along with a suitable use of partitions of unity to decouple boundary regions of the scatterer for a high-order specialized treatment. The interactions from interior regions, aided by these partitions of unity, can be computed efficiently and accurately through an existing FFT based methodology leading to an overall efficient and rapidly converging algorithm.

1 Introduction

We present a high-order methodology for solution of scalar volumetric scattering problems in two dimensions. Among fast numerical schemes for this problem, only a couple of techniques converge with second order for discontinuous scattering configurations – one that rely on the use of "discontinuous FFT" [6] while the other uses FFT for accelerated evaluation of convolution in polar coordinates after a suitable decomposition of the Green's function via addition theorem [5]. Another high-order convergent method for acoustic volumetric scattering problem, introduced in [1], [2], is designed to be computationally efficient only for "thin"scatterers. Our present approach, in fact, extends the ideas presented in [1] to obtain a solver for general scattering configurations while retaining high-order accuracy even in the presence of material discontinuity.

The integral equation formulation for acoustic scattering problem by penetrable scatterers is given by [3], $u(\boldsymbol{x}) + k^2 K[u](\boldsymbol{x}) = u^i(\boldsymbol{x})$, where $K[u](\boldsymbol{x}) = \int_\Omega G(\boldsymbol{x},\boldsymbol{x'}) m(\boldsymbol{x'}) u(\boldsymbol{x'}) d\boldsymbol{x'}$ with kernel $G(\boldsymbol{x},\boldsymbol{x'}) = (i/4)H_0^1(k|\boldsymbol{x}-\boldsymbol{x'}|)$ and $m(\boldsymbol{x}) = 1 - n(\boldsymbol{x})^2$, n being the refractive index which is assumed to be 1 outside the bounded scattering medium Ω.

Rapid convergence of Nyström scheme is achieved by designing a high-order accurate quadrature for approximation of the integral $K[u](\boldsymbol{x})$. We start by covering the scatterer Ω by P number of overlapping coordinate patches where the p^{th} patch is homeomorphic to an open set $(0,1)^2$ via a smooth invertible parameterization $\boldsymbol{x}_p = \boldsymbol{x}_p(s,t)$. With the help of a partitions of unity $\{w_p(\boldsymbol{x}) : p = 1, ..., P\}$ subordinate to this covering, $K[u](\boldsymbol{x})$ is rewritten as a sum of P integrals, $K[u](\boldsymbol{x}) = \sum_{p=1}^{P} K_p[u](\boldsymbol{x})$ where

$$K_p[u](\boldsymbol{x}) = \int_0^1 \int_0^1 G(\boldsymbol{x}, \boldsymbol{x_p}(s',t')) \phi_p^u(s',t') ds' dt', \quad (1)$$

$\phi_p^u(s,t) = m\big(\boldsymbol{x}_p(s,t)\big) u\big(\boldsymbol{x}_p(s,t)\big) w_p\big(\boldsymbol{x}_p(s,t)\big) J_p(s,t)$, with J_p as the Jacobian of the transformation $\boldsymbol{x}_p$. Clearly, $K_p[u](\boldsymbol{x})$ accounts for the interaction of the p^{th} patch with the target point $\boldsymbol{x}$. The difficulty in numerical calculations of such interactions when $\boldsymbol{x}$ lies within the patch is primarily due to singular nature of the kernel. Another aspect that demand varying strategy in computations of $K_p[u](\boldsymbol{x})$ arise due to differences in the behavior of integrands at boundaries of individual patches. Indeed, we see that w_p vanishes to high-order on the boundary of only those patches whose closures do not intersect with the boundary of Ω, i.e., interior patches. Using this criterion, we divide these patches into a set of interior patches, and a set of boundary patches, which require different schemes. As a result of these variations, we break the computation of integral operator in (1) into four different imteractions that are described next.

Boundary-Boundary Interactions: When the integration region is a boundary patch and the target point happens to lie again on one of the boundary patches but outside of the integration patch, then the integrand is smooth, and can be integrated accurately using a high-order quadrature rule. The singular nature of the integrand in the case when the target point belongs to the integration, on the other hand, requires a more careful treatment for obtaining accurate approximations. A change of variable in s' not only analytically removes the logarithmic singularity in G, but also resolves the near singular behavior of the integrand in t'.

Interior-Boundary Interactions: This case occurs when $\boldsymbol{x}$ lies in an interior patch while integrat-

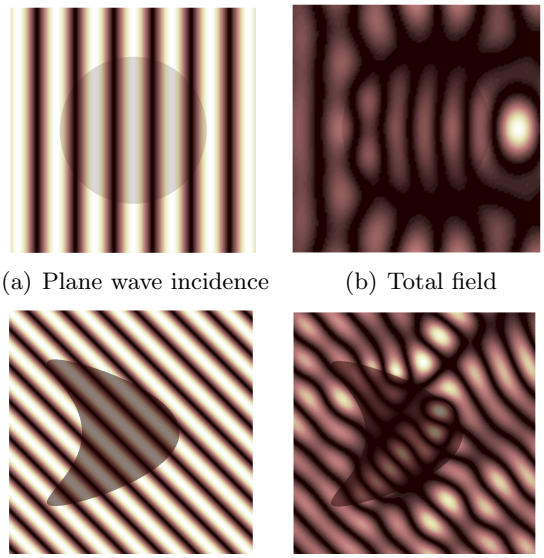

(a) Plane wave incidence (b) Total field

(c) Plane wave incidence (d) Total field

Figure 1: : (a), (b) – Scattering of a plane wave by a penetrable disc — numerical approximations on a $3\times64\times64$ grid with 0.01 % error; (c), (d) - Scattering computations for bean shaped obstacle

ing over a boundary patch. Within this scenario, if $\boldsymbol{x}$ does not belong to any boundary patches then the integrand can be integrated accurately using a high-order accurate quadrature rule, already discussed in Boundary-Boundary interaction. When $\boldsymbol{x}$ happens to lie on a boundary patch, on the other hand, one can interpolate its value from the data computed in the "Boundary-Boundary Interactions" step.

Boundary-Interior Interactions: Similar to previous interactions, if $\boldsymbol{x}$ lies outside the integration patch, then the corresponding integration can be performed using a spectrally accurate trapezoidal rule as, unlike boundary patches, the integrand is smooth as well as periodic in both variables. When $\boldsymbol{x}$ belongs to the integration patch, on the other hand, singularities that arise in the integrand can be surmounted analytically by, for example, going to polar coordinates, which again, can be approximated to high-order by simple use of trapezoidal rule.

Interior-Interior Interactions: Finally, the case when $\boldsymbol{x}$ is in an interior patches and the integration domain itself is an interior patch can be handled in a manner similar to the strategy discussed in the "Boundary-Interior" interactions. These interactions, however, can be computed in a more efficient manner using the approach introduced in [5]. The computation of "Interior-Boundary" and "Boundary-Interior" interactions can also be accelerated by a suitable use of two face equivalent source approximations on Cartesian grids, introduced in [7], that has already been employed in [1], to accelerate "Boundary-Boundary" interactions.

2 Numerical results

We present, in subfigures (a) and (b) of Fig. 1, a comparison of our approximate scattering solution on a computational grid of 64×64 in each patch against the Mie series solution for a disc shaped scatterer of the size of 12-wavelengths with a constant refractive index of $\sqrt{2}$. A similar computation for an incident plane wave shown in (c) by a $\sqrt{2}$ refractive index bean shaped scatterer is presented in (d) to demonstrate method's adaptability and applicability in dealing with complex scattering configurations.

References

[1] A. Anand, *An efficient high-order algorithm for scattering from penetrable thin structures*, Ph.D. Thesis, University of Minnesota, February 2006.

[2] A. Anand and F. Reitich, *An efficient high-order algorithm for acoustic scattering from penetrable thin structures in three dimensions*, Journal of Acoustical Society of America, **121** (2007), pp. 2503–2514.

[3] D. Colton and R. Kress, *Inverse Acoustic and Electromagnetic Scattering Theory.* Springer-Verlag second edition, 1998.

[4] E. M. Hyde and O. P. Bruno, *A fast, higher-order solver for scattering by penetrable bodies in three dimensions*, Journal of Computational Physics, **202** (2005), pp. 236–261.

[5] E. M. Hyde, *Fast, high-order methods for scattering by inhomogeneous media*, Ph.D. Thesis, California Institute of Technology Pasadena, California, 2003

[6] A. Zhu and S. Gedney, *A quadrature-sampled pre-corrected FFT method for the electromagnetic scattering from inhomogeneous objects*, IEEE Antennas Wireless Propagation Letters, **2** (2003), pp. 50–53.

[7] O. P. Bruno and L. A. Kunyansky, *A Fast, High-Order Algorithm for the Solution of Surface Scattering Problems: Basic Implementation, Tests, and Applications*, Journal of Computational Physics, **110** (2001), pp. 80–110.

Fast Multipole Accelerated Boundary Element Method for problems in an elastic half-space

Stéphanie Chaillat[1,*], **Marc Bonnet**[1]
[1] Poems (UMR CNRS-INRIA-ENSTA 7231), ENSTA, Palaiseau, France
*Email: stephanie.chaillat@ensta-paristech.fr, mbonnet@ensta.fr

Abstract

We present a fast multipole-accelerated boundary element method (FM-BEM) for the simulation of elastic waves in semi-infinite media. To avoid the costly discretization of large portions of the free surface, our new FM-BEM is based on the elastic half-space Green's tensor satisfying a traction-free condition on the infinite boundary of the half-space, for which a multipole-type expansion is established. The efficiency of this new approach is demonstrated on numerical examples involving up to $6\,10^5$ DOFs.

1 Context

In a previous study [2], we developed a FM-BEM based on the elastodynamic full-space fundamental solution. This approach has been shown to perform well for the simulation of elastic waves in semi-infinite media, but nevertheless suffers from the drawback of requiring a BE discretization of the free surface. In practice, the free-surface was truncated at an empirically chosen radius "large enough" for achieving a good accuracy in the target domain of study. A large number of BEM degrees of freedom (DOFs) was thus required on the free-surface for the sole purpose of enforcing the traction-free boundary condition. To avoid both the computational burden entailed by discretizing the free surface and the truncation issue, one can preferably use a Green's tensor that satisfies a traction-free boundary condition on a planar unbounded surface bounding an elastic half-space, thereby reducing the overall size of the BE model since the planar part of the free surface is no longer discretized (Figure 1). The derivation and implementation of this Green's tensor [4] are involved. In particular, unlike its full-space counterpart, the half-space Green's tensor cannot be expressed in terms of simpler kernels (e.g. Laplace or Helmholtz fundamental solutions) having already-known multipole expansions. Its multipole expansion thus cannot be obtained in a simple way and requires a specific approach [3], to which this communication is devoted.

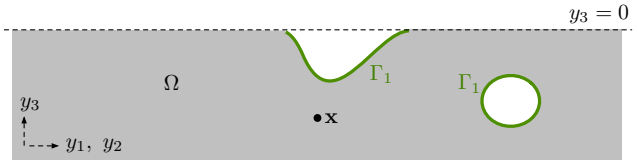

Figure 1: Support of the BE discretization (in green) when using the half-space Green's tensor.

2 Methodology

First, the Green's tensor $\boldsymbol{U}_{\rm HS}$ (resp. $\boldsymbol{T}_{\rm HS}$) is additively decomposed into three terms: the full-space fundamental solution $\mathbf{U}_\infty$ (resp. $\mathbf{T}_\infty$), the image full-space fundamental solution $\bar{\mathbf{U}}_\infty$ (resp. $\bar{\mathbf{T}}_\infty$) and a complementary term $\mathbf{U}_C$ (resp. $\mathbf{T}_C$) to satisfy the traction-free condition on the free-surface:

$$\boldsymbol{U}_{\rm HS} = \mathbf{U}_\infty + \bar{\mathbf{U}}_\infty + \mathbf{U}_C, \quad \boldsymbol{T}_{\rm HS} = \mathbf{T}_\infty + \bar{\mathbf{T}}_\infty + \mathbf{T}_C.$$

The single-layer and double-layer potentials involved in integral equations are then similarly decomposed:

$$\mathcal{S}[\boldsymbol{t}](\mathbf{x}) := \int_{\Gamma_1} \boldsymbol{U}_{\rm HS}(\mathbf{x},\cdot)\mathbf{t}\,{\rm d}S = \big[\mathcal{S}_\infty + \bar{\mathcal{S}}_\infty + \mathcal{S}_C\big](\mathbf{x}),$$

$$\mathcal{D}[\boldsymbol{u}](\mathbf{x}) := \int_{\Gamma_1} \boldsymbol{T}_{\rm HS}(\mathbf{x},\cdot)\mathbf{u}\,{\rm d}S = \big[\mathcal{D}_\infty + \bar{\mathcal{D}}_\infty + \mathcal{D}_C\big](\mathbf{x}).$$

The key to the proposed treatment then lies in expressing $\mathbf{U}_C$ as a 2D Fourier transform w.r.t. spatial coordinates parallel to the free surface, as this formulation (not shown here for brevity) is found to achieve the separation of variables required by the FMM [3]. Substituting that representation of $\boldsymbol{U}_{\rm C}$ into the definition of the complementary single-layer potential $\boldsymbol{\mathcal{S}}_{\rm C}[\boldsymbol{t}](\boldsymbol{x})$ and rearranging terms, one obtains

$$\boldsymbol{\mathcal{S}}_{\rm C}[\boldsymbol{t}](\boldsymbol{x}) = \frac{1}{4\pi^2 k_{\rm S}^2 \mu} \sum_{a,b={\rm P,S}} \int_0^{+\infty} \xi A_{ab}(\xi) \Big\{ \int_0^{2\pi} \boldsymbol{\mathcal{R}}^u_a(\xi,\alpha)\big[\,\exp(\boldsymbol{q}^-_b(\xi,\alpha)\cdot\boldsymbol{x})\,\boldsymbol{V}^-_b(\xi,\alpha)\,\big]\,{\rm d}\alpha \Big\}\,{\rm d}\xi$$

where the multipole moments are given by

$$\boldsymbol{\mathcal{R}}^u_a(\xi,\alpha) := \Big\{ \int_{\Gamma_1} \exp(\boldsymbol{q}^+_a(\xi,\alpha)\boldsymbol{y})\,\boldsymbol{t}(\boldsymbol{y})\,{\rm d}S_y \Big\} \cdot \boldsymbol{V}^+_a(\xi,\alpha)$$

and the scalar functions A_{ab} and vector-valued functions $\boldsymbol{V}^+_{a,b}$, $\boldsymbol{q}^+_{a,b}$, $\boldsymbol{V}^-_{a,b}$, $\boldsymbol{q}^-_{a,b}$ are known [3] (details omitted for brevity). The Fourier integral is in practice

evaluated by means of a product quadrature rule so that one has

$$\boldsymbol{\mathcal{S}}_{\mathrm{C}}[\boldsymbol{t}](\boldsymbol{x}) = \frac{1}{4\pi^2 k_{\mathrm{S}}^2 \mu} \sum_{a,b=\mathrm{P,S}} \sum_{i=1}^{n_\xi} w_i^\xi \xi_i A_{ab}(\xi_i) \Big\{ \sum_{j=1}^{n_\alpha} w_j^\alpha \boldsymbol{\mathcal{R}}_a^u(\xi_i,\alpha_j) \big[\exp(\boldsymbol{q}_b^-(\xi_i,\alpha_j)\boldsymbol{x})\, \boldsymbol{V}_b^-(\xi_i,\alpha_j) \big] \Big\} + E(n_\xi, n_\alpha)$$

where $(\xi_i, w_i^\xi)_{1\le i\le n_\xi}$ and $(\alpha_j, w_j^\alpha)_{1\le j\le n_\alpha}$ denote the sets of nodes and weights used for the radial and angular quadratures, respectively, and $E(n_\xi, n_\alpha)$ is the quadrature error. In the same way, the double-layer complementary potential has the form

$$\boldsymbol{\mathcal{D}}_{\mathrm{C}}[\boldsymbol{u}](\boldsymbol{x}) = \frac{1}{4\pi^2 k_{\mathrm{S}}^2} \sum_{a,b=\mathrm{P,S}} \int_0^{+\infty} \xi B_{ab}(\xi) \Big\{ \int_0^{2\pi} \boldsymbol{\mathcal{R}}_a^t(\xi,\alpha) \big[\exp(\boldsymbol{q}_b^-(\xi,\alpha)\boldsymbol{x})\, \boldsymbol{V}_b^-(\xi,\alpha) \big]\, \mathrm{d}\alpha \Big\} \mathrm{d}\xi$$

where the multipole moments are given by

$$\boldsymbol{\mathcal{R}}_a^t(\xi,\alpha) := \Big\{ \int_{\Gamma_1} \exp(\boldsymbol{q}_a^+(\xi,\alpha)\boldsymbol{y})\, \boldsymbol{u}(\boldsymbol{y})\, \mathrm{d}S_y \Big\} \boldsymbol{W}_a^+(\xi,\alpha),$$

amd the scalar functions B_{ab} and vector-valued functions $\boldsymbol{W}_a^+$ are also known. The computational complexity of the evaluation of $\boldsymbol{\mathcal{S}}_{\mathrm{C}}[\boldsymbol{t}](\boldsymbol{x})$ and $\boldsymbol{\mathcal{D}}_{\mathrm{C}}[\boldsymbol{u}](\boldsymbol{x})$ is thus of order $O(n_\xi n_\alpha N)$ (where n_ξ and n_α depend on N), since the computational work for a given quadrature node is clearly proportional to the $O(N)$ number of BE DOFs. Actual computation of $\boldsymbol{\mathcal{S}}_{\mathrm{C}}[\boldsymbol{t}]$ and $\boldsymbol{\mathcal{D}}_{\mathrm{C}}[\boldsymbol{u}](\boldsymbol{x})$ exploit generalized Gaussian quadrature (GGQ) rules, generated using a method proposed in [1] and customized for the present needs, for the radial integration.

To compute, in an optimal manner, the contributions $\mathcal{S}_\infty + \bar{\mathcal{S}}_\infty$ and $\mathcal{D}_\infty + \bar{\mathcal{D}}_\infty$ we use previous work [2] on the FMM based on $\mathbf{U}_\infty$ while extending the method developed in acoustics in a half space [5].

3 Numerical efficiency of the new FM-BEM

We first show numerically that the proposed formulation achieves a complexity significantly lower than using the non-multipole version of the Green's tensor (Fig. 2). Then, the accuracy of this new FM-BEM (which does not require meshing the free surface) is compared to that of the FM-BEM based on the elastic full-space fundamental solutions (which requires meshing the free surface). Moreover, the numerical efficiency of both approaches is compared

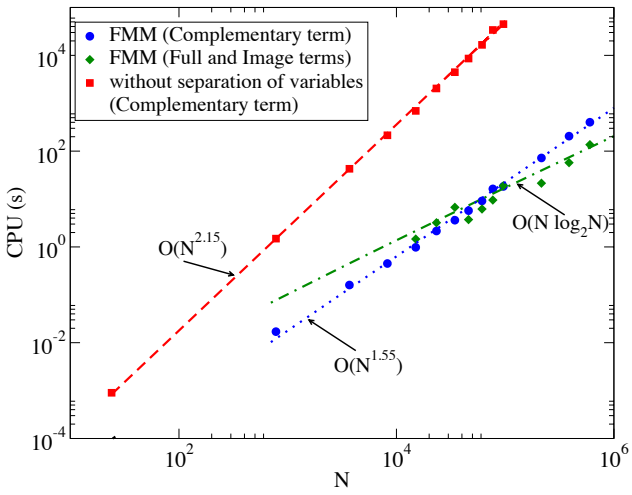

Figure 2: CPU time for the evaluation of $\boldsymbol{\mathcal{S}}[\boldsymbol{t}]$ as a function of the DOF count N: $\boldsymbol{\mathcal{S}}_{\mathrm{C}}[\boldsymbol{t}]$ without FMM (red) and with FMM (blue); $(\boldsymbol{\mathcal{S}}_\infty + \bar{\boldsymbol{\mathcal{S}}}_\infty)[\boldsymbol{t}]$ with FMM (green).

on seismology-oriented examples such as the scattering of plane waves by a cavity embedded in an elastic half-space. Despite the additional computational effort required by the evaluation of the proposed FM-capable form of the half-space fundamental solution, the new approach is shown to reduce several-fold the overall analysis time, thus establishing the net benefit brought by removing the free-surface mesh.

References

[1] J. Bremer, Z. Gimbutas, V. Rokhlin, *A nonlinear optimization procedure for generalized Gaussian quadrature*, SIAM J. Sci. Comput. **32**:1761–1788 (2010).

[2] S. Chaillat, M. Bonnet and J.F. Semblat, *A multi-level fast multipole BEM for 3-D elastodynamics in the frequency domain*, Comput. Meth. Appl. Mech. Eng. **197**:4233-4249 (2008).

[3] S. Chaillat and M. Bonnet, *A new Fast Multipole Formulation for the Elastodynamic Half-space Green's tensor*, under review.

[4] L. Pan, F. Rizzo and P.A. Martin, *Some efficient boundary integral strategies for time-harmonic wave problems in an elastic halfspace*, Comput. Meth. Appl. Mech. Eng. **164**:207–221 (1998).

[5] Y. Yasuda, K. Higuchi, T. Oshima and T. Sakuma, *Efficient technique in low-frequency fast multipole boundary element method for plane-symmetric acoustic problems*, Eng. Anal. Bound. Elem. **36**:1493-1501 (2012).

Reduced basis strategies for aeroacoustic simulations

F. Casenave[1,2,*], **A. Ern**[1], **T. Lelièvre**[1,3], **G. Sylvand**[2]
[1] Université Paris-Est, CERMICS, École des Ponts-Paristech, Marne-la-Vallée, France
[2] EADS-IW, Toulouse, France
[3] INRIA Rocquencourt, Le Chesnay, France
[*] Email: casenavf@cermics.enpc.fr

Abstract

Herein, two aeroacoustic problems solved by means of finite element and boundary element method are considered. The Reduced Basis method, a model reduction technique for parametrized partial differential equations, is applied. The considered formulations are stable at all frequencies, which is required, especially when the frequency is a parameter of interest.

Introduction

Under environmental pressures, aircraft manufacturers have developed tools to simulate acoustic waves propagation. We consider herein two cases of interest: acoustic scattering by an impedant surface by means of a Boundary Element Method (BEM) formulation; and acoustic scattering under a potential convective flow by means of a coupled Boundary Element Method - Finite Element Method (BEM-FEM) formulation [1]. For applications like propagation of uncertainty studies and optimization problems, one has to solve a parametric problem for many values of the parameters. In this context, model reduction techniques provide a way to reduce computation costs.

After presenting the two cases of interest, we give elements to justify their well posedness and we apply the Reduced Basis (RB) method.

1 Scattering by an impedant surface

We consider a solid object in the air at rest, see Figure 1. The surface Γ of the object is Lipschitz and impedant, meaning that any incident wave will be partially absorbed and partially scattered. The proportion of absorbed and scattered parts are quantified by an impedance coefficient, which is used in a Robin boundary condition at Γ. A monopole source is located in Ω^+.

A two-current BEM formulation is used, leading to a problem well-posed at all frequencies of the source [2], [3]. Figure 2 shows an example of scattered pressure field. A RB strategy is carried-out on this test case (see [4] for an application of the RB method with integral equations).

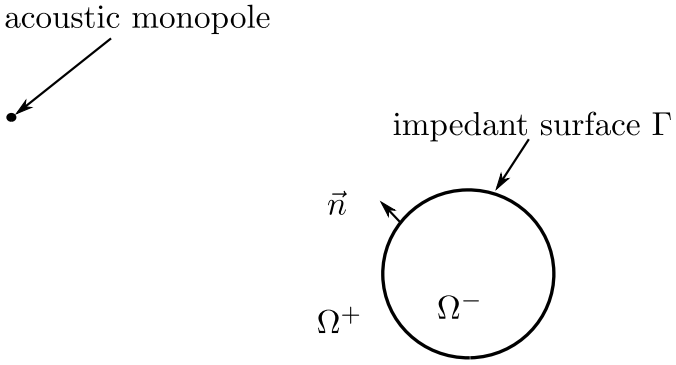

Figure 1: Geometry of the first test-case

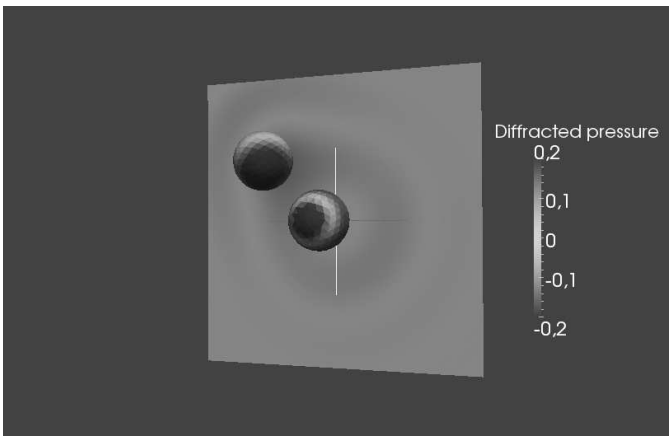

Figure 2: An example of scattered field for the second test-case with two impedant surfaces

2 Scattering under a potential convective flow

We consider a solid object in a flow, see Figure 3. We suppose that the flow around the object is potential in a neighbourhood Ω^- of the object, and uniform in the exterior domain Ω^+. The common boundary between Ω^- and Ω^+ is a Lipschitz surface denoted Γ_∞. The flow is continuous through Γ_∞. A monopole source is located in Ω^+

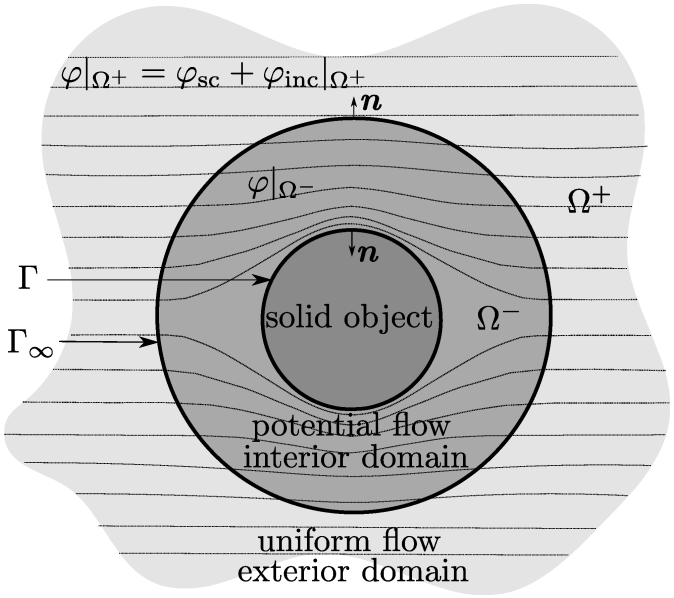

Figure 3: Geometry of the second test-case

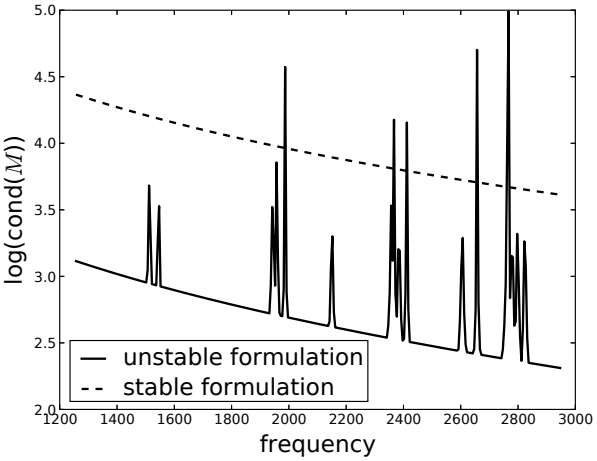

Figure 4: Condition number of the matrices obtained after discretization of the unstable and stabilized formulations

To compute the scattered acoustic field, we first apply a Prandtl–Glauert transformation to kill the convective term in the exterior domain. Then, we write a direct coupling between a FEM resolution in Ω^- and a BEM resolution on Γ_∞. The Prandtl–Glauert transformation enables to recover the classical integral equations for the Helmholtz equation.

It is proven in [2] that the obtained formulation is well-posed, except for given frequencies of the source. We propose a new formulation based on Hipmair and Meury stabilization procedure [5], that is well-posed for all frequency of the source, see Figure 4.

Once we dispose of a well-posed formulation for all frequencies of the source, we can consider a RB strategy for which the frequency is the parameter of interest. Since the dependence of the operator in the frequency is not affine, we have to consider strategies like the Empirical Interpolation Method [6].

3 Conclusion

For our two problems of interest, we derived integral formulations well-posed at all frequencies and for any Lipschitz surface. This enable to consider robust model reduction techniques like the Reduced Basis method. The next step is to use the derived surrogate models in a many queries context, like optimization or propagation of uncertainty.

References

[1] N. Balin, F. Casenave and G. Sylvand, *3D coupled resolution of acoustic waves propagation between a potential flow and uniform flow*, Waves 2011, Conference proceedings.

[2] F. Casenave, A. Ern, T. Lelièvre and G. Sylvand, *A coupled boundary element / finite element method for the convected Helmholtz equation with non-uniform flow in a bounded domain*, submitted.

[3] F. Casenave, A. Ern and T. Lelièvre, *Accurate and efficient evaluation of the a posteriori error estimator in the reduced basis method*, submitted, `http://arxiv.org/abs/1212.0970`.

[4] M. Fares, J.S. Hesthaven, Y. Maday, and B. Stamm. The reduced basis method for the electric field integral equation. *Journal of Computational Physics*, 230(14):5532 – 5555, 2011.

[5] R. Hiptmair and P. Meury, *Stabilized FEM-BEM coupling for Helmholtz transmission problems*. SIAM J. Numer. Anal., 44(5):2107–2130, 2006.

[6] M. Barrault, Y. Maday, N.C. Nguyen and A.T. Patera, *An empirical interpolation method: application to efficient reduced-basis discretization of partial differential equations*. Comptes Rendus Mathematique, 339(9):667–672, 2004.

An Efficient Multigrid Calculation of the Far Field Map for Helmholtz Equations

S. Cools[1,*], **B. Reps**[1,2] **and W. Vanroose**[1,*]
[1] Dept. Math. & Comp. Sc., University of Antwerp, Middelheimlaan 1, 2020 Antwerp, Belgium
[2] Intel® ExaScience Lab, Kapeldreef 75, B-3001 Leuven, Belgium.
*Email: siegfried.cools@ua.ac.be, wim.vanroose@ua.ac.be

Abstract
In this work we present a new highly efficient calculation method for the far field amplitude patterns that arise from scattering problems governed by the d-dimensional Helmholtz equation. The method is based upon a reformulation on a complex contour of the standard real-valued Green's function integral expression for the far field amplitude. On this complex contour the scattered wave can be calculated efficiently using the iterative multigrid method, resulting in a fast and scalable calculation of the far field mapping. The new approach is successfully validated on model problems in two and three spatial dimensions.

Introduction
This paper focuses on calculating the far field map resulting from a Helmholtz scattering problem. The calculation of the far field mapping is typically a two step process. First a Helmholtz problem with absorbing boundary conditions (PML, ECS) is solved on a finite numerical box covering the object of interest. In the second step a volume integral over the Green's function involving the numerical solution yields the angular dependency of the far field amplitude. The main computational bottleneck generally lies within the first step, since it requires a suitable (iterative) method for the solution of a high dimensional indefinite Helmholtz system.
Preconditioned Krylov subspace methods are currently among the most efficient numerical algorithms for the solution of high dimensional positive definite systems. A generalization of this approach led to the development of the Complex Shifted Laplacian (CSL) preconditioner, proposed in [1] as an effective Krylov subspace method preconditioner for Helmholtz problems. The key idea behind CSL is the formulation of a perturbed Helmholtz problem which includes a complex valued wave number. This implies a damping in the problem, thus making the preconditioning system solvable using multigrid in contrast to the original Helmholtz problem. Recently a variation on CSL by the name of Complex Stretched Grid (CSG) was proposed [2], introducing a complex valued grid distance (complex rotation) in the preconditioner.
The far field map computation proposed in this work reformulates the integral over the Green's function on a complex contour. Hence, one requires the solution of the Helmholtz equation on a complex contour. It is shown that the latter problem is equivalent to a CSL problem that can be solved very efficiently using a multigrid method. However, whereas CSL was previously only used as a preconditioner, the proposed complex-valued far field map calculation effectively allows for multigrid to be used as a solver.

1 The far field map for Helmholtz problems

The Helmholtz equation is a mathematical representation of the physics behind a wave scattering at an object O located within a domain $\Omega \subset \mathbb{R}^d$. The equation is

$$\left(-\Delta - k^2(\boldsymbol{x})\right) u(\boldsymbol{x}) = k_0^2 \chi(\boldsymbol{x}) u_{in}(\boldsymbol{x}), \quad \boldsymbol{x} \in \Omega, \quad (1)$$

where $\chi(\boldsymbol{x}) = (k^2(\boldsymbol{x}) - k_0^2)/k_0^2$ represents the object of interest. Note that $\chi(\boldsymbol{x}) = 0$ for $\boldsymbol{x} \in \Omega \setminus O$. The above equation can in principle be solved in a numerical box (i.e. a discretized subset of Ω) covering the support of χ, with absorbing boundary conditions along all boundaries, yielding a numerical solution denoted by u^N. The far field scattered wave then satisfies the following inhomogeneous Helmholtz equation with constant wave number

$$\left(-\Delta - k_0^2\right) u(\boldsymbol{x}) = g(\boldsymbol{x}), \quad \boldsymbol{x} \in \mathbb{R}^d, \quad (2)$$

where $g(\boldsymbol{x}) = k_0^2 \chi(\boldsymbol{x})(u_{in}(\boldsymbol{x}) + u^N(\boldsymbol{x}))$. The analytical solution to (2) is given by the Green's integral

$$u(\boldsymbol{x}) = \int_\Omega G(\boldsymbol{x}, \boldsymbol{x}')\, g(\boldsymbol{x}')\, d\boldsymbol{x}', \quad \boldsymbol{x} \in \mathbb{R}^d. \quad (3)$$

Consequently, the asymptotic form of the scattered wave in the direction of the unit vector $\boldsymbol{\alpha} \in \mathbb{R}^d$ is

$$\lim_{\rho \to \infty} u(\rho, \boldsymbol{\alpha}) = D(\rho) F(\boldsymbol{\alpha}), \qquad \boldsymbol{\alpha} \in \mathbb{R}^d, \quad (4)$$

where the far field (amplitude) mapping is given by

$$F(\boldsymbol{\alpha}) = \int_\Omega e^{-ik_0 \boldsymbol{x}' \cdot \boldsymbol{\alpha}} g(\boldsymbol{x}')\, d\boldsymbol{x}'. \quad (5)$$

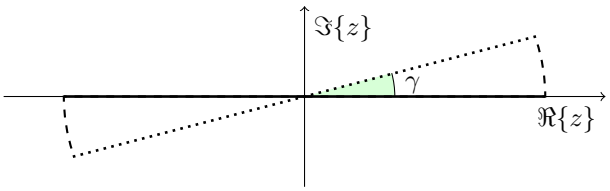

Figure 1: Classical real domain and complex contour far field integral calculation.

$n_x \times n_y \times n_z$	16^3	32^3	64^3	128^3	256^3
CPU time	0.20 s.	0.78 s.	6.24 s.	53.3 s.	462 s.
$\|r\|_2$	3.3e-5	7.9e-5	2.7e-5	1.1e-5	4.6e-6

Table 1: 3D Helmholtz problem solved using one FMG-cycle with GMRES(3) smoother. CPU time and residual norm for various discretizations.

2 Calculation on a complex contour

The far field integral (5) can be split into a sum of two contributions $F(\boldsymbol{\alpha}) = I_1 + I_2$, where

$$I_1 = \int_\Omega e^{-ik_0 \boldsymbol{x}\cdot\boldsymbol{\alpha}} \chi(\boldsymbol{x}) u_{in}(\boldsymbol{x}) d\boldsymbol{x}, \tag{6}$$

$$I_2 = \int_\Omega e^{-ik_0 \boldsymbol{x}\cdot\boldsymbol{\alpha}} \chi(\boldsymbol{x}) u^N(\boldsymbol{x}) d\boldsymbol{x}. \tag{7}$$

Calculation of first integral I_1 is generally easy, since it only requires the expression for the incoming wave. The second integral however requires the solution u^N of the Helmholtz equation on the numerical box, which is known to be notoriously hard to obtain using present-day iterative methods. However, if both u and χ are analytical functions, the integral I_2 can be calculated over a complex contour defined by the rotated real domain $Z_1 = \{\boldsymbol{z} \in \mathbb{C} \,|\, \boldsymbol{z} = \boldsymbol{x}e^{i\gamma} : \boldsymbol{x} \in \Omega\}$, where γ is a fixed rotation angle, followed by the curved segment $Z_2 = \{\boldsymbol{z} \in \mathbb{C} \,|\, z = \boldsymbol{b}e^{i\theta} : \boldsymbol{b} \in \partial\Omega,\ 0 \leq \theta \leq \gamma\}$, as presented schematically on Figure 1. The integral I_2 can then be written as

$$I_2 = \int_{Z_1} e^{-ik_0 \boldsymbol{z}\cdot\boldsymbol{\alpha}} \chi(\boldsymbol{z}) u^N(\boldsymbol{z}) d\boldsymbol{z}, \tag{8}$$

where the integral over Z_2 has vanished because χ is per definition zero everywhere outside O, thus notably in all points of Z_2. The advantage of this approach is that we only need the value of u^N evaluated along this complex contour, where equation (1) is reduced to a damped equation. This problem is equivalent to a CSL problem, and can thus be solved very efficiently using multigrid, resulting in a fast and scalable computation of the far field mapping.

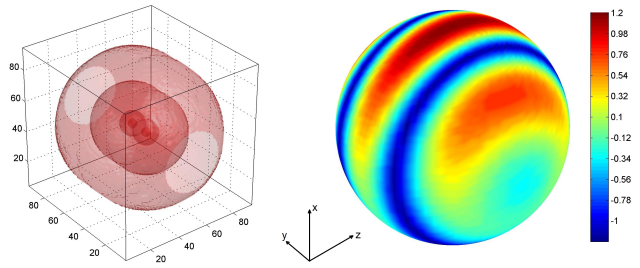

Figure 2: Left: 3D object of interest $|\chi(\boldsymbol{x})|$. $|\chi(\boldsymbol{x})| = c$ isosurfaces for $c =$ `0`, `1e-2`, `1e-10` and `1e-100`. Right: 3D Far field map.

3 Numerical results

The theoretical result presented above is validated on a Helmholtz scattering problem on a 3D cubic domain $\Omega = [-20, 20]^3$ with an object of interest

$$\chi(x, y, z) = -\frac{1}{5}\left(e^{-(x^2+(y-4)^2+z^2)} + e^{-(x^2+(y+4)^2+z^2)}\right)$$

with $(x, y, z) \in \Omega$, representing two spherical point-like objects in 3D space. The incoming wave is defined by

$$u_{in}(\boldsymbol{x}) = e^{ik_0 \boldsymbol{\eta}\cdot\boldsymbol{x}}, \quad \boldsymbol{x} \in \Omega, \tag{9}$$

where $\boldsymbol{\eta}$ is the unit vector in the x-direction. The resulting far field map for $k_0 = 1$ is shown on Figure 2. The complex-valued Helmholtz problem was solved on a $n_x \times n_y \times n_z = 64 \times 64 \times 64$ full complex grid with $\gamma \approx 10°$ using a series of multigrid V-cycles with GMRES(3) smoother up to a residual reduction tolerance of `1e-6`.

Acknowledgments

This research was funded by the *Fonds voor Wetenschappelijk Onderzoek (FWO)* project G.0.120.08 and *Krediet aan navorser* project number 1.5.145.10. Additionally, this work was partly funded by Intel® and by the *Institute for the Promotion of Innovation through Science and Technology in Flanders (IWT).*

References

[1] Y.A. Erlangga, C.W. Oosterlee and C. Vuik, *On a class of preconditioners for solving the Helmholtz equation*, App. Num. Math., **50**(3-4), 2004, pp. 409–425.

[2] B. Reps, W. Vanroose and H. bin Zubair, *On the indefinite Helmholtz equation: Complex stretched absorbing boundary layers, iterative analysis, and preconditioning*, J. Comput. Phys., **229**(22), 2010, pp. 8384–8405.

[3] S. Cools, B. Reps and W. Vanroose, *An efficient multigrid calculation of the far field map for Helmholtz problems*, arXiv:1211.4461.

An efficient Multigrid calculation of the Far Field Map for Schrödinger Equations

W. Vanroose*, **S. Cools and B. Reps**
Department Mathematics and Computer Science,
Universiteit Antwerpen
Middelheimlaan 1, 2020 Antwerpen, Belgium
*Email: wim.vanroose@ua.ac.be

Abstract. In this paper we illustrate how the far field map of a high-dimensional Schrödinger equation can be calculated with the help of a complex valued contour integral. The advantage of the method is that the Schrödinger equation along this contour can be solved with multigrid, an iterative method for sparse linear systems. The method is validated on a model problem and gives the same numerical results as traditional methods but it has a better scalability.

Introduction. Predicting the outcome of collisions between small atomic and molecular systems is of fundamental importance for many areas of science. Understanding their dynamics is crucial for plasma physics, combustion and electron driven chemistry, amongst other examples. However, it is computationally very challenging to predict from first principles the outcome of these collisions since it requires the solution of high–dimensional Schrödinger equations. These are hard to solve even with state-of-the-art iterative methods. To calculate, for example, the breakup reaction rates of the hydrogen molecule requires the solution of a 7–dimensional scattering problem. The reaction rates, also known as the cross sections, are the far field amplitudes of the solution. The development of efficient solvers for this problem remains an important challenge. In this talk we discuss the development of solvers for these scattering problems based on multigrid.

The Schrödinger equation in d-dimensions is

$$(-\frac{1}{2}\Delta + V(\mathbf{x}) - E)\psi(\mathbf{x}) = \phi(\mathbf{x}), \quad \text{for} \quad \mathbf{x} \in \mathbb{R}^d \quad (1)$$

where $V(\mathbf{x})$ is the potential, ψ is the wave function and ϕ is the right hand side that is related to the initial state of the system.

Solving the equation on a complex contour. Scattering problems are described by solutions of (1) with a positive energy E and for these energies the equation is equivalent to a Helmholtz equation

$$(-\Delta - k^2(\mathbf{x}))u = f(\mathbf{x}) \quad (2)$$

with a wave number $k^2(\mathbf{x}) = 2\,(E - V(\mathbf{x}))$ solved with absorbing boundary conditions.

In atomic and molecular scattering problems the use of Exterior Complex Scaling (ECS) as absorbing boundary conditions is wide spread [2], [3]. In ECS the coordinates beyond a certain radius are rotated into the complex plane. This makes outgoing waves decaying and allows the application of homogeneous Dirichlet boundary conditions at the end of the absorbing layers. This is a form of complex stretching as in Chew and Weedow [4].

The far field amplitudes indicate the probability of detecting a certain reaction product with a given energy at a certain space angle in the experiment. The typical calculation is a two step proces [2], [3]. First, the scattering equation is solved on a finite numerical box with absorbing boundary conditions. The box size covers the support of the right hand side of the equation so that it is zero before the start of the absorbing boundary condition. In the second step an integral over the product of a Greens function and the numerical solution is calculated resulting in the far field map.

The first step is computationally most expensive since it requires the solution of a very large sparse linear system that is indefinite and non-Hermitian due to the absorbing boundary condition. For these problems iterative methods such a Krylov methods converge poorly and multigrid fails all together.

However, recent advances in the solution of the Helmholtz problems such as the Complex Shifted Laplacian preconditioner [5] can help us to solve the problem. In these shifted problems the wave number is multiplied with a complex shift such that the Helmholtz equation becomes

$$(-\Delta - (1 + i\beta)k^2(\mathbf{x}))u = f(\mathbf{x}) \quad (3)$$

where the rule of thumb is to take $\beta > 0.5$. Due to the complex shift the problem can be solved by multigrid and (3) is often used as a preconditioner [5].

However, it can also be used as a solver [1]. If the volume integral for the far field map is formulated along a complex contour only the numerical

solution of a complex shifted Schrödinger equation is required to calculate the far field amplitude. Indeed, the potentials in the Schrödinger equation are usually analytical functions so the far field map integral can be calculated along a Complex Scaling contour instead of an Exterior Complex Scaling contour. Result is that the Schr"odinger equation only needs to be solved along the complex scaling contour where it is equivalent to a Complex Shifted Helmholtz problem [1] and can be solved with multigrid.

Numerical Validation. To validate the new approach we illustrate the approach on a model Schrödinger equation derived from a partial wave expansion of a three body problem. The equation is

$$\begin{cases} \left(-\frac{1}{2}\frac{\partial^2}{\partial x^2} - \frac{1}{2}\frac{\partial^2}{\partial x^2} + V(x) + V(y) \right. \\ \left. +V_{12}(x,y) - E\right)\psi(x,y) = \phi(x,y) \quad x,y \geq 0, \\ \psi(x,0) = 0 \quad \forall x \geq 0, \\ \psi(0,y) = 0 \quad \forall y \geq 0, \end{cases} \tag{4}$$

where $V(x) = -4.5\exp(-x^2)$ and $V_{12}(x,y) = 2\exp(-(x+y)^2)$. The coordinates x, y must be interpreted as two radial coordinates.

The system has a single ionized bound state with energy -1.0215. For energies $E = -1.025$ between $E = 0$, the scattering states are single ionization states that are localized along the edges of the problem where either x or y is small. These are solutions of the Schrödinger equation that correspond to a quantum state where one particle is in a bound state and the second particle is in a scattering state. These solution are oscillatory in on direction and smooth in the other direction. They can also be interpreted as evanescant waves. The amplitude of these waves as a function of the energy is shown in Fig. 1.

For energies above $E > 0$ there are both single ionization and double ionization and result in scattering solutions that cover the whole domain. This results in a double ionization amplitude also shown in Fig. 1.

The figure also shows these amplitude calculate with the new method (abbreviated with CC). Both agree with the results calculated in the traditional way. The red line shows the total cross section, single and double ionization calculated with the optical theorem.

Conclusions. This paper discusses the initial application of the complex contour multigrid method originally proposed for the Helmholtz equation in [1] to solve the scattering solution of the Schrödinger

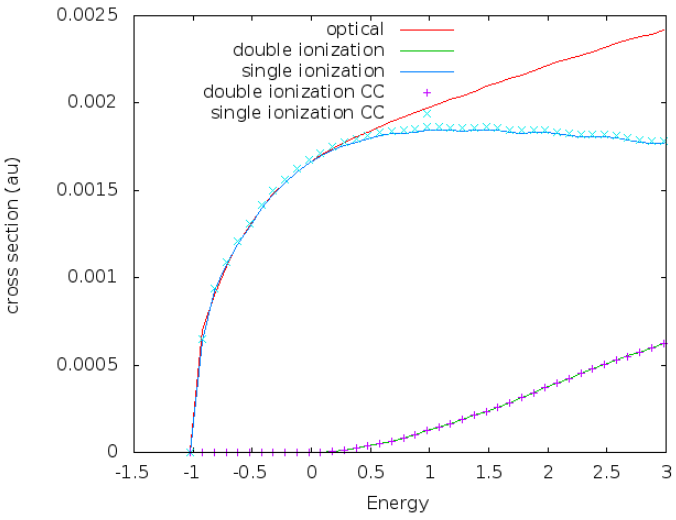

Figure 1: Total cross section for single and double ionization as a function of the energy E for the model problem. The single and double ionization cross sections are calculate both through the traditional way and over the complex valued contour. The later solves the scattering equation along a complex contour and evaluates the integral for the far field along this contour.

equation. The proposed method is attractive since the equation can be solved with a multigrid solver. In this paper we have validated the approach and shown that the results agree with a traditional ECS calculation.

However, further work is necessary to illustrate its performance for problems with long range potentials such as Coulomb potentials that appear in all realistic problems.

References

[1] S. Cools, B. Reps and W. Vanroose, arxiv:1211.4461 (2012).

[2] T.N. Rescigno, M. Baertschy, W.A. Isaacs and C.W. McCurdy, Science, 286, p 2474 (1999).

[3] W. Vanroose, F. Martin, T.N. Rescigno, Science, 310, p 1787, (2005).

[4] W.C. Chew and W.H. Weedon, Microwave and optical technology letters, 7, p599 (1994).

[5] Y.A Erlangga, C.W. Oosterlee and C. Vuik, SIAM journal on Scientific Computing, 27 p 1471 (2006).

Computing Fresnel Integrals via Modified Trapezium Rules

M. Alazah[1,*], **S.N. Chandler-Wilde** [1], **S. La Porte**[2]
[1]University of Reading, UK
[2] Brunel University, UK
*Email: M.A.M.AlAzah@pgr.reading.ac.uk

Abstract

We propose methods for computing Fresnel integrals based on modified trapezium rule approximations to integrals on the real line. Our approximations are exponentially convergent as a function of N, the number of quadrature points, with an explicit error bound which shows that relative accuracies of 10^{-15} uniformly on the real line are achievable with $N = 12$, this confirmed by numerical computations. The approximations we obtain are attractive, additionally, in that they are analytic on the real axis (echoing the analyticity of the Fresnel integrals), and are straightforward to implement.

Introduction

The trapezium rule can be a very accurate method to approximate integrals of the form

$$\int_{-\infty}^{\infty} f(t)\mathrm{e}^{-t^2}\,\mathrm{d}t. \tag{1}$$

In particular, it is well known – the proof uses contour integration and Cauchy's residue theorem and dates back to Turing [1] – that the trapezium rule is exponentially convergent when f is analytic and bounded in a strip surrounding the real axis.

Let $C(x)$, $S(x)$, and $F(x)$ be the Fresnel integrals defined by

$$C(x) := \int_0^x \cos\left(\tfrac{1}{2}\pi t^2\right)\,\mathrm{d}t,\ S(x) := \int_0^x \sin\left(\tfrac{1}{2}\pi t^2\right)\,\mathrm{d}t, \tag{2}$$

and

$$F(x) := \frac{\mathrm{e}^{-\mathrm{i}\pi/4}}{\sqrt{\pi}}\int_x^{\infty} \mathrm{e}^{it^2}\,\mathrm{d}t. \tag{3}$$

F, C, and S are related through

$$\sqrt{2}\,\mathrm{e}^{\mathrm{i}\pi/4}F(x) = \tfrac{1}{2} - C\left(\sqrt{2/\pi}\,x\right) + \mathrm{i}\left(\tfrac{1}{2} - S\left(\sqrt{2/\pi}\,x\right)\right), \tag{4}$$

and our normalisation of F is such that

$$F(x) = 1 - F(-x). \tag{5}$$

Fresnel integrals arise in applications throughout science and engineering, especially in problems of wave diffraction and scattering, so that methods for the efficient and accurate computation of these functions are of wide application.

1 New Methods for Fresnel Integrals

Our approximation of $F(x)$ is built on a method for computation of the complementary error function of complex argument developed by Matta and Reichel [3] and improved by Hunter and Regan [4]. Both these papers propose modifications of the trapezium rule in the case where the integrand has a pole singularity near the real line. These modifications follow naturally, as residue contributions, from the contour integration arguments used to prove that the trapezium rule is exponentially convergent. The starting point for applying the method of [4] is the well-known integral representation (*e.g.*, [4])

$$F(x) = \frac{x}{2\pi}\,\mathrm{e}^{\mathrm{i}(x^2+\pi/4)}\int_{-\infty}^{\infty}\frac{\mathrm{e}^{-t^2}}{x^2+\mathrm{i}t^2}\,\mathrm{d}t, \quad \text{for } x > 0. \tag{6}$$

Our approximation to $F(x)$ is an extension and truncation of the modified trapezium rule approximation of [4] applied to (6). Our approximation is analytic on the real line, in contrast to the piecewise analytic approximation of [4], and our approximation is fully explicit in that we make clear how the trapezium rule step-size should be chosen given a choice of the number of terms $(2N+1)$ to retain in the trapezium rule sum. Explicitly our approximation (see [2]) can be written as

$$F_N(x) = \frac{1}{\exp\left(2A_N x\mathrm{e}^{-\mathrm{i}\pi/4}\right)+1} \tag{7}$$

$$+\frac{x}{A_N}\,\mathrm{e}^{\mathrm{i}(x^2+\pi/4)}\sum_{k=1}^{N}\frac{\mathrm{e}^{-t_k^2}}{x^2+\mathrm{i}t_k^2}, \tag{8}$$

where

$$t_k := \frac{(k-1/2)\,\pi}{\sqrt{(N+1/2)\,\pi}}, \quad A_N := \sqrt{(N+1/2)\pi}. \tag{9}$$

The corresponding approximations to $C(x)$ and $S(x)$ are obtained by substituting this approximation in (4) and separating real and imaginary parts. We note that, echoing (5),

$$F_N(x) = 1 - F_N(-x), \tag{10}$$

so that $F_N(0) = F(0) = 1/2$. Matlab functions for evaluating these approximations are given in [2]. These use (7) for $x \geq 0$ and then extend the approximation to the negative real axis using (10).

2 Error bounds

Our main numerical analysis result is the following bound on the relative error:

Theorem 1 *For the Fresnel integral $F(x)$ and its approximation $F_N(x)$ we have that, for all real x,*

$$\frac{|F(x) - F_N(x)|}{|F(x)|} \leq c_N^* e^{-\pi N}. \tag{11}$$

Here c_N^* is a decreasing sequence of positive constants given explicitly in [2], with $c_1^* \approx 10.4$ and $\lim_{N\to\infty} c_N^* = 100\mathrm{e}^{-\pi/2}/9 \approx 2.3$. The derivation of this result makes use of a bound on the absolute error and a new sharp lower bound on $|F(x)|$ for $x \geq 0$ (see [2] for details).

The bound (11) shows exponential convergence of the relative error, $|F_N(x) - F(x)|/|F(x)|$, uniformly on the real line, in particular that the relative error is $\leq 1.6 \times 10^{-16}$ on the whole real line if $N = 12$.

3 Numerical Results

Numerical computations in [2] confirm and illustrate the theoretical error bound (11), and explore the accuracy and efficiency of our new method. We present some of these results below.

In Figure 1 we plot against x the relative error in $F_N(x)$ for $N = 9$ and the rigorous pointwise upper bound that is equation (51) in [2]. We see that the theoretical error bound is an upper bound as claimed, and that the theoretical upper bound captures the shape of the behaviour of the true error. In Figure 2 we plot against N the maximum value of the relative error, $|F(x) - F_N(x)|/|F(x)|$, on $x \geq 0$, approximating this maximum value on $[0, \infty)$ by computing at 40,000 equally spaced points between 0 and 1,000 and replacing $F(x)$ by $F_{20}(x)$. It can be seen that the exponential convergence predicted by the bound (11) is achieved, indeed this bound overestimates the maximum relative error by at most a factor of 10. Further, with N as small as 12 it appears that we achieve a maximum relative error in $F_N(x)$ which is $< 9.3 \times 10^{-16}$.

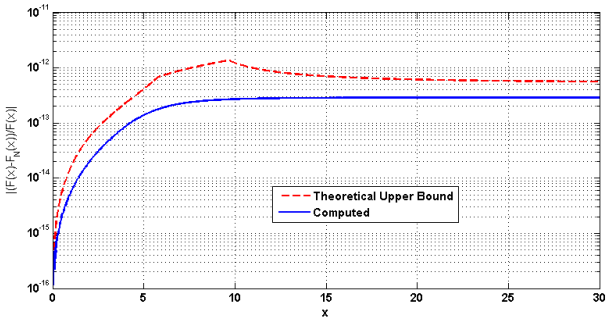

Figure 1: Relative error, $|(F(x) - F_N(x))/F(x)|$, and its upper bound (51) in [2] (−), plotted against x. Here $N = 9$ and $F(x)$ is approximated by $F_{20}(x)$.

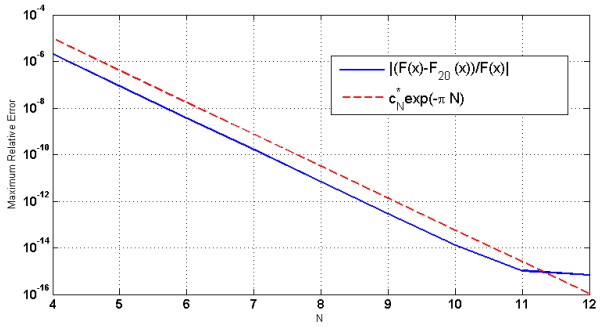

Figure 2: Maximum relative error, $\max_{x\geq 0} |(F(x) - F_N(x))/F(x)|$, and its upper bound (11) (−−), plotted against N, where $F(x)$ is approximated by $F_{20}(x)$.

References

[1] Turing, A. M.: A method for the calculation of the zeta-function, Proc. London Math. Soc. **s2-48**, 180–197 (1943)

[2] M. Alazah, S. N. Chandler-Wilde and S. La Porte, *Computing Fresnel Integrals via Modified Trapezium Rules*, Preprint MPS-2012-20

[3] F. Matta, A. Reichel, *Uniform computation of the error function and other related functions*,J. Math. Phys. **34**, 298–307 (1956)

[4] D. B.Hunter, T. Regan, *A note on evaluation of the complementary error function*, Math. Comp. **26**, 539–541 (1972)

Embedding Circular Material Interfaces in Rectangular Domain Boundaries in Structured Finite-Difference Discretisations of Maxwell's Equations

R. B. Armenta*
Department of Mathematics, Simon Fraser University, Burnaby, BC, Canada
*E-mail: rarmenta@sfu.ca

Abstract

This contribution outlines a robust strategy to generate a structured nonorthogonal finite-difference discretisation of the differential form of Maxwell's equations when a circular material interface is present inside a problem domain with rectangular boundaries.

Introduction

Solving a system of PDEs using a structured discretisation grid when an object with a circular shape is embedded in rectangular domain boundaries can be a challenging problem [1]. This manuscript describes the key issues that must be considered in order to generate a structured nonorthogonal finite-difference discretisation of Maxwell's equations in 2-D when a circular material interface is present inside a problem domain with rectangular domain boundaries. Most of the previously proposed strategies resort to a polygonal approximation of the circular interface to facilitates the enforcement of the field continuity conditions (*e.g.* [2, 3]); however, by using a suitable coordinate mapping and staircased overlapping grid partitions, it is possible to create a structured finite-difference discretisation without introducing any polygonal approximations. The motivation for proposing a new approach that avoids the introduction of geometrical approximations is that, when the geometrical representation of the material interfaces and boundaries of a problem is exact, the global error behaviour is dominated by the local truncation error of the finite-difference approximations used to discretise the partial derivatives of Maxwell's equations rather than by the crudeness of the geometrical representation of the interfaces and boundaries of the problem. This opens up the possibility of exploiting high-order approximations effectively.

Proposed Strategy

Under a structured approach [4], the general strategy for incorporating curved material interfaces and boundaries is to employ a spatial mapping

$$x^p \to u^q \quad \text{for} \quad p, q = 1, 2 \tag{1}$$

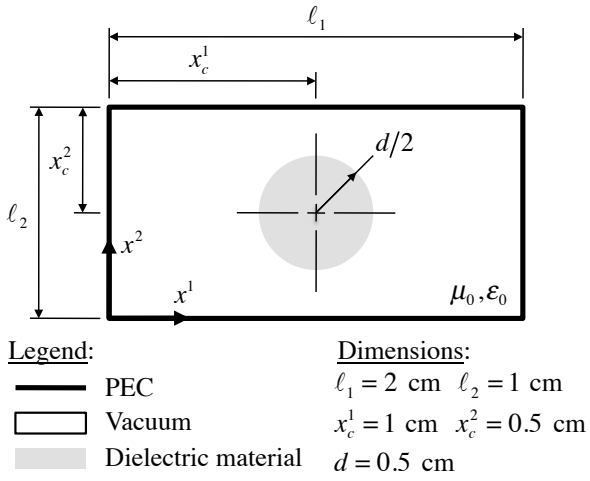

Fig. 1: 2-D cavity with perfect electric conductor (PEC) boundaries and a circular vacuum-dielectric interface.

where u^q stands for the coordinates of a general curvilinear coordinate system and x^p for the two Cartesian coordinates ($x^1 = x$ and $x^2 = y$). The mapping is constructed in such a way that all the material interfaces and boundaries of the problem can be described by u^q coordinate lines, that is to say, by lines specified by equations of the form

$$u^q = \text{constant} \quad \text{for} \quad q = 1, 2. \tag{2}$$

By constructing (1) in this way, a uniform finite-difference discretisation with respect to the u^q coordinates maps onto a structured nonorthogonal discretisation in Cartesian coordinates where the grid cells conform to the curvature of the material interfaces and boundaries of the problem. This approach is easy to formulate when the mapping in (1) transforms the metric tensor from a Kronecker delta in Cartesian coordinates to a second-rank tensor, g_{pq} for $p, q = 1, 2$, whose components are discontinuous only along coordinate lines; however, to have the ability to place a circular material interface inside a domain with rectangular boundaries, it is necessary to allow the components of the metric tensor to have a discontinuity that cuts diagonally across the computational domain along a line described by

$$u^q = \pm u^p + \text{constant} \quad \text{for} \quad p \neq q. \tag{3}$$

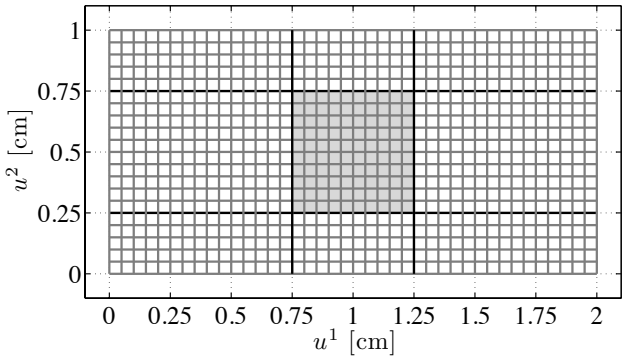

(a)

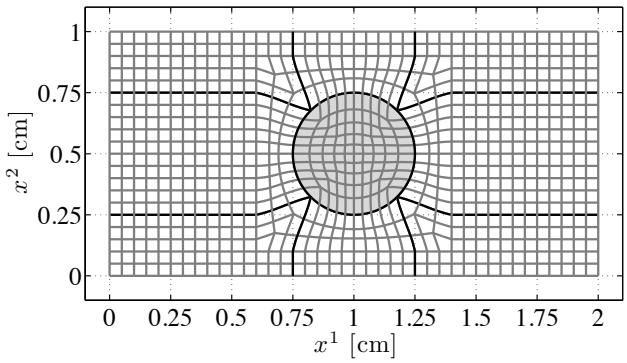

(b)

Fig. 2: Plots for a mapping that can be used to model the problem described in Fig. 1. The coordinate lines plotted in (a) map to the lines plotted in (b).

To illustrate this point, consider the 2-D structure in Fig. 1. Coordinate line plots for one of the mappings that can be used to model this structure are provided in Fig. 2; the mapping was generated by making small modifications to the mapping proposed in [1]. When the coordinate mapping described in Fig. 2 is employed, the metric tensor components are discontinuous along the six black lines marked in Fig. 3. Such discontinuities are the result of employing coordinate lines that have sudden changes in direction (see Fig. 2 (b)). A discontinuity in the metric tensor that lies along a coordinate line can be handled through a conventional grid partition with overlapping regions [5]; nonetheless, when a discontinuity lies along a diagonal line, it is necessary to staircase the grid partition in the adjacent regions to accommodate the structure of the discontinuity. For this reason, when employing the mapping described in Fig. 2, the computational domain must be partitioned as shown in Fig. 3. It is important to understand that staircasing a grid partition is not the same as staircasing the geometry of the circular interface (a strategy that is often employed when discretising directly in Cartesian coordinates). The point of

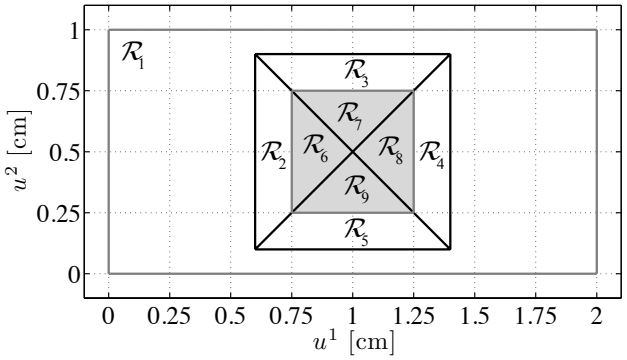

Fig. 3: Proposed partition of the computational domain.

partitioning the computational domain is to create overlapping extensions of the grid along the boundaries of each region (which are typically only a few cells wide) as a way to generate smooth overlapping extensions of the electric and magnetic field profiles that make explicit use of the field continuity conditions to cope with sudden changes in the structure of the metric tensor.

Conclusion

To summarise, the partition of the computational domain outlined in Fig. 3 and the mapping described in Fig. 2 can be used to embed a circular material interface in a rectangular domain without making any polygonal approximations of the interface. Such feature is attractive because it opens up the possibility of exploiting high-order finite-difference approximations in a meaningful way.

References

[1] D. A. Calhoun, C. Helzel and R. J. Leveque, *Logically Rectangular Grids and Finite Volume Methods for PDEs in Circular and Spherical Domains*, SIAM Rev., **50** (2008), pp. 723-752.

[2] S. Dey and R. Mittra, *A Conformal Finite-Difference Time-Domain Technique for Modeling Cylindrical Dielectric Resonators*, **47** (1999), pp. 1737-1739.

[3] A. Mohammadi, H. Nadgaran and M. Agio, *Contour-Path Effective Permittivities for the Two-Dimensional Finite-Difference Time-Domain Method*, Optics Express, **13** (2005), pp. 10367-1038.

[4] M. Farrashkhalvat and J. P. Miles, *Basic Structured Grid Generation*, Butterworth-Heinemann, New York, 2002.

[5] R. B. Armenta and C. D. Sarris, *in Proc. of the 2012 IEEE MTT-S International Microwave Symposium.* © IEEE. doi: 10.1109/MWSYM.2012.6258425.

Approximations to wave propagation problem in the waveguide with statistically rough walls

A. Krynkin[1,*], **K. Horoshenkov**[1]
[1] School of Engineering, Design and Technology, University of Bradford, Bradford, UK
*Email: a.krynkin@bradford.ac.uk

Abstract

In this paper the wave propagation problem is studied for the rectangular waveguide with randomly rough walls. Using the perturbation method and Fourier analysis the eigenvalue correction consistent with that obtained by Bass et al.[1] is derived. The approach is based on the asymptotically consistent boundary-value problems at each asymptotic order and it does not involve the Dyson-type integral equations. The eigenvalue correction describes the attenuation factor in the studied waveguide and it depends on the correlation function of the randomly rough surface. In the plane wave regime the approximations are compared with the numerical results obtained with the finite element method (FEM).

Introduction

The scattering of waves by randomly rough surface has been analyzed with different approaches[2]. For the case of single reflection (i.e. half-space bounded by the rough surface) the small perturbation method (SPM) and Kirchhoff approximations have been developed to find the analytical solution of the wave problem[1], [3], [4].

In the case of multiple reflections occurring in the waveguide with small irregularities SPM can be applied. In works written by Isakovich [5] and Lapin [6] the finite rough section of the waveguide wall is replaced by the extraneous sources and the wave problem is solved with SPM that allows obtaining the intensity of the scattered wave field. The averaged scattered wave field as well as the dispersion relation have been also obtained with SPM [7]. Based on the randomly rough small roughness the Dyson-type integral equation can also be derived to find the Green function and the dispersion relation that involves mass operator of the volume scattering [1].

In this paper the wave propagation problem in the rectangular acoustic waveguide with the randomly rough rigid walls is studied. It is assumed that the rough surface is subject to the Gaussian distribution with the small standard deviation σ compared to the waveguide width h and the typical wavelength L where $h \sim L$. This defines the small parameter $\epsilon = \sigma/h \ll 1$. The smallness of the irregularities is used to decompose the acoustic wave field into the deterministic (averaged) p_a and small random components p_r. The application of the Fourier transform and expansion of the transformed components with respect to the small parameter leads to the the asymptotically consistent boundary value problem at each asymptotic order. The derived approach allows obtaining the correction to the eigenvalue ξ_n of the smooth waveguide. The eigenvalue correction characterises the attenuation in the rough waveguide. In the plane wave regime the averaged acoustic pressure can be approximated by the single exponential function dependent on the derived eigenvalue correction. The approximations are compared with the numerical results obtained with FEM. In the numerical approach realizations of the rough section of the waveguide wall are simulated with random number generator in accordance with the normal distribution.

1 Eigenvalue correction

In this study, total acoustic pressure p is the solution of the Helmholtz equation subject to the boundary conditions

$$\frac{\partial p}{\partial z} = 0, \quad \text{at } z = h, \tag{1}$$

$$\left(-\eta_x \frac{\partial}{\partial x} + \frac{\partial}{\partial z}\right) p = 0, \quad \text{at } z = \eta(x), \tag{2}$$

where $\eta(x)$ describes stochastically rough bottom wall and it is function that belongs to the sample space defined by the Gaussian distribution with the standard deviation σ, correlation length l and zero mean value.

The random component of the solution p is generated by the randomly rough surface. Due to the small irregularities the acoustic pressure can be presented as a superposition of the averaged and random wave fields, i.e.

$$p = p_a^{(0)} + \epsilon p_r^{(1)} + \epsilon^2 p_a^{(2)} + \mathcal{O}(\epsilon^3), \tag{3}$$

where in the leading order $p_a^{(0)}$ is the solution for the smooth waveguide, random component $p_r^{(1)}$ is linked

to the first moment of the probability distribution and scattered solution $p_a^{(2)}$ is defined by the second moment of the probability distribution (i.e. correlation function W(x)).

In order to solve the problem for the given wavelength regime (i.e. $h \sim L$) the Fourier transform $\hat{p}(z,\xi) = \int_{-\infty}^{+\infty} p(x,z)\mathrm{e}^{-\mathrm{i}\xi x}\mathrm{d}x$ is applied first. The wavenumber q in the transformed equation is defined through perturbed eigenvalue $q_n = \sqrt{k^2-\xi_n^2} = \pi n/h$ of the smooth waveguide so that $q^2 = q_n^2 + \epsilon^2 q_{n,2}^2 + \mathcal{O}(\epsilon^4)$. Collecting the same order of smallness in the transformed Helmholtz equation and boundary conditions gives asymptotically consistent boundary value problems. By solving them one can derive the perturbed eigenvalue as

$$\xi = \xi_n + \frac{\mathrm{i}}{2}\frac{\sigma^2}{h^2}\sum_{m=0}^{M}\frac{1}{\xi_n\xi_m^+(1+\delta_{0n})(1+\delta_{0m})}\times \qquad (4)$$
$$\left[(k^2-\xi_n\xi_m^+)^2\hat{W}(\xi_n-\xi_m^+) + (k^2+\xi_n\xi_m^+)^2\hat{W}(\xi_n+\xi_m^+)\right],$$

where M corresponds to the total number of propagating modes in the waveguide. In the plane wave regime the averaged solution is approximated by

$$p_a \approx A_0\mathrm{e}^{\mathrm{i}(k+\xi_{0,2})x}. \qquad (5)$$

within which the excitation coefficient $A_0 = 1$ and eigenvalue correction can be reduced to

$$\xi_{0,2} = \frac{\mathrm{i}}{2}\frac{\sigma^2}{h^2}k^2\hat{W}(2k) \text{ and } \hat{W}(\xi) = \sqrt{\pi}l\mathrm{e}^{-\xi^2l^2/4}. \qquad (6)$$

Figure 1 shows that the attenuation of the propagated wave exhibits minimum in the vicinity of the dimensionless frequency parameter $h/\lambda = 0.24$ with $\lambda = 2\pi c/\omega$. This coincides with the maximum of the eigenvalue correction (6) at

$$\frac{h}{\lambda} = \frac{h}{2\sqrt{2}\pi l} \qquad (7)$$

The accuracy of the approximation (5) is within 5% from the numerical result that was obtained with the finite element method. As the parameter h/λ approaches the first cut on value 1/2 the accuracy deteriorates and the solution (5) should include higher order modes.

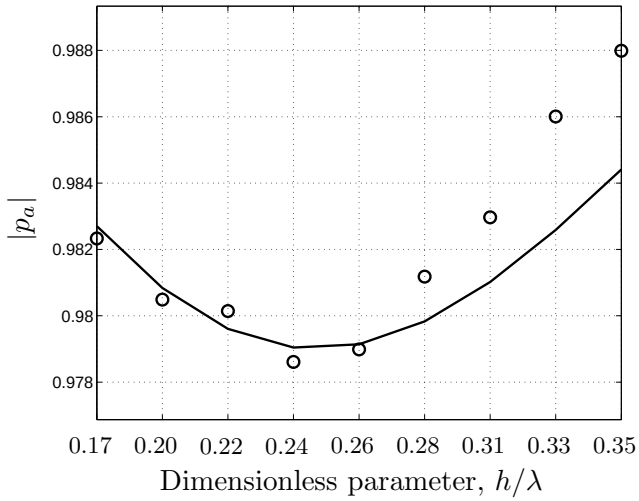

Figure 1: Averaged absolute pressure obtained with FEM ('o') and compared with the approximation (5) ('–') for roughness with $\sigma/h = 0.9/20$ and $l = 1.37d$

References

[1] F. G. Bass and I. M Fuks, *Wave Scattering from Statistically Rough Surfaces*, Pergamon, Oxford, 1979

[2] T.M. Elfouhaily and Charles-Antoine Guerin, *A critical survey of approximate scattering wave theories from random rough surfaces*, Waves Random Media, **14** (2004), R1–R40

[3] M. A. Isakovich, *Wave scattering from a statistically rough surface*, Journal of Experimental and Theoretical Physics, **23** (1952), 305-314 (in Russian)

[4] E.I. Thorsos and D.R. Jackson, *The validity of the perturbation approximation for rough surface scattering using a Gaussian roughness spectrum*, The Journal of the Acoustical Society of America, **86** (1989), 261–277

[5] M. A. Isakovich, "Scattering of acoustic waves at small inhomogeneities in a waveduct", Soviet Physics-Acoustics, **3** 35–45 (1957)

[6] A.D. Lapin, "Sound attenuation in a multimode waveguide by means of periodic wall irregularities and inhomogeneities", Soviet Physics-Acoustics, **23** 515–518 (1977)

[7] G.A. Maximov, E.V. Podjachev, K.V. Horoshenkov, *Attenuation and scattering of axisymmetrical modes in a fluid-filled round pipe with internally rough walls*, The Journal of the Acoustical Society of America, **123** (2008), 1248–1259

Hybrid sweeping preconditioners for the Helmholtz equation

P. N. Childs[1,*], **I. G. Graham**[2,†], **J. D. Shanks**[2‡]
[1] Schlumberger Gould Research, Cambridge UK
[2] University of Bath
*childs4@slb.com †I.G.Graham@bath.ac.uk ‡J.D.Shanks@bath.ac.uk

Abstract

Full waveform inversion (FWI) of seismic data requires repeated solutions of the wave equation in either time or frequency domains. Industry practice is currently to solve the wave equation in the time domain in part due to challenges in devising scalable parallel and fast solvers for the 3D Helmholtz equation. We have investigated the moving perfectly matched layer (PML) sweeping preconditioner of Engquist and Ying [2] and explored modifications for distributed memory clusters. In particular, we use a recursive multilevel form of the sweeping preconditioner coupled with optimized Schwarz methods [4] to avoid issues with distributed memory parallel direct solvers.

Introduction

In seismic inversion, we must solve the wave equation for many different right hand sides: an overview of full waveform inversion is given in [1]. Here we consider the heterogeneous scalar Helmholtz equation $-\frac{\omega^2}{c(x)^2}u - \nabla^2 u = f$, which is well known to be a challenge in designing fast preconditioners [3]. Engquist and Ying [2] proposed the sweeping PML preconditioner for the Helmholtz equation that uses low-rank approximations to half-space Green functions to construct a powerful *fast* preconditioner with complexity $O(N^{\frac{4}{3}})$ setup cost and $O(NlogN)$ per iteration, with $O(NlogN)$ memory requirement. We consider a 3D grid of dimension (n, n, n) with $N = n^3$ the number of unknowns. For 3D models, it is necessary to solve $O(N)$ related quasi-2d problems on slabs of size (n, n, b) where $b = O(1)$. For large-scale parallel applications on a distributed memory cluster, using available parallel direct solvers to factor and solve all the quasi-2D problems in parallel for large n is problematic, not the least because the memory requirement is huge. These methods extend to elastic waves, although we confine this study to the acoustic case in order to explore the key algorithms and parallel implications.

Hybrid preconditioning

Poulson et al. [5] show that a special purpose parallel direct solver, designed around the moving PML problems is very effective for solving 3D problems using the sweeping preconditioner. Here, we investigate replacing the direct solver in each moving PML with a hybrid strategy, aiming to achieve a practical strategy for 3D frequency-domain FWI on general-purpose clusters. Our approach is not weakly scalable.

We explore optimized domain decomposition and recursive application of the sweeping preconditioner, which reduces the work of the direct solver on slabs. Each quasi-2D problem on a slab of size (n, n, b) is decomposed and parallelized in the xy-directions by the optimized Schwarz method of Gander et al [4]. We have a three-level preconditioner: The outer level uses flexible GMRES with the moving PML sweeping preconditioner operating in the z-direction. The second level employs a variant of the optimized Schwarz method of [4] operating across an xy-decomposition in each slab, within a truncated BicgStab or GMRES iterative solver. At the third level, each domain within the Schwarz procedure is further preconditioned by means of a recursive application of the moving PML preconditioner in the x-direction (Figure 1).

We explored truncating the inner solver after a few iterations of the optimized Schwarz method to provide a usable parallel algorithm, with options for multicolouring and overlap. This is ongoing work and conclusions are tentative at this stage, but there are several possibilities for approximation of the transmission conditions in the optimized Schwarz method [4]. The transmission operators are of the form $\frac{\partial}{\partial n}u + Su = 0$ where n is the normal on the domain interface and S is a non-local operator acting along the interface.

Within the moving PML method, it is attractive to explore the PML to construct a DtN operator [6] in the optimized Schwarz method. We compare transmission operators based on Robin conditions and the PML within the sweeping preconditioner. Numerical

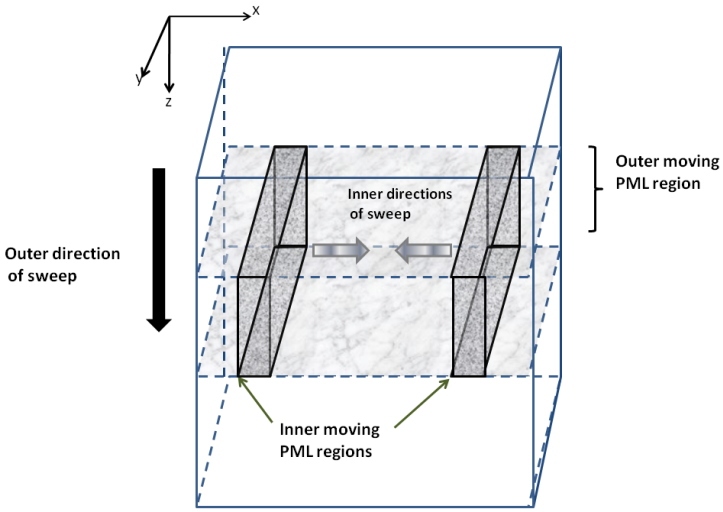

Figure 1: Use of sweeping preconditioner within a single domain. An inner recursive sweep is used within each moving PML

results and preliminary analyses are shown for 3D seismic inversion.

Example

We apply the hybrid preconditioner for the SEG salt model at 7Hz. Figure 2 shows the velocity model. The mesh size is $676\times676\times220$ before adding the PML and employs a Robin condition in the Schwarz iterations. After one outer iteration of the hybrid preconditioner, slices through the wavefield are shown in Figure 3. Here, it was necessary to iterate the second level solver to a 10^{-5} tolerance, imposing a serious performance penalty on the present hybrid method. We are continuing to investigate faster alternatives for parallel inversion applications.

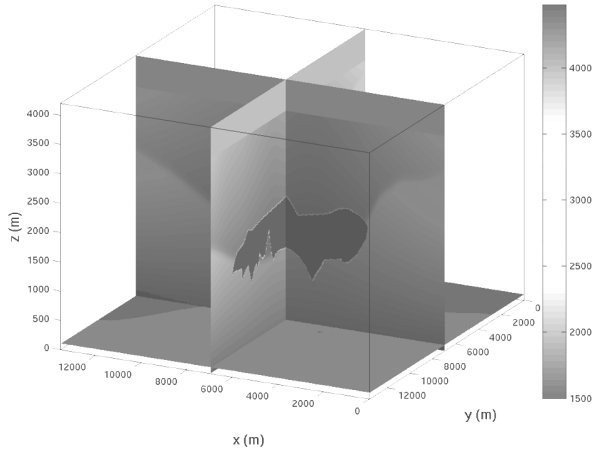

Figure 2: SEG salt model

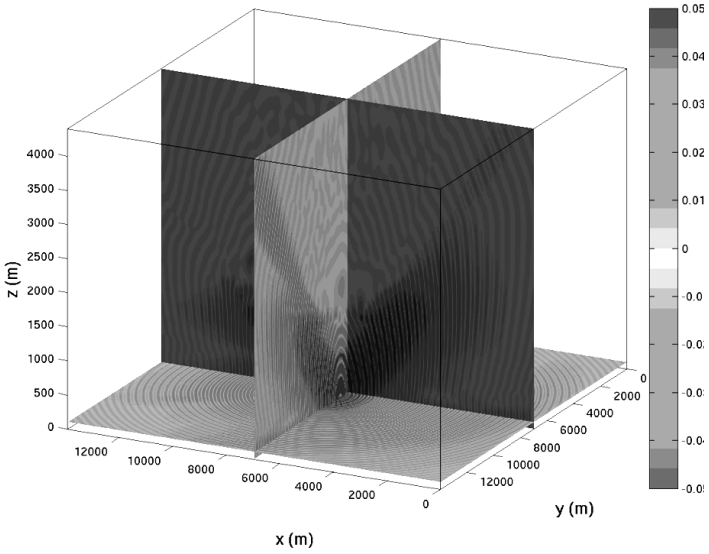

Figure 3: One application of the hybrid sweeping/domain decomposition preconditioner for the SEG model at 7 Hz.

Acknowledgments

We thank Bjorn Engquist, Lexing Ying, Jack Poulson, Martin Gander and Frédéric Nataf for advice.

References

[1] J. Virieux and S. Operto, *An overview of full waveform inversion in exploration geophysics.* Geophysics **74** (2009), pp. WCC127WCC152.

[2] B. Engquist and L. Ying, *Sweeping preconditioner for the Helmholtz Equation: moving perfectly matched layers*, Multiscale Modeling & Simulation, **9** (2011), pp.686–710.

[3] O. Ernst and M. Gander, *Why it is difficult to solve Helmholtz problems with classical iterative methods*, in Analysis of Multiscale Problems, I. Graham, T. Hou, O. Lakkis and R. Scheichl, editors, Springer Verlag (2011).

[4] M. Gander, L. Halpern and F. Magoulès, *An optimized Schwarz method with two-sided Robin transmission conditions for the Helmholtz equation*, Int. J. For Num. Meth. In Fluids, **55** (2007), pp.163–175.

[5] J. Poulson, B. Engquist, S. Fomel, S. Li and L. Ying, *A parallel sweeping preconditioner for high frequency heterogeneous 3D Helmholtz equations*, To appear in SISC (2012).

[6] A. Toselli, *Some results on overlapping Schwarz methods for the Helmholtz equation employing perfectly matched layers*, Courant Institute, TR 765 (1998).

3.12 Absorbing boundary conditions and PMLs

Complete radiation boundary conditions for the Helmholtz equation on a domain with corners

S. Kim[1,*], **T. Hagstrom**[2]
[1] Department of Mathematics, Kyung Hee University, Seoul 130-701, South Korea
[2] Department of Mathematics, Southern Methodist University, Dallas TX 75275, USA
*Email: sikim@khu.ac.kr

Abstract

Complete radiation boundary conditions (CRBCs) are proposed for solving a time-harmonic wave propagation problem in $\mathbb{R}^2$. For numerical computation of wave propagation, the unbounded domain surrounding a wave source is truncated and CRBCs are imposed on the fictitious boundaries. We present that CRBCs provide corner compatibility conditions in case where absorbing boundaries form a corner and verify that the resulting truncated problem supplemented with CRBCs is well-posed. Numerical experiments show that CRBCs are efficient and well-suited for finite elements methods.

Introduction

In this talk, we study the complete radiation boundary conditions applied to time-harmonic wave propagation problems on a domain with corners. The simple model problem under consideration is to find the acoustic pressure u defined in the quarter plane $\Omega_\infty = \{(x,y) \in \mathbb{R}^2 \ : \ x > 0 \text{ and } y > 0\}$ satisfying

$$\Delta u + \omega^2 u = f \text{ in } \Omega_\infty, \tag{1}$$

$$u = 0 \text{ for } x = 0 \text{ or } y = 0, \tag{2}$$

$$\lim_{r\to\infty} r^{1/2}\left(\frac{\partial u}{\partial r} - i\omega u\right) = 0, \tag{3}$$

where ω is positive wavenumber and f is a compactly supported wave source such that $\text{supp}(f) \subset \Omega = (0,1)\times(0,1)$. We truncate the unbounded domain Ω_∞ to the finite computational region Ω and introduce CRBCs on the two artificial boundaries to capture the behavior of the radiating solutions. The original CRBCs [1] were proposed for solving wave propagation in time-domain. For time-domain calculations, CRBCs are derived in term of the auxiliary function formulation, which leads to a more efficient and natural implementation of high order radiation conditions than those proposed by Higdon [2] and by Givoli and Neta [3].

For frequency-domain application, the p-th order CRBCs on the East boundary Γ_E are defined by recursive formulations for auxiliary functions ϕ_j satisfying the Helmholtz equation on a neighborhood of Γ_E: with $\phi_0 = u$

$$(\frac{\partial}{\partial x} + a_j)\phi_j = (-\frac{\partial}{\partial x} + a_j)\phi_{j+1}, \tag{4}$$

$$\phi_{p+1} = 0 \text{ on } \Gamma_E, \tag{5}$$

where $a_j = \sigma_j - i\omega c_j$ are damping parameters such that $0 < c_j < 1$ and $\sigma_j > 0$. The CRBCs for the North boundary Γ_N are defined analogously.

As other high-order absorbing boundary conditions based on Fourier analysis, they are well-understood in such a case where absorbing boundaries are simply lines or segments. However in case that absorbing boundaries form a corner of a truncated domain, corner conditions become a crucial issue for well-posedness and accuracy [4], [5]. In this talk, corner compatibility conditions are provided by investigating a spectral problem associated with CRBCs. We show that the truncation procedure with CRBCs and the corner conditions leads to a well-posed problem.

Eigenfunction expansion

We first study the eigenvalue problem associated with CRBCs to find $\Phi = (\phi_0, \ldots, \phi_{p+1})^t \in (L^2(0,1))^{p+2}$ satisfying $\Phi'' + \lambda^2\Phi = 0$ and the three conditions, $\phi_0(0) = 0$, the recursions (4) given in the interval $(0,1)$ and the terminal condition (5). We prove that the eigenpairs $-\lambda_n^2$ and $\Phi_n = (\phi_{0,n}, \ldots, \phi_{p+1,n})$ for each $n \geq 0$ satisfy

- $\Im(\lambda^2) < 0$
- The asymptotic behavior of the eigenvalues for large n is $\lambda_n^2 = n^2\pi^2 + 4\sum_{j=0}^{p} a_j + O(n^{-1})$
- The eigenfunctions $\{\Phi_n\}_{n=0}^{\infty}$ are complete in $(L^2(0,1))^{p+1}$.

By exploiting the completeness of eigenfunctions, the wave source f can be written as

$$f(x,y) = \sum_{n,m=0}^{\infty} f_{n,m}\phi_{0,n}(x)\phi_{0,m}(y). \tag{6}$$

It then follows that the solution can have the series representation

$$u(x,y) = \sum_{n,m=0}^{\infty} u_{n,m}\phi_{0,n}(x)\phi_{0,m}(y), \qquad (7)$$

where $u_{n,m} = f_{n,m}/(\omega^2 - \lambda_n^2 - \lambda_m^2)$. We notice that the Fourier coefficients of the solution u is well-defined since the imaginary part of λ_n^2 is negative.

Corner compatibility conditions

Denoting

$$\phi_{j,k}(x,y) = \sum_{n,m=0}^{\infty} u_{n,m}\phi_{j,n}(x)\phi_{k,m}(y) \qquad (8)$$

for $j,k = 0,\ldots,p+1$, we observe that the solution u and the doubly indexed auxiliary functions $\phi_{j,k}$ satisfy the Helmholtz equation and the following recursions

$$(\frac{\partial}{\partial x} + a_j)\phi_{j,k} = (-\frac{\partial}{\partial x} + a_j)\phi_{j+1,k} \text{ on } \Gamma_N, \qquad (9)$$

$$(\frac{\partial}{\partial y} + a_k)\phi_{j,k} = (-\frac{\partial}{\partial y} + a_k)\phi_{j,k+1} \text{ on } \Gamma_E \qquad (10)$$

with the terminal conditions $\phi_{j,p+1} = \phi_{p+1,k} = 0$ at the NE corner for $j,k = 0,\ldots,p+1$.

Motivated by the above recursions, we derive the practical boundary conditions of CRBCs with the corner conditions by eliminating all the tangential derivatives on $\Gamma_E \cup \Gamma_N$ and all derivatives at the NE corner. It can be shown that the problem with the practical CRBCs admits a unique solution. See [6] for the derivation of the practical CRBCs and verification of well-posedness.

Illustrations

This section presents numerical examples illustrating the performance of CRBCs. The source function f is prescribed in a way that the analytic solution is given by

$$u(r,\theta) = \chi(r)\sum_{n=1}^{3} \frac{1}{(2n)^2} H_{2n}^1(\omega r)\sin(2n\theta) \qquad (11)$$

in polar coordinates, where $\omega = 10$ and χ is a smooth cut-off function vanishing for $0 < r < 1/4$ and having one for $r > 1/2$. The parameters a_j for CRBCs imposed on $\Gamma_E \cup \Gamma_N$ are chosen to be

$$a_j = \frac{\sin^2\theta_j}{\cos\theta_j} - i\omega\cos(\theta_j), \qquad (12)$$

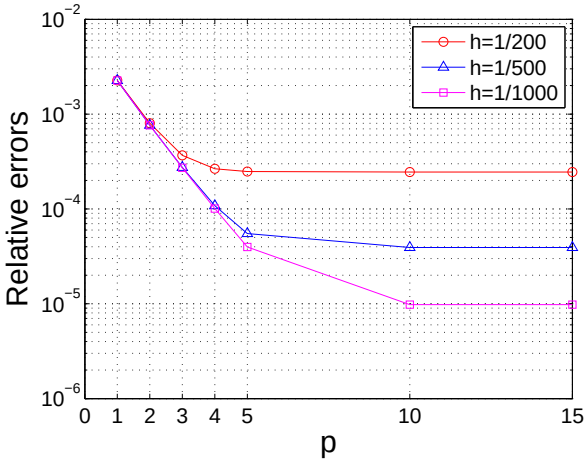

Figure 1: Relative errors as a function of p

where $\theta_j = \pi(j+1)/(2p+4)$ for $j = 0,1,\ldots,p$.

The relative L^2 errors obtained by finite elements with different mesh sizes h are reported in Figure 1. The convergence of approximate solutions satisfying CRBCs can be observed in Figure 1 until the mesh size errors dominate.

References

[1] T. Hagstrom and T. Warburton, *Complete radiation boundary conditions: minimizing the long time error growth of local methods*, SIAM J. Numer. Anal., **47** (2009), pp. 3678–3704.

[2] R. L. Higdon, *Numerical absorbing boundary conditions for the wave equation*, Math. Comp., **49** (1987), pp. 65–90.

[3] D. Givoli and B. Neta, *High-order non-reflecting boundary scheme for time-dependent waves*, J. Comput. Phys., **186** (2003), pp. 24–46.

[4] O. Vacus, *Mathematical analysis of absorbing boundary conditions for the wave equation: the corner problem*, Math. Comp., **74** (2004), pp. 177–200.

[5] D. Rabinovich, D. Givoli, and E. Bécache. *Comparison of high-order absorbing boundary conditions and perfectly matched layers in the frequency domain*, Int. J. Numer. Methods Biomed. Eng., **26** (2010), pp. 1351–1369.

[6] S. Kim and T. Hagstrom, *Complete radiation boundary conditions for the Helmholtz equation II: Domain with corners*, In preparation.

Performance assesment of a fractional radiation boundary condition for the Helmholtz equation

H. Barucq[1,*], C. Bekkey[2], J. Diaz[1]

[1] INRIA Bordeaux Sud-Ouest Research Center, Team Project Magique-3D, LMAP, Université de Pau et des Pays de l'Adour, Pau, France. Emails: firstname.lastname@inria.fr

[2] Department of Mathematics, Faculty of Sciences at Monastir, University of Monastir, Monastir, Tunisia. Email : chokri.bekkey@gmail.com

Abstract

We construct and analyze the performance of a new second-order radiation boundary condition for the Helmholtz equation. The condition involves a fractional power of the wave number which comes from the modeling of grazing waves. By performing a collection of numerical experiments, we show how it impacts on the accuracy of the solution and, in particular, how it outperforms standard second-order conditions like BGT ones.

Introduction

The diffraction of acoustic waves is governed by the Helmholtz equation. Its numerical solution currently involves a truncated problem posed in a bounded computational domain. This is a classical problem that has been widely studied. Regarding its discretization, Finite Element Methods are surely the most efficient but there is always a need in designing new FEM to make for the solution of complex Helmholtz problems involving high frequency and/or heterogenities. Another important issue concerns the performance of the boundary condition which is placed on the outer boundary of the computational domain. This condition, called Radiation Boundary Condition (RBC), should express the exact transmission of the wave field from the truncated domain to the outside to ensure the external surface is fictitious. In practice, reflections are observed and they can be mitigated by improving the modeling effected by RBC. Several attempts have been made to the Helmholtz equation [1,2,3]. In [1], the RBC is improved by taking the variation of the curvatures of the fictitious surface into account. In [3], a new condition is obtained by including evanescent waves into the modeling. In [2], the condition is derived by constructing an analytical extension of the principal symbol of the Dirichlet-to-Neumann (DtN) operator that minimizes the contributions of grazing modes. The construction is possible only if the fictitious boundary is close to the surface of the scatterer. This condition is thus mainly adapted to an On Surface Radiation Condition (OSRC) approach [5]. We propose here a new RBC that includes a fractional power of the wave number. Its construction differs from the condition proposed in [2] because it is based on the representation of the DtN operator for glancing waves. It is more general since its construction applies for general situations, not only in the OSRC context.

1 Problem setting

Let Ω be a bounded domain representing the scatterer and let Γ be its boundary. We denote by n the normal vector defined on Γ and inwardly directed to Ω. The scatterer is supposed to be perfectly conducting and immersed into a fluid Ω_f. It is well-known that an approximate scattered field can be computed by solving the mixed boundary value problem:

$$\Delta p + k^2 p = 0 \qquad \text{in } \Omega_f^t \tag{1}$$

$$p = -p^{inc} \qquad \text{on } \Gamma \tag{2}$$

$$\partial_n p + \alpha p - \beta \Delta_\Sigma p = 0 \qquad \text{on } \Sigma \tag{3}$$

The scalar field p represents the approximate pressure in the fluid and k denotes the wave number. This modeling is obtained by introducing an exterior boundary Σ that modifies Ω_f into the truncated domain Ω_f^t. By this way, the computational domain is bounded and any numerical method based on a grid can be used. The obstacle Ω is illuminated by the incident wave p^{inc} propagating into the exterior fluid. The boundary condition on Σ is an ABC which involves the Laplace-Beltrami operator Δ_Σ and the coefficients α and β are complex valued functions incorporating the geometry of Σ. They are respectively given by:

$$\alpha = \left(\kappa/2 - ik + (ik)^{2/3}(6\kappa)^{1/3} \frac{\Gamma(2/3)}{\Gamma(1/3)} \right)^{-1} \tag{4}$$

and

$$\beta = \alpha \left((ik)^{2/3}(6\kappa)^{1/3} \frac{\Gamma(2/3)}{\Gamma(1/3)} - k^2 \right) (\kappa/2 - ik). \tag{5}$$

2 Construction of the new ABC

Most of the ABCs are obtained as approximations of the DtN operator. The approximation process is based on the fact that the symbol of the DtN operator admits an asymptotic development. The approximation is then valid for a given set of frequencies which is defined in the propagation region [4]. The simplest approximation that includes the geometry of the surface is given by:

$$\partial_n p - ikp + \kappa/2p = 0 \text{ on } \Sigma \tag{6}$$

where κ denotes the curvature of Σ. It is obtained by approximating the symbol of DtN operator by the two first terms of its asymptotic development. This condition can be enriched by considering higher orders of approximation [1]. In that case, the set of frequencies is the same than for the simplest condition but the DtN operator is approximated by using a truncated symbol composed of more than the two first terms of its asymptotic development [1]. This is what we call a regular ABC.

This is not the only way for improving the performance of an ABC. Indeed, another approach consists in combining a regular ABC with another condition that is obtained by considering another set of frequencies. In [3], a condition is obtained for the acoustic wave equation by combining condition (6) with a Robin condition depending on a parameter that is fixed empirically. The combination improves the performance of the regular condition (6) and it outperforms the BGT condition proposed in [1]. The Robin condition corresponds to the simplest approximation of the DtN operator in the set of frequencies corresponding to evanescent waves.

Now, let us consider the principal part of the Helmholtz equation written in a system (r, s) of coordinates representing locally the surface Σ. To consider the principal part of the Helmholtz operator amounts to work with frequencies in the glancing region [6]. In the vicinity of Σ, it is given by:

$$\partial_r^2 p + k^2 p + (1 - 2r\kappa)\Delta_\Sigma p = 0 \tag{7}$$

and by applying a partial Fourier transform in the variable s, we get an Airy equation. By solving this equation, we then get the following result:

Theorem. In the vicinity of glancing points, the symbol of the DtN operator is given by:

$$\sigma(\text{DtN}) = (i\xi)^{2/3}(2\kappa)^{1/3}\frac{Ai'\left((i\xi)^{2/3}(2\kappa)^{1/3}\eta\right)}{Ai\left((i\xi)^{2/3}(2\kappa)^{1/3}\eta\right)} \tag{8}$$

where $\eta = \dfrac{k^2 - \xi^2}{2\xi^2\kappa}$. We then propose to model glancing waves by setting the boundary condition

$$\partial_n p + (ik)^{2/3}(6\kappa)^{1/3}\frac{\Gamma(2/3)}{\Gamma(1/3)}p = 0 \text{ on } \Sigma \tag{9}$$

where Γ denotes the classical gamma function.

An enriched ABC is then obtained by combining (6) with (9) which corresponds to condition (3) after eliminating the term ∂_n^2 thanks to the Helmholtz equation.

3 Performance assessment of the enriched ABC

It is very interesting to observe that the new ABC formulates as BGT-like ABCs. It is thus absolutely relevant to compare their numerical performance since they involve exactly the same computations. Nevertheless, the new ABC includes the behavior of glancing waves while BGT-like conditions represent propagating waves only. This should improve the performance of the condition when Σ is close to the scatterer surface Γ. Indeed, it has been shown in [2] that including the modeling of glancing waves improves regular ABCs. It is now worth noting that the radiation condition obtained in [2] is different from the enriched ABC that we proposed in this work. In particular, the condition in [2] involves $k^{1/3}$ while our condition includes $k^{2/3}$. To compare these two conditions is thus necessary and we will show that our condition is the more efficient in most of the cases.

References

[1] X. Antoine, H. Barucq and A. Bendali, JMAA, **229** (1999), pp. 184-211.

[2] X. Antoine, M. Darbas and Y.Y. Lu, CMAME, **195**, (2006), pp. 4060-4074.

[3] H. Barucq, J. Diaz and V. Duprat, CiCP, **11**, 2 (2012) pp. 674-690.

[4] B. Engquist and A. Majda, Math. of Comp., **31** (1977), pp. 629–651.

[5] G. A. Kriegsmann, A. Taflove and K. R. Umashankar, IEEE Trans. Antennas Propag., **35** (1987), pp. 153–161

[6] M.E. Taylor, Pseudodifferential Operators, Princeton University Press (1981).

A PML for Convex Truncated Domains in Time-Dependent Acoustics with a Discontinuous Galerkin Finite Element Discretization

A. Modave[1,*], **J. Lambrechts**[2], **E. Delhez**[3], **C. Geuzaine**[1]
[1] Montefiore Institute, Université de Liège, Belgium
[2] Institute of Mechanics, Materials and Civil Engineering, Université Catholique de Louvain-la-Neuve, Belgium
[3] Aerospace and Mechanical Engineering Department, Université de Liège, Belgium
*Email: a.modave@ulg.ac.be

Abstract

A new perfectly matched layer (PML) is proposed for convex truncated domains in the context of time-dependent acoustics. With this formulation, the size of the computational domain can be reduced when classical shapes of truncated domains are less appropriate. A numerical discretization based on the discontinuous Galerkin method is then described and validated. An example of realistic three-dimensional application is finally proposed.

Introduction

Perfectly matched layers (PMLs) are used to truncate the computational domain of wave-like problems defined on unbounded spatial domains. Various versions have been proposed in the classical curvilinear coordinate systems to deal with planar, cylindrical or spherical truncations. In [4], the PML is extended to general convex truncated domains in a time-harmonic electromagnetic context. A general convex truncation permits the decrease of the computational cost by diminishing the size of the computational domain when the classical shapes of truncation are less appropriate.

In this paper, we derive a new PML for convex truncations in the time domain. In Section 1, the PML equations are written for three-dimensional problems. In Section 2, we propose a numerical discretization using the discontinuous Galerkin finite element method. The obtained numerical scheme is validated using a three-dimensional reference benchmark. A realistic application is finally presented in Section 3.

1 Governing equations in the PML

We consider the time-evolution of the pressure $p(\boldsymbol{x},t)$ and the velocity $\boldsymbol{u}(\boldsymbol{x},t)$ in the convex bounded domain $\Omega \in \mathbb{R}^3$, that is surrounded by a PML Ω_{pml} with a constant thickness δ. The external boundary Γ of Ω is assumed to be sufficiently smooth.

Employing the strategy proposed in [2], the governing equations in the PML are built by using a complex stretching of spatial coordinates in the frequency domain. For this purpose, the time-harmonic equations are firstly written in a convenient curvilinear coordinate system. Following [4], we consider the system associated to the orthonormal local basis $(\boldsymbol{n}, \boldsymbol{t}_\varphi, \boldsymbol{t}_\theta)$ where, for a point P of Ω_{pml}, the unit vectors $\boldsymbol{n}$, $\boldsymbol{t}_\varphi$ and $\boldsymbol{t}_\theta$ are the external normal and the two principal directions of the surface Γ at the closest point P^Γ of Γ to P. The curvilinear coordinate r associated to the direction $\boldsymbol{n}$, that corresponds to the distance between P and P^Γ, is then stretched using

$$r \quad \rightarrow \quad \tilde{r} = r - \tfrac{1}{i\omega} \int_0^r \sigma(r')dr',$$

where $\sigma(r)$ is the absorption function. Following [3], we use the hyperbolic function $\sigma(r) = cr/(\delta - t)$, that does not require any optimization. Time-dependent cartesian equations are finally obtained by performing an inverse Fourier transform in time, by defining additional differential equations and by moving back to the cartesian coordinate system.

In both Ω and Ω_{pml}, the fields are then governed by the equations

$$\partial_t p + \rho c^2 \, \nabla \cdot \boldsymbol{u} = s_p, \tag{1}$$

$$\partial_t \boldsymbol{u} + \rho^{-1} \, \nabla p = \boldsymbol{s_u}, \tag{2}$$

where ρ and c are positive constants. In Ω, the classical equations are recovered considering the source terms s_p and $\boldsymbol{s_u}$ equal to zero while, in Ω_{pml}, these terms are

$$s_p = -\sigma p_n - \bar{\kappa}_\varphi \bar{\sigma} p_\varphi - \bar{\kappa}_\theta \bar{\sigma}(p - p_n - p_\varphi), \tag{3}$$

$$\boldsymbol{s_u} = -\sigma \boldsymbol{n}(\boldsymbol{n} \cdot \boldsymbol{u}) - \bar{\kappa}_\varphi \bar{\sigma} \boldsymbol{t}_\varphi(\boldsymbol{t}_\varphi \cdot \boldsymbol{u}) - \bar{\kappa}_\theta \bar{\sigma} \boldsymbol{t}_\theta(\boldsymbol{t}_\theta \cdot \boldsymbol{u}),$$

with $\bar{\kappa}_\varphi = (\kappa_\varphi^{-1} + r)^{-1}$, $\bar{\kappa}_\theta = (\kappa_\theta^{-1} + r)^{-1}$, $\bar{\sigma} = \int_0^r \sigma(r')dr'$, where κ_φ and κ_θ are the main curvatures of Γ at P^Γ. Finally, the two additionnal fields p_n and p_φ introduced in the equation (3) are governed by

$$\partial_t p_n + \rho c^2 \, [\boldsymbol{n}(\boldsymbol{n} \cdot \nabla)] \cdot \boldsymbol{u} = -\sigma p_n, \tag{4}$$

$$\partial_t p_\varphi + \rho c^2 \, [\boldsymbol{t}_\varphi(\boldsymbol{t}_\varphi \cdot \nabla)] \cdot \boldsymbol{u} = -\bar{\kappa}_\varphi \bar{\sigma} p_\varphi. \tag{5}$$

2 Numerical scheme

Discontinuous Galerkin method

The equations above are solved using a nodal DG finite element scheme [1] with a mesh made of tetrahedra. The scheme is built by considering the conservative form of the governing equations and by multiplying them by test functions. Integrating the resulting equations over a cell and using integration by part leads to the weak form. The numerical fluxes used in the interface terms of the first two equations (1) and (2) are defined using a Riemann solver, while Lax-Friedrichs fluxes are considered for the two additional equations (4) and (5). Each scalar field and each cartesian component of $\boldsymbol{u}$ is approximated by a first-order Lagrange polynomial. The time-stepping is made with the fourth-order Runge-Kutta method.

Validation

To validate the method, we consider a truncated domain shaped as an ellipsoid of revolution and surrounded by a PML of thickness $\delta = 500$ m. The lengths of the axis of the ellipsoid are 6.6 km ($x-$direction) and 2.4 km ($y-$ and $z-$directions). A Gaussian is prescribed as initial condition on p, *i.e.*

$$p(\boldsymbol{x}, 0) = e^{-\|\boldsymbol{x}-\boldsymbol{x}_0\|^2/R^2}$$

with $\boldsymbol{x}_0 = (-2.45 \text{ km}, 0, 0.4 \text{ km})$ and $R = 150$ m, while the other fields are initially equal to zero. We use $c = 1.5$ km/s and $\rho = 1$ kg/m^3. As time goes by, spherical waves are generated and reach the PML with different incidences.

During the simulation, the numerical solution is compared with the exact solution in the truncated domain Ω. Figure 1 shows the convergence of the relative mean error ξ_r defined by

$$\frac{\int_0^{t_f}\int_\Omega \left(\frac{1}{2\rho c^2}(p_{\text{ana}} - p_{\text{num}})^2 + \frac{\rho}{2}\|\boldsymbol{u}_{\text{ana}} - \boldsymbol{u}_{\text{num}}\|^2\right) d\Omega\, dt}{\int_0^{t_f}\int_\Omega \left(\frac{1}{2\rho c^2}(p_{\text{ana}})^2 + \frac{\rho}{2}\|\boldsymbol{u}_{\text{ana}}\|^2\right) d\Omega\, dt}$$

and computed for the duration $t_f = 4$ s.

3 Realistic benchmark

A submarine is added in the geometry described above. Figure 2 shows the snapshot of p at two instants of the simulation. The spherical waves are not deformed near the external boundary of the domain Ω and are damped in the PML.

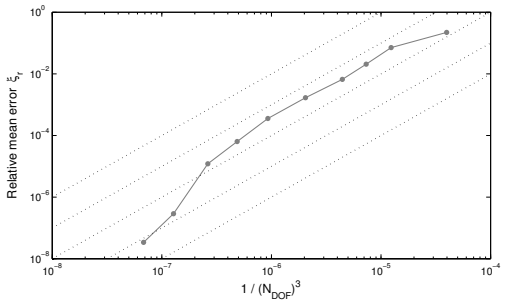

Figure 1: Convergence of the relative mean error. N_{DOF} is the total number of degrees of freedom.

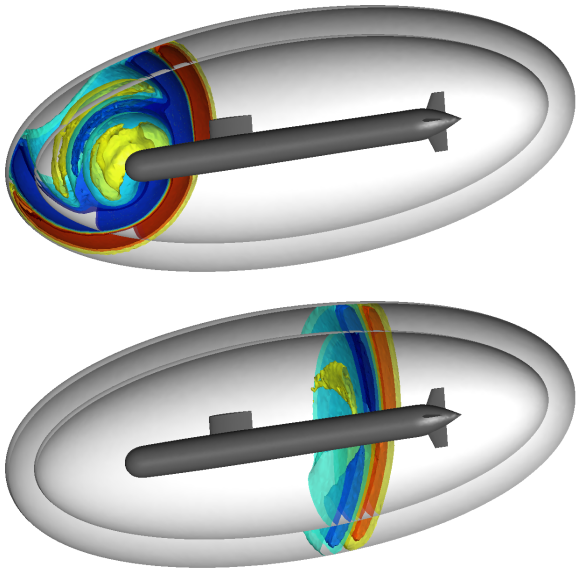

Figure 2: Iso-surfaces of p at $t = 0.8$ s *(top)* and $t = 2.4$ s *(bottom)* for the realistic benchmark.

References

[1] B. Cockburn and C.-W. Shu *The Runge-Kutta Discontinuous Galerkin Method for Conservation Laws V: Multidimensional Systems*, Journal of Computational Physics, **141** (1998), 199-224

[2] F. Collino and P. B. Monk, *The Perfectly Matched Layer in Curvilinear Coordinates*, SIAM J. Sci. Comput., **19** (1998), 2061–2090

[3] A. Modave, E. Delhez and C. Geuzaine, *On the Parameters of the Perfectly Matched Layer in Discrete Contexts*, in Proceedings of the Waves 2011, Vancouver, Canada, pp. 591–594.

[4] F. L. Teixeira and W. C. Chew, *Analytical derivation of a conformal perfectly matched absorber for electromagnetic waves*, Microwave and Optical Technology Letters, **17** (1998), 231–236

Plasmonic cavity modes with sign changing permittivity

A.-S. Bonnet-Ben Dhia[1], C. Carvalho[1,*], L. Chesnel[1], P. Ciarlet Jr.[1]
[1]POEMS, UMR 7231 CNRS-INRIA-ENSTA, Palaiseau, France
*Email : carvalho.camille@ensta-paristech.fr

Abstract

We study a 2D dielectric cavity with a metal inclusion. The permittivity ϵ of the metal depends on the frequency ω and, in a given frequency range, the metal can be (almost) dissipationless ($|Im(\epsilon(\omega))| \ll |Re(\epsilon(\omega))|$) and such that $Re(\epsilon(\omega)) < 0$. We look for the cavity resonance values ω. Due to the dependence of ϵ with respect to ω, this is a non linear eigenvalue problem. Below we consider mainly the linearized-problem where this dependence is frozen. Under some conditions on ϵ and the inclusion's geometry, the linearized-problem principal operator is self-adjoint with compact resolvent. Besides when the inclusion has corners adding to the fact that ϵ is sign changing at the boundaries between the metal and the dielectric, self-adjointness and compactness of the resolvent may be no longer true. This is due to very singular phenomena at the corners, which require a new functional framework for the theoretical analysis, and a specific numerical treatment. The non linear case which requires a fixed point algorithm is briefly discussed.

Introduction

Let's consider a cavity Ω, $\overline{\Omega} = \overline{\Omega_1} \cup \overline{\Omega_2}$, with a dielectric material Ω_1, and a metal inclusion Ω_2. Let's call the interface $\Sigma = \overline{\Omega_1} \cap \overline{\Omega_2}$. We study the following eigenvalue problem :

$$(1)\quad \begin{cases} \text{Find } u \neq 0,\ \omega \in \mathbb{R}\ s.t.\ : \\ -\text{div}(\frac{1}{\epsilon(\omega)}\nabla u) = \omega^2 \mu(\omega) u \quad \text{in } \Omega \\ u = 0 \quad \text{on } \partial\Omega \end{cases}$$

where the electric permittivity $\epsilon(\omega)$ is a non linear real valued function of the frequency ω.

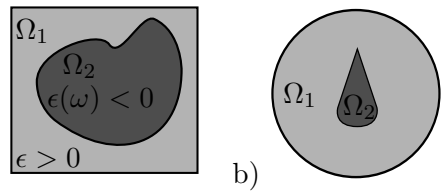

Figure 1: : Examples of a cavity. The configuration b) will provide support for numerical illustrations.

For simplicity we consider the linearized eigenvalue problem in ω, which consists in replacing $\epsilon(\omega)$ by ϵ in (1) and, we focus our attention on the case where $\epsilon < 0$ in the inclusion. More precisely, we take ϵ and μ piecewise constant functions, $\mu > 0$ almost everywhere and ϵ sign changing at the interface Σ. Let's define the principal operator :

$$A : \left| \begin{array}{l} D(A) \subset L^2(\Omega) \longrightarrow L^2(\Omega) \\ \quad u \mapsto -\frac{1}{\mu}\text{div}(\frac{1}{\epsilon}\nabla u) \qquad \text{with} \end{array} \right.$$

$D(A) = \{u \in H_0^1(\Omega), \frac{1}{\mu}\text{div}(\frac{1}{\epsilon}\nabla u) \in L^2(\Omega)\}$ and consider the weighted L^2 inner product $(u, v) \longmapsto \int_\Omega \mu u v \, d\Omega$. Thus our goal is to find the eigenvalues of A. For a given ϵ and depending on the interface Σ, the operator A can be self-adjoint or not. The next part is dedicated to solving the self-adjoint case, the one after that to solving the non self-adjoint case. We also present some computations in each section, with a specific numerical treatment in the second one because of particular phenomena near the corners.

1 The self-adjoint case

When $\epsilon > 0$ almost everywhere, the operator A is self-adjoint with compact resolvent (noted for simplicity SC. in the rest of the paper). The eigenvalues are positive with finite multiplicity and tend to infinity.

When ϵ changes sign, one can still have SC. properties for A under some conditions on ϵ and the interface Σ (precised below)[1], [2] : the eigenvalues then consist in two sequences of real numbers with finite multiplicity tending respectively to $\pm\infty$ (see fig.5a).

For a regular interface Σ (fig.1a), A is SC. if and only if $\frac{\epsilon|_{\Omega_2}}{\epsilon|_{\Omega_1}} \neq -1$. When Σ has corners (fig.1b), the operator is SC. if and only if $\frac{\epsilon|_{\Omega_2}}{\epsilon|_{\Omega_1}}$ doesn't belong to a critical interval containing -1, which is determined by the sharpest corner of the interface.

In this case, we have made computations with standard Finite Element for the geometry fig.1b. We observe stability of the results with respect to the mesh size (see fig.2). In fig.3 we observe that the modes are confined outside or inside the metal inclusion depending on the eigenvalues' sign.

Nodes	3469	7325	32049	132001
1st ev > 0	1.4836	1.4837	1.4807	1.4805
1st ev < 0	-4.083	-4.0771	-4.0762	-4.0758

Figure 2: : First positive and negative eigenvalues (of smallest modulus) for several mesh sizes.

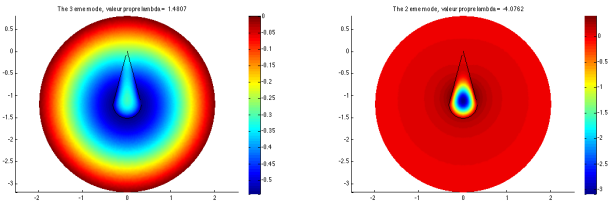

Figure 3: : First positive (left) and negative (right) modes of the SC. operator, associated to the two previous eigenvalues.

2 The non self-adjoint case

For $\frac{\epsilon|_{\Omega_2}}{\epsilon|_{\Omega_1}}$ chosen in the critical interval (excluding $\frac{\epsilon|_{\Omega_2}}{\epsilon|_{\Omega_1}} = -1$), due to singular phenomena at the corners, the SC. properties of A are no longer satisfied in the classical functional framework. In this case, the spectrum of A is the whole complex plane.

In [2], [3] (see also [4]) is given an extension of the operator A which has a compact resolvent, called A^+. It is defined by $D(A^+) = D(A) \oplus \text{span}\{s_1^+, \cdots, s_k^+\} \subset L^2(\Omega)$, where $s_1^+, \cdots, s_k^+$, $k \in \mathbb{N}$ are singular functions at k corners ($k \leqslant$ total corners' number of the interface Σ) that don't belong to H^1. These singularities, selected by a limiting absorption principle (see [3]), can be interpreted as waves propagating along the interface Σ towards the k corners : they are called black-hole plasmonic waves.

Numerically, there is no Finite Element convergence due to these black-hole waves. Thus, in order to capture confined plasmonics waves near the corners, a specific numerical treatment is performed. We operate an original use of PMLs (Perfectly Matched Layers) : by the Euler change of variables $(r, \theta) \longmapsto (log(r), \theta)$ we transform a disk centered at a corner into a waveguide [2] which we can troncate with PMLs. The PMLs domain corresponds to the small hole at the corner in fig.4. Numerical results confirm that the PMLs' method is efficient to ensure the stability of the Finite Element approximation. The A^+'s spectrum contains complex eigenvalues which clearly proves its non self-adjointness. We can prove that the eigenvalues belong to $\{z \in \mathbb{C}\, s.t.\, \text{Im}(z) \leq 0\}$, which is numerically almost satisfied (see fig.5b).

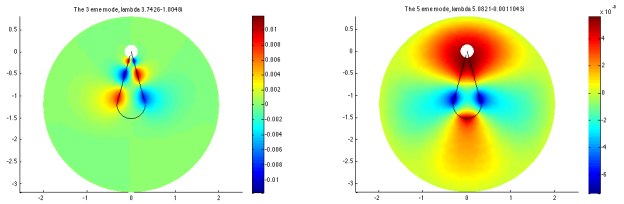

Figure 4: : Third and fifth modes of operator A^+ (associated to the smallest eigenvalues in modulus : $\lambda_3 = 3.7426 - 1.0046i$ and $\lambda_5 = 5.0821 - 1.1043 \times 10^{-3} i$).

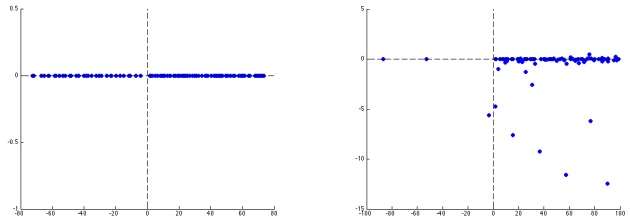

(a) (b)

Figure 5: : (a) Spectrum of the SC. operator in the complex plane. (b) Spectrum of operator A^+ in the complex plane. (The scales are different.)

3 Conclusion/Ongoing work

Once we are able to understand the linearized eigenvalue problem, we could solve in principle our starting non linear problem (1). The cavity modes could be obtained for instance with a fixed point algorithm.

We thank the DGA for financial support.

References

[1] A.-S. Bonnet-Ben Dhia, L. Chesnel, P. Ciarlet Jr., *T-coercivity for scalar interface problems between dielectrics and metamaterials*, Math. Mod. Num. Anal., **46** (2012), pp. 1363–1387.

[2] L. Chesnel, *Étude de quelques problèmes de transmission avec changement de signe. Application aux métamatériaux.*, Ph.D. thesis, 2012.

[3] A.-S. Bonnet-Ben Dhia, L. Chesnel, X. Claeys, *Radiation condition for a non-smooth interface between a dielectric and a metamaterial*, Math. Mod. Meth. App. Sci., Accepted 2012.

[4] A.-S. Bonnet-Ben Dhia, M. Dauge, K. Ramdani, *Analyse spectrale et singularités d'un problème de transmission non coercif*, C. R. Acad. Sci. Paris, Ser. I,**328** (1999), pp. 717–720.

Perfectly Matched Layers for linearized and non linear Shallow Water equation

H. Barucq[1], **J. Diaz**[1], **M. Tlemcani**[2,*]
[1] INRIA Bordeaux Sud-Ouest, Project-Team Magique 3D and LMA, UPPA.
[2]Département de Physique, Université des Sciences et de la Technologie d'Oran.
*Email: mounir.tlemcani@univ-pau.fr

Abstract

We propose a new Perfectly Matched Layer for the linearized Shallow Water Equations. Its construction is similar to the one we proposed in [2], but it does not require the use of an auxiliary variable in the whole computational domain. Moreover, it can be extended to derive an Absorbing Layer for non linear Shallow Water Equations.

Introduction

Shallow Water Equations, which are a simplification of Navier Stokes equations when the vertical length scale is much smaller than the horizontal length scale, are widely used in atmospheric and ocean modeling. A important example of application can be found in meteorological forecasting models which take into account the Earth's rotation (Coriolis Forces). In such applications, the physical domains are huge (for instance the whole ocean) and to compute an accurate numerical solution to these equations is not possible, even with High Performance Computing techniques. The simulations are then performed on smaller domains whose boundaries, which are artificial, should be transparent. In the case of acoustic wave equation, this can be achieved by using Absorbing Boundary Conditions or Perfectly Matched Layers (PML). The principle of this latter consists in surrounding the computational domain by a non-physical absorbing layer. They are called Perfectly Matched because their interface with the computational domain does not generate any reflection, whatever the frequency and the angle of incidence of the waves. However, the extension of this technique to non linear equations is still an open issue. A absorbing layer has been proposed in [1] but it required the introduction of a small damping term to be stable, and is not perfectly matched. In [4], the instabilities in the layer are removed by a filter, which does ensure the perfect matching neither.

In [2], we have proposed a PML for linearized Shallow Water Equations, which required the introduction of an auxiliary variable in the whole computation domain. We propose here a new formulation of this PML which overcomes this drawback, and we show that the technique we use can be extended to construct an efficient Absorbing Layer for the non linear Shallow Water equations.

PML for Shallow Water equations

We consider here the nonconservative form of the 2d-Shallow Water equations on an $f-$plane:

$$\begin{cases} \partial_t \mathbf{h} + \mathbf{u}\partial_x \mathbf{h} + \mathbf{v}\partial_y \mathbf{h} + \mathbf{h}\left(\partial_x \mathbf{u} + \partial_y \mathbf{v}\right) = 0, \\ \partial_t \mathbf{u} + \mathbf{u}\partial_x \mathbf{u} + \mathbf{v}\partial_y \mathbf{u} + g\partial_x \mathbf{h} - f\mathbf{v} = 0, \\ \partial_t \mathbf{v} + \mathbf{u}\partial_x \mathbf{v} + \mathbf{v}\partial_y \mathbf{v} + g\partial_y \mathbf{h} + f\mathbf{u} = 0, \end{cases} \tag{1}$$

where $\mathbf{h}$ is the elevation of the water from $z = 0$, $\mathbf{u}$ and $\mathbf{v}$ are the components of the velocity field, g is the gravity constant and f is the Coriolis parameter. Supposing that $\mathbf{h}$, $\mathbf{u}$ and $\mathbf{v}$ vary weakly around a mean state, denoted respectively by H, U and V, the linearized equations for 2d read as

$$\begin{cases} \left(\partial_t + U\partial_x + V\partial_y\right) h + H\left(\partial_x u + \partial_y v\right) = 0 \\ \left(\partial_t + U\partial_x + V\partial_y\right) u + g\partial_x h - fv = 0 \\ \left(\partial_t + U\partial_x + V\partial_y\right) v + g\partial_y h + fu = 0 \end{cases} \tag{2}$$

where h is the water elevation from the mean value and u and v are such that $\mathbf{u} = U + u$ and $\mathbf{v} = V + v$. We only consider in this work the subsonic regime, i.e. such that $U^2 + V^2 < gH$. The dispersion relations for (2) are known to be

$$\left(\omega + Uk_x + Vk_y\right)^2 = gH\left(k_x^2 + k_y^2\right) + f^2 \tag{3}$$

for inertia-gravity adjustment waves and

$$\omega + Uk_x + Vk_y = 0 \tag{4}$$

for geostrophic adjustment waves. The main difficulty of forming PML equations for oblique mean flow is that both types of waves present inconsistencies between their group and phase velocities. It is well-known [3] that this induces instabilities with classical Perfeclty Matched Layers. However, geostrophic adjusment waves are divergence free and satisfy transparent conditions on the boundary of the computational domain. Hence, an efficient strategy consists in deriving Perfeclty Matched Layers acting only on inertia-gravity adjusment waves and in

absorbing geostrophic waves by a transparent conditions at the end of the layers.However, when considering the 2d shallow water system, this method requires the computation of an additional auxilliary variable in the whole computational domain. To avoid this drawback, we propose to rewrite system (2) by using the divergence of the flow, $\delta = \partial_x u + \partial_y v$ and its rotational $\xi = \partial_x v - \partial_y u$. Then, linear combinations of equations in system (2) yields the following div-rot formulation for the unknowns (h, δ, ξ)

$$\begin{aligned} \mathbf{G}h + H\delta &= 0, & (5)\\ \mathbf{G}\xi + f\delta &= 0, & (6)\\ \mathbf{G}\delta + g\Delta h - f\xi, &= 0 & (7) \end{aligned}$$

where we have denoted $\mathbf{G} = \partial_t + U\partial_x + V\partial_y$.

To uncouple the rotational free waves from the divergent free ones, we formally left multiply (5) by Δ and (7) by $\mathbf{G}$ and substract the first equation from the second one. Using finally (6), we check that the divergent part of the flow satisfies the advective Klein-Gordon equation

$$\mathbf{G}^2\delta - gH\Delta\delta + f^2\delta = 0. \quad (8)$$

The dispersion relation of this equation is once again given by (3). The quantity $\phi = h/H - \xi/f$ is called the potential vorticity and satisfies the transport equation $\mathbf{G}\phi = 0$. Hence, stable PML for the linear shallow water system can be obtained by **a)** applying a preliminary change of variable to remove the inconsistent waves; **b)** applying the PML change of variable only to equation (8) and **c)** applying the inverse change of variable to **a)**.

We have performed numerical simulations in order to assess the performance of the method. The external Rossby deformation radius $r_E = \sqrt{gH}/f$ is set to $r_E = 100Km$ and $g = 10ms^{-2}$. The Coriolis parameter is $f = 1.0285.10^{-4}$ (s^{-1}) (i.e.; evaluated at mid-latitude 45°-northern hemisphere) so that the corresponding mean height is $H = 10.578m$. Assume also that an oblique background flow is moving with constant velocity $U = V = 13.1Km/h$ (orientation of 45°) such that the Froude number defined by $F = \sqrt{U^2 + V^2}/\sqrt{gH}$ is equal to 0.5 flow. Initial conditions for the shallow-water equations are tested with radial Gaussian pulses as follows:

$$\begin{cases} h(x,y,0) = Ae^{-\frac{(x-x_0)^2+(y-y_0)^2}{L^2}} \\ u(x,y,0) = v(x,y,0) = 0 \end{cases}$$

for inertia-gravity waves, and

$$\begin{cases} h(x,y,0) = Ae^{-\frac{(x-x_0)^2+(y-y_0)^2}{L^2}} \\ u(x,y,0) = -\frac{g}{f}\partial_y h(x,y,0) \\ v(x,y,0) = \frac{g}{f}\partial_x h(x,y,0) \end{cases}$$

for geostrophic adjustment waves, where $L = 2.5r_E$ is the width of the Gaussian, A denotes its amplitude and (x_0, y_0) its center placed at the geometric center of the computational domain. Namely, we have set the amplitude $A = 0.5H$ to get nonlinear effects, because the choice of small amplitudes leads simply to level contours approximately the same as in the linear case. We evaluate the effectiveness of the proposed PML model on a domain of width $D = 4000km$ including an absorbing layer of width $l = 10\%D$. To validate our method, we have compared our results to the ones obtained on a larger computational domain $D_{ref} = 24000km$. We have calculated the relative error in time near the upper corner (two grid points points away from the corner). The solid line depicts

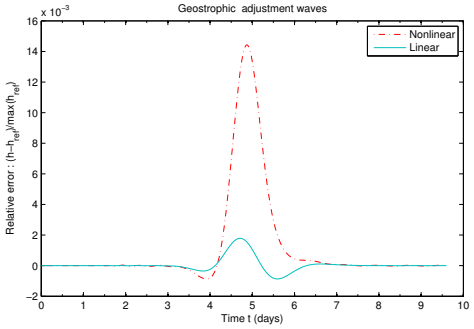

Figure 1: Relative Error near the corner of the PML

the relative error obtained for the linearized Shallow Water equation while the dashed one depicts the relative error obtained for the non-linear Shallow Water equation, using an extension of the new PML to the non linear case. We obtain a relative error below 1% in each case, which shows the efficiency of the method.

References

[1] S. Abarbanel *et al*, Computat. Geosci. (2003).

[2] H. Barucq *et al*, J. Comput. Phys., (2010).

[3] E. Bécache *et al*, J. Comput. Phys.,(2003).

[4] I. M. Navon *et al*, Bull. Am. Met. Soc. (2004).

Boundary waves and stability of a perfectly matched layers I

G. Kreiss[1,*], **K. Duru**[2]
[1] Division of Scientific Computing, Department of Information Technology, Uppsala University, Sweden
[2] Department of Geophysics, Stanford University, USA.
*Email: gunilla.kreiss@it.uu.se

Abstract

We study the stability of a perfectly matched layer (PML) for systems of symmetric second order hyperbolic partial differential equations on a half plane. We are particularly interested in boundary conditions supporting surface waves, and will focus on the elastic wave equation subject to the traction free boundary condition. In the PML the traction free boundary condition must be modified to achieve perfect matching. Using a mode analysis, we can show that for a constant coefficient layer, the boundary condition does not support temporally growing modes. In particular Rayleigh waves decay in the layer. Numerical computations demonstrate the validity of the result also for a variable coefficient layer of finite extent.

.

Introduction

There are many wave propagation problems where boundary phenomenon such as surface waves and wave reflections are important. Typical examples are in non-destructive testing, seismology, earthquake engineering, ultrasonics, and ground penetrating radar technologies. These situations can be modeled by systems of second order symmetric, hyperbolic, timedependent partial differential equations in semi-bounded domains. To perform numerical simulations the domain must be truncated and artificial boundary conditions must be introduced. A popular technique is to surround the artificial boundaries with a perfectly matched layer (PML). In the PML the underlying equations are transformed such that waves decay rapidly in the layer. A very important property of the PML is perfect matching. This means that waves propagate from the physical space into the PML without reflections. A PML is usually derived by assuming a homogeneous media and an infinite domain in all directions. In a domain with physical boundaries, the application of the PML introduces boundary corners where physical boundary conditions interact with the PML. In order to ensure perfect matching, the underlying boundary conditions must be accurately extended from the interior into the PML. We will discuss derivation of layer equations, and explain how to extend boundary conditions.

Even if the PML is perfectly matched, there is no guarantee that solutions decay with time. Analysis of temporal stability of PMLs is therefore a main topic of research. For Cauchy problems, the stability of the PML can be predicted by the geometric stability condition, [2]. Numerical experiments have shown that PMLs which are Cauchy stable can exhibit growth when some physical boundaries are imposed. Below we apply a normal-mode analysis to the half-plane problem for the elastic PML, and show that growing modes are not supported when the boundary condition is correctly extended. The same technique shows that the PML for the elastic wave equations subject to Dirichlet boundary conditions, and to the PML for the curlcurl Maxwells equation subject to insulated walls and perfectly conducting walls boundary conditions do not support temporally growing modes.

We will present numerical computations demonstrating how different types of waves are damped. In particular we show an example with a Rayligh wave. The computations use high-order finite difference discretizations based on the summation-by-parts technique, and impose boundary conditions weakly.

The Elastic Wave Equation

Consider the second order system

$$u_{tt} = (Au_x)_x + (Cu_y)_x + (C^T u_x)_y + (Bu_y)_y,$$

on a half-plane , $0 \geq y > \infty$, $-\infty < x < \infty$. In the standard isotropic case the coefficient matrices are given by

$$A = \begin{pmatrix} 2\mu+\lambda & 0 \\ 0 & \mu \end{pmatrix}, B = \begin{pmatrix} \mu & 0 \\ 0 & 2\mu+\lambda \end{pmatrix}, C = \begin{pmatrix} 0 & \lambda \\ \mu & 0 \end{pmatrix},$$

where μ, λ are the lame parameters. In this paper the parameters will be constant. A boundary condition admitting boundary waves is the free surface condition

$$Bu_y + C^T u_x = 0 \text{ at } y = 0.$$

This initial-boundary-value problem satisfies an energy estimate.

The Perfectly Matched Layer

At $x = L$ we add a layer. The layer equations can be derived by a complex coordinate transformation in the dual space (Laplace transform in time) ,

$$\tilde{x} = \tilde{x}(x),\ \frac{d\tilde{x}}{dx} = 1 + \frac{\sigma(x)}{\alpha + s},$$

see [1]. Here $\sigma(x)$ is a positive, smooth function with $\sigma(L) = 0$ and $\alpha \geq 0$ is the so called complex frequency shift. Before inverting the Laplace transform auxillary variables need to be introduced. The resulting layer system in time domain is

$$\begin{aligned} u_{tt} + \sigma u_t &= (\quad Au_x + Cu_y)_x + (Bu_y + C^T u_x)_y - \\ &- \quad A(\sigma v)_x + B(\sigma w)_y + \sigma\alpha(u - q), \\ v_t &= -(\sigma + \alpha)v + v_x, \\ w_t &= -\alpha w + u_y, \\ q_t &= \alpha(u - q). \end{aligned}$$

To ensure perfect matching boundary conditions must also be transformed as above. In the dual space the traction free boundary condition becomes

$$B\hat{u}_y + \frac{\alpha + s}{\alpha + s + \sigma} C^T \hat{u}_x = 0,$$

which corresponds to

$$Bu_y + C^T u_x + \sigma B w = 0,$$

in physical space.

Normal mode analysis

To understand the effect of the PML on boundary modes we perform a normal mode analysis. Introduce

$$r(x, y, t) = e^{ik_x x + st}\hat{r}(y),$$

for the variables $r = u_1, u_2, v, w, q$ in the frozen coefficient PML system. The auxilary variables can be eliminated, leaving a second order system of ordinary differential equations. The general solution consists of terms of the form

$$\hat{u} = e^{\kappa y}\psi,$$

where κ satisfies a characteristic equation. Only roots with $Re(\kappa) > 0$ are admissible. If $F_0(s, k_x, \kappa) = 0$ is the characteristic equation for the original, undamped system, then the characteristic equation for the PML is

$$F_0(s, \frac{\alpha + s}{\alpha + s + \sigma} k_x, \kappa) = 0.$$

Standard analysis shows that the original system has two admissible roots, which will be admissible roots also in the PML. Thus the general solution consists of two components with unknown coefficients. By inserting the general solution into the boundary condition we obtain a linear system for these coefficients, described by a 2×2 matrix $C_0(s, \tilde{k}_x)$, where $\tilde{k}_x = k_x(\alpha + s)/(\alpha + s + \sigma)$. As above $C_0(s, k_x)$ is the corresponding matrix for the undamped problem. Modal solutions are determined by $|C_0(s, \tilde{k}_x)| = 0$. For the undamped problem

$$|C_0(s, k_x)| = 0$$

is the Rayligh dispersion equation with solutions $s = 0$, $s = \pm i\beta$. The non-zero values correspond to boundary modes, the so-called Rayligh waves, while the zero corresponds to the trivial solution. We can now straightforwardly analyze how the PML changes the temporal behavior of the boundary modes. The result is that the corresponding roots move into the stable half-plane, indicating that the Rayligh waves are damped by the PML.

To rigorously establish well-posedness of the PML we would need to construct and derive an estimate of the solution of the PML equations with forcing only on the boundary. Following the same steps as above we can use Laplace transform technique for the construction. A bound in Laplace-space can then be transformed to physical space. This construction, together with the well-posedness of the corresponding Cauchy problem would leads to well-posedness for the PML problem.

References

[1] K. Duru, G. Kreiss, *A Well–posed and discretely stable perfectly matched layer for elastic wave equations in second order formulation*, Commun. Comput. Phys., 11, 1643–1672, (2012).

[2] E. Bécache, S. Fauqueux, P. Joly, *Stability of Perfectly Matched Layers, Group Velocities and Anisotropic Waves*, J. Comp. Phys., 188,p399-433, (2003).

Boundary waves and stability of perfectly matched layers II : Extensions to first order systems and numerical stability

K. Duru[1,*], **J. E. Kozdon**[2], **G. Kreiss**[3]
[1] Department of Geophysics, Stanford University, Stanford, CA
[2] Department of Applied Mathematics, Naval Postgraduate School, Monterey, CA
[3] Division of Scientific Computing, Uppsala University Uppsala, Sweden
*Email: kduru@stanford.edu

Abstract

In this paper we discuss the stability of the perfectly matched layer (PML) for a first order system of the elastic wave equation on the lower half-plane with free-surface boundary conditions at $y = 0$, and on the left half-plane with characteristics boundary conditions at $x = \delta \geq 0$. In both cases the PML truncates a boundary in the x-direction. Using a modal analysis we prove that the lower half-plane problem and the left half-plane problem do not support temporally growing modes. A stable and high order accurate discretization is developed using summation-by-parts (SBP) operators to approximate spatial derivatives and imposing boundary conditions weakly using penalties. Numerical experiments are presented corroborating the theoretical results.

Introduction

Let us assume that we want to solve the elastic wave equation in the quarter plane $x \leq 0$, $y \leq 0$, where $x = 0$ is a boundary introduced to limit the computational domain. In order to absorb outgoing waves at $x = 0$, we introduce the PML [1] of width $\delta > 0$ outside the quarter plane, that is in $0 \leq x \leq \delta$,

$$\begin{aligned}
\rho \frac{\partial \mathbf{u}}{\partial t} &= \frac{\partial \mathbf{v}}{\partial x} + \frac{\partial \mathbf{w}}{\partial y} - \sigma \mathbf{q}, \\
\frac{\partial \mathbf{v}}{\partial t} &= A \frac{\partial \mathbf{u}}{\partial x} + C \frac{\partial \mathbf{u}}{\partial y} - \sigma A \mathbf{p}, \\
\frac{\partial \mathbf{w}}{\partial t} &= B \frac{\partial \mathbf{u}}{\partial y} + C^T \frac{\partial \mathbf{u}}{\partial x} - \sigma C^T \mathbf{p}, \\
\frac{\partial \mathbf{p}}{\partial t} &= \frac{\partial \mathbf{u}}{\partial x} - (\sigma + \alpha)\, \mathbf{p}, \\
\frac{\partial \mathbf{q}}{\partial t} &= \frac{\partial \mathbf{v}}{\partial x} - (\sigma + \alpha)\, \mathbf{q}.
\end{aligned} \tag{1}$$

Here, ρ is the density of the medium, $\sigma(x) \geq 0$ is the damping function, $\alpha \geq 0$ is the complex frequency shift (CFS), and the unknowns $\mathbf{p} = (p_1, p_2)^T$ and $\mathbf{q} = (q_1, q_2)^T$ are auxiliary variables introduced to localize the PML in time. Inside the domain, $x \leq 0$ and $y \leq 0$, the damping function vanishes $\sigma(x) \equiv 0$ and we recover the elastic wave equation, with $\mathbf{v} = (v_1, v_2)^T$ and $\mathbf{w} = (w_1, w_2)^T$ being the stresses and $\mathbf{u} = (u_1, u_2)^T$ being the velocities. We set the free-surface boundary condition $\mathbf{w} = 0$ on the surface at $y = 0$. In order to complete the statement of the problem we set the characterics boundary condition $\sqrt{A}\mathbf{u} + \mathbf{v} = 0$ at $x = \delta$. The coefficient matrices are given by the Lamé parameters λ, μ:

$$A = \begin{pmatrix} 2\mu + \lambda & 0 \\ 0 & \mu \end{pmatrix}, B = \begin{pmatrix} \mu & 0 \\ 0 & 2\mu + \lambda \end{pmatrix}, C = \begin{pmatrix} 0 & \lambda \\ \mu & 0 \end{pmatrix}.$$

Stability

The stability of the PML (1) is essential in order for it to be computationally useful. For first order hyperbolic systems in unbounded domains the temporal stability of the PML is well known, see [1], [2]. In bounded and semi-bounded domains stability is not as straightforward. For instance, numerical experiments [3] have shown that growth can occur when a free-surface boundary condition is imposed. That said, it has been shown [4] that when (1) is written in second order form the PML is stable when the boundary conditions are correctly chosen. Here, we extend the analysis of [4] to the first order system (1). We also investigate the stability of the boundary condition at $x = \delta$, terminating the PML.

To extend the analysis we freeze all coefficients and split the problem into: 1) a Cauchy problem; 2) a lower half-plane problem with the free-surface boundary condition $\mathbf{w} = 0$ at $y = 0$; 3) a left half-plane problem with the boundary condition $\sqrt{A}\mathbf{u} + \mathbf{v} = 0$ at $x = \delta$. Each of the three problems above can be analyzed separately. The Cauchy problem 1) is analyzed using standard Fourier methods as in [1]. Since the elastic medium is isotropic, we know from [1] that the Cauchy problem is stable. One of the major contributions of this work is showing stability of the half-plane problems 2) and 3) using normal mode analysis. That is we prove that there are no non-trivial solutions of 2) and 3) on the form $\Psi_a = \hat{\Psi}_a(y) \exp(st + ik_x x)$, $|\hat{\Psi}_a| < \infty$ and

$\Psi_b = \hat{\Psi}_b(x)\exp(st + ik_y y)$, $\quad |\hat{\Psi}_b| < \infty$, respectively, with $\Re s \geq 0$.

Extending the analysis above to discrete approximations to prove numerical stability without further simplifications is not trivial. The second major contribution of this work is proving stability of the discrete problem, a non-trivial task. This is done by constructing a semi-discrete energy estimate for sufficiently small damping $\sigma > 0$ which mimics the continuous estimate.

Numerical experiments

Consider a rectangular waveguide with the domain $(x, y) \in [-50, 50] \times [0, 50]$. A free-surface boundary condition $\mathbf{w} = 0$ is used at $y = 50$ and a characteristics boundary condition $\sqrt{B}\mathbf{u} - \mathbf{w} = 0$ is imposed at $y = 0$. In the x-direction we introduce two additional layers, having $50 \leq |x| \leq 50 + \delta$ in which the PML equations are solved. The PML is terminated with the boundary conditions $\sqrt{A}\mathbf{u} \pm \mathbf{v} = 0$ at $x = \pm(50 + \delta)$. The initial data for the velocities is $u_1 = u_2 = \exp\left(-\ln(2)\left(x^2 + (y - 25)^2\right)/9\right)$, and zero initial data is used for the stresses and auxiliary variables. The damping profile is a cubic monomial $\sigma(x) = d_0\Big(\left(|x| - 50\right)/\delta\Big)^3$, where $d_0 \geq 0$ is the damping strength; in all experiments $d_0 = 2$ and $\alpha = 0.5$. A 6th–order SBP operator is used for the spatial discretization with all boundary conditions enforced weakly. Temporal discretization is done with the classical fourth order accurate Runge–Kutta scheme using the time step $k = 0.5/\sqrt{3\mu + \lambda}h$. In the first experiment we evaluate the numerical errors , i.e., artificial reflections. We consider an aluminum waveguide defined by the velocity ratio $\gamma = c_s/c_p = 0.4593$, where c_p, c_s are the P–wave and the S–wave velocities, defined by $c_p = \sqrt{2\mu + \lambda/\rho}$, $\quad c_s = \sqrt{\mu/\rho}$. Note that a PML for this material has also been investigated in the frequency domain [5]. To quantify the numerical reflections we use a wide PML width, $\delta = 50$. We compute the solution until $t = 40$. We also compute a reference solution in a larger domain without the PML. Defining the error as the maximum difference between the two solutions we see $\mathcal{O}(h^4)$ convergence as shown in table 1.

To investigate the long time stability of the PML we use a spatial step $h = 0.5$, and run the simulation to $t = 5000$ using a PML width $\delta = 10$, i.e., a width closer to what would be used in practical calculations. Figure 1 shows the time history of the maximum energy for simulations with $\gamma = 0.1, 0.2, \ldots, 0.5$. As seen for all values of γ the energy decays down to 10^{-3}, showing the stability of the PML. This is particularly noteworthy, because in [3] numerical instabilities were seen to be more severe for small γ.

h	**error**	**rate**
1.0	2.32×10^{-7}	–
0.5	8.81×10^{-9}	4.72
0.25	5.05×10^{-10}	4.12
0.125	3.10×10^{-11}	4.03

Table 1: Numerical errors and convergence rate.

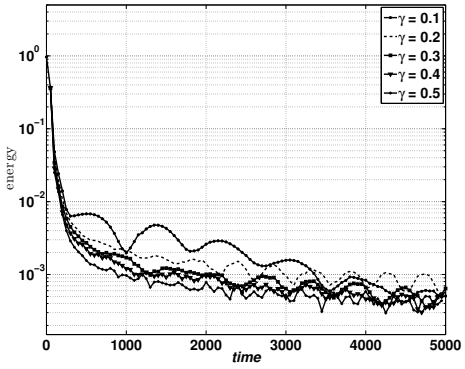

Figure 1: *Time history of the maximum energy for* $\gamma = 0.1, 0.2, 0.3, 0.4, 0.5$.

References

[1] D. Appelö and G. Kreiss. *A new absorbing layer for elastic waves*, J. Compt. Phys. **215** (2006), pp. 642–660.

[2] E. Bécache, S. Fauqueux, P. Joly, *Stability of Perfectly Matched Layers, Group Velocities and Anisotropic Waves*, J. Comp. Phys. **188** (2003), pp. 399–433.

[3] C. Zeng, J. Xia, R. Miller and G. Tsoflias, *Application of the multi-axial perfectly matched layer (M-PML) to near-surface seismic modeling with Rayleigh waves.* Geophysics **76** (2011), pp. 43–52.

[4] K. Duru and G. Kreiss, *Boundary waves and stability of the perfectly matched layer.* Dept. Info. Tech., Uppsala University, (2012), Tech. rep. 2012–007.

[5] E. A. Skelton, S.D.M. Adams and R. V. Craster, *Guided elastic waves and perfectly matched layers,* Wave Motion, **44** (2007) pp. 573–592.

Perfectly Matched Layers and Harmoniously Matched Layers: a numerical comparison for 2D acoustic propagation in heterogeneous media

L. Halpern[1], L. Métivier[2,*], J. Rauch[3]
[1]LAGA, Université Paris 13, Sorbonne Paris Cité, CNRS, UMR 7539, F-93430, Villetaneuse, France.
[2]LJK- Université Joseph Fourier - CNRS, UMR 5224, F-38041, Grenoble, France.
[3]University of Michigan, Ann Arbor, USA.
* Email: ludovic.metivier@ujf-grenoble.fr

Abstract

The Harmoniously Matched Layers (HML) were introduced by Halpern et al. in 2011 [2] for general hyperbolic operators. This method is based on an extrapolation of solutions using first-order layers. For constant coefficient problems, its numerical performances are comparable to those of Bérenger's PML [1], while preserving the strong well-posedness of the hyperbolic system. In homogeneous media, the PML are nonreflecting and absorbing. This is no longer true in heterogeneous media. In that case, other methods may become more attractive. Numerical experiments involving the propagation of 2D acoustic waves in an inhomogeneous medium show smaller amplitude reflections at the interface for the HML.

Introduction

The numerical simulation of wave propagation in unbounded media occurs in numerous industrial applications, such as radar detection or seismic imaging. In these contexts, the use of Perfectly Matched Layer (PML), introduced by Bérenger for the Maxwell system, has rapidly become the state-of-the-art technique to perform such simulations [1]. The domain of interest is surrounded with a damping layer, where the incident waves should be absorbed without reflections for any incidence angle. The original unknowns of the hyperbolic system related to the wave equation are split into non-physical unknowns, and a damping factor is introduced in the resulting equations. Years of successful applications due to its efficiency and its ease of implementation have followed Bérenger's discovery.

In the context of variable background coefficients, the model can still be used, but needs some care in the implementation and the mathematical analysis, as the reflectivity of the layer becomes non negligible, and strong well-posedness can be lost [3]. In this study, we are interested in a new layer method, introduced by Halpern et al [2], named Harmoniously Matched Layers (HML). This method is designed to keep the well-posedness of the original hyperbolic system by using a classical first-order damping layer (named SMART layer in the sequel). The reflectivity of the layer is controlled by an extrapolation technique which annihilates first-order reflections in the high frequency regime. The aim of this study is to compare PML and HML methods in the simple case of 2D acoustic waves propagation.

PML and HML formulation for 2D acoustic wave propagation within the subsurface

Consider the first-order velocity-stress formulation for the 2D propagation of acoustic waves in $\Omega = [0, L]^2 \subset \mathcal{R}^2$, with variable density $\rho(x_1, x_2)$ and velocity $c(x_1, x_2)$[1],

$$\left\{ \begin{array}{rcll} \partial_t u - \dfrac{1}{\rho}\nabla p & = & 0 & u(x_1, x_2, 0) = 0, \\ \partial_t p - \rho c^2 \mathrm{div} u & = & 0, & p(x_1, x_2, 0) = p_0(x_1, x_2). \end{array} \right. \tag{1}$$

Here, $u = (u_1, u_2)$ is the displacement velocity vector, p is the pressure wavefield, and p_0 is the initial pressure wavefield. The PML equations associated with system (1) are defined on $\Omega_l = [-l; L+l]^2 \subset \mathcal{R}^2$

$$\left\{ \begin{array}{l} \partial_t u_j - \dfrac{1}{\rho}\partial_j (p_1 + p_2) + \sigma_j u_j = 0 \\ \partial_t p_j - \rho c^2 \partial_j u_j + \sigma_j p_j = 0 \end{array} \right. \tag{2}$$

where p_j denote the non-physical split pressure wavefields, and $\sigma_j(x_j)$ are the absorbing coefficients non zero only in $\Omega_l \backslash \Omega$. This system is weakly well posed: for piecewise continuous velocity and impedance, energy estimates with one loss of derivatives have been obtained in [4]. The SMART equations add to the operator the zero order perturbation defined by the projectors on the relevant eigenspaces in each direc-

[1]For convenience, we restrict our notations to the square domain case. Extension to rectangular domains is straightforward.

tion.

$$\begin{cases} \partial_t u_j - \frac{1}{\rho}\partial_j p + \frac{1}{1+\rho^2 c^2} F_j(u,p) \\ \partial_t p - \rho c^2 \mathrm{div} u + \frac{\rho c}{1+\rho^2 c^2} \sum_{j=1,2} F_j(u,p) = 0. \\ F_j(u,p) = \left[\sigma_j^+ (u_j + \rho c p) + \sigma_j^- (u_j - \rho c p)\right] \end{cases} \tag{3}$$

where $\sigma_j^+ = (\sigma_j)_{|[L;L+l]}, \sigma_j^- = (\sigma_j)_{|[-l;0]}$ (see [2] for a detailed derivation of these equations). The SMART equations keep the strong well-posedness of the original system (1). Denote $U(\sigma) = (u_1, u_2, p)$ the solution of the SMART system for an absorption $\sigma = (\sigma_1, \sigma_2)$. The HML strategy consists in computing an extrapolation U_{HML} such that

$$U_{HML} = U(2\sigma) - 2U(\sigma). \tag{4}$$

Numerical study of reflectivity in a varying medium

Consider Ω and Ω_l such that $L = l = 5$. The density ρ is taken constant equal to 1. The non constant velocity c is

$$c(x_1, x_2) = 2 + \sin(3(x_1 - L)). \tag{5}$$

The absorption coefficients σ_j are the usual order 3 polynomials (exact formula are given for instance in [4]). Homogeneous Dirichlet boundary conditions are imposed at the boundary of Ω_l. We choose the initial condition p_0 such that, for $\mathbf{x} = (x_1, x_2)$, $\mathbf{x}_C = (4.5, 2)$, $\mathbf{v} = (1, -1)$, $k = 3$, $r = 0.8$:

$$\begin{aligned} p_0(x_1, x_2) &= f(x_1, x_2)\chi_{\|\mathbf{x}-\mathbf{x}_C\| \le r} \\ f(x_1, x_2) &= \cos^2\left(\pi \tfrac{\|\mathbf{x}-\mathbf{x}_C\|}{r}\right) \cos\left(k\pi \tfrac{\mathbf{v}.(\mathbf{x}-\mathbf{x}_C)}{r}\right) \end{aligned} \tag{6}$$

A "beam" centered on x_C propagates along the line $x = -z$ and hits the absorbing layer with an non-normal incidence angle. We present on figure 1 the resulting pressure wavefield at time $t = 0.75$ s and the difference of the PML, SMART and HML solution with the exact solution. The PML layer generates a reflected wave at the interface with the interest domain, whose infinity norm is close to 10^{-4}. The reflection generated by the SMART layer reaches 10^{-3} in infinity norm. Conversely, the extrapolation technique used for the HML method yield a significant decrease of the reflection, which only reaches 10^{-7} in infinity norm in this case.

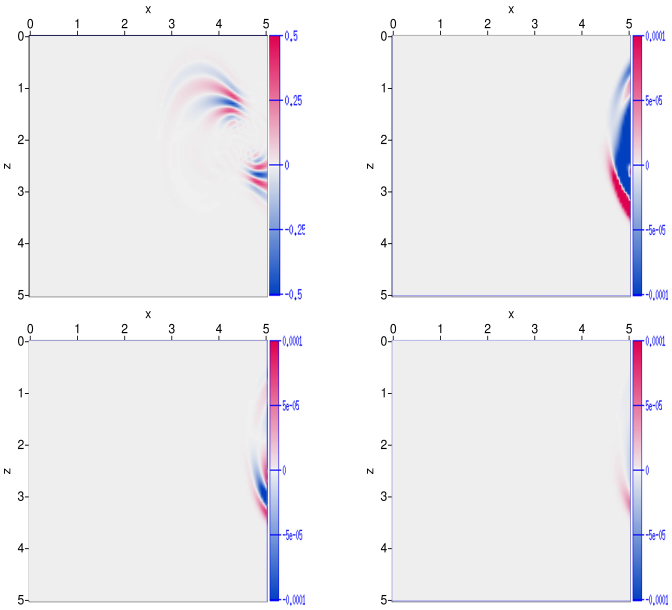

Figure 1. Exact pressure wavefield (top left). Difference between exact and results from SMART (top right), PML (bottom left), HML (bottom right).

Conclusion and perspectives

This preliminary experiment demonstrates that, for variable coefficients problems, the HML method can yield improvements in terms of reflectivity compared to the PML method. Another advantage is that the HML formulation keeps the well-posedness of the initial set of equations, which may yield more robust absorbing layer formulations for the simulation of wave propagating in elastic and anisotropic medias. The mathematical analysis of these models is undergoing.

References

[1] J.-P. BERENGER, *A perfectly matched layer for absorption of electromagnetic waves*, Journal of Computational Physics, 114 (1994), pp. 185–200.

[2] L. HALPERN, S. PETIT-BERGEZ, AND J. RAUCH, *The Analysis of Matched Layers*, Confluentes Mathematici, 3 (2011), pp. 159–236.

[3] J. HESTHAVEN, *On the analysis and construction of perfectly matched layers for the linearized euler equations*, Journal of Computational Physics, 142 (1998), pp. 129–147.

[4] L. MÉTIVIER, *Utilisation des équations Euler-PML en milieu hétérogène borné pour la résolution d'un problème inverse en géophysique.*, ESAIM: Proc., 27 (2009), pp. 156–170.

Dirichlet-to-Neumann boundary conditions for viscous acoustic equations

A. Semin[1,*], **K. Schmidt**[1]
[1] DFG research center MATHEON, TU Berlin, Berlin, Germany.
*Email: semin@math.tu-berlin.de

Abstract

In this study, we are investigating the acoustic equations which arise by perturbation techniques of the compressible Navier-Stokes equations around a stagnant uniform fluid, with mean density ρ_0, mean velocity c_0 and without heat flux on an unbounded domain. Our goal is to derive a Dirichlet-to-Neumann boundary condition to limit the computation domain. We give here the way to compute this Dirichlet-to-Neumann map and give some properties when the viscosity η tends to 0.

1 Formulation of the problem

Let $\Omega \subset \mathbb{R}^2$ be a compact perturbation of a flat semi-infinite waveguide of width L (see figure 1).

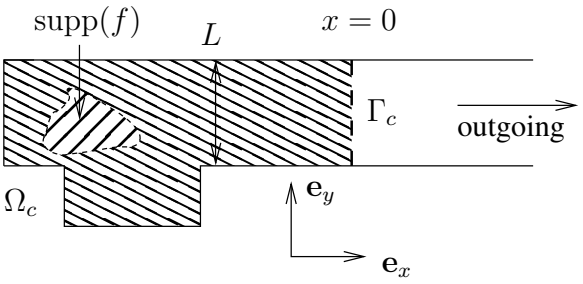

Figure 1: Perturbed waveguide Ω

We consider time-harmonic acoustic velocity $\mathbf{v}$ and acoustic pressure p (the time regime is $\exp(-\mathrm{i}\omega t)$, $\omega > 0$) which are described by the coupled system in the framework of Landau and Lifshitz [1], [2]

$$\omega^2\rho_0\mathbf{v} + c_0^2\rho_0\nabla(\operatorname{div}\mathbf{v}) - \mathrm{i}\omega\eta\Delta\mathbf{v} = \mathrm{i}\omega\mathbf{f}, \text{ in } \Omega, \quad (1a)$$

$$-\mathrm{i}\omega p + \rho_0 c_0^2 \operatorname{div}\mathbf{v} = 0, \text{ in } \Omega, \quad (1b)$$

$$\mathbf{v} = \mathbf{0}, \text{ on } \partial\Omega. \quad (1c)$$

In the *momentum equation* (1a) with some known source term $\mathbf{f}$ the viscous dissipation in the momentum is not neglected. The *continuity equation* (1b) relates the acoustic pressure linearly to the divergence of the acoustic velocity. The system is completed by *no-slip* boundary conditions (1c). Here we assume that $\mathbf{f} = 0$ on $\partial\Omega$ and $\mathbf{f}(x, y) = 0$ for $x \geqslant 0$. The associated variational formulation on the bounded domain Ω_c with artificial boundary Γ_c defined by

$$\begin{aligned}\Omega_c &= \{(x, y) \in \Omega \ / \ x < 0\} \\ \Gamma_c &= \{(x, y) \in \Omega \ / \ x = 0\}\end{aligned} \quad (2)$$

is, denoting by $\mathbf{n} = \mathbf{e}_x$ the unit normal vector and $\mathbf{t} = -\mathbf{e}_y$ the unit tangential vector of Ω_c on Γ_c:

$$\begin{aligned}-(\rho_0 c_0^2 - \mathrm{i}\eta\omega)\int_{\Omega_c} \operatorname{div}\mathbf{v}\operatorname{div}\varphi + \omega^2\rho_0\int_{\Omega_c}\mathbf{v}\cdot\varphi \\ -\mathrm{i}\eta\omega\int_{\Omega_c}\operatorname{curl}_{2D}\mathbf{v}\operatorname{curl}_{2D}\varphi + (\rho_0 c_0^2 - \mathrm{i}\eta\omega)\int_{\Gamma_c}\operatorname{div}\mathbf{v}(\varphi\cdot\mathbf{n}) \\ +\mathrm{i}\omega\int_{\Gamma_c}\eta\operatorname{curl}_{2D}\mathbf{v}(\varphi\cdot\mathbf{t}) = \mathrm{i}\omega\int_{\Omega_c}\mathbf{f}\cdot\varphi\end{aligned} \quad (3)$$

Our goal is to build a Dirichlet-to-Neumann (DtN) map that links both $\operatorname{div}\mathbf{v}$ and $\eta\operatorname{curl}_{2D}\mathbf{v}$ to both components of $\mathbf{v}$.

2 Projection on Fourier modes

We introduce w_p the normalized Fourier basis of $\mathrm{L}^2(0, L)$:

$$w_{-j}(y) = \sqrt{\frac{2}{L}}\sin\left(\frac{2j\pi y}{L}\right),\ w_0(y) = \sqrt{\frac{1}{L}},\ w_j(y) = \sqrt{\frac{2}{L}}\cos\left(\frac{2j\pi y}{L}\right)$$

and we decompose $\mathbf{v}$ over the Fourier basis, using the following ansatz

$$\mathbf{v}(x, y) = \begin{pmatrix} \sum_{j\geqslant 0}\alpha_j\exp(\lambda_j x)w_j(y) + \beta_j\exp(\mu_j x)w_{-j}(y) \\ \sum_{j\geqslant 0}\gamma_j\exp(\lambda_j x)w_{-j}(y) + \delta_j\exp(\mu_j x)w_j(y)\end{pmatrix} \quad (4)$$

with the convention $\beta_0 = \gamma_0 = 0$. We use ansatz (4) in (1a) and get, for any $j \geqslant 1$:

$$M(\lambda_j)\begin{pmatrix}\alpha_j \\ \gamma_j\end{pmatrix} = \begin{pmatrix}0 \\ 0\end{pmatrix} \quad (5)$$

$$M(\lambda_j)\begin{pmatrix}\beta_j \\ -\delta_j\end{pmatrix} = \begin{pmatrix}0 \\ 0\end{pmatrix} \quad (6)$$

with matrix $M(\lambda_j)$ that depends only on j and the physical parameters of the problem. Systems (5), (6) have trivial solution unless there exists $\lambda_j \in \mathbb{C}$ with negative real part such that

$$\det(M(\lambda_j)) = 0 \quad (7)$$

Equation (7) admits two different solutions that correspond to two different behaviours:

- a "fast" solution that corresponds to

$$\eta\lambda_{j,f}^2 = \eta\left(\frac{2j\pi}{L}\right)^2 - \mathrm{i}\omega\rho_0 \qquad (8)$$

  One can see in (8) that $\sqrt{\eta}|\lambda_{j,f}|$ tends to a constant as η tends to 0

- a "slow" solution that corresponds to

$$\lambda_{j,s}^2 = \left(\frac{2j\pi}{L}\right)^2 - \frac{c_0^2\omega^2 + \mathrm{i}\frac{\eta}{\rho_0}\omega^3}{c_0^4 + \omega^2\frac{\eta^2}{\rho_0^2}} \qquad (9)$$

  One can see in (9) that $\lambda_{j,s}$ tends, as η tends to 0, to

$$\mathrm{i}\sqrt{\frac{\omega^2}{c_0^2} - \left(\frac{2j\pi}{L}\right)^2}, j < \frac{\omega L}{2c_0\pi}, \quad -\sqrt{\left(\frac{2j\pi}{L}\right)^2 - \frac{\omega^2}{c_0^2}}, j > \frac{\omega L}{2c_0\pi}$$

For $j = 0$, systems (5) and (6) become degenerated and lead to the following equations

$$\begin{aligned}\alpha_0\left(\omega^2\rho_0 + c_0^2\rho_0\lambda_{0,s}^2 - \mathrm{i}\omega\eta\lambda_{0,s}^2\right) &= 0\\ \delta_0\left(\omega^2\rho_0 - \mathrm{i}\omega\eta\lambda_{0,f}^2\right) &= 0\end{aligned} \qquad (10)$$

and have the following solutions

$$\lambda_{0,s}^2 = \frac{-c_0^2\omega^2 - \mathrm{i}\frac{\eta}{\rho}\omega^3}{c_0^4 + \omega^2\frac{\eta^2}{\rho_0^2}} \text{ and } \lambda_{0,f}^2 = \frac{-\mathrm{i}\omega\rho_0}{\eta}$$

that corresponds formally to (9) and (8) taking $j = 0$.

3 Building the DtN maps

According to results of the previous section, we modify the ansatz (4) to:

$$\mathbf{v}(x,y) = \begin{pmatrix} \alpha_0\exp(\lambda_{0,s}x)w_0(y) \\ \quad + \sum_{j\geqslant 1}\alpha_{j,f}\exp(\lambda_{j,f}x)w_j(y) + \sum_{j\geqslant 1}\beta_{j,f}\exp(\lambda_{j,f}x)w_{-j}(y) \\ \quad + \sum_{j\geqslant 1}\alpha_{j,s}\exp(\lambda_{j,s}x)w_j(y) + \sum_{j\geqslant 1}\beta_{j,s}\exp(\lambda_{j,s}x)w_{-j}(y) \\ \delta_0\exp(\lambda_{0,f}x)w_0(y) \\ \quad + \sum_{j\geqslant 1}\delta_{j,f}\exp(\lambda_{j,f}x)w_j(y) + \sum_{j\geqslant 1}\gamma_{j,f}\exp(\lambda_{j,f}x)w_{-j}(y) \\ \quad + \sum_{j\geqslant 1}\delta_{j,s}\exp(\lambda_{j,s}x)w_j(y) + \sum_{j\geqslant 1}\gamma_{j,s}\exp(\lambda_{j,s}x)w_{-j}(y) \end{pmatrix} \qquad (11)$$

where $(\alpha_{j,i}, \gamma_{j,i})$ and $(\beta_{j,i}, \delta_{j,i})$, for $i = \{f, s\}$ are linked through (5) and (6). In addition, we have the following

$$\begin{aligned}\alpha_{j,f} + \alpha_{j,s} &= \langle\mathbf{v}(x=0)\cdot\mathbf{n}, w_j\rangle\\ \beta_{j,f} + \beta_{j,s} &= \langle\mathbf{v}(x=0)\cdot\mathbf{n}, w_{-j}\rangle\\ \gamma_{j,f} + \gamma_{j,s} &= -\langle\mathbf{v}(x=0)\cdot\mathbf{t}, w_{-j}\rangle\\ \delta_{j,f} + \delta_{j,s} &= -\langle\mathbf{v}(x=0)\cdot\mathbf{t}, w_j\rangle\end{aligned} \qquad (12)$$

where $\langle\cdot\,\cdot\rangle$ is the L^2 scalar product on $(0, L)$. To solve the systems defining $(\alpha_{j,i}, \gamma_{j,i})$ and $(\beta_{j,i}, \delta_{j,i})$, for $i = \{f, s\}$ let us rewrite $\mathbf{v}$ in (11) in terms of normal and tangential traces. Finally, we build our DtN maps computing $\operatorname{div}\mathbf{v}(x=0)$ and $\eta\operatorname{curl}_{2D}\mathbf{v}(x=0)$ as functions of $\mathbf{v}$:

$$\begin{aligned}\operatorname{div}\mathbf{v}(x=0) = &\sum_{j\in\mathbb{Z}} D_{|j|,\mathbf{n}}\langle\mathbf{v}\cdot\mathbf{n}, w_j\rangle w_j\\ &-\sum_{j\in\mathbb{Z}}\operatorname{sgn}(j)D_{|j|,\mathbf{t}}\langle\mathbf{v}\cdot\mathbf{t}, w_{-j}\rangle w_j\end{aligned} \qquad (13)$$

$$\begin{aligned}\eta\operatorname{curl}_{2D}\mathbf{v}(x=0) = &-\sum_{j\in\mathbb{Z}} R_{|j|,\mathbf{t}}\langle\mathbf{v}\cdot\mathbf{t}, w_j\rangle w_j\\ &-\sum_{j\in\mathbb{Z}}\operatorname{sgn}(j)R_{|j|,\mathbf{n}}\langle\mathbf{v}\cdot\mathbf{n}, w_{-j}\rangle w_j\end{aligned} \qquad (14)$$

with $D_{|j|,\mathbf{n}}$, $D_{|j|,\mathbf{t}}$, $R_{|j|,\mathbf{n}}$ and $R_{|j|,\mathbf{t}}$ depending on $\lambda_{j,i}$ and physical parameters. The boundary terms of variational formulation (3) with DtN maps (13),(14) becomes:

$$\begin{aligned}&\left(\rho_0 c_0^2 - \mathrm{i}\eta\omega\right)\int_{\Gamma_c}\sum_{j\in\mathbb{Z}} D_{|j|,\mathbf{n}}\langle\mathbf{v}\cdot\mathbf{n}, w_j\rangle\langle\varphi\cdot\mathbf{n}, w_j\rangle\\ -&\left(\rho_0 c_0^2 - \mathrm{i}\eta\omega\right)\int_{\Gamma_c}\sum_{j\in\mathbb{Z}}\operatorname{sgn}(j)D_{|j|,\mathbf{t}}\langle\mathbf{v}\cdot\mathbf{t}, w_{-j}\rangle\langle\varphi\cdot\mathbf{n}, w_j\rangle\\ &-\mathrm{i}\omega\int_{\Gamma_c}\sum_{j\in\mathbb{Z}} R_{|j|,\mathbf{t}}\langle\mathbf{v}\cdot\mathbf{t}, w_j\rangle\langle\varphi\cdot\mathbf{t}, w_j\rangle\\ &-\mathrm{i}\omega\int_{\Gamma_c}\sum_{j\in\mathbb{Z}} R_{|j|,\mathbf{n}}\langle\mathbf{v}\cdot\mathbf{n}, w_{-j}\rangle\langle\varphi\cdot\mathbf{t}, w_j\rangle\end{aligned}$$

One can remark that the limit behaviour of these coefficients is

$$\lim_{\eta\to 0} D_{j,\mathbf{n}} = -\frac{\omega^2}{c_0^2\lim_{\eta\to 0}\lambda_{j,s}} \text{ and } \lim_{\eta\to 0} D_{j,\mathbf{t}} = 0$$

$$\lim_{\eta\to 0} R_{j,\mathbf{n}} = 0 \text{ and } \lim_{\eta\to 0} R_{j,\mathbf{t}} = 0$$

which is expected (we obtain formally these DtN maps considering $\eta = 0$ in (1)).

References

[1] Landau, L. D. and Lifshitz, E. M.: Fluid Mechanics. Course of theoretical physics, Vol. 6. Pergamon press, New York, 1959.

[2] Schmidt, K. and Thöns-Zueva, A. *Asymptotic analysis for acoustics in viscous gases close to rigid walls.* Preprint 2012-4, Inst. f. Math., TU Berlin, 2012

New transparent boundary condition for time harmonic acoustic diffraction in anisotropic media.

A.-S. Bonnet-Ben Dhia[1], **S. Fliss**[1], **A. Tonnoir**[1,*]
[1] POEMS (UMR 7231 CNRS-ENSTA-INRIA)
*Email: antoine.tonnoir@ensta.fr

Introduction

Many industrial applications require to check the quality of structures such as plates, for instance in aircraft design. A common way to inspect structures is to propagate ultrasonic waves and detect from the experimental results the presence or not of a defect or a crack. However, in aeronautics, structures are often complex media like anisotropic elastic plates for which the interpretation of these results is complicated. Therefore, efficient and accurate numerical methods of simulation are required.

In our work, we want to study the diffraction of a time harmonic wave by a bounded defect in an anisotropic elastic plate. In order to study the diffraction properties of the defect, we consider it in an infinite plate. Since the defect has an arbitrary geometry, we want to use a finite element method in a box that surrounds the defect. On the boundary of this artificial box, we need to find transparent conditions to simulate an infinite domain.

To develop this method, we start with the acoustic, dissipative and isotropic case for which we present the construction of new transparent boundary conditions that can be easily extended to the anisotropic case. We mainly use the ideas developed in [1], [2].

1 Model problem and reformulation

Let us consider

$$\begin{cases} \Delta u + k_\epsilon^2 u = f \text{ in } \Omega \\ \partial_\nu u = 0 \text{ on } \partial\mathcal{O} \end{cases} \qquad (P_\Omega)$$

where $\mathcal{O}$ is a bounded obstacle, ν the exterior normal of $\partial\mathcal{O}$, Ω is defined as $\mathbb{R}^2 \setminus \mathcal{O}$, and f is compactly supported. We suppose that $k_\epsilon^2 = k^2 + i\epsilon$ with $\epsilon > 0$ so that the problem (P_Ω) has a unique solution in $H^1(\Omega)$.

We intend to formulate an equivalent problem defined on a bounded domain. Let surround $\mathcal{O}$ and the support of f by an artificial square denoted Σ_{aa}, centered in $(0,0)$ and of length $2a$. We also define a second square denoted Σ_{bb} of length $2b > 2a$ (see figure 1) and denote by Ω_i the domain $[-b,b]^2 \setminus \mathcal{O}$.

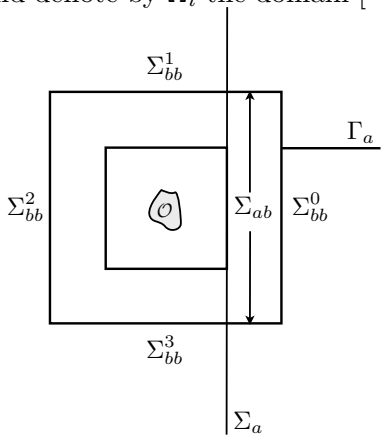

Figure 1: Geometry and notations

To make the presentation easier, we consider that f and $\mathcal{O}$ are symmetric with respect to $\{y = x\}$, $\{y = -x\}$ and $\{x = 0\}$. In this case, we will see in the following that the problem can be restricted to a coupled system where the only unknowns are

- u_i, the restriction of u in Ω_i,
- φ_a, the trace of u on $\Sigma_a = \{x = a\} \times \mathbb{R}$.

First, let us remark that by definition the unknowns verify

$$\begin{cases} \Delta u_i + k_\epsilon^2 u_i = f \text{ in } \Omega_i \\ \partial_\nu u_i = 0 \text{ on } \partial\mathcal{O} \\ \varphi_a = u_i \text{ on } \Sigma_{ab} = \{x = a\} \times [-b,b]. \end{cases} \qquad (P)$$

Let us introduce for all $\varphi_a \in H^{\frac{1}{2}}(\Sigma_a)$, $u_H(\varphi_a)$ the unique solution in $H^1(\Omega_H)$ of

$$\begin{cases} \Delta u_H + k_\epsilon^2 u_H = 0 \text{ in } \Omega_H = \{x \geq a\} \times \mathbb{R} \\ u_H = \varphi_a \text{ on } \Sigma_a. \end{cases} \qquad (P_H)$$

This half space problem can be analytically solved by using a Fourier transform in y and solving the ODE in x. We can then determine analytically two operators defined by

- $D : \varphi \in H^{\frac{1}{2}}(\Sigma_a) \to D\varphi \in H^{\frac{1}{2}}(\Gamma_a)$ where $D\varphi = u_H(\varphi)|_{\Gamma_a}$ where $\Gamma_a =]b, +\infty[\times\{y = a\}$,
- $\Lambda : \varphi \in H^{\frac{1}{2}}(\Sigma_a) \to \Lambda\varphi \in H^{-\frac{1}{2}}(\Sigma^0_{bb})$ where $\Lambda\varphi = \partial_x u_H(\varphi)|_{\Sigma^0_{bb}}$.

Using continuity of the normal trace of u on Σ^0_{bb}, we have $\partial_x u_i = \Lambda\varphi_a$ on Σ^0_{bb} and by symmetry og u_i with respect to $\{y = x\}$ and $\{y = -x\}$, we can deduce

$$\partial_{\nu_i} u_i = \Lambda\varphi_a \text{ on } \Sigma^i_{bb} \tag{1}$$

where ν_i is the exterior normal of Ω_i. Moreover, by symmetry with respect to $\{y = x\}$, we have

$$\varphi_a|_{\{y\geq b\}} = D\varphi_a \tag{2}$$

and by symmetry with respect to $\{x = 0\}$, we have $\varphi_a = D\varphi_a$ for $y \leq -b$ too.
The coupled system that satisfy (u_i, φ_a) is then

$$\begin{cases} \Delta u_i + k_\epsilon^2 u_i = f \text{ in } \Omega_i \\ \partial_\nu u_i = 0 \text{ on } \partial\mathcal{O} \\ \partial_\nu u_i = \Lambda\varphi_a \text{ on } \Sigma^i_{bb} \\ \varphi_a = u_i \text{ on } \Sigma_{ab} \\ \varphi_a|_{\{\pm y\geq b\}} = D\varphi_a \end{cases} \tag{P}$$

Let us remark that even if the thickness $b > a$ is not natural, we expect that it will have the same benefit for an iterative resolution as an overlap for decomposition domain methods. Using [1], we know that for the case $b = a$, this problem has a unique solution. For $b > a$, this is still an open question.
Contrary to the usual method for isotropic media (using Fourier series or Green function), this formulation can be extended to a homogeneous anisotropic medium since it only use Fourier transform.

2 Numerical validation

The main difficulty in discretizing (P) is that the operators D and Λ have an integral form.

2.1 Computation of φ_a

We first focus on the problem satisfied by φ_a which can be reduced, using again symmetry with respect to $\{x = 0\}$, to

$$\begin{cases} \varphi_a = g \text{ on } [0, b] \\ \varphi_a = D\varphi_a \text{ on } [b, +\infty[\end{cases} \tag{P_{Σ_a}}$$

for a given $g \in H^{\frac{1}{2}}([0, b])$. To compute this problem, we approximate φ_a by a piecewise P_1 function, and the Fourier integral is replaced by a quadrature formula.

To validate this discretization, we suppose that g is the trace of the Hankel function (ie $H(k_\epsilon\sqrt{x^2 + y^2})$) on Σ_{ab} and we know that we should find φ_a as the trace of this Hankel function on Σ_a. On figure 2, we see that the reconstruction (cross line) matches with the exact solution (continuous line).

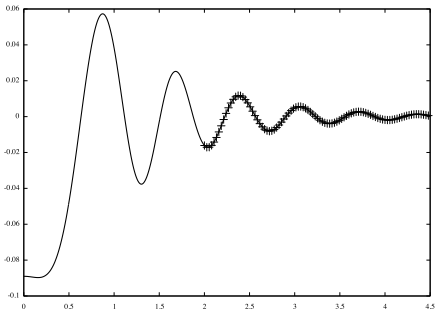

Figure 2: Solution of (P_{Σ_a}) $(b = 2)$

2.2 Solution of the coupled system

We use to approximate u_i a classical finite element discretization. To validate the numerical method, we compute the solution for $\mathcal{O}$ a circle of radius $r < a$ and $\partial_\nu u = 1$ on $\partial\mathcal{O}$. We obtain a solution of the coupled system (P), represented in Figure 3, which is as expected an approximation of the Hankel function.

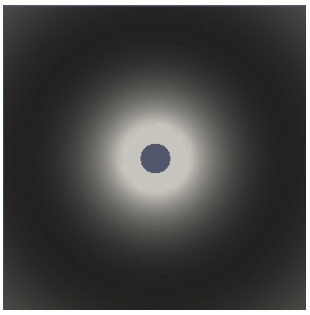

Figure 3: Solution of (P_{Σ_a})

References

[1] S. Fliss, P. Joly, *Exact boundary conditions for time-harmonic wave propagation in locally perturbed periodic media*, Applied Numerical Mathematics, **59** (2009), pp. 2155–2178.

[2] A.-S Bonnet-Ben Dhia, A. Tillequin, *A generalized mode matching method for scattering problems with unbounded obstacles*, Journal of Computational Acoustics, **9** (2001), pp. 1611–1631

An exact NRBC for 2D wave equation problems in unbounded domains

S. Falletta[1,*], **G. Monegato**[2]
[1,2] DISMA - Politecnico di Torino.
*Email: silvia.falletta@polito.it

Abstract

We consider some 2D wave equation problems defined in an unbounded domain. For their solution, by means of standard finite element or finite difference methods, we propose a non reflecting boundary condition (NRBC) on the chosen artificial boundary $\mathcal{B}$, which is based on a space-time integral equation defining a relationship between the solution of the differential problem and its normal derivative on $\mathcal{B}$. Such a NRBC is exact, non local both in space and time and allows the treatment of incoming and outcoming waves. We discretize it by using a fast convolution quadrature in time, based on a second order BDF rule, and a collocation method in space based on continuous piecewise linear approximants. The proposed NRBC has the property of being suitable for artificial boundaries of general shapes (even of non-convex type, and having also corners, if necessary). From the computational point of view, it is competitive with well known existing NRBCs of local type. Furthermore, it allows the treatment of far field sources that do not have to be necessarily included in the finite computational domain.

Introduction

Let $\Omega^i \subset \mathbb{R}^2$ be an open bounded domain with a sufficiently smooth boundary Γ; define $\Omega^e = \mathbb{R}^2 \setminus \bar{\Omega}^i$. We consider the following wave propagation problem in Ω^e:

$$\begin{cases} u^e_{tt}(\mathbf{x},t) - \Delta u^e(\mathbf{x},t) &= f(\mathbf{x},t) \quad \text{in } \Omega^e \times (0,T) \\ u(\mathbf{x},t) &= g(\mathbf{x},t) \quad \text{in } \Gamma \times (0,T) \\ u^e(\mathbf{x},0) &= u_0(\mathbf{x}) \quad \text{in } \Omega^e \\ u^e_t(\mathbf{x},0) &= v_0(\mathbf{x}) \quad \text{in } \Omega^e, \end{cases}$$

where the initial condition u_0, the initial velocity v_0 and the source term f are either trivial or have local supports. We truncate the infinite domain Ω^e by introducing an artificial smooth boundary $\mathcal{B}$. This boundary divides Ω^e into two sub-domains: a finite computational domain Ω, which is bounded internally by Γ and externally by $\mathcal{B}$, and an infinite residual domain $\mathcal{D}$.

The artificial boundary is chosen in such a way that it detects the region where one is interested in computing the solution. This region does not necessarily have to contain the supports of the source term and of the initial data. When the support of a datum is contained in the residual domain $\mathcal{D}$, the datum is taken into account by a corresponding term of the artificial boundary condition.

We impose on $\mathcal{B}$ the integral relation that the solution u and its outward normal derivative $\partial_{\mathbf{n}_\mathcal{D}} u$ have to satisfy. This is:

$$\begin{aligned} \frac{1}{2}u(\mathbf{x},t) &= \mathcal{V}\partial_{\mathbf{n}_\mathcal{D}} u(\mathbf{x},t) - \mathcal{K}u(\mathbf{x},t) + I_{u_0}(\mathbf{x},t) \\ &\quad + I_{v_0}(\mathbf{x},t) + I_f(\mathbf{x},t) \quad \mathbf{x} \in \mathcal{B}, \end{aligned}$$

$$\mathcal{V}\lambda(\mathbf{x},t) := \int_0^t \int_\mathcal{B} G(\mathbf{x}-\mathbf{y}, t-\tau)\lambda(\mathbf{y},\tau) d\mathcal{B}_\mathbf{y} d\tau,$$

$$\mathcal{K}\varphi(\mathbf{x},t) = \int_0^t \int_\mathcal{B} \partial_{\mathbf{n}_\mathcal{D}} G(\mathbf{x}-\mathbf{y}, t-\tau)\varphi(\mathbf{y},\tau) d\mathcal{B}_\mathbf{y} d\tau,$$

where $G(\mathbf{x},t)$ is the wave equation fundamental solution in $\mathbb{R}^2$, I_{u_0}, I_{v_0} and I_f are possible "volume" terms generated by the non trivial source and the non homogeneous initial conditions whose supports are in $\mathcal{D}$ (see [1]).

1 Restriction of the model problem to the domain of interest

Let $X = \{u \in H^1(\Omega), u = g \,\text{on}\, \Gamma\}$ and $X_0 = \{u \in H^1(\Omega), u = 0 \,\text{on}\, \Gamma\}$; denote by $\lambda(\mathbf{x},t) = \lambda(t)(\mathbf{x}) := \partial_\mathbf{n} u(\mathbf{x},t)$, which is defined only on the boundary $\mathcal{B}$, and set $u(t)(\mathbf{x}) = u(\mathbf{x},t)$. We consider the weak formulation: find $u(t) \in C^0([0,T]; X) \cap C^1([0,T]; L^2(\Omega))$ and $\lambda(t) \in C^0([0,T]; H^{-1/2}(\mathcal{B}))$ such that for all $w \in X_0$

$$\begin{cases} \frac{d^2}{dt^2}(u(t),w)_\Omega + a(u(t),w) - (\lambda(t),w)_\mathcal{B} &= (f(t),w), \\ \frac{1}{2}u(\mathbf{x},t) + \mathcal{V}\lambda(\mathbf{x},t) + \mathcal{K}u(\mathbf{x},t) &= 0 \ \text{ on } \mathcal{B} \\ u(0) &= u_0 \\ \frac{du}{dt}(0) &= v_0. \end{cases}$$

for $t \in (0,T]$ (here for simplicity we suppose that the supports of u_0, v_0 and f are contained in Ω, so that $I_{u_0} = I_{v_0} = I_f = 0$).

1.1 *FEM/ Lubich-collocation method coupling*

To solve the problem in the finite computational domain Ω, we discretize the space-time integral equation by combining a second order (in time) BDF convolution quadrature (see [2]) with a classical space collocation method. Such a discretization is then coupled with an unconditionally stable ODE time integrator and a FEM in space. If we use, for example, the Crank-Nicolson ODE rule, the final global linear system takes the following form:

$$\begin{aligned}\Big(\mathbf{M}+\frac{\Delta_t^2}{4}\mathbf{A}\Big)\mathbf{U}_{n+1} \quad &- \quad \frac{\Delta_t^2}{4}\mathbf{Q}\mathbf{\Lambda}_{n+1} = \Big(\mathbf{M}-\frac{\Delta_t^2}{4}\mathbf{A}\Big)\mathbf{U}_n \\ +\frac{\Delta_t^2}{4}\mathbf{Q}\mathbf{\Lambda}_n \quad &+ \quad \Delta_t\mathbf{M}\mathbf{V}_n+\frac{\Delta_t^2}{4}\Big(\mathbf{F}_{n+1}+\mathbf{F}_n\Big)\end{aligned}$$

$$\begin{aligned}\left(\frac{1}{2}\mathbf{I}+\mathbf{K}_0\right)\mathbf{U}^{\mathcal{B}}_{n+1}+\mathbf{V}_0\mathbf{\Lambda}_{n+1} \quad &= \quad -\sum_{j=0}^{n}\mathbf{K}_{n+1-j}\mathbf{U}^{\mathcal{B}}_j, \\ &- \quad \sum_{j=0}^{n}\mathbf{V}_{n+1-j}\mathbf{\Lambda}_j.\end{aligned}$$

where M, A and Q are the finite element mass, stiffness and boundary mass matrices respectively; $\mathbf{V}_n$ and $\mathbf{K}_n$ represent the discretizations of the single and double layer operators in terms of the Lubich/collocation technique. For each row index, the corresponding row elements of all the matrices $\mathbf{V}_n$ and $\mathbf{K}_n$ can be computed simultaneously by means of the FFT algorithm. Moreover, when the boundary $\mathcal{B}$ is that of a circle, and a uniform partition of it is considered, then all the matrices $\mathbf{V}_j$ and $\mathbf{K}_j$, $j=0,\cdots,N$ have a Toeplitz structure. This property reduces significantly the storage and the computational cost of this ABC. When we have to deal with a general boundary, or with a nonuniform partition, then the above property does not hold. Nevertheless, the matrices $\mathbf{V}_j$ and $\mathbf{K}_j$, $j=0,\cdots,N$ can be approximated by corresponding very sparse matrices. This phenomenon is even more relevant in the 3D case. Thus, also in the case of a boundary $\mathcal{B}$ with no special properties, the computational cost of our NRBC can be drastically cut down. Memory and computational cost issues of the proposed approach will be discussed, as well as other features that can allow a significant save of storage and computational overhead. Its generalization to 3D domains is straightforward. We will present some results we have obtained in the case of non trivial initial data, sources which are away from the computational domain Ω, multi-scattering and artificial boundaries with corners.

Figure 1: Example 1. Snapshots of the solution with a non trivial initial datum u_0, at different times.

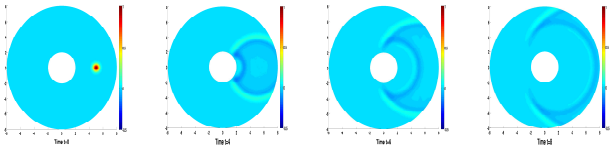

Figure 2: Example 2. Snapshots of the solution at different times: a non trivial initial datum with two humps and a nut shape artificial boundary.

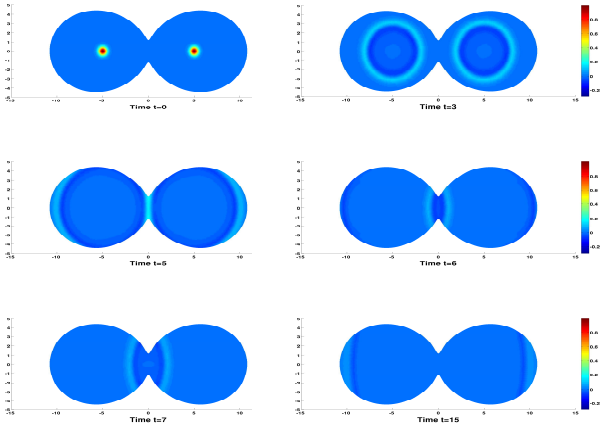

Figure 3: Example 3. An example of artificial boundary with corners: comparison between the approximate and the exact solution at the point P

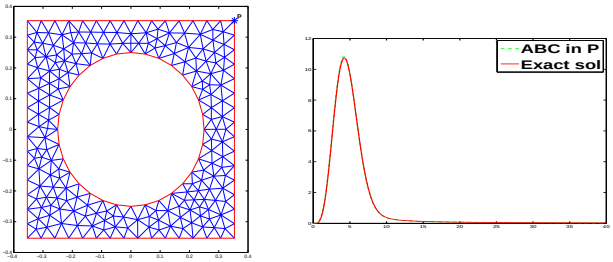

References

[1] S. Falletta, G. Monegato and L. Scuderi, *A space-time BIE method for nonhomogeneous exterior wave equation problems. The Dirichlet case*, IMA J. Numer. Anal., **32** (2012), pp. 202–226.

[2] Ch. Lubich, *Convolution quadrature and discretized operational calculus. I*, Num. Math.,**52** (1988), pp. 129–145.

3.13 High frequency approximation and numerics

Error Estimates for Helmholtz Gaussian Beam Superpositions

H. Liu[1], J. Ralston[2], O. Runborg[3,4,*], N. Tanushev[5]
[1] Department of Mathematics, Iowa State University
[2] UCLA Department of Mathematics
[3] Department of Mathematics, KTH
[4] Swedish e-Science Research Center (SeRC)
[5] Z-Terra Inc.
[*]Email: olofr@math.kth.se

Abstract

In this work we construct and estimate the error in Gaussian beam superposition approximations to solutions of the high frequency Helmholtz equation with a localized source.

Introduction

We are interested in the accuracy of Gaussian beam approximations to solutions of the high frequency Helmholtz equation,

$$\Delta u + (i\alpha k + k^2)n^2 u = f, \qquad x \in \mathbb{R}^d. \tag{1}$$

Here $k > 0$ is the wave number, assumed to be large, $n(y)$ is the index of refraction and $f(y;k)$ is a source function which in general also depends on k. The nonnegative parameter α represents absorption.

Gaussian beams constitutes a high frequency asymptotic model for wave propagation [6], [1]. It is closely related to geometrical optics [3] and assumes a solution of the form

$$u = ae^{ik\phi}, \tag{2}$$

where ϕ is the phase, and a is the amplitude. Unlike geometrical optics, the phase ϕ is complex-valued, and there is no breakdown of this model at caustics. The solution is concentrated near a single ray of geometrical optics. The phase function is real-valued along the ray and its imaginary part is chosen so that the solution decays exponentially away from the central ray, maintaining a Gaussian-shaped profile. More general high frequency solutions that are not necessarily concentrated on a single ray can be described by superpositions of Gaussian beams.

We study the accuracy in terms of k of Gaussian beams superpositions for (1). This would give a rigorous foundation for beam based numerical methods used to solve (1) in the high frequency regime. In the time-dependent case several such error estimates have been derived in recent years, see e.g. [4] and references therein. There have, however, not been any rigorous error estimates of this type available for the Helmholtz equation.

Direct numerical simulation of (1) becomes expensive when the wave number k is high, since a large number of grid points is then needed to resolve the wave oscillations. Numerical methods based on Gaussian beam superpositions have a much weaker cost dependence on the frequency. They go back to the 1980's but in the past decade there has been a renewed interest in such methods for waves following their successful use in seismic imaging. Development of new beam based methods are now the subject of intense interest in the numerical analysis community, see e.g. [2] for a survey.

1 Construction of Gaussian beams

The construction of the phases and amplitudes for Gaussian beams has become standard (see, for example, [6]). For first order beams

$$\phi(y) = S(s) + (y - x(s)) \cdot p(s) + \frac{1}{2}(y - x(s)) \cdot M(s)(y - x(s)),$$

and

$$a(y) = A_0(s),$$

where s is a function of y (see below). Each beam concentrates on a geometrical optics ray $\gamma = \{x(s) : s \in \mathbb{R}\}$, which is the spatial part of the bicharacteristics $(x(s), p(s))$ defined by the ODEs,

$$\dot{x} = 2p, \quad \dot{p} = -\partial_x n^2(x). \tag{3}$$

The ODEs for S, M, A_0 are

$$\dot{S} = 2n^2(x(s)) \qquad \dot{M} = (n^2)_{xx}(x(s)) - 2M^2$$
$$\dot{A}_0 = -\mathrm{tr}(M(s))A_0 - \alpha n^2(x(s))A_0.$$

With these definitions, the phase ϕ can be any function satisfying $\phi(x(s)) = S(s)$, $\phi_x(x(s)) = p(s)$ and $\phi_{xx}(x(s)) = M(s)$. However, to write down such a

function we need to have s as a function of y. We let $x(s(y))$ be the closest point on γ to y. This is only well-defined in a tubular neighborhood of γ. Therefore, we also restrict the support of u to this neighborhood by multiplying it with a smooth cutoff function. Note that $s(y)$ is constant on planes orthogonal to γ. Higher order beams can be constructed in a similar way.

1.1 Source

To define how the source function generates beams, we introduce the surface $\Sigma = \{x : \rho(x) = 0\}$ with $|\nabla\rho| = 1$ on Σ. We construct Gaussian beams $u^{\pm}$ centered on the forward ($s > 0$) and backward ($s < 0$) portions of a ray that leaves Σ in the normal direction when $s = 0$. Hence, both u^+ and u^- will have the form (2) but they will correspond to γ traced in opposite directions. The initial data of the corresponding bicharacteristics satsifies $x^{\pm}(0) =_{def} x_0 \in \Sigma$ and $p^{\pm}(0)$ is normal to Σ at x_0. We next choose the two beam phases $\phi^{\pm}$ so that $\phi^+ = \phi^-$ and $\nabla\phi^+ = -\nabla\phi^-$ on Σ. If their amplitudes $A^{\pm}$ are chosen so that $A^+ = A^- = A$ on Σ, then $u_{GB} = u^+ + u^-$ will satisfy

$$\Delta u_{GB} + (i\alpha k + k^2)n^2 u_{GB} = \left[ik\left(\frac{\partial\phi^+}{\partial\nu} - \frac{\partial\phi^-}{\partial\nu}\right)A + \frac{\partial A^+}{\partial\nu} - \frac{\partial A^-}{\partial\nu}\right]e^{ik\phi^+}\delta(\rho) + f_{GB} =_{def} g_0\delta(\rho) + f_{GB}, \tag{4}$$

where $\nu = \nabla\rho$ is the unit normal to Σ. We consider the singular part of the right hand side $g_0\delta(\rho)$ as a fundamental source term, and f_{GB} as the error from the Gaussian beam construction; it tends to zero with increasing k. Note that $g_0 = g_0(y, x_0, k)$ where x_0 is the initial point.

1.2 Superpositions

To construct superpositions of Gaussian beams we denote by $u_{GB}(y; z)$ the Gaussian beam constructed above for starting point $z \in \Sigma$. Then

$$u(y) = \left(\frac{k}{2\pi}\right)^{\frac{d-1}{2}} \int_\Sigma u_{GB}(y; z)h(z)dA_z \tag{5}$$

is an approximation to the exact solution for the source

$$g(y, k)\delta(\rho) =_{def} \left(\frac{k}{2\pi}\right)^{\frac{d-1}{2}} \int_\Sigma g_0(y, z, k)\delta(\rho)h(z)dA_z, \tag{6}$$

where g_0 is the fundamental source term in (4) and $h(z)$ is any smooth compactly supported function.

2 Error estimate

We now state our main result on the error for superposition (5). We assume that there is a number $R > 0$ such that the (smooth) index of refraction satisfies $n(x) \equiv 1$ when $|y| > R$ and that the source function $g(y, k)$ in (6) is compactly supported in $\{|y| < R\}$. The essential additional hypothesis for our estimate is that the index of refraction does not lead to trapped rays, more precisely that there is an L such that $|x(L)| > 2R$ for all solutions of (3) with $|x(0)| < R$ and $|p(0)| = n(x(0))$. We then have

Theorem 2.1 *Let u_E be the exact solution to (1) with the source in (6), and let u be the Gaussian beam superposition defined in (5). Under the assumptions above, we then have the following estimate*

$$\|u - u_E\|_{L^2(|x|\le R)} \le Ck^{-1/2}, \tag{7}$$

where C is independent of x and k, but may depend on R.

We note that this is the same error dependence on k that has previously been derived for time-dependent wave equations [4]. As in that case, for higher order beams we expect $k^{-1/2}$ be replaced by $k^{-n/2}$ where n is the beam order.

In the proof the Gaussian beam solution u_{GB} is first modified at infinity by a version of the procedure used in [5], such that it satisfies (1) exactly for large enough $|y|$, but also slightly modifying f_{GB} for small $|y|$. The small change in f_{GB} is estimated by stationary phase arguments and techniques similar to those in [4] are used to estimate f_{GB} itself. Finally, the estimates derived by Vainberg [7] for compactly supported sources can be applied to $u_E - u$.

References

[1] V. C. Červený, M. M. Popov, and I. Pšenčík. *Geophys. J. R. Astr. Soc.*, 70:109–128, 1982.

[2] S. Jin, P. Markowich, and C. Sparber. *Acta Numerica*, pages 1–89, 2012.

[3] J. Keller. *J. Opt. Soc. Amer*, 52, 1962.

[4] H. Liu, O. Runborg, and N. M. Tanushev. *Math. Comp.*, In Press 2012.

[5] A. Majda, and J. Ralston. *Duke Math. Journal*, Vol. 45(1978), 183-196

[6] J. Ralston. volume 23 of *MAA Stud. Math.*, pages 206–248. Math. Assoc. America, 1982.

[7] B. Vainberg. *Uspekhi (Russian Math. Surveys)*, 30(2):1–58, 1975.

On justification of a NLS model for laser beams in photopolymers

D. Pelinovsky[1], **D. Ponomarev**[2,*]
[1] Department of Mathematics, McMaster University, Hamilton, Ontario, Canada, L8S 4K1
[2] APICS team, INRIA Sophia Antipolis Méditerranée, 06902 Biot, France
*Email: dmitry.ponomarev@inria.fr

Abstract

A nonstationary model that relies on the spatial nonlinear Schrödinger (NLS) equation with the time-dependent refractive index describes laser beams in photopolymers. We consider a toy problem, when the rate of change of refractive index is proportional to the squared amplitude of the electric field and the spatial domain is a plane. In the present work, we derive the NLS approximation from a two-dimensional quasi-linear wave equation and rigorously justify this model for appropriately small time intervals and smooth initial data. Numerical simulations illustrate the approximation result in the one-dimensional case.

1 Introduction

Mathematical models for laser beams in photochemical materials used in physical literature [2] are based on a spatial nonlinear Schrödinger (NLS) equation with a time-dependent refractive index. These models are normally derived from Maxwell equations using heuristic arguments and qualitative approximations (see e.g. [3]). Numerical simulations of such models are performed by experimentalists [1], [6] for theoretical explanations of complicated dynamics of laser beams in photopolymers. The complexity of the NLS equation modeling photochemical materials is related to the fact that the spatial coordinate in the direction of the beam propagation serves as an evolution time in the NLS equation, whereas the nonlinear refractive index depends slowly on the temporal coordinate. Physically, laser beams described by the NLS approximation induce waveguides in polymers, which affect the shape and dynamics of laser beams via nonlinear refractive index. In the present work we study how to justify a time-dependent NLS model derived from a toy model resembling the Maxwell equations. The toy model is written as a system of a two-dimensional quasilinear wave equation and an empirical relation for the change of the refractive index.

2 Model and results

A photopolymer occupies typically a half-space $z \geq 0$ and its face $z = 0$ is exposed to a laser beam. If the beam is localized in the x-direction and uniform in the y-direction, then the electric field has polarization in the y-direction with the amplitude E being y-independent, hence $\mathbf{E}(x,z,t) = (0, E(x,z,t), 0)$ is the electric field. The initial beam is assumed to be spatially wide-spreaded, small in amplitude, and monochromatic in time.

Neglecting polarization effects and uniform material losses, the electric field satisfies a one-dimensional quasilinear wave equation in the form

$$\partial_x^2 E + \partial_z^2 E - n^2 \partial_t^2 E = 0, \tag{1}$$

where n is referred to as the refractive index of the photopolymer. The refractive index n changes in time t because of the nonlinear effects induced by the squared amplitude of the electric field E.

Let us write the squared refractive index in the form $n^2 = 1 + m$ and assume that the rate of change of m is governed by the empirical relation

$$\frac{\partial m}{\partial t} = E^2. \tag{2}$$

The system (1)-(2) resembles approximation of a more complicated system of governing equations in physical literature [2]. We note that all physical constants in this system are normalized to unity.

Asymptotic solution to the system is given by the multi-scale expansion [5]

$$E(x,z,t) = \epsilon^{\frac{s+2}{2}} A(X,Z,T) e^{i\omega_0(z-t)} + \text{c.c.} \tag{3}$$

$$m(x,z,t) = \epsilon^2 M(X,Z,T), \tag{4}$$

where c.c. stands for complex conjugated terms, $X = \epsilon x$, $Z = \epsilon^2 z$, $T = \epsilon^s t$ are slow variables and $s \geq 2$.

If $s = 2$, the leading-order terms read as follows:

$$\partial_X^2 A + 2i\omega_0 (\partial_Z A + \partial_T A) + \omega_0^2 M A = 0 \tag{5}$$

and

$$\partial_T M = 2|A|^2, \tag{6}$$

which will be the subject of our studies.

If $s > 2$, at the leading order, we have the spatial NLS equation

$$\partial_X^2 A + 2i\omega_0 \partial_Z A + \omega_0^2 M A = 0. \qquad (7)$$

Because M depends on T by means of the same equation (6), A depends on T implicitly in the spatial NLS equation (7). The system (6)-(7) was used in the previous works on photochemical materials (see review in [2]). While justification of the system (6)-(7) still remains an open problem, we focus on the system (5)-(6). We shall consider solutions of the original system (1)-(2) in an unbounded domain for $(x, z) \in \mathbb{R}^2$ supplemented by the initial conditions at $t = 0$. We hence work with the scaling $X = \epsilon x$, $Z = \epsilon^2 z$, $T = \epsilon^2 t$ and represent exact solution to the system (1)-(2) as

$$E(x,z,t) = \epsilon^2 \left(A(X,Z,T) e^{i\omega_0(z-t)} + \text{c.c.} \right) + U(x,z,t) \qquad (8)$$

and

$$m(x,z,t) = \epsilon^2 M(X,Z,T) + N(x,z,t), \qquad (9)$$

where $U(x,z,t)$ and $N(x,z,t)$ are error terms to estimate. Feeding (8)-(9) into (1)-(2) and assuming validity of (5)-(6), we arrive at the system

$$\begin{aligned} \partial_x^2 U + \partial_z^2 U - \left(1 + \epsilon^2 M + N\right) \partial_t^2 U &= -\epsilon^2 R_1 N \\ &- \epsilon^6 R_2 \end{aligned} \qquad (10)$$

and

$$\partial_t N = \epsilon^4 R_3 + \epsilon^2 R_4 U + U^2, \qquad (11)$$

where $R_1, \ldots, R_4$ are some functions of A and its derivatives.

In our work [4], we establish local well-posedness of the systems (1)-(2) and (5)-(6), formulate a criterion for continuation of local solutions of (1)-(2) and obtain *a priori* energy estimates from residual equations derived from (10)-(11) by suitable near-identity transformations. As a main outcome, we have the following justification result for initial pulses lying in Sobolev Hilbert space $H^k\left(\mathbb{R}^2\right) := W^{k,2}\left(\mathbb{R}^2\right)$ with sufficiently high index k.

Theorem. *Given initial data $A_0 \in H^8\left(\mathbb{R}^2\right)$, let A, M be local solutions to the system (5)-(6) for $T \in [0, T_\infty)$, where $T_\infty > 0$ is the maximal existence time. There exist $\epsilon_0 > 0$ and $T_0 \in (0, T_\infty)$ such that for every $\epsilon \in (0, \epsilon_0)$ there is a unique solution E, m of the system (1)-(2) for $t \in \left[0, T_0/\epsilon^2\right]$ satisfying*

$$\sup_{t \in [0, T_0/\epsilon^2]} \left\| E - \epsilon^2 \left(A e^{i\omega_0(z-t)} + c.c. \right) \right\|_{H^3(\mathbb{R}^2)} = \mathcal{O}\left(\epsilon^{5/2}\right),$$

$$\sup_{t \in [0, T_0/\epsilon^2]} \left\| m - \epsilon^2 M \right\|_{H^2(\mathbb{R}^2)} = \mathcal{O}\left(\epsilon^{5/2}\right).$$

3 Discussion and further challenges

We expect justificaton analysis of the NLS model (5)-(6) to be easily extended to the case of time evolution of a pulse in $\mathbb{R}^3$. But, in view of conventional experimental set-up, it would be more interesting to reformulate a problem in a half-space setting. However, justification happens to be problematic since the applied technique is incompatible with spaces in which we are able to prove well-posedness of the system (5)-(6). Moreover, in *a priori* energy estimates, there are non-vanishing boundary terms arising from integration by parts. In case of the spatial NLS model (6)-(7) for $X \in \mathbb{R}$, $Z \in \mathbb{R}_+$, the inapplicability of the energy method is obvious because $\|A\|_{L^2(\mathbb{R}\times\mathbb{R}_+)}$ becomes infinite due to conservation in Z of $L^2_X(\mathbb{R})$-norm of solution of the NLS equation (7).

References

[1] Kasala K., Saravanamuttu K., "An experimental study of the interactions of self-trapped white laser beams in a photopolymer", Appl. Phys. Lett. **93** (2008), 051111 (3 pages).

[2] Monro T. M., de Sterke C. M., Polladian L., "Catching light in its own trap", J. Mod. Opt. **48** (2001), 191–238.

[3] Newell A., Moloney J., "*Nonlinear Optics*", Westview Press, 2003.

[4] Pelinovsky D., Ponomarev D., "Justification of a nonlinear Schrödiger model for laser beams in photopolymers", ZAMP (submitted).

[5] Pelinovsky D. E., "*Localization in Periodic Potentials: From Schrödinger Operators to Gross-Pitaevskii Equation*", Cambridge University Press, Cambridge, 2011.

[6] Villafranca A. B., Saravanamuttu K., "An experimental study of the dynamics and temporal evolution of self-trapped laser beams in a photopolymerizable organosiloxane", J. Phys. Chem. C **112** (2008), 17388–17396.

Gaussian Beam Propagation through Irregular Interfaces

Protasov M.I.
Institute of Petroleum Geology and Geophysics, 3, Koptyug st., Novosibirsk, Russia 630090
Email:ProtasovMI@ipgg.sbras.ru

Abstract

In this study, it is presented a method that aims to overcome some of the limitations of beam propagation based on high- frequency ray tracing in complex velocity models that contain complex interfaces. The method is based on local smoothing of the interface. With a modest increase in computational cost, the method presented captures the wave kinematics and dynamic that are comparable to finite-difference wave propagation with higher fidelity while staying within the ray-tracing framework, without requiring processing or alteration to the original model. There is presented comparison of the method with finite-difference wave propagation in numerical simulations.

Introduction

In the paper [3] there were presented frequency-dependent ray-tracing through rugose interfaces. This approach is based on usage of boundary integrals. Outside the boundary it is a conventional ray tracing. And on the boundary this is way of wave length smoothing. This smoothing depends on Fresnel volume that depends on frequency, ray direction and ray length.

Gaussian beams are ray based solutions and therefore they have all the problems that are connected with ray tracing through rugose interfaces. Moreover Gaussian beams have additional dependency with respect to curvature of the interface (see [2]). Therefore Gaussian beam propagation through non flat boundaries has additional restrictions on the shape of the boundaries (see [1]).

In this paper is suggested the way of Gaussian beams propagation on the basis of frequency dependent ray tracing through rugose interfaces. This way is similar with the method presented in [3] but here is specified for the beam propagation. Outside the boundary it is a conventional dynamic ray tracing. And on the boundary this is way of smoothing. This smoothing depends on the incident Gaussian beam itself not just on Fresnel volume like in [3]. Also this smoothing gives beam dependent interface curvature that is crucial thing for beam propagation.

Method

Gaussian beam propagation through smooth interfaces is described in [2]. There were derived conditions that connect dynamic parameters of an incident beam and dynamic parameters of reflected/transmitted beam. These connections depend on curvature of an interface. Particularly, on an interface connecting two homogeneous layers these conditions for the transmitted beam are:

$$P^t = D(\frac{1}{c^t\cos(\gamma^i)} - \frac{1}{c^i\cos(\gamma^t)})Q^i + \frac{\cos(\gamma^i)}{\cos(\gamma^t)}P^i,$$

$$Q^t = \frac{\cos(\gamma^t)}{\cos(\gamma^i)}Q^i, \qquad (1)$$

here Q^i, P^i - dynamic parameters of an incident beam on the interface, Q^t, P^t - dynamic parameters of the transmitted beam, γ^i - angle between interface normal and incident ray, γ^t - angle between interface normal and transmitted ray, D - curvature of the interface in the point of incidence. As one can see the main influence on the dynamic parameters gives high frequency Snell's law that connects incident and transmitted ray directions and curvature of the interface. Also the main restrictions of beam propagation are connected with high frequency Snell's law and interface curvature (see [2],[1]).

In the paper [3] were shown there is effective interface that describes physical ray propagation through irregular boundaries. In a similar fashion in order to overcome some of the restrictions of Gaussian beam propagation it is suggested to get effective interface, effective interface normals and effective interface curvature. It is proposed local smoothing of the interface that depends on incident Gaussian beam itself:

$$\overline{X}_{eff}(\overline{x}^i, u^i_{gb}) = \int_{\overline{x}^i-\epsilon}^{\overline{x}^i+\epsilon} |u^i_{gb}(\overline{x}^s;\overline{x}^i;\omega)|\cdot\overline{x}^s ds. \qquad (2)$$

The same trick is done for the interface tangent (or normal) vector and for the interface curvature:

$$\overline{K}_{eff}(\overline{x}^i, u^i_{gb}) = \int_{\overline{x}^i-\epsilon}^{\overline{x}^i+\epsilon} |u^i_{gb}(\overline{x}^s;\overline{x}^i;\omega)|\cdot\overline{k}(\overline{x}^s) ds. \qquad (3)$$

$$D_{eff}(\overline{x}^i, u^i_{gb}) = \int_{\overline{x}^i-\epsilon}^{\overline{x}^i+\epsilon} |u^i_{gb}(\overline{x}^s; \overline{x}^i; \omega)| \cdot D(\overline{x}^s) ds. \quad (4)$$

After that we will get effective point of incidence and effective local plane boundary. And we can apply conventional Snell's law with respect to this effective local plane boundary and get effective incident angle γ^i_{eff} and effective transmitted angle γ^t_{eff}. Finally effective curvature D_{eff} and effective angles $\gamma^i_{eff}, \gamma^t_{eff}$ are used in formula (1) in order to get dynamic parameters for the effective transmitted beam.

Illustrations

We compare the Gaussian beam results obtained using the averaging method and high frequency approximation with finite-difference modeling. For this, we consider a velocity model that is composed of two homogeneous mediums with an oscillating interface. We choose the velocities of the upper and lower mediums to be 1500 m/s and 4500 m/s, which correspond to the speed of sound in water and salt, respectively. The interface is chosen to be a sine function. In the Figure 1 are presented seismograms for both solutions. Red one is finite-difference solution and blue one is high frequency ray based solution. In the Figure 2 are presented seismograms for both solutions also. Again red one is finite-difference solution and blue one is effective beam solution. In this specific case high frequency ray and effective ray are the same. But the widths of the high frequency Gaussian beam and effective beam are crucially different. The same we can say about the beam front curvature. Seismograms show that results obtained by smoothing method are rather close to the results obtained by finite-difference modeling while results obtained by high frequency solution are rather different. The method has been applied on the Sigsbee synthetic data set whose results are left for our final presentation.

Conclusions

It is suggested and investigated solution that describes beam propagation through irregular boundaries. This solution gives effective interface, effective interface normal and effective interface curvature that depends on incident beam. Also this solution describes physical beam propagation while staying in the framework of conventional dynamic ray tracing. It is computationally cheap and stable with respect to interface perturbations. Suggested solution can

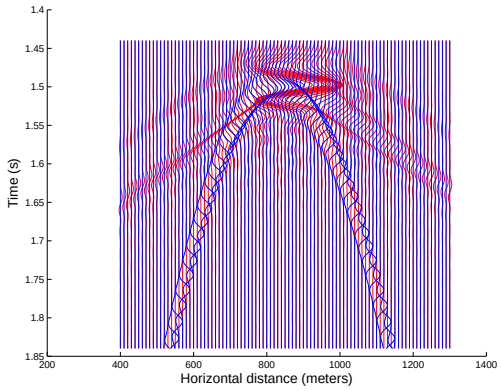

Figure 1: Seismogram of finite difference based beam (red) and high frequency ray based beam (blue).

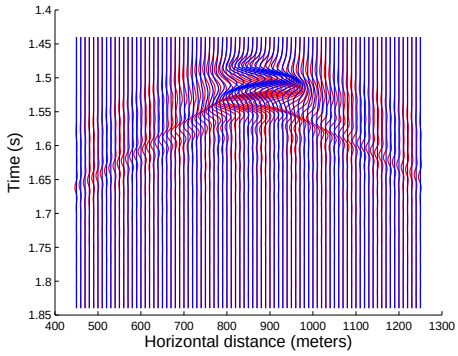

Figure 2: Seismogram of finite difference based beam (red) and high frequency ray based beam (blue).

improve results of beam based applications. For example it can improve subsalt beam imaging results.

References

[1] Ben-Menahem A., Beydoun W., 1985, *Range of validity of seismic ray and beam methods in general inhomogeneous media-I. General theory*, Geophys. J. R. astr. Soc.,**v.82**, 1985, pp.207-234.

[2] Popov M.M., *Ray theory and gaussian beam method for geophysicists*, EDUFBA, 2002.

[3] Protasov, M.I. Yarman C.Y., Nichols D., Osypov K., and Xin Cheng, *Frequency-dependent ray-tracing through rugose interfaces* , SEG Expanded Abstracts of the 81st Annual International Meeting, San-Antonio, USA, 18-23 September 2011, pp. 2992-2996.

A high-order algorithm for wave propagation in stochastic media

M. Ganesh[†,*], **S. C. Hawkins**[‡]
[†] Department of Applied Mathematics and Statistics, Colorado School of Mines, CO 80228, USA
[‡]Department of Mathematics, Macquarie University, NSW 2109, Australia
[*]Email: mganesh@mines.edu

Abstract

We develop an efficient high-order algorithm for simulation of the statistical properties of quantities of interest (QoI) in a class of stochastic acoustic wave propagation models. In particular, the moments of the QoI play an important role in quantifying random uncertainty in the multiple obstacle acoustic scattering and absorption models. The stochastic nature of configurations governing the models may include randomness in location and orientations of the obstacles, their shapes, and their material properties.

1 A model problem and QoI

Let $\Omega^M(\omega)$ denote a two (or three) dimensional configuration of M disjoint particles $D_I(\omega)$ for $I = 1, \ldots, M$. Dependence of $\Omega^M(\omega)$ on ω indicates random uncertainty in the configuration that may include the location and orientations of the particles, their shapes, and their material properties. The nature of the randomness in the configuration is specified through the choice of a probability space $(\mho, \mathcal{F}, \mathbb{P})$ where $\mho$ is a sample space, $\mathcal{F}$ is a σ-algebra, and $\mathbb{P}$ is a probability measure on $(\mho, \mathcal{F})$. In particular, all of the uncertain properties of the configuration are described by $\omega \in \mho$.

We assume that the configuration is illuminated by the incident plane wave $u^{\rm inc}(\boldsymbol{x}) = e^{ik\boldsymbol{x}\cdot\widehat{\boldsymbol{d}}}$ with wavenumber $k = 2\pi/\lambda$ where λ is the wavelength, and incident direction given by the unit vector $\widehat{\boldsymbol{d}}$. When illuminated by the plane wave the stochastic configuration $\Omega^M(\omega)$, with ω in the probability space, induces a time-harmonic scattered random field $u^{\rm s}(\boldsymbol{x}, \omega)$ that satisfies the n-dimensional ($n = 2, 3$) exterior Helmholtz equation

$$\triangle u^{\rm s}(\boldsymbol{x}, \omega) + k^2 u^{\rm s}(\boldsymbol{x}, \omega) = 0, \quad \boldsymbol{x} \in \mathbb{R}^n \setminus \overline{\Omega^M(\omega)}, \tag{1}$$

and the Sommerfeld radiation condition

$$\lim_{|x|\to\infty} |\boldsymbol{x}|^{(n-1)/2} \left(\frac{\partial u^{\rm s}}{\partial |\boldsymbol{x}|}(\boldsymbol{x}, \omega) - iku^{\rm s}(\boldsymbol{x}, \omega) \right) = 0, \tag{2}$$

uniformly in all directions $\widehat{\boldsymbol{x}} = \boldsymbol{x}/|\boldsymbol{x}|$. Let $u^{\rm tot} = u^{\rm inc} + u^{\rm s}$ be the total exterior field and let $u^{\rm int}$ be field inside those particles in $D_I(\omega)$ that are penetrable. If $D_I(\omega)$ is a penetrable obstacle for some $I = 1, \ldots, M$, then the restriction of $u^{\rm int}$ to $D_I(\omega)$ satisfies the interior Helmholtz equation in $D_I(\omega)$ with corresponding interior wavenumber $k_I^{\rm int}$. Each particle $D_I(\omega)$ in the configuration is assumed to be either sound-soft, or sound-hard, or absorbing or penetrable (in the electromagnetic case TM-polarized dielectric), and hence the total field $u^{\rm tot}(\boldsymbol{x})$ satisfies one of the following boundary conditions for $\boldsymbol{x} \in \partial D_I(\omega)$

$$u^{\rm tot}(\boldsymbol{x}) = 0\,, \tag{3}$$

$$\frac{\partial u^{\rm tot}}{\partial \boldsymbol{n}}(\boldsymbol{x}) = 0\,, \tag{4}$$

$$u^{\rm tot}(\boldsymbol{x}) + \mu_I \frac{\partial u^{\rm tot}}{\partial \boldsymbol{n}}(\boldsymbol{x}) = 0\,, \quad \mu_I \in \mathbb{C}, \tag{5}$$

$$u^{\rm tot}(\boldsymbol{x}) = u^{\rm int}(\boldsymbol{x}), \qquad \frac{\partial u^{\rm tot}}{\partial \boldsymbol{n}}(\boldsymbol{x}) = \frac{\partial u^{\rm int}}{\partial \boldsymbol{n}}(\boldsymbol{x}). \tag{6}$$

Thus we have mixed boundary conditions on the stochastic boundary $\partial\Omega^M(\omega)$ and hence the induced scattered field $u^{\rm s}(\boldsymbol{x}, \omega)$ is a random process.

In applications, typically the QoI is derived from the far field

$$u^\infty(\widehat{\boldsymbol{x}}, \omega) = \lim_{|\boldsymbol{x}|\to\infty} |\boldsymbol{x}|^{(n-1)/2} e^{-ik|\boldsymbol{x}|} u^{\rm s}(\boldsymbol{x}, \omega), \quad \widehat{\boldsymbol{x}} = \frac{\boldsymbol{x}}{|\boldsymbol{x}|}. \tag{7}$$

It is useful to expand our notation for the far field to indicate that the far field depends on the incident direction $\widehat{\boldsymbol{d}}$, thus we write $u^\infty(\widehat{\boldsymbol{x}}, \widehat{\boldsymbol{d}}, \omega)$. We denote the QoI by $f(\widehat{\boldsymbol{x}}, \omega)$ and it is typically of the form

$$f(\widehat{\boldsymbol{x}}, \omega) = (\mathcal{F}\boldsymbol{u}^\infty)(\widehat{\boldsymbol{x}}, \omega)$$

where $\mathcal{F}$ is an appropriate operator. For example, the scattering cross section [6] of the configuration as a function of incident direction is given by

$$(\mathcal{F}\boldsymbol{u}^\infty)(\widehat{\boldsymbol{x}}, \omega) = \int_{\mathbb{S}} |\boldsymbol{u}^\infty(\widehat{\boldsymbol{y}}, \widehat{\boldsymbol{x}}, \omega)|^2 \, ds(\widehat{\boldsymbol{y}}),$$

where $\mathbb{S}$ is the set of all unit vectors in $\mathbb{R}^n$. This QoI is important in atmospheric science applications [1],[2].

Important moments metrics of the dependence of the QoI on ω are the expected value

$$\mathbb{E}[f(\widehat{\boldsymbol{x}}, \cdot)] = \int_\Omega f(\widehat{\boldsymbol{x}}, \omega) \, \mathrm{d}\mathbb{P}(\omega) \tag{8}$$

and the variance

$$\mathrm{var}[f(\widehat{\boldsymbol{x}},\cdot)] = \mathbb{E}\Big[f(\widehat{\boldsymbol{x}},\cdot) - \mathbb{E}[f(\widehat{\boldsymbol{x}},\cdot)]\Big]. \qquad (9)$$

These are measures of the mean and spread, respectively, of the QoI.

2 A high-order algorithm for QoI

A standard tool for computing the expected value and the variance is the Monte-Carlo method

$$\mathbb{E}_{\mathrm{MC}}\left[f(\widehat{\boldsymbol{x}},\cdot)\right] = \frac{1}{N}\sum_{j=1}^{m} f(\widehat{\boldsymbol{x}},\boldsymbol{z}_j), \qquad (10)$$

where $\boldsymbol{z}_j$ for $j = 1,\ldots,N$ are independent samples of the random vector $\boldsymbol{z}(\omega)$. For each sample $\boldsymbol{z}_j$, the QoI $f(\widehat{\boldsymbol{x}},\boldsymbol{z}_j)$ is computed by a scattering simulation involving solving the governing equations (1)–(6) for a fixed configuration described by $\boldsymbol{z}_j$. A disadvantage of the Monte-Carlo method (10) is its slow $1/\sqrt{N}$ convergence rate, which necessitates a very large number of simulations even for a couple of digits accuracy.

In this work we reduce the number of simulations using a fully discrete version of the high-order polynomial chaos Fourier-Galerkin projection of the QoI. The resulting stochastic high-order pseudospectral method (based on approximating integrals in the coefficients of the projection by high-order quadratures) belongs to the well known class of the generalized Polynomial Chaos (gPC) methods [7].

Our hybrid approach is based on developing (i) efficient high-order decomposition approximations of the QoI; (ii) high-order approximations of the forward acoustic model in the spatial variable (using the methods developed by the authors [3], [4], [5]); and (iii) fully discrete spectrally accurate approximations of the process in the stochastic variable. Efficient approximations for the forward model are required because of the need to simulate for tens of thousands of incident waves, for each realization. Consequently, we obtain substantial reductions in both the number of simulations and efficient computations for each realizations. Figure 1 demonstrates the efficiency of our high-order algorithm, compared to the standard Monte Carlo based simulations.

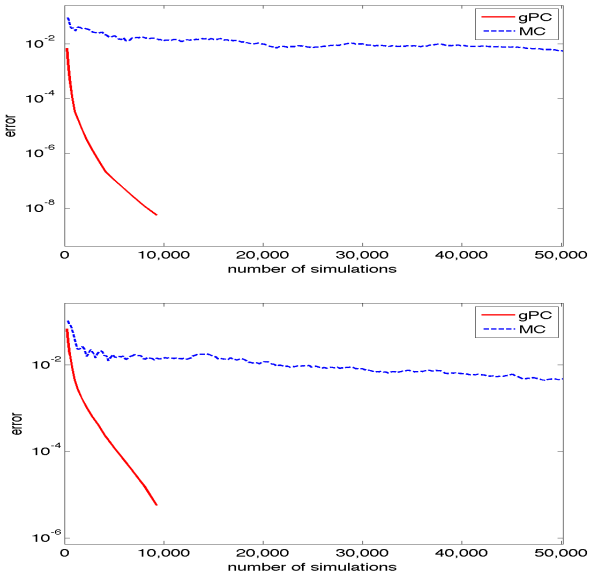

Figure 1: Comparison of the supremum norm error using the Monte Carlo method (MC) and our high-order gPC based algorithm, in the computed expected value [top] and variance [bottom] plotted against number of simulations for a stochastic two dimensional configuration with the three (distinctly shaped sound-soft, sound-hard, and penetrable) scatterers each with acoustic size 20 wavelengths and random orientations with normal and log-normal distributions.

References

[1] A. Baran, From the single-scattering properties of ice crystals to climate prediction: A way forward, *Atmospheric Research*, 112 (2012), 45-69.

[2] A. B. Davis and A. Marshak, Solar radiation transport in the cloudy atmosphere: A 3D perspective on observations and climate impacts, *Reports on Progress in Physics*, 73 (2010), 1–70.

[3] M. Ganesh and S. C. Hawkins Simulation of acoustic scattering by multiple obstacles in three dimensions, *ANZIAM*, 50 (2008), c31–c45.

[4] M. Ganesh and S. C. Hawkins A high-order algorithm for multiple electromagnetic scattering in three dimensions, *Numer. Algorithms*, 50 (2009), 469–510.

[5] M. Ganesh, S. C. Hawkins, and R. Hiptmair Convergence analysis with parameter estimates for a reduced basis acoustic scattering T-matrix method, *IMA J. Numer. Anal.*, 32 (2012), 1348–1374.

[6] H. C. van de Hulst. *Light scattering by small particles*. Dover, 1957.

[7] O. P. Le Maître and O. M. Kino. *Spectral Methods for Uncertainty Quantification*. Springer, 2010.

A high frequency boundary element method for scattering by two-dimensional screens

S. N. Chandler-Wilde[1], D. P. Hewett[1], S. Langdon[1,*], A. Twigger[1]
[1] Department of Mathematics and Statistics, University of Reading, Reading, U.K.
*Email: s.langdon@reading.ac.uk

Abstract

We propose a numerical-asymptotic boundary element method for problems of time-harmonic acoustic scattering of an incident plane wave by a sound-soft two-dimensional (2D) screen. Standard numerical schemes have a computational cost that grows at least linearly with respect to the frequency of the incident wave. Here, we enrich our approximation space with oscillatory basis functions carefully designed to capture the high frequency behaviour of the solution. We show that in order to achieve any desired accuracy it is sufficient to increase the number of degrees of freedom only in proportion to the logarithm of the frequency, as the frequency increases, and for fixed frequency we demonstrate exponential convergence with respect to the number of degrees of freedom.

Introduction

There has been much recent interest (see, e.g., [1]) in the development of numerical-asymptotic boundary element methods for time-harmonic scattering problems. In these methods, knowledge of the high frequency asymptotic behavior of the solution is incorporated into the approximation space, leading to improved performance at high frequencies and, in many cases, rigorous error estimates demonstrating sublinear (often logarithmic) growth in the number of degrees of freedom required to maintain accuracy as frequency increases. Here, we apply this idea to the problem of scattering by a 2D screen. This represents the first application of this approach (supported by error estimates) to any problem of scattering by separated multiple scatterers (in this case the separate components of the screen).

1 Problem statement

We consider the 2D problem of scattering of the time harmonic incident plane wave $u^i(\mathbf{x}) = \mathrm{e}^{\mathrm{i}k\mathbf{x}\cdot\mathbf{d}}$, where $\mathbf{x} = (x_1, x_2) \in \mathbb{R}^2$, $k > 0$ is the wavenumber and $\mathbf{d}$ is a unit direction vector, by a sound soft screen $\Gamma := \{(x_1, 0) \in \mathbb{R}^2 : x_1 \in \tilde{\Gamma}\}$. Here $\tilde{\Gamma} \subset \mathbb{R}$ is a union of disjoint open intervals, i.e. $\tilde{\Gamma} = \cup_{j=1}^{n_i}(s_{2j-1}, s_{2j})$, where $0 = s_1 < \ldots < s_{2n_i} = L$, with n_i denoting the number of intervals making up $\tilde{\Gamma}$ and L being the length of the screen in the case $n_i = 1$. We denote the propagation domain by $D := \mathbb{R}^2\backslash\bar{\Gamma}$, where $\bar{\Gamma}$ is the closure of Γ.

The boundary value problem (BVP) we wish to solve is: given the incident field u^i, determine the total field $u \in C^2(D) \cap H^1_{loc}(D)$ such that

$$\Delta u + k^2 u = 0 \text{ in } D, \quad u = 0 \text{ on } \Gamma,$$

and the scattered field $u^s := u - u^i$ satisfies the Sommerfeld radiation condition. The precise sense in which $u = 0$ holds on Γ is explained in [2].

For the solution of the above BVP, a form of Green's representation theorem holds:

$$u(\mathbf{x}) = u^i(\mathbf{x}) + \int_\Gamma \Phi_k(\mathbf{x}, \mathbf{y}) \left[\frac{\partial u}{\partial \mathbf{n}}\right](\mathbf{y})\, \mathrm{d}s(\mathbf{y}), \quad \mathbf{x} \in D,$$

where $\Phi_k(\mathbf{x}, \mathbf{y}) = \frac{\mathrm{i}}{4} H_0^{(1)}(k\,|\mathbf{x} - \mathbf{y}|)$ is the fundamental solution of the Helmholtz equation and $\left[\frac{\partial u}{\partial \mathbf{n}}\right]$ is the jump in the normal derivative $\frac{\partial u}{\partial \mathbf{n}}$ across Γ. It is shown in [2] that $\phi = \left[\frac{\partial u}{\partial \mathbf{n}}\right]$ satisfies the boundary integral equation

$$S_k\phi(\mathbf{x}) = u^i(\mathbf{x}), \quad \mathbf{x} \in \Gamma, \tag{1}$$

where $S_k\phi(\mathbf{x}) := \int_\Gamma \Phi_k(\mathbf{x}, \mathbf{y})\phi(\mathbf{y})\, \mathrm{d}s(\mathbf{y})$, $\mathbf{x} \in \Gamma$.

2 Analyticity and regularity of solutions

Our approximation space for the solution of (1) is adapted to the high frequency asymptotic behaviour of the solution, which we now consider. Representing $\mathbf{x} \in \Gamma$ parametrically by $\mathbf{x}(s) := (s, 0)$, where $s \in \tilde{\Gamma} \subset (0, L)$, the following theorem is proved in [2]:

Theorem 2.1 *Let $k \geq k_0 > 0$. Then for any $j = 1, \ldots, n_i$ there exists a constant $C > 0$, dependent only on k_0 and $\min_{m=1,\ldots,2n_i-1}\{s_{m+1} - s_m\}$, such that*

$$\phi(\mathbf{x}(s)) = \Psi(\mathbf{x}(s)) + v_j^+(s - s_{2j-1})\mathrm{e}^{\mathrm{i}ks} + v_j^-(s_{2j} - s)\,\mathrm{e}^{-\mathrm{i}ks}, \tag{2}$$

for $s \in (s_{2j-1}, s_{2j})$, where $\Psi := 2\partial u^i/\partial \mathbf{n}$, and the functions $v_j^\pm(s)$ are analytic in the right half-plane $\mathrm{Re}\,[s] > 0$, where they satisfy the bound

$$\left|v_j^\pm(s)\right| \leq C(1 + kL)k\,|ks|^{-\frac{1}{2}}.$$

3 Approximation space

Using the representation (2) we can now design an appropriate approximation space $V_{N,k}$ to represent

$$\varphi(s) := \frac{1}{k}\left(\left[\frac{\partial u}{\partial \mathbf{n}}\right](\mathbf{x}(s)) - \Psi(\mathbf{x}(s))\right), \quad s \in \tilde{\Gamma}.$$

The function φ, which we seek to approximate, can be thought of as the scaled difference between $[\partial u/\partial \mathbf{n}]$ and its "Physical Optics" approximation Ψ, with the $1/k$ scaling ensuring that φ is nondimensional. As alluded to earlier, instead of approximating φ directly by conventional piecewise polynomials we instead use the representation (2) with v_j^+ and v_j^- replaced by piecewise polynomials (of order p) supported on overlapping geometric meshes (each with n layers) on each interval (s_{2j-1}, s_{2j}), graded towards the singularities at $s = s_{2j-1}$ and $s = s_{2j}$ respectively. This leads to an identical approximation space on each interval to that used on each side of a convex polygon in [3]. For full details we refer to [2], where the following best approximation result is shown.

Theorem 3.1 *Let n and p satisfy $n \geq cp$ for some constant $c > 0$ and suppose that $k \geq k_0 > 0$. Then there exist constants $C, \tau > 0$, dependent only on n_i, k_0, c and $\min_{m=1,\ldots,2n_i-1}\{s_{m+1} - s_m\}$, such that*

$$\inf_{v \in V_{N,k}} \|\varphi - v\|_{\tilde{H}_k^{-\frac{1}{2}}(\tilde{\Gamma})} \leq Ck^{1/2}L^{3/2}\mathrm{e}^{-p\tau}.$$

Whereas our estimates for classes of polygons (see, e.g., [1], [3]) hold in L^2, here we need to work in appropriate Sobolev spaces. For a precise definition of the k-dependent norm $\|\cdot\|_{\tilde{H}_k^{-\frac{1}{2}}(\tilde{\Gamma})}$, we refer to [2].

4 Galerkin method

Having designed an appropriate approximation space $V_{N,k}$, we use a Galerkin method to select an element so as to efficiently approximate φ. That is, we seek $\varphi_N \in V_{N,k}$ such that

$$\langle S_k\varphi_N, v\rangle_\Gamma = \frac{1}{k}\langle u^i - S_k\Psi, v\rangle_\Gamma, \quad \forall v \in V_{N,k}, \quad (3)$$

where the duality pairings in (3) can be evaluated simply as L^2 inner products. The following error estimate is proved in [2].

Theorem 4.1 *If the assumptions of Theorem 3.1 hold, then there exist constants $C, \tau > 0$, dependent only on n_i, k_0, c and $\min_{m=1,\ldots,2n_i-1}\{s_{m+1} - s_m\}$, such that*

$$\|\varphi - \varphi_N\|_{\tilde{H}_k^{-1/2}(\tilde{\Gamma})} \leq CkL^2\mathrm{e}^{-p\tau}.$$

5 Numerical results

We now present numerical results for the solution of (3). We take $\mathbf{d} = (1/\sqrt{2}, -1/\sqrt{2})$, $n_i = 1$, and $L = 2\pi$. We take the same number of layers $n = 2(p+1)$ on each graded mesh, giving a total number of degrees of freedom $N = 4(p+1)^2$. Since N depends only on p, we write $\psi_p(s) := \varphi_N(s)$. In Figure 1 we plot on a logarithmic scale the relative L^1 errors $\|\psi_6 - \psi_p\|_{L^1(\tilde{\Gamma})} / \|\psi_6\|_{L^1(\tilde{\Gamma})}$ (used for simplicity of computation) against p for a range of k. The linear plots demonstrate exponential decay as

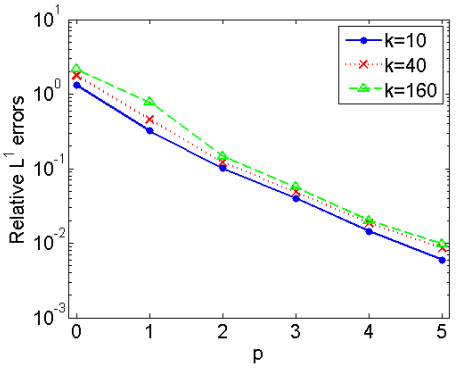

Figure 1: Convergence results

the polynomial degree, p, increases, as we might expect from Theorem 4.1. For fixed p, the relative error increases only very slowly as k increases. For further numerical results, see [2], [4].

References

[1] S. N. Chandler-Wilde, I. G. Graham, S. Langdon and E. A. Spence, *Numerical-asymptotic boundary integral methods in high-frequency acoustic scattering*, Acta Numer., **21** (2012), pp. 89–305.

[2] S. N. Chandler-Wilde, D. P. Hewett, S. Langdon and A. Twigger, *A high frequency hp boundary element method for scattering by a two-dimensional screen*, in preparation (2013).

[3] D. P. Hewett, S. Langdon and J. M. Melenk, *A high frequency hp boundary element method for scattering by convex polygons*, SIAM J. Numer. Anal., to appear (2013).

[4] A. Twigger, *Boundary element methods for high frequency scattering*, PhD thesis, University of Reading (2013).

An edge source integral equation for the scattering from a flat plate

A. Asheim[1,*], **U.P. Svensson**[2]
[1] University of Leuven, Department of Computer Science, Heverlee, Belgium
[2] Norwegian University of Science and Technology, Department of Electronics and Telecommunication, Trondheim Norway.
*Email: andreas.asheim@cs.kuleuven.be

Abstract

We consider the problem of time-harmonic scattering of waves by a flat convex plate. The total diffracted field can be expressed in terms of the solution of an integral equation [1]. This does, in fact, constitute a novel formulation of the scattering problem, not restricted to high frequency ranges. We shall present an exploration of this integral equation formulation and the advantages and disadvantages it poses for numerical computations.

Introduction

Consider the time-harmonic scattering of scalar spherical and plane waves, u^i, by a flat convex plate, D, subject to a Neumann boundary condition. Letting u^s denote the scattered wave, it satisfies an equation

$$\Delta u^s + k^2 u^s = 0 \quad \mathbb{R}^3 \backslash D \tag{1}$$
$$\frac{\partial u^s}{\partial n} + \frac{\partial u^i}{\partial n} = 0 \quad \text{on} \quad \partial D,$$

in addition to a radiation condition, which ensures that the scattered field is outgoing. Solving the PDE as posed in (1) is one option for solving this problem. This involves truncating the unbounded space somehow, which is why a BEM method might be favoured, where one solves an integral equation on ∂D [2]. This is thus a second option for solving this problem. In high frequency ranges, $k \gg 0$, the solution u^s as well as surface fields are oscillatory, and CPU time goes up dramatically; the number of unknown needed to represent the solution is at least $\mathcal{O}(k^3)$ for PDE methods and $\mathcal{O}(k^2)$ for BEM. In this case, asymptotics, such as geometrical optics, GTD, UTD etc., [3], are favoured. However, the usefulness of asymptotics is limited in intermediate frequency ranges, since only limited accuracy can be attained with such methods.

An alternative is hybrid methods: Combining asymptotics and numerics has come a long way in reducing the work and storage load to something closer to $\mathcal{O}(1)$. An extensive review of such efforts is presented in a recent survey paper in Acta Numerica [5]. We particularly note pp. 264–269 in [5], where a problem of the type (1) is treated.

The topic of this work is an exploration of a third option, which is particularly well suited for the given problem, Eq. (1). In a recent work by the authors, [1], it has been shown that the total diffracted field from such a scattering setup can be expressed in terms of an integral equation for an unknown edge source density. However, this integral equation is of a non-standard form, and there is potential to solve it in efficient ways, especially for intermediate frequencies. As such this formulation can be useful for bridging the gap between asymptotics and FEM/BEM.

1 Edge source integral equation

Taking the view of geometric optics, we can decompose the total field in terms of direct, reflected and diffracted components,

$$u^i + u^s = u_{\text{dir.}} + u_{\text{refl.}} + u_{\text{diff.}}.$$

Computing the direct and reflected components is straightforward. Note that $u_{\text{dir.}}$ and $u_{\text{refl.}}$ are discontinuous fields, and by the continuity of the total field $u_{\text{diff.}}$ is discontinuous as well. Computing a first order diffracted field, $u^{(1)}_{\text{diff.}}$, in terms of edge diffraction has been demonstrated in [4]. Letting x_S denote the source position, and x_R the receiver position, we have

$$u^{(1)}_{\text{diff.}}(x_R) = \int_\Gamma \frac{\mathrm{e}^{\mathrm{i}k|x_S - z|}}{|x_S - z|} \frac{\mathrm{e}^{\mathrm{i}k|x_R - z|}}{|x_R - z|} \Omega(x_R, z, x_S) \mathrm{d}s_z, \tag{2}$$

where Γ denotes the edge of D. The function Ω is a function which only depends on the sender and receiver *direction*, relative to an edge point z. For a given edge point z denote by θ_R and θ_S the angle of the directions to x_R and x_S from z with respect to the plate plane, measured from a reference side. Likewise ϕ_R and ϕ_S the angles with respect to the edge tangent at z. Then

$$\Omega(x_R, z, x_S) \quad = \quad -\frac{\gamma}{2\pi} \sum_{\pm} \frac{\cos(\frac{\theta_S \pm \theta_R}{2})}{\gamma^2 - \sin(\frac{\theta_S \pm \theta_R}{2})},$$

where

$$\gamma = \frac{\cos(\frac{\phi_S - \phi_R}{2})}{\sqrt{\sin\phi_S \sin\phi_R}}.$$

In [1] it is shown that the sum of all higher order diffracted components can be written in terms of a directional monopole density $q : \Gamma \times \Gamma \to C$, which solves the integral equation,

$$q(z_1, z_2) = q_0(z_1, z_2) + \int_\Gamma q(z_2, z) \frac{\mathrm{e}^{\mathrm{i}k|z_2 - z|}}{|z_2 - z|} \Omega(z_1, z_2, z) \mathrm{d}s_z, \quad (3)$$

where now q_0 represents the first order diffracted field, and Ω is evaluated in the plane, and thus simplifies,

$$\Omega(z_R, z, z_S) = -\frac{1}{\pi} \frac{\sqrt{\cos\phi_S \cos\phi_R}}{\cos(\frac{\phi_S - \phi_R}{2})}.$$

Under an assumption that all diffraction can be expressed in terms of type (2) and higher order rediffractions of these, an assumption that appears to hold in the current setting, the total diffracted field is given as

$$u_{\text{diff.}}(x_R) = u^1_{\text{diff.}}(x_R) + \iint_{\Gamma\times\Gamma} q(z_1, z_2) \frac{\mathrm{e}^{\mathrm{i}k|z_1 - z_2|}}{|z_1 - z_2|} \frac{\mathrm{e}^{\mathrm{i}k|x_R - z_1|}}{|x_R - z_1|} \Omega(x_R, z_1, z_2) \mathrm{d}s_{z_1} \mathrm{d}s_{z_2}. \quad (4)$$

2 Numerical considerations

The numerical advantage of using this formulation is two-fold. First, the integral equation (3) is not expressed with a global operator, unlike in the Kirchhoff-Helmholtz integral equation. In practical terms, this means that a discretisation of (3) can be sparse. Secondly, the unknown q is non-oscillatory in terms of its first argument – this can be realised by studying (3), given that q_0 is non-oscillatory in terms of its first argument. This should mean that the number of unknowns needed to represent the solution is only $\mathcal{O}(k)$. A disadvantage is that the fields we are computing are discontinuous, and thus need special numerical treatment.

Initial numerical tests confirm these observations. Brute-force computing does show that the discontinuity of the geometrical optics fields are canceled by the diffracted field, providing a qualitatively correct field, see Fig. 1.

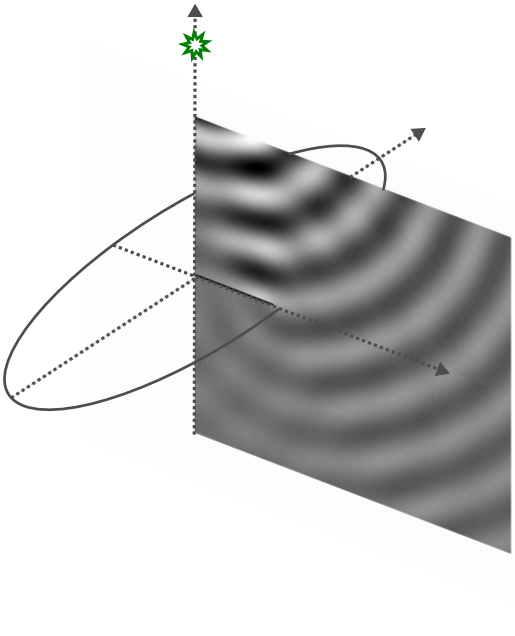

Figure 1: Computed field from the scattering of a field from a point-source at $z = 3$, $k = 10$, impinging on an ellipse in the xy-plane with semi-axes of length 1 and 3.

References

[1] A. Asheim and U.P. Svensson, *An edge diffraction integral equation for the scattering from flat plates and polyhedra*, University of Leuven, Dept. CS, Technical report, TW610 (2012)

[2] Nèdèlec, J.-C., *Acoustic and Electromagnetic Equations: Integral Representations for Harmonic Problems*. Springer, New York, 2001.

[3] Babich, V.M. and Buldyrev, V.S., *Asymptotic Methods in Short-Wavelength Diffraction Theory* . Alpha, Oxford, 2009.

[4] U. P. Svensson, R. Fred, and J. Vanderkooy, *An analytic secondary source model of edge diffraction impulse responses*, in J.Acoust. Soc. Am, **106** (5) (1999), pp. 2331–2344.

[5] Chandler-Wilde, S. N., Graham, I. G., Langdon, S., and Spence, E. A. *Numerical-asymptotic boundary integral methods in high-frequency acoustic scattering.* Acta Numerica, **2**1(1) (2012), pp. 89–305.

Robust methods for highly oscillatory integrals with weak singularities and stationary points

V. Domínguez[1,*], **I.G. Graham** [2], **T. Kim**[2]
[1] Universidad Pública de Navarra, Tudela de Navarra, Spain
[2] University of Bath, Bath, United Kingdom.
*Email: victor.dominguez@unavarra.es

Abstract

The computation of highly oscillatory integrals has enjoyed renewed interest in the last years, fueled by new applications such as high frequency scattering problems (see [1] and references therein).

We show how to approximate efficiently such integrals by combining: (a) non-linear changes of variable to rewrite the oscillations in a simpler way; (b) Filon-Clenshaw-Curtis rules for approximating these new integrals; and (c) graded meshes for an adequate treatment of the singularities in the integrand.

We prove that the use of these techniques gives rise to a simple, efficient and robust method. In fact, the rule converges very fast for non-, mildly and highly oscillatory integrals. Furthermore, we show that the error decreases, for fixed number of quadrature nodes, as the oscillations become stronger.

1 Introduction

This work is devoted to showing an efficient way to approximate

$$I_k^{[a,b]}(f,\psi) := \int_a^b f(x)\exp(\mathrm{i}k\psi(x))\,\mathrm{d}x$$

with ψ and f smooth except possibly at a where f is allowed to have an integrable singularity and ψ is allowed to have a stationary point.The methods extend in an obvious way to the case where singularities or stationary points may appear (not necessarily at the same place) in the interior of (a,b). Without loss of generality, we will assume that $\psi'(x) > 0$ for $x \in (a,b]$ and that $k > 0$.

Such integrals appear in many areas of numerical analysis. For instance, we can find them in boundary element methods for scattering problems where $k > 0$ is the wave-number and (in 2D) f may have a logarithmic singularity. In high frequency problems where $k \gg 1$, the integrand becomes strongly oscillating so that the use of classical quadrature rules is prohibitively expensive.

Clearly, the phase function ψ governs greatly the behavior of the integral. We will show first how the problem can be reduced to a simpler one, namely with a linear oscillator $\psi(x) = x$ via a non-linear change of variables. If a is stationary point, i.e. if $\psi'(a) = 0$, this change of variables adds a new singularity to the non-oscillatory part of the transformed integrand. One of the contributions of this paper is a characterization of this singularity.

For the linear oscillator we present a modified Clenshaw-Curtis rule for which we derive convergence rates in terms of k, the number of nodes N and the regularity of f. For smooth functions f the rule is robust, converges superalgebraically respect N and both the absolute and relative error decrease, for fixed N, as $k \to \infty$. If f is singular at a, either because so was the original function or due to the existence of a stationary point in the phase function ψ, we must consider instead compound rules which give in this context better results. Thus, we show how to construct graded meshes to restore the very good convergence properties fulfilled in the smooth case.

2 General oscillator

Clearly, in the notation introduced before,

$$I_k^{[a,b]}(f,\psi) = I_k^{[\psi(a),\psi(b)]}(g,x)$$

where $g := (f\circ\psi^{-1})\big(\psi'\circ\psi^{-1}\big)^{-1}$. Obviously if $\psi'(a) \neq 0$, then f and g enjoy the same regularity properties. Otherwise, if a is a stationary point of order n, i.e. $\psi^{(j)}(a) = 0$ for $j = 0,\dots,n$, we face a very different situation.

To explore properly the smoothness of the new function g we introduce for $\beta \in (-1,1)\backslash\{0\}$ and $m \geq 1$, the Banach space $\mathcal{C}^m_\beta[a,b]$ endowed with the norm,

$$\|f\|_{m,\beta,[a,b]} := \max\Big\{\Big\|\frac{(x-a)^{-\beta}}{1+(x-a)^{-\beta}}f\Big\|_{L^\infty_{(a,b)}}, \|(x-a)^{j-\beta}f^{(j)}\|_{L^\infty_{(a,b)}},\ j=1,\dots,m\Big\} \quad (1)$$

Clearly, if $f \in C_\beta[a,b]$, then when $\beta < 0$, f can blow up at a whereas for $\beta > 0$, its derivatives may blow up. The definition can be extended in an obvious way to allow log singularities for $\beta = 0$ [3].

Theorem 1 ([3]) *Under the notations and hypotheses stated above, if a is a stationary point of order n and $f \in \mathcal{C}^m[a,b]$ then $g \in \mathcal{C}^m_\beta[\psi(a),\psi(b)]$ with $\beta = -1/(n+1)$.*

The computation of g is feasible in practice, since ψ^{-1} could be efficiently computed by using secant-type solvers as the Dekker's method.

3 Linear oscillator

In view of the previous result, we can concentrate our attention to the case of linear oscillators

$$I_k^{[a,b]}(f) := I_k^{[a,b]}(f,x) = \int_a^b f(x)\exp(\mathrm{i}kx)\,\mathrm{d}x.$$

3.1 Simple Clenshaw-Curtis rules

For $N \geq 0$, we define the "product" or "modified Clenshaw-Curtis" quadrature rule

$$I_{k,N}^{[a,b]}(f) := \int_a^b \mathcal{Q}_N f(x)\exp(\mathrm{i}kx)\,\mathrm{d}x$$

where

$$\mathbb{P}_N \ni \mathcal{Q}_N f \;\text{ s.t. }\; \mathcal{Q}_N f(s_j) = f(s_j), \quad j = 0,\ldots,N,$$

with $s_j := (a+b)/2 + ((b-a)/2)\cos(j\pi/N)$. That is, $\mathcal{Q}_N f$ interpolates f at Chebyshev nodes. Implementation of this rule requires the integration of $\exp(\mathrm{i}kx)$ against a suitable polynomial basis - this can be done efficiently and stably for all N and k [2].

Theorem 2 ([3]) *Let $r \in [0,2]$ and $0 \leq m \leq N+1$. There exists constants $\sigma_{m,N}$ independent of f so that*

$$|I_k^{[a,b]}(f) - I_{k,N}^{[a,b]}(f)| \leq \sigma_{m,N} k^{-r} N^{-m+\rho(r)} (b-a)^{m+1-r} \|f^{(m)}\|_{L^\infty(a,b)}$$

where $\rho(r) = r$, if $r \in [0,1]$ and $\rho(r) = 7r/2 - 5/2$.

It turns out that $\sigma_{m,N} \to C_m < \infty$ for fixed m as $N \to \infty$, and so this result implies superalgebraic convergence with respect to N. Actually, for fixed N, both, the absolute and relative error (the integral can be proved to be $\mathcal{O}(k^{-1})$), decrease as $k \to \infty$. If the rule is going to be applied in a composite manner, the key point is the power $(b-a)$ appearing in the estimate. This is exploited in next section.

3.2 Compound rules for singular functions f

For M a positive integer we will consider the mesh $\{x_j\}_{j=0}^M := \{a + (j/M)^q (b-a)\}_{j=0}^M$. In these meshes, first proposed in [4], the parameter $q > 1$ controls the refinement of the grid at a. For fixed $N \geq 2$, consider then the composite rule

$$I_{k,M,N}^{[a,b]}(f) := \widetilde{I}_k^{[a,x_1]}(f) + \sum_{j=1}^{M-1} I_{k,N}^{[x_j,x_{j+1}]}(f)\,,$$

where $\widetilde{I}_k^{[a,x_1]}(f) = 0$ for $\beta \in (-1,0)$, and $\widetilde{I}_k^{[a,x_1]}(f) = I_{k,2}^{[a,x_1]}(f)$, a two-point rule, for $\beta \in (0,1)$.

Theorem 3 ([3]) *Let $f \in \mathcal{C}^{N+1}_\beta[a,b]$ with $\beta \in (-1,1)\setminus\{0\}$. Then for $r \in [0, 1+\beta)$, and $q > (N+1-r)/(\beta+1-r)$ there exists $C > 0$ independent of f so that*

$$|I_{k,M,N}^{[a,b]}(f) - I_k^{[a,b]}(f)| \leq C k^{-r} M^{-N-1+r} \|f\|_{N+1,\beta,[a,b]}.$$

Remark 4 *As mentioned above, functions with logarithmic singularities can be accommodated as the case $\beta = 0$, with an appropriate definition of $C_{N+1,0,[a,b]}$. In this case we can show that for $r \in [0,1)$ and $q > (N+1-r)/(1-r)$*

$$|I_{k,M,N}^{[a,b]}(f) - I_k^{[a,b]}(f)| \leq C(k^{-1}\log k)^r M^{-N-1+r}(\log M)\,\|f\|_{N+1,0,[a,b]}.$$

References

[1] S. N. Chandler-Wilde, I. G. Graham, S. Langdon and E. A. Spence. Numerical-asymptotic boundary integral methods in high frequency acoustic scattering. Acta Numerica, 21, 89-305, 2012.

[2] V. Domínguez, I.G. Graham, V.P. Smyshlaev. Stability and error estimates for Filon-Clenshaw-Curtis rules for highly-oscillatory integrals. IMA Journal of Numerical Analysis **31** (2011), 1253-1280.

[3] V. Domínguez, I.G. Graham, T. Kim. Filon-Clenshaw-Curtis rules for highly-oscillatory integrals with algebraic singularities and stationary points. Submitted

[4] J. R. Rice. On the degree of convergence of nonlinear spline approximations, in Approximations with Special Emphasis on Spline functions, (I. J. Schoenburg, Ed.) Academic Press, New York, 1969.

Hybrid numerical-asymptotic approximation of high frequency scattering by penetrable convex polygons

S. P. Groth[1,*], **D. P. Hewett**[1], **S. Langdon**[1]
[1] Department of Mathematics and Statistics, University of Reading, Reading, UK.
*Email: s.groth@pgr.reading.ac.uk

Abstract

We consider time-harmonic scattering by penetrable convex polygons. Standard numerical methods for such problems become prohibitively expensive in the high frequency regime. High frequency asymptotic methods, on the other hand, are non-convergent and may be insufficiently accurate at low to medium frequencies. Here, we describe a beam tracing algorithm that calculates the leading order high frequency asymptotics and we present an ansatz for the oscillatory remaining terms which represent the diffracted field. We demonstrate that including oscillatory basis functions in the approximation space enables an accurate approximation of the solution on the boundary of the scatterer with a cost independent of frequency.

Introduction

We consider the two-dimensional problem of scattering of a time-harmonic wave by a penetrable convex polygon, Ω. We wish to determine the total field u_1 in the exterior domain D and the total field u_2 within the polygon such that

$$\Delta u_1 + k_1^2 u_1 = 0, \quad \text{in } D, \tag{1}$$

$$\Delta u_2 + k_2^2 u_2 = 0, \quad \text{in } \Omega, \tag{2}$$

$$u_1 = u_2 \quad \text{and} \quad \frac{\partial u_1}{\partial n} = \frac{\partial u_2}{\partial n} \quad \text{on } \partial\Omega, \tag{3}$$

where k_1, k_2 are the exterior and interior wavenumbers, respectively. An example solution for Ω an equilateral triangle is shown in Figure 1.

This problem arises in numerous areas of physical interest in which the relative size of the particle to the wavelength can vary between one and thousands. Conventional numerical methods using piecewise polynomial approximation spaces suffer from the limitation that a fixed number of degrees of freedom is required per wavelength in order to represent the oscillatory solution. This leads to prohibitive computational expense when the size of the scatterer is large relative to the wavelength.

Much work has been done on developing Hybrid Numerical-Asymptotic (HNA) methods (see [1] and the references therein) which overcome this limitation by approximating the solution, u, in a Boundary Element Method (BEM) framework using an ansatz of the form

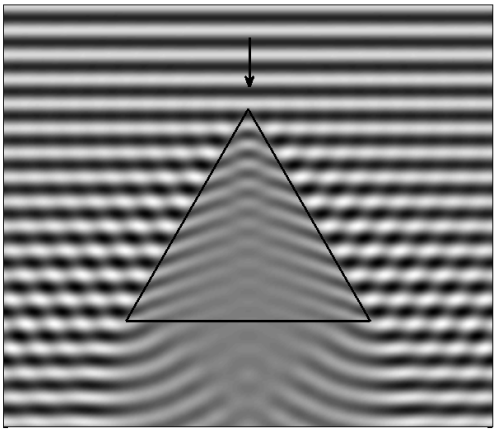

Figure 1: Scattering by a highly absorbing penetrable equilateral triangle.

$$u(x,k) \approx u_{go}(x,k) + \sum_{m=1}^{M} v_m(x,k) \exp(\mathrm{i}k\psi_m(x)), \; x \in \partial\Omega. \tag{4}$$

In this representation, u_{go} is the known leading order high frequency asymptotics, namely the Geometrical Optics (GO), the phases ψ_m are chosen *a priori* using knowledge of the high frequency asymptotics and the amplitudes v_m are approximated numerically. The expectation is that if u_{go} is calculated correctly and ψ_m are chosen wisely, the amplitudes v_m will be much less oscillatory than u and so can be efficiently approximated by piecewise polynomials.

To date, the HNA approach has been applied solely to problems of scattering by *impenetrable* scatterers. The main difficulty in the generalisation of the HNA method to the penetrable case is that the high frequency asymptotic behaviour is much more complicated than in the impenetrable case. In particular, the diffracted waves are reflected infinitely many times within the scatterer, so there are infinitely many phases ψ_m in (4). This complicates the development of our ansatz because, to create a viable

method, we must choose a finite number of these phases.

In this paper, we briefly describe a Beam Tracing Algorithm (BTA) for determining u_{go} and then go on to make a sensible choice of ψ_m in the ansatz (4). This involves truncating the infinite series of diffracted terms. To do this, we begin by examining highly absorbing scatterers for which relatively few terms are required and then investigate how to include additional terms as the absorption is reduced.

Beam Tracing Algorithm

The GO term, u_{go}, in (4) is calculated using a BTA. Consider the hexagon in Figure 2 illuminated from the top left by a plane wave u^i. This wave strikes 3 sides, from each side part of the wave is reflected and part is transmitted into the hexagon, as depicted in Figures 2a, 2b, 2c, obeying Snell's laws of reflection and refraction and the Fresnel formulae. The transmitted portions or 'beams' go on to strike further interfaces giving rise to more beams as shown in Figures 2d, 2e, 2f. This process continues indefintely, however we terminate it when the amplitudes or the beams reflected back into the shape are smaller than a user defined tolerance.

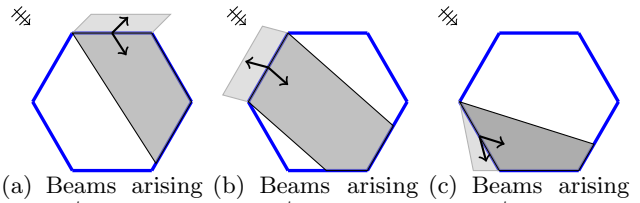

(a) Beams arising from u^i.

(b) Beams arising from u^i.

(c) Beams arising from u^i.

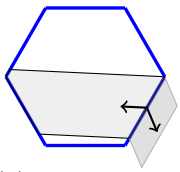

(d) Beams arising from transmitted beam in (a).

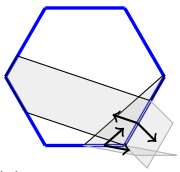

(e) Beams arising from transmitted beam in (b).

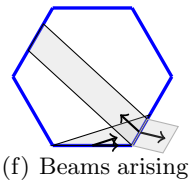

(f) Beams arising from transmitted beam in (c).

Figure 2: Beam tracing in a hexagon

Ansatz for highly absorbing scatterers

For large absorption we anticipate that the influence of diffraction on each side is only due to adjacent corners, so a sensible ansatz for the solution on one side is

$$u \approx u_{go} + v_1^+ \mathrm{e}^{\mathrm{i}k_1 s} + v_2^+ \mathrm{e}^{\mathrm{i}k_2 s} + v_1^- \mathrm{e}^{-\mathrm{i}k_1 s} + v_2^- \mathrm{e}^{-\mathrm{i}k_2 s}, \quad (5)$$

where $v_1^+, v_2^+, v_1^-, v_2^-$ are slowly varying amplitudes to be approximated using piecewise polynomials on overlapping graded meshes as shown in Figure 3. In

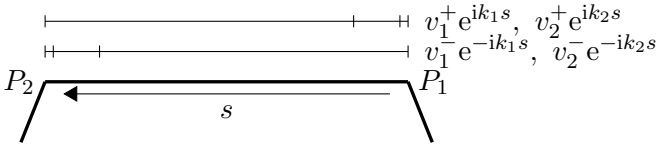

Figure 3: Approximate v_1^+, v_2^+, v_1^-, v_2^- by piecewise polynomials on overlapping meshes, graded towards the corners.

order to demonstrate the suitability of this ansatz, we perform a least squares fit of (5) to a reference solution, u, obtained using a standard BEM. This is done at varying frequencies and the error examined. Table 1 shows how the error in the best fit U compares to the error in using the GO alone. We see a significant improvement over GO using a small, fixed number (168) of degrees of freedom.

k	$\frac{\|u-u_{go}\|}{\|u\|}$	$\frac{\|u-U\|}{\|u\|}$
5	1.88×10^{-1}	1.66×10^{-2}
10	1.37×10^{-1}	1.03×10^{-2}
20	1.00×10^{-1}	8.41×10^{-4}
40	7.25×10^{-2}	2.23×10^{-4}
80	5.19×10^{-2}	2.58×10^{-4}
160	3.69×10^{-2}	2.31×10^{-4}

Table 1: Best fit and GO errors for a highly absorbing triangle.

Reducing absorption

Reducing the scatterer's absorption causes the influence of diffraction from non-adjacent corners to become significant so we add terms of the form $\mathrm{e}^{\mathrm{i}k_1 r_j}$ to the ansatz (5), where r_j is the distance from the non-adjacent corner P_j. With these additions, we show that an accuracy similar to that in Table 1 can be achieved for absorptions down to 0.0125i. In fact, in the far-field, better than 1% accuracy can be achieved for all levels of absorption.

References

[1] S. N. Chandler-Wilde, *Numerical-asymptotic boundary integral methods in high-frequency acoustic scattering*, Acta Numerica (2012), pp. 89–305.

3.14 Asymptotic modelling

Equivalent source modelling of small heterogeneities in the context of $3D$ time-domain wave propagation equation

V. Mattesi[1,2,*], **S. Tordeux**[1,2]
[1] Projet Magique-3D, INRIA Bordeaux Sud-Ouest
[2] LMA-UMR CNRS 5142, Université de Pau et des Pays de l'Adour
*Email: vanessa.mattesi@inria.fr

Abstract
In the context of time harmonic wave equation, we are interested in the computation of the scattered field by a small obstacle. The result of a high performance direct numerical simulation is compared to an approximate solution derived by the method of matched asymptotic expansions.

Introduction
In the context of acoustic imaging, it is rather difficult to observe heterogeneities with characteristic length smaller than the wave length emitted by the scanner. However, it is possible to detect small heterogeneities in homogeneous media by using high performance computing. In this work, we will propose a way to compute the field scattered by a small obstacle with low computation burden based on the matched asymptotic expansions.

1 The considered problem

1.1 Domain definition

Let us consider a small obstacle B_ε equipped with Dirichlet boundary conditions :

$$B_\varepsilon = \varepsilon \hat{B} = \left\{(x,y,z) : \left(\frac{x}{\varepsilon}, \frac{y}{\varepsilon}, \frac{z}{\varepsilon}\right) \in \hat{B}\right\}, \quad (1)$$

with $\hat{B}$ a reference shape and $\partial B_\varepsilon = \varepsilon \partial \hat{B}$ its boundary. The propagation domain Ω_ε consists of the exterior to the obstacle B_ε :

$$\Omega_\varepsilon = \mathbb{R}^3 \backslash B_\varepsilon. \quad (2)$$

1.2 The system of partial differential equations

We denote by $f \in \mathcal{D}\left(\mathbb{R}^3 \times \overline{\mathbb{R}_+}\right)$ a source term satisfying : there exists $\varepsilon_0 > 0$ such that

$$f(\mathbf{x},t) = 0, \quad \text{for } \|\mathbf{x}\| < \varepsilon_0 \text{ and } t \geq 0. \quad (3)$$

Let us consider the solution of the $3D$ time-domain wave equation :

$$\frac{\partial^2 u_\varepsilon}{\partial t^2}(\mathbf{x},t) - \Delta u_\varepsilon(\mathbf{x},t) = f(\mathbf{x},t), \quad \mathbf{x} \in \Omega_\varepsilon,\ t \geq 0,$$

equipped with the Dirichlet boundary condition :

$$u_\varepsilon(\mathbf{x},t) = 0, \quad \mathbf{x} \in \partial\Omega_\varepsilon,\ t > 0 \quad (4)$$

and homogeneous initial conditions :

$$u_\varepsilon(\mathbf{x},0) = 0, \quad \partial_t u_\varepsilon(\mathbf{x},0) = 0. \quad (5)$$

Remark. For the sake of simplicity we have assumed that the wave speed is equal to 1.

2 Matching of asymptotic expansions

The matching of asymptotic expansions [1] is an asymptotic domain decomposition method with overlapping. It consists in representing the solution with a far-field expansion far away from the obstacle and a near-field expansion near the obstacle. These two expansions are matched in a transition zone with the so-called Van Dyke matching conditions. This approach is equivalent [3] to the corrector method [2].

2.1 The far-field expansion

The far-field expansion is defined on the far-field domain $\Omega_* = \mathbb{R}^3 \setminus \{\mathbf{0}\}$ consisting of the limit of Ω_ε for ε varying to 0. It takes the form of a Taylor series :

$$u_{\varepsilon,I}(\mathbf{x},t) = \sum_{i=0}^{I} u_i(\mathbf{x},t)\varepsilon^i. \quad (6)$$

The first term of this expansion $u_0 : \mathbb{R}^3 \longrightarrow \mathbb{R}$ is the limit of u_ε for ε varying to 0. It is a regular solution over all $\mathbb{R}^3$ of the time-domain wave equation :

$$\frac{\partial^2 u_0}{\partial t^2}(\mathbf{x},t) - \Delta u_0(\mathbf{x},t) = f(\mathbf{x},t), \quad \mathbf{x} \in \mathbb{R}^3,\ t > 0,$$

equipped with the initial conditions :

$$u_0(\mathbf{x},0) = 0, \quad \partial_t u_0(\mathbf{x},0) = 0, \quad \mathbf{x} \in \mathbb{R}^3. \quad (7)$$

The next coefficients $u_i : \Omega_* \longrightarrow \mathbb{R}$ of this expansion are solutions of the homogeneous time-domain wave equation :

$$\begin{cases} \dfrac{\partial^2 u_i}{\partial t^2}(\mathbf{x},t) - \Delta u_i(\mathbf{x},t) = 0, & \mathbf{x} \in \Omega_*,\ t > 0, \\ u_i(\mathbf{x},0) = 0, \quad \partial_t u_i(\mathbf{x},0) = 0, & \mathbf{x} \in \Omega_*, \end{cases}$$

which are singular in the neighbourhood of $\mathbf{x} = 0$. This power series aims at approximating the solution u_ε at fixed $\mathbf{x} \neq \mathbf{0}$:

$$u_\varepsilon(\mathbf{x},t) - u_{\varepsilon,I}(\mathbf{x},t) = \underset{\varepsilon\to 0}{O}(\varepsilon^{I+1}). \tag{8}$$

2.2 The near-field expansion

The near-field domain $\widehat{\Omega}$ consists in the normalization of the original domain Ω_ε :

$$\widehat{\Omega} = \frac{\Omega_\varepsilon}{\varepsilon} = \left\{(X,Y,Z) \in \mathbb{R}^3 : \varepsilon X, \varepsilon Y, \varepsilon Z \in \Omega_\varepsilon\right\} \tag{9}$$

The near-field expansion takes the form :

$$\sum_{i=0}^{+\infty} U_i(\mathbf{X},t)\varepsilon^i, \tag{10}$$

which aims at approximating $U_\varepsilon(\mathbf{X},t) = u_\varepsilon(\varepsilon\mathbf{X},t)$ at fixed $\mathbf{X} \in \widehat{\Omega}$. The coefficients of the near field expansion satisfy the hierarchical Laplace equation :

$$\Delta U_i(\mathbf{X},t) = \partial_t^2 U_{i-2}(\mathbf{X},t), \quad \mathbf{X} \in \widehat{\Omega},\ t > 0, \tag{11}$$

equipped with the Dirichlet boundary condition :

$$U_i(\mathbf{X},t) = 0, \quad \mathbf{X} \in \partial\widehat{\Omega}, \tag{12}$$

where we have used the convention $U_i \equiv 0$ for $i < 0$.

2.3 The second order far-field expansion

In the case of a spherical obstacle, $B_\varepsilon = \left\{\mathbf{X} \in \mathbb{R}^3 : \|\mathbf{X}\| \leq \varepsilon\right\}$, the second order far-field expansion is given by :

$$u_{\varepsilon,2}(\mathbf{x},t) = u_0(\mathbf{x},t) - \varepsilon\frac{u_0(0,t-t_0)}{R} - \varepsilon^2\left(\frac{\partial_t u_0(0,t-t_0)}{R}\right),$$

where $t_0 = \frac{R}{c}$ and $R = \sqrt{x^2+y^2+z^2}$.

3 Results

In this section, we present the results of a numerical experiment. Let us first describe the context of this experiment.

We are in $3D$, our computational domain is $B = \left\{\mathbf{X} \in \mathbb{R}^3 : \|\mathbf{X}\| \leq 1\right\}$ and the obstacle is B_ε with $\varepsilon = 0.05$. For the direct numerical simulation, the domain is $B \backslash B_\varepsilon$ whereas for the computation of the far-field expansion, the domain is the whole sphere B. The source term consists in a Rickert localized at point $S = (0, 0.3, 0.3)$.

We compare the second order far-field expansion given in section (2.3) to a direct numerical approximation of u_ε achieved with an Interior Penalty Discontinuous Galerkin Method (IPDG) associated to a second order BGT absorbing boundary condition and to a local space-time mesh refinement [4]. Numerically, we observe that at point $A = (0, 0.5, 0)$, the relative error defined by :

$$e_{rel}^\varepsilon = \left| \frac{u_\varepsilon(A,t) - u_{\varepsilon,2}(A,t)}{\max\limits_{\mathrm{t}} |u_\varepsilon(A,t)|} \right| \tag{13}$$

is lower than 6%.

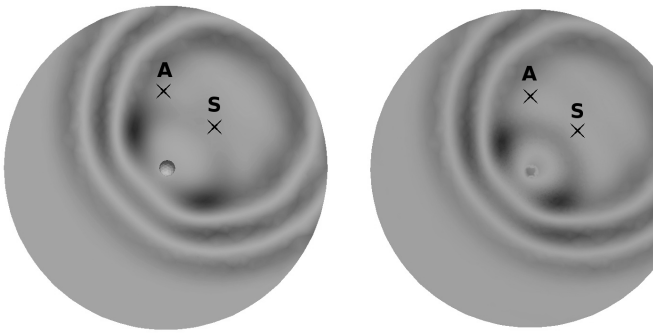

Figure 1: Comparison between the direct numerical computation of u_ε (left) and its far-field expansion (right)

References

[1] A. M. Il'in, *Matching of asymptotic expansions of solutions of boundary value problems*, American Mathematical Society, 1992.

[2] V. Maz'ya, S. Nazarov and B. Plamenevskij, *Asymptotic theory of elliptic boundary value problems in singularly perturbed domains*, Birkhuser Verlag, Basel . Boston . Berlin, 2000.

[3] M. Dauge, S. Tordeux and G. Vial, *Self-similar perturbation near a corner : matching versus multi-scale expansions for a model problem.*

[4] J. Diaz and M.J. Grote *Energy conserving explicit local time stepping for second-order wave equations* SIAM J. SCI. COMPUT., vol. 31, No. 3, pp. 1985-2014.

[5] S. Tordeux, *Méthodes asymptotiques pour la propagation des ondes dans les milieux comportant des fentes* Thèse de l'Université de Versailles, 2004.

Perturbation of transmission eigenvalues due to small inhomogeneities in the media

F. Cakoni[1] **and S. Moskow**[2,*]
[1]Department of Mathematical Sciences, University of Delaware, Newark, Delaware 19716, USA.
[2] Department of Mathematics, Drexel University, 3141 Chestnut Street, Philadelphia, PA 19104, USA.
*Email: moskow@math.drexel.edu

Abstract

The transmission eigenvalue problem is a new class of eigenvalue problems that have recently appeared in inverse scattering theory for inhomogeneous media. Such eigenvalues provide information about material properties of the scattering media [3] and can be determined from scattering data [2]. Hence they can play an important role in a variety of inverse problems in target identification and nondestructive testing. The transmission eigenvalue problem is non-selfadjoint and nonlinear, which makes its mathematical investigation interesting and challenging. In this work we investigate how transmission eigenvalues corresponding to a given inhomogeneous medium are perturbed if small volume inhomogeneities are introduced in this medium. Our analysis is based on the asymptotic techniques developed in in [1] and [4], here applied to a fourth order inhomogeneous bi-Laplacian type equation.

Formulation of the problem

We consider an inhomogeneous medium with support $D \subset \mathbb{R}^d$, $d = 2, 3$, which is a bounded connected region with smooth boundary ∂D and outward unit normal ν. Let $n_0(x) \in C^2(D)$ be the refractive index of this medium such that $n_0(x) \geq n_0 > 0$. Furthermore we assume that inside D there are m small subregions $\epsilon B_i \subset D$, $i = 1 \dots m$ where each $B_i \subset \mathbb{R}^d$ is a bounded connected reference domain which is a smooth deformation of a ball centered at $z_i \in D$, and $\epsilon > 0$ is a small parameter. We denote $W_\epsilon := \bigcup_{i=1}^m \epsilon B_i$. In each small subregion we consider a real valued function n_i, $i = 1 \dots m$ where again $n_i \in C^2(\epsilon B_i)$ is such that $n_i(x) \geq n_i > 0$ and $n_i(x) \neq n_0(x)$ for $x \in \epsilon B_i$. The refractive index of the medium with inhomogeneities is n_ϵ where

$$n_\epsilon(x) := \begin{cases} n_0(x) & x \in D \setminus W_\epsilon \\ n_i(x) & x \in \epsilon B_i. \end{cases}$$

Figure 1: Dark red regions indicate small inhomogeneities B_i inside the square medium D.

The transmission eigenvalues associated with the scattering by the medium D with small inhomogeneities W_ϵ situated in a homogeneous background with refractive index $n = 1$ are the values of k for which the interior transmission problem

$$\Delta v + k^2 v = 0 \quad \text{in } D \tag{1}$$
$$\Delta w + k^2 n_\epsilon(x) w = 0 \quad \text{in } D \tag{2}$$
$$w = v \quad \text{on } \partial D \tag{3}$$
$$\frac{\partial w}{\partial \nu} = \frac{\partial v}{\partial \nu} \quad \text{on } \partial D \tag{4}$$

has a nontrivial solution $v \in L^2(D)$, $w \in L^2(D)$ such that $w - v \in H^2(D)$. It is well-known that an infinite set of *real* transmission eigenvalues exist provided that either $n_\epsilon(x) - 1 \geq \alpha > 0$ or $0 < \beta \leq 1 - n_\epsilon(x) < 1$ [3]. Since the transmission eigenvalue problem is non-selfadjoint, complex eigenvalues may exist, but their existence to date has been proven only for the spherically stratified media. Note that transmission eigenvalues are related to non-scattering wave numbers associated with the medium $n_\epsilon(x)$. It is known that (1)-(4) is equivalent to the eigenvalue problem for $u = w - v \in H_0^2(D)$ satisfying the fourth order equation

$$\left(\Delta + k^2 n_\epsilon\right) \frac{1}{n_\epsilon - 1} \left(\Delta + k^2\right) u = 0 \tag{5}$$

which in variational form, after integration by parts, is formulated as finding a function $u \in H_0^2(D)$ such that for all $v \in H_0^2(D)$

$$\int_D \frac{1}{n_\epsilon - 1} (\Delta u + k^2 u)(\Delta \overline{v} + k^2 n_\epsilon \overline{v})\, dx = 0.$$

Setting $k^2 := \tau$, the latter can be written in the operator form

$$\mathbb{A}_\epsilon u + \tau \mathbb{B}_\epsilon u + \tau^2 \mathbb{C}_\epsilon u = 0$$

where $\mathbb{A}_\epsilon, \mathbb{B}_\epsilon, \mathbb{C}_\epsilon : H_0^2(D) \to H_0^2(D)$ are defined by mean of the Riesz representation theorem

$$(\mathbb{A}_\epsilon u, v)_{H^2(D)} = \int_D \frac{1}{n_\epsilon - 1} \Delta u\, \Delta \overline{v}\, \mathrm{d}x,$$

$$(\mathbb{B}_\epsilon u, v)_{H^2(D)} = \int_D \frac{1}{n_\epsilon - 1} \left(\Delta u\, \overline{v} + n_\epsilon u\, \Delta \overline{v}\right)\, dx,$$

$$(\mathbb{C}_\epsilon u, v)_{H^2(D)} = \int_D \frac{n_\epsilon}{n_\epsilon - 1} u\, \overline{v}\, dx.$$

The above quadratic eigenvalue problem can be rewritten as an eigenvalue problem for the non-selfadjoint compact operator $\mathbf{K}_\epsilon : H_0^2(D) \times H_0^2(D) \to H_0^2(D) \times H_0^2(D)$ given by

$$\mathbf{K}_\epsilon := \begin{pmatrix} -\mathbb{A}_\epsilon^{-1}\mathbb{B}_\epsilon & -\mathbb{A}_\epsilon^{-1}\mathbb{C}_\epsilon^{1/2} \\ \mathbb{C}_\epsilon^{1/2} & 0 \end{pmatrix}.$$

Our main goal is to show that as $\epsilon \to 0$ the spectrum of the operator $\mathbf{K}_\epsilon$ (i.e. transmission eigenvalues and eigenvectors corresponding to the medium with small inhomogeneities) converges to the spectrum of $\mathbf{K}_0$ (i.e. to the transmission eigenvalues corresponding to the reference medium without inhomogeneity, i.e. with refractive index n_0). Furthermore we provide explicit formulas for the main term in the related asymptotic expansion and in particular for the transmission eigenvalues which can potentially be used to obtain information about small inhomogeneities.

1 Convergence analysis and asymptotical formulas

First, analyzing each term of the matrix valued operator $\mathbf{K}_\epsilon$ and $\mathbf{K}_0$, we show that

$$\mathbf{K}_\epsilon \to \mathbf{K}_0, \quad \text{as } \epsilon \to 0$$

in the operator norm. Furthermore, assuming for simplicity of presentation that n_0 and n_i are constants, we obtain the following asymptotic formulas: if $u, \phi \in H_0^2(D) \bigcap C^2(D)$ then

$$((\mathbb{B}_\epsilon - \mathbb{B}_0)u, \phi) = \sum_{j=1}^N \epsilon^d |B_j| \left[\left(\frac{1}{n_j - 1} - \frac{1}{n_0 - 1} \right) \Delta u(z_j) \overline{\phi(z_j)} + \left(\frac{n_j}{n_j - 1} - \frac{n_0}{n_0 - 1} \right) u(z_j) \Delta \overline{\phi(z_j)} \right] + o(\epsilon^d),$$

$$((\mathbb{C}_\epsilon - \mathbb{C}_0)u, \phi) = \sum_{j=1}^N \epsilon^d |B_j| \left(\frac{n_j}{n_j - 1} - \frac{n_0}{n_0 - 1} \right) u(z_j) \overline{\phi(z_j)} + o(\epsilon^d),$$

and if $w_\epsilon = \mathbb{A}_\epsilon^{-1} u$ and $w_0 = \mathbb{A}_0^{-1} u$,

$$(w_\epsilon - w_0, \phi) = \sum_{j=1}^N \epsilon^d \left(1 - \frac{n_0 - 1}{n_j - 1} \right) m_j \Delta w_0(z_j) \Delta \overline{\phi}(z_j) + o(\epsilon^d) \quad \text{where}$$

$$m_j = |B_j| + \left(\frac{1}{n_0 - 1} - \frac{1}{n_j - 1} \right) \int_{\partial B_j} \frac{\partial v_{B_j}}{\partial \nu_y} d\sigma_y$$

acts in place of what was a polarization tensor in the case of small volume conductivity inhomogeneities [1], [4]. Note that here we no longer have a tensor, but we have a scalar m_j with a form similar to the polarization tensor. Finally, combining all the above and applying an important theorem by Osborn in [5], we obtain asymptotic formulas for transmission eigenvalues. In particular, for a simple real transmission eigenvalue this formula takes the form:

$$\frac{1}{\tau_\epsilon} - \frac{1}{\tau_0} = \sum_{j=1}^N \epsilon^d |B_j| \left(\frac{1 + n_0}{n_0 - 1} - \frac{1 + n_j}{n_j - 1} \right) \Delta u(z_j) u(z_j) + \frac{1}{\tau_0} \sum_{j=1}^N \epsilon^d \left(\frac{1}{n_0 - 1} - \frac{1}{n_j - 1} \right) m_j |\Delta u(z_j)|^2 + o(\epsilon^d),$$

where u is the eigenfunction corresponding to τ_0. Similar expressions can be obtained for multiple eigenvalues as well as complex eigenvalues.

References

[1] H. Ammari and S. Moskow, *Asymptotic expansions for eigenvalues in the presence of small inhomogeneities*, Math. Meth. Appl. Sci., 26 2003, 67-75.

[2] F. Cakoni, D. Colton and H. Haddar, *On the determination of Dirichlet or transmission eigenvalues from far-field data*, C. R. Acad. Sci. Paris, 348, 2010, pp. 379-383.

[3] F. Cakoni and H. Haddar, *Transmission Eigenvalues in Inverse Scattering Theory*, Inside Out II, MSRI Publications, 2012, pp. 527-578

[4] DJ. Cedio-Fengya, S. Moskow and M. Vogelius, *Identification of conductivity imperfections of small diameter by boundary measurements. Continuous dependence and computational reconstructions*, Inverse Problems, 14, 1998, pp. 553-595.

[5] JE. Osborn, *Spectral approximations for compact operators*, Mathematics of Computation, 29, 1975, 712725.

Time domain computation of the scattering of waves by small heterogeneities

X. Claeys[3] **S. Marmorat**[1,2*], **P. Joly**[2]
[1]CEA LIST, F-91191, Gif-sur-Yvette, France.
[2] POEMS (UMR 7231 CNRS-INRIA-ENSTA), ENSTA Paristech, Palaiseau, France.
[3] Laboratoire Jacque-Louis Lions, Université Paris VI, Paris, France.
*Email: simon.marmorat@inria.fr

Introduction

This research is developed in the context of the numerical modelling of non-destructive testing experiments by ultrasounds. Some slowly varying background media may be disturbed by small heterogeneities presenting a strong contrast of physical parameters (for instance gravels inside concrete). Simulating the propagation of waves inside such medium is challenging for classical numerical tools, due to the small size of the heterogeneities. In figure 1, we present a result of a numerical simulation obtained with a full discretization including the use of local mesh refinement and local time stepping around each small heterogeneity. To reduce complexity and computational cost, we aim at proposing an approximate model 'easier' to solve than the original one.

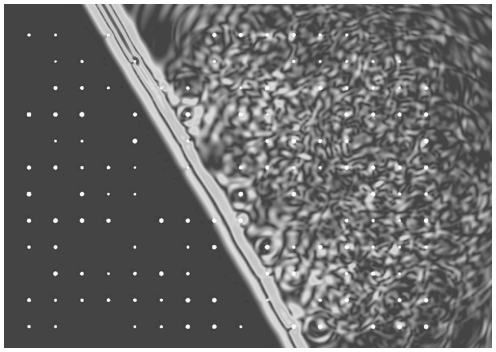

Figure 1: Snapshot of an acoustic plane wave scattered by many small obstacles.

1 A model problem

We consider the diffraction of an acoustic wave by a small inclusion in $\mathbb{R}^d, d \leq 3$, $B_\delta := \delta B$ where B is a reference domain of diameter 1 and $\delta > 0$ is small. For simplicity, we will only consider a variation of the density $\rho > 0 \in L^\infty(\mathbb{R})$ of the reference medium: find $u^\delta : t \to u^\delta(t) \in U := H^1(\mathbb{R}^d)$ such that

$$(P_\delta) \begin{cases} \rho^\delta \, \partial_t^2 u^\delta - \Delta u^\delta = f, & x \in \mathbb{R}^d, \ t \in \mathbb{R}^+, \\ u^\delta(x,0) = \partial_t u^\delta(x,0) = 0, & x \in \mathbb{R}^d, \end{cases}$$

where $\rho^\delta = \rho(1 + a\chi^\delta)$, $a \neq 0$, $a > -1$, (so that $\rho^\delta > 0$) and χ^δ is the indicator function of B_δ.

Remark. *It would not be difficult to generalize what follows to a fixed (maybe large) number of inclusions, namely if*

$$\rho^\delta = \rho\,(1 + \sum_{j=1}^{J} a_j \chi_j^\delta).$$

2 A numerical approach

Our approach is inspired by the Born approximation method which consists in seeing the "medium" ρ^δ as a perturbation of the medium ρ and rewriting:

$$\rho\, \partial_t^2 u^\delta - \Delta u^\delta = f - a\, \rho\, \chi^\delta\, \partial_t^2 u^\delta.$$

In the spirit of [2], we reintroduce the second source term as an additional unknown : $v^\delta = \lambda\ \chi^\delta\, u^\delta$ where $\lambda \neq 0$ is a real parameter whose interest will appear later, and to rewrite (P_δ) as a system:

Find $(u, v) : t \to (u(t), v(t)) \in U \times V_\delta$ such that

$$(\tilde{P}_\delta) \begin{cases} \rho\, \partial_t^2 u^\delta - \Delta u^\delta + \dfrac{\rho a}{\lambda} \partial_t^2 v^\delta = f, & x \in \mathbb{R}^d, \ t \in \mathbb{R}^+, \\ \rho\, v^\delta = \lambda\ \chi^\delta\, \rho\, u^\delta, & x \in B_\delta, \ t \in \mathbb{R}^+, \\ u^\delta(x,0) \ = \ \partial_t u^\delta(x,0) = 0, & x \in \mathbb{R}^d. \end{cases}$$

with variational formulation

$$(VF) \begin{cases} \dfrac{d^2}{dt^2}\, m(u^\delta, \widetilde{u}) + a(u^\delta, \widetilde{u}) + \dfrac{a}{\lambda} \dfrac{d^2}{dt^2}\, b(v^\delta, \widetilde{u}) = L(\widetilde{u}) \\ m^\delta(v^\delta, \widetilde{v}^\delta) = \lambda\, b(\widetilde{v}^\delta, u^\delta) \end{cases}$$

for all $(\widetilde{u}, \widetilde{v}^\delta) \in U \times V_\delta$. The bilinear forms are given by (we omit the obvious definition of $L(\cdot)$)

$$\begin{cases} m(u, \widetilde{u}) = \displaystyle\int_{\mathbb{R}^d} \rho\, u\, \widetilde{u}\, dx, & \forall (u, \widetilde{u}) \in U^2, \\ a(u, \widetilde{u}) = \displaystyle\int_{\mathbb{R}^d} \nabla u \cdot \nabla \widetilde{u}\, dx, & \forall (u, \widetilde{u}) \in U^2, \\ m^\delta(v^\delta, \widetilde{v}^\delta) = \displaystyle\int_{B_\delta} \rho\, v^\delta\, \widetilde{v}^\delta\, dx, & \forall\ (v^\delta, \widetilde{v}^\delta) \in V_\delta^2, \\ b(v^\delta, u) = \displaystyle\int_{B_\delta} \rho\, v^\delta\, u\, dx, & \forall\ (v^\delta, u) \in V_\delta \times U. \end{cases}$$

To simplify the problem, the idea is that, when δ is small, v^δ should be accurately represented by replacing the space V_δ by a finite dimensional subspace (still denoted V_δ for simplicity):

$$V_\delta = \underset{j=1,\dots,N}{span} \big[\, w_j(\cdot/\delta)\,\big], \text{ with } w_j : B \longrightarrow \mathbb{R}$$

This relies on an asymptotic analysis which moreover provides a characterization of the w_j's. Doing so we get a family of approximate problem where the unknown v^δ is "finite-dimensional". An important point is the stability in δ of these approximate problems. We get it by an energy approach that will lead us to fix λ. Choosing $\widetilde{u} = \frac{d}{dt}u^\delta =: \dot{u}^\delta$ in the first equation of (VF) leads to

$$\frac{1}{2}\frac{d}{dt}\Big(m(\dot{u}^\delta,\dot{u}^\delta) + a(u^\delta,u^\delta)\Big) + \frac{a}{\lambda}\, b(\ddot{v}^\delta,\dot{u}^\delta) = 0. \quad (1)$$

Next, we differentiate once in time the second equation of (VF) and choose $\widetilde{v} = \ddot{v}^\delta$ to get

$$\frac{1}{2}\frac{d}{dt}\, m^\delta(\dot{v}^\delta,\dot{v}^\delta) - \lambda\, b(\ddot{v}^\delta,\dot{u}^\delta) = 0. \quad (2)$$

Adding (1) and (2) leads to

$$\begin{aligned}\frac{1}{2}\frac{d}{dt}\Big(m(\dot{u}^\delta,\dot{u}^\delta) + m^\delta(\dot{v}^\delta,\dot{v}^\delta) + a(u^\delta,u^\delta)\Big)\\ + \big(\frac{a}{\lambda} - \lambda\big)\, b(\ddot{v}^\delta,\dot{u}^\delta) = 0.\end{aligned} \quad (3)$$

Finally, we differentiate twice in time the second equation of (VF) and choose $\widetilde{v} = \dot{v}^\delta$ to obtain

$$\lambda\, b(\dot{v}^\delta,\ddot{u}^\delta) = \frac{1}{2}\frac{d}{dt}\, m(\dot{v}^\delta,\dot{v}^\delta) = \lambda\, b(\ddot{v}^\delta,\dot{u}^\delta), \quad \text{by (2)}.$$

Therefore, (2) gives $\dfrac{d}{dt}\Big(E_c^\delta + \dfrac{1}{2}a(u^\delta,u^\delta)\Big) = 0$ where

$$\begin{aligned}E_c^\delta &= \tfrac{1}{2}\Big(m(\dot{u}^\delta,\dot{u}^\delta) + m^\delta(\dot{v}^\delta,\dot{v}^\delta) + \big(\tfrac{a}{\lambda} - \lambda\big)\, b(\dot{v}^\delta,\dot{u}^\delta)\Big)\\ &= \frac{1}{2}\int_{\mathbb{R}^d}\rho\,\Big(\,|\partial_t u^\delta|^2 + |\partial_t v^\delta|^2 + \big(\frac{a}{\lambda} - \lambda\big)\,\partial_t u^\delta\,\partial_t v^\delta\,\Big)\end{aligned}$$

Choosing λ such that $a/\lambda - \lambda = 2$ (which is possible since $a \geq -1$) gives $E_c^\delta = \frac{1}{2}\int_{\mathbb{R}^d}\rho\,|\partial_t u^\delta + \partial_t v^\delta|^2$. This provides uniform estimates with respect to δ of u^δ.

For space discretization, we simply approximate the space U with classical finite elements. We then get an algebraic problem of the form

$$\begin{cases}\mathbf{M}_h\dfrac{d^2\mathbf{U}_h^\delta}{dt^2} + \mathbf{A}_h\mathbf{U}_h^\delta + \dfrac{a}{\lambda}\,\mathbf{B}_h^\delta\dfrac{d^2\mathbf{V}_h^\delta}{dt^2} = F_h\\ \mathbf{M}^\delta\,\mathbf{V}_h^\delta = \lambda\ {}^t\mathbf{B}_h^\delta\,\mathbf{U}_h^\delta\end{cases}$$

which appears as a coupling of a standard finite element approximation of the propagation in the reference medium coupled with a finite number of ordinary differential equations.

3 Construction of V_δ via asymptotic analysis

The choice of the space V_δ is guided by the asymptotic expansion of u^δ inside B_δ:

$$u^\delta(x) = \sum_{j=0}^{N} u_j^\delta(t)\, w_j(\frac{x}{\delta}) + \varepsilon_N(\delta)$$

with $\varepsilon_j(\delta) \to 0$, when $\delta \to 0$ and $\varepsilon_{j_k+1}(\delta) = o\big(\varepsilon_{j_k}(\delta)\big)$ for some sequence $j_k \to +\infty$.

There are many methods for analysing the asymptotic behaviour of u^δ, particularly for time harmonic problems (see for instance [1]). There are much fewer results for time dependent problems [3]. In this work, we use the method of matched asymptotic expansions, which lead to characterize the profile functions w_j as the restriction to B of solutions of elliptic transmission problems between B and $\mathbb{R}^d \setminus B$.

The $d+1$ first terms do not depend on B

$$w_0(x) = 1, w_j(x) = x_j, \quad 1 \leq j \leq d$$

$\varepsilon_0(\delta) = \delta$ and $\varepsilon_{d+1}(\delta) = \delta^2$. The higher order terms require to be determined numerically (except, for instance, when B is a ball).

At the conference, we shall present various numerical simulations to illustrate the accuracy and the efficiency of our approximate model. Moreover, some insights about the error analysis will be given.

References

[1] V.G. Maz'ya, S.A. Nazarov, and B.A. Plamenevskii. *Asymptotic Theory of Elliptic Boundary Value Problems in Singularly Perturbed Domains.* Birkhauser Verlag, 2000.

[2] X. Claeys and F. Collino, *Augmented Galerkin Scheme for the Solution of Scattering by small obstacles*, Num. Math. 116 (2010) no. 2, 246-268

[3] H.Ammari *An inverse initial boundary value problem for the wave equation in the presence of imperfections of small volume*, Siam J. ControlL Optim.. Vol. 41, No. 4, pp. 1190-1211, 2002

An asymptotic boundary element method for thin conducting sheets

K. Schmidt[1,*], **R. Hiptmair**[2]
[1] DFG research center MATHEON, TU Berlin, Berlin, Germany.
[2] Seminar for Applied Mathematics, ETH Zurich, Zürich, Switzerland.
*Email: kersten.schmidt@math.tu-berlin.de

Abstract

Industrial and technical applications involve very small or thin structures, often much smaller than a whole device at least in one dimension. Examples are thin sheets of a particular material, or layers with a microscopic structure. To overcome the difficulty to generate a mesh and to compute with many small cells for the thin and possibly microscopic structures one applies transmission conditions which approximate the solution outside the thin sheets directly and via post-processing inside. Using boundary element methods for the transmission problems the problem reduces further to only a discretisation of an interface. We propose and analyse a boundary element method for thin conducting sheets in the eddy current model [1].

Introduction

Let Γ be the smooth midline of a thin sheet of constant thickness $d > 0$. Let $x_\Gamma(t)$ the parametrisations of Γ (dashed line in Fig. 1), where the sheet can be parametrised as $x(t,s) = x_\Gamma(t) + sn(t)$ with n the normal vector. The traces and the normal-derivates from the two sides of Γ are defined by

$$(\gamma_0^\pm U)(t) := \lim_{s\to+0} U(x(t,\pm s)),$$
$$(\gamma_1^\pm U)(t) := \lim_{s\to+0} \nabla U(x(t,\pm s))\cdot n,$$

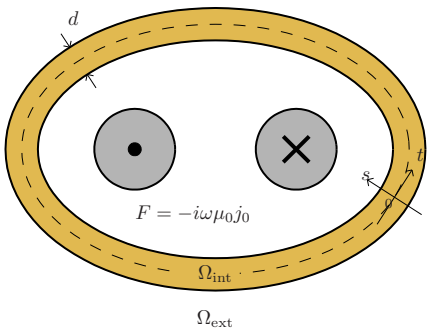

Figure 1: Geometrical setting with thin conducting sheet and current carrying wires.

and we use the notation $[\cdot]$ for the jump and $\{\cdot\}$ for the mean of $\gamma_\ell^\pm$, $\ell = 0, 1$, which are given by

$$[\gamma_\ell U](t) := (\gamma_\ell^+ U)(t) - (\gamma_\ell^- U)(t),$$
$$\{\gamma_\ell U\}(t) := \tfrac{1}{2}\left((\gamma_\ell^+ U)(t) + (\gamma_\ell^- U)(t)\right).$$

In this study we investigate the transmission problem

$$-\Delta U = F \quad \text{in } \mathbb{R}^2\backslash\Gamma, \tag{1a}$$
$$[\gamma_1 U] - \beta\{\gamma_0 U\} = 0 \quad \text{on } \Gamma, \tag{1b}$$
$$[\gamma_0 U] = 0 \quad \text{on } \Gamma, \tag{1c}$$

which arise for example by different asymptotic expansions of the eddy current problem (TM mode) with a thin conducting sheet [2], [3]. The approximated eddy current problem is given with $\xi^2 = \mathrm{i}\omega\varepsilon\mu\sigma$

$$-\Delta E(x) - \xi^2(x)E(x) = F(x), \quad \text{in } \mathbb{R}^2, \tag{2}$$

where ω is the angular frequency, ε, μ and σ the permeability, permittivity and conductivity of the thin conducting sheet and $\xi = 0$ outside the sheet. The thin conducting sheet acts as a shielding of electromagnetic sources $F = -\mathrm{i}\omega\mu_0 j_0$ due to currents j_0 in live wires. See Fig. 2 for an illustration of the shielding phenomena. Three of the eight studied transmission conditions in [3], that are ITC-1-0, ITC-1-1 and ITC-2-0, are of the form (1) which differ only by the

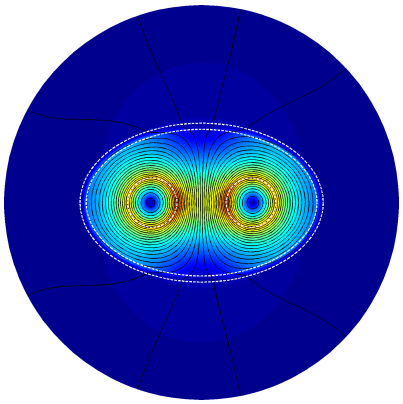

Figure 2: Magnetic field for a thin conducting sheet shielding two live wires.

constant β:

$$\beta_{\text{ITC-1-0}} = \xi^2 d, \quad \beta_{\text{ITC-1-1}} = \xi^2 d \left(1 + \tfrac{1}{6}\xi^2 d^2\right),$$

$$\beta_{\text{ITC-2-0}} = \frac{2\,\xi \sinh\left(\xi \frac{d}{2}\right)}{\cosh\left(\xi \frac{d}{2}\right) - \xi \frac{d}{2} \sinh\left(\xi \frac{d}{2}\right)}.$$

Boundary integral formulation

The solution of (1) can be written with the representation formula [4, Thm. 3.1.8]

$$U = -S\left[\gamma_1 U\right] + D\left[\gamma_0 U\right] + N\,F \quad \text{in } \mathbb{R}^2 \setminus \Gamma,$$

where S and D are the single and double layer potentials and N the Newton potential. Taking the mean trace on Γ and using (1b) and (1c) we can write for the new unknown $\phi = [\gamma_1 U]$ the boundary integral equation (BIE) of second kind

$$(Id + \beta V)\,\phi = \beta \gamma_0 N F, \tag{3}$$

where V is the usual one-sided single layer operator [4]. We can state (3) in variational form: Seek $\phi \in L^2(\Gamma)$ such that for all $\phi' \in L^2(\Gamma)$

$$\left\langle \phi, \phi' \right\rangle + \beta \left\langle V\phi, \phi' \right\rangle = \beta \left\langle \gamma_0 N F, \phi' \right\rangle. \tag{4}$$

Theorem 1 (Existence and uniqueness)**.** *Let* $\beta \notin -\mathbb{R}^+$, $F \in H^{-1}_{\text{comp}}(\mathbb{R}^2)$. *Then* (4) *provides a unique solution* $\phi \in L^2(\Gamma)$.

For the three transmission conditions ITC-1-0, ITC-1-1 and ITC-2-0 the condition is fulfilled as β has an imaginary part.

Boundary element method

We construct a mesh Γ_h of (curved) panels K_j, $j = 1, \ldots, N_h$ by partitioning of the midline Γ. The length of the largest panel is denoted by h. We call the space of piecewise constant functions as $S_0^{-1}(\Gamma_h)$ and that of piecewise linear, continuous functions as $S_1^0(\Gamma_h)$. Replacing $L^2(\Gamma)$ in (4) by the finite-dimensional subspaces $S_0^{-1}(\Gamma_h)$ or $S_1^0(\Gamma_h)$ we obtain

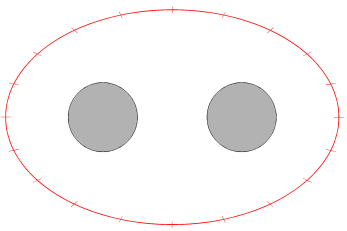

Figure 3: Mesh Γ_h of the interface Γ.

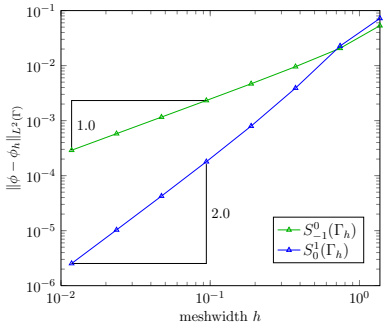

Figure 4: Convergence of the BEM.

linear systems of equations for the approximate solution ϕ_h.

Theorem 2. *Let* $\beta \notin -\mathbb{R}^+$, $F \in H^{-1}_{\text{comp}}(\mathbb{R}^2)$. *Then* (3) *with* $L^2(\Gamma)$ *replaced by a subspace* $S(\Gamma_h)$ *provides a unique solution* $\phi_h \in S(\Gamma_h)$. *Furthermore, we have for* $S(\Gamma_h) = S_0^{-1}(\Gamma_h)$

$$\|\phi - \phi_h\|_{L^2(\Gamma)} \leq C\,h$$

and for $S(\Gamma_h) = S_1^0(\Gamma_h)$

$$\|\phi - \phi_h\|_{L^2(\Gamma)} \leq C\,h^2.$$

In the implemenation of the method we approximate all integrals by replacing the curved by planar panels which will not influence the order of the method essentially (see [4, Chap. 8]).

Numerical experiments for an elliptic sheet justify the convergence orders of Theorem 2, see Fig. 4. The reference solution has been computed by high-order FEM with the numerical C++ library CONCEPTS (see `www.concepts.math.ethz.ch`).

References

[1] Schmidt, K. and Hiptmair, R. *Asymptotic boundary element methods for thin conducting sheets*, in preparation.

[2] Schmidt, K. and Tordeux, S. *High order transmission conditions for thin conductive sheets in magneto-quasistatics* ESAIM:M2AN, 2011, 45, pp. 1115–1140.

[3] Schmidt, K. and Chernov, A. *A unified analysis of transmission conditions for thin conducting sheets in the time-harmonic eddy current model.* Preprint 2012-36, Inst. f. Math., TU Berlin, 2012.

[4] Sauter, S. and Schwab, C. *Boundary element methods* Springer-Verlag, Heidelberg, Germany, 2011.

Effective Transmission Conditions for Thin-Layer Transmission Problems in Elastodynamics

M. Bonnet[1] **A. Burel**[1,2*], **P. Joly**[1]
[1] POEMS (UMR 7231 CNRS-INRIA-ENSTA), ENSTA Paristech, Palaiseau, France.
[2]Equipe Analyse Numérique et Equations aux Dérivées Partielles, Université Paris-Sud XI, Orsay, France.
*Email: alienor.burel@inria.fr

Introduction

This research is developed in the framework of the numerical modeling of non-destructive testing experiments by ultrasounds. Some media involve thin layers (for instance of resin), which are difficult to handle in numerical computations due to the very small element size required for meshing them. Analogous problems arise for the treatment of thin coatings (see [2] and [3]). To overcome this issue, one idea consists in using effective transmission conditions (ETCs) across the two interfaces bounding the layer. This work aims at establishing such ETCs by means of a formal asymptotic analysis with respect to the (small) layer thickness, in the spirit of [1] for Maxwell's equations.

1 Problem Setting

We consider the case of a thin layer of an isotropic elastic material, the strip $\Omega_\eta^i = \mathbb{R} \times [-\frac{\eta}{2}, \frac{\eta}{2}]$, let Ω_η^+ (resp. Ω_η^-) be the upper domain (resp. lower domain) of the thin layer. We call $\partial\Omega_\eta^+$ and $\partial\Omega_\eta^+$ the upper and lower boundaries of the layer connected to each outside domain. We assume that the layer material is isotropic and homogeneous, with mass density ρ^i and Lamé coefficients λ^i, μ^i. We denote by ρ, λ, and μ the (possibly heterogeneous) coefficients of the material in $\Omega^\pm$.

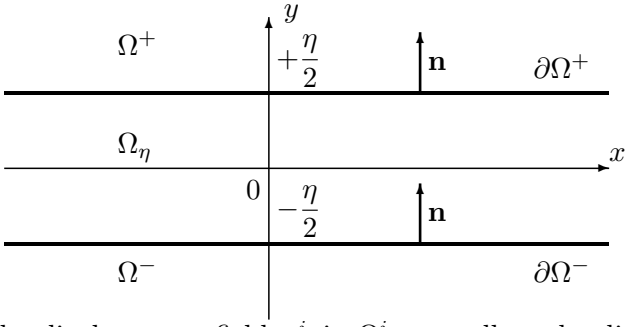

The displacement field $\mathbf{u}_\eta^i$ in Ω_η^i, as well as the displacement fields $\mathbf{u}_\eta^\pm$ inside $\Omega_\eta^\pm$ satisfy the elastodynamics equations:

$$\rho^i \frac{\partial^2 \mathbf{u}_\eta^i}{\partial t^2} - \text{ div } \sigma^i(\mathbf{u}_\eta^i) = 0, \qquad \text{in } \Omega_\eta^i, \quad (1)$$

$$\rho \frac{\partial^2 \mathbf{u}_\eta^\pm}{\partial t^2} - \text{ div } \sigma(\mathbf{u}_\eta^\pm) = 0, \qquad \text{in } \Omega_\eta^\pm. \quad (2)$$

where $\sigma(\mathbf{u})$ and $\sigma^i(\mathbf{u})$ respectively denote the stress tensor in the surrounding and layer material, respectively, given by Hooke's law applied to a given displacement $\mathbf{u}$. Equations (1) and (2) are coupled with transmission conditions on the interfaces $\partial\Omega^\pm$ (we omit the time variable t for simplicity):

$$\begin{cases} \mathbf{u}_\eta^\pm\Big(x, \pm\frac{\eta}{2}\Big) = \mathbf{u}_\eta^i\Big(x, \pm\frac{\eta}{2}\Big) \\ \mathbf{t}(\mathbf{u}_\eta^\pm)\ \Big(x, \pm\frac{\eta}{2}\Big) = \mathbf{t}^i(\mathbf{u}_\eta^i)\ \Big(x, \pm\frac{\eta}{2}\Big), \end{cases} \quad (3)$$

where $\mathbf{t}(\mathbf{u}) := \sigma(\mathbf{u})\mathbf{n}$ and $\mathbf{t}^i(\mathbf{u}) := \sigma^i(\mathbf{u})\mathbf{n}$ are the traction vectors relative to $\Omega^\pm$ and Ω_η and $\mathbf{n}$ is the normal vector to $\partial\Omega^\pm$ (see the figure above).

Eliminating formally $\mathbf{u}_\eta^i$, we can write a transmission problem for $\mathbf{u}_\eta := (\mathbf{u}_\eta^+, \mathbf{u}_\eta^-)$. For any function $f : \mathbb{R}^2 \to \mathbb{R}^d$, if we use the notation:

$$\{f\}_\eta = \big([f]_\eta, \langle f\rangle_\eta\big) : \mathbb{R} \to \mathbb{R}^{2d}$$
$$[f]_\eta(x) := f(x, \eta/2) - f(x, \eta/2),$$
$$\langle f\rangle_\eta(x) := \big(\, f(x, \eta/2) + f(x, \eta/2)\,\big)/2$$

this transmission condition can be written in the form

$$\{\mathbf{t}(\mathbf{u}_\eta)\}_\eta + \mathbf{T}_\eta\{\mathbf{u}_\eta\}_\eta = 0$$

where $\mathbf{T}_\eta$ is a (nonlocal) DtN transmission operator that can easily be defined implicitly from the solution of the interior Dirichlet problem in the strip Ω_η^i. The next idea is that, when η tends to 0, $\mathbf{T}_\eta$ becomes local and that one can get explicit analytical approximations of it.

2 Principle of construction of ETC's

This construction is based on an ansatz for the interior solution $\mathbf{u}_\eta^i$ of the form

$$\mathbf{u}_\eta^i(x,y) = \mathbf{U}^0\big(x, \frac{y}{\eta}\big) + \eta\, \mathbf{U}^1\big(x, \frac{y}{\eta}\big) + \eta^2\, \mathbf{U}^2\big(x, \frac{y}{\eta}\big) + ... \quad (4)$$

where $\mathbf{U}^0 : \Omega_1^i \to \mathbb{R}^2$. This implies in particular an analogous expansion for the traces

$$\mathbf{u}_\eta^i(x, \pm\frac{\eta}{2}) = \mathbf{u}_\pm^0(x) + \eta\, \mathbf{u}_\pm^1(x) + \eta^2\, \mathbf{u}_\pm^2(x) + ... \quad (5)$$

Substituting (4) into (1) allows us to compute explicitly the $\mathbf{U}_k$ from the $\mathbf{u}^k_\pm$ by induction on k: these are polynomial functions in y. These expressions lead us to introduce a family of differential operators of order ℓ, $\mathcal{A}_\ell(\partial_x, \partial_t), \ell \geq 0$, such that

$$\mathcal{A}_0(\partial_x, \partial_t)\{\mathbf{u}^0\} = 0 \tag{6}$$

and

$$\mathbf{t}^i(\mathbf{u}^i_\eta)\left(x, \pm\frac{\eta}{2}\right) = \mathbf{t}^0_\pm(x) + \eta\,\mathbf{t}^1_\pm(x) + \eta^2\,\mathbf{t}^2_\pm(x) + \ldots \tag{7}$$

$$\text{where} \quad \{\mathbf{t}^k\} = \sum_{j=0}^{k+1} \mathcal{A}_{k+1-j}(\partial_x, \partial_t)\{\mathbf{u}^j\} \tag{8}$$

and where we have defined

$$\{\mathbf{t}^k\} = \big([\mathbf{t}^k], \langle\mathbf{t}^k\rangle\big),\ [\mathbf{t}^k] = \mathbf{t}^k_+ - \mathbf{t}^k_-,\ \langle\mathbf{t}^k\rangle = \frac{\mathbf{t}^k_+ + \mathbf{t}^k_-}{2}$$

and the same for $\{\mathbf{u}^k\}$. Note that from (5) and (7)

$$\begin{cases} \{\mathbf{u}^i_\eta\}_\eta = \{\mathbf{u}^0\} + \eta\,\{\mathbf{u}^1\} + \eta^2\,\{\mathbf{u}^2\} + \ldots \\ \{\mathbf{t}^i(\mathbf{u}^i_\eta)\}_\eta = \{\mathbf{t}^0\} + \eta\,\{\mathbf{t}^1\} + \eta^2\,\{\mathbf{t}^2\} + \ldots \end{cases} \tag{9}$$

We rewrite the transmission conditions (3) as

$$\{\mathbf{t}(\mathbf{u}_\eta)\}_\eta = \{\mathbf{t}^i(\mathbf{u}^i_\eta)\}_\eta, \quad \{\mathbf{u}_\eta\}_\eta = \{\mathbf{u}^i_\eta\}_\eta$$

so that, using (9) and (8), we get

$$\eta\,\{\mathbf{t}(\mathbf{u}_\eta)\}_\eta = \sum_{k\geq 0} \eta^{k+1} \Big(\sum_{j=0}^{k+1} \mathcal{A}_{k+1-j}(\partial_x, \partial_t)\{\mathbf{u}^j\} \Big)$$

which, thanks to (6), can be rearranged as

$$\begin{aligned} \eta\,\{\mathbf{t}(\mathbf{u}_\eta)\}_\eta &= \Big(\sum_{\ell} \eta^\ell \mathcal{A}_\ell(\partial_x, \partial_t) \Big) \Big(\sum_{j} \eta^j \{\mathbf{u}^j\} \Big) \\ &= \Big(\sum_{\ell=0}^{k} \eta^\ell \mathcal{A}_\ell(\partial_x, \partial_t) \Big) \{\mathbf{u}^\eta\} + O(\eta^{k+1}) \end{aligned}$$

The transmission condition of order $k+1$ is then obtained formally by dropping the $O(\eta^{k+1})$ term.

3 A third order transmission condition

Applying the above method with $k = 2$ leads to the following transmission conditions

$$\begin{cases} A[\mathbf{u}^\eta]_\eta = \eta\,\langle\mathbf{t}(\mathbf{u}^\eta)\rangle_\eta - \eta\,BJ\,\langle\partial_x\mathbf{u}^\eta\rangle_\eta, \\ [\mathbf{t}(\mathbf{u}^\eta)]_\eta = \eta\,\rho\,\langle\partial_t^2\mathbf{u}^\eta\rangle_\eta - \eta\,JAJ\,\langle\partial_x^2\mathbf{u}^\eta\rangle_\eta \\ \qquad\qquad - JB\,[\partial_x\mathbf{u}^\eta]_\eta, \end{cases} \tag{10}$$

where A, B and J are the following 2×2 matrices:

$$A = \begin{pmatrix} \mu^i & 0 \\ 0 & \lambda^i + 2\mu^i \end{pmatrix},\ B = \begin{pmatrix} \mu^i & 0 \\ 0 & \lambda^i \end{pmatrix},\ J = \begin{pmatrix} 0 & 1 \\ 1 & 0 \end{pmatrix}. \tag{11}$$

A fundamental point is the well-posedness and uniform stability in η of the transmission problem (2, 10). This is in fact a consequence of an energy conservation result: any smooth enough solution of (2, 10) satisfies:

$$\frac{d}{dt}\Big(\mathcal{E}_\eta + \mathcal{E}^i_\eta\Big) = 0 \tag{12}$$

where

$$\mathcal{E}_\eta = \frac{\rho}{2}\int_{\Omega_\eta} |\partial_t\mathbf{u}^\eta|^2\ dx + \frac{1}{2}\int_{\Omega_\eta} \sigma(\mathbf{u}^\eta) : \varepsilon(\mathbf{u}^\eta)\ dx$$

$$\mathcal{E}^i_\eta = \frac{\eta\,\rho}{2}\int_{\mathbb{R}} |\langle\partial_t\mathbf{u}^\eta\rangle|^2\ dx + \frac{\eta}{2}\int_{\mathbb{R}} Q\Big(\partial_x\mathbf{u}^\eta, \frac{[\mathbf{u}^\eta]}{\eta}\Big)\ dx$$

and $Q(\mathbf{x},\mathbf{y}) : \mathbb{R}^2\times\mathbb{R}^2 \to \mathbb{R}$ is the symmetric quadratic form ($J^T = J$ and $(BJ)^T = JB$):

$$Q(\mathbf{x},\mathbf{y}) := \mathbf{x}^T JAJ\,\mathbf{x} + 2\,\mathbf{x}^T JB\,\mathbf{y} + \mathbf{y}^T A\,\mathbf{y} \tag{13}$$

The well-posedness and stability result is then a consequence of the:

Theorem. *The quadratic form $Q(\mathbf{x},\mathbf{y})$ is positive.*

At the conference, we shall present various numerical simulations to illustrate the accuracy and the efficiency of our approximate model. Moreover, some insights about the error analysis will be given.

References

[1] S. Chun, H. Haddar and J.S. Hesthaven, *High-order accurate thin layer approximations for time-domain electromagnetics, Part II: Transmission layers*, in J. Comp. Appl. Math., **8** (2010), pp. 2587–2608.

[2] H. Haddar and P. Joly *Stability of thin layer approximation of electromagnetic waves scattering by linear and non linear coatings*, in Nonlinear Partial Differential Equations and their Applications Collège de France Seminar Volume XIV, Elsevier, **31** (2002), pp. 415–456.

[3] A. Bendali and K. Lemrabet *The effect of a thin coating on the scattering of a time-harmonic wave for the Helmholtz equation*, in SIAM J. Appl. Math., **6**(56) (1996), pp. 1664–1693.

Impedance boundary conditions for viscous acoustic equations close to rigid walls

A. Thöns-Zueva[1,*], **K. Schmidt**[1]
[1] DFG research center MATHEON, TU Berlin, Berlin, Germany.
*Email: anastasia.thoens@math.tu-berlin.de

Introduction

In this study we are investigating the acoustic equations as a perturbation of the Navier-Stokes equations around a stagnant uniform fluid, with mean density ρ_0 and without heat flux. For gases the (dynamic) viscosity η is very small and leads to *viscosity boundary layers* close to walls. To resolve the boundary layers with (quasi-)uniform meshes the mesh size has to be at the same order which leads to very large linear systems to be solved. This is especially the case for the very small boundary layers of acoustic waves. We propose effective *impedance boundary conditions* for curved boundaries by a multiscale analysis, which separate velocity and pressure into *far field* and correcting *near field* [1].

Formulation of the problem

Let $\Omega \subset \mathbb{R}^2$ be a bounded domain with smooth boundary $\partial\Omega$. We consider dimensionless time-harmonic acoustic velocity $\mathbf{v}$ and acoustic pressure p (the time regime is $e^{-\mathrm{i}\omega t}$, $\omega \in \mathbb{R}^+$) which are described by the coupled system in the framework of Landau and Lifshitz [2]

$$-\mathrm{i}\omega\mathbf{v} + \nabla p - R^{-1}\Delta_\eta \mathbf{v} = \mathbf{f}, \text{ in } \Omega, \tag{1a}$$
$$-\mathrm{i}\omega p + \operatorname{div}\mathbf{v} = 0, \text{ in } \Omega, \tag{1b}$$
$$\mathbf{v} = \mathbf{0}, \text{ on } \partial\Omega. \tag{1c}$$

In the *momentum equation* (1a) with some known source term $\mathbf{f}$ the viscous dissipation in the momentum is not neglected as we consider near wall regions. Here, $R^{-1} = \eta/(\rho_0 cL) \ll 1$ is a dimensionless number, c the sound velocity, L the characteristic length of the domain, and $\Delta_\eta := \Delta + (\frac{1}{3} + \zeta/\eta)\nabla \operatorname{div}$ with $\zeta \geq 0$ the second (volume) viscosity. The *continuity equation* (1b) relates the acoustic pressure linearly to the divergence of the acoustic velocity. The system is completed by *no-slip* boundary conditions (1c). Here we assume that $\mathbf{f} = 0$ on $\partial\Omega$, more general results can be found in [1].

Asymptotic expansion

The acoustic equations (1) show a viscosity boundary layer of thickness $O(\sqrt{R^{-1}})$ for the tangential component of the velocity. Introducing the small parameter $\varepsilon = \sqrt{R^{-1}}$ and curvilinear coordinates (t, s) close to the boundary where t is the tangential variable and s the normal one, we write the solution of (1) inspired by the framework of Vishik and Lyusternik [3] as

$$\mathbf{v} = \sum_{j=0}^{\infty} \varepsilon^j \left(\mathbf{v}^j + \varepsilon\, \mathbf{curl}_{2D}\, \phi^j\right);\ p = \sum_{j=0}^{\infty} \varepsilon^j p^j, \tag{2}$$

where $\mathbf{v}^j(x, y)$ and $p^j(x, y)$ are terms of the *far field* expansion, the *near field* terms $\phi^j(t, \frac{s}{\varepsilon})$ represent the boundary layer close to the wall, and $\mathbf{curl}_{2D} = (\partial_y, -\partial_x)^\top$.

The method of multiscale expansion separates the far and near field terms. The far field velocity terms $\mathbf{v}^j$ satisfy the partial differential equation (PDE)

$$\nabla \operatorname{div}\mathbf{v}^j + \omega^2 \mathbf{v}^j = \mathrm{i}\omega\mathbf{f} \cdot \delta_{j=0} + \mathrm{i}\omega\Delta_\eta \mathbf{v}^{j-2}, \tag{3a}$$
$$\mathbf{v}^j(t, 0) \cdot \mathbf{n} = \partial_t \phi^{j-1}(t, 0), \tag{3b}$$

where $\phi^{-j} \equiv 0$ for $j < 0$, $\delta_{j=0}$ the Kronecker symbol which is 1 if $j = 0$ and 0 otherwise, and $\mathbf{n}$ the outer normal vector. The far field pressure terms follow as

$$p^j = -\frac{\mathrm{i}}{\omega} \operatorname{div}\mathbf{v}^j. \tag{4}$$

The near field terms $\phi^j(t, S)$ for $S \in [0, \infty)$ are defined by the ordinary differential equation (ODE)

$$\begin{aligned}\mathrm{i}\omega\phi^j + \partial_S^2\phi^j = {} & \kappa\big(3\,\mathrm{i}\omega S + 3S\partial_S^2 + \partial_S\big)\phi^{j-1} - \partial_t^2\phi^{j-2} \\ & + \big(-3\,\mathrm{i}\omega\kappa^2 S^2 - 3\kappa^2 S^2\partial_S^2 - 2\kappa^2 S\partial_S\big)\phi^{j-2} \\ & + \big(\mathrm{i}\omega\kappa^3 S^3 + \kappa^3 S^3\partial_S^2 + \kappa^3 S^2\partial_S + \kappa S\partial_t^2 - \kappa' S\partial_t\big)\phi^{j-3},\end{aligned}$$

with the boundary condition

$$\partial_S \phi^j(t, 0) = \mathbf{v}^j(t, 0) \cdot \mathbf{n}^\perp,$$

and decay condition for $S \to \infty$. Here, $\mathbf{n}^\perp = (n_2, -n_1)^\top$ and κ are tangential vector and curvature on $\partial\Omega$.

The far field velocity term $\mathbf{v}^0$ has only a vanishing normal component, and the tangential component

gets zero only if $\varepsilon\,\mathbf{curl}_{2D}\,\phi^0(t,\frac{s}{\varepsilon})$ is added, see (1c), where the zeroth order near field function for $S=\frac{s}{\varepsilon}$

$$\phi^0\left(t,\frac{s}{\varepsilon}\right)=\frac{1-\mathrm{i}}{\sqrt{2\omega}}\exp\left(-\frac{(1+\mathrm{i})}{\sqrt{2}}\frac{\sqrt{\omega}s}{\varepsilon}\right)\mathbf{v}^0(t,0)\cdot\mathbf{n}^\perp$$

decays exponentially away from the boundary. The sum $\mathbf{v}^0+\varepsilon\,\mathbf{curl}_{2D}\,\phi^0(t,\frac{s}{\varepsilon})$ has a non-zero, but small normal component and is therefore corrected by $\varepsilon\mathbf{v}^1$.

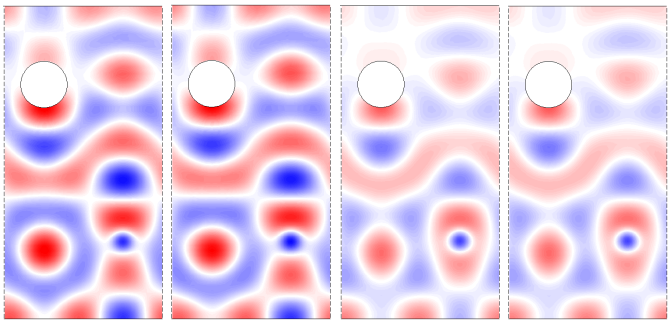

Figure 1: Comparison of pressure.

Impedance boundary conditions

Outside a $O(\varepsilon)$-neighbourhood of the boundary the far field velocity $\mathbf{v}^{\varepsilon,N}:=\sum_{j=0}^N\varepsilon^j\mathbf{v}^j$ and $p^{\varepsilon,N}:=\sum_{j=0}^N\varepsilon^j p^j$ serve as accurate approximation to $\mathbf{v}$ and p, where the error is the smaller the higher N. Approximations $\mathbf{v}_{\mathrm{appr},N}\approx\mathbf{v}^{\varepsilon,N}$ and $p_{\mathrm{appr},N}\approx p^{\varepsilon,N}$ shall be defined by a single PDE, respectively, using again $R^{-\frac{1}{2}}$ instead of ε. In this way we can define PDEs with impedance boundary conditions for the pressure only, which can be directly computed and not in post-processing like for the exact model.

Impedance boundary conditions for the pressure. The approximative models are for $N=0$

$$\Delta p_{\mathrm{appr},0}+\omega^2 p_{\mathrm{appr},0}=\operatorname{div}\mathbf{f},$$
$$\nabla p_{\mathrm{appr},0}\cdot\mathbf{n}=0,$$

for $N=1$

$$\Delta p_{\mathrm{appr},1}+\omega^2 p_{\mathrm{appr},1}=\operatorname{div}\mathbf{f},$$
$$\nabla p_{\mathrm{appr},1}\cdot\mathbf{n}+\tfrac{1+\mathrm{i}}{\sqrt{2\omega R}}\partial_t^2 p_{\mathrm{appr},1}=0,$$

and for $N=2$

$$\left(1-(\tfrac{4}{3}+\tfrac{\zeta}{\eta})\tfrac{\mathrm{i}\omega}{R}\right)\Delta p_{\mathrm{appr},2}+\omega^2 p_{\mathrm{appr},2}=\operatorname{div}\mathbf{f},$$
$$\nabla p_{\mathrm{appr},2}\cdot\mathbf{n}+\tfrac{1+\mathrm{i}}{\sqrt{2\omega R}}\partial_t^2 p_{\mathrm{appr},2}+\tfrac{\mathrm{i}}{2\omega R}\partial_t(\kappa\partial_t p_{\mathrm{appr},2})=0.$$

Error estimate

Lemma If ω^2 is not a Neumann eigenvalue of $-\Delta$, then, there exist a constant C such that for $N=0,1,2$

$$\|p-p_{\mathrm{appr},N}\|_{H^1(\Omega)}\le CR^{-\frac{N+1}{2}}.$$

For a rectangular domain with omitted disk we have performed numerical simulations for the exact model (1) and the approximative pressure models, see Fig. 1. We have used high-order finite elements within the numerical C++ library *Concepts* (`www.concepts.math.ethz.ch`) to push the discretisation error below the modelling error. Figure 2 shows the modelling error in dependance of the viscosity.

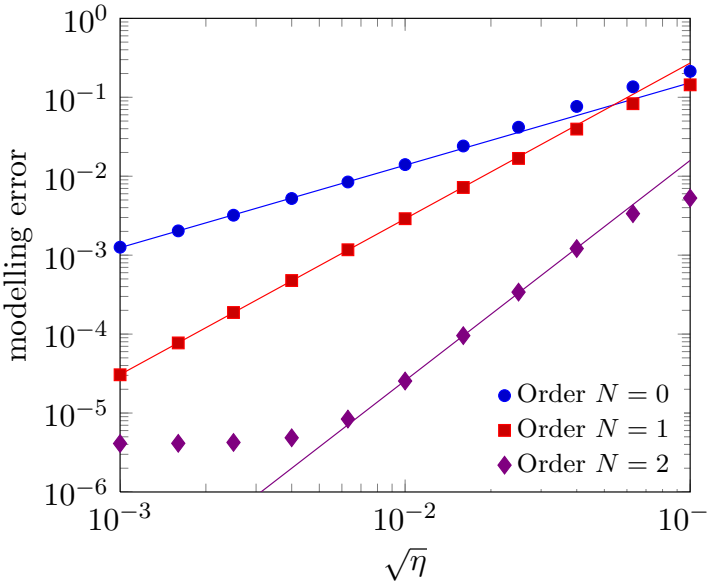

Figure 2: The modelling error, $N=0,1,2$.

References

[1] Schmidt, K. and Thöns-Zueva, A. *Asymptotic analysis for acoustics in viscous gases close to rigid walls.* Preprint 2012-4, Inst. f. Math., TU Berlin, 2012

[2] Landau, L. D. and Lifshitz, E. M.: Fluid Mechanics. Course of theoretical physics, Vol. 6. Pergamon press, New York, 1959.

[3] Vishik, M.I. and Lyusternik, L.A. *The asymptotic behaviour of solutions of linear differential equations* Russian Math. Surveys, 1960, 15, pp. 23–91.

Asymptotic analysis of transmission eigenvalues for perfect conducting body coated by a thin dielectric layer

F. Cakoni[1], N. Chaulet[2,*], H. Haddar[2]
[1]Department of Mathematical Sciences, University of Delaware, Newark, Delaware 19716-2553 USA.
[2] CMAP, Ecole Polytechnique, Route de Saclay, 91128 Palaiseau Cedex, France.
*Email: nicolas.chaulet@inria.fr

Abstract

The interior transmission eigenvalues play an important role in the area of inverse scattering problems for inhomogeneous media. These eigenvalues can actually be determined from multi-static far field data, thus, they could be used in non destructive testing and others areas of applications. Here, we focus on the case where the obstacle is a perfectly conducting body coated by a thin layer of dielectric material. We derive and justify the asymptotic expansion of the first interior transmission eigenvalue with respect to the thickness of the coating for the TM electromagnetic polarization. This expansion provides interesting qualitative information about the behavior of the first interior transmission eigenvalue and also gives an explicit formula to compute the thickness of the coating.

Introduction

A new eigenvalue problem, the so-called interior transmission eigenvalue problem (ITEP), appeared in the nineteen eighties in the context of inverse scattering problems (see [5]). More precisely, the interior transmission eigenvalues are related to non scattering frequencies, which means that when such eigenvalue exists, it corresponds to a frequency for which there exists an incident wave that almost does not scatters. Moreover, recently, it has been noticed that these eigenvalues may be computed from multi static far field data (see [2]) and therefore they can be used for non destructive testing of materials (see [1]). For a survey on the ITEP we refer to [4].

We focus here on the ITEP related to the scattering by an inhomogeneity which is a perfectly conducting body coated by a thin dielectric layer of thickness δ. Existence of such eigenvalues for the TM electromagnetic polarization has been proven in [3] for small index of refraction of the coating (see Theorem 1.2). We go further in understanding the problem by providing a rigorous asymptotic development of the first transmission eigenvalue with respect to δ up to the second order.

1 The interior transmission eigenvalue problem

Let Ω be a bounded domain of $\mathbb{R}^2$ simply connected and denote Γ its boundary of class C^∞. For $\delta > 0$ we denote by $\mathcal{U}_\delta = \{x \in \Omega \text{ such that } d(x,\Gamma) < \delta\}$ a thin layer of interior boundary $\Gamma_\delta = \{x \in \Omega \text{ such that } d(x,\Gamma) = \delta\}$ that defines a bounded and simply connected domain Ω_δ (see Figure 1). Here $d(x,\Gamma)$ stands for the distance function to the surface Γ. The interior transmission eigenvalue problem

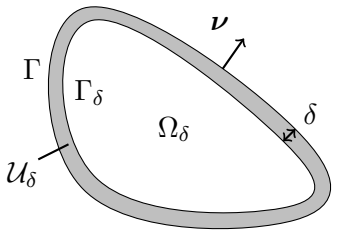

Figure 1: Thin layer geometry.

then writes: find $k_\delta > 0$ such that there exists a non trivial solution (w_δ, v_δ) to the following coupled problem

$$\begin{cases} \Delta w_\delta + k_\delta^2 n w_\delta = 0 \quad \text{in } \mathcal{U}_\delta, \\ \Delta v_\delta + k_\delta^2 v_\delta = 0 \quad \text{in } \Omega, \\ \dfrac{\partial v_\delta}{\partial \boldsymbol{\nu}} = \dfrac{\partial w_\delta}{\partial \boldsymbol{\nu}}, \quad v_\delta = w_\delta \quad \text{on } \Gamma, \\ w_\delta = 0 \quad \text{on } \Gamma_\delta \end{cases} \tag{1}$$

where $n \in L^\infty(\mathcal{U}_\delta)$ denotes the refractive index of the layer and $\boldsymbol{\nu}$ denotes the outward unit normal to Ω.

Definition 1.1 *The values $k_\delta^2 > 0$ for which (2) has a non trivial solution (w_δ, v_δ) are called interior transmission eigenvalues; the functions w_δ and v_δ are the associated eigenvectors.*

There is no guaranty of the existence of such eigenvalues for any n, nevertheless we have the following theorem (see [3]).

Theorem 1.2 *Assume that* $0 < n_* < n(x) < n^* < 1$. *There exist an infinite discrete set of transmission eigenvalues with* $+\infty$ *the only accumulation point.*

In the following, we assume that n is a constant such that $0 < n < 1$.

2 Asymptotic development of the first eigenvalue

Let λ_1^δ be the first interior transmission eigenvalue. First of all, by using the Max-Min principle we obtain

$$\lambda_D^1(\Omega) \leq \lambda_\delta^1 \leq \lambda_D^1(\Omega_\delta)$$

where for any Lipschitz bounded domain $\mathcal{D}$, $\lambda_D^1(\mathcal{D})$ stands for the first Dirichlet eigenvalue of $-\Delta$ in $\mathcal{D}$. Hence we obtain a first asymptotic development for λ_δ^1:

$$\lambda_\delta^1 = \lambda_D^1(\Omega) + \mathcal{O}(\delta).$$

where $\mathcal{O} : \mathbb{R} \to \mathbb{R}$ is a regular function such that

$$|\mathcal{O}(x)| \leq C|x|$$

for all $x \in \mathbb{R}$ and some constant $C > 0$.

To go further in the asymptotic development, we first compute a formal asymptotic development of λ_δ^1 and its associated eigenvectors (v_δ^1, w_δ^1). In a second step, we justify these developments recursively by using a regularity result for elliptic equations which does not depend on the parameter δ, and the Max-Min principle for the first eigenvalues. The regularity estimates allows us to apply some convergence results for the $-\Delta$ operator with Dirichlet boundary conditions to justify the expansion of the eigenvectors, whereas the Max-Min principle provides the convergence of the eigenvalues' expansion. Finally, we are able to prove the following result.

Theorem 2.1 *The following expansion for the first transmission eigenvalue holds:*

$$\lambda_\delta^1 = \lambda_D^1(\Omega) + \delta\lambda_1 + \delta^2\lambda_2 + \mathcal{O}(\delta^3)$$

where

$$\lambda_1 := \int_\Gamma \left|\frac{\partial v_0}{\partial \boldsymbol{\nu}}\right|^2 ds,$$

$$\lambda_2 := -\int_\Gamma \left(\frac{\kappa}{2}\frac{\partial v_0}{\partial \boldsymbol{\nu}} - \frac{\partial v_1}{\partial \boldsymbol{\nu}}\right)\frac{\partial v_0}{\partial \boldsymbol{\nu}}\, ds.$$

Here κ *is the curvature of* Γ, v_0 *is the Dirichlet eigenvector associated with* $\lambda_D^1(\Omega)$ *and* v_1 *is the unique solution in* $H^1(\Omega)$ *of*

$$\begin{cases} \Delta v_1 + \lambda_0 v_1 = -\lambda_1 v_0 & \text{in } \Omega, \\ v_1 = \dfrac{\partial v_0}{\partial \boldsymbol{\nu}} & \text{on } \Gamma, \\ \displaystyle\int_\Omega v_0 v_1 dx = 0. \end{cases}$$

This Theorem provides a formula to compute the thickness δ of the layer from the knowledge of the first interior transmission eigenvalue λ_δ^1 and the geometry Γ.

Remark 2.2 *One may observe that* λ_1 *and* λ_2 *are in fact the first and second order shape derivative of* $\lambda_D^1(\Omega)$ *in the direction* $-\boldsymbol{\nu}$. *Hence*

$$\lambda_\delta^1 = \lambda_D^1(\Omega_\delta) + \mathcal{O}(\delta^3).$$

3 An equivalent eigenvalue problem

From the asymptotic obtained in Theorem 2.1 one can build an equivalent eigenvalue problem: find $\lambda_\delta^{\text{imp}} > 0$ such that there exists a non trivial solution $v_\delta^{\text{imp}} \in H^1(\Omega)$ to

$$\begin{cases} \Delta v_\delta^{\text{imp}} + \lambda_\delta^{\text{imp}} v_\delta^{\text{imp}} = 0 & \text{in } \Omega, \\ \dfrac{\partial v_\delta^{\text{imp}}}{\partial \nu} - \dfrac{1}{\delta} v_\delta^{\text{imp}} = 0 & \text{on } \Gamma. \end{cases} \tag{2}$$

And then, for the first positive $\lambda_\delta^{\text{imp}}$ (which exists) we have

$$\lambda_\delta^1 = \lambda_\delta^{\text{imp}} + \mathcal{O}(\delta^2).$$

References

[1] F. Cakoni, M. Cayören and D. Colton, *Transmission eigenvalues and the nondestructive testing of dielectrics*, Inverse Problems, 24 (2008).

[2] F. Cakoni, D. Colton and H. Haddar, *On the determination of Dirichlet or transmission eigenvalues from far-field data*, C. R. Acad. Sci. Paris, 348, 2010, pp. 379-383.

[3] F. Cakoni, A. Cossonnière and H. Haddar, *Transmission eigenvalues for inhomogeneous media containing obstacles*, Inverse Problems and Imaging, 6(3), 2012, pp. 373-398.

[4] F. Cakoni and H. Haddar, *Transmission Eigenvalues in Inverse Scattering Theory*, Inside Out II MSRI Publications (Ed.), 2012, pp. 527-578

[5] A. Kirsch, *The denseness of the far field patterns for the transmission problem*, IMA Jour. Appl. Math. 37 (1986), pp. 213-225.

Equivalent Conditions for Elasto-Acoustics

J. Diaz[1], **V. Péron**[1,2,*]
[1] INRIA Bordeaux Sud-Ouest, Team Magique 3D
[2] Université de Pau et des Pays de l'Adour.
*Email: victor.peron@univ-pau.fr

Abstract

We present Equivalent Conditions (ECs) for the diffraction problem of elasto-acoustic waves in a solid medium surrounded by a thin region of fluid medium. This problem is well suited for the notion of ECs : since the thickness of the layer is small with respect to the wavelength, the effect of the fluid on the solid is as a first approximation local. These conditions approximate the acoustic waves which propagate in the fluid region. We present numerical results to illustrate the accuracy of ECs.

1 Introduction

Equivalent Conditions (ECs) are usually used in the modeling of wave propagation phenomena to reduce the domain of interest. The main idea consists to replace an "exact" model inside a part of the domain by an approximate condition. This idea is pertinent when the EC can be readily handled for numerical computations.

The coupling of elastic and acoustic waves equations is essential to reproduce geophysical phenomena such as an earthquake on the Earth's surface. We can thus take into account the effects of the ocean on the propagation of seismic waves. In the context of this application, we consider that the medium consists of land areas surrounded by fluid zones whose thickness ε is very small. This raises the difficulty of applying a FEM on a mesh that combines fine cells in the fluid and much larger cells in the solid. To overcome this difficulty we use an asymptotic method to replace the fluid part by an EC. This condition is then coupled with the elastic equation and a FEM can be applied to solve the resulting boundary value problem.

We first introduce the mathematical model. Then, we present ECs up to the second order, stability and convergence results for the elastic displacement. Numerical results illustrate the accuracy of ECs.

The Mathematical Model

We consider an elasto-acoustic waves transmission problem in time-harmonic regime

$$\begin{cases} \Delta \mathsf{p}_\varepsilon + \kappa^2 \mathsf{p}_\varepsilon = 0 & \text{in} \quad \Omega_{\mathsf{f}}^\varepsilon \\ \nabla \cdot \underline{\underline{\sigma}}(\mathbf{u}_\varepsilon) + \omega^2 \rho \mathbf{u}_\varepsilon = 0 & \text{in} \quad \Omega_{\mathsf{s}} \\ \partial_{\mathbf{n}} \mathsf{p}_\varepsilon = \rho_{\mathsf{f}} \omega^2 \mathbf{u}_\varepsilon \cdot \mathbf{n} - \partial_{\mathbf{n}} \mathsf{p}_i & \text{on} \quad \Gamma \\ \mathbf{T}(\mathbf{u}_\varepsilon) = -\mathsf{p}_\varepsilon \mathbf{n} - \mathsf{p}_i \mathbf{n} & \text{on} \quad \Gamma \\ \mathsf{p}_\varepsilon = 0 & \text{on} \quad \Gamma^\varepsilon \ , \end{cases} \tag{1}$$

set in a smooth bounded simply connected domain $\Omega^\varepsilon \subset \mathbb{R}^2$ made of a smooth connected subdomain Ω_{s} embedded in a subdomain $\Omega_{\mathsf{f}}^\varepsilon$. The domain $\Omega_{\mathsf{f}}^\varepsilon$ is a thin layer of uniform thickness ε. We denote by $\mathbf{n}$ the unit normal to Γ oriented from Ω_{s} to $\Omega_{\mathsf{f}}^\varepsilon$; $\Gamma^\varepsilon := \partial\Omega^\varepsilon$ and $\Gamma := \partial\Omega_{\mathsf{f}}^\varepsilon \cap \partial\Omega_{\mathsf{s}}$. In the system (1), the unknowns are the elastic displacement $\mathbf{u}_\varepsilon$ and the acoustic pressure p_ε. The time-harmonic wave field with angular frequency ω is characterized by using the Helmholtz equation for p_ε, and by using an anisotropic discontinuous linear elasticity system for $\mathbf{u}_\varepsilon$. The physical constants are the acoustic wave number $\kappa = \omega/c$, the speed of the sound c, the density of the solid ρ, and the density of the fluid ρ_{f}.

In the elastic equation, $\nabla\cdot$ is the divergence operator for tensors and $\underline{\underline{\sigma}}(\mathbf{u})$ is the stress tensor given by Hooke's law $\underline{\underline{\sigma}}(\mathbf{u}) = \underline{\underline{C}}\ \underline{\underline{\varepsilon}}(\mathbf{u})$. Here $\underline{\underline{\varepsilon}}(\mathbf{u}) = (\underline{\underline{\nabla}}\mathbf{u} + \underline{\underline{\nabla}}\mathbf{u}^T)/2$ is the strain tensor, $\underline{\underline{\nabla}}$ denotes the gradient operator for tensors, and $\underline{\underline{C}} = \underline{\underline{C}}(\mathbf{x})$ is the elasticity tensor, where $\mathbf{x} \in \mathbb{R}^3$ are the cartesian coordinates. The components of $\underline{\underline{C}}$ are the elasticity moduli $C_{ijkl} \in \mathbb{R} : \underline{\underline{C}} = (C_{ijkl}(\mathbf{x}))$. The *traction operator* $\mathbf{T}$ is a surfacic differential operator defined on Γ as $\mathbf{T}(\mathbf{u}) = \sigma(\mathbf{u})\mathbf{n}$. The right-hand side p_i represents an incident wave with support on Γ.

In the framework above we address the issue of ECs for $\mathbf{u}_\varepsilon$ as $\varepsilon \to 0$. This issue is linked with the issue of ε-uniform estimates for the displacement $\mathbf{u}_\varepsilon$ and the pressure p_ε solutions of (1) since it is a main ingredient in the justification of ECs. To answer these questions, we work under usual assumptions (symmetry and positiveness) on the tensor $\underline{\underline{C}}$. Some resonant frequencies may appear in the solid domain. However,

we prove uniform estimates for the elasto-acoustic field $(\mathbf{u}_\varepsilon, \mathsf{p}_\varepsilon)$ as well as ECs for $\mathbf{u}_\varepsilon$ when $\varepsilon \to 0$ under a spectral assumption :

Assumption 1.1 *The angular frequency ω is not an eigenfrequency of the problem*

$$\begin{cases} \nabla \cdot \underline{\underline{\sigma}}(\mathbf{u}) + \omega^2 \rho \mathbf{u} = 0 & \text{in} \quad \Omega_\mathsf{s} \\ \mathbf{T}(\mathbf{u}) = 0 & \text{on} \quad \Gamma \ . \end{cases}$$

2 Statement of Equivalent Conditions

We derive a hierarchy of ECs for $\mathbf{u}_\varepsilon$ set on Γ and satisfied by $\mathbf{u}_\varepsilon^k$ for all $k \in \{0,1,2\}$, i.e. $\mathbf{u}_\varepsilon^k$ solves

$$\begin{cases} \nabla \cdot \underline{\underline{\sigma}}(\mathbf{u}_\varepsilon^k) + \omega^2 \rho \mathbf{u}_\varepsilon^k = 0 & \text{in} \quad \Omega_\mathsf{s} \\ \mathbf{T}(\mathbf{u}_\varepsilon^k) + \mathsf{B}_{k,\varepsilon}(\mathbf{u}_\varepsilon^k \cdot \mathbf{n})\,\mathbf{n} = \mathsf{h}_{k,\varepsilon}\mathbf{n} & \text{on} \quad \Gamma \ . \end{cases} \tag{2}$$

Here $\mathsf{B}_{k,\varepsilon}$ is a surfacic differential operator acting on functions defined on Γ, and $\mathsf{h}_{k,\varepsilon}$ is a data which depends on the source term p_i and ε. ECs write

$$k=0 \ : \quad \mathbf{T}(\mathbf{u}_0) = -\mathsf{p}_i\mathbf{n} \quad \text{on} \quad \Gamma \ , \quad (\mathbf{u}_0 = \mathbf{u}_\varepsilon^0)$$

$$k=1 \ : \quad \mathbf{T}(\mathbf{u}_\varepsilon^1) - \varepsilon\omega^2\rho_\mathsf{f}\mathbf{u}_\varepsilon^1 \cdot \mathbf{n}\,\mathbf{n} = -\mathsf{p}_i\mathbf{n} - \varepsilon\partial_\mathbf{n}\mathsf{p}_i\mathbf{n} \ ,$$

$$k=2 \ : \quad \mathbf{T}(\mathbf{u}_\varepsilon^2) - \varepsilon\omega^2\rho_\mathsf{f}\left(1 - \frac{\varepsilon}{2}\mathrm{c}(t)\right)\mathbf{u}_\varepsilon^2 \cdot \mathbf{n}\,\mathbf{n} = \mathsf{h}_{2,\varepsilon}\mathbf{n} \ .$$

Here, t is an *arc-length coordinate* on the curve Γ, and $\mathrm{c}(t)$ denotes the scalar *curvature* of Γ in $\mathbf{x}(t)$. These conditions show the successive corrections brought when increasing the order. For $k=0$ the effect of the thin layer is completely neglected. The effect of the fluid part appears at the order 1 with the fluid density ρ_f. The influence of the geometry of Γ appears at the order 2 with its scalar curvature.

Stability and Convergence results

The validation of ECs consist to prove estimates for $\mathbf{u}_\varepsilon - \mathbf{u}_\varepsilon^k$, where $\mathbf{u}_\varepsilon^k$ is the solution of the approximate model (2), and $\mathbf{u}_\varepsilon$ solves the problem (1).

Theorem 2.1 *Under Assumption 1.1, for all $k \in \{0,1,2\}$ there exists constants $\varepsilon_k, C_k > 0$ such that for all $\varepsilon \in (0, \varepsilon_k)$, the problem (2) with data $\mathsf{h}_{k,\varepsilon} \in \mathrm{L}^2(\Gamma)$ has a unique solution $\mathbf{u}_\varepsilon^k \in \mathbf{H}^1(\Omega_\mathsf{s})$ and*

$$\|\mathbf{u}_\varepsilon - \mathbf{u}_\varepsilon^k\|_{1,\Omega_\mathsf{s}} \leqslant C_k \varepsilon^{k+1} \ . \tag{3}$$

The well-posedness result for the problem (2) is proved in [2]. To estimate the difference $\mathbf{u}_\varepsilon - \mathbf{u}_\varepsilon^k$, we use a multiscale expansion for $\mathbf{u}_\varepsilon$ in power series of ε and introduce truncates series $\mathbf{u}_{k,\varepsilon}$ up to the order ε^k as intermediate quantities. The error analysis is split into two steps. We first prove uniform estimates for the difference $\mathbf{u}_\varepsilon - \mathbf{u}_{k,\varepsilon}$ [2, Thm 5.2]. Then we prove uniform estimates for the difference $\mathbf{u}_{k,\varepsilon} - \mathbf{u}_\varepsilon^k$ [2, §6.2].

3 Numerical Results.

In the numerical experiments, the computational domain for the solid Ω_s is an aluminum disk with a radius $R = 0.01$m embedded in water [1]. The source term is an incident wave defined as $\mathsf{p}_i(\mathbf{x}) = \exp(i\omega\mathbf{x}\cdot\mathbf{d})$ with $\mathbf{d} = (1,0)$. The angular frequency is $\omega = 1.5\times10^6$Hz. In the domain Ω_s, we consider the Lamé system : $\mu\Delta\mathbf{u} + (\lambda+\mu)\nabla\,\mathrm{div}\,\mathbf{u} + \omega^2\rho\mathbf{u} = 0$, with the coefficients $\mu \simeq 26.32\times10^9$ and $\lambda \simeq 51.08\times10^9$. The physical constants are $c = 1500$ m.s^{-1}, $\rho_\mathsf{f} = 1000$ kg.m^{-3}, and $\rho_\mathsf{s} = 2700$ kg.m^{-3}.

We use a Discontinuous Galerkin Method (IPDGM) and curved $\mathbb{P}_3$-finite elements available in the Finite Element Library Hou10ni. We compute the L^2-errors between the analytical solution of the problem (1) and each analytical solution associated with an EC of order $k \in \{0,1,2\}$. We also compute the L^2-errors for each numerical solution associated with an EC, see Fig. 1. We observe that the numerical convergence rate coincides with the theory since the L^2 error is of order ε^k.

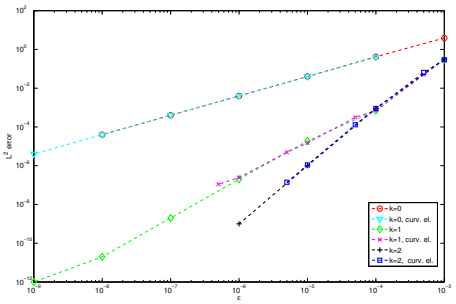

Figure 1: L^2-errors $\|\mathbf{u}_\varepsilon - \mathbf{u}_\varepsilon^k\|_{0,\Omega_\mathsf{s}}$ with respect to ε.

References

[1] T. Huttunen, J. P. Kaipio and P. Monk, *An ultra-weak method for acoustic fluid-solid interaction*, J. Comput. Appl. Math., **213** (2008), pp. 166–185.

[2] V. Péron, *Equivalent Boundary Conditions for an Elasto-Acoustic Problem with a Thin Layer*, Research Report RR-8163, INRIA, 2012.

3.15 Discontinuous methods

Enriching a Hankel Basis by Ray Tracing in the Ultra Weak Variational Formulation

C. J. Howarth[1,*], **S.N. Chandler-Wilde**[1], **S. Langdon**[1], **P.N. Childs**[2]
[1] University of Reading, Reading, UK
[2] Schlumberger Gould Research, Cambridge, UK
*Email: c.j.howarth@pgr.reading.ac.uk

Abstract

The Ultra Weak Variational Formulation (UWVF) is a new generation finite element method for approximating time harmonic acoustic and electromagnetic wave propagation. We use the UWVF to solve the Helmholtz equation in two dimensions. Often a plane wave basis is used; here we implement a Hankel basis, allowing greater flexibility in terms of direction and curvature of the basis set. We augment this basis type using ray tracing techniques for the case of a smooth, convex scatterer. Some initial results are presented, demonstrating the reduction in the computational size of the problem for a given level of accuracy when ray tracing techniques are used.

Introduction

Acoustic wave propagation is currently an area of intensive study. With seismic, defence, and medical applications, accurate numerical methods for simulating how waves interact with structures are required by many. The Ultra Weak Variational Formulation is a form of discontinuous Galerkin method which assumes wave like behaviour on each element, but otherwise allows flexibility in the approximation space. Here we exploit this flexibility by combining the numerical method with ray tracing solutions, in order to find accurate solutions at a lower computational cost than the standard UWVF.

Time harmonic acoustic wave scattering is modelled in 2D by the Helmholtz problem

$$\nabla \cdot \left(\frac{1}{\rho}\nabla u\right) + \frac{\kappa^2}{\rho}u = 0, \qquad \text{in } \Omega, \tag{1}$$

$$\left(\frac{1}{\rho}\frac{\partial u}{\partial \nu} - i\sigma u\right) = Q\left(-\frac{1}{\rho}\frac{\partial u}{\partial \nu} - i\sigma u\right) + g, \qquad \text{on } \Gamma, \tag{2}$$

where Ω is a polygonal domain with boundary Γ. The wavenumber κ is complex with $\Im(\kappa) \geq 0$ and $\Re(\kappa) > 0$, the density ρ and impedance parameter σ are real and positive, the source term is g, and Q is complex with $|Q| \leq 1$.

1 The UWVF with a Hankel Basis

In the implementation of the UWVF, the domain Ω is discretised into triangular finite elements Ω_k, $k = 1, \ldots, K$, upon which local solutions are found, with κ and ρ assumed constant over each element. The approximation takes the form of a linear combination of basis functions $\phi_{k,l}$, $l = 1, \ldots, p_k$, each of which is required to solve the homogeneous Helmholtz equation, so incorporating the oscillatory behaviour of the solution. Much current literature uses an equally spaced plane wave basis on each element, see [1], [2], with a Bessel function basis used in [3].

As an alternative, we instead use a Hankel basis. The basis functions are defined as

$$\phi_{k,l}(x) = \begin{cases} H_0^1(\kappa_k|x - y_{k,l}|), & \text{in } \Omega_k, \\ 0, & \text{elsewhere,} \end{cases} \tag{3}$$

where κ is taken to be piecewise constant with $\kappa_k \equiv \kappa|_{\Omega_k}$. These are cylindrical waves originating from source points $y_{k,l} \notin \Omega_k$. The choice of $y_{k,l}$ allows flexibility in both the direction and the level of curvature of the basis function over the element.

2 Ray Tracing

At high frequencies a ray model gives a good understanding of the direction of propagation of a wave. We use the ideas of ray tracing to find a good a-priori choice of basis function.

Consider a domain Ω enclosing a smooth, convex scatterer with no straight edges, the boundary of which we denote by Γ_1, and call the exterior boundary Γ_2. Let the incident field u_i be a plane wave and the wavenumber be constant in Ω: ray directions perpendicular to the wavefronts are parallel, until they reach the scatterer, reflect, and continue in a straight line. For any given point in the illuminated region $\mathbf{x} \in \Omega$, by tracing the ray through this point back, we can find the point of interaction $\mathbf{z} \in \Gamma_1$ where the incident ray hits the scatterer, and the angle of reflection $\theta = \theta_i = \theta_r$.

For points inside an element Ω_k, we consider the local scattered field to be originating from a single centre of curvature, which we can find by considering

the intersection of rays from points which are close to one another. Let a second point $\mathbf{x_0} \in \Omega$ be reached by a ray that reflects at an angle of reflection θ_0, at point of interaction $\mathbf{z_0} \in \Gamma_1$. If we extend the rays that travel through $\mathbf{x}$ and $\mathbf{x_0}$ back through the scatterer, they will cross at some point $\mathbf{P}$ either within or on the opposite side of the scatterer. Taking the limit as $\mathbf{x} \to \mathbf{x_0}$, we take this intersection point as the centre of curvature $\mathbf{x_C}$. This is illustrated for a circular scatterer in Figure 1.

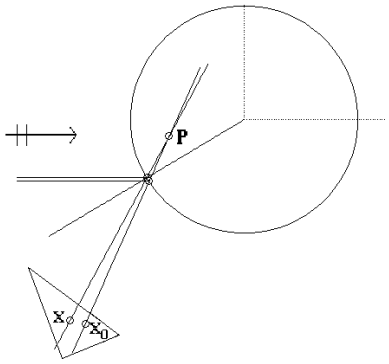

Figure 1: Centre of curvature of rays at x is $x_C := \lim_{x \to x_0} P$.

3 The Ray Enhanced UWVF Method

For Dirichlet boundary conditions on the surface of the scatterer Γ_1 we take $Q = -1$ and we take the source term $g = 0$. On the outer boundary of the domain Γ_2 we take $Q = 0$, for impedance boundary conditions, and we take source term $g = \frac{\partial u}{\partial n} - i\kappa u$, where u is the exact solution (allowing us to focus attention on the value of the ray tracing augmentation).

The UWVF can be extended to incorporate the ray traced directions and centres of curvature into the Hankel basis, using just two basis functions per element: one a single plane wave representing the incident field and the other a point source centred at $\mathbf{x_C}$, found by the ray tracing algorithm of §2, representing the scattered field. The remainder of the basis functions on the element are taken as plane waves in equally spaced directions.

We begin our numerical examples by using just the two ray traced basis functions per element for a circular scatterer. For $\kappa = 80$, we get an L^2 relative error of under 9% using $K = 482$ and 0.4 degrees of freedom per wavelength. If only a more general idea of the wave interaction is needed rather than high accuracy, perhaps as an initial guess of state, then this approach suggests potential computational savings compared to more standard methods.

To achieve higher accuracy we require more basis functions per element. In addition to including the ray traced basis representing the incident field direction, we also include a further $p_k - 2$ directions, equally spaced around a circle of radius $R >> 1$ (thus simulating plane waves), together with a final point source centred at the centre of curvature $\mathbf{x_C}$ given by our ray tracing algorithm. Figure 2 compares these results to those achieved using an equally spaced plane wave basis, for $\kappa = 10$. Including just these two Hankel functions in the basis, with locations determined by ray tracing, leads to a reduction in the overall number of degrees of freedom required to achieve a given level of accuracy.

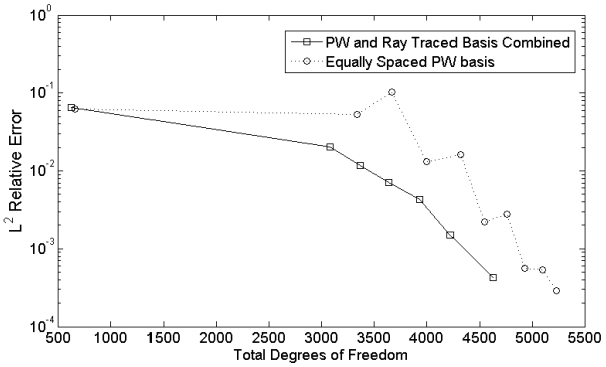

Figure 2: L^2 Relative Error over the domain for scattering by a circle, $\kappa = 10$. Approximation by an equally spaced plane wave basis and an equally spaced plane wave basis enhanced with ray tracing.

References

[1] T. Huttunen, P. Monk, J.P. Kaipio, *Computational Aspects of the Ultra-Weak Variational Formulation*, J. Comput. Phys., **182** (2002), pp. 27–46.

[2] O. Cessenat and B. Després, *Application of an Ultra-Weak Variational Formulation of Elliptic PDEs to the two-dimensional Helmholtz Problem*, SIAM J. Numer. Anal., **35** (1998), pp. 255–299.

[3] T. Luostari, T. Huttunen, P. Monk, *The Ultra Weak Variational Formulation Using Bessel Basis Functions*, Comm. Comput. Phys., **11.2** (2012), pp. 400-414.

About numerical approximation of Maxwell's equations with singular solutions

B. Després[1,2], **L.-M. Imbert-Gérard**[1,2,*]
[1] UPMC Univ Paris 06, UMR 7598, Laboratoire Jacques-Louis Lions, F-75005, Paris, France
[2] CNRS, UMR 7598, Laboratoire Jacques-Louis Lions, F-75005, Paris, France
*Email: imbert@ann.jussieu.fr

Abstract

Hybrid resonance is a physical mechanism for the heating of a magnetic plasma. In our context it is a solution of the time harmonic Maxwell's equations with smooth coefficients, where the permittivity tensor is a non diagonal hermitian matrix. This presentation is dedicated to the description and numerical approximation of a mathematical solution of the hybrid resonance with the limit absorption principle. The corresponding analysis is to be found in [1], as well as in [2], and shows that the mathematical solution is **singular**. As a consequence, it is difficult to approximate it by any numerical method.

Both a simple one dimensional model and the full two dimensional system will be approximated.

Introduction

Starting from Maxwell's equations, we want to focus on the so-called eXtraordinary propagation mode (X-mode) with a limit absorption principle to handle the **anisotropic** permittivity tensor's singularity. The regularization parameter will be denoted μ.

$$\overrightarrow{curl}(curl\ E) - (\varepsilon_\perp + i\mu I)E = 0. \tag{1}$$

Considering coefficients that do not depend on the y variable, we can perform a one dimension reduction by taking the Fourier transform with respect to y. As a result, the system modelling the propagation of X-mode waves in plasmas described in [1] is

$$\left\{\begin{array}{cccc} W & +i\theta U & -V' & = 0, \\ i\theta W & -(\alpha(x)+i\mu)U & -i\gamma(x)V & = 0, \\ -W' & +i\gamma(x)U & -(\alpha(x)+i\mu)V & = 0, \end{array}\right.$$

where (U, V) represents (E_x, E_y) and W represents $curl\ E$. Here the notation $'$ denotes the derivative with respect to the x variable. The domain is

$$\Omega = \left\{(x,y) \in \mathbb{R}^2, \quad -L \le x, \quad y \in \mathbb{R}, \quad L > 0\right\},$$

the coefficient γ can be a positive constant and $\alpha(x) = x$ around zero and constant for x higher than a threshold H. The singularity stems from the fact that around zero the non-diagonal part of $\varepsilon_\perp$ takes the lead over its diagonal part.

A convenient choice is then to consider the ordinary differential system

$$\frac{d}{dx}\left(\begin{array}{c} V^{\theta,\mu} \\ W^{\theta,\mu} \end{array}\right) = A^{\theta,\mu}(x)\left(\begin{array}{c} V^{\theta,\mu} \\ W^{\theta,\mu} \end{array}\right) \tag{2}$$

with

$$A^{\theta,\mu}(x) = \left(\begin{array}{cc} \frac{\theta\gamma(x)}{\alpha(x)+i\mu} & 1 - \frac{\theta^2}{\alpha(x)+i\mu} \\ \frac{\gamma(x)^2}{\alpha(x)+i\mu} - \alpha(x) - i\mu & -\frac{\theta\gamma(x)}{\alpha(x)+i\mu} \end{array}\right). \tag{3}$$

Then $U^{\theta,\mu}$ can be deduced from the equation

$$i\theta W^{\theta,\mu} - (\alpha + i\mu)U^{\theta,\mu} - i\gamma(x)V^{\theta,\mu} = 0. \tag{4}$$

We would like to present the numerical validation of some features of the theoretical analysis of the system (2). For a given μ, the matrix (3) is well defined and smooth, so that the system can be solved with an ODE solver, as long as it is adapted to stiff problems.

A high order numerical method for the X-mode system, based on adapted basis functions, and generalizing the Ultra-Weak Variational Formulation will also be introduced. The design of these basis functions will be developed.

1 The first basis function

1.1 Definition and behavior at infinity

The first basis function

$$\mathbf{U}_1^{\theta,\mu} = \left(U_1^{\theta,\mu}, V_1^{\theta,\mu}, W_1^{\theta,\mu}\right) \in \mathbb{X}^{\theta,\mu} \tag{5}$$

is the natural one which is smooth at the origin: $U_1^{\theta,\mu}(0) = 0$.

Remark that this solution blows up at large scales, and that it is uniformly bounded on $(-L, H)$, $H > 0$.

1.2 Numerical approximation

Starting from the initial boundary condition at $x = 0$, the first basis function can be computed for $x \le 0$ and $x \ge 0$. See figure 1.

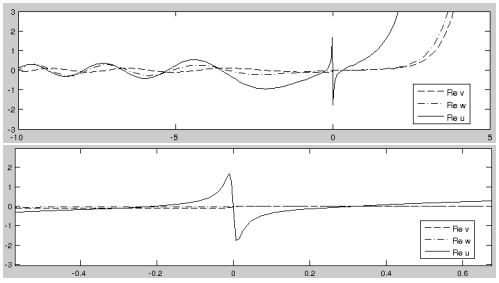

Figure 1: First basis function and zoom on $x = 0$, with $\theta = 1$ and $\mu = 10^{-2}$.

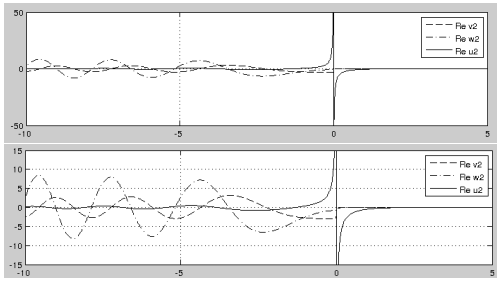

Figure 2: Second basis function and zoom on $x = 0$, with $\theta = 1$ and $\mu = 10^{-2}$.

2 The second basis function

2.1 Definition

We would like to get a second basis function that would be exponentially decreasing at large scales, and linearly dependent of the first basis function regardless the value of μ. Consequently, instead of considering an initial condition at $x = 0$, the idea is to study the behavior of the solution on (H, ∞). Since the coefficients are constant there, the general solution is known explicitly as a linear combination of two exponentials

$$\mathbf{U}(x) = c_+ R_+ e^{\lambda^{\theta,\mu} x} + c_- R_- e^{-\lambda^{\theta,\mu} x}, \quad H \leq x,$$

where $(R_+, R_-) \in (\mathbb{C}^3)^2$, $Re(\lambda^{\theta,\mu}) > 0$ and $\pm\lambda^{\theta,\mu}$ are the eigenvalues of $A^{\theta,\mu}$. Then the second basis function is built with two requirements.

- It is exponentially decreasing at infinity, that is $\exists\ c_- \in \mathbb{C}, s.t. \mathbf{U}_2^{\theta,\mu}(x) = c_- R_- e^{-\lambda^{\theta,\mu} x}, H \leq x.$
- Its value at the origin is normalized with the requirement $i\mu U_2^{\theta,\mu}(0) = 1$.

Note that the limit solution is singular, constituted of a Dirac mass at the origin plus a principle value and a smooth square integrable function.

2.2 Numerical approximation

Starting from the exact boundary condition at D satisfied by $\mathbf{U}_3$, the third basis function is computed. It is then normalized to get $\mathbf{U}_2$. The singularity expected, namely $1/(-x + i\mu)$, appears on figure 2.

The convergence $\mu \to 0$ can be observed as long as the competition with the limit $x \to 0$ is captured by a small enough discretization step.

The choice of a positive or negative regularization parameter μ give different solutions. The relation

$$U_2^{\theta,+}(x) - U_2^{\theta,-}(x) = \frac{-2i\pi}{\alpha'(0)} U_1^{\theta}(x) \qquad x < 0. \quad (6)$$

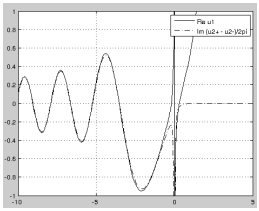

Figure 3: Left and Right hand side of equation (6).

is also satisfied by the numerical solutions (fig. 3).

3 Numerical method for X-mode equations

The UWVF is based on basis functions that are exact solution of the equation. No exact solutions for (1) are known for generic coefficients α and γ, even if the local qualitative features are provided by the previous analysis. In order to adapt the UWVF in this case, the idea is to design basis functions that are approximated solutions, in the following sense: since $div(\varepsilon_\perp E) = 0$, there is φ such that $E = \overrightarrow{curl}\varphi$. Looking for φ as e^P, with $P \in \mathbb{C}[X, Y]$, and inspired by the classical plane wave basis functions, the idea is to design the polynomial function P in order to ensure that $\left(curl\left(\varepsilon_\perp^{-1}\overrightarrow{curl}\varphi\right) - \varphi\right)/\varphi \approx 0$, using Taylor expansions.

We will explain precisely the design process and illustrate some simulation results, which may be compared to the 1D solutions described previously.

References

[1] B. Després, L.-M. Imbert-Gérard, R. Weder, *Hybrid resonance of Maxwell's equations in slab geometry*, (ArXiv, Submitted on 2 Oct 2012).

[2] B. Després, *Singular solutions of anisotropic Maxwell's equations and the third kind integral equation.* Waves 2013 talk.

Discontinuous enrichment method for smoothly variable wavenumber medium-frequency Helmholtz problems

R. Tezaur[1,*], **I. Kalashnikova**[2], **C. Farhat**[1]
[1] Department of Aeronautics and Astronautics, Stanford University, Stanford, CA 94305, USA
[2] Numerical Analysis and Applications Department, Sandia National Lab, Albuquerque, NM 87185, USA.
*Email: rtezaur@stanford.edu

Abstract

The discontinuous enrichment method (DEM) offers superior performance to the classical FEM for a number of constant wavenumber Helmholtz problems and compares very favorably to competing methods that also use plane waves. Here the method is developed for the first time for a smoothly variable wavenumber Helmholtz equation. Plane waves based on a piecewise constant approximation of the wavenumber are considered alone, as well as in a combination with discontinuous polynomial basis functions. A new basis based on solutions of the Helmholtz equation with a linearly changing square of the wavenumber, the so-called Airy waves, is also developed. The new elements are shown to outperform their continuous polynomial FEM counterparts by a substantial degree on a benchmark problem.

Introduction

Methods employing plane waves in the discretization of the Helmholtz equation have been shown to alleviate the pollution effect and improve the unsatisfactory pre-asymptotic convergence of the classical FEM in the medium frequency regime. Such methods include the ultra-weak variational formulation (UWVF), the partition of unity method, the discontinuous Galerkin method, the least squares method, and the method considered here - DEM [1]. In this method, the standard FE polynomial field is enriched within each element by free-space solutions of the homogeneous PDE to be solved. Such enrichment functions can be seen as the fine scales of the solution and are typically discontinuous across element interfaces. Lagrange multipliers are introduced there to enforce a weak continuity of the solution. The method has been shown to outperform the classical FEM in applications that include wave propagation, structural vibration, and advection-diffusion.

While solutions of a homogeneous, free-space Helmholtz equation with a constant wavenumber are easy to find, such solutions are not readily available for this equation with a spatially variable wavenumber, which is encountered, e.g., in underwater acoustics in large domains. This opens the question of how the above methods can be generalized to the variable coefficient scenario. Some progress for the case of a smoothly variable wavenumber has been reported [2] in 1D for the UWVF by using exponentials of polynomials. Here, three types of DEM elements are proposed and tested.

1 Discontinuous enrichment method for the variable wavenumber Helmholtz equation

The following boundary value problem for the Helmholtz equation is considered:

$$\begin{aligned} -\Delta u - \kappa^2 u &= 0 \quad \text{in} \quad \Omega \\ \tfrac{\partial u}{\partial \boldsymbol{\nu}} &= g_N \quad \text{on} \quad \partial\Omega_N \\ \tfrac{\partial u}{\partial \boldsymbol{\nu}} - i\kappa u &= g_R \quad \text{on} \quad \partial\Omega_R, \end{aligned} \tag{1}$$

where $\boldsymbol{\nu}$ denotes the normal derivative on the domain boundary $\partial\Omega = \partial\Omega_N \cup \partial\Omega_R$, $\partial\Omega_N \cap \partial\Omega_R = \emptyset$, and g_N and g_R are prescribed Neumann and Robin data. DEM relies on a partitioning of the domain Ω into n_{el} elements such that $\overline{\Omega} = \cup_{j=1}^{n_{el}} \overline{\Omega}_j$ and $\Omega_j \cap \Omega_k = \emptyset, k \neq j$. Let $\Gamma_j = \partial\Omega_j$ and the edges between elements be denoted by $\Gamma_{jk} = \Gamma_j \cap \Gamma_k$. Let $\mathcal{U} = \{v \in L^2(\cup_{j=1}^{n_{el}}\Omega_j) : v|_{\Omega_j} \in H^1(\Omega_j)\}$, be the space of functions representing the solution and $\mathcal{W} = \prod_{j=1}^{n_{el}} \prod_{k=1,j<k}^{n_{el}} H^{-1/2}(\Gamma_{jk})$. the space of functions for the dual unknowns, the Lagrange multipliers (LMs). The hybrid variational formulation of DEM can be written as [1]: Find $(u, \lambda) \in \mathcal{U} \times \mathcal{W}$ such that

$$\begin{aligned} a(u,v) + b(\lambda, v) &= r(v) \quad \forall v \in \mathcal{U}, \\ b(\mu, u) &= 0 \quad \forall \mu \in \mathcal{W}, \end{aligned} \tag{2}$$

where a and b are bilinear forms and r is a linear form. For BVP (1), these are defined by

$$\begin{aligned} a(u,v) &= \int_\Omega (\nabla u \cdot \nabla v - \kappa^2 uv) d\Omega - \int_{\partial\Omega_R} i\kappa uv d\Gamma, \\ b(\mu, v) &= \sum_{k=1}^{n_{el}} \sum_{j=1,j<k}^{n_{el}} \int_{\Gamma_{jk}} \mu(v_j - v_k)\, d\Gamma, \\ r(v) &= \int_{\partial\Omega_N} v g_N \, d\Gamma + \int_{\partial\Omega_R} v g_R \, d\Gamma. \end{aligned} \tag{3}$$

In discretization, the spaces $\mathcal{U}$ and $\mathcal{W}$ are replaced by suitably chosen finite dimensional subspaces. For

a spatially constant wavenumber, the enrichment space in the original DEM was selected as a superposition of plane waves of the form $e^{i\kappa \mathbf{d}\cdot\mathbf{x}}$, where $\mathbf{d}$ is a unit vector of the direction of the wave. The plane waves solve the constant wavenumber, homogeneous, free-space Helmholtz equation. Since free-space solutions to the Helmholtz equation with a spatially variable wavenumber are in general not available, three approximate choices based on a local element-by-element approximation are considered (and only briefly summarized here due to lack of space):

- A family of elements Q-en_w-en_λ, where n_w is the number of uniformly distributed plane waves with the wavenumber locally frozen within the element. The Lagrange multipliers numbering n_λ per edge are similar to the complex exponential LMs in the constant wavenumber case [3], but they are based on the wavenumber that now varies along the edge.
- A family of elements Q-en_w,px-en_λ derived from Q-en_w-en_λ by adding an element to element discontinuous polynomial field. The discontinuous field can be condensed out on the element level and does not add to the global number of variables that is given by the number of LMs.
- A family of elements Q-an_w-an_λ based on solutions of the Helmholtz equation with a linearly changing square of the wavenumber are considered. These involve the Airy functions and they are constructed in the form resembling plane waves. Corresponding LMs are also derived.

2 Numerical experiment

A problem modeling sound-hard scattering by a disk submerged in an acoustic fluid with a variable speed of sound is considered. The total pressure is computed by solving the BVP (1) with $g_N = 0$, on the scatterer boundary Γ_N formed by a circle of $r = 0.5$, and $g_R = i\kappa(\boldsymbol{\nu}\cdot\mathbf{d} - 1.0)e^{i\kappa d\cdot\mathbf{x}}$ that imposes an incident plane wave on the absorbing boundary Γ_R, a circle of $R = 1.5$. The wavenumber varies linearly in the radial direction from 120 near the scatterer to 40. Relative l_2 errors are computed for solutions on meshes of different resolutions discretized by the bi-polynomial elements Q_p, and the three families of DEM elements outlined above. Figure 1 shows that high order convergence of the element Q-e16-e4 is limited by the degree of approximation of the wavenumber, but the other new DEM elements achieve the same accuracy as the bi-quartic element with 4 times fewer dofs. Figure 2 illustrates a similar improvement by DEM elements with Airy waves over elements bi-polynomial elements Q_p.

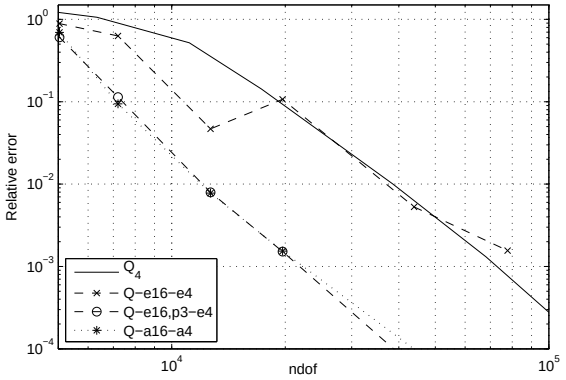

Figure 1: Convergence comparison of Q_4, Q-e16-e4, Q-e16,p3-e4, and Q-a16-a4

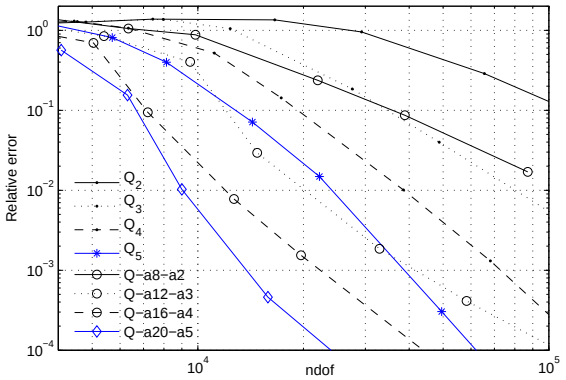

Figure 2: Convergence comparison of Q_p and DEM elements with Airy waves Q-an_w-an_λ

References

[1] C. Farhat, I. Harari and L. P. Franca. *The Discontinuous Enrichment Method.* CMAME, **190** (2001), pp. 6455–6479.

[2] L.-M. Imbert-Gerard and B. Després. *Generalized plane wave numerical methods for magnetic plasma. Proceedings of the 10th Int. Conf. on the Math. and Numerical Aspects of Waves, Vancouver, Canada*, 2011, pp. 233–236.

[3] D. Wang, R. Tezaur, J. Toivanen, and C. Farhat, *Overview of the discontinuous enrichment method, the ultra-weak variational formulation, and the partition of unity method for acoustic scattering in the medium frequency regime and performance comparisons. IJNME*, **89(4)** (2012), pp. 403–417.

Local Basis Set Optimization to Efficiently Solve Helmholtz Problems

M. Amara[1,2], S. Chaudhry[3], R. Djellouli[3], J. Diaz[2,1], S. L. Fiedler[3,*]
[1]LMA/CNRS UMR 5142, Université de Pau et des Pays de l'Adour, France.
[2]INRIA Bordeaux Sud-Ouest Research Center, Team Project Magique-3D, France.
[3]Interdisciplinary Research Institute for the Sciences (IRIS) and Department of Mathematics
California State University, Northridge, Northridge, CA
[*]Email: sfiedler@csun.edu

Abstract

The proposed approach supplements existing plane wave-based methods to facilitate solution of wave problems in the high-frequency regime. The approach is developed to maintain a low number of basis functions which are systematically rotated to best match the direction of field propagation. In this manner, a better approximation of the field is anticipated and numerical instabilities associated with high discretization and large basis sets are mitigated. Determination of the direction of propagation of the scattered field is formulated as a minimization problem, solved by the Newton method with Jacobians and Hessians evaluations yielding the requisite Fréchet derivatives of the field. To assess performance, the field scattered by a prototypical disk-shaped, sound-hard object is approximated with comparisons made to both the analytical solution and the solution obtained by the Least-Squares Method (LSM). Results illustrate that a significant reduction in system size is achievable by this proposed wave-tracking approach as taken with respect to LSM.

Introduction

It has long been recognized that the discretization required to attain a given level of accuracy for Helmholtz's problems, is greater than linearly proportional to the frequency of the field. While the oscillatory nature of plane wave basis function model allow good numerical field approximation and a multitude of plane wave-based approaches have been proposed [1], mid- and high-frequency fields require a significantly higher level of discretization and/or an increased number of basis functions to achieve a given level of accuracy. Both approaches, unfortunately, can create numerical instabilities. To circumvent the above issues, we developed an iterative algorithm that can allow a small basis set to locally rotate in each element to best align one function with the direction of field propagation. Termed Wave-Tracking (WT) for this study, the principle was recently demonstrated [2] to improve the approximation for a rectangular wave guide problem by a factor of 10^8 when used in conjunction with LSM [3]. Here, the WT approach is extended to systematically approximate fields that possess multiple directions of propagation.

The Approach

The considered scattering problem can be expressed as the following boundary value problem,

$$\begin{aligned} \Delta u + k^2 u &= 0 && \text{in } \Omega, \\ \partial_n u &= -\partial_n e^{ik\vec{x}\cdot\vec{d}} && \text{on } \Gamma, \\ \partial_n u &= \mathrm{i}ku && \text{on } \Sigma, \end{aligned} \tag{1}$$

where Ω is a two-dimensional computational domain, $\mathbf{n}$ is the unitary outward normal vector to the inner and outer boundaries, Γ and Σ respectively, k is a positive number representing the wavenumber, and $\vec{d}$ is a unit vector representing the direction of the incident plane wave. The computational domain, Ω, is partitioned into a regular triangulation τ_h of N_h quadrilateral-shaped elements, K, and solution of the Helmholtz equation, by plane-wave-based finite element methods, can proceed by minimization of a cost function J,

$$J(u_h) = \inf_{v \in X_h} J(v), \tag{2}$$

with the global subspace $X_h \subset L^2(\Omega)$ defined as,

$$X_h = \left\{ v \in L^2(\Omega); \forall\, K \in \mathcal{T}_h,\ v_{|_K} = \sum_{j=1}^{n^K} \xi_j^K \phi_j^K \right\}, \tag{3}$$

with element $K \in \mathcal{T}_h$ possessing n^K basis functions. The set of basis functions in each element can be realigned through use of rotational matrices, and this accommodation can be expressed in an expanded cost function:

$$J(u_h(\theta)) = \inf_{\alpha \in \mathcal{D}_h} \inf_{v \in X_h(\alpha)} J(v) \tag{4}$$

with $\mathcal{D}_h$ as the space corresponding to all possible directions of propagation of the field in the domain Ω:

$$\mathcal{D}_h = \left\{\alpha \in L^2(\Omega); \forall\, K \in \mathcal{T}_h,\ \alpha_{|_K} = \alpha^K \ \in [0, 2\pi)\right\}. \tag{5}$$

The field is thus represented at the element level by basis functions and expansion coefficients that possess an angular dependence:

$$u_h(\alpha^K)|_K = \sum_{j=1}^{n_b} \xi_j^K(\alpha^K)\ e^{ik\vec{d}_j(\alpha^K)\cdot\vec{r}}. \tag{6}$$

For simplicity, the second minimization in (4) can be expressed as a collapsed cost function, L,

$$J(u_h(\hat{\theta})) \ = \ \inf_{\hat{\alpha}\in\mathcal{D}_h} L(\hat{\alpha}) \tag{7}$$

Extremum values of L can be determined by seeking roots of the Jacobian, $\vec{L}'(\hat{\alpha})$. To solve this non-linear system, the Newton method was employed in this study, for a given iteration m:

$$\mathbf{L}''(\hat{\alpha}^{(m)})\delta\hat{\alpha}^{(m)} = -\vec{L}'(\hat{\alpha}^{(m)}) \tag{8}$$

with $\mathbf{L}''(\hat{\alpha})$ as the Hessian, and $\delta\hat{\alpha}$ as the angular update. For each iteration, m, the update was applied to the set of basis functions,

$$\hat{\alpha}^{(m+1)} = \hat{\alpha}^{(m)} + \delta\hat{\alpha}^{(m)}. \tag{9}$$

Illustrative Results

To apply the WT approach, we consider the system represented by Eq. 1, with the boundaries Γ and Σ defined as circular to enable analytical calculation of the exact solution, used as a reference for the numerical results. To enhance efficiency, radially adjacent elements in the computational domain were grouped, with basis functions in each element of the group locked to a common value. Initially, the field was numerically approximated by LSM with errors obtained by comparison to analytical values [2]. Subsequently, the above (WT) iterative algorithm was applied to allow each elemental basis set to rotate. Evolution of the optimal basis set orientations within a given radial group, shown in Figs. 1a and 2a, allows a precipitous decline in the relative error of the resultant fields, Figs. 1b and 2b . Comparison of the H^1-norm relative error [2], demonstrates the applicability of the proposed method to achieve a sizable reduction in computational costs. In order to achieve an error of 10% for frequency ka=5, the WT strategy reduced system size by a factor of 300 over LSM.

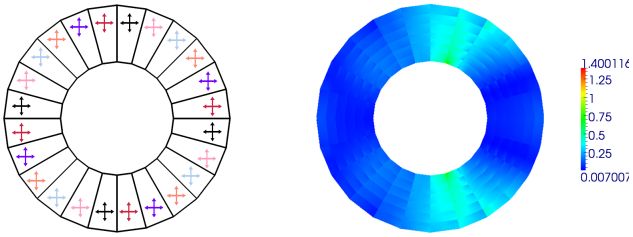

a) Basis set orientation b) Pointwise relative error

Figure 1: Scattered field as computed by LSM, $ka = 1$, h^{-1}=6, with a four plane waves basis set. H^1 relative error = 22%.

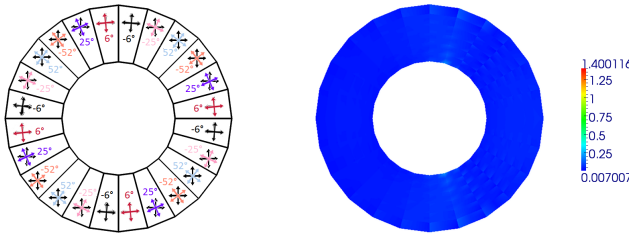

a) Basis set evolution b) Pointwise relative error

Figure 2: Scattered field of the system defined in Fig. 1 after 3 successive WT iterations. H^1 relative error = 10%

Acknowledgments

The authors acknowledge the support by INRIA/CSUN Associate Team Program and by IRIS. Any opinions, findings, conclusions or recommendations expressed in this material are those of the authors and do not necessarily reflect the views of CSUN, INRIA, or IRIS.

References

[1] I. G. Graham, Th. Y. Hou, R. Scheichl (Ed.), Numerical Analysis of Multiscale Problems, Springer, 2012 and references therein.

[2] S. Chaudhry, Efficient Solution Methodology Based on a Local Wave Tracking Strategy for Mid- and High-Frequency Helmholtz Problems, Master's thesis, Department of Mathematics, California State University, Northridge (November 2012).

[3] P. Monk and D. Q. Wang, *A least-squares method for the Helmholtz equation*, Comput. Meths. Appl. Mech. Engrg. Papers, **175** (1999), pp. 121–136.

Numerical Analysis of a reduced formulation of an elasto-acoustic scattering problem

H. Barucq[1,*], J. Chabassier[1], J. Diaz[1], E. Estecahandy[1]
[1] INRIA Bordeaux Sud-Ouest Research Center, Team Project Magique-3D, LMAP, Université de Pau et des Pays de l'Adour, PAU, France.
*Emails: firstname.lastname@inria.fr

Abstract

We present a reduced formulation for the elasto-acoustic scattering problem. The modeling is based on the On Surface Radiation Condition method. It leads to a discrete system which solution is assessed when using Discontinuous Finite Elements.

Introduction

The numerical reconstruction of the shape of a solid immersed into a fluid is an interesting issue both from a mathematical and a practical point of view. Indeed, if engineers have solved this problem from a while in relatively simple configurations, it continues to deserve attention because its solution requires to invert a sparse linear system composed of two discretized Helmholtz equations which are known to be very sensitive to the values of the frequency [1]. The computational costs are then very high and become quickly prohibitive in particular in 3D. Solution methodologies that are able to decrease the computational burden are thus welcome. Obviously, they can be minimized by choosing suitable finite elements [2], [3]. In this work, we propose to investigate a different approach by using a reduced problem that can be solved with lower computational costs. For the construction of the reduced problem, we propose to play with the boundary condition that is used to limit the fluid domain. This is an absorbing boundary condition that is set on a surface which can be more or less far from the solid. Now in the simplest case of a sound-soft or hard obstacle, Kriegsmann *et al.* [4], have shown that it is possible to compute an approximate solution by setting the ABC directly on the surface of the scatterer. The corresponding reduced problem is then given by an equation called On Surface Radiation Condition (OSRC) that is set on the boundary of the scatterer and that requires less computations than the initial problem. The interest of OSRC methodology has been demonstrated later for solving the scattering problem of a penetrable object immersed into a fluid [5] and to the best of our knowledge, it has not been investigated in the case of an elasto-acoustic problem. The accuracy of the OSRC method depends on the geometry of the scatterer and on the frequency regime and it can not provide an accurate solution in all the situations. Nevertheless, it can certainly quickly deliver a solution that could be used as an initial guess for the solution of the inverse problem.

1 Problem setting

Let Ω_s be a bounded domain representing the solid and let Γ be the boundary of Ω_s. We denote by n the normal vector defined on Γ and outwardly directed to Ω_s. The solid is immersed into a fluid Ω_f which is limited by a surface Σ that has been introduced for numerical reasons. We then consider the mixed boundary value problem:

$$\nabla \cdot \sigma(u) + \omega^2 \rho_s \, u = 0 \qquad \text{in } \Omega_s \tag{1}$$

$$\Delta p + (\omega^2 / c_f^2)\, p = 0 \qquad \text{in } \Omega_f \tag{2}$$

$$\omega^2 \rho_f u \cdot n = \partial_n p + \partial_n p^{inc} \qquad \text{on } \Gamma \tag{3}$$

$$\sigma(u) n = -pn - p^{inc} n \qquad \text{on } \Gamma \tag{4}$$

$$\partial_n p + \alpha p - \beta \Delta_\Sigma p = 0 \qquad \text{on } \Sigma \tag{5}$$

to model the behavior of the pair (u, p) representing the displacement u into the solid and the pressure p in the fluid. ρ_f and ρ_s are the density moduli of the fluid and the solid, c_f is the propagation velocity in the fluid and the positive constant ω is the pulsation. In the following, we set $k_f = \omega / c_f$. The stress tensor $\sigma(u)$ is defined by $\sigma(u) = C\varepsilon(u) = \frac{1}{2} C \left(\nabla u + \nabla^t u\right)$, where C is the elasticity tensor. The solid S is illuminated by the incident wave p^{inc} propagating into the fluid and impinging the surface Γ according to the transmission conditions. Now let x be a generic point in $\mathbb{R}^2$ and γ_δ be the level set defined by $\gamma_\delta = \{x := \tau + \delta n\}$ where $\tau := \tau(s)$ denotes the orthogonal projection of x onto γ_δ and s is the curvilinear abscissa. We then have $\gamma_0 = \Gamma$ and we choose $\Sigma = \gamma_R$ for a given $R > 0$. By this way, Γ and Σ are parallel and the parameter δ measures the distance between the two surfaces. The boundary condition on Σ is an ABC which involves the Laplace-Beltrami operator Δ_Σ and the coefficient α incorporates the geometry of Γ and depends on δ. For instance, fol-

lowing the same ideas than in [6], we get :

$$\alpha = (\xi - \kappa_\delta/2 + ik_f)^{-1}(\xi(\kappa_\delta + ik_f) - k_f^2) \qquad (6)$$

where κ_δ denotes the curvature of Σ defined by:

$$\kappa_\delta = \frac{\kappa}{1 + \delta\kappa}$$

with κ the curvature of Γ. Regarding β, we have:

$$\beta = (\xi - \kappa_\delta + ik_f)^{-1}. \qquad (7)$$

In the above definitions, ξ is a positive parameter which is determined empirically.

2 Reduced problem

The construction of a reduced formulation begins with assuming that γ and Σ are close enough to be merged. It is well-known that if p and $\partial_n p$ can be computed on Γ, it is possible to reconstruct the pressure field p in the fluid by using an integral representation. Based on this remark, we propose to replace $\partial_n p$ on Γ in the transmission condition (3) by using the ABC (5). By this way, we get the reduced problem composed of Eq.(1) combined with a modified version of (3) given by

$$\omega^2 \rho_f u \cdot n = -\alpha p + \beta \Delta_\Gamma p + \partial_n p^{inc}, \qquad (8)$$

and Eq.(4). The solution to the reduced problem is then given by the pair $(u, p_{|\Gamma})$ and the computation are performed in Ω_s only.

To compute the solution to the elasto-acoustic scattering problem, we thus propose to solve a discrete system related to Eq. (1) set in the bounded domain Ω_s combined with the boundary conditions (8) and (4) at first. The pressure field can next be reconstructed by computing $\partial_n p_{|\Gamma}$ thanks to (5) set on Γ, which enables to get the expression of p in Ω_f thanks to the Kirchhoff integral formulation. While (4) is included in the variational formulation of (1), Condition (8) is weakly taken into account by a surfacic variational formulation on Γ.

To get an approximate solution of this problem, we propose to use an Interior Penalty Discontinuous Galerkin (IPDG) method. We denote by Ω_h (resp. Γ_h) a triangulation of Ω (resp. Γ) and we consider the spaces

$$V_h = \left\{ u \in L^2(\Omega) \,|\, u_{|T} \in P^r(T),\, \forall T \in \Omega_h \right\} \text{ and}$$

$$W_h = \left\{ u \in L^2(\Gamma) \,|\, p_{|\Sigma} \in P^r(\Sigma),\, \forall \Sigma \in \Gamma_h \right\},$$

where $P^r(T)$ denotes the space of polynomials of degree r on T. We denote by $\Phi = (\phi_i)_{i=1..N_s}$ (resp. $\Psi = (\psi_i)_{i=1..N_f}$) a basis of V_h (resp. W_h). It is worth noting that N_f is very small compared to N_s since we only compute an approximation of p on the boundary Γ. The linear system to be solved reads as

$$\begin{array}{rcrcl} (M_s + K_s)U & + & B_{sf}P & = & F_1, \\ B_{fs}U & + & (M_f + K_f)P & = & F_2, \end{array} \qquad (9)$$

where U and P are two vectors of size N_s and N_f containing the components of the approximation of u and p in the basis Φ and Ψ. M_s and M_f are block-diagonal mass matrices of size $N_s \times N_s$ and $N_f \times N_f$ defined by

$$(M_s)_{i,j} = \int_\Omega \phi_i \cdot \phi_j d\Omega \text{ and } (M_f)_{i,j} = \int_\Gamma \alpha \psi_i\, \psi_j d\Gamma.$$

K_s and K_f are stiffness matrices of size $N_s \times N_s$ and $N_f \times N_f$ defined by

$$(K_s)_{i,j} = a(\phi_i\,,\, \phi_j) \text{ and } (K_f)_{i,j} = b(\psi_i\,,\, \psi_j),$$

where $a(.,.)$ and $b(.,.)$ are the bilinear forms obtained by the IPDG discretization of the operators $\nabla \cdot \sigma(u)$ and $-\beta\Delta_\Gamma$. Finally, B_{sf} and B_{fs} are two coupling matrices of size $N_s \times N_f$ and $N_f \times N_s$ defined by

$$(B_{sf})_{i,j} = -\int_\Gamma \phi_i \cdot \psi_j n d\Gamma \text{ and } (B_{fs})_{i,j} = \omega^2 \rho_f (B_{sf})_{j,i}.$$

We present numerical results that illustrate the performance of the reduced model. We also assess the impact of parameter δ on the accuracy of the solution.

References

[1] I. M. Babuska, and S. A. Sauter, SIAM Review, **42(3)** (2000), pp. 451–484.

[2] P. Monk and D.Q. Wang, Comput Methods Appl Mech Eng, **175** (1999), pp. 121–@136.

[3] M. Amara, H. Calandra, R. Djellouli, and M. Grigoroscuta, Computers and Structures (2012), **106-107**, pp. 258–272.

[4] G. A. Kriegsmann, A. Taflove and K. R. Umashankar, IEEE Trans. Antennas Propag., **35** (1987), pp. 153–161

[5] X. Antoine, H. Barucq, and L. Vernhet, Asymptotic Analysis; **26**, 3-4 (2001), pp. 257–283.

[6] H. Barucq, J. Diaz and V. Duprat, Communications in Computational Physics **11**, 2 (2012) pp. 674-690.

Trefftz-discontinuous Galerkin methods: *hp*-version and exponential convergence

R. Hiptmair[1], **A. Moiola**[2,*], **I. Perugia**[3], **Ch. Schwab**[1]
[1] Seminar of Applied Mathematics, ETH Zürich, Switzerland.
[2] Department of Mathematics and Statistics, University of Reading, UK.
[3] Department of Mathematics, University of Pavia, Italy.
*Email: a.moiola@reading.ac.uk

Abstract

Trefftz schemes are FEMs whose trial functions are piecewise solution of the considered PDE. They are becoming increasingly popular for medium-frequency acoustic, electromagnetic and elastic problems. We consider the *hp*-version of a Trefftz-discontinuous Galerkin method based on plane/circular waves and the approximation estimates necessary for its exponential convergence in term of the number of DOFs.

1 Trefftz methods in time-harmonic regime

The propagation and the interaction of acoustic, electromagnetic and elastic linear waves in time-harmonic regime, with wavenumber $k > 0$, are modelled by Helmholtz (1), Maxwell (2) and Navier (3) equations, respectively:

$$-\Delta u - k^2 u = 0, \quad (1)$$

$$\nabla \times (\nabla \times \mathbf{E}) - k^2 \mathbf{E} = \mathbf{0}, \quad (2)$$

$$(\lambda + 2\mu)\nabla(\nabla \cdot \mathbf{u}) - \mu \nabla \times (\nabla \times \mathbf{u}) + k^2 \rho\, \mathbf{u} = \mathbf{0}. \quad (3)$$

The finite element method (FEM), in its numerous variations, is a widely used tool for the discretisation of these PDEs. However, as soon as the wavelength $\lambda = 2\pi/k$ becomes small compared to the diameter L of the domain, simulations become very expensive, indeed infeasible for larger values of L/λ. This is due to the highly oscillatory structure of the solutions in the high frequency regime and to the accumulation of phase error, called *numerical dispersion*, that affects any local discretisation via the FEM.

To cope with these fundamental difficulties, several recent methods incorporate information about the equations in the design of the trial space. This can be achieved by choosing basis functions defined from plane waves (functions $\mathbf{x} \mapsto \exp(ik\mathbf{xd})$, with propagation direction $\mathbf{d}$), or from circular, spherical and angular waves, fundamental solutions or more exotic solutions of the underlying PDEs. Prominent examples of such methods are the *ultra weak variational formulation* (UWVF) of Cessenat and Després [2]; the *partition of unity finite element method* (PUM or PUFEM) of Babuška and Melenk; the *discontinuous enrichment method* (DEM/DGM) of Farhat and co-workers; the *variational theory of complex rays* (VTCR) of Ladevéze; and the *wave based method* (WBM) of Desmet. The UWVF, the DEM, the VTCR and the WBM are *Trefftz methods*, i.e., test and trial functions are piecewise solutions of the underlying PDE. For a more extensive discussion of Trefftz schemes and for more references, see [10, §1.2].

1.1 The TDG method

We focus on a family of Trefftz-discontinuous Galerkin (TDG) schemes, firstly introduced in [3], that include the UWVF as a special case. In the case of the Helmholtz equation, a priori error estimates for the *h*- and the *p*-convergence were proved in [3] and [4], respectively. The proof of these bounds is made possible by the special DG framework used, which ensures unconditional stability and quasi-optimality (i.e., control of the error for any value of the wavenumber and the meshsize), and by the use of new approximation estimates (from [11]) for plane, circular and spherical waves, which ensure high order convergence. The method was then generalised to the Maxwell equations in [5]; for the Navier equation we refer to the UWVF scheme of [8].

In [1], it was demonstrated that it is possible to improve the TDG by estimating the dominant propagation directions of the BVP solution and using them to define the (modulated) plane waves spanning the trial space; the extension to problems with varying speed of sound was also considered.

2 The *hp*-version of the TDG

Considerations about numerical dispersion suggest that the *h*-versions of FEMs are not effective for medium and high frequency problems. In the case of complicated geometries or scatterers with sharp corners, *p*-methods are also not viable. Thus an *hp*-version that combines the strengths of both strategies is advisable. Indeed, a priori *hp*-FEM for the Helmholtz equation saw an increased interest in the

last years; but the analyses to date are limited to polynomial-based schemes

In the case of the TDG, a special choice of the numerical flux parameters allows to prove a priori error estimates in L^2-norm for meshes that are locally refined, for example near the corners of a scatterer, [6]. These can be combined with the local approximation estimates of [11] to achieve convergence estimates that, in every element K, are explicit the local meshwidth h_K, the number p_K of degrees of freedom (DOFs) and the solution regularity s_K, which can all vary across the domain (see [6, §5] for the 2D case).

However, in order to obtain better results in terms of the number of DOFs in quite general meshes, the approximation bounds can still be improved.

2.1 Harmonic polynomial approximation estimates

The approximation estimates [11] for Helmholtz Trefftz spaces rely on bounds for the approximation of harmonic functions by harmonic polynomials; in 2D they where obtained by Melenk in [9]. They are based on analogous complex variable results, proved with the use of Hermite's representation formula for the interpolation error applied with special interpolation points and integration contours which are, in turn, defined through conformal mappings.

The position of these level lines can be estimated in greater detail for a wide class of domains, namely those that are star-shaped with respect to an open set. In [7] we have proved the following result.

Theorem 1. *Let $D \subset \mathbf{R}^2$ be an open domain with diameter 1, containing the ball B_ρ and star-shaped with respect to B_{ρ_0}, $0 < \rho_0 < \rho \leq 1/2$. Let u be a harmonic function in the neighbourhood $D_\delta = D + B_\delta$, with $\delta > 0$. Then, there exists a sequence of harmonic polynomials $\{Q_p\}_{p\geq 1}$ of degree p, such that*

$$\|u - Q_p\|_{L^\infty(D)} \leq C\, e^{-bp}\, \|u\|_{W^{1,\infty}(D_\delta)}.$$

The positive constants C and b are made explicit and depend only on ρ, ρ_0 and δ.

2.2 Exponential convergence of Trefftz hp-dGFEM

These result can be immediately used to prove exponential convergence of a Trefftz *hp*-DG method based on harmonic polynomials, for Laplace BVPs. In particular, on a graded mesh, we have proved in [7] that the error (in DG energy norm) decays as $\exp(-b\sqrt{N})$, N being the number of degrees of freedom and $b > 0$; this is an improvement over standard schemes which achieve only $\exp(-b\sqrt[3]{N})$.

The extension of this result to the Helmholtz case and plane/circular wave spaces, relying on Vekua's theory [10, Ch. 2], is currently under way.

References

[1] T. Betcke, J. Phillips, *Approximation by dominant wave directions in plane wave methods*, J. Sound Vib., 2012, submitted.

[2] O. Cessenat, B. Després, *Application of an ultra weak variational formulation of elliptic PDEs to the two-dimensional Helmholtz equation*, SIAM J. Numer. Anal., **35** (1) 1998, pp. 255–299.

[3] C.J. Gittelson, R. Hiptmair, I. Perugia, *Plane wave discontinuous Galerkin methods: analysis of the h–version*, M2AN Math. Model. Numer. Anal., **43** (2) 2009, pp. 297–332.

[4] R. Hiptmair, A. Moiola, I. Perugia, *Plane wave discontinuous Galerkin methods for the 2D Helmholtz equation: analysis of the p-version*, Siam J. Numer. Anal., **49**(1) 2011, pp. 264–284.

[5] R. Hiptmair, A. Moiola, I. Perugia, *Error analysis of Trefftz-discontinuous Galerkin methods for the time-harmonic Maxwell equations*, Math. Comput., **82**(281) 2013, pp. 247–268.

[6] R. Hiptmair, A. Moiola, I. Perugia, *Trefftz discontinuous Galerkin methods for acoustic scattering on locally refined meshes*, SAM report 2012-06, ETH Zürich (accepted for publication).

[7] R. Hiptmair, A. Moiola, I. Perugia, Ch. Schwab, *Approximation by harmonic polynomials in star-shaped domains and exponential convergence of Trefftz hp-dGFEM*, SAM report 2012-38, ETH Zürich.

[8] T. Huttunen, P. Monk, F. Collino, J.P. Kaipio, *The ultra-weak variational formulation for elastic wave problems*, SIAM J. Sci. Comput., **25** (5) 2004, pp. 1717–1742.

[9] J.M. Melenk, *On generalized finite element methods*, PhD thesis, Univ. of Maryland, 1995.

[10] A. Moiola, *Trefftz-discontinuous Galerkin methods for time-harmonic wave problems*, PhD thesis, ETH Zürich, 2011.

[11] A. Moiola, R. Hiptmair, I. Perugia, *Plane waves approximation of homogeneous Helmholtz solutions*, ZAMP, **62**(5) 2011, pp. 809–837.

Dispersion of the Lowest Order DPG Method for Helmholtz Equation with Scaled Norms

J. Gopalakrishnan[1], **I. Muga**[2,*], **N. Olivares**[1]
[1] Fariborz Maseeh Department of Mathematics and Statistics, Portland State University, Portland, USA.
[2] Instituto de Matemáticas, Pontificia Universidad Católica de Valparaíso, Valparaíso, Chile.
*Email: ignacio.muga@ucv.cl

Abstract

We study the discrete dispersion (cf.[1]) of the lowest order DPG method for acoustics proposed in [2], in terms of a modified ε-scaling in one of the components of the test norm. Theoretically, we are able to show that the scaled norm acts as a stabilizer of the method when $\varepsilon \to 0^+$. Our numerical approach only considers the traces and fluxes variables, which in the lowest order case ($p = 1$ for traces and $p = 0$ for fluxes) leads to a 21-point stencil analysis.

Introduction

In acoustics and other wave propagation problems, numerical methods of the FEM-type have long sufered from dispersion errors: Computed and exact waves are increasingly out of phase as frequency grows. An overview of the subject can be found in the book of Ihlenburg [1].

Plane waves, $\psi(\vec{x}) \equiv e^{i\vec{k}\cdot\vec{x}}$, are exact solutions of the Helmholtz equation with zero sources (and are often used to represent other solutions). Here the wave vector $\vec{k}$ is of the form $\vec{k} = \omega(\cos(\theta), \sin(\theta))$ for some $0 \le \theta < 2\pi$ representing the direction of propagation. The objective of a dispersion analysis is to find similar solutions of a discrete (Helmholtz) homogeneous system. Accordingly, the regular assumption is that the discrete solution is interpolating a plane wave of the type

$$\psi_h(\vec{x}) = a(\vec{x})e^{i\vec{k}_h\cdot\vec{x}}, \tag{1}$$

where $\vec{k}_h = \omega_h(\cos(\theta), \sin(\theta))$ and $a(\vec{x})$ is an amplitude function. Within the context and framework of the DPG method proposed in [2], we would like to find such discrete wavenumbers ω_h as a function of the exact wavenumber ω, the direction of propagation θ and some of the discretization and stabilization parameters. The idea is to compare how far is ω_h with the exact wavenumber ω. For our DPG approach, ω_h is a complex number. Its real part indicates the discrete phase, while its imaginary part indicates a diffusive behavior.

1 Theoretical Background

Here we describe the basic setting we use for the DPG method. Let $V(\Omega) = H(\mathrm{div}, \Omega) \times H^1(\Omega)$ and (the *wave operator*) $A : V(\Omega) \longmapsto L^2(\Omega)^N \times L^2(\Omega)$ be defined for $v = (\vec{v}, \eta)$ by

$$Av := (i\omega\vec{v} + \nabla\eta, i\omega\eta + \vec{\nabla}\cdot\vec{v}).$$

Let Ω_h be a disjoint partitioning of Ω into open elements K. such that $\overline{\Omega} = \cup_{K\in\Omega_h}\overline{K}$. Let

$$V(\Omega_h) := \big\{(\vec{v}, \eta) : (\vec{v}, \eta)|_K \in H(\mathrm{div}, K) \times H^1(K)\big\}.$$

The operator $A_h : V(\Omega_h) \longmapsto L^2(\Omega)^N \times L^2(\Omega)$ will be defined in the same way as A, except that derivatives are taken element-wise. For global $v = (\vec{v}, \eta) \in V(\Omega_h)$ and global $w = (\vec{w}, \psi) \in V(\Omega)$, an important (element-wise) integration by parts formula is:

$$(Aw, v) = -(w, A_h v) + < w, v >_h, \tag{2}$$

where $(\cdot, \cdot)$ denotes the usual inner product on $L^2(\Omega)^N \times L^2(\Omega)$ and $< \cdot, \cdot >_h$ denotes the boundary contribution:

$$< w, v >_h := \sum_{K\in\Omega_h} \int_{\partial K} (\vec{w}\cdot\vec{n})\overline{\eta} + \psi\overline{(\vec{v}\cdot\vec{n})} \quad d\sigma. \tag{3}$$

We introduce some notation for such traces. Define

$$tr_h : V(\Omega) \mapsto \prod_K H^{-1/2}(\partial K) \times H^{1/2}(\partial K)$$

as follows: for any $w = (\vec{w}, \psi) \in V(\Omega)$, the restriction of $tr_h(w)$ on the boundary of any mesh element ∂K takes the form $(\vec{w}\cdot\vec{n}|_{\partial K}, \psi|_{\partial K}) \in H^{-1/2}(\partial K) \times H^{1/2}(\partial K)$.

1.1 An ultraweak formulation

To derive the DPG method for the Helmholtz problem to find $u = (\vec{u}, \phi)$ such that

$$Au = = f, \qquad \text{on } \Omega, \tag{4a}$$
$$\phi = 0, \qquad \text{over } \partial\Omega, \tag{4b}$$

we use the integration by parts formula (2) to get

$$-(u, A_h v) + < tr_h(u), v >_h = (f, v)$$

for all $v = (\vec{v}, \eta) \in V(\Omega_h)$. Now we let the trace $tr_h(u)$ be an independent unknown $\hat{u} \in Q = tr_h(H(\mathrm{div}, \Omega) \times H_0^1(\Omega))$. Defining the bilinear form $b((u, \hat{u}), v) = -(u, A_h v) + < \hat{u}, v >_h$, we obtain the ultraweak formulation of [2]: Find $u \in L^2(\Omega)^N \times L^2(\Omega)$ and $\hat{u} \in Q$ satisfying

$$b((u, \hat{u}), v) = (f, v), \qquad \forall v \in V(\Omega_h). \tag{5}$$

The wellposedness of this formulation follows from [2] (except for a countable set of wavenumers ω).

1.2 The ideal DPG method

Let $U_h \subset U := L^2(\Omega)^N \times L^2(\Omega) \times Q$ be a finite dimensional trial space. The standard *DPG method* finds $u_h \in U_h$ satisfying

$$b(u_h, v_h) = (f, v_h), \tag{6}$$

for all v_h in the test space V_h, defined by

$$V_h = T U_h, \tag{7}$$

where $T : U \mapsto V$ is defined by

$$(Tw, v)_V = b(w, v), \qquad \forall v \in V, \tag{8}$$

and the V-inner product $(\cdot, \cdot)_V$ is the inner product generated by the ε-scaled norm

$$\|v\|_V^2 = \|A_h v\|^2 + \varepsilon^2 \|v\|^2. \tag{9}$$

Here $\varepsilon \in (0, 1]$ is an arbitrary scaling parameter. The case of $\varepsilon = 1$ was treated in [2].

Theorem 1 *The DPG solution u_h admits the following quasioptimal error estimate:*

$$\|u - u_h\|_U \leq (1 + \varepsilon\, C(\omega)) \inf_{w_h \in U_h} \|u - w_h\|_U.$$

□

The lowest order case assumes piecewise constants for field variables and numerical fluxes, while using globally continuous piecewise linear functions for traces. Field variables can be condensed out, letting to a 8×8 element stiffness matrix for numerical traces and fluxes. We follow the approach proposed in [3] to compute the discrete wavenumber.

2 Numerical Result

We fix the angular frequency to be $\omega = 1$ and the element size to be $h = 2\pi/4$ (four elements per wavelength). Figure 1 shows the dependence of $\Re(\vec{k}_h)$ in terms of the propagation angle θ, for several values of the ε parameter. The exact wavevector is given by the solid circle while the discrete wavevectors are in dashed lines. We observe that as ε decreases, the dashed curves approach the solid line, which indicates control of dispersion when $\varepsilon \to 0^+$, as predicted in Theorem 1.

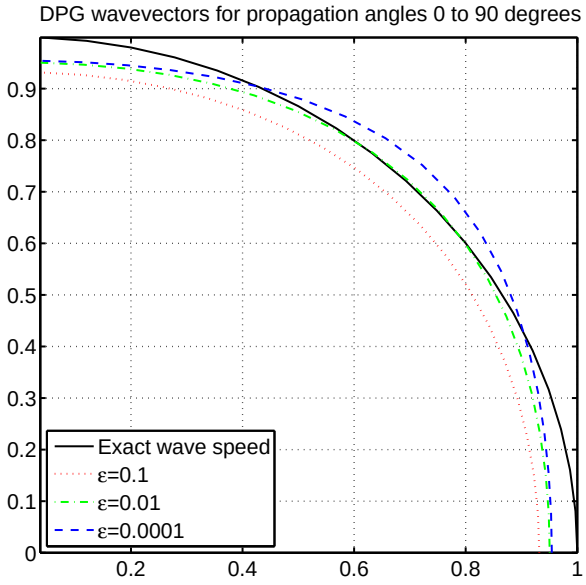

Figure 1: Dependence of $\Re(\vec{k}_h)$ on ε and θ.

References

[1] F. Ihlenburg, *Finite element analysis of acoustic scattering*, volume 132 of *Applied Mathematical Sciences*, Springer-Verlag, 1998.

[2] L. Demkowicz, J. Gopalakrishnan, I. Muga and J. Zitelli, *Wavenumber explicit analysis of a DPG method for the multidimensional Helmholtz equation*, Computer Methods in Applied Mechanics and Engineering, **213-216** (2012), pp.126–138.

[3] A. Deraemaeker, I. Babuska, and P. Bouillard, *Dispersion and pollution of the FEM solution for the Helmholtz equation in one, two and three dimensions*, International Journal for Numerical Methods in Engineering, **46**(4) (1999), pp. 471–499.

3.16 Waveguides

Decomposition domain methods for scattering problems in elastic waveguides

V. Baronian[1,*], **A.-S. Bonnet-Ben Dhia**[2], **S. Fliss**[2], **A. Tonnoir**[1,2]
[1] CEA, LIST, Gif-sur-Yvette, France
[2] POEMS (UMR 7231 CNRS-ENSTA-INRIA), Palaiseau, France
*Email: vahan.baronian@cea.fr

Introduction

In this work, we consider an elastic waveguide with one infinite direction and we focus on the study of wave scattering phenomena by an arbitrary localized defect. It is typically a situation for which standard PML techniques cannot work because of the presence of backward propagating modes. However, other approaches can be used to bound the computational domain surrounding the defect :

- absorbing layers (constituted of viscoelastic materials) which lead to solve a sparse but large linear system;
- transparent boundary conditions (involving modal expansion) developped in [1] giving rise to a small but partially dense linear system.

The idea is to gather advantages of these two approaches (inversion of a sparse and small matrix). To achieve this purpose, a decomposition domain (DD) method is proposed. The principle is to split the domain in two parts, a bounded one containing the defect, where finite elements are used to handle wave scattering, and an infinite regular one, where a modal decomposition is used to propagate the diffracted elastodynamic field. Moreover an overlapping is introduced between these two domains in order to get advantages for the iterative resolution as in usual DD methods.
Even if this approach may not converge for all frequencies, it has the features to design an efficient preconditioned GMRES solver.

1 DD method for elastic waveguides

We consider an isotropic elastic waveguide of geometry Ω decomposed in two subdomains Ω_1 and Ω_2 (figure 1). Let $u = (u_x, u_y)$ be the displacement field which verifies :

$$\begin{cases} -\mathrm{div}\sigma(u) - \omega^2\rho u = f \text{ in } \Omega, \\ \sigma(u).\nu = 0 \text{ on } \partial\Omega, \end{cases} \tag{1}$$

where $\sigma(u)$ is the stress tensor, $\omega > 0$ the pulsation, ρ the density, f a compactly supported source

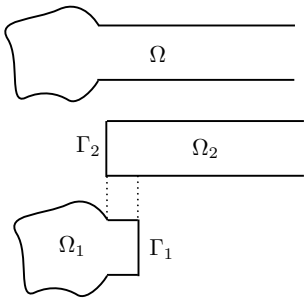

Figure 1: Decomposition of the waveguide Ω in two subdomains Ω_1 and Ω_2

and x the propagation axis. To formulate the iterative algorithm, we need to set conditions on artificial boundaries Γ_1 and Γ_2. Since we want to use a modal expansion of the solution in Ω_2, we impose a condition on Γ_2, expressed in terms of mixed vectors originally introduced in [2]

$$X = \begin{pmatrix} u_x \\ t_y \end{pmatrix} \text{ or } Y = \begin{pmatrix} u_y \\ t_x \end{pmatrix} \tag{2}$$

where t_i ($i = x$ or y) equals $(\sigma.\nu)_i = \sigma_{ix}$ and ν is the outgoing normal on Γ_2. Imposing X or Y on Γ_2 is suitable for decoupling guided elastic modes.
In practice, we use a Robin condition (a linear combination of u and t with a complex coefficient) on Γ_1 to ensure well-posedness of the problem in Ω_1.

However, for the convergence analysis, let us consider a separable geometry (Ω_1 is rectangular) and an appropriate condition on Γ_1 which enables us to make analytical calculations (ie use a modal decomposition also in Ω_1) :

$$\begin{cases} \mathrm{div}\sigma(u_1^{n+1}) + \omega^2\rho u_1^{n+1} = -f \text{ in } \Omega_1, \\ \sigma(u_1^{n+1})\nu = 0 \text{ on } \partial\Omega \cap \partial\Omega_1, \\ X_1^{n+1} = X_2^{n+1} \text{ on } \Gamma_1, \end{cases} \tag{3}$$

$$\begin{cases} \mathrm{div}\sigma(u_2^{n+1}) + \omega^2\rho u_2^{n+1} = 0 \text{ in } \Omega_2, \\ \sigma(u_2^{n+1})\nu = 0 \text{ on } \partial\Omega \cap \partial\Omega_2, \\ Y_2^{n+1} = Y_1^{n} \text{ on } \Gamma_2. \end{cases} \tag{4}$$

The eigenvalues of the operator A which links u_1^{n+1} and u_1^n are given by

$$\lambda_k = \frac{(e^{i\beta_k a} + e^{-i\beta_k a})e^{i\beta_k l}}{e^{i\beta_k (l+a)} - e^{-i\beta_k (l+a)}} \tag{5}$$

where l is the distance between Γ_1 and Γ_2, and (β_k, u_k) is the family of right going modes. Let us remind that there are only a finite number of propagative modes (whose β_k are real) and an infinite set of (possibly oscillating) evanescent modes such that $\beta_k \in \mathbb{C}$ and $\mathrm{Im}(\beta_k)$ tends to $+\infty$.

The convergence is obtained if $|\lambda_k| < 1 \ \forall k$.
In the case of no overlapping ($l = 0$), the above expression becomes $\lambda_k = -i/tan(\beta_k a)$. Therefore $\lambda_k \sim -1$ when k goes to $+\infty$ and the method does not converge. In the case of overlapping ($l > 0$), $\lambda_k \sim e^{-2Im(\beta_k)l}$, so $|\lambda_k|$ tends to 0 when k tends to $+\infty$ for all $l > 0$.
Figure 2 represents the location of λ_k in the vicinity of the unit disk at a given frequency $F = \omega/2\pi$, for different values of l/h (h denotes the thikness of the regular waveguide). The overlap l can be chosen

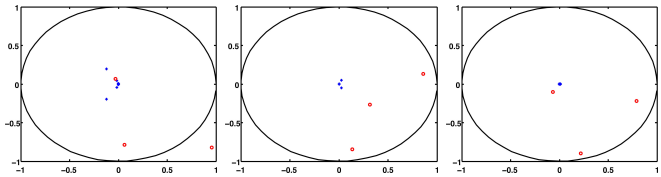

Figure 2: λ_k for $l/h = 1, 2, 3$ - F.h = 350 kHz.mm.

to have all λ_k in the unit disk for this particular frequency.
But, it seems that this "naive" iterative algorithm will not converge at any frequency, even if we add an overlap: see figure 3 where the frequency is fixed and we represent $max_k|\lambda_k|$ with respect to l. However, we observe that only a finite number of eigenvalues are far from 0, which is a good property for a preconditioned GMRES algorithm. Let us remark that we can show the same property for general geometries using the fact that thanks to the overlap, the operator A is compact (and then λ_k tends to 0 when k tends to $+\infty$).

2 Numerical experiments using a preconditioned GMRES algorithm

We use now a GMRES algorithm to solve our scattering problem for which we only need to invert a sparse matrix (corresponding to the Finite Element discretisation of problem in Ω_1) and to make a matrix-vector

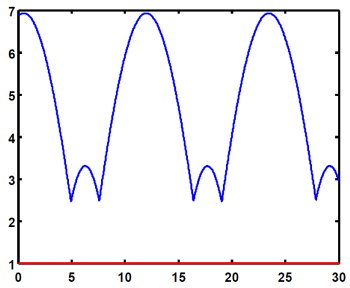

Figure 3: $\underset{k>0}{max}(|\lambda_k|)$ vs l/h (F.h = 420 kHz.mm.)

product (corresponding to the modal decomposition in Ω_2).
In order to validate this approach, we have computed a mode of the guide. We represent the numerical solution on figure 4 and the relative error is lower than 0.1%.
Finally, we show in the following table the gain ob-

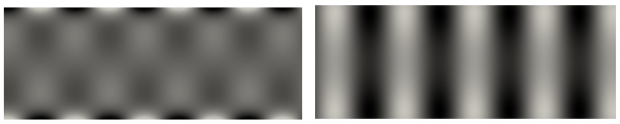

Figure 4: Real part of u_x and u_y F.h = 1020 kHz.mm.

tained by the overlapping on the convergence rate.

Overlap l/h	0	0.3	0.5	1	3	5	7
Number of iterations	113	16	17	16	9	8	8

Acknowledgement: this work was partially supported by DIGITEO.

References

[1] Vahan Baronian, Anne-Sophie Bonnet-BenDhia, Eric Lunéville, *Transparent boundary conditions for the harmonic diffraction problem in an elastic waveguide*, J. Comput. Appl. Math, **234(6)** (2009), pp. 1945–1952.

[2] Vincent Pagneux, Agnès Maurel, *Lamb wave propagation in elastic waveguides with variable thickness*, Proceedings of the Royal Society A: Mathematical, Physical and Engineering Science, **462** (2006), pp. 1315–1339.

A Spectral Volumetric Integral Equation Method for Ocean Acoustics with Depth-Dependent Background Sound Speed

T. Rienmüller
ZeTeM, Zentrum für Technomathematik, Universität Bremen, Germany.
Email: rienmueller@uni-bremen.de

Abstract

The scattering of time-harmonic acoustic waves in a flat ocean can be modelled by the Helmholtz equation, however, reasonable models for sound propagation over large distances imperatively require a depth-dependent background sound speed. Lechleiter and Nguyen present in [1] a spectral volumetric integral equation method to compute sound fields in a homogeneous ocean with constant background sound speed. Inspired by [1], we introduce fundamentals ingredients for the numerical analysis of a spectral volumetric integral equation method applied to ocean acoustics with depth-dependent background sound speed.

1 Sound Waves in a Flat Ocean

First, we introduce some model assumptions. The domain of interest is a waveguide $\Omega = \mathbb{R}^2 \times (0,h)$, where $h > 0$ is the constant depth of the ocean. The propagation of time-harmonic waves in an inhomogeneous ocean is modelled by the Helmholtz equation

$$\Delta u + k^2 n^2 u = 0 \quad \text{in } \Omega, \tag{1}$$

where

$$k(x_3) = \frac{\omega}{c_0(x_3)}, \quad x_3 \in (0,h),$$

is the real-valued depth-dependent wave number, ω is the frequency and c_0 is the speed of sound depending on the depth of the ocean. Furthermore, n is the refractive index and we assume that $n = 1$ outside some bounded and open set D. Hence, n models a local perturbation inside an inhomogeneous waveguide Ω. Next, we define the contrast by

$$q(x) := n^2(x) - 1 \text{ for } x \in \Omega.$$

Second, we model the free surface of the ocean by a sound soft boundary

$$u = 0 \text{ on } \Gamma_0 := \{x \in \mathbb{R}^3 : x_3 = 0\},$$

and the seabed of the ocean by a sound hard boundary

$$\frac{\partial u}{\partial x_3} = 0 \text{ on } \Gamma_h := \{x \in \mathbb{R}^3 : x_3 = h\}.$$

Third, we formally expand u in (1) by separation of variables into horizontal and vertical coordinates. To this end, we establish for a point x in the wave guide Ω the notation $x = (x_1, x_2, x_3)^T = (\tilde{x}, x_3)^T$. Then

$$u(\tilde{x}, x_3) = \sum_{m \in \mathbb{N}_+} w_m(\tilde{x}) u_m(x_3), \tag{2}$$

for $|x|$ large enough. Consequently, we deduce from the Helmholtz equation (1) that

$$\frac{\partial^2 u_m}{\partial x_3^2} + k^2(x_3) u_m = \lambda_m u_m, \text{ in } (0,h), m \in \mathbb{N}_+, \tag{3}$$

and

$$\Delta_{\tilde{x}} w_m + \lambda_m w_m = 0 \text{ in } \mathbb{R}^2. \tag{4}$$

We investigate equation (3) with corresponding boundary conditions on Γ_0 and Γ_h, $u_m(0) = 0$ and $\frac{\partial u_m}{\partial x_3}(h) = 0$. It is well known that for $k^2 \in L^\infty(0,h)$ the eigenvalues $\lambda_m \in \mathbb{R}$ and corresponding eigenvectors $u_m \in H^2(0,h)$ exist, since the eigenvalue problem is selfadjoint.

To obtain a radiating solution u in (2), the functions w_m need to satisfy a radiation condition for the wave number $\sqrt{\lambda_m} (= i\sqrt{|\lambda_m|}$, if $\lambda_m < 0)$. Since $\lambda_m \to -\infty$ for $m \to \infty$, only finitely many square roots $\sqrt{\lambda_m}$ are real, and for those m we prescribe Sommerfeld's radiation condition

$$\lim_{|\tilde{x}| \to \infty} \sqrt{\tilde{x}} \Big(\frac{\partial w_m}{\partial |\tilde{x}|} - i\lambda_m w_m \Big) = 0, \text{ uniformly in } \frac{\tilde{x}}{|\tilde{x}|}. \tag{5}$$

If $\lambda_m < 0$, we prescribe that u_m must be a bounded solution to (4), yielding an evanescent mode.

Finally, we introduce the Green's function

$$G(x,y) = \frac{i}{4} \sum_{m \in \mathbb{N}_+} \phi_m(x_3) \phi_m(y_3) H_0^{(1)}(\sqrt{\lambda_m} |\tilde{x} - \tilde{y}|),$$

where $\tilde{x} \neq \tilde{y}$, $H_0^{(1)}$ denotes the Hankelfunction of the first kind of order zero, ϕ_m is the eigenfunction and λ_m is the corresponding eigenvalue solving (3).

2 Integral Equation

The aim is to derive a volumetric integral equation of the second kind, the so called Lippmann-Schwinger equation, that is equivalent to the scattering problem (1), the given boundary conditions and the radiation condition. Xu states in [2, Lem.3.4] that the volumetric integral equation $\mathcal{V}f$, formally defined for a function $f : D \to \mathbb{C}$ by

$$\mathcal{V}f = \int_D G(\cdot, y) f(y) dy \qquad \text{for } f \in L^2(\Omega),$$

is a bounded operator from $L^2(D)$ into $H^2_{loc}(\Omega)$. Roughly speaking, for constant wave number k it is possible to separate the volumetric integral operator $\mathcal{V}$ into one bounded part defined via the free-space Green's function and a second, compact part that corrects the boundary conditions on Γ_0 and Γ_h. For a wave number depending on the x_3-coordinate, however, this is more challenging. We present an alternative proof.

For analytic aspects we restrict ourselves to the domain $\Lambda_\rho := \{x \in \Omega : |\tilde{x}|_\infty < \rho\}$, where $\rho > 0$ and introduce $\tilde{\Lambda}_\rho := \{x \in \mathbb{R}^2 : |\tilde{x}|_\infty < \rho\}$.

Lemma 2.1 *Consider the operator $\mathcal{V}_m$ defined by*

$$\mathcal{V}_m : L^2(\tilde{\Lambda}_\rho) \to L^2(\tilde{\Lambda}_\rho),$$
$$f \mapsto \int_{\tilde{\Lambda}_\rho} H_0^{(1)}(\sqrt{|\lambda_m|}|\tilde{x} - \tilde{y}|) f(\tilde{y}) d\tilde{y}, \quad m \in \mathbb{N}_+.$$

Then $\mathcal{V}_m$ is a bounded operator from $L^2(\tilde{\Lambda}_\rho)$ into $H^1(\tilde{\Lambda}_\rho)$, and

$$\|\mathcal{V}_m f\|^2_{H^1(\tilde{\Lambda}_\rho)} \leq \frac{C}{m} \|f\|^2_{L^2(\tilde{\Lambda}_\rho)}. \tag{6}$$

For a fixed m, boundedness of $\mathcal{V}_m$ follows directly from the weak singularity of the kernel. The estimate (6) requires slightly more careful arguments to get an explicit dependence on m. By Fourier theory we obtain the representation

$$L^2(\Lambda_\rho) = \Big\{ f : \Lambda_\rho \to \mathbb{C}, f(x) = \sum_{m \in \mathbb{N}_+} \hat{f}_m(\tilde{x}) \phi_m(x_3),$$
$$\sum_{m \in \mathbb{N}_+} \int_{\tilde{\Lambda}_\rho} |\hat{f}_m(\tilde{x})|^2 d\tilde{x} = \|f\|^2_{L^2(\Lambda_\rho)} < \infty \Big\},$$

and a corresponding representation as a direct sum,

$$L^2(\Lambda_\rho) = \bigoplus_{m=1}^{\infty} L^2(\tilde{\Lambda}_\rho).$$

Consequently, we find

$$\|\mathcal{V}f\|^2_{L^2(\Lambda_\rho)} = \sum_{m \in \mathbb{N}_+} \|\mathcal{V}_m \hat{f}_m(\tilde{y})\|^2_{L^2(\tilde{\Lambda}_\rho)} \leq C \|f\|^2_{L^2(\Lambda_\rho)}. \tag{7}$$

Similarly to this idea we use a representation by Fourier theory to deduce

$$H^1(\Lambda_\rho) = \Big\{ f(x) = \sum_{m \in \mathbb{N}_+} \hat{f}_m(\tilde{x}) \phi_m(x_3),$$
$$\sum_{m \in \mathbb{N}_+} (1 + m^2) \|\hat{f}_m(\tilde{y})\|^2_{L^2(\tilde{\Lambda}_\rho)}$$
$$+ \sum_{i=1,2} \sum_{m \in \mathbb{N}_+} \|\frac{\partial}{\partial x_i} \hat{f}_m(\tilde{y})\|^2_{L^2(\tilde{\Lambda}_\rho)} < \infty \Big\}.$$

This permits like in (7) to show boundedness of $\mathcal{V}$ from $L^2(\Lambda_\rho)$ into $H^1(\Lambda_\rho)$. Furthermore, for every $f \in L^2(\Omega)$, with compact support, the function $\mathcal{V}f \in H^2_{loc}(\Omega)$ solves $\Delta \mathcal{V}f + k^2 \mathcal{V}f = -f$. When an incident wave solving (1) for $n^2 \equiv 1$, scatters from the inhomogeneity D, it creates a scattered field u^s such that the total field

$$u(x) = u^i(x) + u^s(x), \quad x \in \Omega,$$

solves the Helmholtz equation (3) and the boundary conditions.

This scattering problem can equivalently be described by the Lippmann-Schwinger integral equation

$$u^s - \mathcal{V}(k^2 q u^s)|_D = \mathcal{V}(k^2 q u^i)|_D.$$

in $L^2(D)$, where we note again that the function k^2 is x_3-dependent.

This integral equation can now be employed to introduce a periodic Lippmann-Schwinger equation and to do numerical calculations using a combined spectral/multipole method.

References

[1] Lechleiter, A. and Nguyen, D. L., *Spectral volumetric integral equation methods for acoustic medium scattering in a 3D waveguide.* IMA Num. Anal., **32(3)**, 2010, pp. 813-844.

[2] Xu, Y., *Radiation condition and scattering problem for time-harmonic acoustic waves in a stratified medium with a nonstratified inhomogeneity.* IMA App. Math., **54(1)**, 1995, pp. 9-29.

Computation of leaky modes in three-dimensional open elastic waveguides

K. L. Nguyen[1,*], **F. Treyssède**[1], **A.-S. Bonnet-BenDhia**[2], **C. Hazard**[2]
[1] IFSTTAR, Centre de Nantes, Route de Bouaye, 44344 Bouguenais Cedex, France.
[2] ENSTA ParisTech, 828, Boulevard des Maréchaux, 91762 Palaiseau Cedex, France.
*Email: khac-long.nguyen@ifsttar.fr

Abstract

Elastic guided waves are of interest for inspecting structures due to their ability to propagate over long distances. When the guiding structure is embedded into a solid matrix, waveguides are open and waves can be trapped or leaky. With numerical methods, one of the difficulty is that leaky modes attenuate along the axis (complex wavenumber) and exponentially grow along the transverse direction. The goal of this work is to propose a numerical approach for computing modes in open elastic waveguides combining the so-called semi-analytical finite element method (SAFE) and a perfectly matched layer (PML) technique.

Introduction

The simulation of open waveguides can be done through a simple numerical method which consists in using absorbing layers of artificially growing viscoelasticity [1]. To circumvent the transverse exponential growth of leaky modes, an alternative approach is to use a PML method instead of absorbing layers. Such a technique has already been applied to the scalar wave equation [2], [3]. In the present work, a SAFE-PML approach is applied to the equation of elastodynamics (non-scalar) in order to compute leaky modes in three-dimensional waveguides of arbitrary cross-section.

1 SAFE-PML formulations

1.1 Cartesian PML

One assumes a linearly elastic material in a domain $\Omega = \{S, z\}$. The time harmonic dependence is chosen as $e^{-i\omega t}$. z is the waveguide axis, S is the transverse section of the waveguide. $S = (x, y)$ in Cartesian coordinates or (r, θ) in cylindrical coordinates. Acoustic sources and external forces are suppressed for the purpose of studying propagation modes.

The 3D variational formulation governing elastodynamics is given by:

$$\int_\Omega \delta\tilde{\boldsymbol{\epsilon}}^T \tilde{\boldsymbol{\sigma}} d\tilde{\Omega} - \omega^2 \int_\Omega \tilde{\rho}\delta\tilde{\mathbf{u}}^T \tilde{\mathbf{u}} d\tilde{\Omega} = 0 \qquad (1)$$

where $d\tilde{\Omega} = d\tilde{x}d\tilde{y}dz = \tilde{r}d\tilde{r}d\theta dz$ (the tilde notation will be explained later). The variational formulation holds for any kinematically admissible trial displacement field $\delta\mathbf{u}$. $\delta\tilde{\boldsymbol{\epsilon}}$ denotes the virtual strain vector and $\tilde{\boldsymbol{\sigma}}$ is the stress vector. The superscript T denotes the matrix transpose. $\tilde{\rho}$ is the material density.

The stress-strain relationship is $\tilde{\boldsymbol{\sigma}} = \tilde{\mathbf{C}}\tilde{\boldsymbol{\epsilon}}$, where $\tilde{\mathbf{C}}$ is the matrix of material properties.

With a Cartesian PML in the x, y direction, the formulation (1) can be interpreted as the analytical continuation of the equilibrium equations into the complex spatial coordinate $\tilde{x}$, $\tilde{y}$, with:

$$\tilde{x} = \int_0^x \gamma_x(\xi)d\xi, \ \tilde{y} = \int_0^y \gamma_y(\xi)d\xi \qquad (2)$$

γ_x is a complex-valued function of x, satisfying $\gamma_x(x)$=1 for $|x| \leq d_x$; $Im\{\gamma_x(x)\} > 0$ for $|x| > d_x$. The definition of γ_y is analogous. d_x, d_y are the interfaces between the PML and physical domains.
From Eq. (2), the change of variables $\tilde{x} \mapsto x$ yields for any function $\tilde{f}$:

$$\frac{\partial\tilde{f}}{\partial\tilde{x}} = \frac{1}{\gamma_x}\frac{\partial f}{\partial x}, \ \frac{\partial\tilde{f}}{\partial\tilde{y}} = \frac{1}{\gamma_y}\frac{\partial f}{\partial y}, \ d\tilde{x} = \gamma_x dx, \ d\tilde{y} = \gamma_y dy \qquad (3)$$

where $\tilde{f}(\tilde{x}(x), \tilde{y}(y)) = f(x, y)$.
In addition to the PML technique, the SAFE method is applied, which consists in assuming an e^{ikz} dependence, where k is the axial wavenumber. Combining SAFE and PML approach, the strain-displacement relation can be written as follows by separating transverse from axial derivatives:

$$\boldsymbol{\epsilon} = (\mathbf{L}_{\tilde{x}\tilde{y}} + ik\mathbf{L}_z)\,\mathbf{u} \qquad (4)$$

where $\boldsymbol{L}_{\tilde{x}\tilde{y}}$ is the operator containing derivatives with respect to transverse direction $(\tilde{x}, \tilde{y})$.

$$\boldsymbol{L}_{\tilde{x}\tilde{y}} = \begin{bmatrix} \frac{1}{\gamma_x}\frac{\partial}{\partial x} & 0 & 0 \\ 0 & \frac{1}{\gamma_y}\frac{\partial}{\partial y} & 0 \\ 0 & 0 & 0 \\ \frac{1}{\gamma_y}\frac{\partial}{\partial y} & \frac{1}{\gamma_x}\frac{\partial}{\partial x} & 0 \\ 0 & 0 & \frac{1}{\gamma_x}\frac{\partial}{\partial x} \\ 0 & 0 & \frac{1}{\gamma_y}\frac{\partial}{\partial y} \end{bmatrix}, \ \boldsymbol{L}_z = \begin{bmatrix} 0 & 0 & 0 \\ 0 & 0 & 0 \\ 0 & 0 & 1 \\ 0 & 0 & 0 \\ 1 & 0 & 0 \\ 0 & 1 & 0 \end{bmatrix}. \qquad (5)$$

Finally, the FE discretization of the variation formulation (1) along the transverse directions x, y yields:

$$\{\mathbf{K}_1 - \omega^2\mathbf{M} + ik(\mathbf{K}_2 - \mathbf{K}_2^T) + k^2\mathbf{K}_3\}\mathbf{U} = \mathbf{0} \quad (6)$$

with the following elementary matrices:

$$\begin{gathered}\boldsymbol{K}_1^e = \int_{S^e} \boldsymbol{N}^{eT}\boldsymbol{L}_{\tilde{x}\tilde{y}}^T\boldsymbol{C}\boldsymbol{L}_{\tilde{x}\tilde{y}}\boldsymbol{N}^e\gamma_x\gamma_y dxdy \\ \boldsymbol{K}_2^e = \int_{S^e} \boldsymbol{N}^{eT}\boldsymbol{L}_{\tilde{x}\tilde{y}}^T\boldsymbol{C}\boldsymbol{L}_z\boldsymbol{N}^e\gamma_x\gamma_y dxdy \\ \boldsymbol{K}_3^e = \int_{S^e} \boldsymbol{N}^{eT}\boldsymbol{L}_z^T\boldsymbol{C}\boldsymbol{L}_z\boldsymbol{N}^e\gamma_x\gamma_y dxdy \\ \boldsymbol{M}^{\boldsymbol{e}} = \int_{S^e} \rho\boldsymbol{N}^{eT}\boldsymbol{N}^e\gamma_x\gamma_y dxdy\end{gathered}$$

where the column vector $\mathbf{U}$ contains nodal displacements and $\mathbf{N}^e$ is a matrix of nodal interpolating functions of displacement on the element.
Given ω and finding k, the eigenproblem (6) is quadratic. The linearization of this eigensystem is detailed in [4] for instance.

1.2 Cylindrical PML

The cylindrical PML defines the complex radial coordinate $\tilde{r}$:

$$\tilde{r} = \int_0^r \gamma(\xi)d\xi \quad (7)$$

where $\gamma(r)$=1 for $r \leq d_r$; $Im\{\gamma(r)\} > 0$ for $r > d_r$.
By using the change of variable $\tilde{r} \to r$ and a SAFE method, the strain-displacement relation becomes:

$$\boldsymbol{\epsilon} = (\mathbf{L}_{\tilde{r}\theta} + ik\mathbf{L}_z)\,\mathbf{u} \quad (8)$$

Before FE discretization, the formulation (1) and Eq. (8) are rewritten in Cartesian coordinates. For paper conciseness, the operator matrix $L_{\tilde{r}\theta}$ in Cartesian coordinates is not presented here.
Finally, it can be shown that the FE discretization of the variation formulation (1) along the transverse section yields the same equation as Eq.(6) with the elementary matrices obtained by replacing $\boldsymbol{L}_{\tilde{x}\tilde{y}}$ with $\mathbf{L}_{\tilde{r}\theta}$ and $\gamma_x\gamma_y$ with $\tilde{r}\gamma/r$.

2 Results

A numerical test is taken from the literature [1], consisting of a steel bar buried in a concrete infinite domain. The continuity of displacements and stresses is enforced at each interface, i.e. between the core and semi-infinite layers. Following the suggestion of [2], [3], the PML layer is close to the core in order to reduce the effects of the exponential growth of leaky modes on the numerical results. A Dirichlet condition is chosen at the exterior boundary of truncated domain. Finite elements are triangles with six nodes. γ_x, γ_y, γ in Eqs. (2) and (7) should be chosen as smooth as possible to minimize numerical reflection [5]. They are parabolic functions in this work.

A difficulty is that the method will not only provide trapped and leaky modes but also non-intrinsic modes corresponding to continua of radiation modes which are mainly resonating in the artificial layers and depend on the characteristics of these layers. A modal filtering step consists in identifying and separating physical modes from unwanted modes. The filtering criterion used for our tests is the ratio of kinetic energy in the PML region over the kinetic energy in the whole domain. Physical modes are then identified if this criterion is smaller than a user-defined value.

Numerical results will be shown during the conference to validate the SAFE-PML methods.

Further work will consist in extending the proposed approach to twisted waveguides in order to simulate helical structures buried in infinite solid media.

References

[1] Michel Castaings and Michael Lowe. Finite element model for waves guided along solid systems of arbitrary section coupled to infinite solid media. *Journal of the Acoustical Society of America*, 123(2):696–708.

[2] A. S. Bonnet-BenDhia, B. Goursaud, C. Hazard and A. Prieto. Finite element computation of leaky modes in stratified waveguides. In *5th Meeting of the Anglo-French-Research-Group*, volume 128, pages 73–86.

[3] B. Goursaud. *Étude mathématique et numérique de guides d'ondes ouverts non uniformes, par approche modale (Mathematical and numerical study of non uniform open waveguides, modal approach, in French)*. PhD thesis, École Polytechnique, 2010.

[4] F. Treyssède. Elastic waves in helical waveguides. *Wave Motion*, 45:457-470.

[5] F. Treyssède, K.-L. Nguyen, A.-S. Bonnet-BenDhia and C. Hazard. On the use of a a SAFE-PML technique for modeling 2D open elastic waveguides. *Acoustic 2012*, Nantes (France), April 23-27, 2012.

Wave trapping in slowly-varying waveguides

S. N. Gaulter[1,*], **N. R. T. Biggs**[1]
[1] Dept of Mathematics and Statistics, University of Reading
*Email: s.n.gaulter@pgr.reading.ac.uk

Abstract

The problem of determining the trapped modes present in various waveguides of slowly-varying cross section is discussed. By 'trapped mode', we refer to eigenmodes of the waveguide featuring a finite region of oscillatory energy, with exponential decay elsewhere.

The waveguide cross section changes over a length-scale L_x which is much larger than the characteristic cross section width, L_{yz}. Thus $\epsilon = L_{yz}/L_x \ll 1$ is a small parameter which can be exploited to develop an asymptotic scheme for determining the eigenfrequencies. The method is introduced by considering first the case of an acoustic waveguide with slowly-varying cross section, and is shown to be accurate to leading order, whilst computationally advantageous compared to a numerical scheme. It is then adapted to the problem of approximating solutions to the elastodynamic wave equation in similarly perturbed elastic plates, and we highlight the similarities and differences between the two cases.

Introduction

Motivated by prior research in, e.g., [2], we employ an asymptotic approach to first approximate the trapped mode solutions in the case of acoustic propagation in a smooth three-dimensional waveguide with a simply connected, but otherwise arbitrary cross section, with a slowly varying localised bulge, symmetric around the centre of its longitudinal axis, as in [1].

Comparing the eigenvalues obtained via this asymptotic analysis with those obtained numerically from a three-dimensional spectral collocation method, we find them to be in excellent agreement. Interestingly, we find that the relative error remains favourably small when the 'small' parameter is increased to unity.

Finally, we apply an analogue of this method to the problem of elastic propagation in a semi-infinite elastic plate, with a similarly slowly varying perturbation, symmetric around one longitudinal coordinate and constant in the other.

1 Acoustic waveguide

Orienting a three-dimensional waveguide along the x-axis, we take its cross section to be some simply connected domain $D(\epsilon x) \subset \mathbb{R}^2$, which depends smoothly on x. The waveguide is slowly-varying in the sense that $\epsilon = L_{yz}/L_x \ll 1$, where the waveguide cross section changes over a length scale L_x and L_{yz} is the characteristic waveguide width. In non-dimensional coordinates $(\xi, \eta, \zeta) = (x/L_x, y/L_{yz}, z/L_{yz})$, the governing Helmholtz equation is

$$\epsilon^2\phi_{\xi\xi} + \phi_{\eta\eta} + \phi_{\zeta\zeta} + k^2\phi = 0,$$

in which k is the non-dimensional wavenumber, to be solved subject to either Dirichlet ($\phi = 0$) or Neumann ($\phi_\nu = 0$) conditions on the waveguide boundary.

We apply a WKBJ-type ansatz of the form

$$\phi = (A_0 + \epsilon A_1 + \ldots)\exp\left(\epsilon^{-1}P_{-1} + \epsilon P_1 \ldots\right) \quad (1)$$

and equate coefficients of ϵ to find, to leading order, that the solutions are given by

$$\phi_n(\xi, \eta, \zeta) = \mathcal{A}_n|f_n'|^{-1/2}E_n \exp\left\{\epsilon^{-1}f_n\right\} + O(\epsilon),$$

where

$$f_n(\xi) = \begin{cases} \pm i\displaystyle\int^{\xi} \sqrt{k^2 - \lambda_n^2(\bar{\xi})}\,\mathrm{d}\bar{\xi} & \text{for } k \geq \lambda_n(\xi), \\ \pm\displaystyle\int^{\xi} \sqrt{\lambda_n^2(\bar{\xi}) - k^2}\,\mathrm{d}\bar{\xi} & \text{for } k \leq \lambda_n(\xi), \end{cases}$$

for constants $\mathcal{A}_n$ and where $\{\lambda_n(\xi), E_n(\xi; \eta, \zeta)\}$ is the n-th eigensolution over the waveguide cross section $D = D(\xi)$.

We hence see that the either oscillatory or decaying nature of the solution is determined by the relative magnitudes of the wavenumber, k, and the eigenvalues of the duct cross section at ξ, from which we can determine the region of trapping.

Since the symmetry of the waveguide tells us that $D(\xi) = D(-\xi)$, we may restrict our attention to the region $\xi \in [0, \infty)$. At the turning point, $\xi = \xi_n^* > 0$, defined as the solution of $k = \lambda_n(\xi_n^*)$, the solution breaks down, and a local analysis shows that there is a nonuniform region surrounding this point of width

$O(\epsilon^{2/3})$. The solution within this region is readily determined, and its form motivates the derivation of the uniform approximation.

We hence take a new ansatz, expanding in a basis of Airy functions, and generate a uniformly valid leading order solution, valid for $\xi \in [0, \infty)$,

$$\phi_n = \mathcal{B}_n |g'_{0;n}|^{-1/2} E_n \operatorname{Ai}\left(\epsilon^{-2/3} g_{0;n}\right) + O(\epsilon^{2/3}), \quad (2)$$

where $\mathcal{B}_n$ are constants and

$$g_{0;n} = \begin{cases} -\left(\frac{3}{2}\int_{\xi}^{\xi_n^*} \sqrt{k^2 - \lambda_n^2(\bar{\xi})}\,\mathrm{d}\bar{\xi}\right)^{2/3} & \text{for } \xi \le \xi_n^*, \\ \left(\frac{3}{2}\int_{\xi_n^*}^{\xi} \sqrt{\lambda_n^2(\bar{\xi}) - k^2}\,\mathrm{d}\bar{\xi}\right)^{2/3} & \text{for } \xi \ge \xi_n^*. \end{cases} \quad (3)$$

Given (2)–(3), we may solve the trapping problem for symmetric or antisymmetric modes, by imposing the additional conditions $\phi \to 0$ as $\xi \to \pm\infty$ and $\phi_\xi(0, \eta, \zeta) = 0$ or $\phi(0, \eta, \zeta) = 0$, respectively.

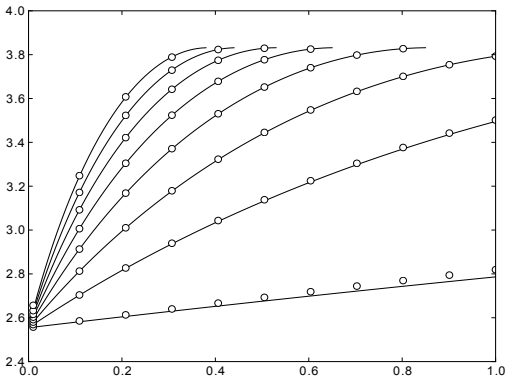

Figure 1: Asymptotic (lines) and numerical (circles) wavenumbers for the duct described by $\sqrt{\eta^2 + \zeta^2} \equiv h(\xi) = 1 + 0.5\operatorname{sech}\xi$, for varying small parameter $\epsilon \in [0.01, 1]$.

Figure 1 shows a comparison between the first eight wavenumbers obtained with this asymptotic scheme against a spectral collocation method for a sample waveguide with circular cross section, in which we see an excellent level of accuracy, even as the 'small' parameter, ϵ, approaches unity.

2 Elastic waveguide

The method described above is then applied to the different problem of the trapping of elastic waves within an elastic plate with slow perturbation along x, described by $z \equiv \pm h_\pm(\epsilon x)$ and constant in y. Because of plane strain on the plate, we assume no displacement in y and express the displacement vector as $\boldsymbol{u} = (u, 0, w)$, so that we may essentially treat the problem as two-dimensional. Then, by decomposing the displacement into dilational and rotational components,

$$\boldsymbol{u} = \nabla\phi + \nabla \times \boldsymbol{\psi}$$

where $\boldsymbol{\psi} = (0, \psi, 0)$, we may write the displacement vector as $\boldsymbol{u} = (\phi_x - \psi_z, 0, \phi_z + \psi_x)$, where $\phi(x, z)$ and $\psi(x, z)$ satisfy

$$\left(\nabla^2 + k_d^2\right)\phi = 0, \qquad \left(\nabla^2 + k_s^2\right)\psi = 0$$

individually, for the dilational and shear wavenumbers $k_{d,s} = \omega/c_{d,s}$. Thus the shear and dilational waves propagate independently inside the waveguide, but assuming clamped boundary conditions

$$\mp h'_\pm u + w = 0, \qquad u \pm h'_\pm w = 0$$

on $z = \pm h_\pm$, we find that the wave types are coupled on the boundary of the plate.

After non-dimensionalising the problem by mapping it onto a flat plate with the transformations

$$\xi = \epsilon x, \qquad \eta = -1 + \frac{2\,(z + h_-)}{h_+ + h_-}$$

the method described above for the acoustic case can be followed. In particular, expanding each of ϕ and ψ in the WKBJ-type ansatz as in (1), we find to leading order the compressionally symmetric solution

$$\phi \sim \alpha_0 \cosh(\nu_d \eta) \exp\left(\epsilon^{-1} f\right),$$
$$\psi \sim \frac{iwf' \cosh\nu_d}{2\nu_s \cosh\nu_s} \alpha_0 \sinh(\nu_s \eta) \exp\left(\epsilon^{-1} f\right)$$

where $w(\xi)$ denotes the plate width. The phase, $f(\xi)$, and transverse eigenvalues, $\nu_s(\xi)$ and $\nu_d(\xi)$, satisfy the Rayleigh-Lamb frequency equation

$$\frac{(wf')^2}{4\nu_d\nu_s} = \frac{\tanh\nu_d}{\tanh\nu_s},$$

and $\alpha_0(\xi)$ is determined at next order. Further results will be discussed in the presentation.

References

[1] S. N. Gaulter and N. R. T. Biggs. Acoustic trapped modes in a three-dimensional waveguide of slowly varying cross section. *Proc. R. Soc. Lond. A*, 469(2149), 2013.

[2] D. Gridin, R. V. Craster, and A. T. I. Adamou. Trapped modes in curved elastic plates. *Proc. R. Soc. Lond. A*, 461(2056):1181–1197, 2005.

3.17 Elastic waves

Surface Waves in Almost Incompressible Elastic Materials

K. Virta[1,*], **G. Kreiss**[1]
[1] Division of Scientific Computing, Department of Information Technology, Uppsala.
*Email: kristoffer.virta@it.uu.se

Abstract

A recent study shows that the classical theory concerning accuracy and points per wavelenghth is not valid for surface waves in almost incompressible elastic materials. The gridsize must instead be proportional to $(\frac{\mu}{\lambda})^{(1/p)}$ to achieve a certain accuracy. Here p is the order of the scheme and μ and λ are the Lame parameters. This accuracy requirement becomes very restrictive close to the incompressible limit where $\frac{\mu}{\lambda} \ll 1$, especially for low order methods. We present results concerning how to choose the number of gridpoints for 6th and 8th order summation-by-parts finite difference schemes. The result is applied to Lambs problem in an almost incompressible material.

Introduction

Consider the half - plane problem for the two - dimensional elastic wave equation in a homogeneous isotropic material. With time scaled to give unit density the displacement field $(u, v)^T$ is governed by

$$\begin{aligned} &u_{tt} = \mu\Delta u + (\lambda+\mu)(u_x + v_y)_x, \\ &v_{tt} = \mu\Delta v + (\lambda+\mu)(u_x + v_y)_y, \\ &(x, y) \in (-\infty, \infty) \times [0, \infty), t \geq 0. \end{aligned} \tag{1}$$

Initial data for $(u, v)^T$ and $(u_t, v_t)^T$ is given at $t = 0$. On the boundary $y = 0$ we consider normal stress boundary conditions,

$$\begin{aligned} &v_y + \tfrac{\lambda}{\lambda+2\mu} u_x = g(x, t), \\ &u_y + v_x = 0. \end{aligned} \tag{2}$$

It is well known that (1) - (2) admits compressional and shear waves as well as Rayleigh surface waves ([1]). For a fixed temporal frequency the wave length of the compressional and shear waves are proportional to $\sqrt{\lambda+2\mu}$ respective $\sqrt{\mu}$. The wavelength of the Rayleigh waves are proportional to $c_R\sqrt{\mu}$ where c_R depends on μ and λ and $0 < c_R < 1$. The classical theory ([2]) states that when using a finite difference scheme an accurate solution is guaranteed if the shortest wavelength is not smaller than a constant number of grid sizes, where the constant depends on the order of accuracy of the method. For the Rayleigh waves this corresponds to using a grid size proportional to $c_R\sqrt{\mu}$. However, in [3] H-O.Kreiss and N.A.Petersson show that to accurately simulate Rayleigh surface waves, the grid size should be proportional to $\left(\frac{\mu}{\lambda}\right)^{(1/p)}$. Here p is the order of accuracy of the method. The implications of this accuracy requirement become evident in almost incompressible media ($\lambda \gg \mu$). Then a larger than predicted number of grid points per Rayleigh wavelength is needed for an accurate solution.

Higher order methods

In [3] a 4th order method is used to illustrate the theory by comparing results obtained with a 2nd order method. We continue along this line and use the 6th and 8th order schemes of [4] to illustrate the benefits of using higher order methods to simulate Rayleigh surface waves. We use an analytic expression for a periodic train of Rayleigh surface waves to measure the relative max error obtained with a pth order method, e_p. The error is measured when the waves have propagated 10 periods. The number of points per wavelength,P, is increased until an relative max error of at most 5% is obtained. An example of results from this experiment with $\frac{\mu}{\lambda} = 10^{-3}$ is shown in Table 1. Here the superiority of methods of order higher than 4 becomes apparent. In fact, the 4th order scheme uses about 4 times as many points per wavelength predicted by the classical theory for an accuracy of 5%. These results are then used in the next section to predict the number of grid points needed to accurately solve Lambs problem [5] in an almost incompressible material.

P	e_4	e_6	e_8
13	5.7×10^{0}	6.6×10^{-1}	7.5×10^{-2}
25	9.4×10^{-1}	2.7×10^{-2}	4.3×10^{-3}
49	8.8×10^{-2}	-	-
97	6.3×10^{-3}	-	-

Table 1: Relative max error, e_p at time $T = 33.104$, with $\lambda = 1, \mu = 10^{-3}$

Application: Lambs problem in almost incompressible media

We solve a version of Lambs problem ([5]) in which the surface of a half - space is subjected to a periodic array of line sources with loading normal to the surface. Under these conditions compressional, shear and Rayleigh waves are generated. The normal stress forcing of (2) is then

$$g(x,y) = f(t)\delta(x - kM), M > 0, k = 0, \pm 1, \ldots,$$

where M is the distance between the sources and δ the Dirac delta function. We let f be the wavelet given by

$$f(t) = \begin{cases} \sin(2\pi\omega t) - \frac{1}{2}\sin(4\pi\omega t), & 0 \leq t \leq \frac{1}{\omega} \\ 0, \text{ else.} \end{cases}$$

f is shown as an inset in Fig 1(a) with $\omega = 1$. With $\lambda = 1, \mu = 10^{-3}$ the Rayleigh wave speed

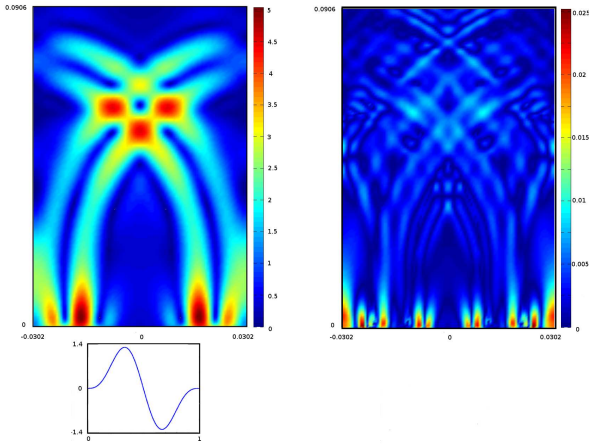

(a) Numerical solution (b) Relative error

Figure 1: The numerical solution (a) and the relative error (b) at time $t = 3.2$

becomes $c_R\sqrt{\mu} = 0.0302$. The highest significant frequency with $\omega = 1$ in the time function f is 2. The corresponding shortest wavelength is then $L_{\min} = \frac{c_R\sqrt{\mu}}{2} = 0.0151$. We choose the domain $[-2L_{\min}, 2L_{\min}] \times [0, 6L_{\min}]$, $M = 4L_{\min}$ and solve numerically until time $t = 3.2$. Figure 1(a) shows the magnitude of the displacement field. Periodic boundary conditions are applied at the vertical boundaries and the domain is truncated above with a perfectly matched layer ([6]). To estimate the required number of points per wavelength to achieve an relative max error of at most 5% with a 6th order method we consult Table 1 to conclude that 25 points per wavelength should suffice. To ascertain this claim a reference solution with 200 points per shortest wavelength is constructed. As a comparison a solution using 10 points per shortest wavelength, a quantity predicted by the classical theory to yield a relative error lower than 5%, is also computed. The results presented in Table 2 verifies the claim for this application. Figure (1(b)) shows the relative error in the magnitude of the displacement field. It is interesting to see that the main bulk of the error is seen to be located in the vicinity of the surface. Which is in accordance with the theory in [3], which predicts that the Rayleigh waves are much more sensitive to discretization errors than the shear and preassure waves.

P	e_6
10	7.5×10^{-1}
25	2.7×10^{-2}

Table 2: Points per shortest wavelength and corresponding relative max error.

References

[1] K.F.Graff, *Wave Motion In Elastic Solids*, Dover Publications, 1991

[2] B. Gustafsson, H-O. Kreiss and J. Oliger, *Time Dependent Problems and Difference Methods*, Wiley, 1995

[3] H-O. Kreiss, N.A. Petersson, *Boundary Estimates for the Elastic Wave Equation in Almost Incompressible Media*, SIAM. J. Numer. Anal, **50**, No 3, 2012, pp. 1556 - 1580

[4] K.Duru, G.Kreiss, K.Mattsson, *Accurate and Stable Boundary Treatments for Elastic Wave Equations in Second Order Formulation*, submitted manuscript, 2012

[5] H. Lamb, *On the propagation of tremors over the surface of an elastic solid*, Phil. Trans. R. Soc. **A203**, 1904, pp. 1-42

[6] K.Duru, G. Kreiss, *A Well - Posed and Discretely Stable Perfectly Matched Layer for Elastic Wave Equations in Second Order Formulation*, Commun. Comput. Phys, **11**, 2012, pp 1643 - 1672

Reflection of an elastic wave by a continuous, non differentiable acoustic velocity

O. Lafitte[1,2]
[1] LAGA, UMR 7539, Université Paris 13, Sorbonne-Paris-Cité, 99, avenue J.B. Clement, F-93430 Villetaneuse.
[2] CEA/DM2S, Centre d'études de Saclay, F-91 191 Gif sur Yvette Cedex.
*Email: olivier.lafitte@mines.org

Abstract

In this paper, we study a wave equation with index of refraction depending on the variable Z, such that $n^2(Z)$ has a C^1 discontinuity at $Z = 0$. For the simple case $n^2(Z) = n^2(0)1_{z<0} + n^2(0)(1 + \lambda Z)1_{Z>0}$, we exhibit an exact solution which is incoming from $-\infty$, which reflects on $Z = 0$ and we calculate the reflection operator on the interface $Z = 0$.

Introduction and statement of the physical problem

The notion of reflection coefficient is standard for waves propagating in a medium with a discontinuity along a planar interface. For a jump in the wave speed, or in the index of refraction, the Fresnel equations predict the amplitudes of the reflected and transmitted waves as a function of the angle of incidence. The Zoeppritz equations achieve the same result, and also predict mode conversion, in the case of discontinuous density and elastic Lamé parameters.

It is much less well known how to deal with other kinds of singularities in the medium properties, such as square root or ramp singularities. It was argued on physical grounds that reflection about a fractional interface should be the result of a fractional integrator of the same order on the incident wave, see for instance [3],[4]. Recognizing the fine structure of a reflector from the particular shape of the oscillations of the recorded waves in a seismic trace is an important method of interpretation in lithology, though one that has not been properly justified yet.

One may hope that the "fractional integrator" heuristic can be made precise by characterizing the reflection coefficient as a pseudodifferential operator of fractional order. We concentrate in this presentation to the case of a ramp, that is the model case described in the Abstract, before treating the general case (see [2]).

After partial Fourier transform in transverse variables and in time, and by choosing the adequate scaling of the variable z, one is left to:

"find the unique solution of $\frac{d^2}{dz^2}u + \omega^2(1 - \eta^2 + \lambda z)u = 0$ which coincides to the incoming wave from $-\infty$ equal to $u(z) = e^{-i\omega(1-\eta^2)^{\frac{1}{2}}z}$ for $z < 0$. and find the transmission and reflection coefficient on respectively outgoing at $+\infty$ and outgoing at $-\infty$ waves".

This will need precise definitions of incoming and outgoing waves both at $-\infty$ and $+\infty$ and of the unique representant of each of these waves, which is the aim of the next section.

Note that the time dependency chosen in this set-up is $e^{i\omega t}$, with $\omega > 0$, which accounts to $e^{-i\omega(1-\eta^2)^{\frac{1}{2}}z}$ being an incoming wave from $-\infty$ (with wave front $t = (1 - \eta^2)^{\frac{1}{2}}z$), and an outgoing wave to $-\infty$ is, similarly, $e^{i\omega(1-\eta^2)^{\frac{1}{2}}z}$. This classification is obvious in a constant coefficients medium, but needs to be clarified in a general medium (see next section).

1 Outgoing and incoming waves: definitions and properties

We deal with solutions of

$$\frac{d^2}{dz^2}u(z,\eta,\omega) + \omega^2(1 - \eta^2 + \lambda z)u(z,\eta,\omega) = 0 \quad (1)$$

Definition 1 *A outgoing solution to $+\infty$ of (1) is $u(z,\eta,\omega_0)$, $\omega_0 > 0$, such that, for $\omega = \omega_0(1 + i\sigma)$, $\sigma < 0$, the limit of $u(z,\eta,\omega)$ at $z \to +\infty$ is zero and the limit of $u(z,\eta,\omega)$ when $\sigma \to 0_-$ is $u(z,\eta,\omega_0)$.*

Definition 2 *An incoming solution from $+\infty$ of (1) is $u(z,\eta,\omega_0)$ such that, for $\omega = \omega_0(1+i\sigma)$, $\sigma > 0$, the limit of $u(z,\eta,\omega)$ at $z \to +\infty$ is zero and the limit of $u(z,\eta,\omega)$ when $\sigma \to 0_+$ is $u(z,\eta,\omega_0)$.*

A problem is to define the base solution in the space of incoming or outgoing solutions, because the above definitions do define vectorial spaces of dimension 1. In [2], we adopt a definition linked with the behavior at $+\infty$, because we do not know the values at $z = 0$. However, in the model case of this paper, we consider that the base outgoing solution (as well as the base incoming solution) is equal to 1 at $z = 0$. It is possible and straightforward thanks to properties of the Airy functions.

2 Exact solution of the problem and its properties

2.1 Explicit solutions in $z > 0$

The problem that we consider here is

$$\Delta\tilde{u} + \omega^2 n^2(z)\tilde{u} = 0, \tag{2}$$

with $n^2(z) = 1_{z<0} + (1+\lambda z)1_{z>0}$. Note that n^2 is continuous, with a discontinuity in the derivative on the surface $z = 0$.

The first part of the analysis of this problem is to consider the partial Fourier transform in (x, y), the associated wave number being $\omega(\eta_1, \eta_2)$, with $\eta_1^2 + \eta_2^2 = \eta^2, \eta \geq 0$. One then reverts to

$$\partial_{z^2}^2 u + \omega^2(n^2(z) - \eta^2)u = 0, \tag{3}$$

We first consider (3) in $z > 0$:

$$u'' + \omega^2(1 - \eta^2 + \lambda z)u = 0. \tag{4}$$

Introducing $w_\pm(X) = Ai(e^{\pm i\frac{\pi}{3}}X)$ a pair of satisfactory solutions of $U'' = -XU$, one checks that a pair of independent solutions of (4) is $(w_+(\theta(z + \frac{1-\eta^2}{\lambda})), w_-(\theta(z + \frac{1-\eta^2}{\lambda})))$, where $\theta^3 = \omega^2\lambda$, $\theta > 0$ We introduce $Z_0 = (1-\eta^2)\theta\lambda^{-1}$. In $z > 0$, one has

$$u(z) = Aw_+(\theta(z + \frac{1-\eta^2}{\lambda})) + Bw_-(\theta(z + \frac{1-\eta^2}{\lambda}))).$$

2.2 Outgoing and incoming solutions at $+\infty$ for (3)

We show in this paragraph that the decomposition of solutions of (3) on w_+, w_- is the suitable decomposition to study outgoing and incoming solutions at $+\infty$. Indeed, we have

Proposition 1 *The function w_- is in the space of incoming solutions from $+\infty$, and the function w_+ is in the space of outgoing solutions to $+\infty$ for (3).*

Proof: Let Ai and Bi be the classical solutions of $u'' = xu$ (see [1]). We have

$$Ai(Xe^{\pm i\frac{\pi}{3}}) = \frac{e^{\pm i\frac{\pi}{3}}}{2}[Ai(-X) \pm iBi(-X)]. \tag{5}$$

Using 10.4.59 of [1] and noticing that $X^{\frac{3}{2}} = \omega\lambda^{\frac{1}{2}}(z + \frac{1-\eta^2}{\lambda})^{\frac{3}{2}}$, and replacing ω by $\omega(1+i\sigma)$, $\sigma > 0$, and letting $z \to +\infty$, the solution w_+ corresponds to a phase behavior $e^{-(e^{i\frac{\pi}{3}})^{\frac{3}{2}}\omega(1+i\sigma)\frac{2}{3}(z+\frac{1-\eta^2}{\lambda})^{\frac{3}{2}}\lambda^{\frac{3}{4}}}$, which goes to 0 when $z \to +\infty$, hence is in the class of outgoing solutions to $+\infty$.

As the roots of the Airy are on the negative real axis, w_+ and w_- never vanish, hence the unique incoming solution from $+\infty$ on $[0, +\infty[$ is thus $\frac{w_-(\theta(z+\frac{1-\eta^2}{\lambda}))}{w_-(Z_0)}$, and the unique outgoing solution to $+\infty$ on $[0, +\infty[$ is $\frac{w_+(\theta(z+\frac{1-\eta^2}{\lambda}))}{w_+(Z_0)}$.

We have now, in $z > 0$ as well as in $z < 0$, the description of outgoing solutions to $+\infty$ and incoming solutions from $+\infty$ (Proposition 1) and outgoing solutions to $-\infty$ and incoming solutions from $-\infty$ (described in the Introduction) of (3). We want to study the reflected and the transmitted coefficients R and T when the incoming wave from $-\infty$. The situation is thus the following:

- in $]-\infty, 0[$, $u(z) = Re^{i\omega(1-\eta^2)^{\frac{1}{2}}z} + e^{-i\omega(1-\eta^2)^{\frac{1}{2}}z}$,
- in $]0, +\infty[$, $u(z) = T\frac{w_+(\theta(z+\frac{1-\eta^2}{\lambda}))}{w_+(Z_0)}$.

Note that, from $n^2 \in L^\infty$, u is in $W^{2,\infty}$ hence u is continuous, and u' is continuous. This yields:

$$\begin{cases} R + 1 = T \\ i\omega(1-\eta^2)^{\frac{1}{2}}(R-1) = T\theta\frac{w_+'(Z_0)}{w_+(Z_0)} \end{cases}$$

2.3 Reflection operator

Noting that $Z_0^{\frac{1}{2}} = (1-\eta^2)^{\frac{1}{2}}\frac{\omega}{\theta}$, this rewrites

$$\begin{cases} R + 1 = T \\ iZ_0^{\frac{1}{2}}(R-1) = T\frac{w_+'(Z_0)}{w_+(Z_0)} \end{cases}$$

The reflection coefficient is thus

$$R(\omega, \eta) = \frac{iZ_0^{\frac{1}{2}} + \frac{w_+'(Z_0)}{w_+(Z_0)}}{iZ_0^{\frac{1}{2}} - \frac{w_+'(Z_0)}{w_+(Z_0)}}. \tag{6}$$

Note that it is a pseudo differential operator, hence obtaining the result sought.

Proposition 2 *The reflection operator $\mathcal{R}(\omega, \xi)$ for the ramp problem is defined by its pseudo differential symbol $R(\omega, \frac{\xi}{\omega})$. There exists two sequences α_k, β_k such that*

$$R(\omega, \eta) \simeq i\frac{\lambda}{\omega}(1-\eta^2)^{-\frac{3}{2}}\frac{\sum_{k\geq 0}\alpha_k(\frac{\omega}{\lambda})^{-n}(1-\eta^2)^{-\frac{3n}{2}}}{\sum_{k\geq 0}\beta_k(\frac{\omega}{\lambda})^{-n}(1-\eta^2)^{-\frac{3n}{2}}}. \tag{7}$$

Away from the glancing rays ($1 - \eta^2 \geq \epsilon_0 > 0$ or, equivalently $\omega^2 - \xi^2 \geq \frac{\epsilon_0}{2-\epsilon_0}(\omega^2 + \xi^2)$), it is an operator of order -1.

Proof: We use explicitly the expansion of the Airy function (10.4.59 of [1] and 10.4.61 of [1]):

$$\frac{Ai'(u)}{Ai(u)} \simeq -u^{\frac{1}{2}} \frac{\sum(-1)^k c_k (\frac{2}{3})^{-k} u^{-\frac{3k}{2}}}{\sum(-1)^k (\frac{2}{3})^{-k} d_k u^{-\frac{3k}{2}}}$$

with $c_0 = d_0 = 1$, and for $u = e^{i\frac{\pi}{3}}(1-\eta^2)(\frac{\omega}{\lambda})^{\frac{2}{3}}$, for which $-e^{i\frac{\pi}{3}}u^{\frac{1}{2}}$ is equal to $-iZ_0^{\frac{1}{2}}$ and $-u^{-\frac{3}{2}} = iZ_0^{-\frac{3}{2}}$, we deduce the relation

$$R(\omega,\eta) = \frac{\sum_k (i\frac{2}{3})^{-k} Z_0^{-\frac{3k}{2}} (c_k - d_k)}{\sum_k (i\frac{2}{3})^{-k} Z_0^{-\frac{3k}{2}} (c_k + d_k)}$$

hence with $c_0 = d_0$ the expansion (7), which leads to the the estimate in (ω,ξ), valid thanks to $\omega^2 - \xi^2 \in (\omega^2+\xi^2)[\frac{\epsilon_0}{2-\epsilon_0}, 1]$.

Extensions of this method, in which the most difficult thing is to identify the incoming or outgoing solutions in $[0,+\infty[$, suggest that the reflection operator is of order $-\alpha$, where $\alpha > 1$ is the fractional regularity of $n^2(Z)$ at $Z = 0$, and can be expressed through Jost integrals (see [2]).

2.4 Extension to a layer

Assume now that the index of refraction is continuous, and that the size of the layer in which n^2 has a ramp is δ. Denote by $Z_\delta = (\frac{1-\eta^2}{\lambda} + \delta)\theta$. We know that the base outgoing solution at $+\infty$ in $[\delta,+\infty[$ is $e^{-i\omega(1-\eta^2+\lambda\delta)^{\frac{1}{2}}(z-\delta)}$ (and the conjugate function is the unique incoming solution). We denote by R_1 and T_1 the reflected (resp transmitted) coefficient. One has:

- in $]-\infty,0[$: $u(z) = R_1 e^{i\omega(1-\eta^2)^{\frac{1}{2}}z} + e^{-i\omega(1-\eta^2)^{\frac{1}{2}}z}$,
- in $]0,\delta[$: $u(z) = Aw_+(z) + Bw_-(z)$,
- in $]\delta,+\infty[$: $u(z) = T_1 e^{-i\omega(1-\eta^2+\lambda\delta)^{\frac{1}{2}}(z-\delta)}$.

From the condition at $z = \delta$, one deduces the relation:

$$Aw'_+(Z_\delta) + Bw'_-(Z_\delta) = -iZ_\delta^{\frac{1}{2}}(Aw_+(Z_\delta) + Bw_-(Z_\delta)),$$

The condition at $z = 0$ yields

$$\begin{cases} R_1 + 1 = Aw_+(Z_0) + Bw_-(Z_0) \\ iZ_0^{\frac{1}{2}}(R_1 - 1) = Aw'_+(Z_0) + Bw'_-(Z_0) \end{cases}$$

from which one deduces R_1. By investigation, R_1 is a pseudodifferential of order -1 as well, thanks to the equality $R_1 = \frac{D_1(\omega,\eta)}{D(\omega,\eta)}$, with

$$D = \begin{vmatrix} -1 & w_+(Z_0) & w_-(Z_0) \\ -iZ_0^{\frac{1}{2}} & w'_+(Z_0) & w'_-(Z_0) \\ 0 & w'_+(Z_\delta) + iZ_\delta^{\frac{1}{2}} w_+(Z_\delta) & w'_-(Z_\delta) + iZ_\delta^{\frac{1}{2}} w_-(Z_\delta) \end{vmatrix}$$

and

$$D_1 = \begin{vmatrix} 1 & w_+(Z_0) & w_-(Z_0) \\ -iZ_0^{\frac{1}{2}} & w'_+(Z_0) & w'_-(Z_0) \\ 0 & w'_+(Z_\delta) + iZ_\delta^{\frac{1}{2}} w_+(Z_\delta) & w'_-(Z_\delta) + iZ_\delta^{\frac{1}{2}} w_-(Z_\delta) \end{vmatrix}$$

Define $Q_\pm = \frac{w'_\pm(Z_0)}{w_\pm(Z_0) iZ_0^{\frac{1}{2}}}, Q_\pm^\delta = \frac{w'_\pm(Z_\delta)}{w_\pm(Z_\delta) iZ_\delta^{\frac{1}{2}}}, T_\pm = \frac{w_\pm(Z_\delta)}{w_\pm(Z_0)}$. One obtains

$$\frac{D}{iZ_0^{\frac{1}{2}} w_+(Z_0) w_-(Z_0)} = \begin{vmatrix} -1 & 1 & 1 \\ -1 & Q_+ & Q_- \\ 0 & (1+Q_+^\delta)\frac{Z_\delta^{\frac{1}{2}}}{Z_0^{\frac{1}{2}}} T_+ & (1+Q_-^\delta)\frac{Z_\delta^{\frac{1}{2}}}{Z_0^{\frac{1}{2}}} T_- \end{vmatrix}$$

$$\frac{D_1}{iZ_0^{\frac{1}{2}} w_+(Z_0) w_-(Z_0)} = \begin{vmatrix} 1 & 1 & 1 \\ -1 & Q_+ & Q_- \\ 0 & (1+Q_+^\delta)\frac{Z_\delta^{\frac{1}{2}}}{Z_0^{\frac{1}{2}}} T_+ & (1+Q_-^\delta)\frac{Z_\delta^{\frac{1}{2}}}{Z_0^{\frac{1}{2}}} T_- \end{vmatrix}$$

hence the same regularity result on the reflection coefficient.

3 Conclusions

For the simplest model of C^1 discontinuity (namely where $n^2(x,y,z) = 1+\lambda z$ for $z > 0$, and $n^2(x,y,z) = 1$ for $z < 0$), we are able to define outgoing and incoming solutions at $+\infty$. From these definitions we derive the reflection operator, which is a pseudodifferential operator of order -1. This result holds also for a layer in which n^2 has a ramp. It agrees with the arguments of [3], [4] mentioned in the Introduction. Under investigations are the analysis of the relations between micro local outgoing solutions and outgoing solutions, as well as the generalization to a general fractional singularity of the interface (see [2]).

References

[1] M. Abramovitz and I.A. Stegun *H*andbook of mathematical functions Dover Books, 9th Edition.

[2] L. Demanet and O. Lafitte, *The reflection operator for a fractional reflector*, in preparation.

[3] F. J. Herrmann Singularity characterization by mono scale analysis: application to seismic imaging *Appl. Comput. Harmon. Anal.* 11:64-88 (2001)

[4] F. J. Herrmann Multi-fractional splines: application to seismic imaging *Proc. SPIE Wavelets X*, San Diego, 2003

[5] O. Vallee and M. Soarez *Airy functions and applications to physics*, World Scientific Press 2004.

Existence of surface waves in an elastic half-plane with impedance boundary conditions

E. Godoy[1,*], **M. Durán**[2], **J.-C. Nédélec**[3]
[1]Ingenieros Matemáticos Consultores Asociados S.A. (INGMAT), Santiago, Chile
[2] Facultad de Ingeniería, Pontificia Universidad Católica de Chile, Macul, Santiago, Chile.
[3] Centre de Mathématiques Appliquées, École Polytechnique, 91128 Palaiseau Cedex, France.
*Email: eduardo.godoy@ingmat.com

Abstract

In this work, the problem of surface waves in an isotropic elastic half-plane with impedance boundary conditions (IBCs) is investigated. It is assumed that the boundary is free of normal traction and the shear traction varies linearly with the tangential displacement times the frequency, where the impedance corresponds to the constant of proportionality. The standard traction-free boundary conditions are then retrieved for zero impedance. The secular equation for surface waves with IBCs is given in explicit form. The existence and uniqueness of the Rayleigh wave is properly established, and it is found that its velocity varies with the impedance. Moreover, we prove that an additional surface wave exists in a particular case, whose velocity lies between those of the longitudinal and the transverse waves. Numerical results are presented.

1 Introduction and basic equations

Elastic surface waves are of particular importance in seismology, because they are the most destructive in earthquakes. In a geological context, it is usually assumed that the bounding surfaces are traction-free, which is mathematically expressed by Neumann boundary conditions, whereas other types of boundary conditions as IBCs are far less frequent. Some authors that have previously studied elastic surface waves with IBCs are Tiersten [1], Malischewsky [2] and Bövik [3]. The present work considers elastic surface waves in an isotropic elastic half-plane with particular IBCs prescribed on its surface (cf. [4]).

Given Cartesian coordinates (x_1, x_2), we consider the half-plane $x_2 > 0$ occupied by an isotropic elastic solid with constant density ρ. For $1 \leq i \leq 2$, the displacement components are denoted by u_i. The components of the stress tensor, denoted by σ_{ij}, are given in terms of u_i through the Hooke's law for isotropic materials: $\sigma_{ij} = \lambda u_{k,k} + \mu(u_{i,j} + u_{j,i})$, where λ, μ stand for the Lamé's constants. The time-harmonic waves are governed by the equation $\sigma_{ij,j} + \rho\omega^2 u_i = 0$, where ω is the angular frequency.

2 Impedance boundary conditions and secular equation

Malischewsky [2] proposed a general form of IBCs in seismology. In the 2D case, it is given by (summation convention does not hold for underlined indices):

$$\sigma_{i2} + \varepsilon_{\underline{i}} u_{\underline{i}} = 0, \qquad \text{for } x_2 = 0, \tag{1}$$

where the impedance parameters ε_i have the dimensions of stress/length. The associated secular equation (or dispersion relation) for surface waves is

$$\begin{aligned} &\big(2s^2 - s_T^2\big)^2 - 4s^2\sqrt{s^2 - s_L^2}\sqrt{s^2 - s_T^2} \\ &+\frac{1}{\mu\omega}\, s_T^2\Big(\varepsilon_1\sqrt{s^2 - s_T^2} + \varepsilon_2\sqrt{s^2 - s_L^2}\Big) \\ &-\frac{1}{\mu^2\omega^2}\,\varepsilon_1\varepsilon_2\Big(s^2 - \sqrt{s^2 - s_L^2}\sqrt{s^2 - s_T^2}\Big) = 0, \end{aligned} \tag{2}$$

where the unknown s is the surface wave slowness (reciprocal of velocity), $s_L = \sqrt{\rho/(\lambda + 2\mu)}$ is the longitudinal wave slowness, and $s_T = \sqrt{\rho/\mu}$ is the transverse wave slowness ($s_T > s_L$).

We assume that the surface $x_2 = 0$ is free of normal traction, and the shear traction varies linearly on the tangential component of the displacement times the frequency, that is, $\varepsilon_1 = \omega Z$ and $\varepsilon_2 = 0$ in (1) and (2), where $Z \in \mathbb{R}$ is an impedance parameter that has the dimensions of stress/velocity. The IBCs are then obtained from (1):

$$\sigma_{12} + \omega Z u_1 = 0, \quad \sigma_{22} = 0, \qquad \text{for } x_2 = 0. \tag{3}$$

and the corresponding secular equation from (2):

$$\begin{aligned} \big(2s^2 - s_T^2\big)^2 - 4s^2\sqrt{s^2 - s_L^2}\sqrt{s^2 - s_T^2} \\ +\frac{Z}{\mu}\, s_T^2\sqrt{s^2 - s_T^2} = 0. \end{aligned} \tag{4}$$

If $Z = 0$ we retrieve in (3) the usual traction-free boundary conditions and (4) becomes the classic secular equation for Rayleigh waves. Only real solutions of (4) have physical meaning, since a complex slowness gives rise to displacements that do not tend to zero at infinity which is inadmissible. As (4) only depends on s^2, it suffices to consider $s > 0$.

3 Surface wave analysis

The following propositions provide some characteristics of the solutions to the secular equation (4).

Proposition 1. *For each impedance $Z \in \mathbb{R}$ the secular equation* (4) *has a unique solution in the range $s > s_T$. This solution corresponds to the Rayleigh wave slowness and is strictly increasing in Z.*

Proposition 2. *If the impedance Z takes the positive value $Z^* \equiv 2\mu\sqrt{s_T^2/2 - s_L^2}$, then the secular equation* (4) *has one real solution in the range $s_L < s < s_T$. This solution is given by $s^* \equiv s_T/\sqrt{2}$ and corresponds to the slowness of an additional surface wave.*

Proposition 3. *Let us assume a perturbed value of the impedance $Z = Z^*(1+\varepsilon)$, where ε is a real parameter satisfying $|\varepsilon| << 1$. Then the secular equation* (4) *has a complex solution s satisfying $s_L \leq \mathfrak{Re}\{s\} \leq s_T$. Locally, this solution can be approximated as $s = s^*\big(1 + a\,\varepsilon + (b + \mathrm{i}c)\varepsilon^2\big) + o(\varepsilon^3)$, where a, b and c are real numbers, with $c > 0$.*

Proposition 1 generalises the standard Rayleigh wave to the case of IBCs. Proposition 2 establishes the existence of an additional surface wave in the range $s_L < s < s_T$ for a particular value of Z. Proposition 3 states that the associated slowness becomes complex if this value of Z is perturbed, hence it corresponds to a local uniqueness result of the additional wave.

4 Numerical results

We present next some numerical results for three elastic materials. The secular equation (4) was numerically solved in function of Z. The Rayleigh solution is presented in Fig. 1 and the additional solution is shown in Figs. 2 and 3. These results agree with the analysis performed in the previous section.

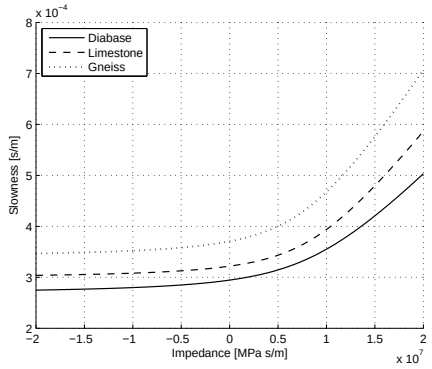

Figure 1: Rayleigh solution as a function of the impedance.

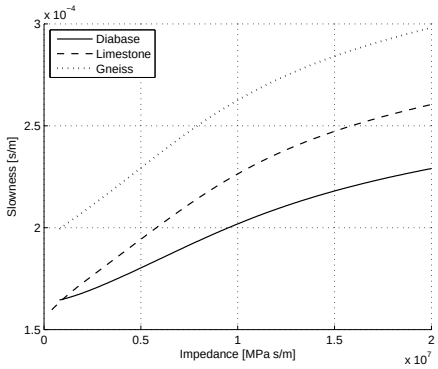

Figure 2: Real part of the additional solution as a function of the impedance.

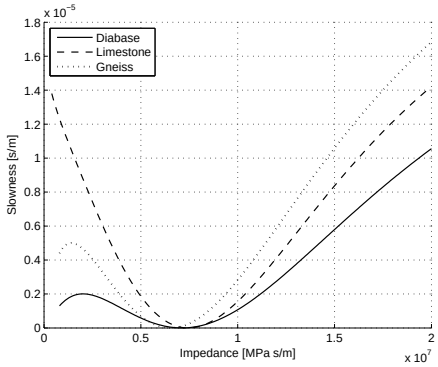

Figure 3: Imaginary part of the additional solution as a function of the impedance.

Acknowledgements

The first author was supported by the program Advanced Human Capital Job Insertion in the Industry, CONICYT, Chile.

References

[1] H. F. Tiersten, *Elastic surface waves guided by thin films*, J. Appl. Phys., **40** (1969), pp. 770–789.

[2] P. G. Malischewsky, *Surface Waves and Discontinuities*, Elsevier, Amsterdam, 1987.

[3] P. Bövik, *A comparison between the Tiersten model and $O(h)$ boundary conditions for elastic surface waves guided by thin layers*, Transactions of the ASME, **63** (1996), pp. 162–167.

[4] E. Godoy, M. Durán and J.-C. Nédélec, *On the existence of surface waves in an elastic half-space with impedance boundary conditions*, Wave Motion, **49** (2012), pp. 585–594.

Multi-wavelength sized finite elements for three-dimensional elastic wave problems

M.S. Mahmood[1], **O. Laghrouche**[1,*], **J. Trevelyan**[2]
[1] Institute for Infrastructure and Environment, Heriot-Watt University, Edinburgh EH14 4AS, UK
[2] School of Engineering and Computing Sciences, Durham University, Durham DH1 3LE, UK.
*Email: o.laghrouche@hw.ac.uk

Abstract

The aim of this work is to develop finite elements capable of containing many wavelengths per nodal spacing for three dimensional elastic wave problems. This will be achieved by applying the plane wave basis decomposition to the three dimensional elastic wave equation. The proposed elements will allow us to relax the traditional requirement of around ten nodal points per wavelength, used in polynomial based finite elements, and therefore solve elastic wave problems without refining the mesh of the computational domain at each frequency. The accuracy and effectiveness of the proposed technique will be determined by comparing solutions for selected problems with available analytical solutions.

Theory and preliminary results

Plane wave basis finite elements were developed and implemented to solve acoustic [1]and elastic wave problems [2]. The idea consist to relax the grid density by the incorporation of the physical features of the problem in the finite element space. Many other techniques have been developed for the same objective such as the discontinuous enrichment method, the ultra weak variational formulation, the partition of unity boundary element method, the least-squares method and the oscillated polynomials based finite elements. These approaches led to elements capable of containing many wavelengths per nodal spacing and have been very successful in reducing the computing effort associated to the high frequency.

Let Ω be a spacial domain in $\mathbb{R}^3$, occupied by an elastic medium and Γ its boundary. We will denote by $(\mathbf{e}_1, \mathbf{e}_2, \mathbf{e}_3)$ the cartesian vector system and by $\mathbf{x} = x_1\mathbf{e}_1 + x_2\mathbf{e}_2 + x_3\mathbf{e}_3$ a generic point in $\mathbb{R}^3$. Under the assumption that Ω is linear, homogenous and isotropic, and in the absence of a body force, the following homogeneous Navier equation holds

$$-\rho\omega^2\mathbf{u} - \nabla\cdot\boldsymbol{\sigma}(\mathbf{u}) = 0, \tag{1}$$

where the stress tensor $\boldsymbol{\sigma}$ is defined, via the classical Hooke's law, by $\boldsymbol{\sigma}(\mathbf{u}) = \lambda\nabla\cdot\mathbf{u}\,\mathbf{I} + \mu(\nabla\mathbf{u} + \nabla\mathbf{u}^\top)$ for a given displacement field $\mathbf{u} = u_1\mathbf{e}_1 + u_2\mathbf{e}_2 + u_3\mathbf{e}_3$, $\mathbf{I}$ is the identity matrix, λ and μ are the Lamé parameters of the elastic material, ω is the circular frequency, ρ is the density of the medium, assumed constant, and $\nabla\mathbf{u} = (\nabla u_1, \nabla u_2, \nabla u_3)^\top$. Let us denote, respectively, by $\mathbf{n}$ and $\mathbf{t}$ the outward unit normal and tangent vectors to the boundary Γ. The time harmonic elastic wave equation (1) is completed by a Robin type boundary condition on Γ

$$\begin{aligned}\boldsymbol{\sigma}(\mathbf{u})\mathbf{n} &= \mathrm{i}[(\lambda+2\mu)k_P(\mathbf{u}\cdot\mathbf{n})\mathbf{n} \\ &+ \mu k_S(\mathbf{u}\cdot\mathbf{t})\mathbf{t}] + \mathbf{g},\end{aligned} \tag{2}$$

where $\mathrm{i} = \sqrt{-1}$ is the imaginary unit number, k_P and k_S are, respectively, the P and S wave numbers, and $\mathbf{g}$ is a source term.

We first derive the variational formulation. Let us introduce the usual Sobolev space $\mathbf{V} = H^1(\Omega)\times H^1(\Omega)$. Taking into account (2), multiplying (1) by the complex conjugate of a test function $\mathbf{v}$ in $\mathbf{V}$ and integrating by parts over Ω we get the following variational problem:

Find $\mathbf{u}$ in $\mathbf{V}$ such that for all $\mathbf{v}$ in $\mathbf{V}$,

$$\begin{aligned}&- \omega^2\rho\int_\Omega \mathbf{u}\cdot\bar{\mathbf{v}}\,d\Omega + \int_\Omega \boldsymbol{\sigma}(\mathbf{u})\cdot\nabla\bar{\mathbf{v}}\,d\Omega \\ &- \mathrm{i}\int_\Gamma((\lambda+2\mu)k_P(\mathbf{u}\cdot\mathbf{n})\,(\bar{\mathbf{v}}\cdot\mathbf{n}) \\ &+ \mu k_S(\mathbf{u}\cdot\mathbf{t})\,(\bar{\mathbf{v}}\cdot\mathbf{t}))\,d\Gamma = \int_\Gamma \mathbf{g}\cdot\bar{\mathbf{v}}\,d\Gamma.\end{aligned} \tag{3}$$

Let us consider a finite element mesh containing n nodes, denoted z, $z = 1, n$. We denote by $\{N_z\}$ the partition of unity by polynomial finite element shape functions, and respectively by m_P and m_S the numbers of approximating P and S plane waves. The displacement $\mathbf{u}$ is approximated as follows

$$\begin{aligned}\mathbf{u}_h &= \sum_{z=1,n}\sum_{l=1,m_P} N_z A^P_{z,l}\exp(\mathrm{i}k_P\mathbf{x}\cdot\mathbf{d}^l_P)\mathbf{d}^l_P \\ &+ \sum_{z=1,n}\sum_{l=1,m_S} N_z A^{S,1}_{z,l}\exp(\mathrm{i}k_S\mathbf{x}\cdot\mathbf{d}^l_S)\mathbf{d}^{l,1}_{S,\perp} \\ &+ \sum_{z=1,n}\sum_{l=1,m_S} N_z A^{S,2}_{z,l}\exp(\mathrm{i}k_S\mathbf{x}\cdot\mathbf{d}^l_S)\mathbf{d}^{l,2}_{S,\perp},\end{aligned} \tag{4}$$

where h is the computational mesh size. The vectors $\mathbf{d}_{S,\perp}^{l,1}$ and $\mathbf{d}_{S,\perp}^{l,2}$ are orthogonal to each other and lie in the orthogonal plane to $\mathbf{d}$. For convenience, the directions $\mathbf{d}_P^l$ and $\mathbf{d}_S^l$ are chosen uniformly distributed in space. This latter remark raises a problem as it is very restrictive and not straightforward to uniformly distribute an arbitrary number of directions in space. The problem (3) leads to an invertible linear algebraic system provided that the approximating plane waves are linearly independent. The integration of the element matrices is performed using high order Gauss-Legendre scheme involving large numbers of integration points. Hence, at this stage, the computational effort shifts from the solver to the assembling process. The global matrix of the resulting system is symmetrical and block banded. The solution of the final system is obtained via a direct solver based on LDL^T decomposition where L^T is the transpose of the lower triangular matrix L and D is a diagonal matrix.

Let us consider the case of displacements caused by progressive plane waves, in a three dimensional elastic infinite medium, of the form $\mathbf{u} = \exp(\mathrm{i}k_P\mathbf{x}\cdot\mathbf{d}_P)\mathbf{d}_P + \exp(\mathrm{i}k_S\mathbf{x}\cdot\mathbf{d}_S)\mathbf{d}_{S,\perp}^1 + \exp(\mathrm{i}k_S\mathbf{x}\cdot\mathbf{d}_S)\mathbf{d}_{S,\perp}^2$. The source term $\mathbf{g}$ of expression (2) is evaluated and prescribed on Γ. All parameters λ, μ and ρ are taken equal to 1 with their respective corresponding units. The finite elements used here are 8-noded cubes and their geometry is interpolated via Lagrange polynomials. We consider three uniform mesh grids denoted by h_1, $h_{\frac{1}{2}}$ and $h_{\frac{1}{4}}$ for the domain $1 \le x_1, x_2, x_3 \le 3$. The coarser mesh h_1 has 8 elements and the finer mesh $h_{\frac{1}{4}}$ has 512 elements. Table 1 shows the L_2 error given by $||\mathbf{u}_h - \mathbf{u}||_{L_2(\Omega)}/||\mathbf{u}||_{L_2(\Omega)} \times 100\%$, where the Euclidean norm of the real part of $\mathbf{u}_h$ is given by $|Re(\mathbf{u}_h)|$, for increasing number of approximating plane waves and for different values of the circular frequency $\omega = 1, 5, 10$, respectively.

From the numerical results it is obvious that h-refinement improves the accuracy of the scheme for all cases of frequencies and plane wave enrichments. This is expected as a refinement of the mesh leads to a higher number of degrees of freedom (DOF) per wavelength. Increasing the number of approximating plane waves, however, did improve the results only at the highest considered frequency, $\omega = 10$, while it did not have any effect at $\omega = 1$ and 5. This is most likely due to the ill conditioning, which is an inherent feature of the plane wave basis finite elements, especially at low frequencies and for high numbers of DOF per wavelength. Such behaviour was also noticed in previous work related to acoustic wave modelling for which the benefit of using such elements was obvious at high frequencies and for low DOF per wavelength. Extensive numerical testing is currently underway to properly assess the effectiveness of the developed elements for three dimensional elastic wave problems, including the effect of conditioning. At this stage, the evaluation of the element matrices is carried out using a high-order Gauss-Legendre quadrature, which involves many integration points depending on the nodal spacing in terms of the characteristic wavelength of the problem. This latter issue requires significant computational time for increasing nodal spacing, in terms of the wavelength, and hence a semi-analytical integration scheme becomes necessary in order to run simulations in practical times.

(m_P, m_S)	(10,10)	(26,26)
h_1	0.137	0.137
$h_{\frac{1}{2}}$	0.100	0.100
$h_{\frac{1}{4}}$	0.075	0.075
h_1	1.221	0.727
$h_{\frac{1}{2}}$	0.395	0.396
$h_{\frac{1}{4}}$	0.205	0.208
h_1	27.454	6.126
$h_{\frac{1}{2}}$	1.673	0.780
$h_{\frac{1}{4}}$	0.531	0.255

Table 1: L_2 error in % for $\omega = 1$ (top), $\omega = 5$ (middle) and $\omega = 10$ (bottom).

References

[1] E. Perrey-Debain, O. Laghrouche, P. Bettess and J. Trevelyan, Plane wave basis finite elements and boundary elements for three dimensional wave scattering, *Phil. Trans. R. Soc. Lond. A*, **362** (2004), pp.561-577.

[2] A. El Kacimi and O. Laghrouche, Numerical modelling of elastic wave propagation in frequency domain by the partition of unity finite element method, *Int. J. Numer. Meth. Engng*, **77** (2009), pp. 1646-1669.

Index